Inhibition of UHRF1 protein by epigenetic partners and epi-drugs

Tanveer Ahmad

UNIVERSITÉ DE STRASBOURG

ÉCOLE DOCTORALE DES SCIENCES DE LA VIE ET DE DA SANTE

Laboratoire de Bioimagerie et Pathologies – LBP UMR 7021

THÈSE présentée par :

Tanveer AHMAD

Soutenue le : **20 Novembre 2019**

Pour obtenir le grade de : **Docteur de l'Université de Strasbourg**

Discipline/ Spécialité : DOCTORAT Sciences Pharmacologie-Pharmacocinétique

Inhibition de la protéine UHRF1 par les partenaires épigénétiques et les épi-drogues

THÈSE dirigée par :

M. MOUSLI Marc	Chargé de Recherche, INSERM, UMR 7021

RAPPORTEURS :

Mme. EYMIN Béatrice	Directeur de Recherche, Institut pour l'Avancée des Biosciences, Université Grenoble Alpes
M. CARTRON Pierre-François	Chargé de Recherche**,** Centre de Recherche en Cancérologie et Immunologie, Nantes-Angers

AUTRE MEMBRE DU JURY (EXAMINATEUR) :

Mme. DANTZER Françoise	Directeur de Recherche, ESBS, UMR7242

MEMBRES INVITÉS :

Mme. DUBREZ Laurence	Chargé de Recherche, Université de Bourgogne
M. BRONNER Christian	Chargé de Recherche, IGBMC

THIS DISSERTATION IS DEDICATED TO MY BELOVED PARENTS

ACKNOWLEDGEMENTS

I acknowledge all the people who helped me to complete this dissertation:

In the first place, to Dr. Marc MOUSLI, my mentor, for his remarkable guidance, extraordinary mentoring, unconditional support, extensive motivation and impressive scientific discussions during last four years. In particular, I am grateful for his time and efforts dedicated to different aspects of my scientific growth including, but not limited to, augmenting productivity, learning of experimental & technical skills, improving scientific thinking and communication skills. I would also like to express my gratitude to my co-supervisor Dr. Christian Bronner for his precious time, worthwhile suggestions, essential support and critical comments regarding project.

On a special note, I am indebted to Professor Yves MELY for his outstanding support, valuable time, extraordinary knowledge, fruitful advices & discussions and his prime example of scientific leadership which inspired me a lot.

I really appreciate my jury members Dr. Béatrice EYMIN, Dr. Laurence DUBREZ, Dr. Françoise DANTZER and Dr. Pierre-François CARTRON for accepting our request to evaluate this thesis.

I am thankful to members of my thesis advisory committee Dr. Ali HAMICHE and Dr. Christian D. MULLER for their time, evaluation, critical discussion, suggestions and providing me lab facilities to complete this project.

Many thanks to Dr. Ludovic RICHERT and Dr. Pascal DIDIER for helping me in acquisition and analysis of FLIM experiments. Thanks a lot to members of Plateforme d'Imagerie Quantitative Romain VAUCHELLES, Dr. Philippe CARL and Philippe RONDE for their help in confocal microscopy and live cell imaging experiments. I would also like to thank Dr. Abdulkhaleg IBRAHIM for his help in protein purification and cell line preparations.

I truly appreciate the permanent staff of Laboratory of Bioimaging and Pathologies for their scientific discussions and help, Dr. Christian BOUDIER, Dr. Emmanuel BOUTANT, Dr.

Julien GODET, Dr. Eleonore REAL, Dr. Nicolas HUMBERT, Dr. Patrice RASSAM, Tania STEFFAN and Thiebault LEQUEU.

Special thanks to Marlyse WERNERT and Ingrid BARTHEL for always helping me in administrative procedures.

Sincere thanks to my small UHRF1 team: Waseem ASHRAF and Liliyana Zaayter. Their amazing personalities, faithful company and endless laughs during good and bad times made this journey easier for me. I really appreciate your care, support and guidance.

Thanks to the current and past lab mates Rajhans, Lesia, Manu, Redouane, Vanille, Krishna, Maaz, Jaganaath, Sarwat, Marianna, Nina, Oleksi, Raphael, Stefano, Tannoo, Hasan, Nario, Tina, Soraya, Sara, Imtiaz, Sani, Antoine, Mario and Marléne for their help, motivation, discussion and enjoyable company. Special and sincere thanks to Malak Abbas, M. Faisal Nadeem and Waseem Ashraf for their kind support, precious time, positive discussions and motivation at each and every step of this journey.

I am grateful to Strasbourg Family especially Wahid, Bilal, Raman, Tajith, Yasmin, Imtiaz, Asad, Salman, Akmal, Sara, Hira Hasan, proteomic friend Arslan, Hira, Aabid, Hanna Gsell, Fareeha, Kareem, Ameer, Irshad, Camille, Jean Martin and Astrid. I cannot forget their unlimited support, time, encouragement, and unforgettable memories.

I would also like to acknowledge Higher Education Commission of Pakistan and Campus France for providing me the financial support to continue my Ph.D in France.

Lastly, it was not possible without pure love, care, sincerity and motivation of my father, mother, sister and brothers who supported me at each phase of my life. They made me what I am today. This thesis belongs to them.

Thank you very much.

Tanveer

TABLE OF CONTENTS

LIST OF ABBREVIATIONS

5-mC	5-methylcytosine
17-AAG	17-Allylamino-17-demethoxygeldanamycin
Acetyl CoA	Acetyl-Coenzyme A
AdoMet	S-Adenosylhomocysteine (SAH)
AHAQ	2-Amino-3-Hydroxyanthraquinone
AR	Androgen Receptor
ATM	Ataxia Telangiectasia Mutated
BAH	Bromo-adjacent Homology
BAX	Bcl-2-Associated X Protein
BCL2	B Cell Lymphoma
BPC	4-Benzylpiperdine-1-Carboximidamide
BRCA1	Breast Cancer 1
Caspase	Cysteine Aspartate Protease
CCL	Chronic Lymphocytic Leukemia
CDK	Cyclin kinase dependent
CFP1	CXXC Finger Protein 1
CpG	Cytosine-phosphate Guanine
CRD	Chromodomain
DAPI	4',6-diamidino-2-phenylindole
DDR	DNA Damage Response
DHA	Dihydroartemisnin
DHAQ	1,3-Dihydroxy-9,10-Anthraquinone-2-carboxylic acid
DHNQ	5,8-Dihydroxy-1,4-Naphthoquinone
DMAPD	DNA methyltransferase-associated protein 1 domain
DMEM	Dulbecco's modified Eagle's Medium
DNA	Deoxyribonucleic Acid
DNMT1	DNA Methyltransferase 1
E2F1	E2F Transcription Factor 1
EDTA	Ethylenediaminetetraacetic acid
EdU	5-Ethynyl-2´-deoxyuridine
EGCG	Epigallocatechin-3-Gallate
EHMT2 (G9a)	Euchromatic Histone-Lysine N-Methyltransferase 2
EMT	Epithelial-Mesenchymal Transition
ER	Estrogen Receptor
ERCC1	Excision Repair Cross-Complementing group 1

ESCs	Embryonic Stem Cells
Esa1	Essential Sas family acetyltransferase
EZH2	Enhancer of Zeste 2 Polycomb Repressive Complex 2 subunit
eGFP	enhanced Green Fluorescent Protein
FACS	Fluorescence-Activated Cell Sorting
FLIM	Fluorescence Lifetime Imaging Microscopy
FRET	Fluorescence Resonance Energy Transfer
FRET	Förster Resonance Energy Transfer
FQI1	Factor Quinolinone Inhibitor
GSK-3	Glycogen Synthase Kinase-3
H3K9me2	Histone 3 Lysine 9 dimethylation
H3K9me3	Histone 3 Lysine 9 Trimethylation
H3R2	Histone 3 Arginine 2
H4K16Ac	Histone 4 Lysine 16 Acetylation
HAT	Histone Acetyltransferase
HCC	Hepatocellular Carcinoma
HDAC1	Histone Deacetylase 1
HDM	Histone Demethylase
HIV	Human Immunodeficiency Virus
HMT	Histone Methyltransferase
HNSCC	Head and Neck Squamous Cell Carcinoma
HPV	Human Papilloma Virus
HSP90	Heat Shock Protein 90
ICBP90	Inverted CCAAT box Binding Protein of 90 kDa
ING	Inhibitor of Growth protein
LIG1	DNA Ligase 1
LOPAC	Library of Pharmacologically Active Compounds
LSF	Late SV40 Factor
MBD	methyl-CpG binding domain proteins
MBPs	Methyl-binding domain proteins
Mdm2	Mouse double minute 2
MPTE	Maritime Pine Tannin Extract
MOF	Males-absent on the first protein
miRNA	microRNA
mTOR	Mammalian Target of Rapamycin
MYST	MOZ, Ybf2/Sas3, Sas2 and TIP60
ncRNA	non-coding RNA
NFκB	Nuclear Factor Kappa B
NPAT	Nuclear Protein coactivator of histone Transcription
NR	Nuclear Receptor

PBD	PCNA-binding domain
PBR	Polybasic Region
PCNA	Proliferation Cell Nuclear Antigen
PDE1	Phosphodiestrase 1
PHC	Pericentromeric Heterochromatin
PHD	Plant Homeo Domain
PI	Propidium iodide
PI5P	Phosphatidylinositol 5-Phosphate
PKB	Protein Kinase B also known as Akt
PML	Promyelocytic Leukemia
PMSF	Phenylmethylsulfonyl fluoride
PRAK	p38-Regulated/Activated protein Kinase
PRMT5	Protein Arginine Methyltransferase 5
PUMA	p53 Upregulated Modulator of Apoptosis
RFTD	Replication foci-targeting domain
RFTS	Replication foci- targeting sequence
RING	Really Interesting New Gene
RNA	Ribonucleic acid
ROS	Reactive Oxygen Species
Rb	Retinoblastoma
SAM	S-adenosyl-L-methionine
SIRT1	Sirtuin 1
SRA	Set and Ring Associated
SRSF2	Serine and Arginine rich Splicing Factor 2
STAT3	Signal Transducer and Activator of Transcription 3
SUMO	Small Ubiquitin-like Modifier
SUV39H1	Suppressor of Variegation 39-Homolog 1
TCL	T Cell Receptor
TET	Ten Eleven Translocation
TIP60	Tat Interactive Protein 60 kDa
TSGs	Tumor Suppressor Genes
TRD	Target Recognition Domain
TR-FRET	Time Resolved-FRET
TTD	Tandem Tudor Domain
TQ	Thymoquinone
UBB	Ubiquitin-B or Polyubiquitin-B
UBC	Ubiquitin-C or Polyubiquitin-C
Ubc9	Ubiquitin Carrier protein 9
UBL	Ubiquitin-Like Domain
UIM	Ubiquitin Interacting Motif
UHRF1	Ubiquitin like with PHD and Ring Finger domains 1

USP7 also known as	Ubiquitin-specific-processing protease 7
HAUSP	Herpesvirus-associated ubiquitin-specific protease

INTRODUCTION

I- INTRODUCTION

1. Epigenetics

To answer the diversity of phenotypes within a population arising from the same genome has always attracted the attention of scientists. How stem cells having same genomic sequence can have different phenotypes and they can differentiate into different type of cells and tissues? How homozygote twins or cloned animals having identical DNA sequence can have different phenotypes?

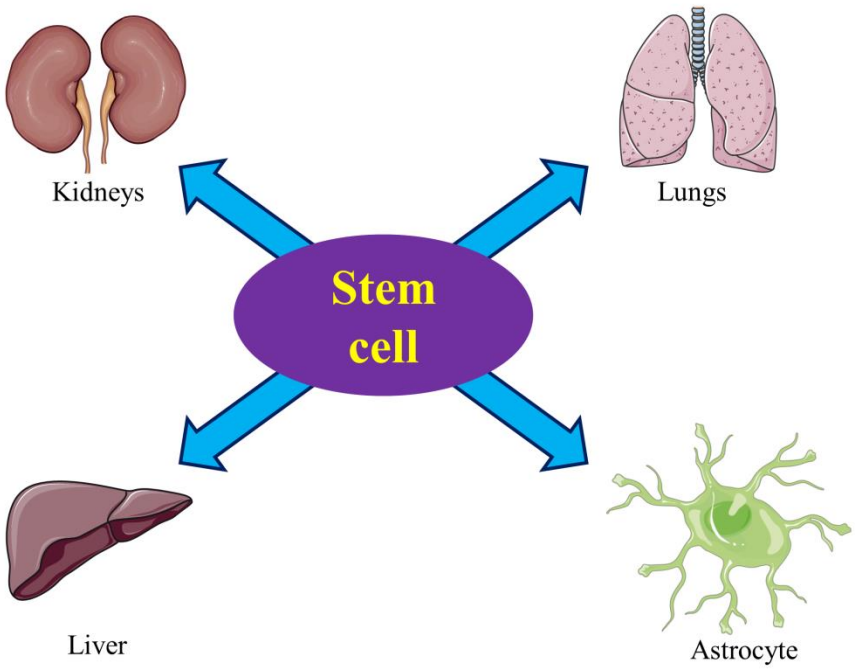

Figure 1: Same genome but different phenotypes. Stem cells of same origin having identical DNA sequence have developed different phenotypes with specialized functions. Images used in figure are taken from Servier Medical Arts http://servier.com/Powerpoint-image-bank.

Life cycle of a butterfly is a classic example of metamorphosis in insects which explains the essential role of DNA at different stages of life cycle (Figure 2). During different stages (egg, caterpillar, pupa and adult butterfly), butterfly has the same DNA so how it is possible to have four different phenotypes? To answer this question according to genetics is an enigma. A same DNA sequence (genotype) producing different form (phenotypes) indicates that DNA sequence alone is not controlling life patterns.

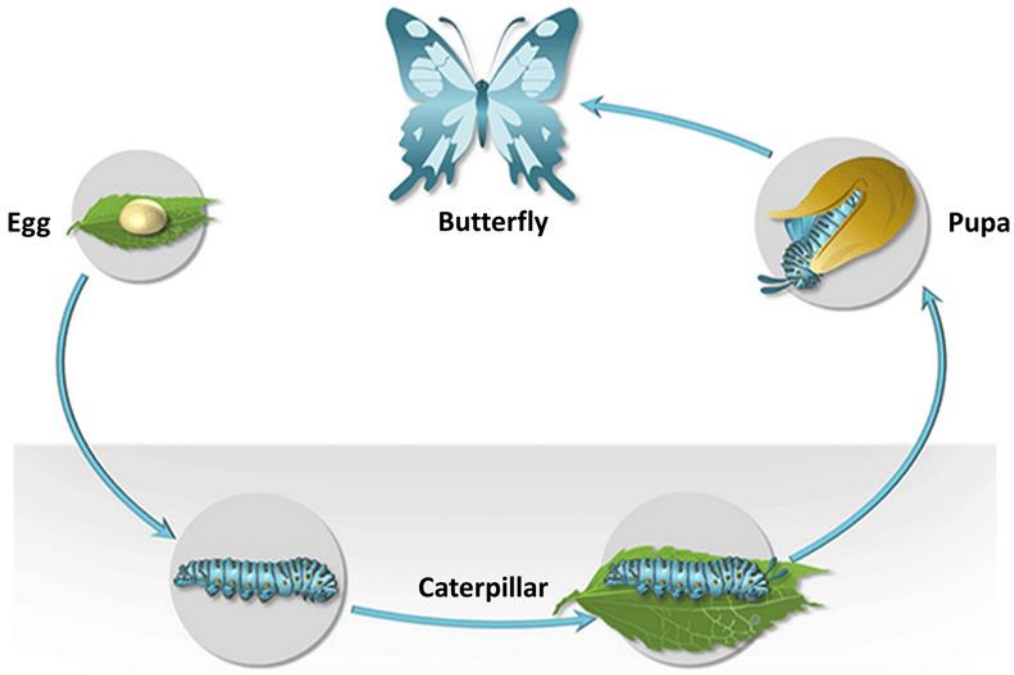

Figure 2: Metamorphosis of a butterfly (Rhopalocera).

Classic genetics alone may not be able to answer these questions. However, epigenetics can answer these questions. Term epigenetics was introduced by C.H.Waddington in 1939 and it is defined as "the casual interactions between genes and their products, which bring phenotype into being." Later it was defined as "heritable changes in gene function that are not due to any alterations in the DNA sequence" (Esteller, 2008). Arthur Riggs and colleagues defined epigenetics as "the study of mitotically and/or meiotically heritable changes in gene function that cannot be explained by changes in DNA sequence (Russo *et al.*,1996). Then Adrian Bird summarized the definition as "the structural adaptation of chromosomal regions so as to register, signal or perpetuate altered activity states" (Bird, 2007).

Cells and tissues with different phenotypes are controlled by the gene state which is regulated through epigenetic mechanisms. Epigenetic mechanisms involve chemical modifications on DNA, RNA and proteins. Epigenetic modifications include DNA methylation, histone modifications and non-coding RNAs. Through these modifications epigenetic mechanisms can alter the chromatin accessibility to transcriptional regulation both at local and global level. These mechanisms are very important in cellular functions. Dysregulation of epigenetic mechanisms can persuade to transformed gene activity and pathological state like cancer. Global alterations in genome are hallmark of cancer (Lund & van Lohuizen, 2004; Esteller, 2008; Sharma *et al.*, 2010; Bennett & Licht, 2018).

Queen honeybee and her coworker bees have the identical DNA sequence, but which factor makes one as a queen and others as workers? Scientists are now able to answer this with the help of epigenetics. This is because of DNA methylation which decides the rank in honeybee. Through analysis of brain tissues of reproductive and sterile honeybee workers, scientists have discovered more than 550 genes in which DNA methylation patterns are significantly different. It was found that methylation sites were clustered in in areas of genes where splicing of RNA occurs. Methylation can affect splicing which can generate different phenotypes (Lyko *et al.*, 2010).

Figure 3: Caste of honeybee. Queen produces scent (pheromones) and lays eggs. Worker bees represent majority of population and perform all the necessary work (defense, nectar collection, feeding queen and drones). Drone bees are a small percentage of population and they produce offspring with queen. Figure adapted from http://www.madegood.org/beekeeping/honey-bee-caste/.

2. Chromatin organization

In eukaryotes DNA is assembled into regularly arranged nucleosomes. This organized packing of DNA is very important for gene regulation. Crystal structure has shown that two replicas of each core histone protein (H2A, H2B, H3 and H4) are packed in an octamer form. 145-147 base pair DNA is coiled around this octamer to generate nucleosome. Repeating nucleosomes are organized in arrays to build higher-order structure which is stabilized by H1 linker histone (Figure 4) (Luger *et al.*, 1997; Cole *et al.*, 2016).

Nucleosome being a principal packaging unit of DNA in nucleus determines the accessibility to DNA for gene regulation. Based on its compactness, chromatin is divided into euchromatin and heterochromatin. In euchromatin, DNA is roughly coiled over histones octamer permitting transcription factors to bind and activate transcription. While in heterochromatin, DNA is tightly packed around histones and there is no access for the transcription factors to bind (Figure 5). Chromatin conformation is affected by DNA methylation, histone modifications (phosphorylation, methylation acetylation and ubiquitination), exchange of histone variants (H2A to H2A.Z) and chromatin remodeling complexes which can change

DNA and histone interaction. Changing in chromatin dynamics can influence transcription, recombination, replication and DNA repair mechanisms (Allis & Jenuwein, 2016).

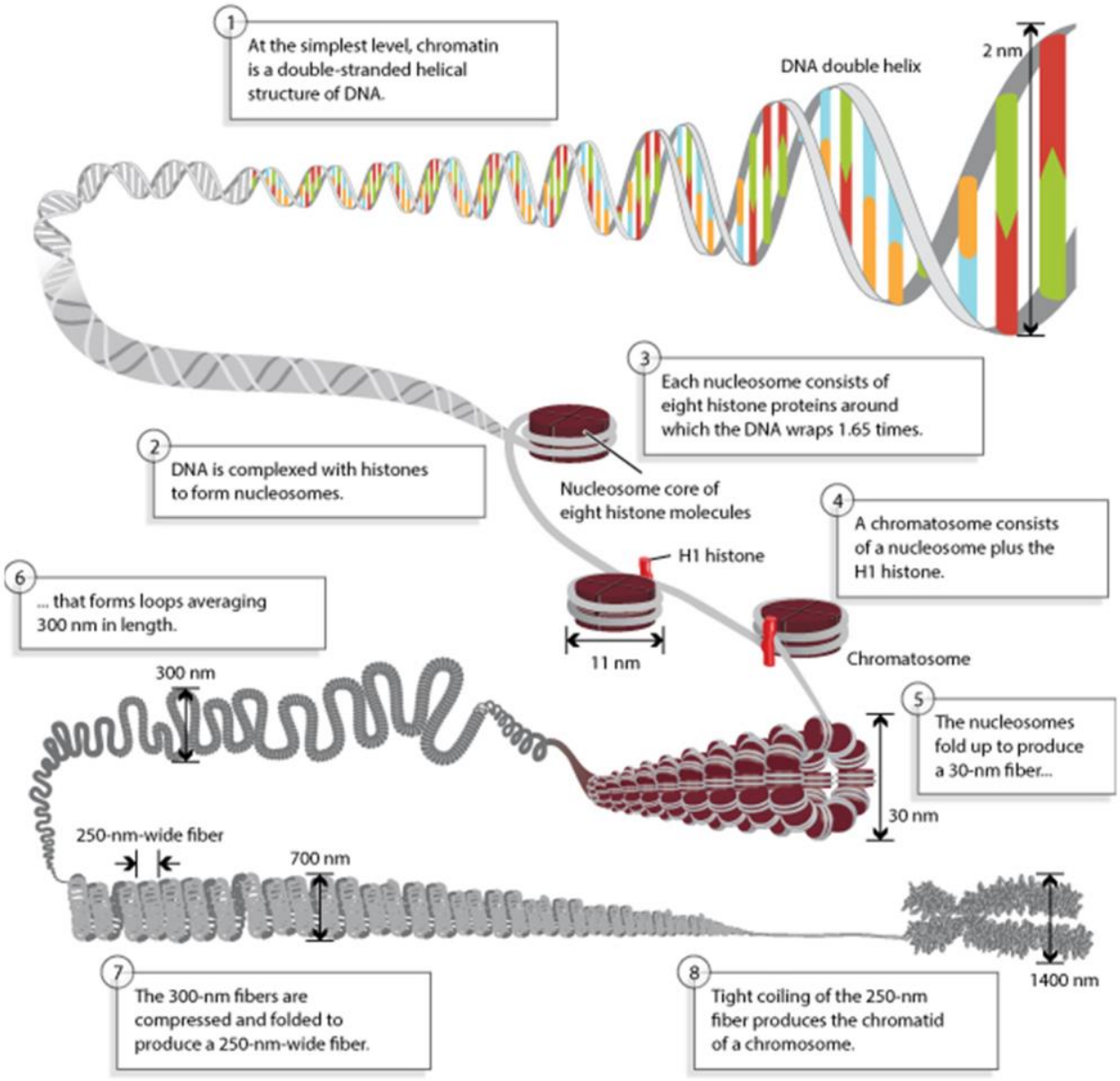

Figure 4: Chromatin organization. DNA is tightly wrapped around histones to form chromosome. Positively charged proteins strongly adhered to negatively charged DNA to build nucleosome. Adapted from (Genetics: A Conceptual Approach, 2nd edition. Pierce 2012).

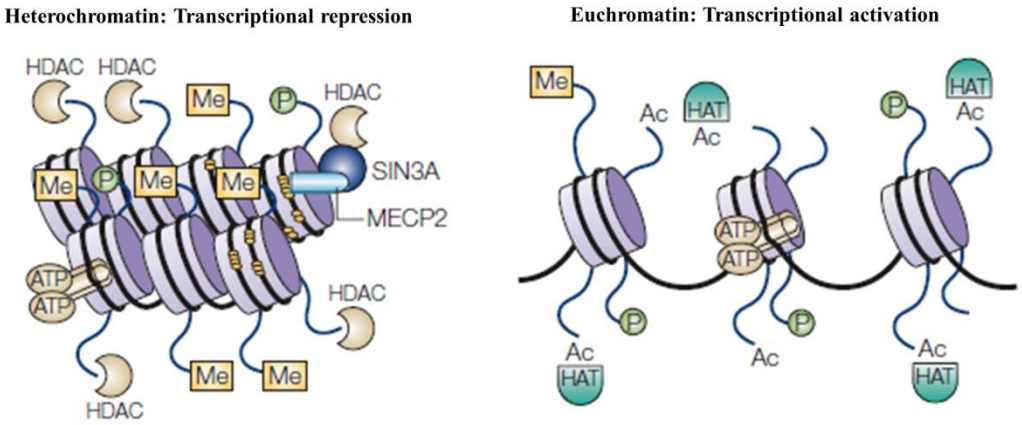

Figure 5: Transcription is regulated by chromatin state. Closed chromatin state represses transcription while open chromatin state favors transcription. Adapted from (Johnstone 2002).

3. Epigenetic modifications

3.1.A. DNA methylation

DNA methylation is remarkably studied epigenetic modification. First time DNA methylation was identified in calf thymus DNA by Hotchkiss in 1948. Now it is a well-established epigenetic mechanism which is involved in imprinting, control of gene expression, embryonic development, X chromosome inactivation, immune system development, genome integrity, brain function and cellular reprogramming. Abnormal methylation levels are linked with psychological, neurological, atherosclerosis, osteoporosis and immunological diseases as well as associated with initiation and progression of cancer (Robertson, 2005; Jurkowska *et al.*, 2011; Li *et al.*, 2018; Ehrlich, 2019). There are many questions linked with DNA methylation like how methylation marks are settled initially and how they are preserved throughout life cycle? Which are the environmental factors that can affect DNA methylation? Scientists are trying to address these questions but still there are some challenges. DNA methylation impressions are established by *de novo* methylation process while maintenance methylation process is liable for the faithful transmission and preservation of methylation marks from parent to daughter cells.

a. DNA methylation chemistry

DNA methylation involves methylation of cytosine at 5th position in CpG dinucleotide (Figure 6). DNMTs (DNA methyltransferases) enzymes carry out the methylation of cytosine.

DNMTs transfer methyl group (-CH_3) from -CH3 donating cofactor *S*-adenosyl-L-methionine (SAM) to intended cytosine (Robertson, 2005).

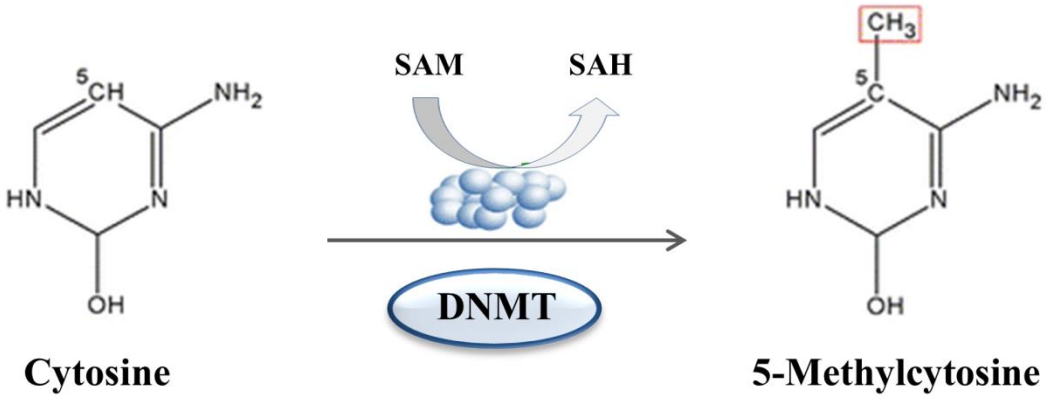

Figure 6: Transfer of methyl group from methyl donating cofactor (SAM) to targeted cytosine with help of the DNA methyltransferase enzyme (DNMT).

b. Enzymes involved in DNA methylation

There are four representatives of DNMT (DNA methyltransferases) family: DNMT1, DNMT3A, DNMT3B and DNMT3L. Above mentioned proteins are very essential and their knockout leads to developmental deformities and fatality of embryo (Takebayashi *et al.*, 2007; Liao *et al.*, 2015). DNMT3L lacks enzymatic activity. DNMT1 is the maintenance methyltransferase while DNMT3A and DNMT3B are *de novo* methyltransferases (Xu *et al.*, 2010; Jurkowska *et al.*, 2011; Jin & Robertson, 2013). DNMT1 maintains the transfer of methylation marks from parent strand to daughter strand by methylating the hemi-methylated (HM) DNA with the help of its interacting partners (UHRF1, PCNA). UHRF1 through its SRA domain perceives HM DNA and engages DNMT1 for preservation of DNA methylation impressions (Bostick *et al.*, 2007; Sharif *et al.*, 2007; Arita *et al.*, 2008; Avvakumov *et al.*, 2008). DNMT3A and DNMT3B hold comparable affinity for HM or non-methylated DNA. While, DNMT3L which lacks catalytic activity, promotes DNMT3A and DNMT3B to perform their role (Xu *et al.*, 2010). Generally, DNMTs have similar structure (Figure 7). DNMTs have two functional parts (C- and N-terminus parts) which are separated by KG repeat. Catalytic center is situated inside the C-terminus domain and this domain has the entire amino acids sequence motifs characteristic for cytosine-C5 methyltransferase fold (Jeltsch & Jurkowska, 2016). Motif I and IX are essential for binding of flipped cytosine and AdoMet (S-adenosyl-L-methionine) (Song *et al.*, 2012) Motif IV, VI and VIII are involved in

catalysis (transfer of methyl group). TRD (Target Recognition Domain) which is a non-conserve region located between motif VIII and IX implicates DNA identification and distinction (Jeltsch, 2002; Jurkowska & Jeltsch, 2016). The N-terminus part consists of different domains and this part collaborates with multiple proteins and chromatin and is responsible for focusing and governance of DNMTs (Jeltsch, 2006; Jurkowska & Jeltsch, 2016). N-terminus part guides DNMTs for nuclear localization and helps their communication with proteins, regulative nucleic acids and chromatin (Jurkowska & Jeltsch, 2016).

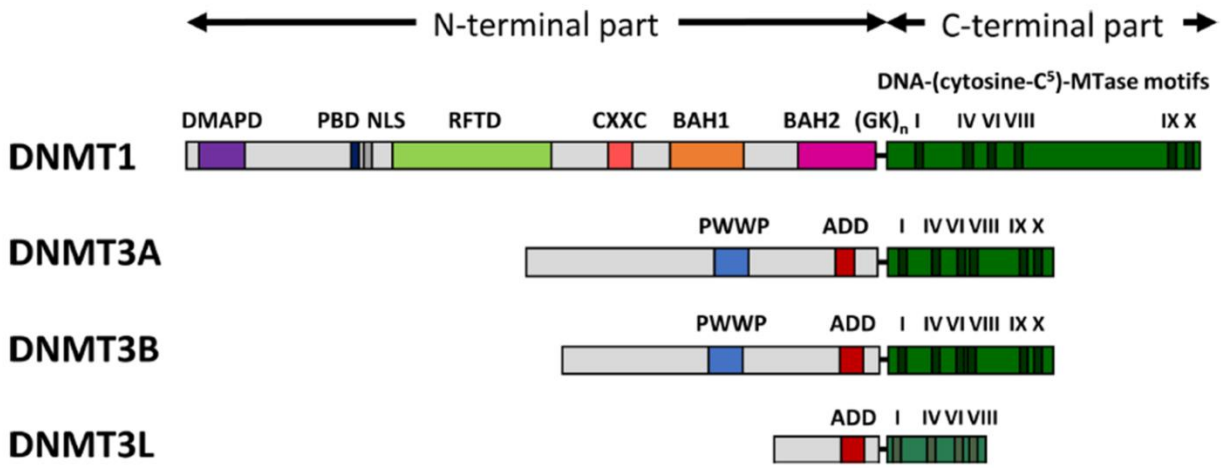

Figure 7: Architecture of DNMTs and their functional domains. Abbreviations used: *DMAPD* (DNA methyltransferase-associated protein1), *PBD* (PCNA-binding domain), *NLS* (nuclear localization signal), RFTD (replication foci-targeting domain), *CXXC* (CXXC domain), *BAH1* and *BAH2* (bromo-adjacent homology domains 1 and 2), GK_n glycine-lysine repeats, *PWWP* (PWWP domain), *ADD* (ATRX-DNMT3-DNMT3L) domain. Adapted from (Jeltsch & Jurkowska, 2016).

c. Methylation sites

In humans 70-80% of genomic CpG can undergo methylation (Bird, 2002). These methylated CpG dinucleotides are localized to repetitive elements, centromeres and coded regions of operative genes. Methylation of these distinctive sites is very essential for genomic stability and transcription of gene body (Portela & Esteller, 2010; Biswas & Rao, 2017). Un-methylated CpG dinucleotides are present in promoter region of 70% of human genome. Here CpG nucleotides are clustered in a region called as “CpG island”. CpG island is defined as region having a length of 550 bps and a ratio of observed to statistically expected CpG frequencies of at least 0.6 (Portela & Esteller, 2010; Jurkowska *et al.*, 2011). Approximately 60% of gene promoters are related with CpG and they are normally un-methylated in normal cells. However, a small fraction of these CpG (6%) become methylated during early

development or during differentiation of tissues (Portela & Esteller, 2010). Generally, CpG methylation is linked with suppression of genes and transcription repression but not in all contexts. As distribution of CpG is not uniform, their methylation patterns are also not uniform. Methylation patterns of CpG dinucleotides can vary dramatically regarding disease state, cell type and functional state (Ehrlich, 2019; Singer, 2019) (Figure 8). Silencing of gene activity and transcription could be enhanced through two mechanisms. First mechanism involves recognition of CpG islands methylation which can bind with MBPs (methyl-binding domain proteins). MBPs can engage HDACs (histone deacetylases) and other complexes that can mark the chromatin into a repressive state (Wade, 2001; Jurkowska *et al.*, 2011). Second mechanism suggests that methyl group interferes with binding of transcription factors and so supporting repressive state of transcription (Watt & Molloy, 1988; Santoro & Grummt, 2001; Bogdanović & Lister, 2017). Aberrations in methylation of promoter region can cause serious problems like malignant transformation of normal cells. Many studies have reported that hypermethylation in promoter region of various TSGs (like *p16, p73, BRCA1, RASSF1, TIMP3, CDH1, CDH13, ESR1, MLH1, CASP8 and ALKBH3*) has been observed in different cancers. In result, these genes are silenced which allows malignant cells to proliferate in an uncontrolled manner (Merlo *et al.*, 1995; Van Den Broeck *et al.*, 2010; Pei *et al.*, 2011; Stefansson *et al.*, 2011; Stefansson *et al.*, 2017; García-Martínez *et al.*, 2018; Ma *et al.*, 2018; Botezatu *et al.*, 2019; Liyanage *et al.*, 2019). DNA hypermethylation-mediated silencing of pro-apoptotic genes in cancer cells confers resistance against apoptosis which is a hallmark of tumorogenesis (Hervouet *et al.*, 2013).

Global hypomethylation is a hallmark of cancer which favors expression of oncogenes and provokes tumor malignancy and invasion (Ehrlich, 2009; Dawson & Kouzarides, 2012; Hervouet *et al.*, 2013; Klein Hesselink *et al.*, 2017; Veland *et al.*, 2017). Study has suggested that promoter hypermethylation and global hypomethylation can serve as a prognostic marker of cancer (Li *et al.*, 2014; Ehrlich, 2019). Recently, a link between aging and cancer has been suggested as both shared similar genomic distribution of hyper- and hypomethylation patterns. But still there is a need to investigate the methylation pattern relation between aging and cancer in detail (Pérez *et al.*, 2018).

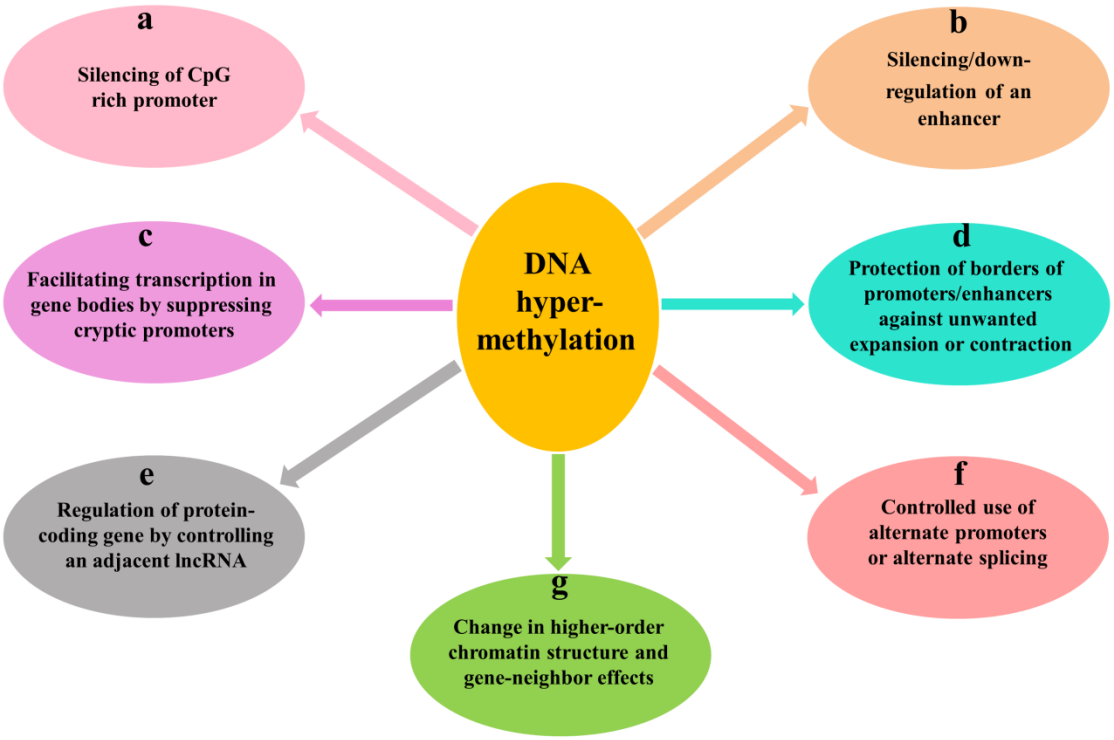

Figure 8: DNA hypermethylation regulates gene expression in different fashions. (a) and (b) silencing of gene expression through suppression of CpG rich promoters and enhancers. (c) and (d) specific cooperation of DNA hypermethylation with gene expression. (e) and (g) positive or negative connection with gene function. (f) effects on nature of transcript which can be established without changing the regulatory state of the transcript. Adapted from (Ehrlich, 2019).

d. Maintenance of DNA methylation patterns

DNA methylation has a critical role in selection and preservation of cell integrity (Bogdanović & Lister, 2017). Once DNA methylation patterns are set then it is very important to maintain and faithfully transfer these methylation patterns. DNMT1 is the main player in maintenance and transmission of methylation patterns during replication (Leonhardt *et al.*, 1992; Singer, 2019). Preference of DNMT1 for binding with hemi-methylated DNA (Jeltsch & Jurkowska, 2014) and its localization at replication fork in S phase favor DNMT1 as a maintenance enzyme.

3.1.B. DNMT1

a. Structure and domain architecture of DNMT1

DNMT1 is a substantial enzyme composed of 1616 amino acids. Due to alternative splicing or use of a substitute promoter, this enzyme exists in different isoforms.

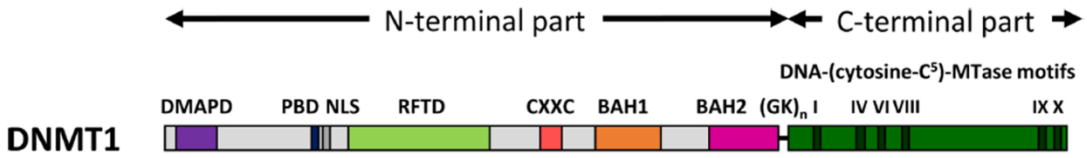

Figure 9: Domain composition of DNMT1. Adapted from (Jurkowska & Jeltsch, 2016)

DNMT1 has C- and N-terminus parts which are joined through a KG repeats. N-terminal chunk works as a podium concerning attachment of different proteins which are participating in chromatin remolding and gene activity. DMAPD (DNA methyltransferase-associated protein 1 domain) helps DNMT1 to interact with a transcription repressor (DMAP1) and is also involved in DNMT1 stability. PBD (PCNA-binding domain) recruits DNMT1 to replication fork in S phase. RFTD (replication foci-targeting domain) targets DNMT1 to replication foci and centromere chromatin. It also helps DNMT1 to interact with UHRF1 and ubiquitinated H3. Eight cysteine residues linked with zinc atoms construct CXXC domain which binds with un-methylated DNA. BAH1 and BAH2 (bromo-adjacent homology 1 and 2) domains act as protein-protein modules. C-terminus part harbors catalytic center of DNMT1. For catalytic activity it needs all motifs to be present. Catalytic domain is under the allosteric control of N-terminus domain (Jurkowska & Jeltsch, 2016; Edwards *et al.*, 2017; Ren *et al.*, 2018).

b. DNMT1 expression

DNMT1 expression is low in non-dividing cells while its levels are high in proliferating cells (Robertson *et al.*, 1999). Significant increase in expression levels of DNMT1 mRNA was observed in S phase while before completion of DNA synthesis mRNA expression returned back to basal level (Szyf *et al.*, 1991). Transcriptional regulation of DNMT1 is persuaded by Ras-AP-1 signaling network (Bigey *et al.*, 2000) and pRb-E2F1 pathway (Jung *et al.*, 2007).

c. Target selectivity of DNMT1

DNMT1 has a high processivity because of its ability to mark methylation tags to long stretches of hemi-methylated DNA. During this process, DNMT1 is not dissociated from substrate. In fact, DNMT1 slides along the DNA (Hermann *et al.*, 2004; Jurkowska & Jeltsch, 2016). DNMT1 also exhibits specificity for hemi-methylated DNA as compared to un-methylated one (Fatemi *et al.*, 2001; Bashtrykov *et al.*, 2012; Song *et al.*, 2012). Inherent tendency of DNMT1 for HM DNA was evaluated approximately 30-40 fold as compared to un-methylated DNA (Jeltsch, 2006; Song *et al.*, 2012; Jeltsch & Jurkowska, 2014). Crystal framework of murine DNMT1 complex with HM DNA has been reported to reveal the preference of DNMT1. Methyl group of methyl cytosine is located inside the hydrophobic pocket within TRD domain. TRD domain is composed of Cysteine 1501, Leucine 1502, Tryptophan 1512, Leucine 1515 and Methionine 1535. This complex formation involves both major (2 TRD loop) and minor (catalytic loop) grooves. Cytosine targeted for methylation is flipped out from DNA duplex and it is fitted inside the catalytic domain which is very close to SAM (Song *et al.*, 2012).

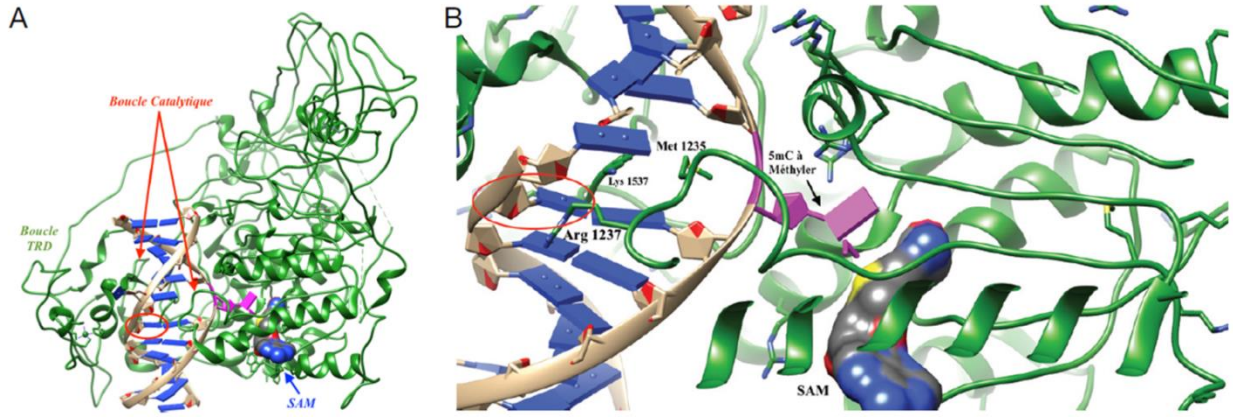

Figure 10: A, Crystal structure of murine DNMT1 with hemi-methylated DNA. DNMT1 (indicated in green color), bases (indicated in blue color), phosphate bridges (indicated in beige color), targeted cytosine for methylation (indicated in magenta color) and 5mC corresponding to parent strand (indicated as red circle). B, Zoomed on stabilization site of opened DNA duplex. Adapted from (Barthes *et al.*, 2016).

Besides processivity and intrinsic preference of DNMT1, an autoinhibitory regulatory mechanism of DNMT1 at un-methylated CpG sites, has also been proposed. Non-methylated DNA is removed from operating spot of DNMT1 through interaction of CXXC domain. On the other hand, autoinhibitory CXCC-BAH1 linker blocks access of DNA within catalytic pocket of DNMT1 by positioning itself between the substrate DNA and catalytic pocket of enzyme. Next, BAH2-TRD loop gradually pull TRD loop in such a position that TRD is no

more able to bind with major groove of DNA. This mechanism suggests that un-methylated CpG sites are preserved from *de novo* methylation through binding of CXXC domain. In this way efficiency of maintenance methylation increases through inhibition of *de novo* methylation (Song *et al.*, 2011).

Another study has indicated that several structural changes are necessary for faithful conservation of DNA methylation. First, RFTS domain of DNMT1 resides inside catalytic pocket so DNA cannot access that place. RFTS position is very unique in N-terminus. And its release is very crucial for initiation of DNA methylation activity (Takeshita *et al.*, 2011). Recent study has shown that UHRF1 can release RFTS from catalytic center to help DNMT1 to attain its active conformation (Bashtrykov *et al.*, 2014). Second, CXXC domain occupies the place where DNA has to bind as reported by Song *et al*. Further, complex with AdoMet flips out C1229 towards the targeted cytosine. C1229 is expected to bind covalently with sixth position of cytosine (Takeshita *et al.*, 2011).

d. Interaction of DNMT1 with other partners

An important partner of DNMT1 is PCNA (proliferating cell nuclear antigen) which is associated not only in DNA replication but also plays an essential role in DNA repair and cell cycle. PCNA serves as a hub which interacts with approximately one hundred proteins including ligases, polymerases, DNA modification enzymes and epigenetic factors. DNMT1 is recruited at replication site which is characterized by PCNA dense regions. Particularly, at its N-terminus DNMT1 has a special PIP box (PCNA interacting protein motif) with a sequence ^{164}QTTITSHF^{171}. DNMT1 is accumulated at replication site in early and mid-S phase. PIP box interacts with PCNA with a comparable binding affinity (Jimenji *et al.*, 2019).

Another important partner of DNMT1 is epigenetic integrator UHRF1. UHRF1 by means of its SRA and PHD domain recruits DNMT1 to the replication site for DNA methylation maintenance and transmission. DNMT1/UHRF1/PCNA complex is committed in maintenance of DNA methylation. DNA hypomethylation induced by interruption of this complex can lead to tumorogenesis and tumor transformation (Pacaud, *et al.*, 2014). UHRF1 is also recruited to replication site but in a different way as compared to DNMT1. UHRF1 binds with DNA ligase (LIG1) which has methylated K126 and leads to UHRF1 localization at DNA replication site (Ferry *et al.*, 2017; Kori *et al.*, 2019). UHRF1-DNMT1 interaction pathway will be discussed in detail in UHRF1 section. CFP1 (CXXC finger protein 1) interacts with DNA and cells lacking CFP1 had shown 60% decrease in DNMT1 activity

(Butler *et al.*, 2008). Peptide-induced specific disruption of DNMT1/CFP1 and DNMT1/DMAP1 interaction can improve response to chemotherapy (Cheray *et al.*, 2013; Cheray *et al.*, 2014). PARP1 also plays a role in stability of DNMT1. It negatively regulates the UHRF1-mediated ubiquitination of DNMT1 (De Vos *et al.*, 2014). Studies in last two decades have reported variety of proteins interacting with DNMT1 (Figure 11). These studies suggested that there are some additional mechanisms which can increase activity of DNMT1.

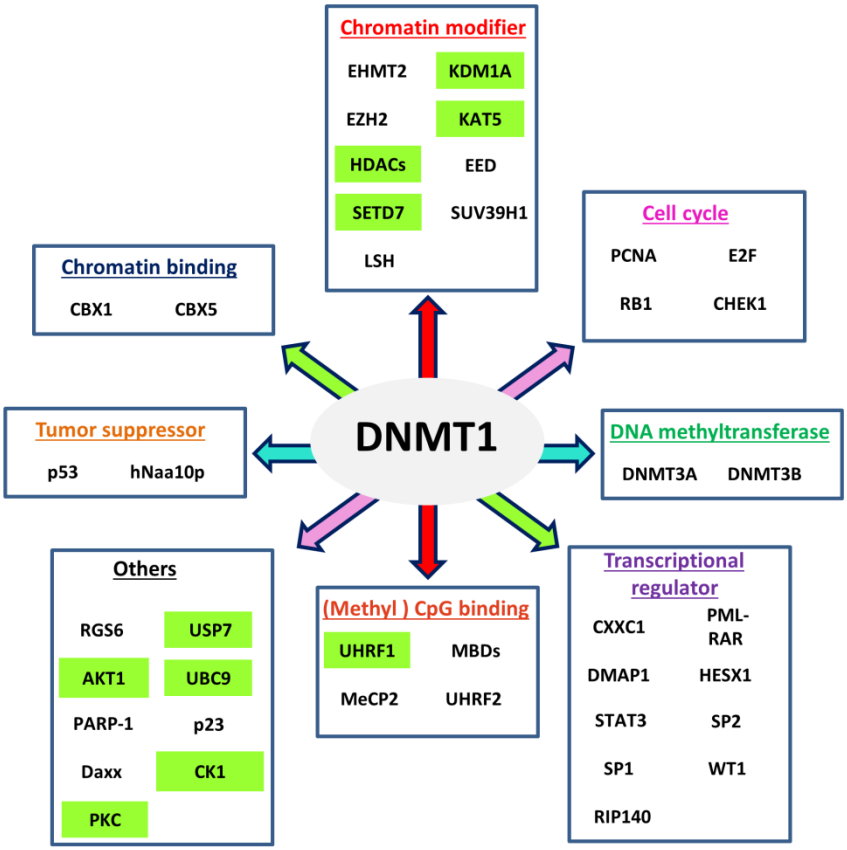

Figure 11: Interacting partners of DNMT1. Among interacting proteins are DNA methyltransferases, transcriptional regulators, chromatin modifiers, DNA binding proteins, cell cycle regulators, tumor suppressors and chromatin binding proteins. Proteins which are involved in post-translational modification (PTM) of DNMT1 are highlighted in green color. Adapted from (Qin *et al.*, 2011).

3.1.C. DNMT2

In comparison with other members of DNMT1 family, information about DNMT2 is less. DNMT2 has all amino acid motifs which are characteristics of DNMT1, and its structure is also similar to DNMT1. But DNMT2 has a very weak DNA methyltransferase activity (Hermann *et al.*, 2003). Study has reported that DNMT2 is a highly specific $tRNA^{Asp}$

methyltransferase. DNMT2 silencing prohibits cellular proliferation and promotes cell senescence (Goll *et al.*, 2006; Lewinska *et al.*, 2018).

3.1.D. DNMT3 family

This family is composed of three members known as DNMT3A, DNMT3B and DNMT3L mainly involved in *de novo* methylation. DNMT3A and DNMT3B play an essential role to set methylation patterns during early development. DNMT1 is involved in maintenance and transmission of DNA methylation but studies have suggested that DNMT3 enzymes are also involved in maintenance methylation (Sykes *et al.*, 1998; Kim *et al.*, 2002; Jones & Liang, 2009; Jeltsch & Jurkowska, 2014; Hervouet *et al.*, 2018). DNMT3L lacks catalytic activity and cannot bind with DNA. DNMT3A and DNMT3B can interact with certain transcription factors to localize on precise DNA strings (Hervouet *et al.*, 2009). DNMT3L can also interact with some transcription factors (like NFκB-p65) with which DNMT3A/B cannot interact. Through this interaction DNMT3L can help DNMT3A/B to localize on specific DNA sequences for *de novo* methylation (Pacaud *et al.*, 2014).

a. De novo methylation

De novo methylation is very important in initial stages of embryonic development. To set totipotency in early embryo, intensive reprogramming of zygote occurs. At this level, demethylation is observed. Methylation patterns are endorsed at the time of procreation by DNMT3 enzymes. Then another stream of *de novo* methylation occurs in germ cells during germ cell development. This process is responsible for establishment of genomic imprinting in gametes. This methylation and demethylation mechanisms generate an epigenetic rhythm in mammals. This is a landmark of mammalian genome (Jurkowska *et al.*, 2011; Langenstroth-Röwer *et al.*, 2017). In contrast with DNMT1, DNMT3A and DNMT3B are not concentrated at replication foci. During DNA replication, DNMT3B can interact with human chromosome-associated proteins and members of condensing complex. This proposes that DNA methylation by DNMT3B is somewhat self-reliant from DNA replication. UHRF1 (member of DNMT1/UHRF1/PCNA/G9a complex) through its SRA domain can interact with N-terminal region of DNMT3A and B independently of DNMT1 existence. DNMT1 is partially involved in *de novo* methylation. *De novo* methylation activity of DNMT1 is increased when it is recruited to previously methylated DNA. DNMT3A-mediated *de novo* methylation also enhances *de novo* methylation activity of DNMT1. Interaction of DNMT1

with USP7 also promotes its inheritance and *de novo* methylation activity (Hervouet *et al.*, 2018). Group of Unoki has reported recently that UHRF1 is involved in *de novo* methylation during oogenesis (Unoki, 2019).

3.1.E. DNA demethylation

In comparison with histone modifications, DNA methylation is relatively considered more stable but there are evidences showing that DNA methylation is a dynamic event especially during embryogenesis and development. This proposes the existence of demethylation machinery that regulates the DNA methylation. This process can occur in an active or passive manner. Passive demethylation (dilution of methylation) is the loss of 5mC mark during repeated cycles of replication in the absence of DNA methylation maintenance machinery. Active demethylation is the modification or removal of methylation mark from 5mC with the help of an enzyme (Kohli & Zhang, 2013). Previously methylation was considered as an irreversible process which can be modified through dilution or *de novo* synthesis of DNA. But now it is clear that erasers of DNA methylation are more involved than passive demethylation mechanism. Active demethylation process can involve following ways: oxidation of 5mC by TET (ten-eleven-translocations) proteins or deamination of methylated or adjacent base through AID (activation induced deaminase). TET can transform 5mC into 5hmC (5-hydroxymethylcytosine) followed by conversion into 5fC (5-formylcytosine) and 5caC (5-carboxylcytosine). Modified base is then removed through BER (base excision repair) pathway. Other pathways of base removal can be nucleotide excision and non-canonical mismatch repair (Schuermann *et al.*, 2016; Bochtler *et al.*, 2017). TET1 can interact with proteins which bind with full/hemi-methylated DNA or chromatin binding proteins. Importantly, interaction of TET1 with PCNA is critical in DNA demethylation (Cartron *et al.*, 2013). Loss of TET function and impaired 5mC demethylation process corresponds with malignancies (Cartron *et al.*, 2013; Bochtler *et al.*, 2017). A study conducted in chronic lymphocytic leukemia (CLL) patients has suggested that dysregulation in DNA methylation and demethylation is very critical in disease progression. This interconnection represents prognostic value. Classifying CLL patients according to levels of 5-cytosine derivatives can improve prognosis (Bagacean *et al.*, 2017). DNMT1 and histone demethylase KDM1A (also known as LSD1) interact in cancer cells and interestingly KDM1A-mediated demethylation of DNMT1 increases stability of DNMT1 protein and this interaction did not affect the DNA methylation levels (Brenner *et al.*, 2016).

3.2. Histone modification

Histones are the proteins which are wrapped around DNA to give it a compact order structure which is known as nucleosome. Histones are composed of a globular shape C-terminal domain and an N-terminal tail. Various PTM (post-translational modifications) can occur on N-terminal histone tail such as methylation, phosphorylation, acetylation, ribosylation, ubiquitination, sumoylation, and deimination. Histone modifications play an essential role in variety of cellular process like transcription, repair, condensation and replication (Sharma *et al.*, 2010; Dawson & Kouzarides, 2012). The role of histone modifications is studied well in transcription while studies are ongoing to investigate role in other DNA processes.

These modifications on histones can activate and repress transcription but this action is not exclusive and static (Figure 12). It is dynamic kind of process which works in a cell-context dependent manner. Additionally, active and repressive states are not always absolute. These modifications construct a "code" that can be identified by transcription factors to establish the transcriptional state of gene. But recent studies have revealed that this mechanism is more complex and involves context and time dependent chromatin signaling pathways for transcriptional regulation. This is called as histone "crosstalk" and is very important in biological processes and abreactions can lead to disease state like cancer (Lee *et al.*, 2010; Dawson & Kouzarides, 2012; Audia & Campbell, 2016; Biswas & Rao, 2017; Michalak *et al.*, 2019; Qin *et al.*, 2019).

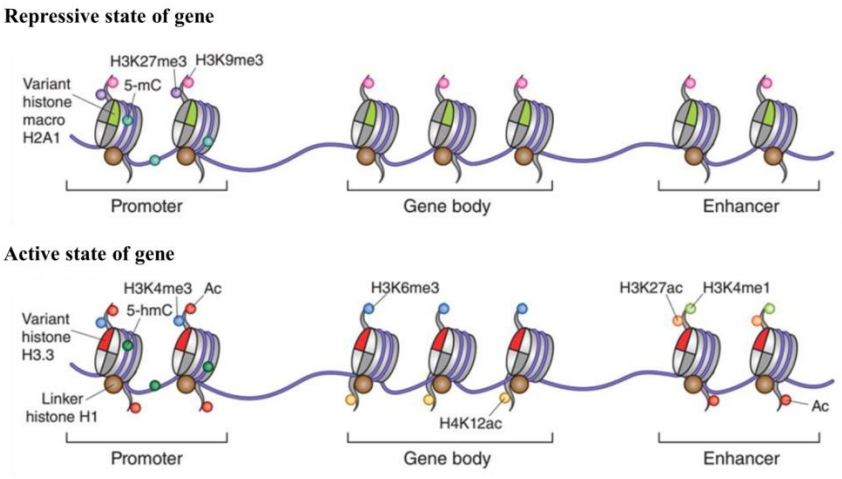

Figure 12: Histone modifications and gene function. Trimethylation at H3K9 or H3K27 represses gene function through compaction of chromatin. While methylation at H3K4, H3K6 or acetylation at H3K27 activates gene capacity through relaxation of chromatin. Adapted from (Jakovcevski & Akbarian, 2012).

Histone modifications are regulated by different enzyme known as “writers” (add histone mark); “erasers” (remove histone mark) and “readers” (read/recognize histone mark). For example, HATs (histone acetyltransferases), HDACs (histone deacetylases) and bromodomains can add, remove or recognize acetylation at histones. Similarly, HMTs (histone methyltransferases), HDMs (histone demethylases) and various domains (chromodomain, Zn finger, PHD and Tudor domain) can write, erase and read methylation marks on histones (Xu *et al.*, 2017).

3.3. Regulatory ncRNAs (non-coding RNAs)

ncRNAs are also involved in governance of epigenetic mechanisms. They incorporate siRNAs (small interfering RNAs, miRNAs (microRNAs) and lncRNAs (long non-coding RNAs). They portray a fundamental role in coding of gene expression at different stages: transcription, RNA splicing, mRNA degradation and translation (Figure 13). siRNAs are dsRNAs (double-stranded RNAs) which can induce post-translational silencing (Inbar-Feigenberg *et al.*, 2013). miRNAs are small (18-24 nucleotides), single-stranded RNAs. They are generally produced from cleavage of precursor RNA through RNA polymerase III enzymes (DROSHA and DICER).

miRNAs target mRNA in a specific manner for degradation and/or translational repression for regulation of gene expression. They can regulate gene expression through changing chromatin conformation by recruiting chromatin-modifying complexes and this gene regulation helps animals to survive under stress conditions (Inbar-Feigenberg *et al.*, 2013; Wang, 2018). lncRNAs are highly conserved in various species. They function as a guide to direct the chromatin-modifying complexes to a specific location in genome and therefore contribute in specific epigenetic modification. lncRNAs participates in genome imprinting and X-chromosome inactivation (Inbar-Feigenberg *et al.*, 2013).

lncRNAs can also induce silencing of their targeted genes by binding to RBP (RNA binding-proteins) complexes. In a study Xiaohua Shen and Naihe Jings groups have suggested that lncRNAs play a role as modulator of gene expression in development and cell differentiation. Localization of ncRNAs and their association with RBP partners affect biological processes but still there is a need of systematic studies to understand this pathway (Wang, 2018).

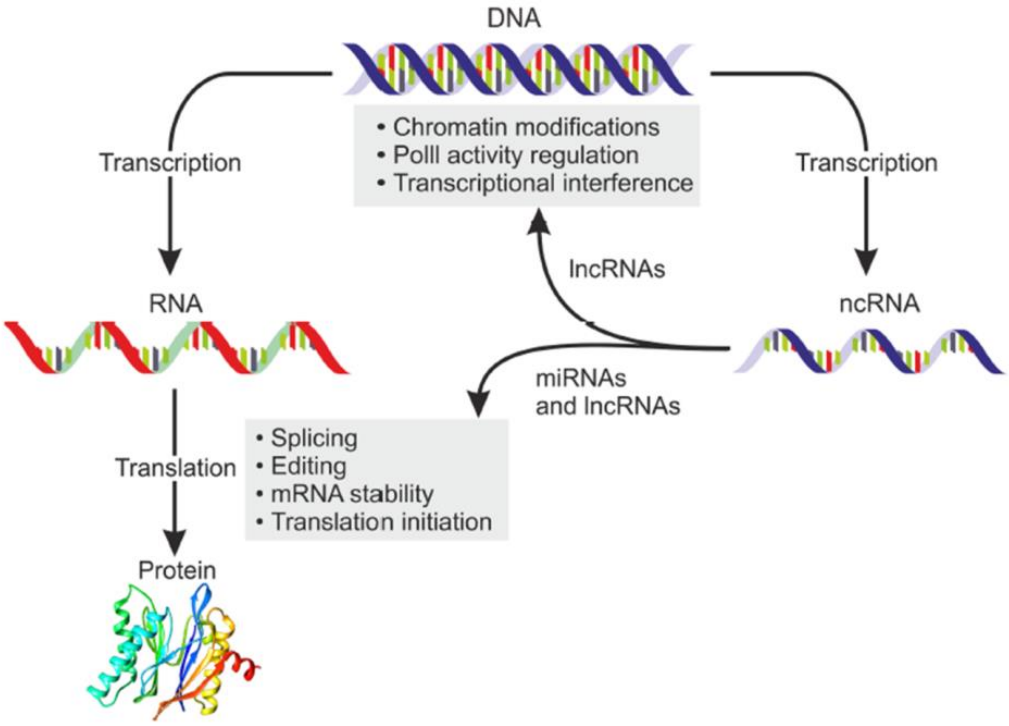

Figure 13: Extension of 'Central dogma' by ncRNAs. Concept of 'central dogma' was given by Francis Crick in 1958. Figure describes that ncRNAs in collaboration with 'central dogma' play role in gene expression regulation. Adapted from (Slaby *et al.*, 2017).

4. Ubiquitin PHD RING Finger (UHRF) family

UHRF family includes three human origin proteins namely: hUHRF1 (ICBP90), hUHRF2 (NIRF) and hUHRF3 (ICBP55). Mouse origin members of this family are mUHRF1 (Np95), mUHRF2 (Np97) and mUHRF3 (ICBP55). Among these members hUHRF1 and mUHRF1 are well studied (Bronner *et al.*, 2007a). UHRF proteins have evolutionary conserved amino acids sequences in vertebrates. mUHRF1 shares 73.4% identity with hUHRF1 whereas Rhesus UHRF1 shares 98% identity with hUHRF1 (Bronner *et al.*, 2007a). Homology between human UHRF2 and mouse UHRF2 is 90.3% (Mousli *et al.*, 2003). Strikingly, UHRF1 equivalent was not identified either in *Drosophila melanogaster* (flybase) or *Caenorhabditis elegans* (wormbase) or in *Saccharomyces cerevisiae* (yeastgenome). Phylogenetic study of *UHRF1* gene conserved sequence in vertebrates has revealed its importance in backbone development. Interestingly, structural domains of UHRF1 have also conserved sequence resemblance which explains its importance throughout the evolution in vertebrates (Bronner *et al.*, 2007a).

Another important family member is hUHRF2. *hUHRF2* gene was mapped at chromosome 9p23-24.1. hUHRF2 is composed of 802 amino acids. Homology between hUHRF1 and hUHRF2 is 53% (Mori *et al.*, 2002). UHRF2 urges an important task in cell cycle network and coordinates between cell cycle, proteasomal degradation and epigenetic machinery. It interacts with many epigenetic partners and leads to cell cycle arrest at G1 phase. In contrast to *UHRF1* gene, *UHRF2* gene has been reported to be lost in tumors and has the potential of being tumor suppressor (Mori *et al.*, 2011; Mori *et al.*, 2012). It contributes in G1/S transition by regulating Cdk2 activity (Li *et al.*, 2004). Unlike UHRF1, UHRF2 does not have a priority for binding to HM DNA. This preference occurs only when UHRF2 binds with H3K9me3 peptide with the help of TTD domain (Pichler *et al.*, 2011). SRA domain of UHRF2 recognizes and binds with hydroxymethylcytosine (Zhou *et al.*, 2014).

4.1.A UHRF1 (Ubiquitin-like, containing PHD and RING Finger domains 1)

UHRF1 (previously called ICBP90 “Inverted CCAAT box binding protein of 90 kDa”) was isolated from Jurkat cells first time in 2000 by using one hybrid system. It was spotted as a novel protein binding to inverted CCAAT box of the human topoisomerase IIα gene promoter region (Hopfner *et al.*, 2000). UHRF1 is composed of 793 amino acids having isoelectric

point of 7.7 and a molecular weight of 90 kDa. *UHRF1* gene is located on chromosome 19p13.3 in telomeric region. It is constructed of 6 coding exons and 2 non-coding exons (Hopfner *et al.*, 2001). Originally ICBP90 was proposed as a transcription factor having role in induction of *topoisomerase IIα gene* at G1/S phase of cell cycle (Mousli *et al.*, 2003). Now it is studied well that UHRF1 is a multi-domain nuclear protein performing an imperative job in faithful transmission of methylation marks, DNA damage response, cell cycle progression and regulation of stability and function of many proteins (Alhosin *et al.*, 2010; Du *et al.*, 2010; Alhosin *et al.*, 2011; Dai *et al.*, 2013; Guan *et al.*, 2013; Alhosin *et al.*, 2016; Ashraf *et al.*, 2017a). UHRF1 has two isoforms. UHRF1 (isoform 1) is the main isoform. Only difference in case of UHRF1 isoform 2 is that it contains additional 13 amino acids at its N-terminus (Zhang *et al.*, 2016).

4.1.B. Structure and function of UHRF1 domains

UHRF1 is a multifunctional and multidomain protein having five conserved domains (Figure 14). On its N-terminal it has ubiquitin-like (UBL) domain followed by tandem Tudor domain (TTD) and a plant homeodomain (PHD). While on its C-terminus it has SRA domain (set and ring associated) and RING domain (really interesting new gene) (Bronner *et al.*, 2007a).

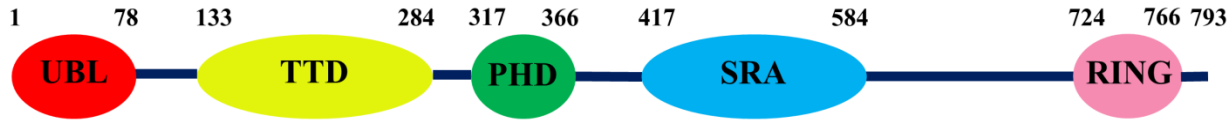

Figure 14: Schematic representation of UHRF1 structure with its domains. "Ubiquitin-like domain" (UBL), "Tandem Tudor domain" (TTD), "Plant homeodomain" (PHD), "SET and RING associated" (SRA) domain and "Really interesting new gene" (RING) domain.

a. Ubiquitin-like domain (UBL)

UBL domain comprises of classical alpha and beta ubiquitin folds. It exhibits three lysine on its surface (K26, K33, K52). K33 and K52 of UBL domain resembles in structure with K29 and K48 of ubiquitin. Poly-ubiquitination of K52 presents signal to proteasomal complex for protein degradation. This domain is present in all members of UHRF family except hUHRF3 and mUHRF3. It is composed of 76 amino acids and has 35% identity with ubiquitin. It has many functions including protein-protein interaction, proteasomal degradation, transcription

and cell cycle progression. It interacts with UIM (ubiquitin-interacting motif) of S5a proteasomal unit and helps in transport of aggresomes (Bronner *et al.*, 2007a). UBL domain deletion cannot assist DNA methylation transfer (Smets *et al.*, 2017). Recently it has been reported that UBL domain binds directly with DNMT1. Interestingly, although UBL has resemblance with ubiquitin but it binds with DNMT1 in a different way in contrast to ubiquitin. Along with RING domain, UBL domain is necessary for nuclear localization of DNMT1 and faithful transfer of methylation patterns (Li *et al.*, 2018). Structural and biochemical study has revealed a bifunctional role of UBL domain. UBL binds with backside of E2 and coordinates with UHRF1 domains to read epigenetic marks and directs ubiquitin to H3. This is important in DNMT1 recruitment to newly synthesized chromatin (DaRosa *et al.*, 2018). Another study has reported that UBL is necessary for stimulation of UHRF1 E3 ligase activity. Hydrophobic chunk present on UBL surface plays a role in establishment of E2/E3/chromatin network and indeed in DNA methylation (Foster *et al.*, 2018).

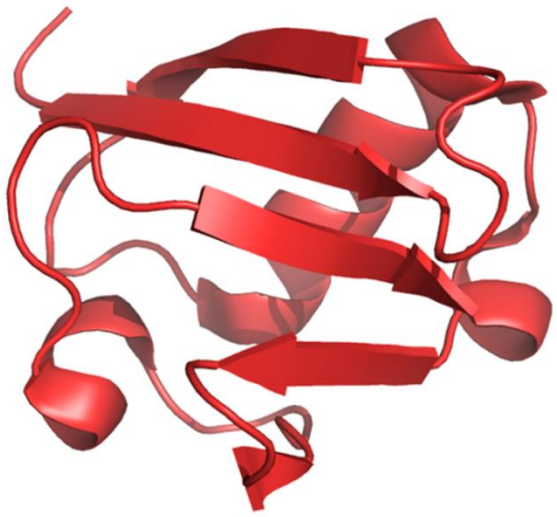

Figure 15: Crystal structure of UBL (Ubiquitin-like) domain of UHRF1 representing peculiar α-helix and β-sheet folds. Adapted from structure deposited at RCSB protein data bank. PDB ID: 2FAZ

b. Tandem Tudor domain (TTD)

TTD mediates a variety of protein-protein interactions which are required in biological processes. This domain helps in reading of various histone marks (Lu & Wang, 2013). It is comprised of two subdomains: TTD_N and TTD_C. Each subdomain exhibits 5-stranded β-barrel folds. Crystal structure of TTD and H3K9me3 complex has validated that aromatic cage (Phe-152, Tyr-188 and Tyr-191) of TTD_N interacts with H3K9's triethylammonium moiety with

the help of two residues (Asn-194 and Asp-145) and thus provides charge for a stable interaction.

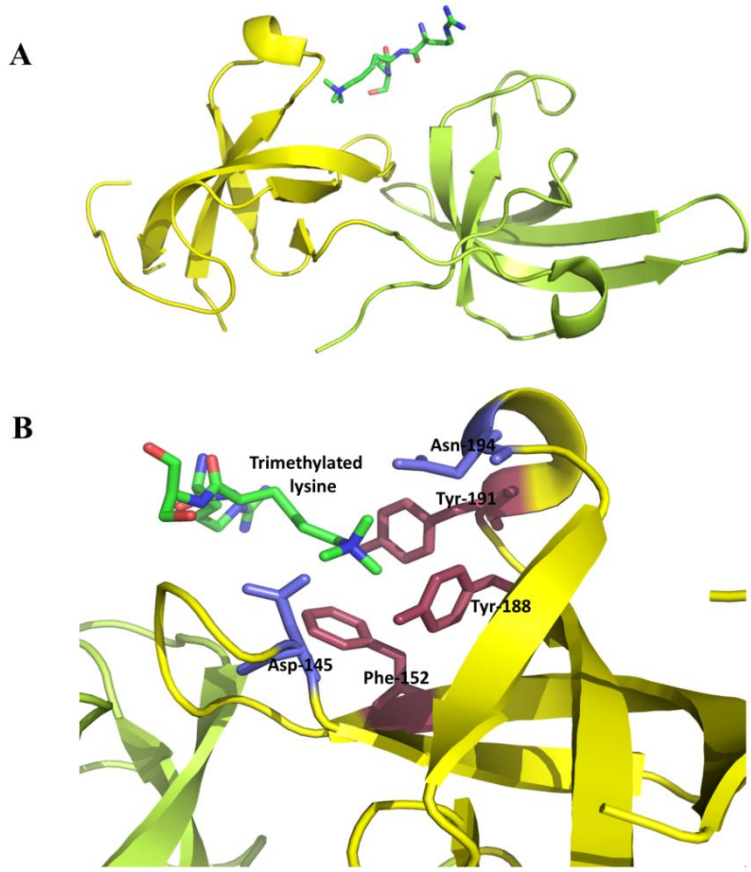

Figure 16: Crystal structure of tandem Tudor domain (TTD). A, Subdomains of TTD (TTD_N and TTD_C are illustrated in yellow and green color respectively) with trimethylated lysine (marked with dark green). B, Aromatic cage of TTD_N Tyr-188, Tyr-191 and Phe-152 (demonstrated in raspberry color) along with Asp-145 and Asn-194 (illustrated in blue) serve as binding pocket for trimethylated lysine residue. Adapted from structure deposited at RCSB protein data bank. PDB ID: 3DB3 (Nady *et al.*, 2011)

Through its conserved aromatic cage in first Tudor subdomain, TTD identifies H3K9me3 while at the same time identifies H3K4 present in groove between two tandem subdomains. In addition, with SRA domain, TTD participates in subnuclear localization of UHRF1 (Nady *et al.*, 2011). TTD interacts with DNA ligase (LIG1) and this interaction enhances recruitment of UHRF1 to replication foci to maintain DNA methylation (Ferry *et al.*, 2017). Another structural study has shown that TTD binds with LIG1K126me3 and this interaction switches closed conformation of UHRF1 into open conformation (Jeltsch, 2019; Kori *et al.*, 2019). Interaction of TTD with poly basic region (PBR) of UHRF1 interferes with H3K9me3 binding with TTD-PHD, and this leads to closed conformation of UHRF1.

Interruption of TTD-PBR interaction with the help of UHRF1 binding with hemi-methylated DNA or USP7 changes closed conformation of UHRF1 into open and facilitates its binding with chromatin (H3K9me3) (Zhang *et al.*, 2015; Fang *et al.*, 2016; Gao *et al.*, 2018). It is well studied that UHRF1 expression levels are high in most of the cancers (Ashraf *et al.*, 2017b) and TTD is essential for UHRF1 functioning. A screening study has reported small molecule antagonists against UHRF1-TTD-H3K9me2/3 interaction which can be further explored to synthesize new probe and inhibitors for anticancer therapy (Senisterra *et al.*, 2018).

c. Plant homeodomain (PHD)

PHD is Zinc-finger domain which reads H3 tail and it has preference for unmethylated H3K4 as compared to methylated H3K4. This interaction is not affected by H3K9 methylation status and needs histone's first two residues H3A1 and H3R2. Recognition of H3R2 by PHD is the main reason for this interaction. Any modification on H3R2 reduces its binding with PHD. Interestingly, PHD can entertain methylated H3K4 without disturbing the complex formation (Lallous *et al.*, 2011; Rajakumara *et al.*, 2011). Previously it was identified that UHRF1 is concentrated to PHC (pericentromeric heterochromatin) (Papait *et al.*, 2007) but now it is known that UHRF1 is also localized to euchromatin playing role in transcription repression (Kim *et al.*, 2009; Daskalos *et al.*, 2011). UHRF1's ability to repress transcription of targeted genes depends on interaction of PHD domain with unmodified arginine and it also indicates a crosstalk between UHRF1 function and histone arginine methylation (Rajakumara *et al.*, 2011; Bronner *et al.*, 2019). Houliston *et al* identified an inhibitor BPC (4-benzylpiperdine-1-carboximidamide) which can target TTD-PHD module to harmonize histone reading function for therapeutic purpose (Houliston *et al.*, 2017).

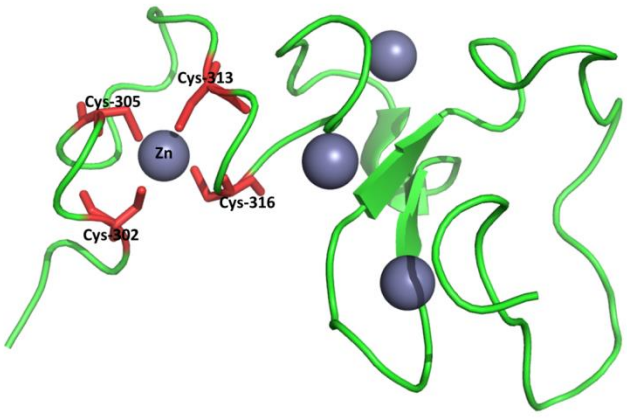

Figure 17: Crystal structure representing pre PHD motif linked to canonical PHD domain of UHRF1. Adapted from structure deposited at RCSB protein data bank. PDB ID: 3SHB (Hu *et al.*, 2011)

d. Set and ring associated (SRA) domain

Among vertebrates, SRA domain has been found only in UHRF family (Bronner *et al.*, 2007a). It plays an important role in DNA methylation patterns transfer by perceiving the hemi-methylated DNA (Arita *et al.*, 2008; Avvakumov *et al.*, 2008; Hashimoto *et al.*, 2008), recruiting DNMT1(Bostick *et al.*, 2007; Felle *et al.*, 2011) and interacting with various epigenetic proteins like HDAC1 (Unoki *et al.*, 2004) and G9a (Kim *et al.*, 2009). SRA domain structure is composed of twisted and flared β-barrel which is covered by α-helicals. At one side of this barrel, α2 helical connects β5 and β6 strands while on other side another helical connects β6 and β7 strands.

Overall DNA-SRA interactions looks like a hand grasping the hemi-methylated DNA while having a binding pocket for 5-methylcytosine in its palm. Two loops representing finger and thumb where finger projects into the major groove while thumb into the minor groove of DNA duplex. Binding pocket of SRA is very specialized which recognizes only 5-methylcytosine which is flipped out of DNA duplex. Tyrosine 478 and Tyrosine 466 stabilize 5-mC into binding pocket through π-stacking interaction (Avvakumov *et al.*, 2008). Finger called as NKR (N489, K490 and R491) identifies 5-mC and flips out methylated cytosine. NKR finger not only recognizes CpG sequence but also differentiates methylation of complementary strand.

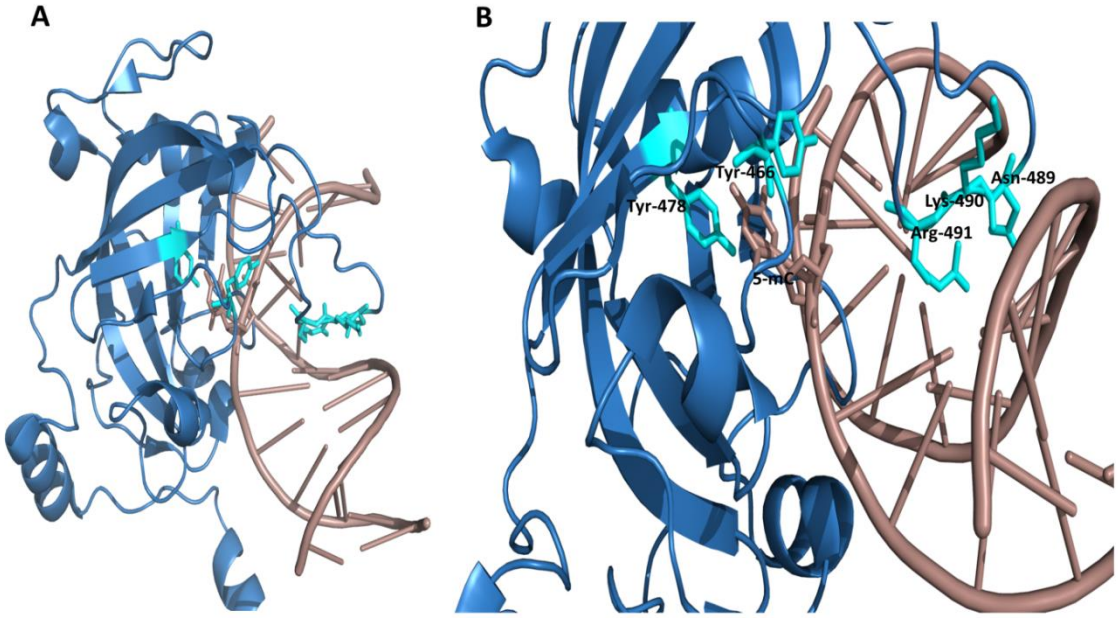

Figure 18: A, Crystal structure showing SRA domain (blue in color) with hemi-methylated DNA (dirty violet color). B, zoomed image showing 5-mC (dirty violet color) flipped out of DNA duplex and stacked between Tyr-

466 and Tyr-478 (Cyan color). NKR finger (Cyan color) is projected into major groove of DNA. Adapted from structure deposited at RSCB protein data bank. PDB ID: 3CLZ (Avvakumov *et al.*, 2008)

Another study has revealed that SRA domain performs dual functions: recognition of DNA and recruitment of DNMT1 to proper place at DNA (Arita *et al.*, 2008). Through recognition and flipping of 5-mC, SRA-DNA interaction supports UHRF1 to hold a place over hemi-methylated CpG sites and to recruit DNMT1 and perhaps some other proteins (Hashimoto *et al.*, 2008). A previous study has suggested a model which depicts that UHRF1 interacts with HM CpG site through SRA domain and followed by DNMT1 recruitment (Vaughan *et al.*, 2018). This model shows that UHRF1 first binds with DNA through its SRA domain which is in accordance with previous studies reporting that SRA moves over DNA in search of hemi-methylated DNA (Bronner *et al.*, 2010; Greiner *et al.*, 2015; Bronner *et al.*, 2019). A recent study has reported that functional SRA domain and its finger loop is very essential for E3 ligase activity of UHRF1 towards H3 which is important for recruitment of DNMT1. This finger loop regulates conformation and activity of UHRF1 (Vaughan *et al.*, 2019).

e. Really interesting new gene (RING) domain

At its C-terminus UHRF1 has a RING domain which has E3 ubiquitin ligase activity. RING domain structure is composed of two zinc-fingers and a special α-helix bundle (Tauber & Fischle, 2015).

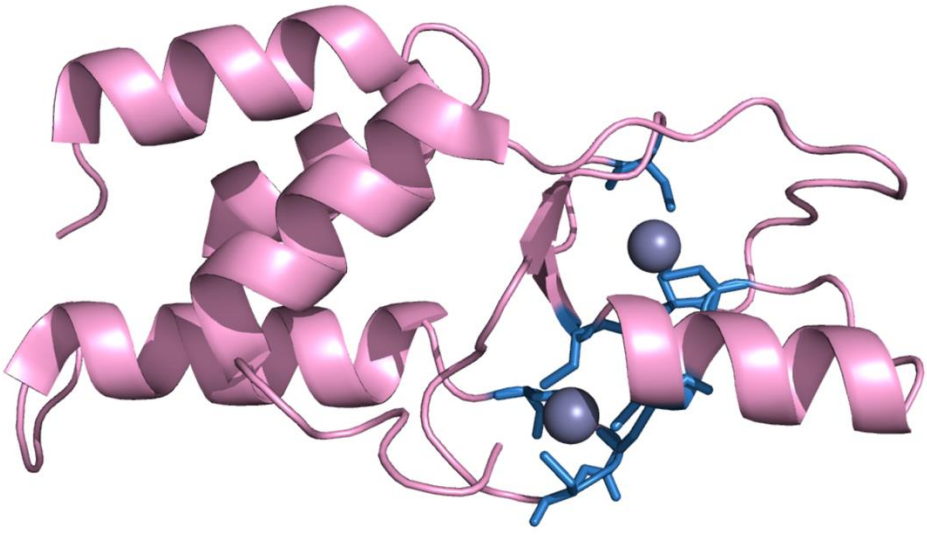

Figure 19: Crystal structure of RING domain. Cysteine residues (blue color) interacting with zinc atoms (gray color) to form zinc fingers which is necessary for interaction with substrates. Adapted from structure deposited at RSCB protein data bank. PDB ID: 3FL2

Due to its intrinsic E3 ligase activity, UHRF1 can either ubiquitinate itself or can ubiquitinate many other proteins including histones and non-histone proteins (Qin *et al.*, 2015; Tauber & Fischle, 2015). A study on mouse embryonic stem cells has shown that RING domain-mediated monoubiquitination of H3K23 is essential for DNMT1 recruitment at replication site (Nishiyama *et al.*, 2013). UHRF1 interacts with DNMT1 and regulates expression and stability of DNMT1 through ubiquitination of DNMT1 (Du *et al*., 2010). On the other hand, PARP1 can regulate the interaction between DNMT1 and UHRF1. It prevents UHRF1-mediated ubiquitination of DNMT1 and stabilizes DNMT1 levels (De Vos *et al*., 2014).

Through complementation assay it has been shown that ligase activity of RING domain is required for H3K18 ubiquitination and finally for DNA methylation maintenance (Qin *et al.*, 2015). As already described, RING domain in connection with UBL domain is essential for DNMT1 nuclear localization (Li *et al.*, 2018). UHRF1 RING domain and its E3 ligase activity are crucial in survival during the presence of cytotoxic agents and also in suppression of promyelocytic leukemia (PML) tumor suppressor protein. Therefore, E3 ligases can be potential targets in anticancer therapy (Jenkins *et al.*, 2005; Kirkin & Dikic, 2011; Guan *et al.*, 2013; Popovic *et al.*, 2014).

4.1.C. Roles of UHRF1

a. Role in DNA and histone methylation

UHRF1 is a member of epigenetic network which plays a decisive role in faithful transmission and maintenance of DNA methylation patterns (Bostick *et al.*, 2007; Bronner *et al.*, 2007a; Bronner *et al.*, 2010). UHRF1 co-localizes and directly interacts with DNMT1 during replication phase and recruits DNMT1 on chromatin. Knockdown of UHRF1 reduced the DNMT1 recruitment on chromatin which shows its crucial role in methylation maintenance (Bostick *et al.*, 2007). SRA domain of UHRF1 showed higher binding affinity for hemi-methylated (HM) DNA and it recognizes hemi-methylated CpG sites which are preferential substrate for DNMT1 (Bostick *et al.*, 2007; Sharif *et al.*, 2007). Recruitment of DNMT1 on replication foci involves PCNA (proliferating cell nuclear antigen) but it is not required absolutely (Sharif *et al.*, 2007).

Structural studies have provided the proof that SRA domain recognizes 5-mC and flips it out from DNA duplex. This base flipping is a signal to engage DNMT1 for methylation of the newly formed daughter strand (Arita *et al.*, 2008; Avvakumov *et al.*, 2008; Hashimoto *et al.*,

2008; Vaughan *et al.*, 2018). Study has reported that UHRF1 knockout in embryonic stem cells (ESC) led to loss of DNMT1 association with chromatin (Bostick *et al.*, 2007; Sharif *et al.*, 2007). Early gestational lethality and developmental arrest was observed in UHRF1 knockout embryos (Sharif *et al.*, 2007).

Later on, it was discovered that SRA is not the only protein involved in DNMT1 targeting. TTD and PHD domains are also associated with recognition of reading histone marks and play an important role to guide DNMT1 to DNA. TTD of UHRF1 binds with H3K9me3 and H3K4 marks which is essential for loading of UHRF1 on chromatin and finally for maintenance of methylation. Mutation in TTD interferes with this interaction (Karagianni *et al.*, 2008; Rottach *et al.*, 2010; Nady *et al.*, 2011; Rothbart *et al.*, 2012; Ferry *et al.*, 2017). UHRF1 is also involved to recruit G9a (histone methyltransferase) to histone lysines which is essential for methylation of histone lysines (Kim *et al.*, 2009). Interestingly another study has shown that G9a regulates UHRF1 expression levels (Kim *et al.*, 2015).

PHD domain has also an important role in methylation. Structural investigations have shown that PHD domain binds with unmodified arginine (H3R2) and this helps UHRF1 to suppress genes by hypermethylation (Hu *et al.*, 2011; Rajakumara *et al.*, 2011; Wang *et al.*, 2011). Any mutation or loss of this interaction can turn out in loss of DNA methylation (Qin *et al.*, 2015; von Meyenn *et al.*, 2016). PHD and RING domains of UHRF1 are necessary for H3 ubiquitination. DNMT1 has a ubiquitin interacting motif (UIM) that mediates its binding with ubiquitinated H3 and this association is important for DNA methylation activity.

Besides recruiting DNMT1, UHRF1 has also the ability to stimulate catalytic activity of DNMT1. Replication foci targeting sequence (RFTS) plugs the catalytic pocket of DNMT1. SRA domain removes this plug to facilitate the binding of hemi-methylated DNA into catalytic pocket of DNMT1 (Bashtrykov *et al.*, 2014; Berkyurek *et al.*, 2014). RING domain-mediated ubiquitination of H3 at K18 and K23 stimulates DNMT1 activity since DNMT1 has more affinity for ubiquitinated H3 (Nishiyama *et al.*, 2013; Qin *et al.*, 2015). RING domain along with UBL domain is involved in DNMT1 nuclear localization (Li *et al.*, 2018).

Two types of models can explain the dialogue between UHRF1 and DNMT1 for DNA methylation. Polybasic region (spacer region between SRA and RING domain) of UHRF1 inhibits binding of TTD with H3K9me3. In closed conformation, UHRF1 is unable to interact with H3K9me3 through its TTD domain, with unmodified H3R2 through PHD domain or with hemi-methylated DNA through SRA domain (Bronner *et al.*, 2019).

In presence of HM DNA, intramolecular interactions are interrupted, and these domains interact with their targets. Interaction of TTD with H3K9me3 can induce RING domain-mediated mono-ubiquitination of H3 at K14, K18 and K23 which is a signal for DNMT1 recruitment (Figure 20A). Probably two mono-ubiquitinated molecules are enough for DNMT1 to bind with H3 (Bronner *et al.*, 2019).

Many studies have validated that UHRF1 and DNMT1 can physically interact with each other. Our group reported that human SRA domain is responsible for interaction with human DNMT1 while another group reported that PHD domain of mouse UHRF1 interacts with DNMT1. And recently a study had reported that UBL domain of UHRF1 can interact with RFTS domain of DNMT1 and stimulates catalytic activity of DNMT1. Spacer region of UHRF1 has an important role in interaction of SRA domain with (HM) DNA (Bronner *et al.*, 2019).

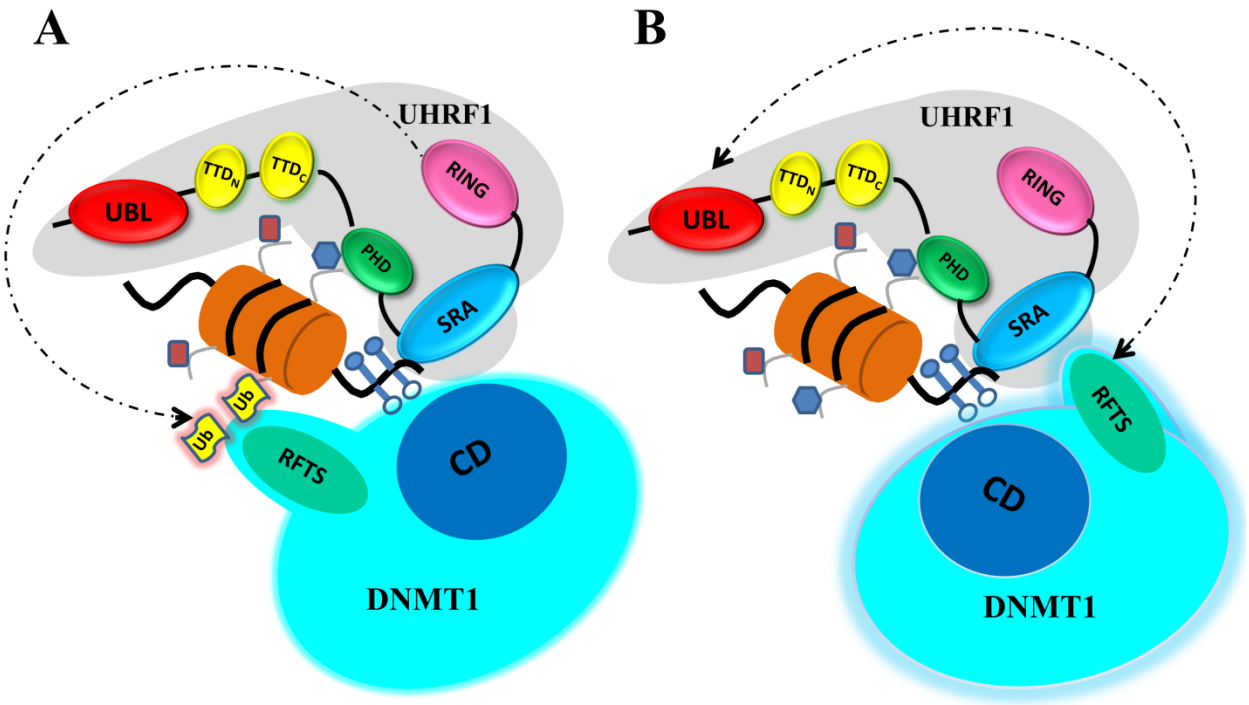

Figure 20: Talk between UHRF1 and DNMT1 in the presence of hemi-methylated DNA . (i) Model A: targeting of DNMT1 to chromatin through H3-mediated ubiquitination. RING domain-mediated ubiquitination (dotted line) on nucleosome serves as a dock for DNMT1 through its RFTS domain (replication focus targeting sequence). This interaction relieves auto-inhibitory effect of RFTS on catalytic domain (CD) of DNMT1. At the same time, TTD interacts with H3K9me2/3 (ocher rectangle on nucleosome) and PHD interacts with unmodified arginine 2 on H3 (blue hexagon). (ii) Model B: targeting of DNMT1 to chromatin through interaction of UHRF1 domains. Interaction of UBL (dotted line) and SRA domain with RFTS domain of DNMT1 allows the release of

CD of DNMT1. Like model A, TTD binds with H3K9me2/3 and PHD binds with unmodified H3R2. Adapted from (Bronner *et al.*, 2019).

This spacer region demonstrates difference between UHRF1 and UHRF2. UHRF2 lacks spacer region as well as maintenance of DNA methylation. So, most likely sites for interaction are SRA and UBL domain of UHRF1 with RFTS domain of DNMT1 (Figure 20B). If both models are correct, then there should be an explanation for compatibility of these models. So, a complete model can explain this in which UHRF1 does not recruit DNMT1 but still they are present in the same macromolecular complex. Both are always present in close proximity while moving along the replication fork, despite a direct transfer of CpG sites from SRA domain to DNMT1 looks not applicable. When SRA domain interacts with HM-CpG dinucleotides, UHRF1 adopts open conformation which allows ubiquitination of H3 and/or auto-ubiquitination by RING domain facilitated by UBL interaction with E2 ubiquitin conjugating enzyme. This is the signal for RFTS domain to relive catalytic domain of DNMT1. At the same time, TTD interacts with H3K9me3. This step allows DNMT1 to come in action but is not enough for its localization (Bronner *et al.*, 2019).

It is also proposed that when UHRF1 flips mC through SRA, UHRF1 can undergo an allosteric change creating contact sites for DNMT1. This leads to interaction of catalytic domain of DNMT1 with HM-DNA with the release of mC by SRA domain. When UHRF1 releases mC it follows other HM-CpG while leaves behind DNMT1 to methylate newly synthesized DNA strand. RFTS first interacts with ubiquitinated H3 and then interacts with SRA to remove UHRF1 from CpG. This explains that DNMT1 cannot methylate the opposite DNA strand until UHRF1 is not removed from there (Bronner *et al.*, 2019).

Replication machinery recruits UHRF1 to replication site with the help of DNA ligase 1 (LIG1). LIG1 is methylated by two methyltransferases (G9a and GLP) which resembles to H3K9me2/3 mark in binding to UHRF1-TTD. Binding of methylated LIG1 enhances recruitment of UHRF1 to replication site (Ferry *et al.*, 2017).

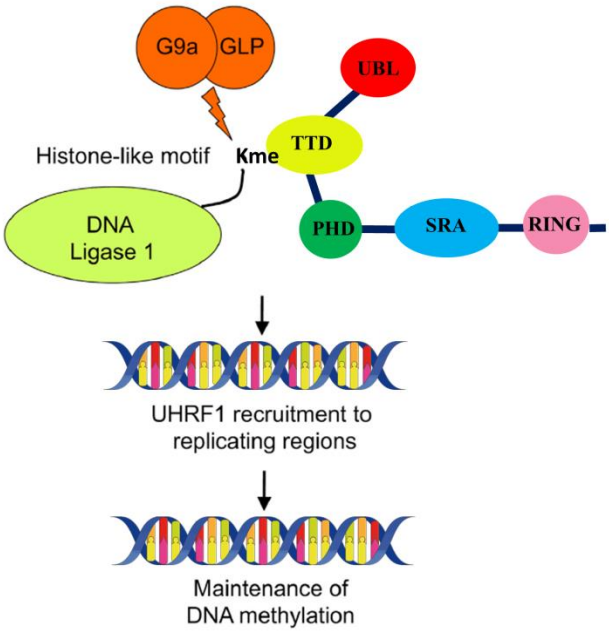

Figure 21: UHRF1-LIG1 interaction is important in maintenance of DNA methylation. G9a and GLP methylate histone mimic LIG1 which enhances interaction of LIG1 with UHRF1. This interaction helps UHRF1 in recruitment to replication foci and maintenance of methylation. Adapted from (Ferry *et al.*, 2017).

b. UHRF1 and its conformational dynamics

UHRF1 is a multidomain protein and through its domains it performs its role in epigenetic modifications. Interactions and roles of these domains are studied very well but information regarding their spatial conformation is still little (Gelato *et al.*, 2014). TTD domain interacts with PBR (polybasic region) or "spacer" region present between SRA and RING domain of UHRF1.

Additionally, PHD domain can collaborate with SRA domain and through this interaction UHRF1 adopts a closed (occluded) conformation. In closed conformation, loading of UHRF1 to chromatin is improbable (Gelato *et al.*, 2014; Zhang *et al.*, 2015; Fang *et al.*, 2016). P15P (Phosphatidylinositol 5-phosphate) (Gelato *et al.*, 2014), Ubiquitin-specific-protease 7 (USP7) (Zhang *et al.*, 2015) or hemi-methylated DNA (Fang *et al.*, 2016) can interfere with interaction of UHRF1 domains and UHRF1 adopts "open" conformation for its loading to chromatin (Figure 22).

USP7 and PI5P interact with "spacer" region of UHRF1 and dissociate PHD from TTD to allow them to read H3R2 and H3K9me3 marks, respectively (Gao *et al.*, 2018). Open conformation of UHRF1 not only enables UHRF1 loading on chromatin but also stimulates UHRF1 to interact with DNMT1.

Recently structure studies have revealed that TTD interacts with LIG1K126me3 helping UHRF1 to come in open conformation (Jeltsch, 2019; Kori *et al.*, 2019). It has also been reported that UBL domain interacts with E2 enzyme and coordinates with other domains helping them in reading histone marks leading to H3 ubiquitination which is important for DNA methylation (DaRosa *et al.*, 2018).

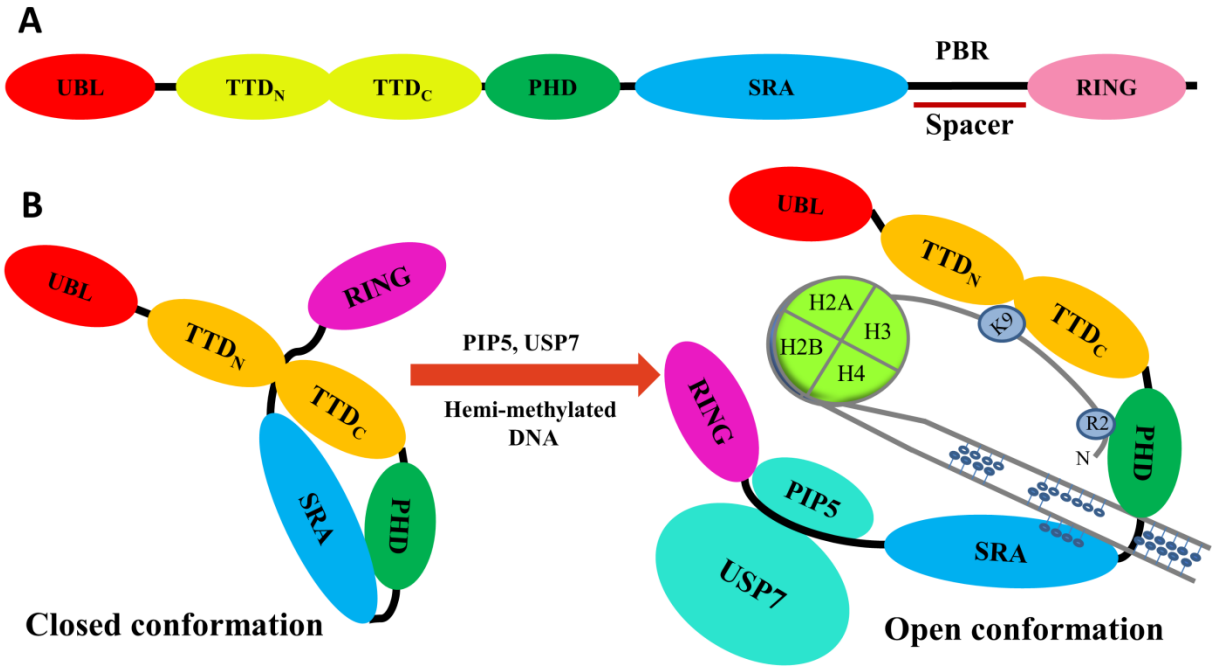

Figure 22: DNA methylation and change in conformation of UHRF1. (**A**) Structure of UHRF1 with polybasic region. (**B**) During replication phase, USP7, PIP5 and hemi-methylated DNA associate with UHRF1 and UHRF1 adopts an "open" conformation from "closed" conformation. Adapted from (Gelato *et al.*, 2014; Zhang *et al.*, 2015; Fang *et al.*, 2016).

4.1.D. UHRF1 regulation through post-translational modifications

As described above, UHRF1 performs critical role in a variety of cellular functions and being a mediator, it recruits many enzymes to their target sites. However, investigation of UHRF1 regulation still needs attention of researchers. UHRF1 can undergo post-translational modifications (PTMs) which can affect its stability and functions. Important PTMs on UHRF1 are described here.

a. Ubiquitination of UHRF1

Ubiquitin is a small protein having a molecular weight around 8.6 kDa and it is expressed ubiquitously in most tissues of eukaryotes. This polypeptide was discovered in 1975

(Goldstein *et al.*, 1975). In human genome ubiquitin is coded by four genes named UBB, UBC, UBA52 and RPS27A. UBB and UBC genes are coded for polyubiquitin precursor protein while UBA52 and RPS27A correspond to single copy of ubiquitin fused with ribosomal proteins L40 and S27a, respectively (Kimura & Tanaka, 2010). Ubiquitination involves addition of either one or several molecules of ubiquitin proteins. This PTM can mark proteins for a variety of functions like protein degradation, intracellular trafficking, regulation of enzymes, receptor down-regulation or internalization, protein complex formation autophagy and DNA repair. Ubiquitination involves three enzymes E1 (ubiquitin-activating enzyme), E2 (conjugating enzyme) and E3 (ligase enzyme) (Kirkin & Dikic, 2011; Popovic *et al.*, 2014; Dubrez, 2017).

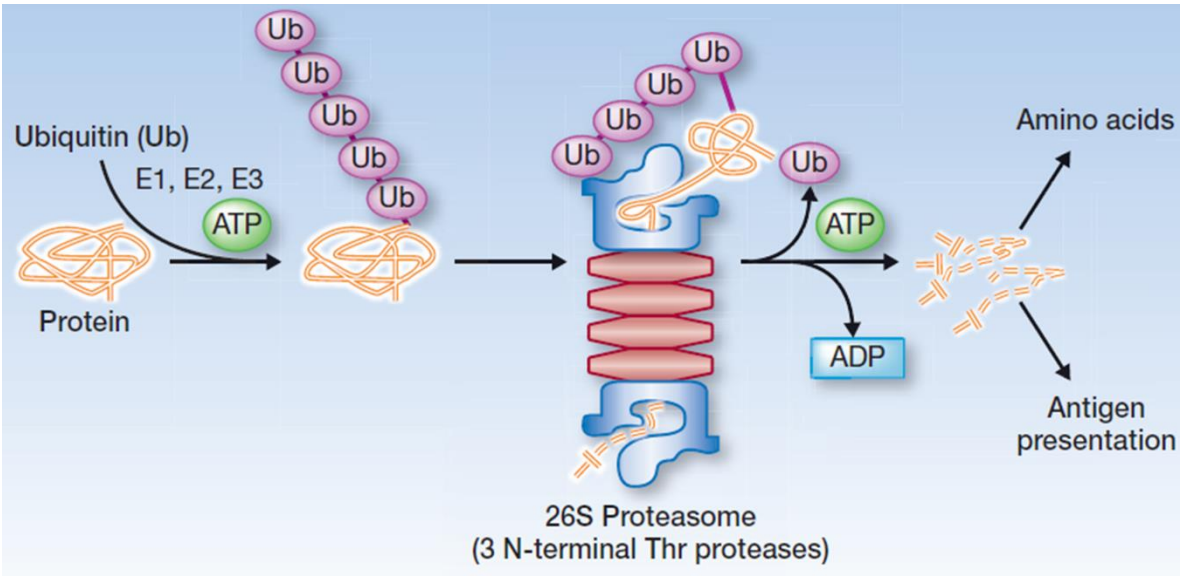

Figure 23: Ubiquitin-proteasome pathway marking protein for degradation. Ubiquitin molecules are added to protein with the action of E1, E2 and E3 enzymes. This ubiquitin-protein complex is transferred to proteasome where ubiquitin molecules are separated, and protein is unfolded by ATP-dependent process. Unfolded protein is transferred deep inside the proteasome complex for degradation. Adapted from (Molineaux 2011).

UHRF1 RING domain has intrinsic E3 ligase activity through which UHRF1 can ubiquitinate either itself or other protein (Jenkins *et al.*, 2005; Tauber & Fischle, 2015). UHRF1 can be polyubiquitinated by $SCF^{\beta\text{-}TrCP}$ enzyme and degraded by proteasomal pathway (Chen *et al.*, 2013). A long noncoding RNA named UPAT intrudes with β-TrCP1 and β-TrCP2-mediated ubiquitination of UHRF1 and stabilizes UHRF1 (Taniue *et al.*, 2016). Interestingly, unmodified histones and nucleosomes reduce auto-ubiquitination of UHRF1 and ultimately enhance UHRF1 stability (Karagianni *et al.*, 2008).

USP7 (de-ubiquitinase enzyme) protects UHRF1 from ubiquitin-mediated degradation during S phase (Felle *et al.*, 2011; Ma *et al.*, 2012). During M phase, USP7-UHRF1 association is interrupted due to UHRF1 phosphorylation. After dissociation, USP7 cannot protect UHRF1 from degradation (Figure 24) (Ma *et al.*, 2012).

In a study Ibrahim *et al* have shown that thymoquinone induced UHRF1's degradation and it was related with corresponding decrease in USP7 and an increase in caspase-3 and p73 levels. UHRF1 degradation was resulted in UHRF1 E3 ligase dependent auto-ubiquitination (Ibrahim *et al.*, 2018). It was studied that UHRF1 interacts with HSP90 (heat shock protein 90). Inhibition of HSP90 resulted in ubiquitination of UHRF1 and this ubiquitination was neither dependent on E3 ligase activity of UHRF1 nor on $SCF^{\beta\text{-}TrCP}$ enzyme (Ding *et al.*, 2016). HSP90 proteins are involved in regulation of many cellular functions such as transcription, DNA repair, epigenetic and chromatin regulation (Dubrez et al., 2019).

Recently, it has been reported that SET8 (also named as PR-SET7, SETD8 and KMT5A) is involved in ubiquitination of UHRF1. SET8 can methylate (monomethylation) of H4K20 and aslo non-histone proteins like p53. SET8 down-regulates UHRF1 in G2/M phase through methylation-mediated ubiquitination. It methylates UHRF1 at K385 and ubiquitinates UHRF1 at K500 and finally degrades UHRF1. In contrast LSD1 stabilizes UHRF1 through its demethylase activity. Through down-regulation of UHRF1, SET8 suppresses post-replication DNA methylation. In this way, SET8 regulates UHRF1 levels in a cell cycle-dependent manner through methylation-mediated ubiquitination (Zhang *et al.*, 2019).

b. Phosphorylation of UHRF1

UHRF1 is a phosphoserine protein and it can be phosphorylated at Ser-298 by protein kinase A in cAMP signaling pathway. This results in enhanced ability of UHRF1 to activate topoisomerase IIα expression which is essential for G1/S phase transition (Trotzier *et al.*, 2004). UHRF1 exhibits consensus sequence pattern for protein kinase 2 (also known as casein kinase 2 /CK2). CK2 can phosphorylate UHRF1 and this can increase transcriptional activity of UHRF1 which supports G1/S transition (Bronner *et al.*, 2004).

Crystal study of TTD and PHD domains of UHRF1 with H3K9me3 peptide has shown that phosphorylation of UHRF1 at S-298 abolishes UHRF1-H3 interaction. Therefore, UHRF1 phosphorylation regulates UHRF1's role in DNA methylation (Arita *et al.*, 2012). It is phosphorylated at Ser-661 by CDK2 along with cyclin A2. This phosphorylation was shown

to be essential in zebrafish embryogenesis as well as in localization of UHRF1 to cytoplasm (Chu *et al.*, 2012). During G1 and S phase, USP7 protects UHRF1 from degradation. In M phase, UHRF1 is phosphorylated at Ser-652 (UHRF1 isoform 2) (Ser-639 in UHRF1 isoform 1) by CDK1-cyclin B which interferes with USP7-UHRF1 association. Unbound UHRF1 is degraded through proteasomal pathway (Figure 24) (Ma *et al.*, 2012).

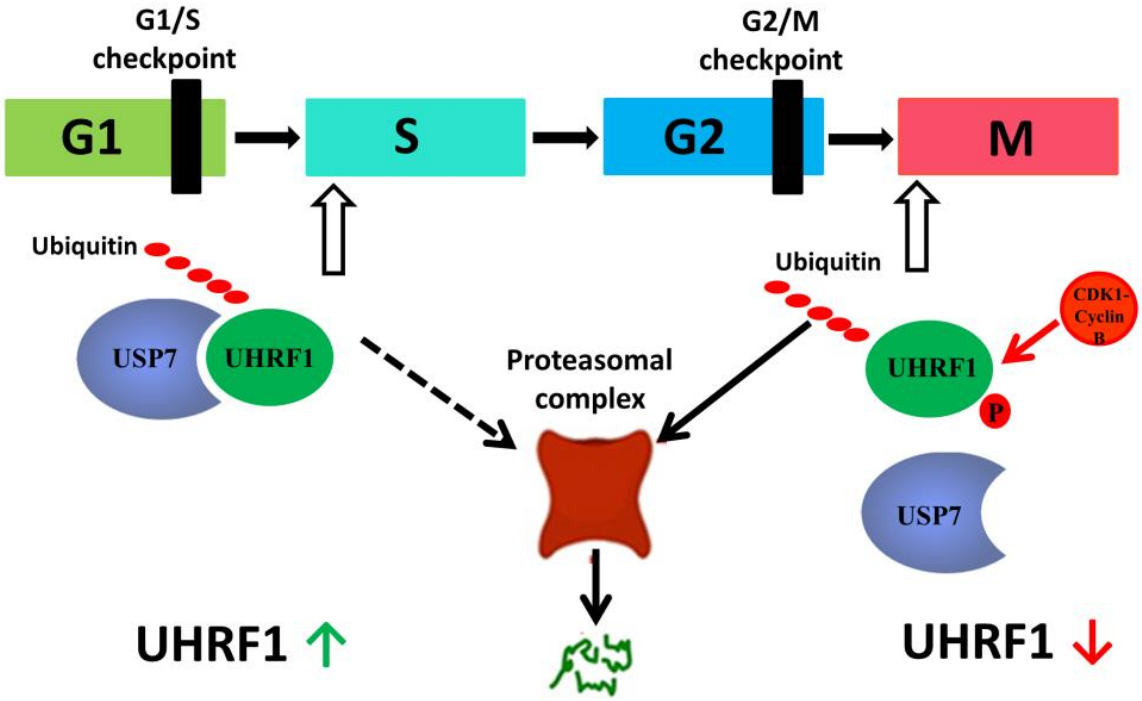

Figure 24: At G1 and S phase of cell cycle, UHRF1 levels are maintained through a fine balance between its ubiquitination and USP7-mediated deubiquitination. During M phase, CDK1-cyclinB phosphorylates UHRF1 which disrupts USP7-UHRF1 association. Unbound UHRF1 is degraded by proteasome pathway. Adapted from (Ma *et al.*, 2012).

Yang *et al* have identified that UHRF1 can be phosphorylated at Ser-311 (isoform 2, Ser-298 in isoform 1) by PIM1 kinase and finally degraded. PIM1 is a proto-oncogene involved in regulation of cellular proliferation, survival, apoptosis and differentiation. PIM1 destabilizes UHRF1 leading to DNA hypomethylation and ultimately senescence (Yang *et al.*, 2017). Phosphorylation of UHRF1 at Ser-95 (isoform 1, Ser-108 in isoform 2) by casein kinase 1δ can also lead to $SCF^{\beta\text{-}TrCP}$-mediated ubiquitination of UHRF1 (Chen *et al.*, 2013).

c. Acetylation of UHRF1

UHRF1 is found in a macro-molecular complex with its interacting partners like TIP60, DNMT1, HDAC1, PCNA and USP7 (Achour *et al.*, 2009; Du *et al.*, 2010). So, there is a

possibility that UHRF1 can be acetylated by an acetyltransferase enzyme like TIP60 or MOF. It has been already shown that TIP60 acetylates DNMT1 during S phase of cell cycle and association between USP7 and acetylated DNMT1 is decreased (Du *et al.*, 2010). So, there are chances that TIP60 can acetylate UHRF1 at its PBR (polybasic region) which comes under the preferential acetylation sequence of TIP60 (Kimura & Horikoshi, 1998). Zhang *et al* identified recombinant TIP60-mediated acetylation of UHRF1 at K659 (isoform 2, 646 in isoform 1) in an *in vitro* acetylation assay (Zhang *et al.*, 2015). Still there is need to explore TIP60-mediated acetylation of UHRF1 *in vivo* to investigate regulation of UHRF1 in more detail.

4.2. UHRF1 regulation and cell cycle

Many signaling pathways are involved in regulation of UHRF1 and activation of these pathways results in reduced levels of UHRF1. ERK1/2 signaling pathway activation suppresses cell proliferation and brings about cell cycle arrest in Jurkat T cells through down-regulation of UHRF1 (Fang *et al.*, 2009). p73 pathway is also involved in UHRF1's regulation. Thymoquinone treated p53 deficient cells showed decreased UHRF1 and increased p73 expression levels. Cell cycle arrest in G_0/G1 and induced apoptosis was also observed (Alhosin *et al.*, 2010). UHRF1 expression levels are also controlled through another pathway known as p53/$p21^{Cip1/WAF1}$ which is activated upon DNA damage. Down-regulation of UHRF1 was because of both transcription suppression and protein degradation (Arima *et al.*, 2004). TCR (T cell receptor) pathway regulates UHRF1 gene expression through pRb/E2F complex. TCR pathway stimulation reduced UHRF1 protein and mRNA expression and induced cell cycle arrest (Abbady *et al.*, 2005). CDK-cyclins are essential for cell cycle progression. CDK-mediated phosphorylation of retinoblastoma (Rb) tumor suppressor protein is involved in cell cycle progression from G1 to S phase. But if Rb is hyperphosphorylated then its association with E2F1 is decreased. E2F1 is very important transcription factor playing a critical role in G1/S phase transition (Dubrez, 2017; Dumétier *et al*., 2019). UHRF1 has three E2F binding sites in its promoter region, so it explains that why UHRF1 is transcriptionally regulated by E2F1 and role of UHRF1 in cell cycle is regulated through these transcription factors (Mousli *et al.*, 2003; Arima *et al.*, 2004; Unoki *et al.*, 2004). UHRF1 expressions are also regulated by some microRNAs. UHRF1 higher expression in cancer cells is related to lower expression of microRNAs which act as tumor suppressor genes. Therefore, abnormal microRNAs level can lead to higher expression of UHRF1 in cancer cells (Sidhu & Capalash, 2017; Choudhry *et al.*, 2018).

4.3. Screening and targeting of UHRF1

4.3.A. Targeting of UHRF1

As described earlier, expression levels of UHRF1 are high in many cancers. Overexpression of UHRF1 is involved in silencing of TSGs, tumor cell proliferation, DNA repair inhibition and resistance towards anti-cancer therapy. While knock down of UHRF1 in cancer cells resulted in inhibition of cellular proliferation, cell cycle arrest, apoptosis, activation of TSGs and better response towards anti-cancer therapy. Advantage to target UHRF1 is that it will have better efficacy, specificity and less side effects as compared to DNMT1 and HDAC inhibitors, as UHRF1 expression levels are low in normal cells. So UHRF1 can be a useful anticancer drug target (Bronner *et al.*, 2007a; Unoki *et al.*, 2009; Bronner *et al.*, 2013; Alhosin *et al.*, 2016; Ashraf *et al.*, 2017b).

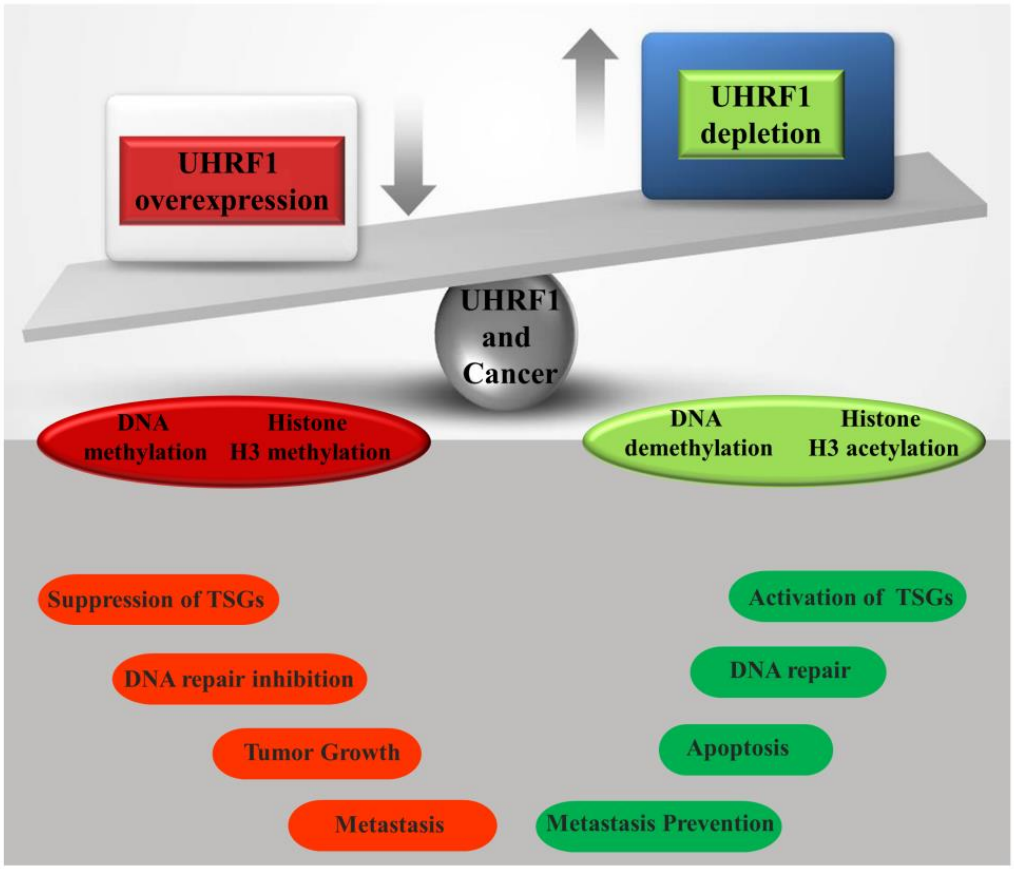

Figure 25: Mis-regulation of UHRF1 in cancers and effects of this mis-regulation on different biological processes. UHRF1 overexpression inhibits TSG, DNA repair and promotes tumor growth and metastasis through

methylation of DNA and H3. Depletion of UHRF1 activates pro-apoptotic pathway through re-activation of TSGs and also inhibits tumor growth. Adapted from (Bronner *et al.*, 2013).

UHRF1 cannot be targeted through antibody therapy because the targeted proteins should be membrane proteins so that antibodies can identify them. As UHRF1 is a nuclear protein, antibody therapy is not useful to target UHRF1. s*iRNAs* therapy can bring excellent benefits in targeting UHRF1, once improved drug delivery systems are established which can protect *siRNAs* from degradation and ensure their delivery at target site. Another strategy is to develop peptides which can interfere with association of UHRF1 and its interacting partners so that functions of UHRF1 can be inhibited. But again, stability issue of peptides is the hurdle in application of peptides as therapy. Cancer vaccine is also another option to stimulate immune system of the patient against oncantigens. This potential targeting is under trials and needs attention of scientists to develop effective and efficient cancer vaccines (Unoki *et al.*, 2009). Relatively an easier and promising strategy is to develop small molecular compounds that can target SRA domain or other domains of UHRF1 (Unoki *et al.*, 2009). We will discuss this in detail here.

a. Chemical compounds targeting UHRF1

A high throughput study has identified a novel small molecule which is HSP90 (90kDa heat-shock protein) inhibitor known as 17-AAG (17-allylamino-17-demethoxygeldanamycin). 17-AAG induced degradation of UHRF1 through proteasomal degradation pathway and inhibited cellular proliferation (Ding *et al.*, 2016).

Small molecule screening study identified a new molecule named BPC (4-benzylpiperidine-1-carboximidamide). BPC interacts with TTD (tandem Tudor domain) groove of UHRF1 protein and encourages open conformation of UHRF1 (TTD-PHD). This open conformation has low binding efficiency with H3K9me3 which affects UHRF1 functionality. Still studies are needed to evaluate its effects in cellular processes (Houliston *et al.*, 2017).

Tandem virtual screening study has identified a potent uracil derivative compound, NSC232003. This molecule was able to fit in 5-mC binding pocket of SRA domain. The interaction between UHRF1 and DNMT1 was disturbed in the presence of this compound. Global hypomethylation was observed which can be due to interference between SRA and hemi-methylated DNA. This study has reported the first evidence for druggability of SRA

domain and it can be used as a molecular tool to investigate new molecules and their effects on UHRF1 functionality (Myrianthopoulos *et al.*, 2016).

Recently a study has reported a unique high-throughput screening approach known as TR-FRET (time-resolved fluorescence resonance energy transfer) which can be used for screening of small molecules that can interfere with SRA domain and hemi-methylated DNA interaction. Through this approach, a library called LOPAC (library of pharmacologically active compounds) was identified containing several SRA inhibitors out of which seven compounds were validated. Out of these commonly used anti-cancer compounds (mitoxantrone, idarubicin, doxorubicin, pixantrone and daunorubicin) unexpectedly inhibited interaction of SRA domain with hemi-methylated DNA. These compounds also showed synergistic effect when combined with DNMT inhibitors (Giovinazzo *et al.*, 2019).

ERK1/2 are involved in cell cycle and cellular proliferation. Their expression levels reported to be up-regulated in breast and liver cancer. Activation of ERK1/2 (extracellular signal-regulated kinase 1/2) is involved in release of E2F which can bind with in promoter region of UHRF1. Inhibitors of ERK1/2 (PD98059, LY294002, GF109203X, AG490 and genistein) inhibited cellular proliferation and colony formation in a dose dependent manner. Treatment of Jurkat cells for 24 h showed significant decrease in phosphorylated ERK1/2 and UHRF1 levels especially PD98059, LY294002 and AG490. PD98059 significantly induced arrest of cell cycle (at G_1/G_0). Results indicate that UHRF1 can be targeted through ERK1/2 signaling pathway (Fang *et al.*, 2009).

Dihydroartemisnin (DHA) has been studied to explore its anti-cancer potential. Anti-proliferation and anti-apoptotic activities of DHA have been reported in prostate cancer cells (Morrissey *et al.*, 2010; Xu *et al.*, 2016). DHA treatment in prostate cancer cells induced down-regulation of UHRF1 and DNMT1 and up-regulation of p16 ^{INK4A}. DHA induced apoptosis and cell cycle arrest at G1/S phase (Du *et al.*, 2017).

mTOR (mammalian target of rapamycin) is overexpressed in HCC (hepatocellular carcinoma) and its inhibition reduced cellular proliferation in HCC. Treatment with an inhibitor of mTOR, Torin-2 significantly inhibited cell growth and induced apoptosis along with down-regulation of UHRF1. UHRF1 down-regulation was partially due to decrease in UHRF1 mRNA levels but still it needs attention to explain the exact mechanism involved (Wang *et al.*, 2015).

LSF (Late SV40 Factor) is a transcription factor and is involved in many biological processes like cell cycle regulation, cell survival, DNA synthesis and regulation of cellular and viral promoters. Overexpression of LSF has been found in HCC (Santhekadur *et al.*, 2012). A novel small molecule named FQI1 (factor quinolinone inhibitor 1) was identified which inhibited LSF binding activity with DNA and also induced death in many cancer cell lines (Grant *et al.*, 2012). LSF binds directly with UHRF1 and DNMT1 while FQI1 inhibits this interaction resulting in altered methylation patterns and cell cycle progression (Chin *et al.*, 2016).

b. Natural compounds targeting UHRF1

Plant-derived drugs can play a vital role in cancer cure due to their higher efficacy and low toxicity as compared to synthetic drugs. Drugs of plant origin like taxol, paclitaxel, vincristine camptothecin and others have shown promising results in anti-cancer regimen. There are several natural compounds which can target signaling pathways of UHRF1. Luteolin is a flavonoid compound obtained from *Reseda luteola* plant. It has anti-proliferative capability and it leads to cell cycle arrest and apoptosis. Luteolin treatment resulted in down-regulation of UHRF1 and DNMT1 and up-regulation of TSG $p16^{INK4A}$ (Krifa *et al.*, 2014). Active constituents (gallocatechin, epigallocatechin and epigallocatechin-3-O-gallate) of *Limoniastrum guyonianum* aqueous gall extract exhibit anticancer properties. Treatment with extract in HeLa cells resulted in cell cycle arrest at G2/M phase and apoptosis. It also reactivated $p16^{INK4A}$ TSG. Down-regulation of UHRF1 and DNMT1 was also observed after extract treatment resulting in global hypomethylation (Krifa *et al.*, 2013).

EGCG (epigallocatechin-3-gallate), a polyphenol found in green tea has the potential to up-regulate various TSGs ($p16^{INK4A}$, *RAR* β, MGMT and hMLH1) via demethylation of promoter regions of these TSGs. It also affected DNMT1 expression and activity. In Jurkat cancer cells, EGCG interfered with UHRF1/DNMT1 interaction in a *p73*-dependent manner (Achour *et al.*, 2013).

Thymoquinone (TQ) is an active constituent of volatile oil of black seeds (*Nigella sativa*). TQ had shown anti-cancer activity against different cancer cell lines. It induces apoptosis in a p53-dependent and p53-independent manner (Gali-Muhtasib *et al.*, 2006; Darakhshan *et al.*, 2015). TQ had been reported to induce cell cycle arrest at G_o/G_1 phase with an increase in p16 expressions (Shoieb *et al.*, 2003; Gali-Muhtasib *et al.*, 2004). In Jurkat cells, TQ treatment led to decrease in UHRF1, DNMT1 and HDAC1 expression levels. Besides this, it also induced

apoptosis through p73 activation (Abusnina *et al.*, 2011; Alhosin *et al.*, 2010). TQ treatment induced ubiquitination-mediated degradation of UHRF1 with a decrease in USP7 and increase in p73 and caspase-3. After TQ treatment, UHRF1 was degraded due to its intrinsic E3 ligase-dependent autoubiquitination (Ibrahim *et al.*, 2018). Recently RNA sequencing study has shown that TQ treatment in Jurkat cells led to down-regulation of UHRF1, DNMT1, G9a, HDAC1 and up-regulation of several TSGs (Qadi *et al.*, 2019).

DHNQ (5,8-dihydroxy-1,4-naphthoquinone, Naphthazarin, Naph) is an 1,4-naphthoquinone derivative of plant origin having anti-cancer properties. DHNQ treatment in human breast cancer cells (MCF-7) inhibited cell viability and in combination with ionizing radiation induced down-regulation of UHRF1, DNMT1 and HDAC1. An increase in p53-dependent p21 expression was also observed. Finally, cell cycle arrest and apoptosis were induced in MCF-7 cells (Kim *et al.*, 2015).

Red wine is a rich source of polyphenols which have beneficial effects on health. Study has found an inverse correlation between moderate use of red wine and cancer. Anti-cancer properties of red wine are linked with resveratrol, which can arrest cell cycle and can induce apoptosis. Treatment with red wine polyphenols (RWPs) reduced cell viability of Jurkat cells in a concentration dependent manner. Treatment also led to cell cycle arrest in G_o/G_1 phase. RWPs also induced down-regulation of UHRF1 and up-regulation of p73 and caspase-3 (Sharif *et al.*, 2010). Another study reported that oral intake of grape-derived polyphenols in rats with C26 tumor reduced tumor growth through inhibition of angiogenesis and induction of apoptosis. Treatment also reduced expression of UHRF1 and enhanced expression of caspase-3, p16, p53 and p73 (Walter *et al.*, 2010).

A naphthoquinone, Shikonin which is derived from traditional Chinese medicine *purple gromwell* (Zi cao) is known to exhibit anticancer potential. Treatment of Shikonin in HeLa and MCF-7 cells reduced UHRF expression and increased expression of $p16^{INK4A}$. Shikonin induced apoptosis through p73 and caspase-3 dependent pathway (Jang *et al.*, 2015).

Berry anthocyanins especially from bilberry (*Vaccinium myrtillus* L.) possess anti-cancer and anti-angiogenesis activities (Mauray *et al.*, 2009). Bilberry extract (Antho 50) treatment in B CLL (B cell chronic lymphocytic leukaemia) induced apoptosis and down-regulation of UHRF1. Treatment activated caspase-3, inhibited Bcl-2 and dephosphorylated Akt and Bad (Alhosin *et al.*, 2015). *Aronia melanocarpa* juice also showed strong anti-tumor activity through redox- sensitive mechanism in Jurkat cells (deficient-p53). Treatment of Jurkat cells

inhibited cell proliferation and induced cell cycle arrest (in G2/M phase) and apoptosis. UHRF1 and cyclin B1 expression levels were decreased while expression levels of p73 and caspase-3 were increased (Sharif *et al.*, 2012).

Hinokitiol (4-isopropyltropolone) is an active bio constituent of essential oil of *Chymacyparis obtuse* and has shown anti-cancer property in various cancer cells through inhibition of cellular proliferation and induction of apoptosis. Treatment of colon cancer cells with Hinokitiol resulted in down-regulation of UHRF1 and DNMT1. It induced demethylation through inhibition of DNMT1/UHRF1 and induction of demethylation protein TET1. It also reactivated several TSGs which are involved in cellular proliferation and biological oxidation (Seo *et al.*, 2017).

Emodin (C_{15} $H_{10}O_5$) isolated from roots and rhizomes of various Chinese herbs had been reported to possess anti-tumor activity. In Raji lymphoma cells, emodin reduced cell viability and decrease in expression of UHRF1. It induced apoptosis through activation of caspase-3, 9 and PARP. In combination with doxorubicin, emodin induced more cell death indicating that may be emodin sensitizes cells to doxorubicin-mediated death (Lin *et al.*, 2017).

Curcumin is extracted from turmeric (*Curcuma longa*) and has been reported *in vitro* and *in vivo* to have anti-tumor activity. Curcumin targets PDE1 (phosphodiestrase 1) which is involved in proliferation of melanoma cells. Treatment induced down-regulation of UHRF1, DNMT1, and cyclin A along PDE1. Cell cycle was delayed and TSGs (p21, p27) were up-regulated (Abusnina *et al.*, 2011). In another study, curcumin treatment in different cancer cell lines reactivated TSG *PAX1* (paired box gene 1) and down-regulated UHRF1. However, hypermethylation of promoter region of *PAX1* was not reversed even with positive control (Parashar & Capalash, 2016).

Anisomycin is an antibiotic which is isolated from *Streptomyces* and can suppress the growth of Jurkat cancer cells in a dose dependent manner. It induced down-regulation of UHRF1 and cell cycle arrest at S and G2/M phase. Treatment showed positive correlation between anisomycin concentration and TSGs (p21, p27 and p53/P-p53) (Yu *et al.*, 2013).

4.3.B. Targeting of SRA domain

As described earlier, SRA domain of UHRF1 recognizes hemi-methylated DNA and also participates in recruitment of DNMT1 to replication site (Arita *et al.*, 2008; Vaughan *et al.*,

2018). Therefore, SRA domain is a potential candidate to explore for screening of new molecules and targeting for therapeutic purposes with lower side effects. Small molecules that bind with SRA domain can compromise UHRF1 binding with hemi-methylated DNA (Figure 26). So in this way, aberrant methylation levels in cancer can be regulated.

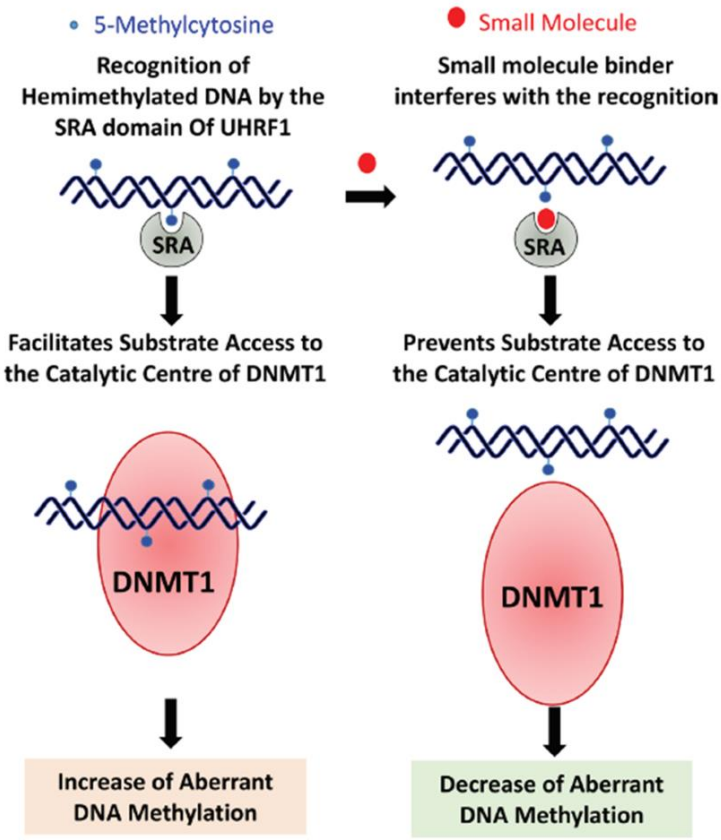

Figure 26: Small molecules that can tie up with SRA domain are anticipated to be effective in cancer therapy. These small molecules can modulate DNA methylation levels. Adapted from (Patnaik *et al.*, 2018).

Mitoxantrone (topoisomerase II inhibitor) was reported to change the binding of SRA domain with hemi-methylated DNA and induced hypomethylation (Parker *et al.*, 2003). First time a tandem virtual screening approach identified a novel compound NSC232003 which binds with SRA binding pocket and modulates UHRF1 function through disruption of UHRF1/DNMT1 interaction (Myrianthopoulos *et al.*, 2016). A tool using two fluorescence nucleobase analogues has provided to have a mechanistic look in 5-mC flipping and it can assist to screen inhibitors flipping to target against UHRF1 (Kilin *et al.*, 2017).

Structure based studies have indicated that Luteolin and Taxifolin are likely to bind with SRA domain (Patnaik *et al.*, 2018). In a recent study, different inhibitors are screened through time-resolved fluorescence resonance energy transfer (TR-FRET) assay, which can interfere with

SRA/hemi-methylated DNA interaction. This screening has confirmed mitoxantrone and four other topoisomerase II inhibitors of anthraquinone family that can inhibit interaction of SRA with hemi-methylated DNA (Giovinazzo *et al.,* 2019).

Through molecular docking approach, Polepalli *et al* have investigated some natural (thymoquinone, emodin and Naphthazarin) and synthetic (nocodazole and propranolol) molecules which can bind within the 5-mC binding site of SRA domain and can be potential UHRF1 inhibitors. Docking of thymoquinone and SRA domain showed that benzoquinone ring was directed towards 5-mC binding pocket. Similarly, naphthazarin has also shown the potential to bind with SRA. Nocodazole and propranolol can significantly develop favorable interactions with SRA domain. Further studies are needed to explore their potential to inhibit UHRF1 in detail (Polepalli *et al.,* 2019).

In a recent study from our lab, we have identified an anthraquinone compound (UM63) which can target the 5-methylcytosine binding pocket of SRA domain to prevent the recognition and flipping of 5-methylcytosine. We also shown that this compound interrupted UHRF1/DNMT1 interaction and hence reduced the methylation levels. This has revealed the integral role of base flipping in DNMT1 recruitment and evidence of druggability of the 5-methylcytosine binding pocket. This molecule can also serve as a molecular tool for investigation of UHRF1 role in the establishment of DNA methylation patterns and also as a foundation for hit-to-lead optimizations (Zaayter *et al.,* 2019).

4.4. UHRF1 partners

UHRF1 is an important player and coordinator of epigenetic complex. UHRF1 works in coordination with other members of the complex like TIP60 (Tat-interacting protein) (Achour *et al*., 2009), DNMT1 (DNA methyltransferase 1) (Bostick *et al*., 2007; Sharif *et al*., 2007), USP7 (Ubiquitin specific protease 7) (Zhang *et al*., 2015), HDAC1 (Histone deacetylase 1) (Unoki *et al*., 2009), PCNA (Proliferating cell nuclear antigen) (Hervouet *et al*., 2010), G9a/EHMT2 (euchromatic histone-lysine N methyltransferase 2) (Kim *et al*., 2009), $SCF^{\beta\text{-}TrCP}$ (E3 ubiquitin ligase) (Chen *et al*., 2013) and SUV39H1 (suppressor of variegation 39-homolog 1) (Babbio *et al*., 2012). Some other members interacting with UHRF1 in complex are DNMT3a, DNMT3b (Meilinger et al., 2009), histone methyltransferases, EZH2 (Enhancer of Zeste 2 Polycomb Repressive Complex 2 subunit) (Babbio *et al*., 2012), BRCA1 (Breast cancer type 1 susceptibility protein) (Zhang *et al*., 2016), PARP1 (Poly [ADP-ribose] polymerase 1) (De Vos *et al*., 2014), PRMT5 (Protein arginine methyltransferase 5) (Sheng *et al*., 2016), LIG1 (DNA ligase 1) (Ferry *et al*., 2017) and MBD4 (Methyl-CpG binding domain 4) (Meng *et al*., 2015).

TIP60 is the most important epigenetic partner of UHRF1. TIP60 deals with an array of biological mechanisms through its acetyltransferase activity. Acetylation of specific lysine by TIP60 is an important post-translational modification (PTM) which affects many cellular functions like protein-protein interactions, binding with DNA and activity of enzymes. This PTM is essential in the maintenance of genomic stability. Acetylation of proteins is a reversible phenomenon which is managed by histone acetyltransferases and histone deacetylases. Acetyltransferases enzymes transfer an acetyl group from acetyl coenzyme A to either the α-amino group of N-terminal amino acids or the ε-amino group of internal lysine residues. In most of the eukaryotic proteins, acetylation mark is added to these proteins during translation. There is a large variety of proteins which can be acetylated including histones, transcription factors, high mobility group proteins and nuclear import factors (Sapountzi *et al.*, 2006). Lysine acetyltransferases are classified in different categories, one of which is MYST family. MYST family is named after its originating members: MOZ, Ybf2/Sas3, Sas2 and TIP60. MYST family members have a highly conserved MYST acetyltransferase domain (Sapountzi *et al.*, 2006). TIP60 is a well-defined member of this family. Role of TIP60 in acetylation and effects of TIP60-mediated acetylation will be discussed in detail.

5. TIP60 (Tat Interactive Protein 60kDa)

5.1.A. Structure of TIP60

By using two-hybrid system in yeast, TIP60 was identified as an interacting partner of HIV-1 Tat protein. They named this protein as Tat interactive protein 60 kDa (Kamine *et al.*, 1996). TIP60 is also known as KAT5 (lysine acetyltransferase 5). It is encoded by HTATIP gene which is located at 11q13.1. There are three spliced variants of TIP60 named: TIP60 isoform 1, TIP60 isoform 2 (TIP60α) and TIP60 isoform 3 (TIP60β/PLA2 interactive protein/PLIP) (Figure 27).

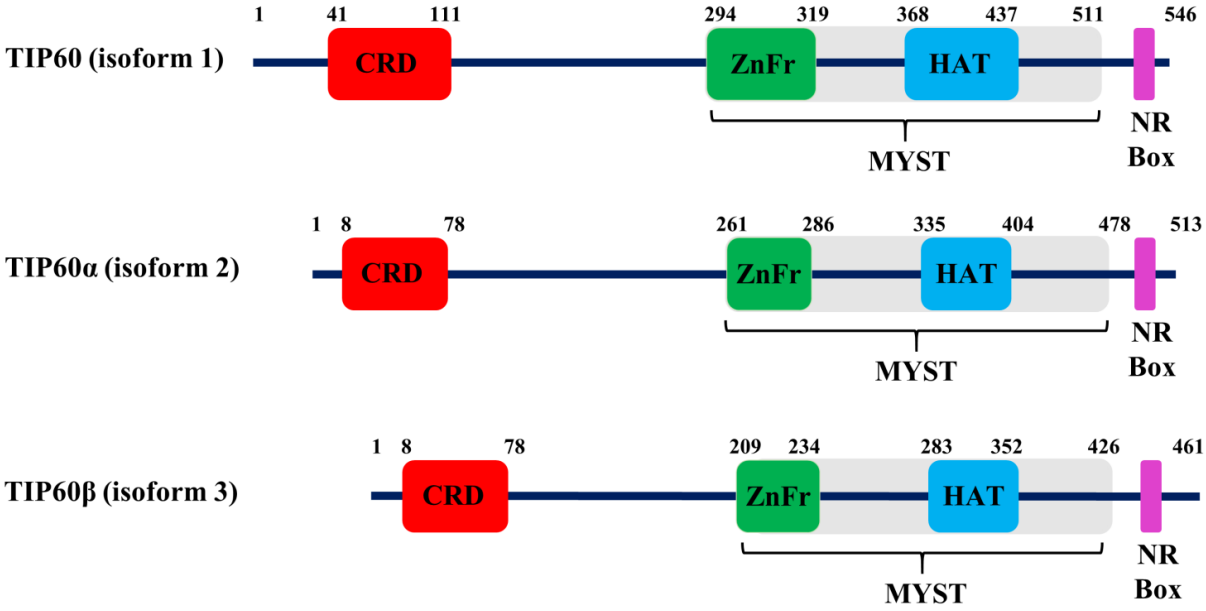

Figure 27: Schematic diagram of TIP60 isoforms.

Isoform 2 is best characterized and studied variant of TIP60 (Sapountzi *et al.*, 2006). Isoform 1 is the longer TIP60 protein which has 33 amino acids insertion at its N-terminal (Legube & Trouche, 2003). TIP60α (isoform 2) protein consists of 513 amino acids having a molecular weight of 58 kDa. This isoform is well studied and is involved in many cellular functions (Sapountzi *et al.*, 2006). Isoform 3 (TIP60β) is an alternatively spliced form of TIP60 which lacks exon 5 which is a proline rich region. TIP60β is expressed in various human tissues and cell lines. It is localized in both nucleus and cytoplasm while TIP60α is present in nucleus only. TIP60β has similar kind of properties and activities like TIP60α (Ran 2000; Sheridan *et al.*, 2001). In mouse four isoforms of TIP60 exist named: TIP60α, TIP60β, LTIP60 and

TIP55. LTIP60 and TIP55 isoforms have different amino acid sequence from TIP60α and TIP60β in chromodomain and MYST domain respectively. So, there is a possibility that mutations in these domains can change functions of TIP60 (Acharya *et al.*, 2018).

TIP60α is a multidomain protein which has a chromodomain on its N-terminal and a highly conserved MYST domain on its C-terminal (Figure 28).

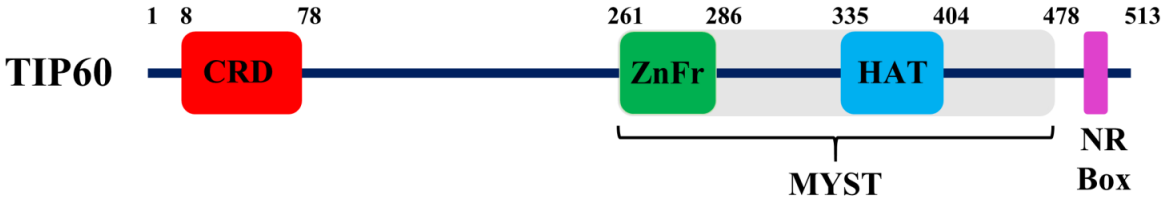

Figure 28: Schematic representation of TIP60 (isoform 2) and its domains.

Chromodomain (CRD) exists in many regulatory proteins and it helps TIP60 to interact with methylated lysines of histones or RNA molecules. CRD of TIP60 can recognize both active and repressive methylated lysines modifications on histones and this is essential in chromatin remodeling and TIP60-mediated DNA damage response (Akhtar *et al.*, 2000; Nielsen *et al.*, 2002; Sun *et al.*, 2010; Jeong *et al.*, 2011; Kim *et al.*, 2015). Phosphorylation of TIP60 stimulates its binding with histone mark (Kaidi & Jackson, 2013).

Figure 29: Crystal structure of an N-terminal HTATIP fragment containing chromodomain (CRD) of TIP60. Adapted from structure deposited at RCSB protein data bank. PDB ID: 4QQG (Zhang *et al.*, 2018)

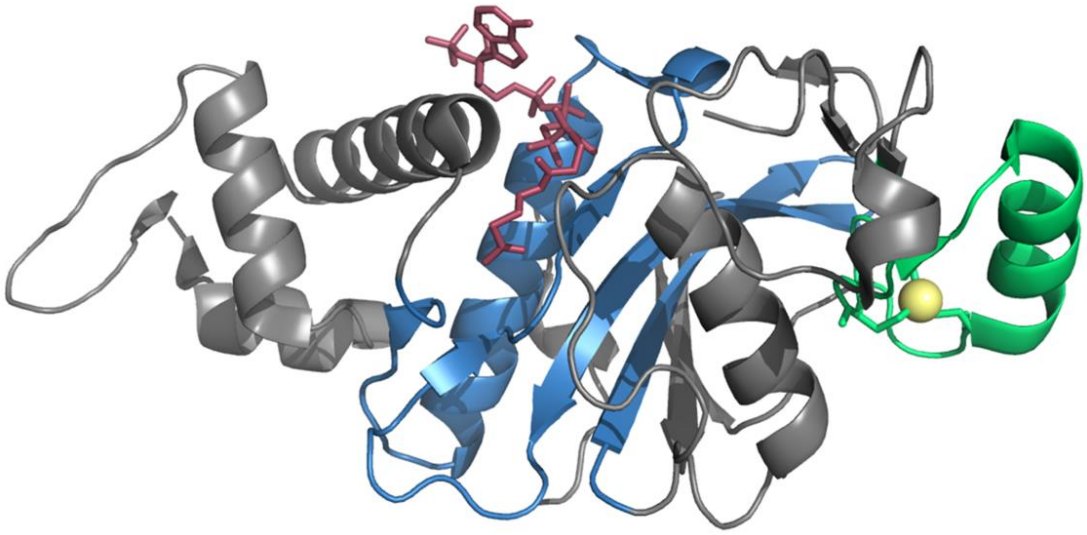

Figure 30: Crystal structure of MYST domain of TIP60. Zinc finger (indicated in green color) in association with zinc atom (indicated in yellow color). HAT domain (indicated in blue color) in connection with Acetyl-CoA (indicated in raspberry color). Adapted from structure deposited at RCSB protein data bank. PDB ID: 2OU2

MYST domain is the catalytic domain and inside it there is a conserved short sequence (335-404) which is known as HAT domain. HAT domain transfers acetyl group from acetyl coenzyme A to substrate protein. This domain is conserved within other acetyltransferase families and has a critical role in normal cellular functions (Sapountzi *et al.*, 2006; Johnson *et al.*, 2013). Inside the MYST domain there is a zinc finger (Cys-Cys-His-Cys) which is crucial for the acetyltransferase activity and it helps TIP60 to interact with other proteins (Sapountzi *et al.*, 2006). Targeting the cysteine residues of zinc finger can affect TIP60-mediated acetylation of histones (H4K16Ac) (Tam *et al.*, 2017). On its C-terminus, TIP60 has a (NR) nuclear receptor-interaction box. Through this NR box, TIP60 interacts with androgen receptors (AR) and augments androgen, estrogen and progesterone receptor-mediated transactivation. Deletion of NR box leads to inefficacy of TIP60 to interact with AR (Gaughan *et al.*, 2001).

5.1.B. Acetyltransferase activity of TIP60

To understand the mechanism of MYST enzymes-mediated acetylation of lysines, scientists used TIP60 orthologue Esa1 (essential Sas family acetyltransferase) in *in vitro* studies. Previously it was believed that MYST proteins transfer acetyl group to targeted lysine through “ping-pong” mechanism. In this mechanism, a conserved Cysteine residue of MYST enzyme (Cysteine 369 in human) builds enzyme-acetyl intermediate complex with acetyl-CoA. Then finally acetyl group is transferred to target lysine (Yan *et al.*, 2000; Yan *et al.*,

2002). But later studies had shown that no intermediate complex formation is involved. Instead, these studies suggest the formation of a ternary complex (MYST enzyme, acetyl-CoA and substrate protein) before catalysis (Berndsen *et al.*, 2007; Wapenaar & Dekker, 2016). Here acetyl-CoA binds first and CoA is the last released product. Conserved glutamic acid 338 of Esa1 extracts a proton from lysine to enhance the nucleophilic attack on acetyl carbonyl-carbon of acetyl-CoA (Berndsen *et al.*, 2007).

MYST domain of TIP60 harbors a structural motif that is also present in acetyltransferases and it was expected that this motif can be a binding site for acetyl-CoA. TIP60 preferentially acetylates amino terminal peptides of core histones H2A (lysine 5), H3 (lysine 14) and H4 (lysine 5, 8, 12, 16) but H2B is not acetylated by TIP60 (Yamamoto & Horikoshi, 1997; Kimura & Horikoshi, 1998). *In vivo* TIP60 is found in complex with its interacting partners, and this complex can acetylate nucleosome (Yamamoto & Horikoshi, 1997; Ikura *et al.*, 2000). *In vitro* studies have shown that TIP60 has acetylation specificity for histone lysines but it doesn't have "consensus" pattern for identification of the substrate. TIP60 has preference for histone lysines that are preceded by glycine or alanine residues, but there are other similar sequences which are not targeted by TIP60 (Kimura & Horikoshi, 1998).

Apart from histones, TIP60 can acetylate non-histone proteins which include transcription factors, post-translational modifiers and epigenetic modulators. Contrary to histones, TIP60 can acetylate non-histone proteins independent of NuA4 complex (Yamada, 2012). TIP60 acetylates p53 (Sun *et al.*, 2005; Sykes *et al.*, 2006; Tang *et al.*, 2006 ; Dai *et al.*, 2013), DNMT1 (Du *et al.*, 2010), MYC (Patel *et al.*, 2004), ATM (Jiang *et al.*, 2006; Sun *et al.*, 2007 ; Kim *et al.*, 2009), p21 (Lee *et al.*, 2012), E2F (Van Den Broeck *et al.*, 2008; Van Den Broeck *et al.*, 2011), SRSF2 (Edmond *et al.*, 2011), RB (Leduc *et al.*, 2005), and androgen receptors (Gaughan *et al.*, 2002). TIP60-mediated acetylation can regulate the stability and activity of these target proteins. TIP60 through its acetylation capacity can act as a coactivator of nuclear receptors (NR) and it can modulate activity and transcription of NR (Jaiswal & Gupta, 2018).

5.1.C. Role of TIP60 in transcription regulation

a. TIP60-mediated regulation of transcription in tumor suppression

TIP60 and p53 share some common properties. Both are involved in cellular DNA damage response, are degraded through Mdm-2-mediated ubiquitination and both are accumulated after exposure to UV irradiation. p53 is one of the major targets of TIP60 and TIP60 is involved in activation of p53 pathway to maintain genomic stability. Knockdown of TIP60 lead to down-regulation of p53 and p53-dependent p21 activation and growth arrest (Legube *et al.*, 2004). After stress or DNA damage, TIP60 acetylates p53 at K120 and this is necessary for p53-induced pro-apoptotic response. But p53-mediated growth arrest can proceed without this acetylation mark (Tang *et al.*, 2006).

TIP60-mediated acetylation mark on p53 is important to decide that p53 activation response will move towards cell cycle arrest or pro-apoptotic pathway. Non-acetylated p53 appears at the p21 promoter for growth arrest while acetylated p53 appears at BAX and PUMA promoters for pro-apoptotic pathway (Sykes *et al.*, 2006). A subunit of TIP60/NuA4 complex, ING3 also supports p53 activation to help p53-induced apoptosis and cell cycle control (Nagashima *et al.*, 2003).

Another member of ING family, ING5 helps TIP60 as a cofactor to acetylate p53 and promotion of BAX-mediated apoptosis in cancer cells (Liu *et al.*, 2013). A recent study has revealed that TIP60 activity is tightly controlled by p53-PTEN-Akt-GSK3-TIP60 complex. Upon low damage or stress, TIP60 acetyltransferase activity is inhibited by Akt to activate p21-mediated growth arrest while on severe damage GSK3 activates TIP60 to acetylate p53 and p53-mediated apoptosis (Wang *et al.*, 2019).

TIP60 interacts with $p14^{ARF}$ and through this interaction both play a tumor suppressor role. TIP60 is a very important mediator of both p53-dependent and p53-independent tumor suppression activity of $p14^{ARF}$. Interaction of TIP60 with $p14^{ARF}$ not only stabilizes TIP60 but also activates ATM repair pathway. TIP60-$p14^{ARF}$ interaction also inhibits TIP60-mediated degradation of tumor suppressor protein RB (retinoblastoma) and activates its tumor suppressor activity (Leduc *et al.*, 2005; Eymin *et al.*, 2006).

TIP60 also interacts with tumor suppressor gene p21 and it can acetylate K161 and K163 of p21 leading to cell cycle arrest in G1 phase. This PTM of p21 stabilizes p21 protein through

protecting it from proteasomal degradation (Lee *et al.*, 2012). In normal cells, p400 (a subunit of TIP60/NuA4 complex) interacts with TIP60, blocks TIP60's activity and represses p21 expression by loading H2AZ on its promoter. Upon DNA damage, p400 and H2AZ are dislodged and TIP60 acetylates p21 and promotes its expression (Gévry *et al.*, 2007; Park *et al.*, 2010).

Oncogenic transcription factors like STAT3 and c-MYB are also regulated by TIP60. STAT3 plays role in apoptosis, cell cycle regulation and mobility of cell in response to growth factors and cytokines. TIP60 inhibits transcription of STAT3 and also its targeted genes by loading HDAC7 to their promoters (Xiao *et al.*, 2003).

c-MYB is a proto-oncogene and TIP60 acetylates it to inhibit its transcription through loading of deacetylases (HDAC1 and HDAC2) on promoter region of c-MYB. In leukemias, c-MYB expression is high which leads to c-MYB-mediated tumorogenesis while TIP60 expression is lower in leukemias which cannot inhibit transcription of this proto-oncogene (Zhao *et al.*, 2012). TIP60 and H3K4 interact and both are localized on same promoters of specific genes in breast cancer cells. TIP60 acetylates H3K4. In ER negative tumors, reduced expression of TIP60 affected H3K4 acetylation and also promoted tumorogenesis (Judes *et al.*, 2018).

b. TIP60-mediated regulation of transcription in tumorogenesis

TIP60-mediated acetylation of some oncogenes can activate their tumorogenesis potential (Figure 31). TIP60 regulates a transcription factor E2F1. E2F1 is involved in a variety of cellular functions. In cisplatin exposed cells, TIP60 acetylates E2F1 (at K120 and K125) and stabilizes E2F1. This interaction loads ERCC1 (excision repair cross-complementing group 1) protein at damage site which repairs cisplatin-induced DNA adducts (Van Den Broeck *et al.*, 2011).

Taubert *et al* had reported that in G1 phase, E2F1 can also engage other subunits of TIP60/NuA4 complex to promoters of E2F1 target genes to acetylate chromatin for signaling pathway activation (Taubert *et al.*, 2004).

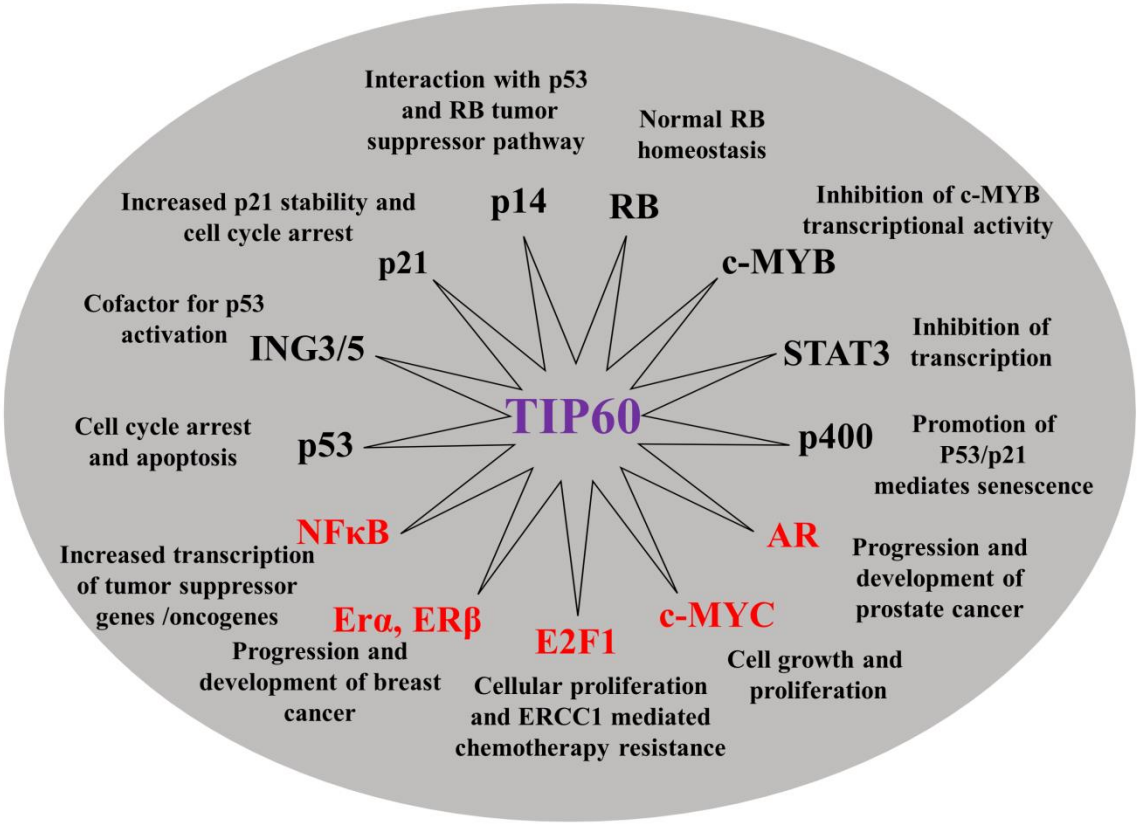

Figure 31: Tumor suppressive and tumorogenesis role of TIP60 through its interaction with other proteins. TIP60 interacting proteins (indicated in red color) are representing tumorogenesis role of TIP60 while other proteins (indicated in black color) are representing tumor suppressive role of TIP60. Adapted from (Avvakumov & Côté, 2007).

An oncoprotein c-MYC involved in cell growth and proliferation, is also regulated by TIP60. TIP60 interacts and stabilizes c-MYC through acetyltransferase activity. c-MYC directly interacts with TIP60 and recruits TIP60/NuA4 complex at chromatin where TIP60 acetylates H4 which facilitates chromatin relaxation for active transcription (Patel *et al.*, 2004; Frank *et al.*, 2003).

NFκB (nuclear factor-kappa B) is involved in inflammatory response, apoptosis, development and oncogenesis. TIP60 is a cofactor of RelA/p65 for transcription of NFκB targeted genes. TIP60 interacts with NFκB subunit RelA/p65 and is recruited on promoters of target genes. Chromatin relaxation because of H3 and H4 acetylation leads to up-regulation of targeted genes expression which promotes oncogenesis (Kim *et al.*, 2012).

At its C-terminus, TIP60 has a nuclear box through which it interacts with nuclear receptors and regulates their functions. It interacts with estrogen (ER) and progesterone receptors (PR) (Brady *et al.*, 1999). TIP60 is a vital administrator of ER-mediated transcription of ERα

subunit targeted genes. Acetylation-induced chromatin relaxation allows enhanced transcription of these genes (Jeong *et al.*, 2011).

TIP60 acetylates androgen receptor (AR) through its interaction with ligand binding domain of AR and increases its transactivation. This acetylation can be reversed by histone deacetylase 1 (Brady *et al.*, 1999; Gaughan *et al.*, 2001; Gaughan *et al.*, 2002). TIP60 expression levels are higher in resistant prostate cancer cells and increase AR signaling activity (Shiota *et al.*, 2010). A recent study has reported that targeting of TIP60 through siRNA decreases TIP60-mediated acetylation of ABCE1 (ATP-binding cassette transporter E1) in lung cancer cells. So, down-regulation of TIP60 inhibited cell proliferation, invasion and migration (Liang *et al.*, 2019).

5.1.D. Role of TIP60 in cell cycle regulation

TIP60 is linked with cell cycle regulation by playing its role at different cell cycle spot-checks. Down-regulation of TIP60 results in mis-regulation of cell cycle checkpoints (Berns *et al.*, 2004). TIP60 maintains genomic stability by regulating the mitotic checkpoints. During cell division, if there is inaccurate chromosome segregation, mitotic checkpoints stop onset of anaphase by inhibiting APC (anaphase promoting complex). Main proteins involved in this security check are Mad1 and Mad 2 (mitotic arrest deficient 1/2) and their expression is regulated by TIP60/NuA4 complex (Sapountzi *et al.*, 2006). TIP60 is also involved in G1/S phase transition. Nuclear protein coactivator of histone transcription (NPAT) is substrate of cyclin E and it is involved in histone transcription activation at G1/S phase. TIP60 is recruited by NPAT and then TIP60 acetylates histone genes (H4) to induce their expression. And suppression of TIP60 or its subunit TRAAP inhibits histone genes expression (DeRan *et al.*, 2008). For efficient DNA repair, cells need a balanced supply of dNTP (deoxyribonucleotide). RNR (ribonucleotide reductase) is accumulated at damage site and it interacts with TIP60 at the damage site. Cells deficient of TIP60-RNR interaction, are not able to rescue DNA damage. TIP60 dependent RNR recruitment ensures balanced dNTP supply (Niida *et al.*, 2010). TIP60 maintains chromosomal segregation in M phase by regulating Mad1/2 and acetylated Aurora B proteins (Li *et al.*, 2004; Mo *et al.*, 2016). It is also very essential in error free DNA repair during S phase (Jacquet *et al.*, 2016).

5.1.E. Regulation of TIP60 in cells

Studies on TIP60 explain that it is an important player of various nuclear and cellular functions. Therefore, for efficient performance TIP60's expression, constancy, activity and localization should be tightly managed in cells. Complex formation of TIP60 with other partners also modifies its acetyltransferase activity. Interaction of TIP60 with Tat protein reduces its activity (Sapountzi *et al.*, 2006). TIP60 is an unstable protein. Depending upon type of cells, TIP60 has a half-life of 30-190 minutes. Basal levels of TIP60 are maintained through Mdm-2-mediated ubiquitination (mono/polyubiquitination) of TIP60. Upon DNA damage, ubiquitination of TIP60 is inhibited and its expression levels are up-regulated to join DNA repair pathways (Legube *et al.*, 2002). Besides Mdm-2, p300/CBP-associated E4 type ubiquitin ligase, EDD1 (E3 identified by differential display) and Cullin-3 ubiquitin ligase are involved in ubiquitination of TIP60 to maintain its normal levels in cells (Col *et al.*, 2005; Bhoumik *et al.*, 2008; Subbaiah *et al.*, 2015).

TIP60 is also regulated through phosphorylation at serine 86 and serine 90. cdc-2 (cyclin B/ cell division cycle 2) phosphorylates TIP60 at serine 90. After phosphorylation, TIP60 is accumulated at G2/M phase. TIP60 is also regulated through circadian transcription factor clock which binds with E box of TIP60 promoter region and promotes its expression levels. Some other E box binding factors like c-MYC, USF1 and Twist cannot affect TIP60 expression levels (Miyamoto *et al.*, 2008). Human papilloma virus (HPV) destabilizes TIP60 and disturbs TIP60/p53-mediated apoptotic pathway through its E6 oncoprotein. TIP60 is degraded through ubiquitination by EDD1 E3 ligase of HPV. This event promotes cell proliferation and endurance of cancer cells (Jha *et al.*, 2010; Subbaiah *et al.*, 2015).

De-ubiquitinase enzyme (USP7) plays an important role in stabilization of TIP60. Pertaining to genotoxic stress, USP7 protects TIP60 from ubiquitination and stabilizes it and its expression levels (Dar *et al.*, 2013). During early adipogenesis, there is also need of higher TIP60 expression levels which are achieved by USP7 (Gao *et al.*, 2013). A stress mediator, ATF3 (activating transcription factor 3) also help TIP60 deubiquitination. Interaction of ATF3 with TIP60 also stimulates TIP60 to activate ATM dependent DNA damage response (Cui *et al.*, 2015; Cui *et al.*, 2016).

5.1.F. TIP60 regulation through post-translational modifications

Different post-translational modifications can affect stability, expression and localization of TIP60.

a. Acetylation of TIP60

Besides acetylation of histones and non-histone proteins, TIP60 itself can undergo acetylation. Autoacetylation of TIP60 is very critical for catalytic activity of TIP60. Autoacetylation can occur on different residues including K76, K80, K104, K150, K187, K327 and K383. Among these residues, acetylation of K327 is very critical. K327 resides in the active and catalytic motif of TIP60 and any mutation of K327 results in loss of not only autoacetylation activity but also intrinsic acetylation activity of TIP60. It was also reported that K327 acetylation regulates catalytic activity, but it is not obligatory (Yang *et al.*, 2012).

TIP60 is also autoacetylated in response to UV radiation which leads to dissociation of TIP60 oligomer and promotes its interaction with its substrates. After autoacetylation, catalytic domain of TIP60 changes its conformation. Acetylated TIP60 is more efficient than un-acetylated one. SIRT1 deacetylates TIP60 and it negatively regulates TIP60. SIRT1 not only interferes with TIP60 autoacetylation, it also inhibits TIP60-mediated acetylation of p53 at K120. Down-regulation of SIRT1 through siRNA treatment restored TIP60 catalytic activity and also p53 acetylation (Wang & Chen, 2010).

Under the influence of HIV-1 Tat protein, p300/CBP acetyltransferase can also acetylate TIP60 at K268 and K282; however, effects of this acetylation are still not known (Col *et al.*, 2005). Autoacetylation of TIP60 at K104 is very critical for TIP60-mediated p53 activation in response to stress and apoptosis initiation. In glucose starved cells, mutation in TIP60 K104 showed weak p53 acetylation and apoptosis. Acetylation at K104 is also necessary for recruitment of TIP60 at promoter of *PUMA* gene (Fang *et al.*, 2018).

HDAC3 can also regulate acetylation of TIP60. HDAC3 deacetylates TIP60 and stabilizes it (Yi *et al.*, 2014). Tat protein of HIV-1 interacts with TIP60 and comprehensively inhibits histone-acetyltransferase activity of TIP60. However, autoacetylation of TIP60 is not influenced by Tat protein (Creaven *et al.*, 1999).

b. Phosphorylation of TIP60

Phosphorylation is a controlled phenomenon which regulates activity of TIP60 protein. Among HAT members, TIP60 is the only known member whose activity is controlled through phosphorylation. TIP60 can be phosphorylated at serine 86 and serine 90. Phosphorylation of TIP60 modulates its acetyltransferase activity. It was also revealed that serine 90 is conserved among homologous of TIP60 in different species so this type of regulation can be conserved during evolution. Serine 90 comes under the consensus of cyclin B/Cdc2 kinase. Phosphorylation of TIP60 was enhanced during G2/M phase while this modification was abolished when an inhibitor of cyclin-dependent kinase (roscovitin) was used (Lemercier *et al.*, 2003; Mo *et al.*, 2016). Phosphorylation at S86 and S90 regulates recruitment of 53BP1 at DNA damage site (Li *et al.*, 2018).

p38 phosphorylates TIP60 at threonine 158 (T158) and stimulates its activity. p38-induced phosphorylation is very imperative for TIP60-mediated p53 acetylation, PUMA induction and apoptosis pathway referring to DNA damage. This shows tumor suppressive role of p38 and TIP60. Phosphorylation of TIP60 is also important to activate PRAK (p38-regulated/activated protein kinase). PRAK induces senescence against oncogenes to maintain genomic stability (Zheng *et al.*, 2013; Xu *et al.*, 2014).

TIP60 can also be phosphorylated at serine 86 by GSK-3 (glycogen synthase kinase-3) *in vitro* and *in vivo*. TIP60 having mutation at serine 86 represents weak activity towards acetylation of p53, and H4. GSK-3 is requisite for induction of PUMA but not for p21 (Charvet *et al.*, 2011). After phosphorylation at serine 86 by GSK3, TIP60 stimulates (acetylates) protein kinase ULKI which is essential for induction of autophagy. GSK3 is activated under starving conditions in cells (Lin *et al.*, 2012).

Phosphorylation of tyrosine of TIP60 is a unique phenomenon. Abl kinase can phosphorylate TIP60 at tyrosine 327 (Y327). This modification results in altered functional activity and subcellular localization of TIP60. After phosphorylation, TIP60 expression was found in nucleus only. Mutation at Y327 with phenylalanine (F) prohibited TIP60 phosphorylation. Catalytic activity of TIP60 was also improved and Go-G1 growth arrest was also observed (Shin & Kang, 2013). Upon exposure to DNA damage, TIP60 is phosphorylated at tyrosine 44 (Y44) by c-Abl tyrosine kinase. This is important for activation of ATM signaling pathway (Kaidi & Jackson, 2013). CDK9 kinase can phosphorylate TIP60 at serine 90 (S90). Mutant lacking S90 phosphorylation showed weak interaction with chromatin, RNA Pol II and H3. It

was also observed that phosphorylation at S90 corresponds to binding with transcription machinery while phosphorylation at S86 regulates HAT activity of TIP60 (Brauns-Schubert *et al.*, 2018).

c. Sumoylation of TIP60

Sumoylation is an important PTM in which members of SUMO (small ubiquitin-like modifier) family are covalently attached with lysines of target protein (Wilkinson & Henley, 2010). Unlike ubiquitination which results in proteins turn over, sumoylation can perform multiple functions like change in protein stability, conducting protein-protein interactions and regulation of protein activity (Wilson, 2017). After exposure to UV radiation induced DNA damage, TIP60 can undergo sumoylation at K430 and K451 through Ubc9 (ubiquitin carrier protein 9). After sumoylation, TIP60 is localized to PML (promyelocytic leukemia) from nucleoplasm and this is important to initiate p53-dependent apoptotic pathway. It was also observed that sumoylation of TIP60 promoted acetyltransferase activity of TIP60 (Cheng *et al.*, 2007). TIP60 was also sumoylated at K430 and K451 by E3 ligase named PIAS4. This sumoylation also stimulated TIP60-mediated p53 acetylation and apoptosis (Naidu *et al.*, 2012).

5.1.G. Deregulation of TIP60 in cancers

A variety of genes in human cancer cells are deregulated. Their overexpression or lack of expression can lead to malignant transformation. Many genetic alterations corresponding to cell signaling, apoptosis, cell cycle and cell invasiveness participates in malignant transition. TIP60 is deregulated in most of cancer types (Idrissou *et al.*, 2018). Low expression levels of TIP60 in cancers are related with cellular proliferation and metastasis. A study reported that *TIP60* mRNA levels were found to be down-regulated in colon and lung cancer cells as compared to normal tissues. Whereas, no considerable difference in mRNA levels of *TIP60* was observed in prostate cancers (LLeonart *et al.*, 2006). However, TIP60 mRNA and protein levels were down-regulated in prostate carcinomas as compared to normal or non-metastatic cancer cells (Kim *et al.*, 2005). This de-regulation of *TIP60* mRNA is related with p53 function (LLeonart *et al.*, 2006). Ras-extracellular signal-related protein kinases 1 and 2 (ERK1/2) pathway has been reported to down-regulate H3K14 acetylation through degrading TIP60, in uveal melanoma (Judes *et al.*, 2018; Li *et al.*, 2019). Sakuraba *et al* also reported that mRNA levels of TIP60 were reduced in colorectal cancer and this was correlated with large tumor size, feeble distinction and metastasis (Sakuraba *et al.*, 2009). TIP60 down-regulation was generally detected in gastric cancer and this can serve as a novel parameter of gastric malignancy (Sakuraba *et al.*, 2011).

A study reported that TIP60 play a tumor suppressive role in a haplo-insufficient and p53-independent manner. TIP60 counteracts c-Myc induced lymphogenesis. Haplo-insufficiency of TIP60 does not cancel the idea that TIP60 is a co-regulator of p53; instead this indicates another way of tumor suppression by TIP60. This tumor suppression activity corresponds to oncogenes mediated DNA damage response (DDR), supporting that DDR signaling pathway is a barrier against tumorogenesis and this barrier does not always depend on p53. Alterations in TIP60-p53 association in cancer cells indicate that they act on parallel pathways and loss of these pathways can synergize during progression of tumors. Down-regulation of *TIP60* mRNA were found in HNSCC (head and neck squamous cell carcinoma), breast cancer and low-grade B-cell lymphomas while down-regulation of TIP60 protein levels were observed in colon, breast, lung and gastric cancers (Gorrini *et al.*, 2007).

Loss of TIP60 in breast cancer can lead to genomic instability. Heterozygous deletion of TIP60 is involved in breast cancer tumorogenesis (Judes *et al.*, 2018). This deletion of TIP60 decreases DNA damage repair response in both normal and breast cancer cells, under normal

as well as in genotoxic stress (Bassi *et al.*, 2016). MicroRNA miR-22 was reported to target TIP60 at its 3'UTR region of mRNA. A negative correlation was observed between TIP60 and miR-22 in breast cancer tissues. TIP60 nominal levels and miR-22 levels were connected with weak endurance in patients. TIP60 down-regulation was also correlated with an alteration in tumor progression known as EMT (epithelial-mesenchymal transition). Blocking of miR-22 resulted in restoration of TIP60 levels and inhibition of migration and invasion in breast cancer cells (Pandey *et al.*, 2015).

Proportion between TIP60 and ATPase p400 was disturbed in colorectal cancers and this imbalanced ratio promotes cancer progression. Interestingly, correction of this imbalance through TIP60 overexpression or siRNA treatment resulted in decreased cancer progression and increased apoptosis. The balanced ratio is also involved in regulation of oncogenes induced DDR and also essential for response to 5-flourouracil treatment in colorectal cancer (Mattera *et al.*, 2009). Low levels of TIP60 are involved in metastasis, cell migration and poor survival in human melanomas and glioblastomas (Chen *et al.*, 2012; Takino *et al.*, 2016). TIP60 expression was significantly decreased in metastatic melanoma and this led to poor survival in primary and metastatic melanoma patients. TIP60 knockdown was linked with cancer progression and TIP60 overexpression inhibited cancer cell progression. This suggests a regulatory role of TIP60 in melanoma. Overexpressed TIP60 levels resulted in improved response to chemotherapy. Finally, it was indicated that TIP60 can be used as a potential biomarker in melanoma patient outcome (Chen *et al.*, 2012). Enhanced TIP60 expression levels in breast, lung and pancreatic cancers reduced cell invasion and improved sensitivity towards chemotherapy (Ravichandran & Ginsburg, 2015; Yang *et al.*, 2017).

TIP60 down-regulation was found in cholangiocarcinoma (CCA) tissues and it was correlated with large tumor size, tumor invasion and poor survival in CCA patients (Zhang *et al.*, 2018). In another study on colorectal cancers, tumor suppressor role of TIP60 has been reported. TIP60 is involved in silencing of ERVs (endogenous retroviral elements) through its interaction with Brd4. Activation of ERVs supports tumor growth (Rajagopalan *et al.*, 2018). TIP60 inhibits tumor cells growth by reducing telomerase enzyme (TERT) levels through acetylation of SP1 (specificity protein1) protein. SP1 protein is involved in induction of TERT gene expression (Rajagopalan *et al.*, 2017).

5.1.H. TIP60 and apoptosis

Dysregulation of cell apoptosis mechanism is a hallmark of cancer. Defect in apoptosis can lead to tumor progression and malignant transformation. TIP60 has been reported to be engaged in apoptotic network. It is very critical in p53-mediated apoptosis pathway. Both proteins are recruited at damage sites after DNA damage to rescue the cells through participation in repair pathways. After DNA damage, p53 pathway activation decides that cell will follow either DNA repair or cell cycle arrest/apoptotic pathway. Growth factor ING3 is a subunit of TIP60/NuA4 complex and it is also involved in p53 pathway activation. In an RNAi screening study, it was identified that TIP60 is very essential for p53-dependent G1/S phase cell cycle arrest in reference to DNA damage (Berns *et al.*, 2004). Cells deficient in HAT activity of TIP60 had shown defects in apoptosis in response to irradiation (Ikura *et al.*, 2000).

TIP60 through its acetyltransferase activity was found to be involved in up-regulation of p21 and p21-mediated cell cycle arrest (Doyon & Côté, 2004). Concerning to stress, p53 levels are up-regulated through acetylation. Acetylation of p53 can be marked by TIP60 (Legube *et al.*, 2004; Tang *et al.*, 2006). TIP60-mediated p53 acetylation harmonize the cellular decision between cell cycle arrest and apoptosis (Tang *et al.*, 2006). It has been reported that there are mutations in p53 K120 acetylation in cancers which indicates the importance of TIP60-mediated acetylation (Deissler *et al.*, 2004; Leitao *et al.*, 2004). Cancer cells having this mutation can grow without any control and these cells are not able to response efficiently to DNA damage (Meyers *et al.*, 1993; Schlechte *et al.*, 1998; Sykes *et al.*, 2006). A preceding study has shown that mutation in K120 of p53 to arginine (K104R) inhibited the binding of TIP60/NuA4 complex and suppressed TIP60 acetyltransferase activity. This resulted in decreased expression of pro-apoptotic genes (NOXA, PUMA) upon glucose starvation. This explains the essential role of TIP60/p53 pathway in response to metabolic stress (Fang *et al.*, 2018). Another protein involved in apoptosis named PDCD5 (programmed cell death 5) interacts with TIP60 and stabilizes TIP60. It acts as co-activator with TIP60 in p53-mediated activation of pro-apoptotic targeted genes (Xu *et al.*, 2009).

In a recent study, a direct interaction between UHRF1 and TIP60 has been reported. UHRF1 can negatively coordinate the interplay between TIP60 and p53 and leads to tumorogenesis (Dai *et al.*, 2013) (Figure 32). UHRF1 through its SRA-RING domain directly interacts with TIP60. TIP60 is ubiquitinated which is independent of degradation of protein. UHRF1

physically interacts with TIP60 and blocks its acetyltransferase activity and compromises p53 acetylation at K120. Therefore, it results in defect of p53-mediated apoptosis. It was observed that down-regulation of UHRF1 enhanced TIP60-mediated p53 activation and induction of p21 and PUMA to induce cell cycle arrest and apoptosis respectively (Dai *et al.*, 2013).

UHRF1 and TIP60 incorporate in many cellular tasks including regulation of stability and functions of many proteins (e.g. DNMT1, p53). So, aberrations in these epigenetic mechanisms can lead towards cancer induction and development. Therefore, it is very pivotal to study the interaction, function and regulation of these essential epigenetic integrators: TIP60 and UHRF1.

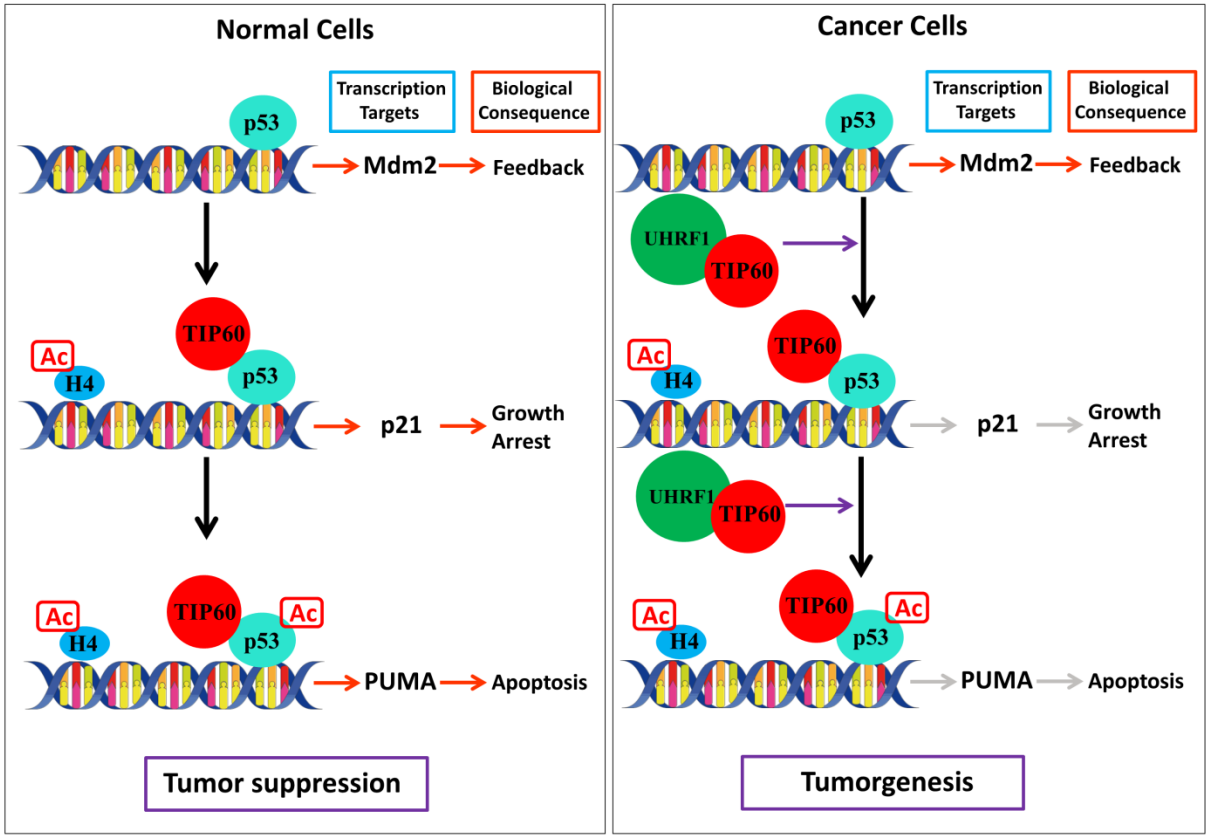

Figure 32: A portrait of tumorogenesis/tumor progression in cells with UHRF1 overexpression. Adapted from (Dai *et al.*, 2013).

OBJECTIVES

II- OBJECTIVES

Epigenetic modifications such as DNA methylation, histone modifications and non-coding RNA actions perform an integral task in regulation of various cellular functions like transcription, replication and DNA damage. These highly precise epigenetic operations are governed through reader, writer or eraser proteins. Genomic alterations/epimutations in regulatory processes can lead to pathologies like cancer. Initially link between cancer and epigenetics was found through investigations on gene expression and DNA methylation. In last few years, epigenetic studies on cancer have improved our insight regarding basic disease mechanisms and better therapeutic regimens (Dawson & Kouzarides, 2012; Inbar-Feigenberg *et al.*, 2013).

In a multiprotein complex, epigenetic proteins usually execute their responsibilities in a coordinated and regulated fashion. The epigenetic integrator UHRF1 deals with DNA methylation and histone modification through its interaction with other epigenetic partners. UHRF1 has oncogenic potential and is overexpressed in different types of cancers which is linked with aberrations in DNA methylation, silencing of tumor suppressor genes (TSGs), cellular proliferation and poor prognosis of cancer (Ashraf *et al.*, 2017b).

Our team investigated another epigenetic member TIP60 which was found to be present in the same epigenetic complex with UHRF1. Both proteins are involved in multiple processes including DNA methylation. It was also reported that UHRF1 negatively regulates TIP60 and p53 interaction to promote tumorogenesis. This project was planned to investigate the interaction of UHRF1 with TIP60 and targeting SRA domain of UHRF1 through small inhibitor molecules.

1. Interaction of UHRF1 and TIP60 inside the cells through FLIM (Fluorescent lifetime imaging microscopy). Both proteins with DNMT1 exist in the same epigenetic complex and are associated with epigenetic code replication during S phase.
2. Identification of TIP60's domain interacting with UHRF1.
3. Effect of TIP60 overexpression in cancer cells. TIP60 displays promising tumor suppressive potential through inhibition of TSGs and proliferation of tumor cells. TIP60 expression is down-regulated in most of cancers; therefore overexpression of TIP60 in cancer cells might revamp normal functioning of TSGs and control proliferation.

4. Effect of TIP60 overexpression on UHRF1 levels and identification of another possible mechanism behind TIP60-mediated regulation of UHRF1.
5. Screen small inhibitor molecules through a precise fluorescent tool “base flipping assay”. This tool speculates interaction dynamics of SRA domain with DNA. Positive hits further will be studied with the help of biophysical techniques (isothermal calorimetry, steady state fluorescence spectroscopy, anisotropy and FLIM-FRET).
6. Evaluation of anti-cancer potential of positive hit on cancer cell lines. To assess the effect of hit molecule on cell proliferation, apoptosis, cell cycle and expression of UHRF1 and DNMT1. Effect of hit candidate on UHRF1-DNMT1 interaction and its impact on DNA methylation maintenance.

MATERIALS AND METHODS

III- MATERIALS AND METHODS

1. Materials

MG-132 ($C_{26}H_{41}N_3O_5$) was purchased from Selleckchem.com Inhibitor Expert (S2619, USA). MG-132 was dissolved in pure DMSO and stored at -80°C. Guanidine HCl (G3272) and Urea (U5378) were purchased from Sigma-Aldrich. Propidium iodide (130-093-233) was purchased from Miltenyi Biotec while Annexin V-iFlourTM 350 conjugate (20090) was purchased from AAT BioquestR. Ni-NTA Agarose was purchased from QIAGEN (30210). Dynabeads™ Protein A (10002D) was purchased from Invitrogen (ThermoFischer Scientific).

1.A. Antibodies

Name	Host	Source	Type
Anti-UHRF1	Mouse	Engineered in lab as described previously in (Hopfner *et al.*, 2000)	Monoclonal
Anti-TIP60	Rabbit	Genetex (GTX 112197)	Polyclonal
Anti-USP7	Rabbit	Abcam (ab4080)	Polyclonal
Anti-DNMT1	Mouse	Proteogenix (PTG-MAB0079)	Monoclonal
Anti-Ubiquitin	Mouse	Merck (05-944)	Monoclonal
Anti-GAPDH	Mouse	Merck Millipore (MAB374)	Monoclonal
Anti-p73	Mouse	BD Biosciences Pharmingen (558785)	Monoclonal
Anti-p53	Mouse	BD Biosciences Pharmingen (554293)	Monoclonal
Anti-Caspase 3	Rabbit	Cell Signaling Technology (9660)	Polyclonal
Anti-eGFP	Mouse	Proteintech (66,002-1-Ig) and Thermo Fisher Scientific (A-11120)	Monoclonal
Anti-mCherry	Rabbit	Genetex (GTX 59788)	Polyclonal
Anti-BCL2	Mouse	Merck-Millipore (05-826)	Monoclonal
Anti-PARP	Mouse	BD Biosciences Pharmingen (51-6639GR)	Monoclonal
Anti-BAX	Rabbit	Merck Millipore (AB2930)	Polyclonal
Anti-His	Mouse	Thermo Fisher Scientific (MA1-21315)	Monoclonal
Anti-GFP	Mouse	Proteintech (66002-1-Ig)	Monoclonal
Anti-Mouse	Goat	HRP Conjugate Promega France (W4021)	Polyclonal
Anti-Rabbit	Goat	HRP Conjugate Promega France (W4011)	Polyclonal

Anti-Mouse	Goat	Invitrogen Alexa-568 (A11031)	Polyclonal
Anti-Mouse	Goat	Molecular probes Alexa-647 (A21237)	Polyclonal
Anti-Rabbit	Goat	Invitrogen Alexa-568 (A11011)	Polyclonal

Name	Tag	Resistance	Vector backbone	Promoter
mCherry	mCherry	Ampicillin	pCMV-mCherry	CMV
UHRF1-mCherry	mCherry at C-terminal	Kanamycin	pCMV-mCherry	CMV
His-Ubiquitin	His at N-terminal	Ampicillin	pCl	CMV
RFP-Ubiquitin	RFP at N-terminal	Kanamycin	EGFP-C1	CMV
eGFP	eGFP	Kanamycin		CMV
TIP60WT-eGFP	eGFP at C-terminal	Kanamycin	pEGFP-N1	CMV
TIP60ΔMYST-eGFP	eGFP at C-terminal	Kanamycin	pEGFP-N1	CMV
TIP60ΔCRD-eGFP	eGFP at C-terminal	Kanamycin	pEGFP-N1	CMV
TIP60ΔZnFr-eGFP	eGFP at C-terminal	Kanamycin	pEGFP-N1	CMV
TIP60ΔHAT-eGFP	eGFP at C-terminal	Kanamycin	pEGFP-N1	CMV
TIP60ΔNLS1-eGFP	eGFP at C-terminal	Kanamycin	pEGFP-N1	CMV
TIP60ΔNLS2-eGFP	eGFP at C-terminal	Kanamycin	pEGFP-N1	CMV
TIP60ΔNLS1&2-eGFP	eGFP at C-terminal	Kanamycin	pEGFP-N1	CMV
GST	GST	Ampicillin	pGEX	tac
GST-UHRF1	GST at N-terminal	Ampicillin	pGEX-4T1	tac
His-TIP60WT	6xHis at N-terminal	Ampicillin	pET-15b	T7
His-TIP60ΔCRD	6xHis at N-terminal	Ampicillin	pET-15b	T7
His-TIP60ΔZnFr	6xHis at N-terminal	Ampicillin	pET-15b	T7
His-TIP60ΔHAT	6xHis at N-terminal	Ampicillin	pET-15b	T7
His-TIP60ΔMYST	6xHis at N-terminal	Ampicillin	pET-15b	T7
His-TIP60(MYST)	6xHis at N-terminal	Ampicillin	pET-15b	T7
Flag-TIP60(MYST)	Flag at N-terminal	Ampicillin	pET-15b	T7
eGFP-DNMT1	eGFP at N-terminal	Kanamycin	pEGFP-C2	CMV

1.B. Plasmid Constructs

TIP60-eGFP Wild type

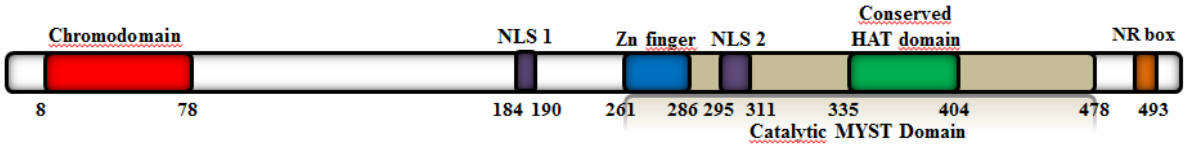

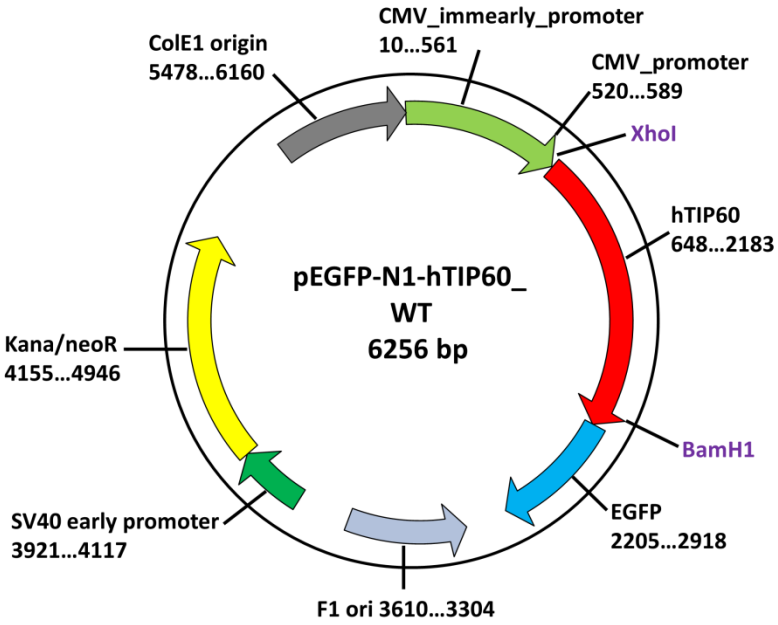

Sequence

atgGCGGAGGTGGGGGAGATA**ATCGAGGGCTGCCGCCTACCCGTGCTGCGGCGGAACCAGGACAACGAAGA**
TGAGTGGCCCCTGGCCGAGATCCTGAGCGTGAAGGACATCAGTGGCCGGAAGCTTTTCTACGTCCATTACAT
TGACTTCAACAAACGTCTGGATGAATGGGTGACGCATGAGCGGCTGGACCTAAAGAAGATCCAGTTCCCCA
AGAAAGAGGCCAAGACCCCCACTAAGAACGGACTTCCTGGGTCCCGTCCTGGCTCTCCAGAGAGAGAGGTGC
CGGCCTCGGCGCAGGCCAGCGGGAAGACCTTGCCAATCCCGGTCCAGATCACACTCCGCTTCAACCTGCCCAA
GGAGCGGGAGGCCATTCCCGGTGGCGAGCCTGACCAGCCGCTCTCCTCCAGCTCCTGCCTGCAGCCCAACCAC
CGCTCAACGAAACGGAAGGTGGAGGTGGTTTCACCAGCAACTCCAGTGCCCAGCGAGACAGCCCCGGCCTCG
GTTTTTCCCCAGAATGGAGCCGCCCGTAGGGCAGTGGCAGCCCAG**CCAGGACGGAAGCGAAAATCG**AATTGT
TTGGGCACTGATGAGGACTCCCAGGACAGCTCTGATGGAATACCGTCAGCACCACGCATGACTGGCAGCCTG
GTGTCTGATCGAAGCCACGACGACATCGTCACCCGGATGAAGAACATTGAGTGCATTGAGCTGGGCCGGCAC
CGCCTCAAGCCGTGGTACTTCTCCCCGTACCCACAGGAACTCACCACATTGCCTGTCCTC**TACCTGTGCGAGTTC**
TGCCTCAAGTACGGCCGTAGTCTCAAGTGTCTTCAGCGTCATTTGACCAAGTGTGACCTACGACATCCTCCAG
GCAATGAGATTTAC**CGCAAGGGCACCATCTCCTTCTTTGAGATTGATGGACGTAAGAACAAGAGT**TATTCCCA
GAACCTGTGTCTTTTGGCCAAGTGTTTCCTTGACCATAAGACACTGTACTATGACACAGAC**CCTTTCCTCTTCTA**
CGTCATGACAGAGTATGACTGTAAGGGCTTCCACATCGTGGGCTACTTCTCCAAGGAGAAAGAATCAACGG

AAGACTACAATGTGGCCTGCATCCTAACCCTGCCTCCCTACCAGCGCCGGGGCTACGGCAAGCTGCTGATCG
AGTTCAGCTATGAACTCTCCAAAGTGGAAGGGAAAACAGGGACCCCTGAGAAGCCCCTCTCAGACCTTGGCC
TCCTATCCTATCGAAGCTACTGGTCCCAGACCATCCTGGAGATCCTGATGGGGCTGAAGTCGGAGAGCGGGGA
GAGGCCACAGATCACCATCAATGAGATTAGTGAAATCACCAGCATCAAGAAGGAGGATGTCATCTCCACTCTG
CAGTACCTCAATCTCATCAACTACTACAAGGGCCAGTACATCCTCACACTGTCAGAGGACATCGTGGATGGCCA
TGAGCGGGCCATGCTCAAGCGGCTCCTGCGGATCGACTCCAAGTGTCTGCACTTCACTCCCAAGGACTGGAGC
AAGAGGGGGAAGTGG

MAEVGEIIEGCRLPVLRRNQDNEDEWPLAEILSVKDISGRKLFYVHYIDFNKRL
DEWVTHERLDLKKIQFPKKEAKTPTKNGLPGSRPGSPEREVPASAQASGKTLPI
PVQITLRFNLPKERE AIPGGEPDQPLSSSSCLQPNHRSTKRKVEVVSPATPVPSE
TAPASVFPQNGAARRAVAAQPGRKRKSNCLGTDEDSQDSSDGIPSAPRMTGSL
VSDRSHDDIVTRMKNIECIELGRHRLKPWYFSPYPQELTTLPVLYLCEFCLKYGR
SLKCLQRHLTKCDLRHPPGNEIYRKGTISFFEIDGRKNKSYSQNLCLLAKCFLDH
KTLYYDTDPFLFYVMTEYDCKGFHIVGYFSKEKESTEDYNVACILTLPPYQRRG
YGKLLIEFSYELSKVEGKTGTPEKPLSDLGLLSYRSYWSQTILEILMGLKSESGER
PQITINEISEITSIKKEDVISTLQYLNLINYYKGQYILTLSEDIVDGHERAMLKRLLR
IDSKCLHFTPKDWSKRGKW

TIP60ΔCRD-eGFP

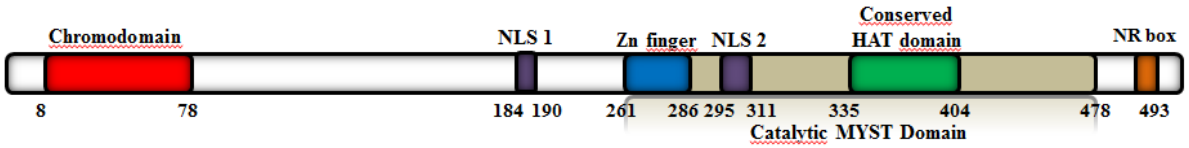

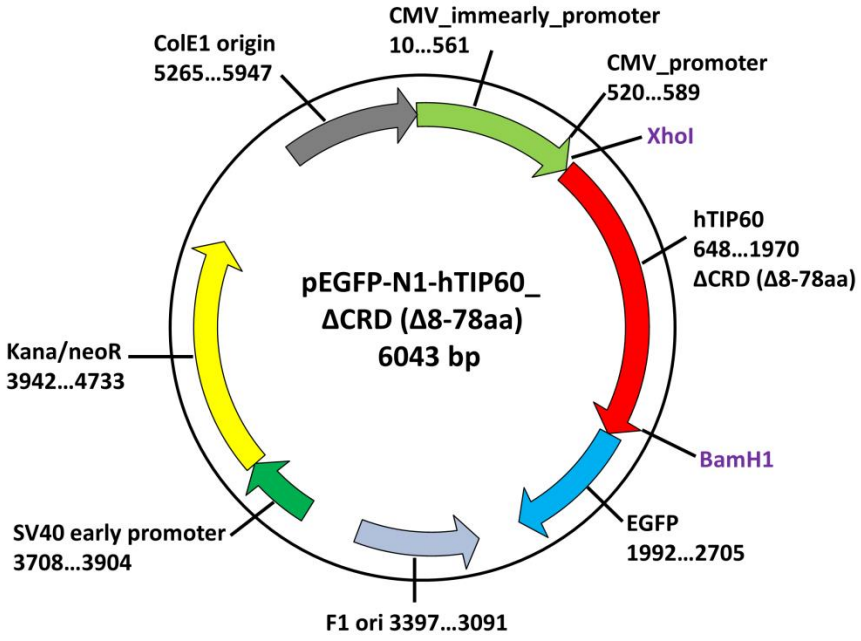

Sequence

atgGCGGAGGTGGGGGAGATA~~ATCGAGGGCTGCCGCCTACCCGTGCTGCGGCGGAACCAGGACAA~~
~~CGAAGATGAGTGGCCCCTGGCCGAGATCCTGAGCGTGAAGGACATCAGTGGCCGGAAGCTTTCT~~
~~ACGTCCATTACATTGACTTCAACAAACGTCTGGATGAATGGGTGACGCATGAGCGGCTGGACCTA~~
~~AAGAAGATCCAGTTCCCCAAGAAAGAGGCCAAGACCCCC~~ACTAAGAACGGACTTCCTGGGTCCCG
TCCTGGCTCTCCAGAGAGAGAGGTGCCGGCCTCGGCGCAGGCCAGCGGGAAGACCTTGCCAATCCC
GGTCCAGATCACACTCCGCTTCAACCTGCCCAAGGAGCGGGAGGCCATTCCCGGTGGCGAGCCTGA
CCAGCCGCTCTCCTCCAGCTCCTGCCTGCAGCCCAACCACCGCTCAACGAAACGGAAGGTGGAGGT
GGTTTCACCAGCAACTCCAGTGCCCAGCGAGACAGCCCCGGCCTCGGTTTTTCCCCAGAATGGAGCC
GCCCGTAGGGCAGTGGCAGCCCAGCCAGGACGGAAGCGAAAATCGAATTGTTTGGGCACTGATGA
GGACTCCCAGGACAGCTCTGATGGAATACCGTCAGCACCACGCATGACTGGCAGCCTGGTGTCTGA
TCGAAGCCACGACGACATCGTCACCCGGATGAAGAACATTGAGTGCATTGAGCTGGGCCGGCACCG
CCTCAAGCCGTGGTACTTCTCCCCGTACCCACAGGAACTCACCACATTGCCTGTCCTCTACCTGTGCG
AGTTCTGCCTCAAGTACGGCCGTAGTCTCAAGTGTCTTCAGCGTCATTTGACCAAGTGTGACCTAC
GACATCCTCCAGGCAATGAGATTTACCGCAAGGGCACCATCTCCTTCTTTGAGATTGATGGACGTAA
GAACAAGAGTTATTCCCAGAACCTGTGTCTTTTGGCCAAGTGTTTCCTTGACCATAAGACACTGTACT
ATGACACAGACCCTTTCCTCTTCTACGTCATGACAGAGTATGACTGTAAGGGCTTCCACATCGTGG
GCTACTTCTCCAAGGAGAAAGAATCAACGGAAGACTACAATGTGGCCTGCATCCTAACCCTGCCTC
CCTACCAGCGCCGGGGCTACGGCAAGCTGCTGATCGAGTTCAGCTATGAACTCTCCAAAGTGGAA
GGGAAAACAGGGACCCCTGAGAAGCCCCTCTCAGACCTTGGCCTCCTATCCTATCGAAGCTACTGG
TCCCAGACCATCCTGGAGATCCTGATGGGGCTGAAGTCGGAGAGCGGGGAGAGGCCACAGATCAC
CATCAATGAGATTAGTGAAATCACCAGCATCAAGAAGGAGGATGTCATCTCCACTCTGCAGTACCTC
AATCTCATCAACTACTACAAGGGCCAGTACATCCTCACACTGTCAGAGGACATCGTGGATGGCCATG
AGCGGGCCATGCTCAAGCGGCTCCTGCGGATCGACTCCAAGTGTCTGCACTTCACTCCCAAGGACTG
GAGCAAGAGGGGGAAGTGG

M A E V G E I ~~I E G C R L P V L R R N Q D N E D E W P L A E I L S V K D I S G R K L F Y V H Y I D~~
~~F N K R L D E W V T H E R L D L K K I Q F P K K E A K T P~~ T K N G L P G S R P G S P E R E V P A S
A Q A S G K T L P I P V Q I T L R F N L P K E R E A I P G G E P D Q P L S S S S C L Q P N H R S T K
R K V E V V S P A T P V P S E T A P A S V F P Q N G A A R R A V A A Q **P G R K R K S** N C L G T D
E D S Q D S S D G I P S A P R M T G S L V S D R S H D D I V T R M K N I E C I E L G R H R L K P W
Y F S P Y P Q E L T T L P V L **Y L C E F C L K Y G R S L K C L Q R H L T K C D L R** H P P G N E I Y **R**
K G T I S F F E I D G R K N K S Y S Q N L C L L A K C F L D H K T L Y Y D T D **P F L F Y V M T E Y D**
C K G F H I V G Y F S K E K E S T E D Y N V A C I L T L P P Y Q R R G Y G K L L I E F S Y E L S K V
E G K T G T P E K P L S D L G L L S Y R S Y W S Q T I L E I L M G L K S E S G E R P Q I T I N E I S E I
T S I K K E D V I S T L Q Y L N L I N Y Y K G Q Y I L T L S E D I V D G H E R A M L K R L L R I D S K C
L H F T P K D W S K R G K W

TIP60ΔZF-eGFP

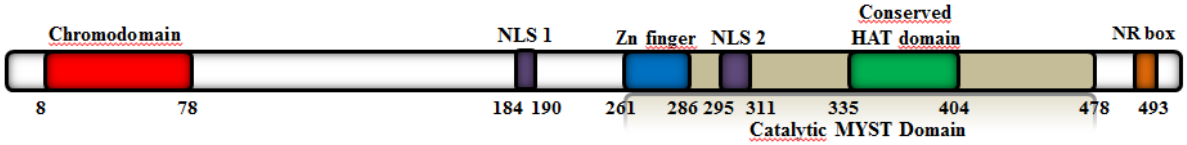

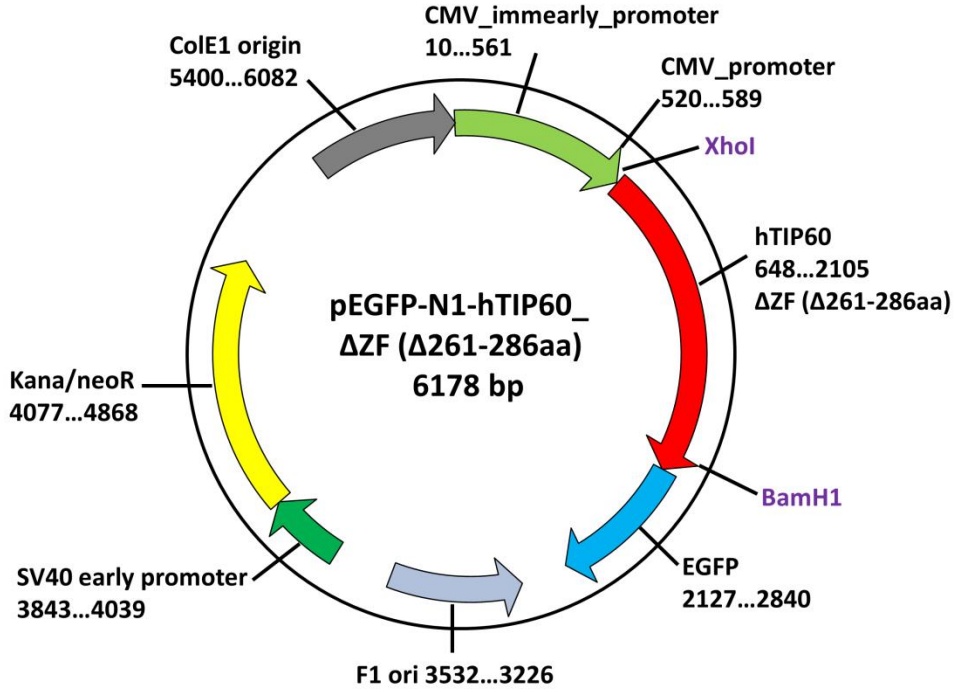

Sequence

atgGCGGAGGTGGGGGAGATA**ATCGAGGGCTGCCGCCTACCCGTGCTGCGGCGGAACCAGGACAACGA**
AGATGAGTGGCCCCTGGCCGAGATCCTGAGCGTGAAGGACATCAGTGGCCGGAAGCTTTTCTACGTCCA
TTACATTGACTTCAACAAACGTCTGGATGAATGGGTGACGCATGAGCGGCTGGACCTAAAGAAGATCC
AGTTCCCCAAGAAAGAGGCCAAGACCCCCACTAAGAACGGACTTCCTGGGTCCCGTCCTGGCTCTCCAGA
GAGAGAGGTGCCGGCCTCGGCGCAGGCCAGCGGGAAGACCTTGCCAATCCCGGTCCAGATCACACTCCG
CTTCAACCTGCCCAAGGAGCGGGAGGCCATTCCCGGTGGCGAGCCTGACCAGCCGCTCTCCTCCAGCTCC
TGCCTGCAGCCCAACCACCGCTCAACGAAACGGAAGGTGGAGGTGGTTTCACCAGCAACTCCAGTGCCCA
GCGAGACAGCCCCGGCCTCGGTTTTTCCCCAGAATGGAGCCGCCCGTAGGGCAGTGGCAGCCCAGCCAG
GACGGAAGCGAAAATCGAATTGTTTGGGCACTGATGAGGACTCCCAGGACAGCTCTGATGGAATACCGT
CAGCACCACGCATGACTGGCAGCCTGGTGTCTGATCGAAGCCACGACGACATCGTCACCCGGATGAAGAA
CATTGAGTGCATTGAGCTGGGCCGGCACCGCCTCAAGCCGTGGTACTTCTCCCCGTACCCACAGGAACTC
ACCACATTGCCTGTCCTC~~TACCTGTGCGAGTTCTGCCTCAAGTACGGCCGTAGTCTCAAGTGTCTTCAGCG~~
~~TCATTTGACCAAGTGTGACCTACGA~~CATCCTCCAGGCAATGAGATTTACCGCAAGGGCACCATCTCCTTCT
TTGAGATTGATGGACGTAAGAACAAGAGTTATTCCCAGAACCTGTGTCTTTTGGCCAAGTGTTTCCTTGAC
CATAAGACACTGTACTATGACACAGAC**CCTTTCCTCTTCTACGTCATGACAGAGTATGACTGTAAGGGCTT**
CCACATCGTGGGCTACTTCTCCAAGGAGAAAGAATCAACGGAAGACTACAATGTGGCCTGCATCCTAAC

CCTGCCTCCCTACCAGCGCCGGGGCTACGGCAAGCTGCTGATCGAGTTCAGCTATGAACTCTCCAAAGTG
GAAGGGAAAACAGGGACCCCTGAGAAGCCCCTCTCAGACCTTGGCCTCCTATCCTATCGAAGCTACTGGT
CCCAGACCATCCTGGAGATCCTGATGGGGCTGAAGTCGGAGAGCGGGGAGAGGCCACAGATCACCATCA
ATGAGATTAGTGAAATCACCAGCATCAAGAAGGAGGATGTCATCTCCACTCTGCAGTACCTCAATCTCATC
AACTACTACAAGGGCCAGTACATCCTCACACTGTCAGAGGACATCGTGGATGGCCATGAGCGGGCCATGC
TCAAGCGGCTCCTGCGGATCGACTCCAAGTGTCTGCACTTCACTCCCAAGGACTGGAGCAAGAGGGGGA
AGTGG

MAEVGEIIEGCRLPVLRRNQDNEDEWPLAEILSVKDISGRKLFYVHYIDFNK
RLDEWVTHERLDLKKIQFPKKEAKTPTKNGLPGSRPGSPEREVPASAQASG
KTLPIPVQITLRFNLPKEREAIPGGEPDQPLSSSSCLQPNHRSTKRKVEVVSP
ATPVPSETAPASVFPQNGAARRAVAAQPGRKRKSNCLGTDEDSQDSSDGIP
SAPRMTGSLVSDRSHDDIVTRMKNIECIELGRHRLKPWYFSPYYPQELTTLPV
LYLCEFCLKYGRSLKCLQRHLTKCDLRHPPGNEIYRKGTISFFEIDGRKNKSY
SQNLCLLAKCFLDHKTLYYDTDPFLFYVMTEYDCKGFHIVGYFSKEKESTED
YNVACILTLPPYQRRGYGKLLIEFSYELSKVEGKTGTPEKPLSDLGLLSYRSY
WSQTILEILMGLKSESGERPQITINEISEITSIKKEDVISTLQYLNLINYYKGQY
ILTLSEDIVDGHERAMLKRLLRIDSKCLHFTPKDWSKRGKW

TIP60ΔHAT-eGFP

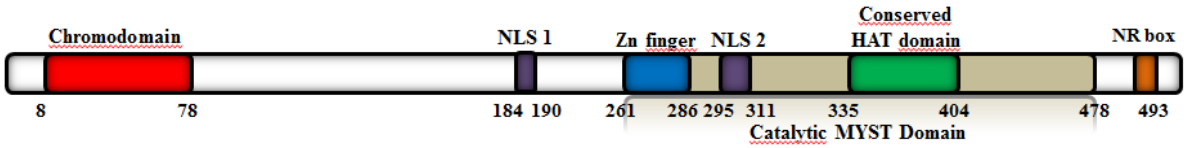

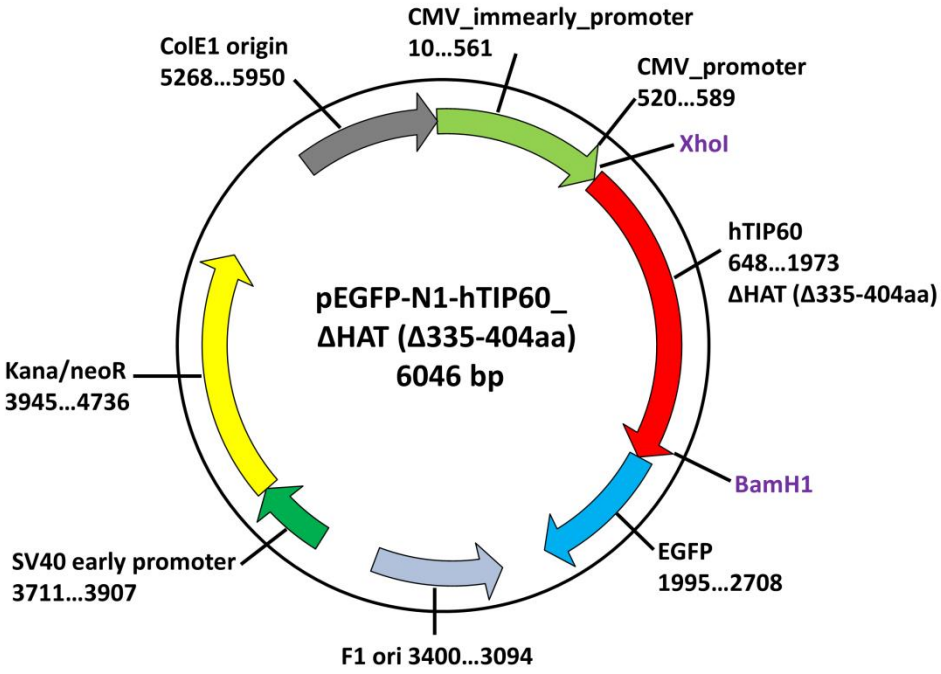

Sequence

atgGCGGAGGTGGGGGAGATA**ATCGAGGGCTGCCGCCTACCCGTGCTGCGGCGGAACCAGGACAACGAAGA**
TGAGTGGCCCCTGGCCGAGATCCTGAGCGTGAAGGACATCAGTGGCCGGAAGCTTTTCTACGTCCATTACAT
TGACTTCAACAAACGTCTGGATGAATGGGTGACGCATGAGCGGCTGGACCTAAAGAAGATCCAGTTCCCCA
AGAAAGAGGCCAAGACCCCCACTAAGAACGGACTTCCTGGGTCCCGTCCTGGCTCTCCAGAGAGAGAGGTGC
CGGCCTCGGCGCAGGCCAGCGGGAAGACCTTGCCAATCCCGGTCCAGATCACACTCCGCTTCAACCTGCCCAA
GGAGCGGGAGGCCATTCCCGGTGGCGAGCCTGACCAGCCGCTCTCCTCCAGCTCCTGCCTGCAGCCCAACCAC
CGCTCAACGAAACGGAAGGTGGAGGTGGTTTCACCAGCAACTCCAGTGCCCAGCGAGACAGCCCCGGCCTCG
GTTTTTCCCCAGAATGGAGCCGCCCGTAGGGCAGTGGCAGCCCAGCCAGGACGGAAGCGAAAATCGAATTGT
TTGGGCACTGATGAGGACTCCCAGGACAGCTCTGATGGAATACCGTCAGCACCACGCATGACTGGCAGCCTG
GTGTCTGATCGAAGCCACGACGACATCGTCACCCGGATGAAGAACATTGAGTGCATTGAGCTGGGCCGGCAC
CGCCTCAAGCCGTGGTACTTCTCCCCGTACCCACAGGAACTCACCACATTGCCTGTCCTC**TACCTGTGCGAGTTC**
TGCCTCAAGTACGGCCGTAGTCTCAAGTGTCTTCAGCGTCATTTGACCAAGTGTGACCTACGACATCCTCCAG
GCAATGAGATTTACCGCAAGGGCACCATCTCCTTCTTTGAGATTGATGGACGTAAGAACAAGAGTTATTCCCA
GAACCTGTGTCTTTTGGCCAAGTGTTTCCTTGACCATAAGACACTGTACTATGACACAGAC~~**CCTTTCCTCTTCTA**~~
~~**CGTCATGACAGAGTATGACTGTAAGGGCTTCCACATCGTGGGCTACTTCTCCAAGGAGAAAGAATCAACGG**~~
~~**AAGACTACAATGTGGCCTGCATCCTAACCCTGCCTCCCTACCAGCGCCGGGGCTACGGCAAGCTGCTGATCG**~~
~~**AGTTCAGCTATGAACTCTCCAAAGTGGAAGGGAAAACAGGGACCCCTGAGAAG**~~CCCCTCTCAGACCTTGGCC
TCCTATCCTATCGAAGCTACTGGTCCCAGACCATCCTGGAGATCCTGATGGGGCTGAAGTCGGAGAGCGGGGA
GAGGCCACAGATCACCATCAATGAGATTAGTGAAATCACCAGCATCAAGAAGGAGGATGTCATCTCCACTCTG
CAGTACCTCAATCTCATCAACTACTACAAGGGCCAGTACATCCTCACACTGTCAGAGGACATCGTGGATGGCCA
TGAGCGGGCCATGCTCAAGCGGCTCCTGCGGATCGACTCCAAGTGTCTGCACTTCACTCCCAAGGACTGGAGC
AAGAGGGGGAAGTGG

Sequence for the mutants

M A E V G E I **I E G C R L P V L R R N Q D N E D E W P L A E I L S V K D I S G R K L F Y V H Y I D F N K R L**
D E W V T H E R L D L K K I Q F P K K E A K T P T K N G L P G S R P G S P E R E V P A S A Q A S G K T L P I
P V Q I T L R F N L P K E R E A I P G G E P D Q P L S S S S C L Q P N H R S T K R K V E V V S P A T P V P S E
T A P A S V F P Q N G A A R R A V A A Q **P G R K R K S** N C L G T D E D S Q D S S D G I P S A P R M T G S L
V S D R S H D D I V T R M K N I E C I E L G R H R L K P W Y F S P Y P Q E L T T L P V L **Y L C E F C L K Y G R**
S L K C L Q R H L T K C D L R H P P G N E I Y **R K G T I S F F E I D G R K N K S** Y S Q N L C L L A K C F L D H
K T L Y Y D T D ~~**P F L F Y V M T E Y D C K G F H I V G Y F S K E K E S T E D Y N V A C I L T L P P Y Q R R G**~~
~~**Y G K L L I E F S Y E L S K V E G K T G T P E K**~~ P L S D L G L L S Y R S Y W S Q T I L E I L M G L K S E S G E R
P Q I T I N E I S E I T S I K K E D V I S T L Q Y L N L I N Y Y K G Q Y I L T L S E D I V D G H E R A M L K R L L R
I D S K C L H F T P K D W S K R G K W

TIP60ΔMYST-eGFP

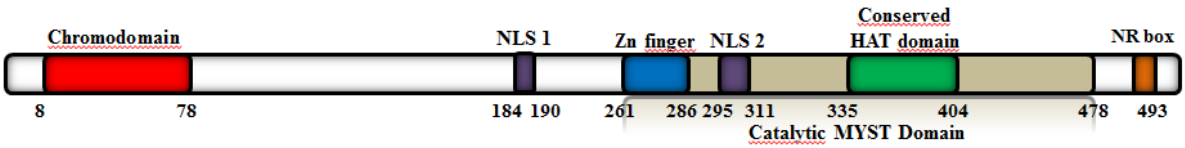

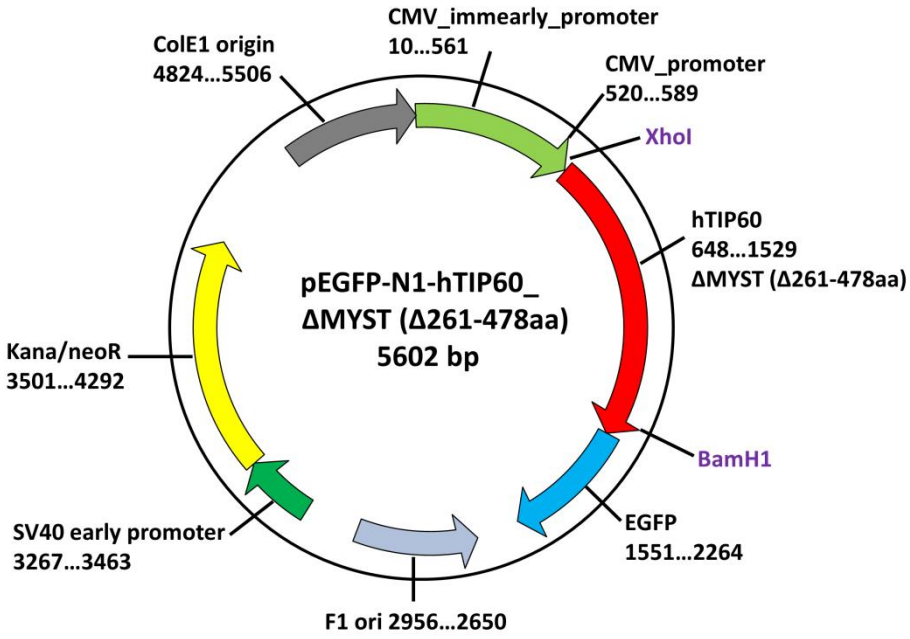

Sequence

atgGCGGAGGTGGGGGAGATA**ATCGAGGGCTGCCGCCTACCCGTGCTGCGGCGGAACCAGGACAACGAAGA**
TGAGTGGCCCCTGGCCGAGATCCTGAGCGTGAAGGACATCAGTGGCCGGAAGCTTTTCTACGTCCATTACAT
TGACTTCAACAAACGTCTGGATGAATGGGTGACGCATGAGCGGCTGGACCTAAAGAAGATCCAGTTCCCCA
AGAAAGAGGCCAAGACCCCCACTAAGAACGGACTTCCTGGGTCCCGTCCTGGCTCTCCAGAGAGAGAGGTGC
CGGCCTCGGCGCAGGCCAGCGGGAAGACCTTGCCAATCCCGGTCCAGATCACACTCCGCTTCAACCTGCCCAA
GGAGCGGGAGGCCATTCCCGGTGGCGAGCCTGACCAGCCGCTCTCCTCCAGCTCCTGCCTGCAGCCCAACCAC
CGCTCAACGAAACGGAAGGTGGAGGTGGTTTCACCAGCAACTCCAGTGCCCAGCGAGACAGCCCCGGCCTCG
GTTTTTCCCCAGAATGGAGCCGCCCGTAGGGCAGTGGCAGCCCAG**CCAGGACGGAAGCGAAAATCG**AATTGT
TTGGGCACTGATGAGGACTCCCAGGACAGCTCTGATGGAATACCGTCAGCACCACGCATGACTGGCAGCCTG
GTGTCTGATCGAAGCCACGACGACATCGTCACCCGGATGAAGAACATTGAGTGCATTGAGCTGGGCCGGCAC
CGCCTCAAGCCGTGGTACTTCTCCCCGTACCCACAGGAACTCACCACATTGCCTGTCCTC~~TACCTGTGCGAGTTC~~
~~TGCCTCAAGTACGGCCGTAGTCTCAAGTGTCTTCAGCGTCATTTGACCAAGTGTGACCTACGA~~CATCCTCCAG
~~GCAATGAGATTTAC~~**~~CGCAAGGGCACCATCTCCTTCTTTGAGATTGATGGACGTAAGAACAAGAGT~~**~~TATTCCCA~~
~~GAACCTGTGTCTTTTGGCCAAGTGTTTCCTTGACCATAAGACACTGTACTATGACACAGAC~~**~~CCTTTCCTCTTCTA~~**
~~CGTCATGACAGAGTATGACTGTAAGGGCTTCCACATCGTGGGCTACTTCTCCAAGGAGAAAGAATCAACGG~~
~~AAGACTACAATGTGGCCTGCATCCTAACCCTGCCTCCCTACCAGCGCCGGGGCTACGGCAAGCTGCTGATCG~~
~~AGTTCAGCTATGAACTCTCCAAAGTGGAAGGGAAAACAGGGACCCCTGAGAAG~~~~CCCCTCTCAGACCTTGGCC~~
~~TCCTATCCTATCGAAGCTACTGGTCCCAGACCATCCTGGAGATCCTGATGGGGCTGAAGTCGGAGAGCGGGGA~~

GAGGCCACAGATCACCATCAATGAGATTAGTGAAATCACCAGCATCAAGAAGGAGGATGTCATCTCCACTCTG
CAGTACCTCAATCTCATCAACTACTACAAGGGCCAGTACATCCTCACACTGTCAGAGGACATCGTGGATGGCCA
TGAGCGGGCCATGCTCAAGCGGCTCCTGCGGATCGACTCCAAGTGTCTGCACTTCACTCCCAAGGACTGGAGC
AAGAGGGGGAAGTGG

MAEVGEIIEGCRLPVLRRNQDNEDEWPLAEILSVKDISGRKLFYVHYIDFNKRL
DEWVTHERLDLKKIQFPKKEAKTPTKNGLPGSRPGSPEREVPASAQASGKTLPI
PVQITLRFNLPKERE AIPGGEPDQPLSSSSCLQPNHRSTKRKVEVVSPATPVPSE
TAPASVFPQNGAARRAVAAQPGRKRKSNCLGTDEDSQDSSDGIPSAPRMTGSL
VSDRSHDDIVTRMKNIECIELGRHRLKPWYFSPYPQELTTLPVLYLCEFCLKYGR
SLKCLQRHLTKCDLRHPPGNEIYRKGTISFFEIDGRKNKSYSQNLCLLAKCFLDH
KTLYYDTDPFLFYVMTEYDCKGFHIVGYFSKEKESTEDYNVACILTLPPYQRRG
YGKLLIEFSYELSKVEGKTGTPEKPLSDLGLLSYRSYWSQTILEILMGLKSESGER
PQITINEISEITSIKKEDVISTLQYLNLINYYKGQYILTLSEDIVDGHERAMLKRLLR
IDSKCLHFTPKDWSKRGKW

TIP60ΔNLS1-eGFP

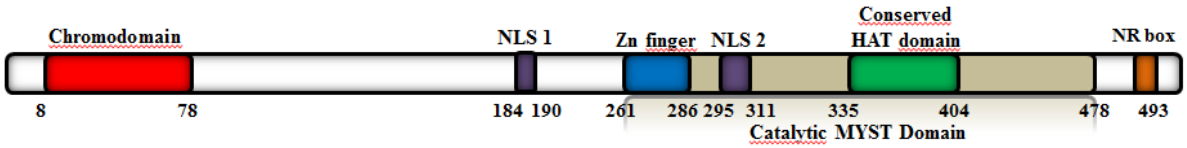

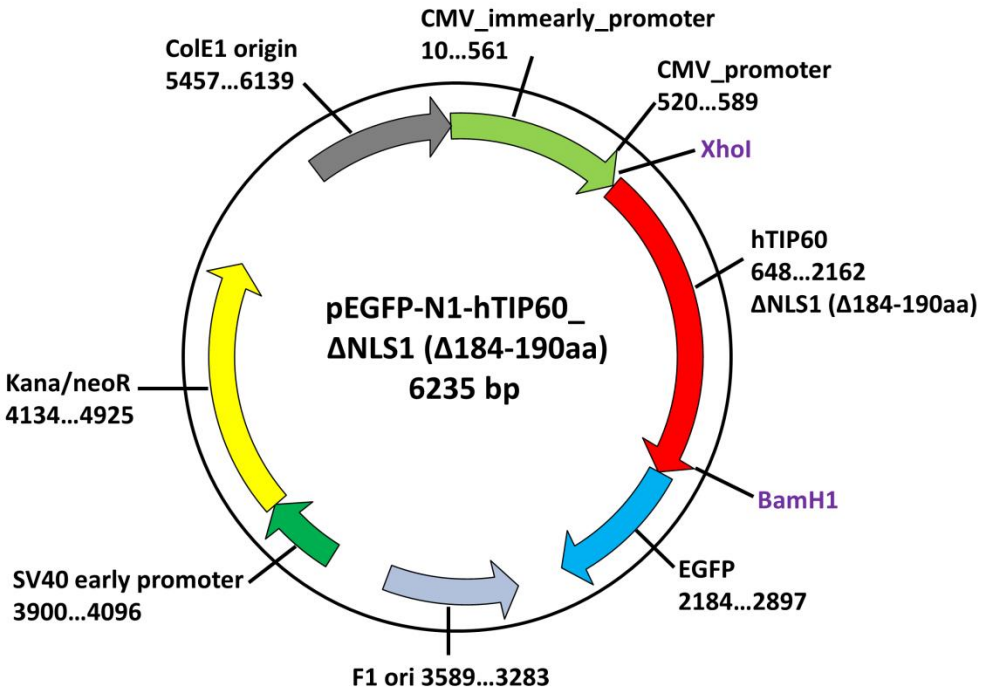

Sequence

atgGCGGAGGTGGGGGAGATA**ATCGAGGGCTGCCGCCTACCCGTGCTGCGGCGGAACCAGGACAACGAAGA**
TGAGTGGCCCCTGGCCGAGATCCTGAGCGTGAAGGACATCAGTGGCCGGAAGCTTTTCTACGTCCATTACAT
TGACTTCAACAAACGTCTGGATGAATGGGTGACGCATGAGCGGCTGGACCTAAAGAAGATCCAGTTCCCCA
AGAAAGAGGCCAAGACCCCCACTAAGAACGGACTTCCTGGGTCCCGTCCTGGCTCTCCAGAGAGAGAGGTGC
CGGCCTCGGCGCAGGCCAGCGGGAAGACCTTGCCAATCCCGGTCCAGATCACACTCCGCTTCAACCTGCCCAA
GGAGCGGGAGGCCATTCCCGGTGGCGAGCCTGACCAGCCGCTCTCCTCCAGCTCCTGCCTGCAGCCCAACCAC
CGCTCAACGAAACGGAAGGTGGAGGTGGTTTCACCAGCAACTCCAGTGCCCAGCGAGACAGCCCCGGCCTCG
GTTTTTCCCCAGAATGGAGCCGCCCGTAGGGCAGTGGCAGCCCAG~~CCAGGACGGAAGCGAAAATCG~~AATTGT
TTGGGCACTGATGAGGACTCCCAGGACAGCTCTGATGGAATACCGTCAGCACCACGCATGACTGGCAGCCTG
GTGTCTGATCGAAGCCACGACGACATCGTCACCCGGATGAAGAACATTGAGTGCATTGAGCTGGGCCGGCAC
CGCCTCAAGCCGTGGTACTTCTCCCCGTACCCACAGGAACTCACCACATTGCCTGTCCTC**TACCTGTGCGAGTTC**
TGCCTCAAGTACGGCCGTAGTCTCAAGTGTCTTCAGCGTCATTTGACCAAGTGTGACCTACGACATCCTCCAG
GCAATGAGATTTAC**CGCAAGGGCACCATCTCCTTCTTTGAGATTGATGGACGTAAGAACAAGAGT**TATTCCCA
GAACCTGTGTCTTTTGGCCAAGTGTTTCCTTGACCATAAGACACTGTACTATGACACAGAC**CCTTTCCTCTTCTA**
CGTCATGACAGAGTATGACTGTAAGGGCTTCCACATCGTGGGCTACTTCTCCAAGGAGAAAGAATCAACGG
AAGACTACAATGTGGCCTGCATCCTAACCCTGCCTCCCTACCAGCGCCGGGGCTACGGCAAGCTGCTGATCG
AGTTCAGCTATGAACTCTCCAAAGTGGAAGGGAAAACAGGGACCCCTGAGAAGCCCCTCTCAGACCTTGGCC
TCCTATCCTATCGAAGCTACTGGTCCCAGACCATCCTGGAGATCCTGATGGGGCTGAAGTCGGAGAGCGGGGA
GAGGCCACAGATCACCATCAATGAGATTAGTGAAATCACCAGCATCAAGAAGGAGGATGTCATCTCCACTCTG
CAGTACCTCAATCTCATCAACTACTACAAGGGCCAGTACATCCTCACACTGTCAGAGGACATCGTGGATGGCCA
TGAGCGGGCCATGCTCAAGCGGCTCCTGCGGATCGACTCCAAGTGTCTGCACTTCACTCCCAAGGACTGGAGC
AAGAGGGGGAAGTGG

Sequence for the mutants

M A E V G E I **I E G C R L P V L R R N Q D N E D E W P L A E I L S V K D I S G R K L F Y V H Y I D F N K R L**
D E W V T H E R L D L K K I Q F P K K E A K T P T K N G L P G S R P G S P E R E V P A S A Q A S G K T L P I
P V Q I T L R F N L P K E R E A I P G G E P D Q P L S S S S C L Q P N H R S T K R K V E V V S P A T P V P S E
T A P A S V F P Q N G A A R R A V A A Q **~~P G R K R K S~~** N C L G T D E D S Q D S S D G I P S A P R M T G S L
V S D R S H D D I V T R M K N I E C I E L G R H R L K P W Y F S P Y P Q E L T T L P V L **Y L C E F C L K Y G R**
S L K C L Q R H L T K C D L R H P P G N E I Y **R K G T I S F F E I D G R K N K S** Y S Q N L C L L A K C F L D H
K T L Y Y D T D **P F L F Y V M T E Y D C K G F H I V G Y F S K E K E S T E D Y N V A C I L T L P P Y Q R R G**
Y G K L L I E F S Y E L S K V E G K T G T P E K P L S D L G L L S Y R S Y W S Q T I L E I L M G L K S E S G E R
P Q I T I N E I S E I T S I K K E D V I S T L Q Y L N L I N Y Y K G Q Y I L T L S E D I V D G H E R A M L K R L L R
I D S K C L H F T P K D W S K R G K W

TIP60ΔNLS2-eGFP

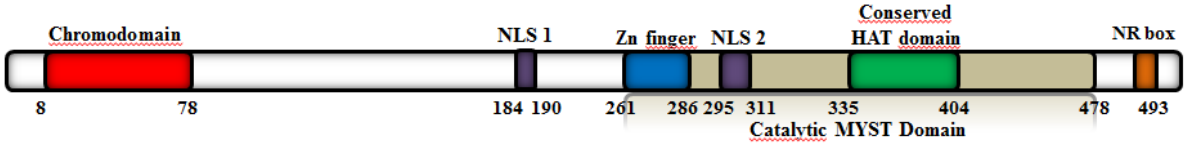

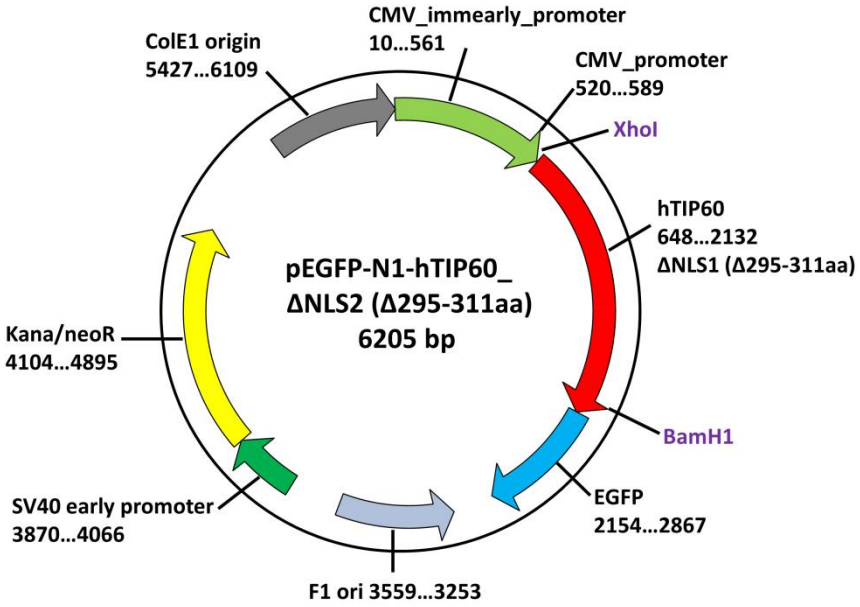

Sequence

atgGCGGAGGTGGGGGAGATA**ATCGAGGGCTGCCGCCTACCCGTGCTGCGGCGGAACCAGGACAACGAAGA**
TGAGTGGCCCCTGGCCGAGATCCTGAGCGTGAAGGACATCAGTGGCCGGAAGCTTTTCTACGTCCATTACAT
TGACTTCAACAAACGTCTGGATGAATGGGTGACGCATGAGCGGCTGGACCTAAAGAAGATCCAGTTCCCCA
AGAAAGAGGCCAAGACCCCCACTAAGAACGGACTTCCTGGGTCCCGTCCTGGCTCTCCAGAGAGAGAGGTGC
CGGCCTCGGCGCAGGCCAGCGGGAAGACCTTGCCAATCCCGGTCCAGATCACACTCCGCTTCAACCTGCCCAA
GGAGCGGGAGGCCATTCCCGGTGGCGAGCCTGACCAGCCGCTCTCCTCCAGCTCCTGCCTGCAGCCCAACCAC
CGCTCAACGAAACGGAAGGTGGAGGTGGTTTCACCAGCAACTCCAGTGCCCAGCGAGACAGCCCCGGCCTCG
GTTTTTCCCCAGAATGGAGCCGCCCGTAGGGCAGTGGCAGCCCAG**CCAGGACGGAAGCGAAAATCG**AATTGT
TTGGGCACTGATGAGGACTCCCAGGACAGCTCTGATGGAATACCGTCAGCACCACGCATGACTGGCAGCCTG
GTGTCTGATCGAAGCCACGACGACATCGTCACCCGGATGAAGAACATTGAGTGCATTGAGCTGGGCCGGCAC
CGCCTCAAGCCGTGGTACTTCTCCCCGTACCCACAGGAACTCACCACATTGCCTGTCCTC**TACCTGTGCGAGTTC**
TGCCTCAAGTACGGCCGTAGTCTCAAGTGTCTTCAGCGTCATTTGACCAAGTGTGACCTACGACATCCTCCAG
GCAATGAGATTTAC~~CGCAAGGGCACCATCTCCTTCTTTGAGATTGATGGACGTAAGAACAAGAGT~~TATTCCCA
GAACCTGTGTCTTTTGGCCAAGTGTTTCCTTGACCATAAGACACTGTACTATGACACAGAC**CCTTTCCTCTTCTA**
CGTCATGACAGAGTATGACTGTAAGGGCTTCCACATCGTGGGCTACTTCTCCAAGGAGAAAGAATCAACGG
AAGACTACAATGTGGCCTGCATCCTAACCCTGCCTCCCTACCAGCGCCGGGGCTACGGCAAGCTGCTGATCG
AGTTCAGCTATGAACTCTCCAAAGTGGAAGGGAAAACAGGGACCCCTGAGAAGCCCCTCTCAGACCTTGGCC

TCCTATCCTATCGAAGCTACTGGTCCCAGACCATCCTGGAGATCCTGATGGGGCTGAAGTCGGAGAGCGGGGA
GAGGCCACAGATCACCATCAATGAGATTAGTGAAATCACCAGCATCAAGAAGGAGGATGTCATCTCCACTCTG
CAGTACCTCAATCTCATCAACTACTACAAGGGCCAGTACATCCTCACACTGTCAGAGGACATCGTGGATGGCCA
TGAGCGGGCCATGCTCAAGCGGCTCCTGCGGATCGACTCCAAGTGTCTGCACTTCACTCCCAAGGACTGGAGC
AAGAGGGGGAAGTGG

MAEVGEIIEGCRLPVLRRNQDNEDEWPLAEILSVKDISGRKLFYVHYIDFNKRL
DEWVTHERLDLKKIQFPKKEAKTPTKNGLPGSRPGSPEREVPASAQASGKTLPI
PVQITLRFNLPKEREAIPGGEPDQPLSSSSCLQPNHRSTKRKVEVVSPATPVPSE
TAPASVFPQNGAARRAVAAQPGRKRKSNCLGTDEDSQDSSDGIPSAPRMTGSL
VSDRSHDDIVTRMKNIECIELGRHRLKPWYFSPYYPQELTTLPVLYLCEFCLKYGR
SLKCLQRHLTKCDLRHPPGNEIY~~RKGTISFFEIDGRKNKS~~YSQNLCLLAKCFLDH
KTLYYDTDPFLFYVMTEYDCKGFHIVGYFSKEKESTEDYNVACILTLPPYQRRG
YGKLLIEFSYELSKVEGKTGTPEKPLSDLGLLSYRSYWSQTILEILMGLKSESGER
PQITINEISEITSIKKEDVISTLQYLNLINYYKGQYILTLSEDIVDGHERAMLKRLLR
IDSKCLHFTPKDWSKRGKW

TIP60ΔNLS1-2-eGFP

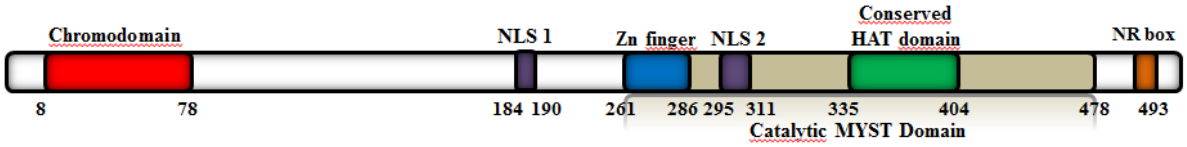

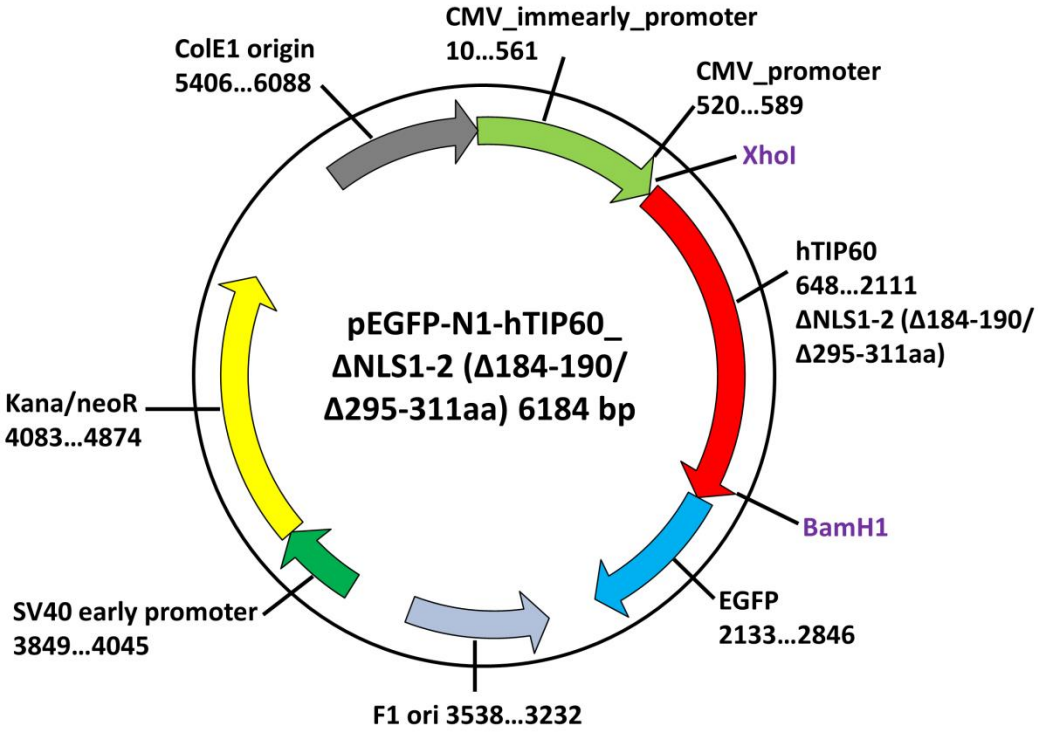

Sequence

atgGCGGAGGTGGGGGAGATA**ATCGAGGGCTGCCGCCTACCCGTGCTGCGGCGGAACCAGGACAACGAAGA**
TGAGTGGCCCCTGGCCGAGATCCTGAGCGTGAAGGACATCAGTGGCCGGAAGCTTTTCTACGTCCATTACAT
TGACTTCAACAAACGTCTGGATGAATGGGTGACGCATGAGCGGCTGGACCTAAAGAAGATCCAGTTCCCCA
AGAAAGAGGCCAAGACCCCCACTAAGAACGGACTTCCTGGGTCCCGTCCTGGCTCTCCAGAGAGAGAGGTGC
CGGCCTCGGCGCAGGCCAGCGGGAAGACCTTGCCAATCCCGGTCCAGATCACACTCCGCTTCAACCTGCCCAA
GGAGCGGGAGGCCATTCCCGGTGGCGAGCCTGACCAGCCGCTCTCCTCCAGCTCCTGCCTGCAGCCCAACCAC
CGCTCAACGAAACGGAAGGTGGAGGTGGTTTCACCAGCAACTCCAGTGCCCAGCGAGACAGCCCCGGCCTCG
GTTTTTCCCCAGAATGGAGCCGCCCGTAGGGCAGTGGCAGCCCAG~~CCAGGACGGAAGCGAAAATCG~~AATTGT
TTGGGCACTGATGAGGACTCCCAGGACAGCTCTGATGGAATACCGTCAGCACCACGCATGACTGGCAGCCTG
GTGTCTGATCGAAGCCACGACGACATCGTCACCCGGATGAAGAACATTGAGTGCATTGAGCTGGGCCGGCAC
CGCCTCAAGCCGTGGTACTTCTCCCCGTACCCACAGGAACTCACCACATTGCCTGTCCTC**TACCTGTGCGAGTTC**
TGCCTCAAGTACGGCCGTAGTCTCAAGTGTCTTCAGCGTCATTTGACCAAGTGTGACCTACGACATCCTCCAG
GCAATGAGATTTAC~~CGCAAGGGCACCATCTCCTTCTTTGAGATTGATGGACGTAAGAACAAGAGT~~TATTCCCA
GAACCTGTGTCTTTTGGCCAAGTGTTTCCTTGACCATAAGACACTGTACTATGACACAGAC**CCTTTCCTCTTCTA**
CGTCATGACAGAGTATGACTGTAAGGGCTTCCACATCGTGGGCTACTTCTCCAAGGAGAAAGAATCAACGG
AAGACTACAATGTGGCCTGCATCCTAACCCTGCCTCCCTACCAGCGCCGGGGCTACGGCAAGCTGCTGATCG
AGTTCAGCTATGAACTCTCCAAAGTGGAAGGGAAAACAGGGACCCCTGAGAAGCCCCTCTCAGACCTTGGCC
TCCTATCCTATCGAAGCTACTGGTCCCAGACCATCCTGGAGATCCTGATGGGGCTGAAGTCGGAGAGCGGGGA
GAGGCCACAGATCACCATCAATGAGATTAGTGAAATCACCAGCATCAAGAAGGAGGATGTCATCTCCACTCTG
CAGTACCTCAATCTCATCAACTACTACAAGGGCCAGTACATCCTCACACTGTCAGAGGACATCGTGGATGGCCA
TGAGCGGGCCATGCTCAAGCGGCTCCTGCGGATCGACTCCAAGTGTCTGCACTTCACTCCCAAGGACTGGAGC
AAGAGGGGGAAGTGG

M A E V G E I**I E G C R L P V L R R N Q D N E D E W P L A E I L S V K D I S G R K L F Y V H Y I D F N K R L**
D E W V T H E R L D L K K I Q F P K K E A K T P T K N G L P G S R P G S P E R E V P A S A Q A S G K T L P I
P V Q I T L R F N L P K E R E A I P G G E P D Q P L S S S S C L Q P N H R S T K R K V E V V S P A T P V P S E
T A P A S V F P Q N G A A R R A V A A Q ~~**P G R K R K S**~~ N C L G T D E D S Q D S S D G I P S A P R M T G S L
V S D R S H D D I V T R M K N I E C I E L G R H R L K P W Y F S P Y P Q E L T T L P V L **Y L C E F C L K Y G R**
S L K C L Q R H L T K C D L R H P P G N E I Y ~~**R K G T I S F F E I D G R K N K S**~~ Y S Q N L C L L A K C F L D H
K T L Y Y D T D **P F L F Y V M T E Y D C K G F H I V G Y F S K E K E S T E D Y N V A C I L T L P P Y Q R R G**
Y G K L L I E F S Y E L S K V E G K T G T P E K P L S D L G L L S Y R S Y W S Q T I L E I L M G L K S E S G E R
P Q I T I N E I S E I T S I K K E D V I S T L Q Y L N L I N Y Y K G Q Y I L T L S E D I V D G H E R A M L K R L L R
I D S K C L H F T P K D W S K R G K W

eGFP-DNMT1

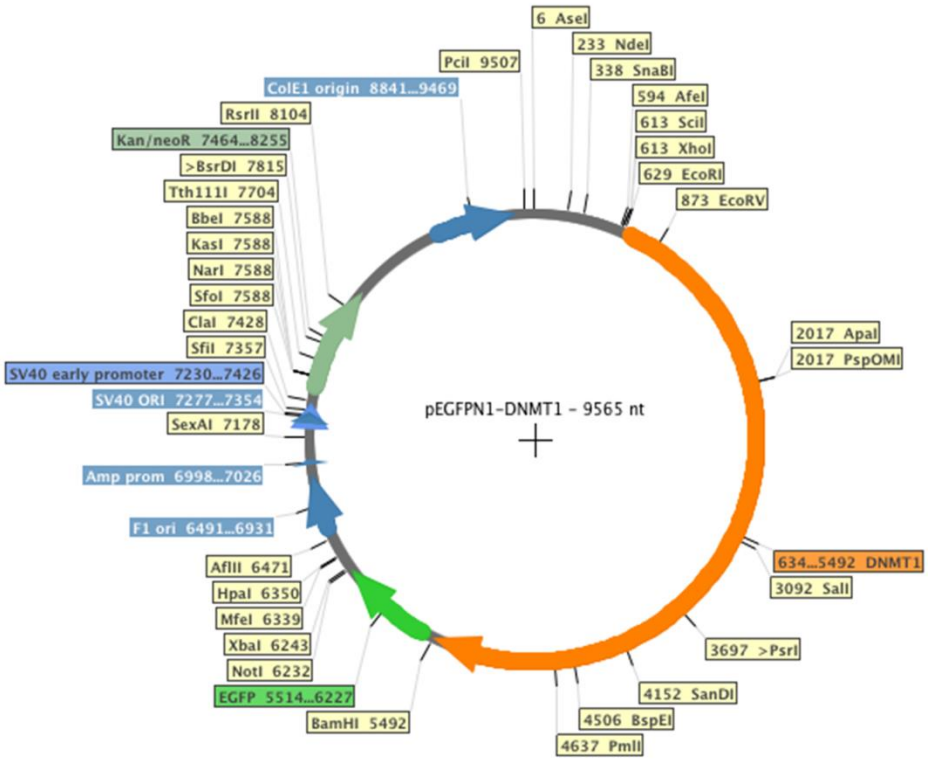

1.C. Bacterial plasmids for expression of TIP60 and its mutants proteins

1. pET15bm-hTIP60-WT

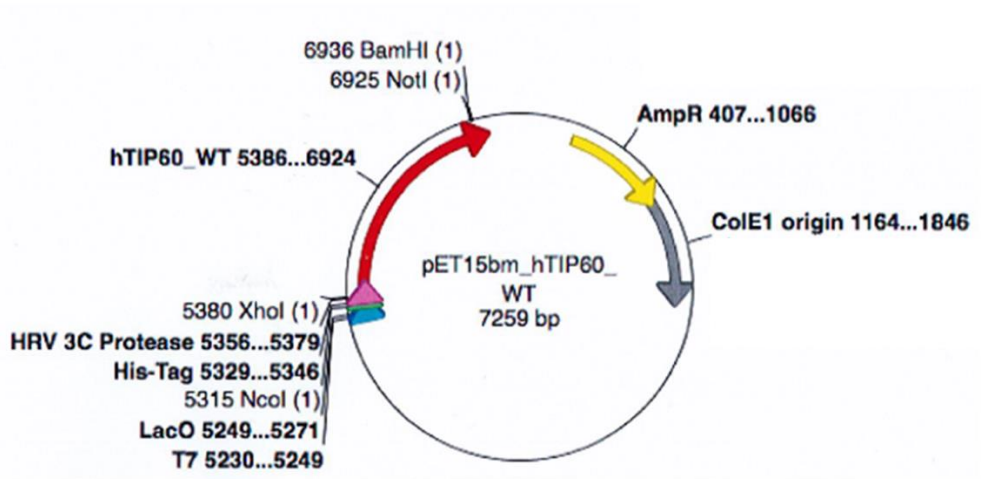

2. **pET15bm-hTIP60ΔCRD**

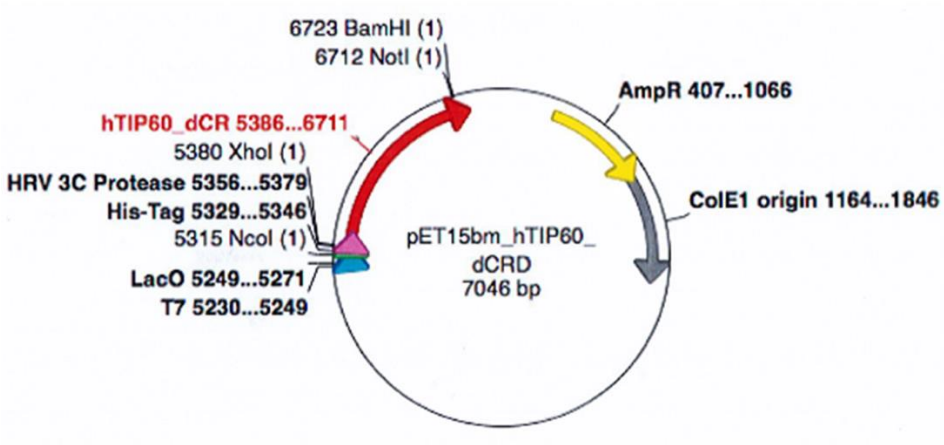

3. **pET15bm-hTIP60ΔZF**

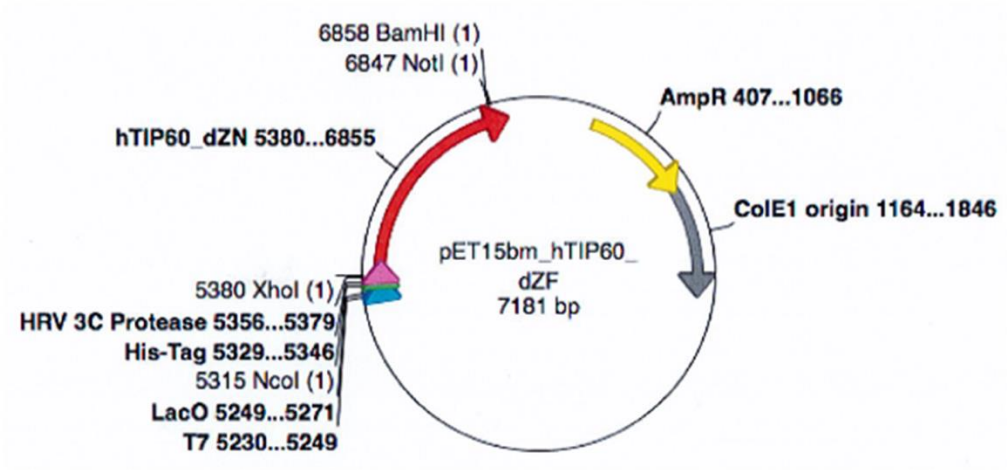

4. **pET15bm-hTIP60ΔHAT**

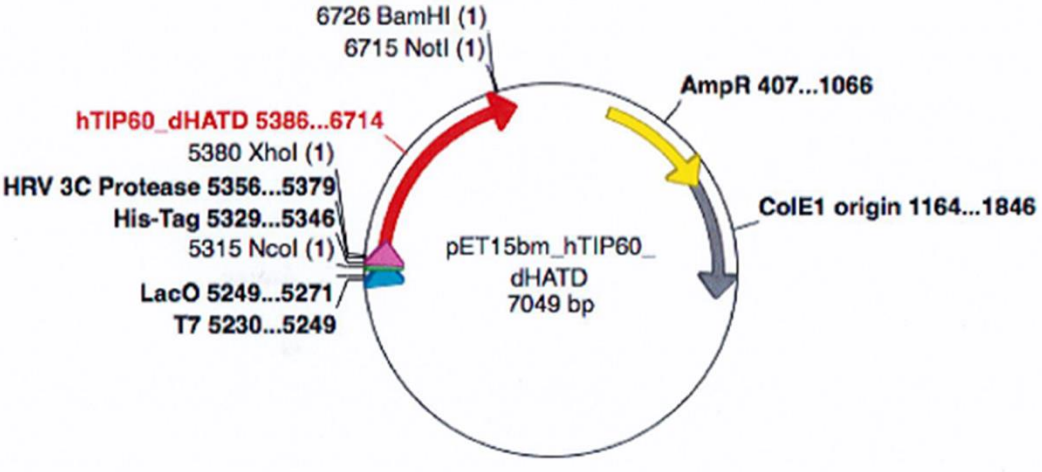

5. **pET15bm-hTIP60ΔMYST**

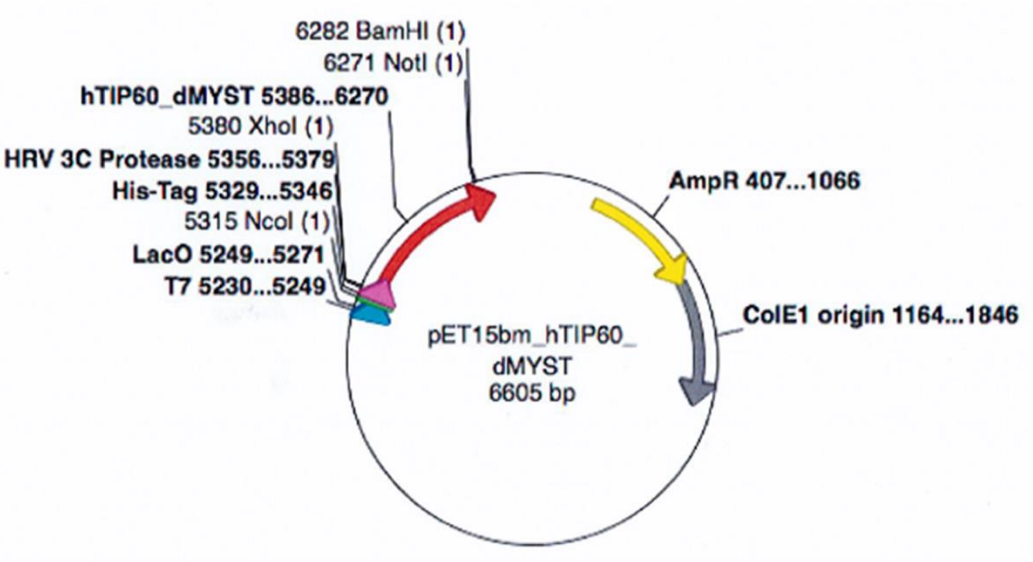

1.D. Cell lines

HeLa cells (ATCC, CCL-2, Amp, Cervical Adenocarcinoma; Human) derived from patient named Henrietta Lacks. She died of cancer in 1951. HeLa cell lines stably expressing GFP-UHRF1 wild type and GFP-UHRF1 RING C724A mutant proteins were prepared as described elsewhere (Ibrahim *et al.*, 2018).

2. METHODS

2.A. Cell Culture

Cells were grown in Dulbecco's Modified Eagle's Medium (DMEM 1X + GlutaMAXTM, Pyruvate, Gibco, Lifetech, France) which was supplemented with 10% fetal bovine serum (Dominique Dutscher), in addition to mixture of penicillin (100 U/ml) and streptomycin (100 U/ml) (Lonza, USA), at 37°C with 5% CO2 in humidified environment.

2.B. Transient transfection

Transfection of foreign DNA in HeLa cells was done with either jetPEI^{TM} or jetPRIME (PolyPlus-transfection, France). jetPEI is composed of linear polyethylenimine molecules.

These molecules cover the DNA to develop positively charged particles. These charged particles interact with proteoglycans (anionic) of cell membrane and are engulfed through endocytosis. PEI assures the integrity of DNA in endosomes and later DNA is released into cytoplasm. Released DNA is transported to nucleus for transcription. According to manufacturer's guidelines, two solutions were prepared for transfection. One solution was containing DNA (plasmid) in 150 mM NaCl while the second solution was containing jetPEI reagent in 150 mM NaCl. jetPEI solution was transferred to first solution containing DNA. Mixture was incubated at room temperature for 20-25 minutes to allow the formation of PEI-DNA particles. Then this solution was added drop by drop into culture media.

2.C. Protein isolation

For protein isolation, cells were collected after transient transfection. Adherent cells were washed with PBS and then trypsinized to collect the cells. Action of trypsin was inhibited with fresh warm media. Cells were collected through centrifugation at 1000 RPM for 4 minutes. Cells were lysed with freshly prepared ice-cold lysis buffer (Tris-HCl pH 7.5 10mM, NaCl 150 mM, EDTA 1 mM, NP40 1% and freshly supplemented with EDTA free protease inhibitors cocktail tablet). Samples were incubated at ice for 25-30 minutes to ensure the complete lysis. Proteins were isolated through centrifugation (14000 g, 25 min at 4°C). Proteins were quantified through Bradford assay. This assay is based on the change in color of Coomassie brilliant blue G-250 dye in response to different concentrations of proteins. Change in color appears because of interaction between acidic Coomassie dye and arginine and aromatic amino acids of protein sample. Change in color is proportional to the amount of protein present in sample. Absorbance is measured at 595. Known concentrations of BSA were used to develop a standard curve to quantify relative concentration of protein samples.

2.D. Western blot

To study the expression of proteins, 30-40 µg from protein lysates of different samples were mixed with Laemmli sample buffer (Bio-Rad, 1610747) and DTT (dithiothreitol). Protein samples were denatured by heating at 95°C for 5-6 minutes. Samples were loaded to SDS-PAGE (1.5 % or 10%) for separation in Tris-Glycine migration buffer (Tris 25 mM, Glycine 192 mM, SDS 0.1%, final pH 8.8) by using minigel system (Bio-Rad). After migration, proteins were transferred to PVDF (polyvinylidene difluoride) membrane in transfer buffer (Tris 25mM, Glycine 192 mM and 30% ethanol, pH 6.8). 7). Before use, PVDF membrane

was activated with absolute ethanol and then equilibrated along the gel with the transfer buffer (1X). Blocking was done with 3% blotting-grade blocker (Bio-Rad 1706404) prepared in TBST (Tris Buffered Saline with Tween 20, pH 8.0) (Sigma-T9039) for 60 min at room temperature. After blocking, membrane was incubated with respective primary antibody at 4°C. Membrane was washed with TBST buffer thrice. HRP-conjugated secondary antibody was used to label the primary antibody. Membrane was incubated with secondary antibody for 60 min at room temperature. Again, washing was done three times. Signals were detected on an Image Quant LAS 4000 apparatus (GE Healthcare Life Sciences, USA) with chemiluminescent ECL system (Clarity^{TM} ECL western blotting substrate, Bio-Rad, France, 170-5060). Image Studio Lite (Li-Core Biosciences, USA) was used to analyze the images.

2.E. Immunoprecipitation

For immunoprecipitation experiments, HeLa cells were transfected as described earlier. Cells were collected 24 hr of post-transfection through trypsinization. Cell pellet was obtained after centrifugation and pellet was resuspended in ice-cold PBS (freshly supplemented with protease inhibitor cocktail). Cells were freezed in liquid nitrogen and were allowed to de-freeze slowly on ice. Then lysis was done through mild sonication. Each sample was sonicated five times and for 5 seconds each time. Proteins were isolated through centrifugation (at 14000 g, 25-30 min, 4°C). Input controls were prepared by taking 40 µg of protein from each sample cell lysate. 1000 µg to 1500 µg of protein lysate were incubated with anti-UHRF1 antibody at 4°C for 3 h or with anti-USP7 antibody at 4°C for overnight. After washing and equilibration, 50 µL of Dynabeads® protein A (Thermo Fischer Scientific, Norway 1002D) were added to the lysate-antibody mixture and incubated for 60 min at 4 °C. Then beads were collected by placing tubes on a magnetic rack. Beads were washed 3-4 times with ice cold PBS freshly supplemented with protease inhibitors tablet. Finally, beads were resuspended in Laemmli sample buffer. Proteins were denatured by heating at 95 °C for 5-6 min and analyzed through Western blotting.

2.F. Cell-based ubiquitination assay

This assay was performed as described by (Dai *et al.,* 2013) with some modifications. HeLa cells were co-transfected (by using jetPEI) with either TIP60-eGFP and His-Ubiquitin or TIP60ΔMYST-eGFP and His-Ubiquitin plasmids. Samples were treated with proteasomal degradation inhibitor MG-132 (final concentration 10 µM) 8 h before cell harvesting. Cells

were collected after trypsinization. Cell pellet was resuspended in PBS. Inputs were prepared by taking 10% of cells from each sample and lysed with lysis buffer. Leftover pellet was lysed with mild sonication in phosphate/guanidine buffer (10 mM Tris-HCl pH 8.0, 6 M Guanidine-HCl, 6.8 mM NaH_2PO_4, 0.1 M $Na_2HPO_4.2H_2O$, 0.2% Triton X-100 freshly supplemented with 5 mM Imidazole and 10 mM β-mercaptoethanol). Sonication was done five times, each time for 5 second. Ni-NTA beads suspension was centrifuged briefly to get beads. Beads were washed and equilibrated with phosphate/guanidine buffer. Then beads were added to sample lysates for 3h at room temperature to pull down His-tagged proteins. Samples were centrifuged at 2000-2500 RPM for 2 minutes. Supernatant was discarded. Ni-NTA captured fractions were washed with phosphate/guanidine and Urea wash buffer (10 mM Tris-HCl pH 8.0, 8 M Urea, 0.1 M $Na_2HPO_4.2H_2O$, 6.8 mM NaH_2PO_4, 0.2% Triton X-100 freshly supplemented with 5 mM Imidazole and 10 mM β-mercaptoethanol). Then these fractions were washed thrice with Wash buffer (10 mM Tris-HCl pH 6.3, 80 mM NaH_2PO_4, 18 mM $Na_2HPO_4.2H_2O$, 0.2% Triton X-100 freshly supplemented with 5 mM Imidazole and 10 mM β-mercaptoethanol). Then precipitates were eluted for 40-60 min in 50 µL of Elution buffer (0.5 M Imidazole, 0.125 M DTT). Finally, samples were denatured and analyzed by Western blotting.

2.G. UHRF1 auto-ubiquitination assay

HeLa cells stably expressing GFP-UHRF1 WT and GFP-UHRF1 C724A mutant protein were transfected with either TIP60 WT or TIP60ΔMYST mutant with jetPRIME reagent. Samples were treated with 10 µM MG-132, 8h before harvesting the cells. Immunoprecipitation (as described above) was performed with anti-GFP antibody to immunoprecipitate the GFP-tagged UHRF1 protein. Samples were resolved by Western blotting.

2.H. Confocal microscopy

Confocal microscopy was used to study the effect of TIP60 overexpression on UHRF1 and DNMT1 levels. HeLa cells were seeded on a glass cover slip. Transient transfection of eGFP or TIP60-eGFP or TIP60ΔMYST-eGFP plasmids was done by using jetPEI^{TM} reagent as described in manufacturer's protocol. Media was removed and cells were washed with PBS 1X. Cells were fixed with 4% paraformaldehyde (PFA) for 10-15 minutes at room temperature. Then PFA was removed and washing was done three times with PBS 1X. Cells were permeabilized with 0.2% Triton X-100 for 15-20 min at room temperature. After that,

triton was removed and again washing was done thrice with PBS 1X. 1% BSA was used for blocking. Freshly prepared BSA was added in each sample and incubated at room temperature for 1 hr. Then, BSA was removed and washing was done. Then cells were labeled with primary antibody against either UHRF1 or DNMT1. Cells were incubated with primary antibody at 4°C for 3 hr. Cells were washed thrice with PBS 1X, each time for 10 min. Then, cells were incubated with secondary antibody labeled with Alexa Fluor 568 at room temperature for 60 min. Again, cells were washed three times with PBS 1X, each time for 10 min. After that DAPI (4', 6-diamidino-2-phenylindole) was used to label the nucleus. Cells were incubated with DAPI for 15-20 minutes at room temperature. Confocal Leica TCS SPE microscope equipped with a 20× air (0.7 NA) immersion lens objective was used for acquisition. For Alexa Flour 568, eGFP and DAPI excitation was performed with a 561 nm laser (10 mW), 405 nm laser (25 mW) and 488 nm laser (25 mW) respectively. The detection range for the three dyes was 570-630 nm, 500-523 nm and 430-480 nm respectively.

To study the co-localization of UHRF1 and Ubiquitin and effect of TIP60 overexpression over this co-localization confocal microscopy experiments were performed. For this, HeLa cells were co-transfected with TIP60-eGFP and RFP-Ubiquitin by using jetPEI^{TM} reagent. Cells transfected with either eGFP or RFP-Ubiquitin were used as control. 8 h before cell fixation, one group of samples was treated with MG-132 (10 µM). After fixation, permeabilization and blocking cells were labeled with anti-UHRF1 as primary antibody and Alexa Flour 647 (goat anti-mouse, A21237, Molecular probes) as secondary antibody. Cells were incubated with DAPI for staining of nucleus. Confocal Leica TCS SPE equipped with an oil immersion objective (HXC PL APO 63×/1.40 OIL CS) was used to image the cells. For RFP, Alexa Flour 647, eGFP and DAPI excitation was performed with a 561 nm laser (10 mW), 635 nm laser (18 mW), 488 nm laser (25 mW), and 405 nm laser (25 mW), respectively. The detection range for the four dyes was 570-630 nm, 640-702, 500-523 nm and 430-480 nm, respectively.

To study the effect of TIP60 overexpression over endogenous expression of UHRF1 and USP7 in the same nucleus, HeLa cells were transfected with either TIP60-eGFP or TIP60ΔMYST-eGFP. 8 h before cell fixation, one group of samples was treated with MG-132 (10 µM). After fixation, permeabilization and blocking cells were labeled with anti-UHRF1 (mouse) and anti-USP7 (rabbit) antibodies overnight at 4 °C. After washing, cells were incubated with secondary antibody labeled with Alexa Flour 568 (goat anti-rabbit) for USP7 and Alexa Fluor 647 (goat anti-mouse) for UHRF1. Cells were incubated with DAPI for

staining of nucleus. Confocal Leica TCS SPE equipped with an oil immersion objective (HXC PL APO 63×/1.40 OIL CS) was used for acquisition. For Alexa Flour 568, Alexa Flour 647, eGFP and DAPI excitation was performed with a 561 nm laser (10 mW), 635 nm laser (18 mW), 488 nm laser (25 mW), and 405 nm laser (25 mW), respectively. The detection range for the four dyes was 570-625 nm, 644-707 nm, 500-531 nm and 430-480 nm, respectively. All the images were processed with Image J software.

2.I. FÖster Resonance Energy Transfer-Fluorescence Lifetime Imaging Microscopy (FRET-FLIM)

To study the interaction between UHRF1 and Ubiquitin, FRET-FLIM experiment was performed. This is an efficient and high-resolution technique to study the protein-protein interactions. FRET-FLIM is now frequently used to investigate the molecular mechanisms involved in various cellular processes like regulation of gene expression, vesicular transport and signal transduction. Basic principle of FRET involves energy transfer from excited donor fluorophore to non-excited acceptor fluorophore through dipole-dipole coupling (Periasamy *et al.*, 2015). After this energy transfer, lifetime of both fluorophores is changed. For FRET to occur, absorption spectra of acceptor fluorophore should overlap with donor fluorophores's emission spectra. Secondly, for efficient FRET two fluorophores should be very close (<10 nm) to each other.

To investigate the interaction between UHRF1 and Ubiquitin, we tagged UHRF1 with GFP (green fluorescent protein) and Ubiquitin with RFP (red fluorescent protein). HeLa cell line was prepared to stably express GFP-UHRF1 protein. For experiment, HeLa cells stably expressing GFP-UHRF1 were seeded (10^5 cells per dish) in a µ-dish (Ibidi) with 35 mm wells. RFP-Ubiquitin plasmid was transfected by using jetPEI™ reagent. Cells were fixed with 4% PFA at different time intervals after RFP-Ubiquitin transfection. Acquisition was performed on a homemade two-photon excitation scanning microscope based on an Olympus IX70 inverted microscope with a 60× 1.2 NA water immersion objective operating in the descanned fluorescence collection mode as described (Clamme *et al.*, 2003; El Meshri *et al.*, 2015; Zaayter *et al.*, 2019).

Two-photon excitation at 930 nm was equipped with an Insight DeepSee laser (Spectra Physics). Fluorescence photons were compiled using a short-pass filter with a cut-off wavelength of 680 nm (F75-680, AHF, Germany) and a band-pass filter of 520 ± 17 nm (F37-

520, AHF, Germany). The fluorescence was guided to a fiber coupled APD (SPCM-AQR-14-FC, Perkin Elmer), which was connected to a time-correlated single photon counting module (SPC830, Becker & Hickl, Germany). FLIM data was analyzed using SPCImage v 7.3 (Becker & Hickel). FRET efficiency was calculated according to $E=1-(\tau_{DA}/\tau_D)$, where τ_{DA} is the lifetime of the donor (GFP) in the presence of acceptor (RFP) and τ_D is the lifetime of GFP in the absence of acceptor.

2.J. Apoptosis analysis

To investigate the TIP60-mediated apoptosis in cancer cells, flow cytometry technique was used. Flow cytometry can determine optical and fluorescence properties of single cells. HeLa cells were seeded in six well plates. Transient transfection of TIP60-eGFP was performed by using jetPEI™ reagent according to manufacturer's protocol. After 24 h of transfection, media was collected, and cells were washed with PBS and collected after trypsinization. Cells were centrifuged at 1200 g for 5 minutes. Supernatant was discarded. Cell pellet was resuspended in fresh media and 200 µl of this cell suspension was added to each well of 96 well plate. Then cell suspension was incubated with Propidium iodide (PI) and Annexin V-iFlour™350 conjugate. Plate was incubated at room temperature for 15-20 minutes. Acquisition of samples was performed by Guava easyCyte™ flow cytometer (Merck Millipore). InCyte Software for Guava (Merck Millipore) was used to analyze the results.

RESULTS

IV- RESULTS

Manuscript I: Interaction of the epigenetic integrator UHRF1 with the MYST domain of TIP60 inside the cell

Ashraf et al. Journal of Experimental & Clinical Cancer Research (2017) 36:188
DOI 10.1186/s13046-017-0659-1

Journal of Experimental & Clinical Cancer Research

RESEARCH Open Access

Interaction of the epigenetic integrator UHRF1 with the MYST domain of TIP60 inside the cell

Waseem Ashraf[1], Christian Bronner[2], Liliyana Zaayter[1], Tanveer Ahmad[1], Ludovic Richert[1], Mahmoud Alhosin[3,4], Abdulkhaleg Ibrahim[2,5], Ali Hamiche[2], Yves Mely[1] and Marc Mousli[1*]

Abstract

Background: The nuclear epigenetic integrator UHRF1 is known to play a key role with DNMT1 in maintaining the DNA methylation patterns during cell division. Among UHRF1 partners, TIP60 takes part in epigenetic regulations through its acetyltransferase activity. Both proteins are involved in multiple cellular functions such as chromatin remodeling, DNA damage repair and regulation of stability and activity of other proteins. The aim of this work was to investigate the interaction between UHRF1 and TIP60 in order to elucidate the dialogue between these two proteins.

Methods: Biochemical (immunoprecipitation and pull-down assays) and microscopic (confocal and fluorescence lifetime imaging microscopy; FLIM) techniques were used to analyze the interaction between TIP60 and UHRF1 in vitro and in vivo. Global methylation levels were assessed by using a specific kit. The results were statistically analyzed using Graphpad prism and Origin.

Results: Our study shows that UHRF1, TIP60 and DNMT1 were found in the same epigenetic macro-molecular complex. In vitro pull-down assay showed that deletion of either the zinc finger in MYST domain or deletion of whole MYST domain from TIP60 significantly reduced its interaction with UHRF1. Confocal and FLIM microscopy showed that UHRF1 co-localized with TIP60 in the nucleus and confirmed that both proteins interacted together through the MYST domain of TIP60. Moreover, overexpression of TIP60 reduced the DNA methylation levels in HeLa cells along with downregulation of UHRF1 and DNMT1.

Conclusion: Our data demonstrate for the first time that TIP60 through its MYST domain directly interacts with UHRF1 which might be of high interest for the development of novel oncogenic inhibitors targeting this interaction.

Keywords: Cancer, Epigenetics, Fluorescence lifetime imaging microscopy (FLIM), Fluorescence resonance energy transfer (FRET), Protein-protein interaction, TIP60, UHRF1, Cell cycle

Background

Ubiquitin-like containing PHD and RING Finger domains 1 (UHRF1) is a multi-domain nuclear protein that plays an important role in epigenetics through the maintenance of DNA methylation patterns during DNA replication [1, 2]. UHRF1 senses hemi-methylated strand through its SRA domain and then recruits the DNA methyltransferase 1 (DNMT1) to duplicate the methylation patterns on the newly formed daughter strand [3–5]. Besides the readout of DNA methylation marks, UHRF1 also reads histone post-translational modifications (H3K9me2/3) via its tandem tudor and PHD domains and ubiquitinylates histone H3 at lysine 23 by its C-terminal RING domain [6–9]. UHRF1 is highly expressed in proliferating cells as compared with differentiated cells and its level peaks during the G1/S phase transition and G2/M phase of the cell cycle [1, 10]. In cancer cells, UHRF1 is mostly up-regulated and its levels are maintained constant throughout the cell cycle. The high levels of UHRF1 found in variety of cancers are often

* Correspondence: marc.mousli@unistra.fr
[1]Laboratoire de Biophotonique et Pharmacologie, UMR 7213 CNRS, Faculté de Pharmacie, Université de Strasbourg, 74, Route du Rhin, 67401 Illkirch Cedex, France
Full list of author information is available at the end of the article

correlated to the epigenetically silencing of tumor suppressor genes, poor prognosis and aggressiveness of the tumor [11–15]. UHRF1 is stabilized in the cells by its association with the ubiquitin specific protease 7 (USP7 or HAUSP) which prevents the proteasomal degradation of UHRF1 [16]. UHRF1 also plays an important role in regulating the stability and functions of other proteins such as DNMT1, promyelocytic leukemia protein (PML) and p53 through its interaction with other proteins such as the Tat-interacting protein 60 kDa (TIP60), USP7 and histone deacetylase 1 (HDAC1) [17–20]. UHRF1 and TIP60 were shown to be in the same epigenetic complex and to play an important role in regulating the stability and activity of DNMT1 [19, 21]. DNMT1 is acetylated by TIP60 which allows UHRF1 to ubiquitinylate DNMT1 and induce its down-regulation [19].

TIP60, initially identified as a partner of the HIV-1 Tat protein, is an evolutionary conserved and ubiquitously expressed acetyltransferase of the MYST family [22–25]. The TIP60 protein contains several domains (Fig. 1a, (i)), including a chromodomain and MYST domain endowed with acetyltransferase activity. Through these domains, TIP60 acetylates both histone and non-histone proteins. Tip60 also interacts with androgenic receptors and transcription factors and is involved in a variety of cellular activities including DNA damage response, chromatin remodeling, gene transcription, cell cycle regulation and apoptosis [26–29]. It also mediates the progression of the cell cycle by facilitating the G1/S phase transition, maintaining the genome integrity during the G1 and S phase and ensuring the faithful chromatin segregation during the M phase [30–33]. TIP60 also plays a role in regulating the activities of p53 in an acetylation-dependent and independent manner [18]. TIP60 mediated K120 acetylation in DNA binding region of p53 is necessary for the induction of apoptosis through Bcl 2-associated X protein (BAX) and p53 upregulated modulator of apoptosis (PUMA) pathway. The knockdown of TIP60 has been shown to abrogate the p21-induced cell cycle arrest after the activation of the tumor suppressor gene p53 in response to DNA damage [34–36]. Of note, UHRF1 by its direct interaction with TIP60 through the SRA and RING domains is thought to perturb the association between TIP60 and p53, preventing this latter from an acetylation-dependent activation and antitumor response [18]. Thus, a new anticancer strategy would be to restore p53 function by hindering UHRF1 to interact with TIP60. Although, the literature [18, 21] clearly suggests the occurrence of such an interaction in cells, its final demonstration is still lacking.

In order to further explore this interaction in cells and identify its determinants, we performed Fluoresecence Lifetime Imaging Microscopy (FLIM) experiments to demonstrate that UHRF1 and TIP60 physically interacts inside the cells. Through the use of deletion mutants of TIP60, we identified the key role of the MYST domain in its interaction with the UHRF1. This interaction also occurs in the S phase of the cell cycle during DNA replication.

Methods

Cell cultures

HeLa cells (ATCC, CCL-2 Amp, HeLa; Cervical Adenocarcinoma; Human) were cultured in Dulbecco's modified Eagle's medium (DMEM + GlutaMAX, Gibco, Lifetech, France) supplemented with 10% of heat inactivated fetal bovine serum and mixture of penicillin (100 U/ml) and streptomycin (100 U/ml) (penicillin/streptomycin: Invitrogen Corporation Pontoise, France) at 37 °C in 5% CO_2. Transfection of the plasmids in HeLa cells was carried by the jetPEI™ reagent (Life Technologies, Saint Aubin, France) according to the manufacturer's protocol.

Plasmid constructs

For HeLa cell transfection, UHRF1 was cloned into pCMV-mCherry vector to express UHRF1-mCherry protein while the TIP60 wild-type and mutants were cloned into a pEGFP-N1 plasmid to express eGFP-labeled TIP60 proteins in cells. For protein purification, UHRF1 was cloned into pGEX-4 T-1 to get the recombinant GST-UHRF1 fusion protein as described in [1]. For in vitro studies, TIP60 wild-type (TIP60-WT) and mutant TIP60 proteins were cloned into pET15b vector with XhoI and BamHI restriction sites to purify His tagged TIP60WT/mutants from bacteria.

Antibodies

Antibodies used in this study include the mouse monoclonal anti-UHRF1 engineered as described previously [1], mouse monoclonal anti-DNMT1 (Stressgen Canada), rabbit polyclonal anti-TIP60 (Genetex GTX 112197), rabbit polyclonal anti-mCherry (Genetex GTX 59788), mouse monoclonal anti-eGFP (Thermo Fisher Scientific A-11120 & Proteintech 66,002–1-Ig), and mouse monoclonal anti-GAPDH (Merck Millipore MAB 374). Mouse monoclonal anti-His and mouse monoclonal anti-GST antibodies were engineered in our core facilities (IGBMC, Illkirch, France).

Protein purification and pull-down assays

For protein purification, the plasmids were transfected in BL21 cells and cells were allowed to grow at 37 °C until the absorbance of the culture reached 0.5–0.6. Expression of the proteins was induced by the addition of 1 mM isopropyl-1-thio-β-D-galactopyranoside (IPTG) and the cells were further incubated at 25 °C for 4 h before collecting the proteins. GST-tagged UHRF1 protein

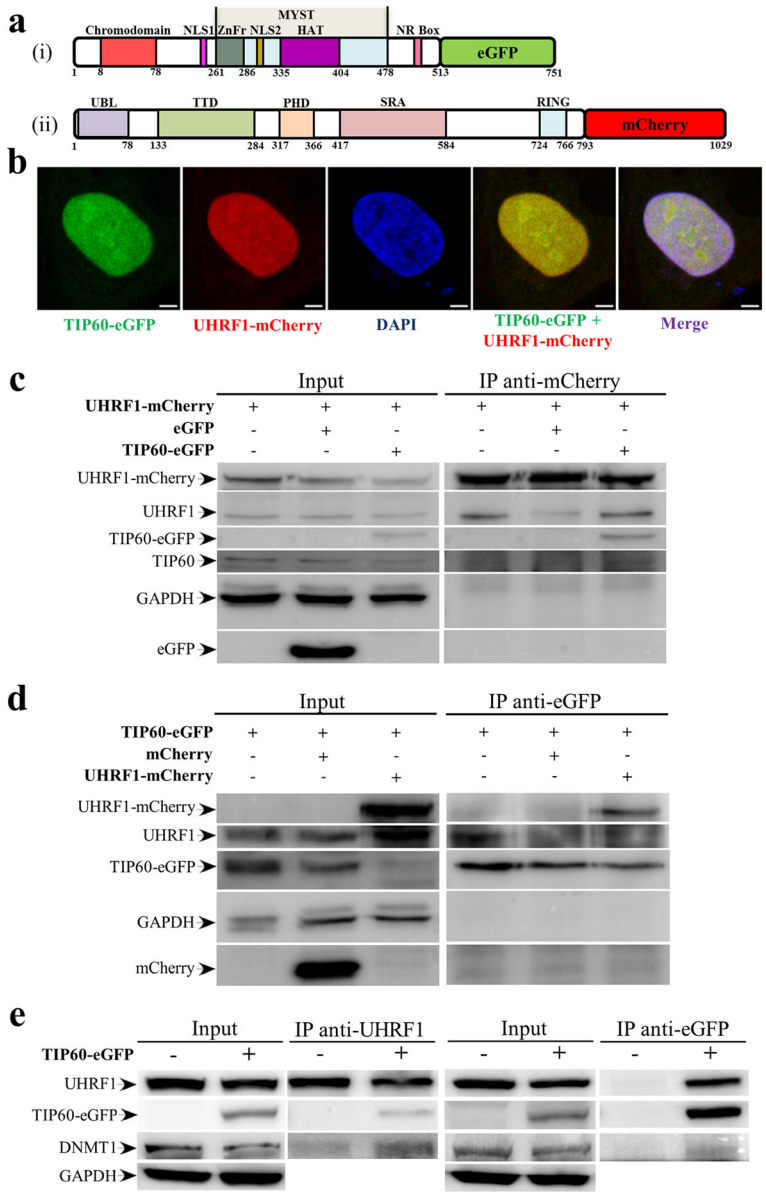

Fig. 1 TIP60 interacts with UHRF1 and DNMT1 in HeLa cells. **a** Schematic diagram of TIP60 wild type tagged with eGFP (i) and UHRF1 tagged with mCherry (ii) at their C-terminus. **b** Transfection of TIP60-eGFP and UHRF1-mCherry in the nucleus of HeLa cells. White bar indicates size of 5 μm. **c** Immunoprecipitation of UHRF1-mCherry with anti-mCherry antibody co-immunoprecipitating exogenous TIP60-eGFP and endogenous TIP60. **d** Reciprocal immunoprecipitation of TIP60-eGFP with anti-eGFP antibody co-immunoprecipitating exogenous UHRF1-mCherry and endogenous UHRF1. **e** DNMT1 co-immunoprecipitate with UHRF1 and TIP60-eGFP using anti-UHRF1 and anti-eGFP antibody respectively

was purified from the cell lysate using Glutathione Sepharose 4B beads (GE Healthcare Life Sciences 17–0756-05) while the His-tagged wild-type and mutant TIP60 proteins were purified using Ni-NTA agarose beads (Qiagen 30,230) in appropriate buffers. Wild-type and mutant TIP60 proteins were immobilized on the Ni-NTA agarose beads and equal quantity of GST-UHRF1 was added in PBS containing 30 mM imidazole and 0.1% triton to study protein-protein interaction. The immobilized beads were washed five times before being analyzed by SDS-PAGE.

Fluorescence lifetime imaging microscopy (FLIM)

For FLIM measurements, 10^5 cells were seeded in a μ-dish 35 mm, glass bottom grid-50 (Ibidi 81,148) wells and were co-transfected with 0.75 μg TIP60-eGFP and 0.75 μg UHRF1-mCherry plasmids by using jetPEI™ reagent as described in manufacturer's protocol. After 24 h of transfection, cells were incubated for 20 min with 10 μM 5-ethynyl-2′-deoxyuridine (EdU) containing media before fixation with 3.7% paraformaldehyde. After fixation, cells were analyzed with a homemade two-photon excitation

scanning microscope based on an Olympus IX70 inverted microscope with an Olympus 60X 1.2 NA water immersion objective operating in the descanned fluorescence collection mode as described [37]. Two-photon excitation at 930 nm was provided by an Insight DeepSee laser (Spectra Physics). Photons were collected using a short pass filter with a cut-off wavelength of 680 nm (F75–680, AHF, Germany) and a band-pass filter of 520 ± 17 nm (F37–520, AHF, Germany). The fluorescence was directed to a fiber coupled APD (SPCM-AQR-14-FC, Perkin Elmer), which was connected to a time-correlated single photon counting module (SPC830, Becker & Hickl, Germany). FLIM data were analyzed using the SPCImage v 4.0.6 (Becker & Hickel) software. The Förster resonance energy transfer (FRET) efficiency was calculated according to $E = 1- (\tau_{DA}/\tau_{D})$, where τ_{DA} is lifetime of donor (eGFP) in the presence of acceptor (mCherry) and τ_{D} is the lifetime of donor in the absence of acceptor.

Confocal microscopy

The cells imaged by FLIM were also imaged by confocal microscopy. The same cells could be imaged by both techniques, by locating the cells with the help of coordinates on the ibidi well. Prior to confocal microscopy the cells in S phase were labeled with the Click-iT® EdU Alexa Fluor® 647 Imaging Kit (Thermo Fisher Scientific USA C10340) according to the manufacturer's protocol. For transfection and localization analysis, cells were co-transfected with TIP60-eGFP WT/mutants and UHRF1-mCherry and were labeled with DAPI after fixation to stain the nucleus. All samples were imaged with a Leica SPE equipped with a 63× 1.4NA oil immersion objective (HXC PL APO 63×/1.40 OIL CS). The images were further processed with Image J software.

Immunoprecipitation and western blotting

For Western blot, cells were harvested 24 h post-transfection by mild trypsinization. After washing with PBS, cells were lysed by ice cold lysis buffer 10 mM Tris-HCl pH 7.5, 150 mM NaCl, 1 mM EDTA and 1% NP40 supplemented with protease inhibitors (complete mini EDTA free protease inhibitor cocktail tablets, Roche Germany 11,836,170,001). Cell lysates (40 μg of the protein) were loaded onto 10% SDS-PAGE gels after denaturation for 5 min in Laemmli sample buffer (Bio-Rad Laboratories USA 1610747). The proteins were identified by anti-UHRF1, anti-eGFP, anti-DNMT1 and anti-GAPDH antibodies with overnight incubation at 4 °C. Primary antibodies were labeled with secondary anti-mouse (Promega, W402B) or anti-rabbit antibodies (Promega, W401B) conjugated with horseradish peroxidase and were visualized with the chemiluminescent ECL system (Clarity™ ECL western blotting substrate, Biorad, 170–5060) on an Image Quant LAS 4000 apparatus. Images were analyzed using the Image Studio Lite (Li-Core Biosciences, USA). For co-immunoprecipitation, the cells were collected and lysed by freeze shock and sonication in PBS supplemented with protease inhibitor cocktail tablet. A fraction of 40 μg of protein from each lysate was saved to serve as input control while 800 μg to 1 mg of protein lysate was incubated with appropriate antibodies for 4 h at 4 °C for subsequent immunoprecipitation. After washing and equilibration, 50 μL of Dynabeads® Protein A (Thermo Fisher Scientific Norway 10002D) were added to the lysate-antibody mixture and incubated for 1 h at 4 °C. Beads were collected later and washed five times in lysis buffer. They were then resuspended in Laemmli sample buffer (Bio-Rad Laboratories, USA). Proteins denatured by heating at 95 °C for 5 min were analyzed through Western blotting.

Global DNA Methylation analysis

HeLa cells were transiently transfected with TIP60-eGFP and mutants and were analyzed for global methylation levels by using Sigma's Imprint® Methylated DNA Quantification Kit Sigma-Aldrich). Briefly DNA was extracted from the cells using QIAamp® DNA Kit (Qiagen) and 200 ng of purified DNA were used for global DNA methylation level analysis according to the manufacturer's protocol.

Statistical analysis

The results were statistically analyzed using GraphPadPrism (version 5.04) and Origin (version 8.6).

Results

UHRF1 and TIP60 interaction inside the cells

In order to study the interaction between TIP60 and UHRF1, we expressed eGFP-tagged TIP60 (Fig. 1a, (i)) and mCherry-tagged UHRF1 (Fig. 1a, (ii)) in HeLa cells. The two proteins were expressed and co-localized with DAPI inside the nucleus of HeLa cells as seen by the merge (Fig. 1b). The interaction between UHRF1 and TIP60 proteins was assessed in vitro by co-immunoprecipitation experiments. Immunoprecipitating UHRF1-mCherry by using anti-mCherry antibody led to the co-immunoprecipitation of both endogenous TIP60 and exogenous TIP60-eGFP while free eGFP which was co-transfected with UHRF1-mCherry did not co-immunoprecipitate with it (Fig. 1c). This shows specific interaction of UHRF1-mCherry with endogenous TIP60 and exogenous TIP60-eGFP. Similarly, reciprocal co-immunoprecipitation experiments were performed by immunoprecipitating TIP60-eGFP with anti-eGFP antibody in cells (Fig. 1d). Immunoprecipitation of TIP60-eGFP led to co-immunoprecipitation of UHRF1-mCherry and endogenous UHRF1 while it did not immunoprecipitate free mCherry suggesting specific interaction between UHRF1 and TIP60 in the cells. Therefore, we can

assume that tagged proteins correctly localize in the nucleus of HeLa cells and can mimic the interaction pattern of endogenous proteins. It is interesting to note that UHRF1-mCherry co-expression resulted in lower levels of TIP60-eGFP recombinant protein (Fig. 1d) as compared with cells transfected with TIP60-eGFP or co-transfected with mCherry alone.

LikeTIP60, DNMT1 has also been reported to be associated with UHRF1 in the same protein complex [21]. So, in order to check the presence of DNMT1 in UHRF1/TIP60 complex, we also performed co-immunoprecipitation experiments. DNMT1 co-immunoprecipitated with the UHRF1 in normal HeLa cells or cells with overexpressed TIP60-eGFP (Fig. 1e). Overexpressed TIP60-eGFP also interacted with endogenous DNMT1 as DNMT1 co-immunoprecipitated with TIP60-eGFP along with UHRF1 showing the presence of the three proteins together in the same complex (Fig. 1e). This supports that the tag of TIP60-eGFP does not hinder it to adequately interact with its partners like DNMT1.

However, the results obtained with immunoprecipitation cannot confirm the interaction of proteins in vivo and do not explain the presence or absence of a close dialogue between the two proteins inside the cell.

Therefore, we studied the interaction between UHRF1 and TIP60 in cells using the FLIM-FRET technique which allows monitoring of very close contact (< 10 nm) between two proteins inside a cell. TIP60-eGFP served as the FRET pair donor because of the mono-exponential decay and high quantum yield of eGFP while the UHRF1-mCherry served as the FRET pair acceptor in these experiments as the absorption spectrum of mCherry falls in the emission spectrum of the eGFP. FRET occurs only when the two fluorophores are in close proximity to each other and can be unambiguously evidenced by a decrease of lifetime of the donor. By using FLIM microscopy, the lifetime of eGFP is calculated and color coded in each pixel of the image. The red to blue color covers lifetime ranging from 1.8 ns to 2.8 ns. FLIM images were recorded for TIP60-eGFP transfected cells (Fig. 2a, (i)) and cells co-transfected with TIP60-eGFP and UHRF1-mCherry (Fig. 2a, (ii)). The resulting distributions of fluorescent lifetimes are given in (Fig. 2a, (iii)). The average lifetime of TIP60-eGFP was 2.52 ± 0.01 ns in the cells transfected with TIP60-eGFP alone (Fig. 2b) or co-transfected with free mCherry (data not shown). However, the lifetime of eGFP was significantly reduced when TIP60-eGFP was co-transfected with UHRF1-mCherry in 1:1 ratio (Fig. 2b). The average lifetime of eGFP in co-transfected cells was 2.15 ± 0.02 ns, which corresponds to a mean FRET efficiency of 14.3 ± 0.6% (Fig. 2b). Altogether, these findings demonstrate that TIP60-eGFP interacts with UHRF1-mCherry in HeLa cells.

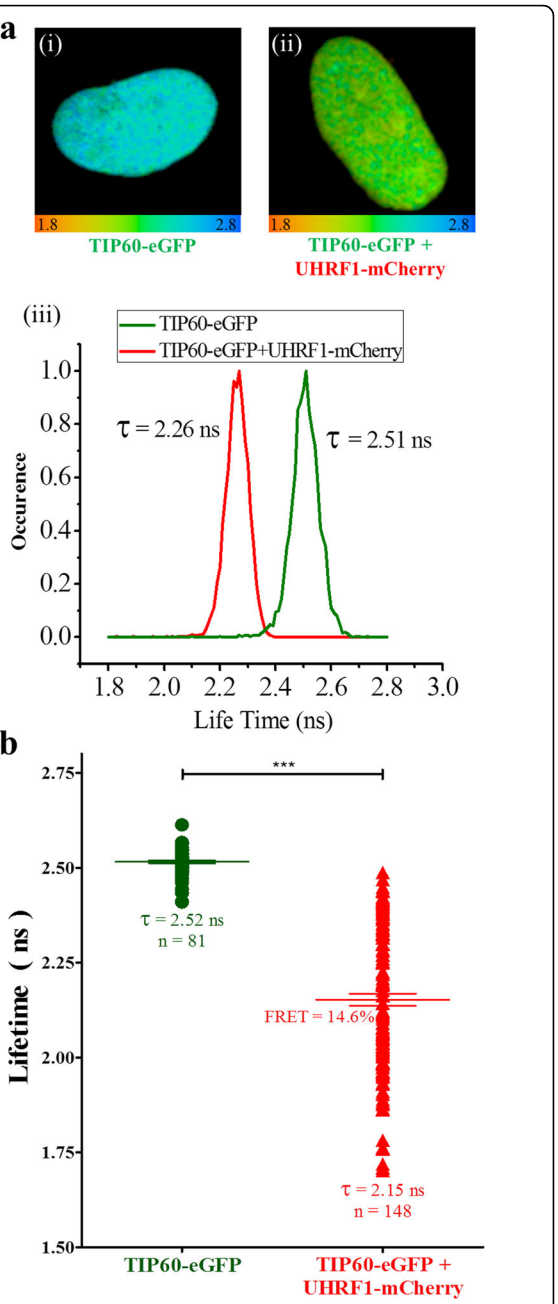

Fig. 2 Interaction of TIP60-eGFP with UHRF1-mCherry evidenced by FRET-FLIM. **a** 25 μm × 25 μm FLIM images of HeLa cells transfected with TIP60eGFP (i) or co-transfected with TIP60-eGFP and UHRF1-mCherry (ii) and lifetime distribution curve (iii). Color coded images indicate the fluorescence lifetime of TIP60-eGFP at each pixel. Color scale codes for lifetimes ranging from 1.8 ns (red) to 2.8 ns (blue). **b** Fluorescence lifetimes in TIP60-eGFP (●) and TIP60-eGFP + UHRF1-mCherry co-transfected cells (▲). Values are means ± SEM from five independent experiments. For statistical analysis, a Student's *t*-test was performed (*** $P < 0.001$)

UHRF1 and TIP60 interaction occurs during S phase of the cell cycle

UHRF1 localization and its association with other proteins dynamically changes during the cell cycle. NP95, the murine homologue of UHRF1 associates with PCNA and chromatin in early and mid S phase of cell cycle. Moreover UHRF1 interaction with DNMT1 for maintenance of DNA methylation pattern is also dependent on the S phase of cell cycle and is more pronounced in mid and late S phase of cell cycle [38–40]. Since both UHRF1 and TIP60 are also regulating the DNMT1 levels [19] and TIP60 is also playing important roles during the G1/S phase transition and S phase of the cell cycle [30, 33], we focused on S phase to decipher the interaction between UHRF1 and TIP60. Therefore, we labeled S phase cells undergoing DNA replication with EdU (thymidine analogue) for 15 min before fixation and then, we performed FLIM analysis (Fig. 3). After this, S phase cells were identified using alexa 647 labeling for confocal microscopy study. Different sub-phases of S phase were identified by the characteristic staining of EdU which gets incorporated into the genome at the sites of active replication [41]. Early S phase cells have numerous replication foci in the nucleus as evident by bright and abundant EdU labeling in nucleus of HeLa cells (Fig. 3a). In mid S phase the replication foci are more localized to periphery of nucleus and surrounding the nucleolus (Fig. 3b) while in late S phase, very few irregular replication foci are found in nucleus at heterochromatin regions of genome (Fig. 3c). The lifetime of the TIP60-eGFP was found to be decreased in the different sub-phases of the S phase (Fig. 3a-c). When the average lifetime of TIP60-eGFP in S phase cells was compared to the total cells, it was decreased to 2.12 ± 0.03 ns and the overall FRET efficiency increased to 16.0 ± 1.2% in the S phase positive cells (Fig. 3d). These results confirm UHRF1/ TIP60 interaction during the S phase of cell cycle.

TIP60 interacts with UHRF1 through its MYST domain

It is known that UHRF1 interacts with TIP60 through its SRA and RING domains and hinders the association of TIP60 with p53 and K120 acetylation of p53 [18]. However, the TIP60 domain responsible for its interaction with UHRF1 remains to be determined. Therefore, in this study we performed in vitro pull-down assay to identify the domain of TIP60 that is responsible for interaction with UHRF1. For this, we used His-tagged mutants of the TIP60 (Fig. 4a) immobilized on Nickel NTA agarose beads and the GST-UHRF1. We observed that full length UHRF1 interacted with TIP60WT in the presence of 150 mM NaCl (Fig. 4b-c) until 500 mM NaCl (data not shown) supporting a strong interaction between both proteins. Deletion of the TIP60 zinc finger domain or the whole MYST domain significantly reduced its association with GST-UHRF1 in the pull-down assay (Fig. 4b-c). In contrast, deletion of the chromodomain and HAT domains did not significantly affect their interaction with UHRF1. Recombinant TIP60 MYST domain also had a strong association with UHRF1 like the wild type TIP60 protein (Fig. 4b-c) and this interaction was stable up to 1 M NaCl salt concentration (data not shown) predicting the TIP60 MYST domain is playing a key role in this interaction.

The FLIM-FRET technique employing different mutants of TIP60 tagged with eGFP (Fig. 5a) was further used to identify the interacting domain of TIP60 with UHRF1-mCherry inside the nucleus of HeLa cells. TIP60-eGFP wild type and mutants were co-transfected with UHRF1-mCherry and the lifetime of eGFP was measured to assess the interaction. We found that the interaction of TIP60 and UHRF1 was marginally affected by removal of TIP60 chromodomain as the average FRET of TIP60ΔCRD-eGFP co-transfected with UHRF1-mCherry was of 12.2 ± 1.3% as compared to 14.3 ± 0.6% for TIP60WT-eGFP (Fig. 5b). All other mutations affecting the MYST domain of TIP60 strongly perturbed the interaction of these mutants with UHRF1. Indeed, the lifetime of TIP60ΔZnFr-eGFP, TIP60ΔHAT-eGFP and TIP60ΔMYST-eGFP co-transfected with UHRF1-mCherry was 2.49 ± 0.01 ns, 2.46 ± 0.01 ns and 2.49 ± 0.01 ns, respectively which is quite similar to that in control sample with 2.52 ± 0.01 ns (Fig. 5b). To check whether this loss of interaction is not a result of an alteration of subcellular localization, we performed a confocal microscopy analysis of co-transfected HeLa cells. We observed that TIP60WT-eGFP and its mutants including TIP60ΔCRD-eGFP, TIP60ΔZnFr-eGFP, TIP60ΔHAT-eGFP and TIP60ΔMYST-eGFP are localized in the nucleus of HeLa cells (Fig. 6). It is also important to note that TIP60WT and mutants co-localized with UHRF1-mCherry as shown in merge panels and were closely associated to DNA labeled by DAPI. This indicates that the loss of interaction between TIP60ΔZnFr, TIP60ΔHAT and TIP60ΔMYST with UHRF1 is not due to protein delocalization.

In order to check the heterogeneity of lifetime populations in TIP60-eGFP wild type or TIP60ΔCRD-eGFP co-transfected cells showing FRET, the FLIM images were also analyzed by a two-component model: $F(t) = \alpha_1 e_1^{-t/\tau} + \alpha_2 e_2^{-t/\tau}$ [37]. This analysis provides the distribution and population of TIP60-eGFP molecules interacting with UHRF1-mCherry (having FRET) and the TIP60-eGFP molecules which are free in nucleus without having interaction with UHRF1-mCherry (having no FRET). The lifetime for the long lifetime component (τ_2) (having no FRET) was fixed according to the lifetime of eGFP in only TIP60-eGFP transfected samples, while the lifetime (τ_1) of the short

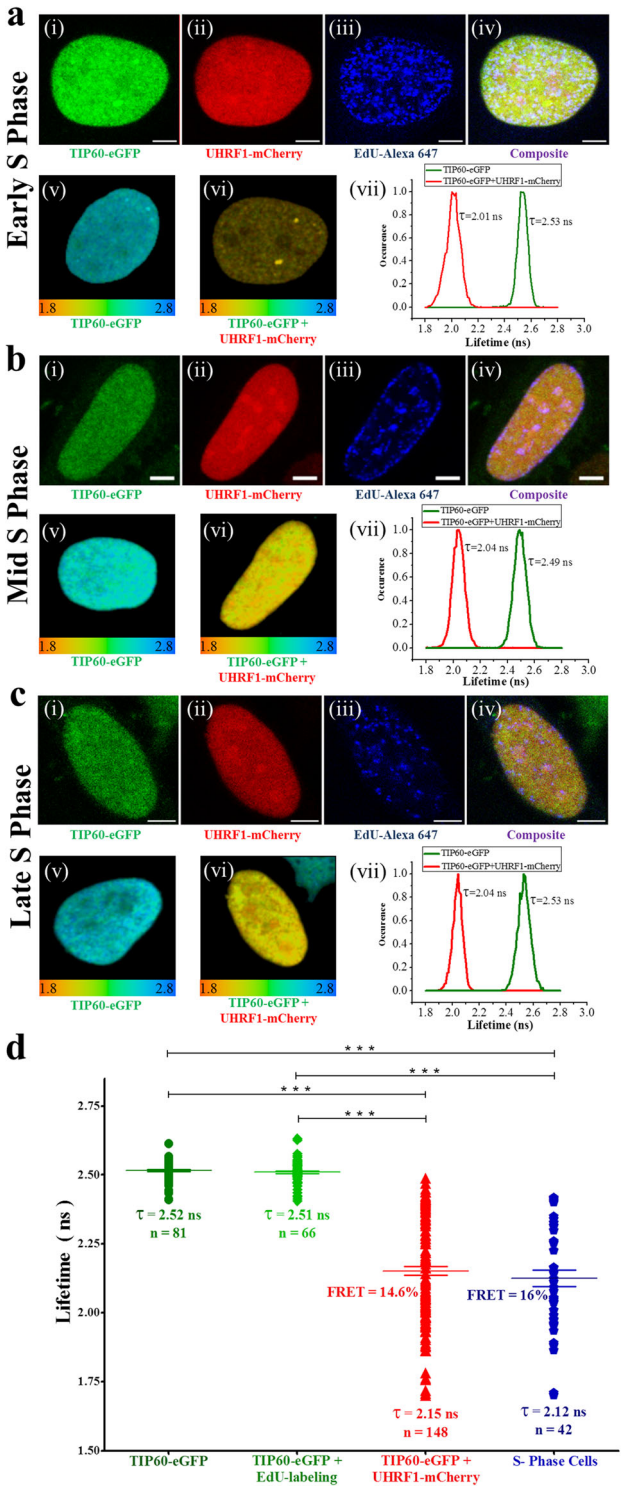

Fig. 3 Interaction between TIP60-eGFP and UHRF1-mCherry in S phase of cell cycle. **a-c** TIP60-eGFP interaction with UHRF1-mCherry in early, mid and late S phases of cell cycle, respectively. Confocal images of cells labeled with TIP60-eGFP, UHRF1-mCherry, EdU-Alexa 647 and merge, respectively (i - iv). The white bar indicates size of 5 μm. 25 μm × 25 μm FLIM images of HeLa cells transfected with TIP60-eGFP (v) or co-transfected with TIP60-eGFP and UHRF1-mCherry (vi) and lifetime distribution curves of the respected cells (vii). Color scale codes for lifetimes ranging from 1.8 ns (red) to 2.8 ns (blue). **d** Fluorescence lifetime distributions of TIP60-eGFP (●), TIP60-eGFP EdU labeled cells (◆), total TIP60-eGFP + UHRF1-mCherry co-transfected cells (▲) and co-transfected cells in S-phase of cell cycle (⬟). Values are means ± SEM from five independent experiments. For statistical analysis, a Student's *t*-test was performed (*** $P < 0.001$)

component (having FRET) and the populations of both component (α_1 and α_2) were obtained from the fits. The short lifetime component (τ_1) in TIP60WT-eGFP and TIP60ΔCRD-eGFP samples having FRET because of interaction with UHRF1-mCherry are shown in green or warmer color in FLIM images (Fig. 7a-b). The lifetime distribution curves of these FRET components for TIP60WT-eGFP and TIP60ΔCRD-eGFP are depicted in Fig. 7c. The mean value of the short lifetime component in TIP60WT-eGFP samples was 1.33 ± 0.01 ns and the average FRET calculated for this component was 45 ± 0.6% indicating close association of TIP60-eGFP with UHRF1-mCherry in HeLa cells. The mean value of the short component in TIP60ΔCRD-eGFP was 1.4 ± 0.03 ns and the average FRET calculated for this component was 43 ± 1.1% (Fig. 7c). Though the short lifetime component had almost similar values in TIP60WT-eGFP and TIP60ΔCRD-eGFP samples, the values of its corresponding population were different in the two samples as shown in Fig. 7d-e. TIP60WT-eGFP had higher population (α_1) of interacting short lifetime component as compared to TIP60ΔCRD-eGFP as its mean value in TIP60WT-eGFP was 37.5 ± 1.2% while it was 19 ± 0.3% in TIP60ΔCRD-eGFP as indicated from their respective distribution curves (Fig. 7f). This shows that TIP60ΔCRD-eGFP can interact with UHRF1-mCherry inside the nucleus but with less efficiency than TIP60WT-eGFP.

TIP60 overexpression down-regulates UHRF1 and DNMT1

Down-regulation of TIP60 has been reported in many cancers [42–45] and TIP60 has a well-established role in regulation of DNMT1. So, we investigated the consequences of TIP60-eGFP overexpression on UHRF1 and DNMT1 in HeLa cells in order to decipher the relationship between these epigenetic partners in the tumorigenesis process. Overexpression of TIP60 led to down-regulation of UHRF1 and DNMT1 in HeLa cells (Fig. 8a). UHRF1 levels were significantly reduced in TIP60-eGFP transfected cells as compared to that in untreated control cells, i.e., without any treatment or cells treated with jetPEI or transfected with eGFP alone (Fig. 8b). Similarly, DNMT1 levels were also significantly reduced in cells overexpressing TIP60-eGFP (Fig. 8c). It is interesting to observe that DNMT1 and UHRF1 levels were not affected by the overexpression of TIP60ΔMYST-eGFP in the nucleus which lacks the acetyltransferase domain of TIP60. Further, we also analyzed the effect of TIP60-eGFP overexpression on global DNA methylation levels. In accordance with the decrease in UHRF1 and DNMT1 levels, global DNA

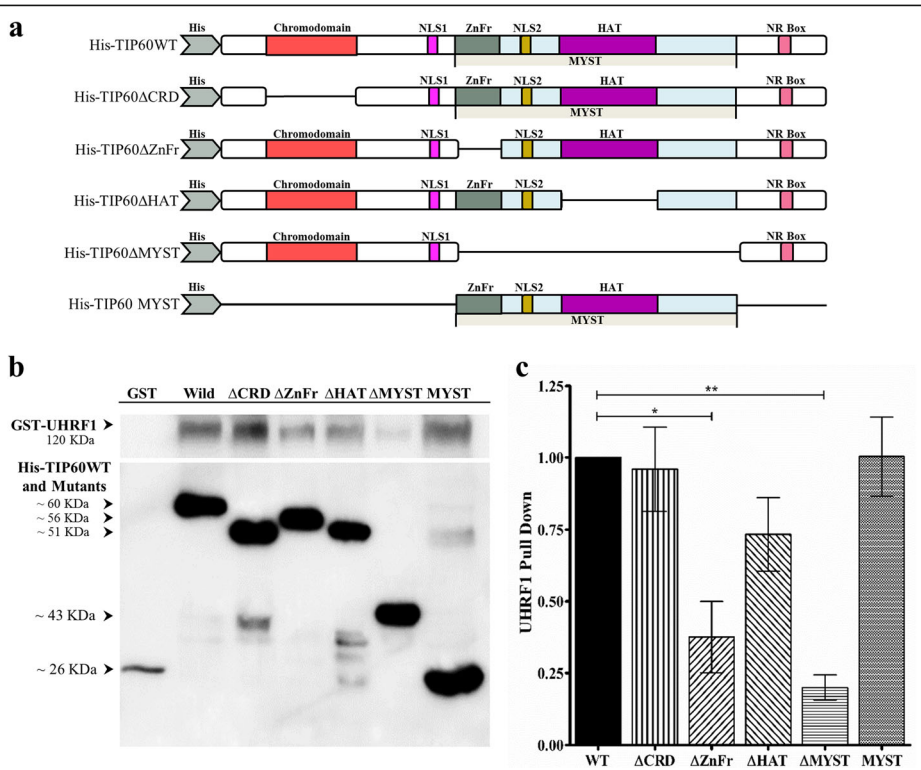

Fig. 4 In vitro pull-down analysis between His-TIP60WT/mutants and GST-UHRF1. **a**, Diagram showing His tag TIP60 wild type and mutants. **b** Western blot of in vitro pull-down assay. His tagged TIP60-WT or mutants were immobilized on Ni-NTA beads and incubated with UHRF1-GST. The complex recovered after washing were subjected to SDS PAGE and analyzed by Western blot. **c**. Western blot images were quantified by Image Studio Lite (Li-Core Biosciences USA) and statistically analyzed by using Student's *t*-test. Values are means ± SEM from three independent experiments (* $P < 0.05$, ** $P < 0.01$)

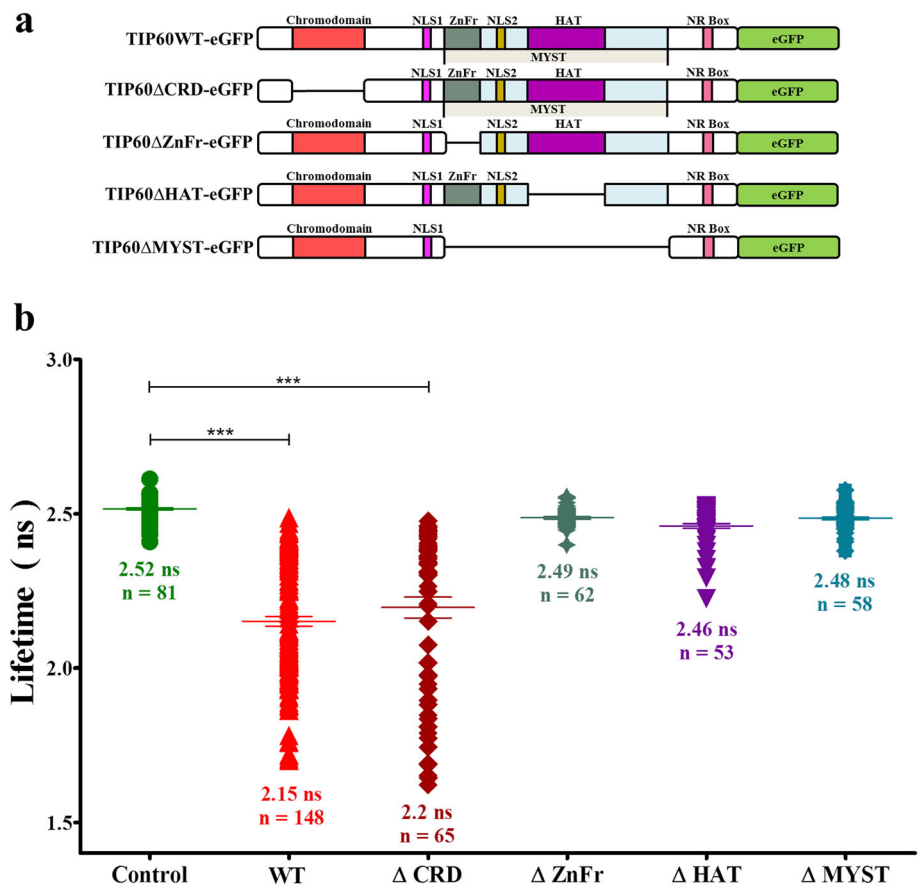

Fig. 5 Interaction between TIP60-eGFP WT/mutants and UHRF1 evidenced by FRET-FLIM. **a** Schematic diagram of TIP60WT/mutants tagged with eGFP at the C-terminus. **b** Lifetime distribution of TIP60-eGFP (●), TIP60 WT-eGFP + UHRF1-mCherry co-transfected cells (▲), TIP60 ΔCRD-eGFP + UHRF1-mCherry co-transfected cells (◆), TIP60 ΔZnFr-eGFP + UHRF1-mCherry co-transfected cells (✦), TIP60 ΔHAT-eGFP + UHRF1-mCherry co-transfected cells (▼), TIP60 ΔMYST-eGFP + UHRF1-mCherry co-transfected cells (✿). Values are means ± SEM from three to five independent experiments. For statistical analysis, a Student's *t*-test was performed (*** $P < 0.001$)

methylation also decreased by 26% after overexpression of TIP60WT-eGFP in 24 h of transfection (Fig. 8d). Overexpression of TIP60ΔCRD-eGFP also decreased the global DNA methylation by 21% (Fig. 8d), however, over expressing TIP60ΔZnFr-eGFP and TIP60ΔMYST-eGFP only lowered the DNA methylation by 9%. Overexpression of TIP60ΔHAT-eGFP had minimal effect on global DNA methylation which decreased only by 5% (Fig. 8d). Altogether these results suggest TIP60 as a regulator of DNMT1, UHRF1 and DNA methylation levels through its enzymatic activity.

Discussion

UHRF1 and TIP60 are part of large protein complexes and their conformation and association with other partners vary with the genomic activity and are regulated during cell cycle [46, 47]. Our results provided evidence for in vivo and in vitro interaction between UHRF1 and TIP60 protein by using the FLIM-FRET technique and pull-down assay. Furthermore, we could also show that MYST domain of TIP60 is playing a major role in its interaction with UHRF1. MYST domain is the conserved part of TIP60 containing a zinc finger involved in protein-protein interaction and a catalytic domain harboring its acetyltransferase activity [47]. In fact, through its MYST domain, TIP60 is able to acetylate both histones and non-histones proteins and regulates the activity of many proteins such as ATM and p53 [25, 36, 48]. Since p53-mediated apoptosis is dependent on its acetylation by TIP60 [35] therefore, interaction of TIP60 through its MYST domain with UHRF1 might impair many cellular functions. This may also explain how overexpressed UHRF1 in cancer negatively regulates the TIP60-p53 interplay in cells by preventing induction of cell cycle arrest and apoptosis. It is interesting to note that although chromodomain is not playing a direct role in its association with UHRF1 as indicated by FLIM and pull-down experiments, its removal can adversely also affect this interaction in vivo. According to two-component model, removal of chromodomain did not

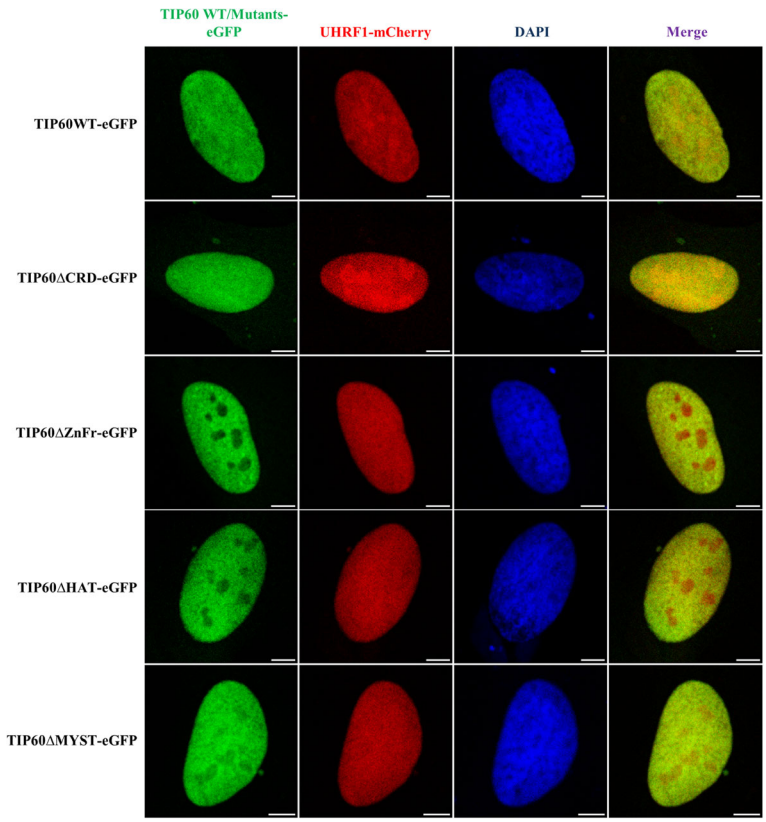

Fig. 6 Expression and localization of TIP60 mutants in HeLa cells. Confocal images show the expression and co-localization of TIP60WT-eGFP and mutants with UHRF1-mCherry in the HeLa cells with DAPI labeling. Green panel indicates TIP60 wild type or mutants tagged with eGFP, red panel shows UHRF1-mCherry, blue panel indicates DAPI and merge panel shows the composite of the TIP60-eGFP and UHRF1-mCherry panels. White bar indicates size of 5 μm

have a big impact on the mean lifetime of short component and FRET efficiencies as compared with wild type. However, the population interacting with UHRF1 was drastically reduced when chromodomain was removed from the structure of TIP60. Chromodomain helps TIP60 in reading out the histone marks and its loading to chromatin which may increase the possibility of TIP60 to interact with UHRF1 present in the same complex [49–51].

UHRF1 is a multi-domain protein which is essential for maintaining the DNA methylation during S phase of cell cycle by recruiting DNMT1 to the replication foci where it forms a multi protein complex with PCNA, DNMT1, TIP60, HDAC1, USP7 and other epigenetic partners [38, 52]. TIP60 is also well known for its role in DNA damage response to interstrand cross linkages or double strand breaks as TIP60-mediated H4K16 acetylation promotes DNA damage repair by homologous recombination (HR) pathway which dominates during the S phase of cell cycle [53, 54]. Recently the role of UHRF1 in DNA damage response has also been reported as it identifies interstrand cross linkages and double strand breaks and facilitates DNA damage repair by the same homologous recombination (HR) pathway through interaction with common partners such as FANCD2 and BRCA1 [55–57]. This predicts that UHRF1 and TIP60 may also work together in coherence to facilitate the DNA damage repair during S phase of cell cycle.

TIP60 along with UHRF1 is known to regulate levels of DNMT1 during cell cycle by inducing proteasomal degradation of DNMT1 through TIP60-mediated acetylation and subsequent ubiquitination by UHRF1 [19, 58, 59]. Accordingly, we have observed increased association of DNMT1 with UHRF1 in TIP60-eGFP transfected samples through co-immunoprecipitation experiments confirming the previous findings. DNMT1 is stabilized in cells by its direct association with USP7, a deubiquitinating enzyme which is present in the same complex. It has been recently reported that TIP60 impairs this protective association of USP7 with DNMT1 by acetylation [60]. Besides DNMT1, UHRF1 is also prevented from proteasomal degradation through its association with USP7 [16, 61, 62] and interruption of this association through cell cycle dependent kinase leads to proteasomal degradation of UHRF1 in M phase [16]. Zang and collaborators have recently suggested an identical role of

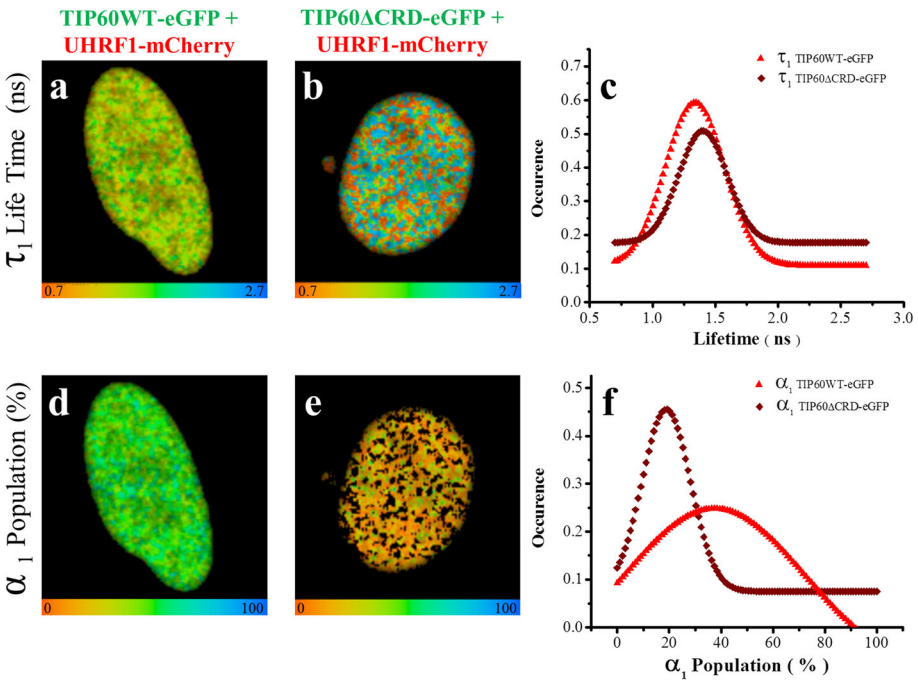

Fig. 7 Two component analyses of the fluorescence decays of TIP60WT-eGFP and TIP60ΔCRD-eGFP lifetime in presence of UHRF1-mCherry. Fluorescence decays were measured at each pixel for the respective cells by using bi-exponential model. In this model, the long-lived lifetime component (τ_2) was fixed to the lifetime of Tip6WT-eGFP when it is transfected alone in HeLa cells (2.52 ns). **a** 25 μm × 25 μm FLIM image of the distribution of τ_1 lifetimes of TIP60WT-eGFP in the presence of UHRF1-mCherry (corresponding to the component undergoing FRET). **b** 25 μm × 25 μm FLIM image of the distribution of τ_1 lifetimes of TIP60ΔCRD-eGFP in the presence of UHRF1-mCherry (corresponding to the component undergoing FRET). Color scale codes for lifetimes ranging from 0.7 ns (red) to 2.7 ns (blue). **c** Distribution of τ_1 lifetimes of TIP60WT-eGFP and TIP60ΔCRD-eGFP transfected cells in presence of UHRF1-mCherry. **d** 25 μm × 25 μm FLIM image of the population α_1 of TIP60WT-eGFP undergoing FRET in the presence of UHRF1-mCherry. **e** 25 μm × 25 μm FLIM image of the population α_1 of TIP60ΔCRD-eGFP undergoing FRET in the presence of UHRF1-mCherry. Color scale codes for population ranging from 0% (red) to 100% (blue). **f** Distribution of population α_1 for TIP60WT-eGFP and TIP60ΔCRD-eGFP transfected cells in presence of UHRF1-mCherry. Values indicated are from 148 TIP60WT-eGFP and UHRF1-mCherry co-transfected cells from five independent experiments and 65 TIP60ΔCRD-eGFP and UHRF1-mCherry co-transfected cells from three independent experiments

TIP60 in regulating the stability of UHRF1 as it regulates the stability of DNMT1. They demonstrated that UHRF1 can be acetylated by TIP60 at the K659 which lies in preferential binding area of USP7 and this acetylation greatly hampered the association of USP7 with UHRF1 [63]. Our results showed that TIP60 interacts with UHRF1 through its enzymatic MYST domain and overexpression of TIP60 in HeLa cells led to downregulation of UHRF1 suggesting another mechanism for the regulation of UHRF1 in cells.

TIP60 is found downregulated in different types of cancers and is believed to have tumor suppressor properties as oncovirus like HPV induces proliferation and tumorigenesis by destabilizing TIP60 in cervical cancer cells [42–45, 64–66]. Downregulation of TIP60 is associated with increased metastasis, decreased DNA damage response to oncogenes and poor survival of patients while enhanced TIP60 levels counters DNMT1-SNAIL2 driven epithelial to mesenchymal transition and inhibits metastasis [67]. UHRF1 on the other hand, is known to play an oncogenic role in cancer as its high expression in cancer is often related to downregulation of tumor suppressor genes through promoter hypermethylation [52, 68]. We observed that overexpression of UHRF1-mCherry decreases the protein level of TIP60-eGFP (Fig. 1d) which might be attributed to promoter hypermethylation or the E3 ligase activity of UHRF1 through which it can ubiquitinate TIP60 and may possibly reduce the level of TIP60-eGFP inside the cells [18]. This is in agreement with our previous findings where knock down of UHRF1 through siRNA upregulated the TIP60 levels in Jurkat cells [21]. It is also reported that targeting UHRF1 and DNMT1 can affect the global methylation [69, 70] and re-expression of tumor suppressor genes [2]. Our results showed that TIP60 overexpression in HeLa cells induced downregulation of UHRF1 and DNMT1, resulting in global DNA hypomethylation.

Conclusion

Epigenetic code replication machinery is a multi-protein complex which is actively involved in maintaining the epigenetic marks after the DNA replication. TIP60 and

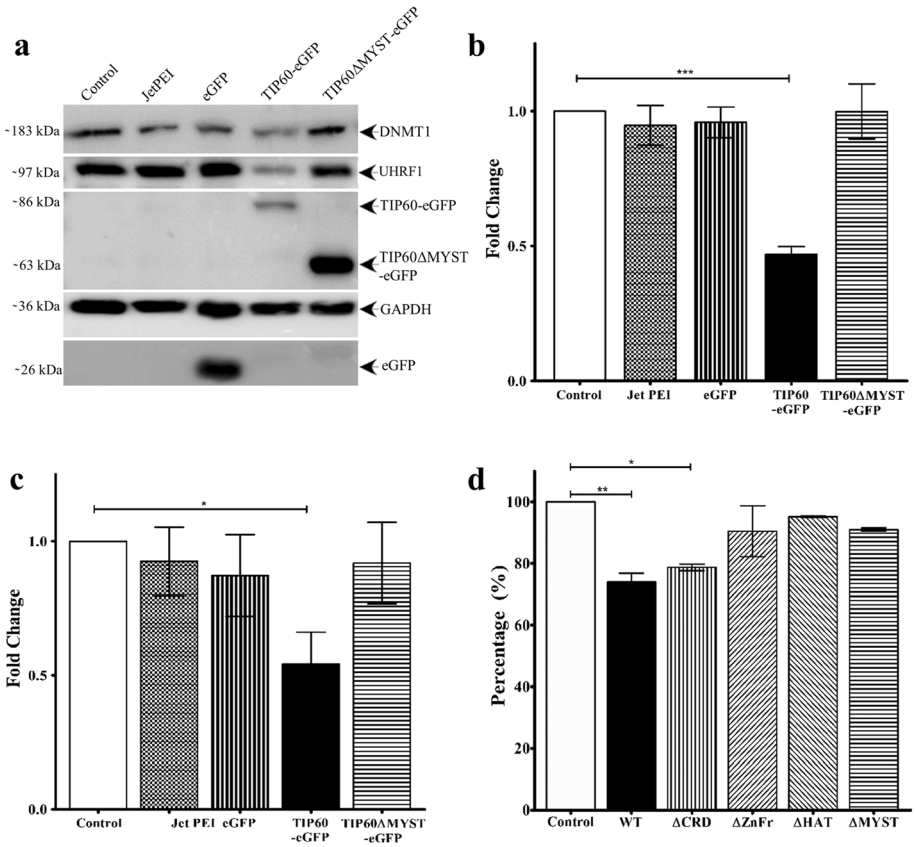

Fig. 8 TIP60 overexpression down-regulates its epigenetic partners UHRF1 and DNMT1. TIP60-eGFP was overexpressed in HeLa cells and the effect of this transient overexpression was compared to that of the control HeLa cells, HeLa cells with transfecting agent (JetPEI), HeLa cells with transfection of eGFP alone or TIP60**Δ**MYST-eGFP. **a** Western blot results showing down-regulation of UHRF1 and DNMT1 in TIP60-eGFP transfected cells. **b** Analysis of effect of TIP60-eGFP overexpression on UHRF1. **c**, Analysis of effect of TIP60-eGFP overexpression on DNMT1. Results indicated are from five independent experiments which are analyzed statistically by Student's *t*-test (* $P < 0.05$, ** $P < 0.01$, *** $P < 0.001$). **d** Effect of TIP60-eGFP overexpression on global DNA methylation. DNA was extracted from HeLa cells transfected with TIP60WT-eGFP and mutants and the methylation levels were compared to control HeLa cells. Results are indicated from three independent experiments and were analyzed by one-way ANOVA with post-hoc Tukey test. (* $P < 0.05$, ** $P < 0.01$, *** $P < 0.001$)

URHF1 are important members of this complex along with DNMT1. Here we conclude that TIP60 directly interacts with UHRF1 during the DNA replication phase of cell cycle and this interaction is dependent on the MYST domain of TIP60. Since UHRF1 interaction with TIP60 is known to perturb TIP60 mediated p53 activation, this study provides us with information to overcome this perturbation and counter the malicious transformations by utilizing the tumor suppressive role of TIP60. Finally, further investigations are required to fully decipher the dialogue within this three-way partnership involving UHRF1, DNMT1 and TIP60.

Abbreviations

ΔCRD: Chromodomain mutant; ΔHAT: Histone acetyltransferase domain mutant; ΔMYST: MYST domain mutant; ΔZnFr: Zinc Finger mutant; DNMT1: DNA methyl transferase 1; eGFP: Enhanced Green Fluorescent Protein; FLIM: Fluorescence Lifetime Imaging Microscopy; FRET: Fluorescence Resonance Energy Transfer; IP: Immunoprecipitation; TIP60: Tat interacting protein 60 kDa; UHRF1: Ubiquitin-like with PHD and RING Finger Domains 1; USP7: Ubiquitin specific protease 7; WB: Western Blotting; WT: Wild type

Acknowledgements

We thank Hugues de Rocquigny and Romain Vauchelles (Plate-forme d'Imagerie Quantitative - PIQ) for their technical support. WA and TA would also like to acknowledge funding support by the Higher Education Commission Pakistan for this work.

Funding

Our work was supported by the Agence Nationale de la Recherche (ANR-12-BS08–0003-02), the Fondation pour la Recherche Médicale (FRM DCM20111223038), Ligue contre le Cancer and by the grant ANR-10-LABX-0030-INRT, a French State fund managed by the Agence Nationale de la Recherche under the frame program Investissements d'Avenir ANR-10-IDEX-0002-02. WA and TA would also like to acknowledge funding support by the Higher Education Commission Pakistan for this work.

Availability of data and materials

Please contact corresponding author for data requests.

Authors' contributions
WA conducted most of the biochemical and cellular experiments with the help of LZ, AI and TA under the supervision of MM and CB. LR helped in the FLIM FRET experiments. WA, MA, CB and MM wrote most of the manuscript with the guidance and help of AH and YM. All authors read and approved the final manuscript.

Ethics approval and consent to participate
Not applicable

Consent for publication
Not applicable

Competing interests
The authors declare that they have no competing interests.

Publisher's Note
Springer Nature remains neutral with regard to jurisdictional claims in published maps and institutional affiliations.

Author details
[1]Laboratoire de Biophotonique et Pharmacologie, UMR 7213 CNRS, Faculté de Pharmacie, Université de Strasbourg, 74, Route du Rhin, 67401 Illkirch Cedex, France. [2]Institut de Génétique et de Biologie Moléculaire et Cellulaire, INSERM U964 CNRS UMR 7104, Université de Strasbourg, Illkirch, France. [3]Department of Biochemistry, Faculty of Science, King Abdulaziz University, Jeddah, Saudi Arabia. [4]Cancer Metabolism and Epigenetic Unit, Faculty of Science, King Abdulaziz University, Jeddah, Saudi Arabia. [5]BioTechnology Research Center (BTRC), Tripoli, Libya.

Received: 9 August 2017 Accepted: 4 December 2017
Published online: 21 December 2017

References
1. Hopfner R, Mousli M, Jeltsch JM, Voulgaris A, Lutz Y, Marin C, et al. ICBP90, a novel human CCAAT binding protein, involved in the regulation of topoisomerase IIalpha expression. Cancer Res. 2000;60(1):121–8.
2. Krifa M, Alhosin M, Muller CD, Gies JP, Chekir-Ghedira L, Ghedira K, et al. Limoniastrum guyonianum aqueous gall extract induces apoptosis in human cervical cancer cells involving p16 INK4A re-expression related to UHRF1 and DNMT1 down-regulation. J Exp Clin Cancer Res. 2013;32:30.
3. Arita K, Ariyoshi M, Tochio H, Nakamura Y, Shirakawa M. Recognition of hemi-methylated DNA by the SRA protein UHRF1 by a base-flipping mechanism. Nature. 2008;455(7214):818–21.
4. Avvakumov GV, Walker JR, Xue S, Li Y, Duan S, Bronner C, et al. Structural basis for recognition of hemi-methylated DNA by the SRA domain of human UHRF1. Nature. 2008;455(7214):822–5.
5. Hashimoto H, Horton JR, Zhang X, Bostick M, Jacobsen SE, Cheng X. The SRA domain of UHRF1 flips 5-methylcytosine out of the DNA helix. Nature. 2008;455(7214):826–9.
6. Liu X, Gao Q, Li P, Zhao Q, Zhang J, Li J, et al. UHRF1 targets DNMT1 for DNA methylation through cooperative binding of hemi-methylated DNA and methylated H3K9. Nat Commun. 2013;4:1563.
7. Nady N, Lemak A, Walker JR, Avvakumov GV, Kareta MS, Achour M, et al. Recognition of multivalent histone states associated with heterochromatin by UHRF1 protein. J Biol Chem. 2011;286(27):24300–11.
8. Nishiyama A, Yamaguchi L, Sharif J, Johmura Y, Kawamura T, Nakanishi K, et al. Uhrf1-dependent H3K23 ubiquitylation couples maintenance DNA methylation and replication. Nature. 2013;502(7470):249–53.
9. Qin W, Wolf P, Liu N, Link S, Smets M, La Mastra F, et al. DNA methylation requires a DNMT1 ubiquitin interacting motif (UIM) and histone ubiquitination. Cell Res. 2015;25(8):911–29.
10. Mousli M, Hopfner R, Abbady AQ, Monte D, Jeanblanc M, Oudet P, et al. ICBP90 belongs to a new family of proteins with an expression that is deregulated in cancer cells. Br J Cancer. 2003;89(1):120–7.
11. Ashraf W, Ibrahim A, Alhosin M, Zaayter L, Ouararhni K, Papin C, et al. The epigenetic integrator UHRF1: on the road to become a universal biomarker for cancer. Oncotarget. 2017;8:51946.
12. Boukhari A, Alhosin M, Bronner C, Sagini K, Truchot C, Sick E, et al. CD47 activation-induced UHRF1 over-expression is associated with silencing of tumor suppressor gene p16INK4A in glioblastoma cells. Anticancer Res. 2015;35(1):149–57.
13. Jeanblanc M, Mousli M, Hopfner R, Bathami K, Martinet N, Abbady AQ, et al. The retinoblastoma gene and its product are targeted by ICBP90: a key mechanism in the G1/S transition during the cell cycle. Oncogene. 2005; 24(49):7337–45.
14. Unoki M, Brunet J, Mousli M. Drug discovery targeting epigenetic codes: the great potential of UHRF1, which links DNA methylation and histone modifications, as a drug target in cancers and toxoplasmosis. Biochem Pharmacol. 2009;78(10):1279–88.
15. Wang F, Yang YZ, Shi CZ, Zhang P, Moyer MP, Zhang HZ, et al. UHRF1 promotes cell growth and metastasis through repression of p16(ink(4)a) in colorectal cancer. Ann Surg Oncol. 2012;19(8):2753–62.
16. Ma H, Chen H, Guo X, Wang Z, Sowa ME, Zheng L, et al. M phase phosphorylation of the epigenetic regulator UHRF1 regulates its physical association with the deubiquitylase USP7 and stability. Proc Natl Acad Sci U S A. 2012;109(13):4828–33.
17. Bronner C. Control of DNMT1 abundance in epigenetic inheritance by acetylation, ubiquitylation, and the histone code. Sci Signal. 2011;4(157):pe3.
18. Dai C, Shi D, Gu W. Negative regulation of the acetyltransferase TIP60-p53 interplay by UHRF1 (ubiquitin-like with PHD and RING finger domains 1). J Biol Chem. 2013;288(27):19581–92.
19. Du Z, Song J, Wang Y, Zhao Y, Guda K, Yang S, et al. DNMT1 stability is regulated by proteins coordinating deubiquitination and acetylation-driven ubiquitination. Sci Signal. 2010;3(146):ra80.
20. Guan D, Factor D, Liu Y, Wang Z, Kao HY. The epigenetic regulator UHRF1 promotes ubiquitination-mediated degradation of the tumor-suppressor protein promyelocytic leukemia protein. Oncogene. 2013;32(33):3819–28.
21. Achour M, Fuhrmann G, Alhosin M, Ronde P, Chataigneau T, Mousli M, et al. UHRF1 recruits the histone acetyltransferase Tip60 and controls its expression and activity. Biochem Biophys Res Commun. 2009;390(3):523–8.
22. Doyon Y, Selleck W, Lane WS, Tan S, Cote J. Structural and functional conservation of the NuA4 histone acetyltransferase complex from yeast to humans. Mol Cell Biol. 2004;24(5):1884–96.
23. Kamine J, Elangovan B, Subramanian T, Coleman D, Chinnadurai G. Identification of a cellular protein that specifically interacts with the essential cysteine region of the HIV-1 tat transactivator. Virology. 1996;216(2):357–66.
24. Lee KK, Workman JL. Histone acetyltransferase complexes: one size doesn't fit all. Nat Rev Mol Cell Biol. 2007;8(4):284–95.
25. Yamamoto T, Horikoshi M. Novel substrate specificity of the histone acetyltransferase activity of HIV-1-tat interactive protein Tip60. J Biol Chem. 1997;272(49):30595–8.
26. Gaughan L, Logan IR, Cook S, Neal DE, Robson CN. Tip60 and histone deacetylase 1 regulate androgen receptor activity through changes to the acetylation status of the receptor. J Biol Chem. 2002;277(29):25904–13.
27. Ikura T, Ogryzko VV, Grigoriev M, Groisman R, Wang J, Horikoshi M, et al. Involvement of the TIP60 histone acetylase complex in DNA repair and apoptosis. Cell. 2000;102(4):463–73.
28. Murr R, Loizou JI, Yang YG, Cuenin C, Li H, Wang ZQ, et al. Histone acetylation by Trrap-Tip60 modulates loading of repair proteins and repair of DNA double-strand breaks. Nat Cell Biol. 2006;8(1):91–9.
29. Squatrito M, Gorrini C, Amati B. Tip60 in DNA damage response and growth control: many tricks in one HAT. Trends Cell Biol. 2006;16(9): 433–42.
30. DeRan M, Pulvino M, Greene E, Su C, Zhao J. Transcriptional activation of histone genes requires NPAT-dependent recruitment of TRRAP-Tip60 complex to histone promoters during the G1/S phase transition. Mol Cell Biol. 2008;28(1):435–47.
31. Mo F, Zhuang X, Liu X, Yao PY, Qin B, Su Z, et al. Acetylation of aurora B by TIP60 ensures accurate chromosomal segregation. Nat Chem Biol. 2016; 12(4):226–32.
32. Niida H, Katsuno Y, Sengoku M, Shimada M, Yukawa M, Ikura M, et al. Essential role of Tip60-dependent recruitment of ribonucleotide reductase at DNA damage sites in DNA repair during G1 phase. Genes Dev. 2010; 24(4):333–8.
33. Taubert S, Gorrini C, Frank SR, Parisi T, Fuchs M, Chan HM, et al. E2F-dependent histone acetylation and recruitment of the Tip60 acetyltransferase complex to chromatin in late G1. Mol Cell Biol. 2004;24(10):4546–56.
34. Berns K, Hijmans EM, Mullenders J, Brummelkamp TR, Velds A, Heimerikx M, et al. A large-scale RNAi screen in human cells identifies new components of the p53 pathway. Nature. 2004;428(6981):431–7.

35. Sykes SM, Mellert HS, Holbert MA, Li K, Marmorstein R, Lane WS, et al. Acetylation of the p53 DNA-binding domain regulates apoptosis induction. Mol Cell. 2006;24(6):841–51.
36. Tang Y, Luo J, Zhang W, Gu W. Tip60-dependent acetylation of p53 modulates the decision between cell-cycle arrest and apoptosis. Mol Cell. 2006;24(6):827–39.
37. El Meshri SE, Dujardin D, Godet J, Richert L, Boudier C, Darlix JL, et al. Role of the nucleocapsid domain in HIV-1 Gag oligomerization and trafficking to the plasma membrane: a fluorescence lifetime imaging microscopy investigation. J Mol Biol. 2015;427(6 Pt B):1480–94.
38. Bostick M, Kim JK, Esteve PO, Clark A, Pradhan S, Jacobsen SE. UHRF1 plays a role in maintaining DNA methylation in mammalian cells. Science. 2007; 317(5845):1760–4.
39. Miura M, Watanabe H, Sasaki T, Tatsumi K, Muto M. Dynamic changes in subnuclear NP95 location during the cell cycle and its spatial relationship with DNA replication foci. Exp Cell Res. 2001;263(2):202–8.
40. Zhang J, Gao Q, Li P, Liu X, Jia Y, Wu W, et al. S phase-dependent interaction with DNMT1 dictates the role of UHRF1 but not UHRF2 in DNA methylation maintenance. Cell Res. 2011;21(12):1723–39.
41. Chakalova L, Debrand E, Mitchell JA, Osborne CS, Fraser P. Replication and transcription: shaping the landscape of the genome. Nat Rev Genet. 2005;6(9):669–77.
42. Bassi C, Li YT, Khu K, Mateo F, Baniasadi PS, Elia A, et al. The acetyltransferase Tip60 contributes to mammary tumorigenesis by modulating DNA repair. Cell Death Differ. 2016;23(7):1198–208.
43. Chen G, Cheng Y, Tang Y, Martinka M, Li G. Role of Tip60 in human melanoma cell migration, metastasis, and patient survival. J Invest Dermatol. 2012;132(11):2632–41.
44. Sakuraba K, Yasuda T, Sakata M, Kitamura YH, Shirahata A, Goto T, et al. Down-regulation of Tip60 gene as a potential marker for the malignancy of colorectal cancer. Anticancer Res. 2009;29(10):3953–5.
45. Sakuraba K, Yokomizo K, Shirahata A, Goto T, Saito M, Ishibashi K, et al. TIP60 as a potential marker for the malignancy of gastric cancer. Anticancer Res. 2011;31(1):77–9.
46. Gelato KA, Tauber M, Ong MS, Winter S, Hiragami-Hamada K, Sindlinger J, et al. Accessibility of different histone H3-binding domains of UHRF1 is allosterically regulated by phosphatidylinositol 5-phosphate. Mol Cell. 2014; 54(6):905–19.
47. Sapountzi V, Logan IR, Robson CN. Cellular functions of TIP60. Int J Biochem Cell Biol. 2006;38(9):1496–509.
48. Sun Y, Jiang X, Chen S, Fernandes N, Price BD. A role for the Tip60 histone acetyltransferase in the acetylation and activation of ATM. Proc Natl Acad Sci U S A. 2005;102(37):13182–7.
49. Kim CH, Kim JW, Jang SM, An JH, Seo SB, Choi KH. The chromodomain-containing histone acetyltransferase TIP60 acts as a code reader, recognizing the epigenetic codes for initiating transcription. Biosci Biotechnol Biochem. 2015;79(4):532–8.
50. Kim MY, Ann EJ, Kim JY, Mo JS, Park JH, Kim SY, et al. Tip60 histone acetyltransferase acts as a negative regulator of Notch1 signaling by means of acetylation. Mol Cell Biol. 2007;27(18):6506–19.
51. Sun Y, Jiang X, Xu Y, Ayrapetov MK, Moreau LA, Whetstine JR, et al. Histone H3 methylation links DNA damage detection to activation of the tumour suppressor Tip60. Nat Cell Biol. 2009;11(11):1376–82.
52. Alhosin M, Sharif T, Mousli M, Etienne-Selloum N, Fuhrmann G, Schini-Kerth VB, et al. Down-regulation of UHRF1, associated with re-expression of tumor suppressor genes, is a common feature of natural compounds exhibiting anti-cancer properties. J Exp Clin Cancer Res. 2011;30:41.
53. Renaud E, Barascu A, Rosselli F. Impaired TIP60-mediated H4K16 acetylation accounts for the aberrant chromatin accumulation of 53BP1 and RAP80 in Fanconi anemia pathway-deficient cells. Nucleic Acids Res. 2016;44(2):648–56.
54. Tang J, Cho NW, Cui G, Manion EM, Shanbhag NM, Botuyan MV, et al. Acetylation limits 53BP1 association with damaged chromatin to promote homologous recombination. Nat Struct Mol Biol. 2013;20(3):317–25.
55. Liang CC, Zhan B, Yoshikawa Y, Haas W, Gygi SP, Cohn MA. UHRF1 is a sensor for DNA interstrand crosslinks and recruits FANCD2 to initiate the Fanconi anemia pathway. Cell Rep. 2015;10(12):1947–56.
56. Tian Y, Paramasivam M, Ghosal G, Chen D, Shen X, Huang Y, et al. UHRF1 contributes to DNA damage repair as a lesion recognition factor and nuclease scaffold. Cell Rep. 2015;10(12):1957–66.
57. Zhang H, Liu H, Chen Y, Yang X, Wang P, Liu T, et al. A cell cycle-dependent BRCA1-UHRF1 cascade regulates DNA double-strand break repair pathway choice. Nat Commun. 2016;7:10201.
58. Qin W, Leonhardt H, Spada F. Usp7 and Uhrf1 control ubiquitination and stability of the maintenance DNA methyltransferase Dnmt1. J Cell Biochem. 2011;112(2):439–44.
59. Shamma A, Suzuki M, Hayashi N, Kobayashi M, Sasaki N, Nishiuchi T, et al. ATM mediates pRB function to control DNMT1 protein stability and DNA methylation. Mol Cell Biol. 2013;33(16):3113–24.
60. Cheng J, Yang H, Fang J, Ma L, Gong R, Wang P, et al. Molecular mechanism for USP7-mediated DNMT1 stabilization by acetylation. Nat Commun. 2015;6:7023.
61. Chen H, Ma H, Inuzuka H, Diao J, Lan F, Shi YG, et al. DNA damage regulates UHRF1 stability via the SCF(beta-TrCP) E3 ligase. Mol Cell Biol. 2013;33(6):1139–48.
62. Felle M, Joppien S, Nemeth A, Diermeier S, Thalhammer V, Dobner T, et al. The USP7/Dnmt1 complex stimulates the DNA methylation activity of Dnmt1 and regulates the stability of UHRF1. Nucleic Acids Res. 2011;39(19): 8355–65.
63. Zhang ZM, Rothbart SB, Allison DF, Cai Q, Harrison JS, Li L, et al. An Allosteric interaction links USP7 to Deubiquitination and chromatin targeting of UHRF1. Cell Rep. 2015;12(9):1400–6.
64. Gorrini C, Squatrito M, Luise C, Syed N, Perna D, Wark L, et al. Tip60 is a haplo-insufficient tumour suppressor required for an oncogene-induced DNA damage response. Nature. 2007;448(7157):1063–7.
65. Jha S, Vande Pol S, Banerjee NS, Dutta AB, Chow LT, Dutta A. Destabilization of TIP60 by human papillomavirus E6 results in attenuation of TIP60-dependent transcriptional regulation and apoptotic pathway. Mol Cell. 2010; 38(5):700–11.
66. Subbaiah VK, Zhang Y, Rajagopalan D, Abdullah LN, Yeo-Teh NS, Tomaic V, et al. E3 ligase EDD1/UBR5 is utilized by the HPV E6 oncogene to destabilize tumor suppressor TIP60. Oncogene. 2016;35(16):2062–74.
67. Zhang Y, Subbaiah VK, Rajagopalan D, Tham CY, Abdullah LN, Toh TB, et al. TIP60 inhibits metastasis by ablating DNMT1-SNAIL2-driven epithelial-mesenchymal transition program. J Mol Cell Biol. 2016;
68. Alhosin M, Omran Z, Zamzami MA, Al-Malki AL, Choudhry H, Mousli M, et al. Signalling pathways in UHRF1-dependent regulation of tumor suppressor genes in cancer. J Exp Clin Cancer Res. 2016;35(1):174.
69. Rothbart SB, Dickson BM, Ong MS, Krajewski K, Houliston S, Kireev DB, et al. Multivalent histone engagement by the linked tandem Tudor and PHD domains of UHRF1 is required for the epigenetic inheritance of DNA methylation. Genes Dev. 2013;27(11):1288–98.
70. Seo JS, Choi YH, Moon JW, Kim HS, Park SH. Hinokitiol induces DNA demethylation via DNMT1 and UHRF1 inhibition in colon cancer cells. BMC Cell Biol. 2017;18(1):14.

Supplementary Results

Interaction of the epigenetic integrator UHRF1 with the MYST domain of TIP60 inside the cell

Waseem Ashraf[1], Christian Bronner[2], Liliyana Zaayter[1], Tanveer Ahmad[1], Ludovic Richert[1], Mahmoud Alhosin[3,4], Abdulkhaleg Ibrahim[2,5], Ali Hamiche[2], Yves Mely[1] and Marc Mousli[1]

[1]Laboratoire de Biophotonique et Pharmacologie, UMR 7213 CNRS, Faculté de Pharmacie, Université de Strasbourg, 74, Route du Rhin, 67401 Illkirch Cedex, France. [2]Institut de Génétique et de Biologie Moléculaire et Cellulaire, INSERM U964 CNRS UMR 7104, Université de Strasbourg, Illkirch, France. [3]Department of Biochemistry, Faculty of Science, King Abdulaziz University, Jeddah, Saudi Arabia. [4]Cancer Metabolism and Epigenetic Unit, Faculty of Science, King Abdulaziz University, Jeddah, Saudi Arabia. [5]BioTechnology Research Center (BTRC), Tripoli, Libya.

Strength of interaction between GST-UHRF1 and His-TIP60 was also determined by varying the salt concentration in the *in-vitro* pull-down analysis. Increasing the salt concentration in the solution usually weakens the interaction between the two proteins. It was observed that there is a strong interaction between GST-UHRF1 and His-TIP60 protein and this interaction was strong enough to endure the 500 mM of NaCl in the interaction buffer (Figure 1).

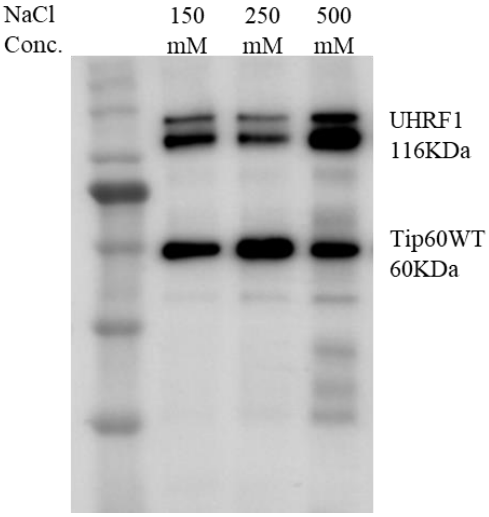

Figure 1: Western blot image of an in-vitro pull-down assay showing strong interaction between UHRF1 and TIP60 proteins which is stable up to 500 mM of NaCl.

Similarly, interaction between GST-UHRF1 and FLAG-MYST was also determined at different salt concentration and was found stable up till 1 M of NaCl concentration (Figure 2). This shows strong association between the UHRF1 and MYST domain of TIP60 protein.

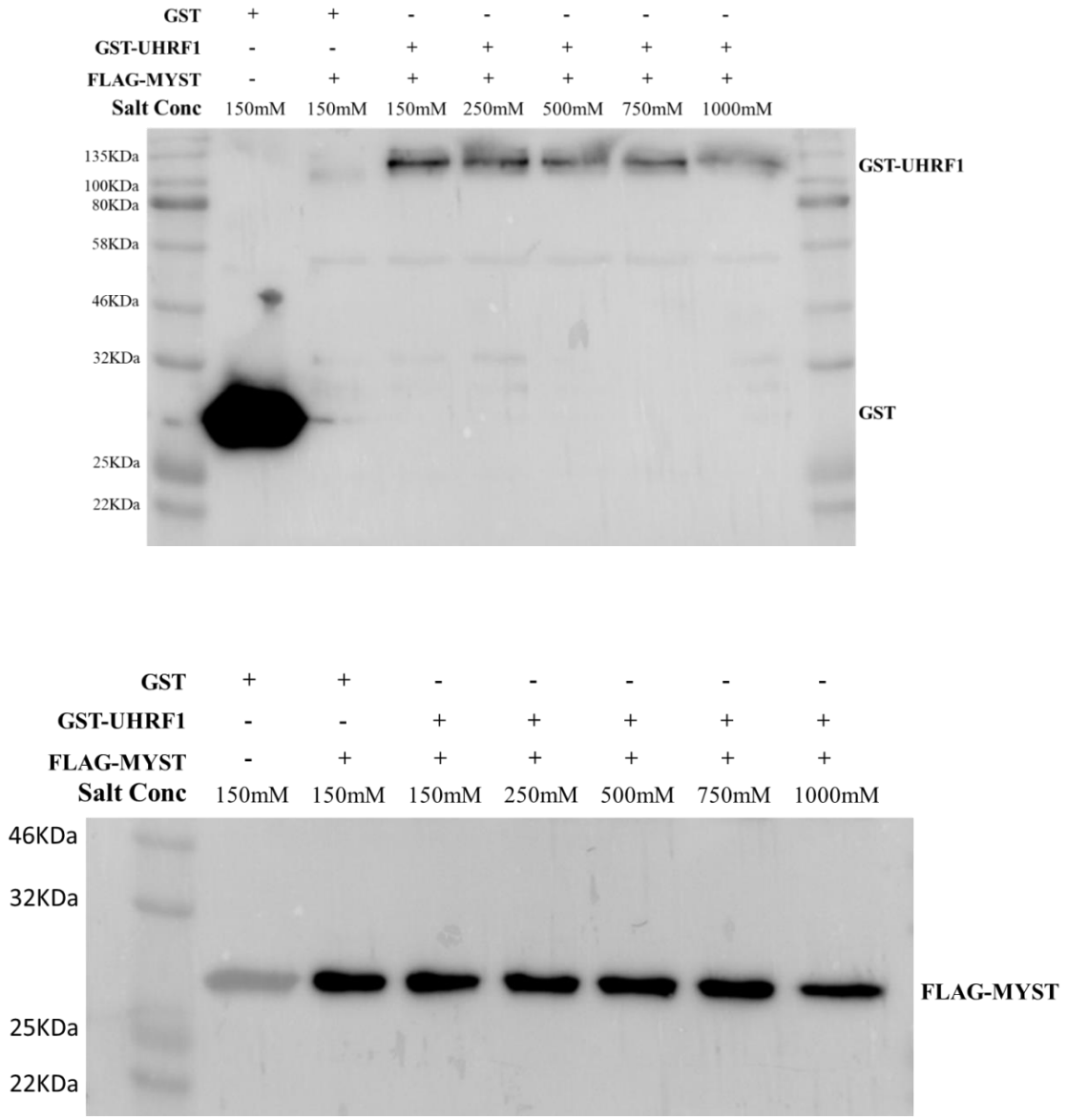

Figure 2: Interaction between UHRF1 and TIP60 at different salt concentration. Western blot analysis showing results of in-vitro pull down assays between GST-UHRF1 and His-TIP60 at different salt concentration. In upper image, blot is revealed by anti-GST antibody while the lower image represents the same blot revealed by anti-FLAG antibody.

Besides the other mutants of TIP60, we also prepared some mutants of TIP60 tagged with eGFP, affecting the localization of TIP60 protein inside the cells (Figure 3). TIP60 was predicted to have two nuclear localization signals (NLS) in its structure by PSORT II prediction program (Hass and Yankner, 2005). One nuclear localization signal PGRKRKS

(NLS1) lies before the MYST domain at position 184 while the second signal RKGTISFFEIDGRKNKS (NLS2) starts at 295 and lies within the MYST domain of TIP60.

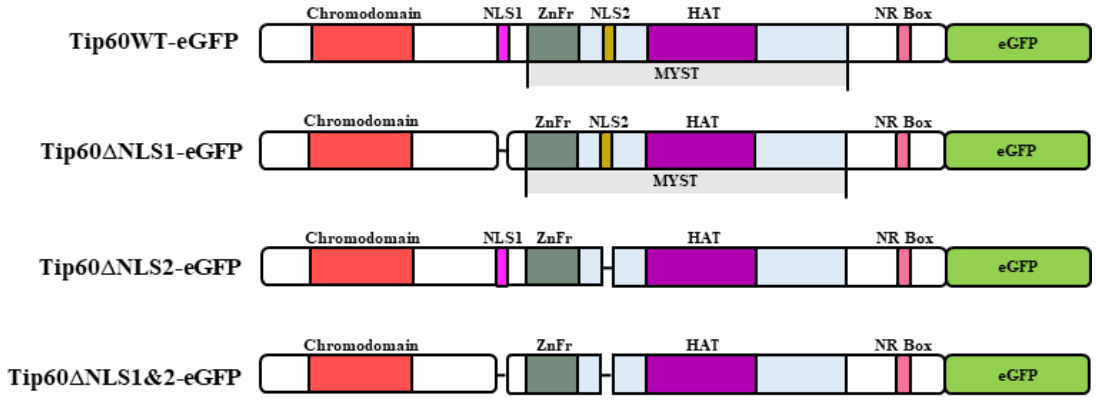

Figure 3: Schematic diagram of mutants of TIP60 affecting its nuclear localization.

Through confocal microscopy, we found that NLS1 is playing a major role in localization of the TIP60 protein to the nucleus of HeLa cells (Figure 4). Deletion of NLS1 resulted in distribution of the protein in both cytoplasm and nucleus of the HeLa cells. While deletion of other localization signal NLS2, did not affect the localization of the expressed eGFP tagged TIP60 protein. When both NLS sequences, *i.e.*, NLS1 & 2 were removed from the structure of TIP60 protein, it specifically localized to the cytoplasm and did not traverse to the nucleus of the cells (Figure 4).

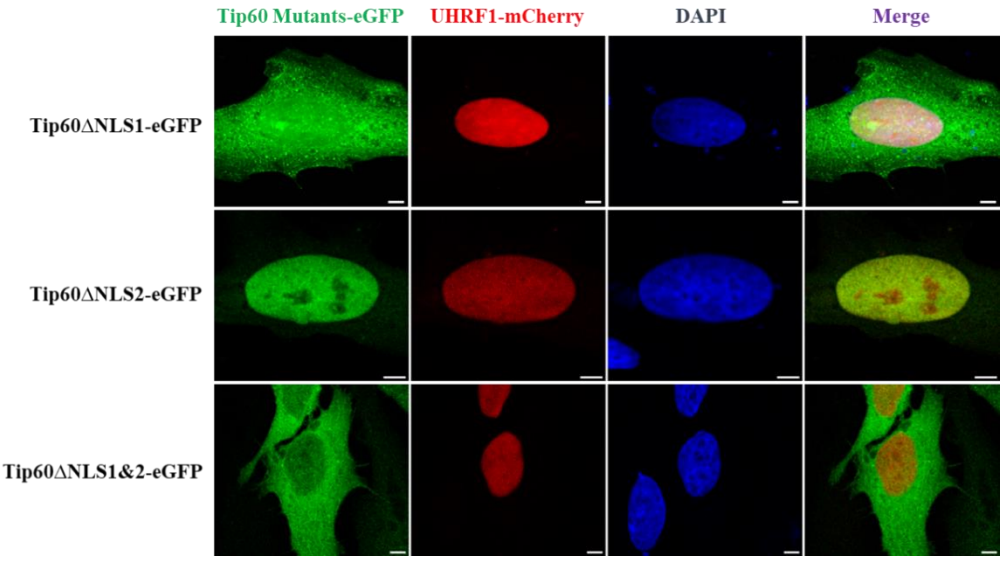

Figure 4: Confocal microscopy image showing localization of different mutants of TIP60 protein. White bar indicates size of 5 µm.

By using FLIM, we also analyzed the interaction of these mutants with UHRF1-mCherry, which specifically localize to the nucleus of cells. There was no significant change in the lifetime of eGFP in these mutants when transfected with UHRF1-mCherry as compared to the controls (Figure 5).

This is probably because of the change in localization of these proteins. TIP60ΔNLS1-eGFP and TIP60ΔNLS1&2-eGFP localized to cytoplasm where there was no UHRF1-mCherry and because of that, there was no global decrease in lifetime of eGFP. TIP60ΔNLS2-eGFP localized to the nucleus of HeLa cells but deletion of this fragment might have resulted in change in three-dimensional structure of the protein, which affected its interaction with UHRF1-mCherry in the nucleus of cells.

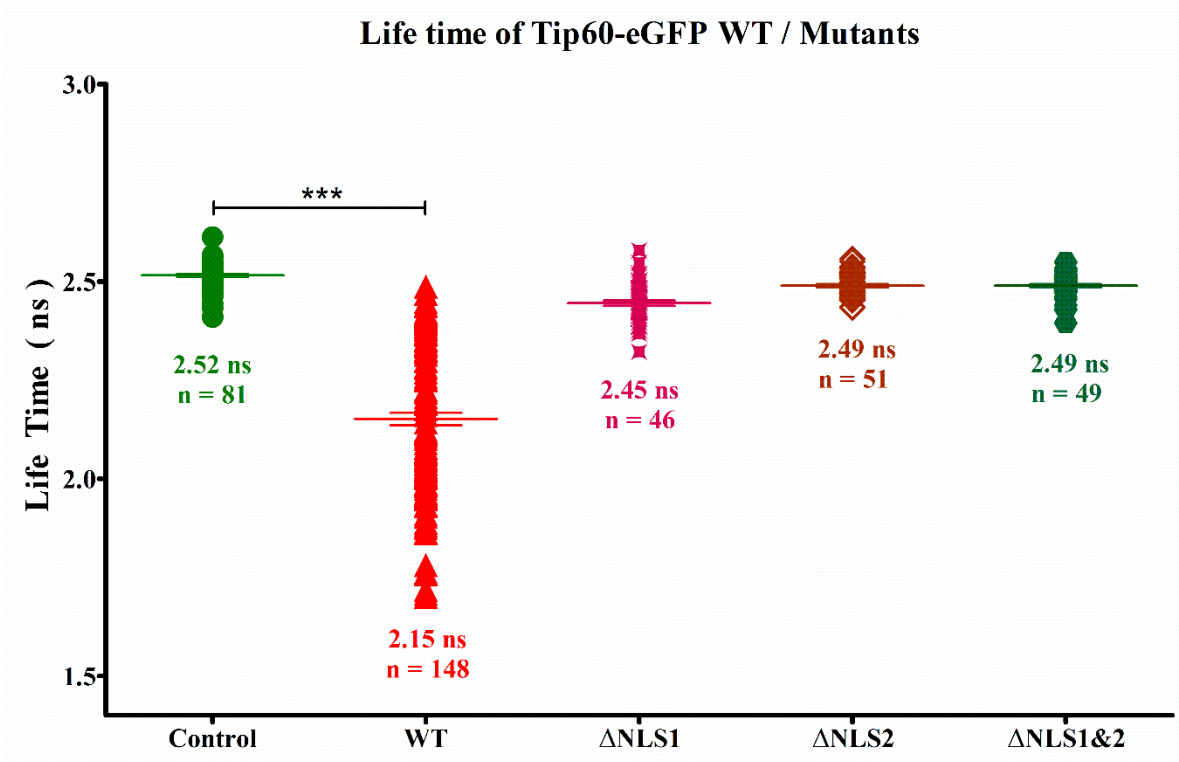

Figure 5: Interaction between Tip60-eGFP WT/mutants in FRET-FLIM analysis. Life time distribution of Tip60-eGFP (●), Tip60 WT-eGFP + UHRF1-mCherry co-transfected cells (▲), Tip60 ΔNLS1-eGFP + UHRF1-mCherry co-transfected cells (✖), Tip60 ΔNLS2-eGFP + UHRF1-mCherry co-transfected cells (◆) and Tip60 ΔNLS1&2-eGFP + UHRF1-mCherry co-transfected cells (⬢). Values are means ± SEM from three to five independent experiments. For statistical analysis, a Student's t-test was performed (*** p>0.001).

Manuscript II: Intracellular regulation of UHRF1 by TIP60 in human cancer cells

Intracellular regulation of UHRF1 by TIP60 in human cancer cells

Tanveer Ahmad[1], Waseem Ashraf[1], Liliyana Zaayter[1], Christian D. Muller[2], Ali Hamiche[3], Yves Mély[1], Christian Bronner[3], Marc Mousli[1, *]

[1] Laboratoire de Bioimagerie et Pathologies, UMR 7021 CNRS, Université de Strasbourg, Faculté de Pharmacie, Illkirch-France

[2] Institut Pluridisciplinaire Hubert Curien, UMR 7178 CNRS Université de Strasbourg, Illkirch, France

[3] Institut de Génétique et de Biologie Moléculaire et Cellulaire (IGBMC), INSERM U964 CNRS UMR 7104, Université de Strasbourg, Illkirch-France.

*Author to whom correspondence should be addressed:
Marc Mousli
Phone No: (+33) 3 68 85 42 49
Email: mousli@unistra.fr;
Permanent address: Laboratoire de Bioimagerie et Pathologies, UMR 7021 CNRS, Université de Strasbourg, Faculté de Pharmacie, 4 route du Rhin (67401) Illkirch Cedex France.

ABSTRACT

The epigenetic regulator UHRF1 (Ubiquitin-like, containing PHD and RING finger domains 1) plays an essential role in faithful transmission of DNA methylation during replication. It has tumorogenesis potential and is overexpressed in cancers. TIP60 (Tat interactive protein, 60 kDa) is an important interacting partner of UHRF1, which performs its role in epigenetic processes through its acetyltransferase activity. TIP60 is believed to have tumor suppressive role and it is down-regulated in many cancers. Both proteins participate in various cellular functions such as chromatin remodeling, cell cycle, DNA damage repair and regulation of stability of other proteins. Herein, our goal is to investigate the role of TIP60 overexpression in regulation of UHRF1 in cancer cells. Our results demonstrated that TIP60 overexpression down-regulated expression levels of proto-oncogenic proteins UHRF1 and DNMT1. TIP60 interfered with USP7-UHRF1 association and regulated degradation of UHRF1 in a ubiquitous way through stimulation of E3 ligase activity of UHRF1 itself. Moreover, TIP60 induced activation of p73 and p53-mediated apoptotic pathway. Taken together, our study suggests an intracellular regulatory event which uncovers TIP60-mediated regulation of UHRF1 in cancer cells which confers a tumor suppressive role to TIP60.

INTRODUCTION

Ubiquitin-like, containing PHD and RING finger domains 1 (UHRF1, also known as ICBP90 in humans and Np95 in mice), a multidomain protein, is an important epigenetic integrator and is responsible for the faithful transmission of DNA methylation patterns from parent strands to daughter strands during DNA replication (1-6). UHRF1 performs this role by recognizing the CpG motifs in hemi-methylated DNA through its SRA domain (SET and RING-associated domain) and by recruiting DNMT1 (DNA methyltransferase 1) (5,7-9). TTD and PHD domains help UHRF1 to read the histone marks (10-12). RING domain of UHRF1 has intrinsic ubiquitin E3 ligase activity by which UHRF1 can ubiquitinate itself or other proteins including histones (13,14). Ubiquitylation of H3K23 and H3K18 is important to create binding sites for DNMT1 (15-17). N-terminal UBL domain binds directly to DNMT1 and increases its enzymatic activity toward chromatin by controlling H3 ubiquitylation (17,18). Besides DNA methylation and histone modification, UHRF1 is also involved in DNA damage response (3,19,20) and regulation of stability and function of other proteins like p53, PML (promyelocytic leukemia protein) and DNMT1 through its interaction with other epigenetics partners such as USP7 (Ubiquitin-specific-processing protease 7), TIP60 (Tat interactive protein, 60 kDa) and HDAC1 (histone deacetylase 1) (3,14,21,22).

UHRF1 has oncogenic potential as reported in studies that its expression levels are high in proliferating cells and tissues as compared to normal ones (1,23). Higher expression of UHRF1 in different types of cancers is correlated with repression of tumor suppressor genes (TSGs), tumor aggressiveness and poor prognosis (3,24-28). Therefore, it can be used as a diagnostic and prognostic biomarker in cancer (3,28-30). UHRF1 is essential for the cell cycle progression and its deletion results in de-regulation of G1 and G2/M phases of cell cycle (31,32). Indeed, UHRF1 is mis-regulated in most of the cancers so; it can be a druggable target for anticancer therapy (21,30,33,34).

TIP60 was recognized originally as an interacting partner of HIV-1 Tat protein (35). TIP60 (also known as KAT5) belongs to MYST family (MOZ, YBF2/SAS3, SAS2, TIP60) having an evolutionary conserved domain which harbors histone acetyltransferase activity (36-39). On its N-terminal, TIP60 has a chromodomain (CRD) while on C-terminal it has conserved enzymatic MYST domain (40). TIP60 reads histone marks (H3K4me2/H3K9me3) through its CRD (41) and translates this message through MYST domain (42). Inside the MYST domain, there is a catalytic domain known as HAT domain which binds to acetyl coenzyme A and

substrate to mark the acetylation. Besides that, there is a zinc finger which helps TIP60 to interact with other proteins and also helps in the acetyltransferase activity (43-45). It can acetylate both histone and non-histone proteins (46,47). Being a multifunctional enzyme, TIP60 is a central player in many key cellular activities like chromatin remodeling, DNA damage response, transcription regulation, genomic integrity, cell cycle and apoptosis (21,44,46,48-50). It interacts and regulates transcription of nuclear hormone receptors, p53, c-MYC and NF-κB (44,49,51). During M-phase, TIP60 is essential for the chromosomal segregation (52) and also supports cell cycle progression by aiding G1/S phase changeover (53-55). Cells lacking TIP60's acetyltransferase activity, loose their ability to repair DNA and ultimately cell cycle control (48). Heterozygous deletion of TIP60 gene (*HTATIP*) has lethal effect on embryo (56). In many cancers, TIP60 levels are low as compared to normal cells. TIP60 suppresses tumorogenesis (21,48,57-63). It regulates p53 activity in an acetylation-dependent (K120 of p53) and independent style (21). Acetylation of p53 activates p21 and PUMA pathway leading to growth arrest and apoptosis, respectively, to maintain cellular and genomic stability and tumor suppression (21). Knockdown of TIP60 brings about failure of p21 (p53 pathway target gene) induced growth arrest (57). Higher levels of UHRF1 interfere with TIP60-p53 interplay and prevent p53 activation which leads to tumorogenesis and/or tumor progression (21). Therefore, targeting UHRF1 in cancer cells would be another strategy to rescue p53 levels and to enhance coordinated dialogue between p53 and TIP60.

UHRF1 levels are regulated through its association and physical interaction with USP7 (also known as HAUSP), in a cell cycle specific manner. Its levels are at peak during G1/S transition and G2/M phase while levels are down-regulated during G_0/G1 (1,23,33). USP7 (a deubiquitinating enzyme) protects the UHRF1 from proteasomal degradation during S-phase, while during M phase USP7 leaves UHRF1 which results in degradation of UHRF1 (64,65). Structural investigation has disclosed that first two UBL domains of USP7 and polybasic region (PBR) of UHRF1are responsible for their interaction (66). This association is not only critical for UHRF1 stability but also has interference in UHRF1's intramolecular TTD-PBR interaction which changeover the UHRF1 closed conformation to an open conformation, facilitating the histone binding (66-69).

UHRF1 and TIP60 are found to be in the same macromolecular complex and interact directly with each other (14,21,70). In our previous study we have shown that UHRF1 interacts with the MYST domain of TIP60 inside the cell (3). TIP60 interferes with DNMT1-USP7 association and acetylates the DNMT1. And finally UHRF1 through its E3 ligase activity,

ubiquitinates DNMT1 to regulate its levels in cell (14,66,71). Although it has been shown already, that TIP60 overexpression leads to down regulate the UHRF1 levels in HeLa cells (3) but mechanism behind TIP60-mediated UHRF1 down-regulation in cancer cells has not been reported yet. Here, we have demonstrated that TIP60 interferes with the UHRF1-USP7 association. After dissociation from USP7, UHRF1 is auto-ubiquitinated by its RING domain's inherent E3 ligase activity. Down-regulation of UHRF1 activates p53 and p73-mediated apoptosis in cancer cells. Thus, these observations provide us with insight about TIP60's tumor suppressive role by maintaining an optimal level of UHRF1 in the cellular milieu.

Results

TIP60 overexpression down-regulates UHRF1 and DNMT1 levels

Studies have shown that TIP60 expression levels are low in cancer cells as compared to normal cells (58-60,62) and it is also well studied that TIP60 has an important role in DNMT1 regulation (14). Therefore, in our previous study we evaluated the role of TIP60 overexpression in regulation of its interacting partners UHRF1 and DNMT1. Western blot results had shown that TIP60 overexpression induced down-regulation of UHRF1 and DNMT1 (3). UHRF1 and DNMT1 levels in TIP60 transfected samples were significantly reduced as compared to control samples i.e. cells without any treatment or cells treated with transfecting agent jetPEI or cells transfected with eGFP alone (3). Interestingly, in TIP60ΔMYST-eGFP (TIP60 mutant lacking acetyltransferase activity) overexpressed sample, levels of these proteins were not affected.

To support our western blot data, confocal microscopy experiments were executed. HeLa cells were transfected with either TIP60-eGFP or TIP60ΔMYST-eGFP. Untreated, jetPEI treated, and eGFP transfected cells were taken as controls. Endogenous UHRF1 and DNMT1 levels were observed by using specific primary antibody against UHRF1 and DNMT1. Then, Alexa 568-labeled secondary antibody was used to detect the signal of these proteins in confocal microscope. TIP60 and UHRF1 were co-localized in the nucleus. Downturn in UHRF1 expression was very obvious in TIP60 transfected cells (cells marked with white arrows) in contrast with either non-transfected cells in the same sample or eGFP transfected cells (Figure 1A). After quantification of mean fluorescence intensity of Alexa 568, a significant drop in UHRF1 fluorescence (50%) was detected in TIP60 WT transfected cells which is comparable to that of control. ΔMYST mutant transfection only marginally affected

UHRF1 fluorescence intensity (13%) (Figure 1B). Similarly, an obvious fall in DNMT1 expression was observed in TIP60 transfected cells as compared to control cells (Figure 1C). Decrease in fluorescence intensity of DNMT1 was significant (40%) as compared to control cells and ΔMYST mutant transfected cells (6%) (Figure 1D).

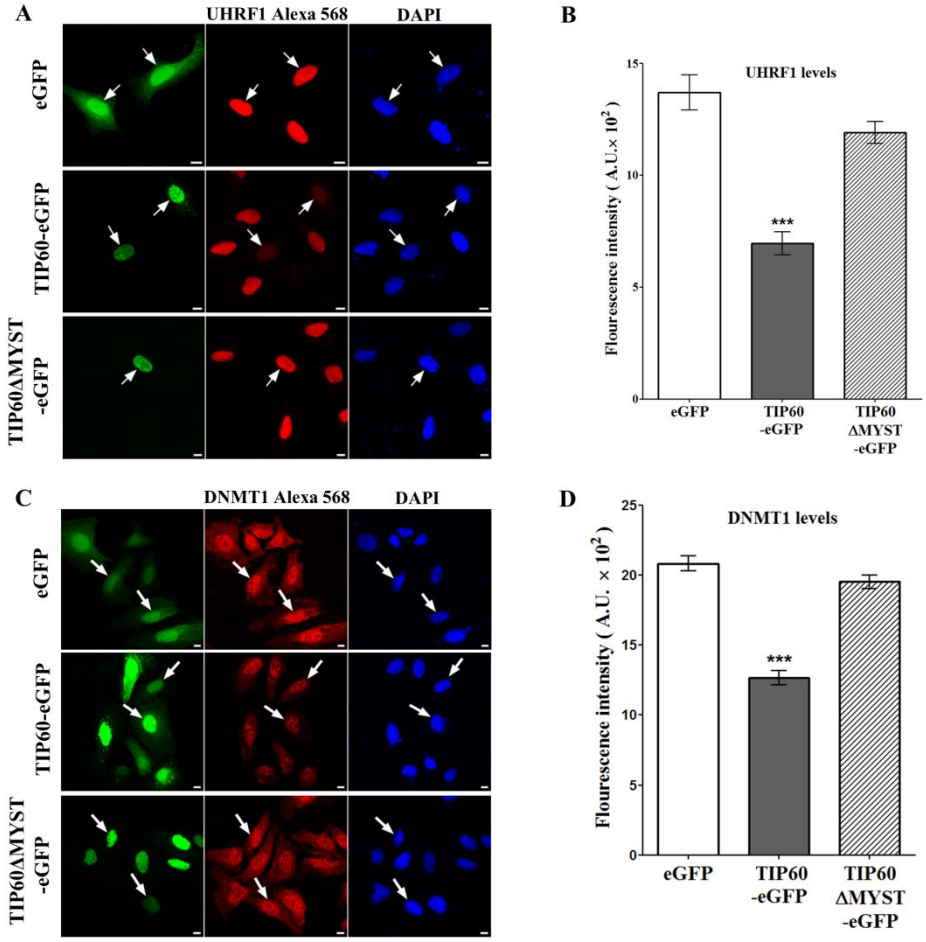

Figure 1. TIP60 overexpression leads to down-regulation of UHRF1 and DNMT1 levels. **(A)** and **(C)** Immunostaining of UHRF1 and DNMT1 in HeLa cells. Either TIP60-eGFP wild type (WT) or TIP60ΔMYST-eGFP mutant was transiently overexpressed. Cells were fixed after transfection and labeled with either anti-UHRF1 or anti-DNMT1 antibody and then with Alexa 568-labeled secondary antibody before visualization in confocal microscopy. White bar indicates size of 10 µm. eGFP transfected cells served as negative control. **(B)** and **(D)** Mean fluorescence intensities representing the levels of UHRF1 and DNMT1 in different samples. Values are means ± S. E. M. for three independent experiments; statistically significant: *** $p < 0.001$ (versus eGFP control group).

TIP60 overexpression induces ubiquitination of UHRF1

Like various proteins, UHRF1 is also regulated by proteasomal degradation pathway in the cell. As we demonstrated that TIP60 overexpression down-regulates UHRF1 levels in cancer cells (3), so we decided to evaluate in detail the possible mechanism involving ubiquitination-mediated UHRF1 down-regulation. HeLa cells were transfected with either TIP60 WT or

TIP60ΔMYST mutant. One group of samples was treated with MG-132 (a proteasome inhibitor). In TIP60 WT transfected sample (Figure 2A, MG-132 group lane 2) UHRF1 levels were reduced significantly as compared with either control or TIP60ΔMYST mutant samples (lane 1 and 3, respectively). Incubation with MG-132 stabilized UHRF1 levels in TIP60 WT overexpressed sample (Figure 2A, +MG-132 group lane 2). Turned over levels of UHRF1 were comparable to that of control and TIP60ΔMYST mutant transfected samples (Figure 2B). Indeed, in TIP60 WT transfected sample we observed a prominent smear over UHRF1 after treatment with MG-132 (Figure 2A, +MG-132 lane 2). Interestingly, after transfection TIP60 expression was very less as compared to its ΔMYST mutant but still ubiquitination smear was more prominent in TIP60 WT transfected sample (Figure 2A). So, this data gave us a notion that in spite of having lower expression, TIP60 may induce the ubiquitination-mediated UHRF1 degradation.

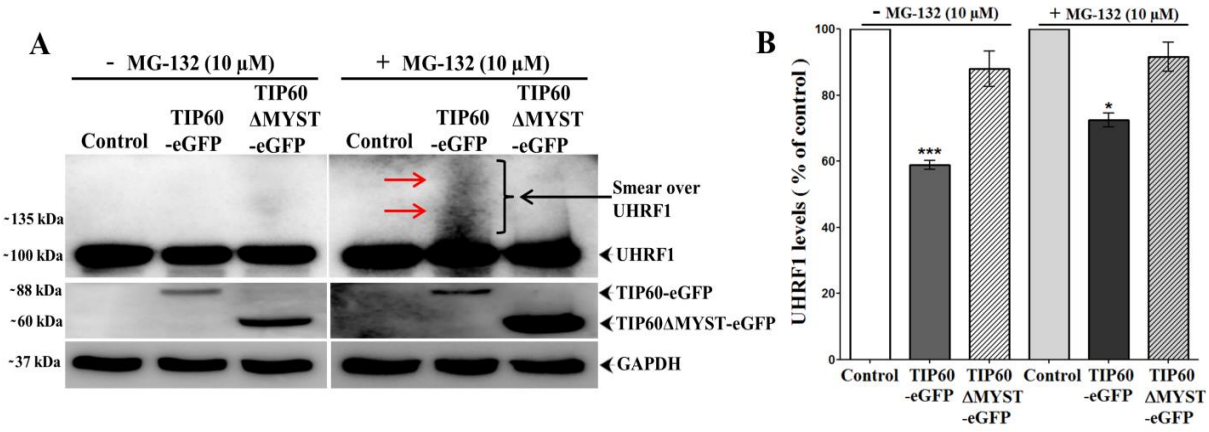

Figure 2. TIP60 overexpression leads to down-regulation of UHRF1 levels while MG-132 treatment stabilizes UHRF1 levels. **(A)** One group of samples was treated with 10 μM of MG-132. Whole cell lysates were immunoblotted with anti-UHRF1 antibody. **(B)** UHRF1 bands were quantified and expressed as means percentage of control ± S. E. M. Results represent five independent experiments which are analyzed statistically by one-way ANOVA (* $p < 0.05$; *** $p < 0.001$ versus control group).

To support our western blot data, we carried out confocal microscopy experiment to gather more detailed evidence regarding UHRF1 degradation inside the nucleus. HeLa cells were co-transfected with TIP60-eGFP + RFP-ubiquitin. Non-treated HeLa cells and eGFP + RFP-ubiquitin co-transfected cells served as controls. Endogenous UHRF1 levels were detected by using specific primary antibody against UHRF1 and Alexa 647-labeled secondary antibody. TIP60, UHRF1 and ubiquitin were well co-localized inside the nucleus (Figure 3). A clearly visible decrease in UHRF1 expression was witnessed in TIP60 and ubiquitin co-transfected

cells as compared to adjacent non-transfected cells in the same sample or control samples (Figure 3A).

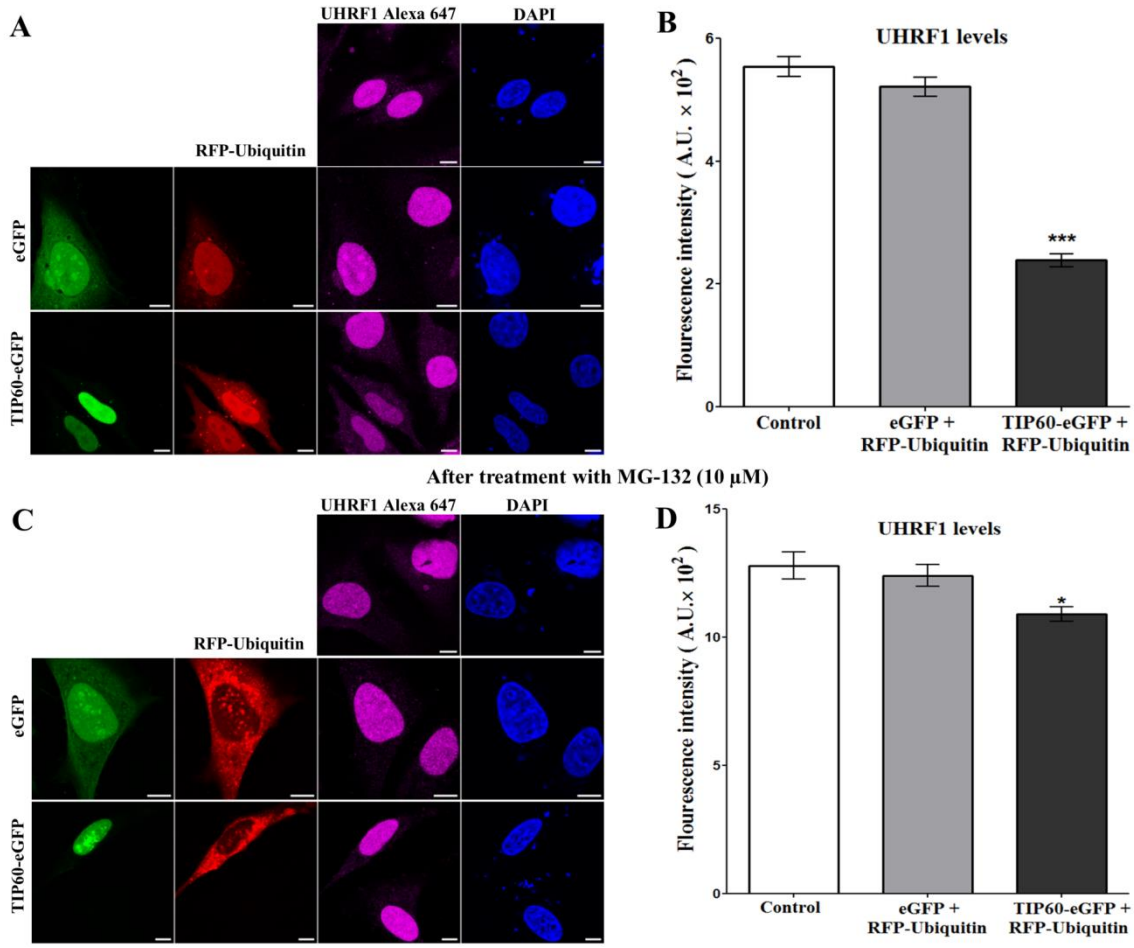

Figure 3. TIP60 and ubiquitin co-transfection induces down-regulation of UHRF1 while MG-132 treatment improved UHRF1 levels. Cells were co-transfected with either TIP60-eGFP (green) and RFP-Ubiquitin (red) or eGFP and RFP-Ubiquitin. Immunostaining of UHRF1 in HeLa cells without **(A)** or with treatment by MG-132 **(C)**. Cells were fixed after transfection and labeled with anti-UHRF1 antibody. Endogenous UHRF1 protein was labeled with Alexa 647-labeled secondary antibody before visualization in confocal microscopy. White bar indicates size of 10 µm. **(B** and **D)** Mean fluorescence intensities representing the levels of UHRF1 in different samples. Values are means ± S. E. M. for three independent experiments; statistically significant: * $p < 0.05$; ** $p < 0.01$; *** $p < 0.001$ (versus control group).

On the base of quantification of mean fluorescence intensity of Alexa 647, a convincing fall in the UHRF1 fluorescence (57%) was examined in TIP60 + ubiquitin co-transfected sample. This drop was comparable to that of control or eGFP + ubiquitin transfected cells (6%) (Figure 3B). Consequently, to empower the ubiquitination mediated degradation mechanism of UHRF1, in next experiment all samples were incubated with MG-132 and analyzed. As anticipated, UHRF1 labeling was improved in TIP60 + ubiquitin co-transfected cells (Figure 3C). Mean fluorescence intensity of UHRF1 was recovered significantly (Figure 3D).

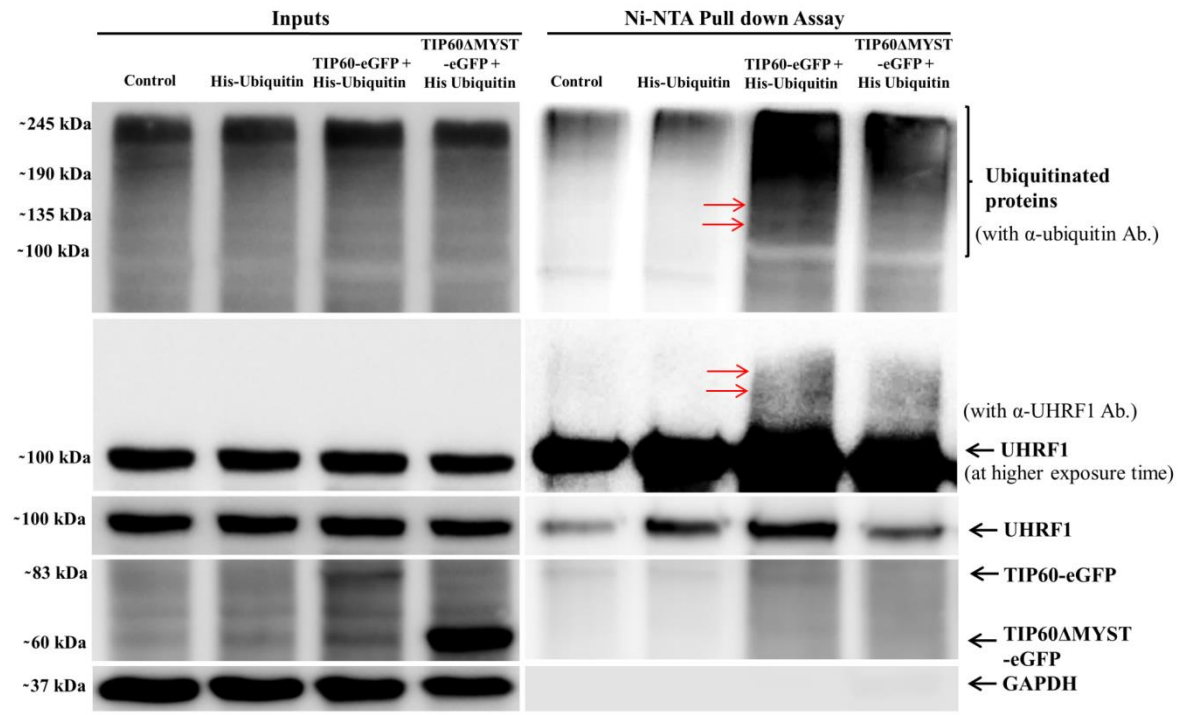

Figure 4. TIP60 induces UHRF1 ubiquitination in HeLa cells. Cells were co-transfected with either TIP60-eGFP WT or TIP60ΔMYST-eGFP mutant in combination with His-Ubiquitin. All samples were treated with 10 μM of MG-132 for 8 hours before harvesting the cells. Whole cell extracts and Ni-NTA affinity-purified fractions were analyzed by SDS-PAGE and then immunoblotted with anti-UHRF1 and anti-Ubiquitin antibodies.

Indeed, we agreed to demonstrate the UHRF1's ubiquitination through specific ubiquitination assay. To identify ubiquitination of cellular UHRF1, HeLa cells were co-transfected with either TIP60 WT + His-Ubiquitin or TIP60ΔMYST mutant + His-Ubiquitin. Untreated HeLa cells and His-Ubiquitin transfected HeLa cells served as controls. Then Ni-NTA (nickel-nitrilotriacetic acid) chromatographic technique was used to examine the TIP60-mediated UHRF1 ubiquitination. Affinity-purified ubiquitin conjugated UHRF1 levels were detected by UHRF1 antibody (Figure 4). Although having low expression (Inputs lane 3), TIP60 (IP lane 3) induced the ubiquitination of UHRF1 (Figure 4). Ni-NTA fractions analysis also revealed more ubiquitinated-UHRF1 levels in TIP60 WT transfected sample (IP lane 3) as compared to either ΔMYST mutant (IP lane 4) or controls (IP lanes 1, 2). We also observed a ubiquitination smear and bands above UHRF1 in TIP60 WT transfected sample (IP lane 3). These bands above UHRF1 were more prominent when incubated with anti-ubiquitin antibody.

Ubiquitination event can occur very early, so we decided to check effect of TIP60 overexpression over ubiquitination of UHRF1 in a kinetic manner (Figure 5).

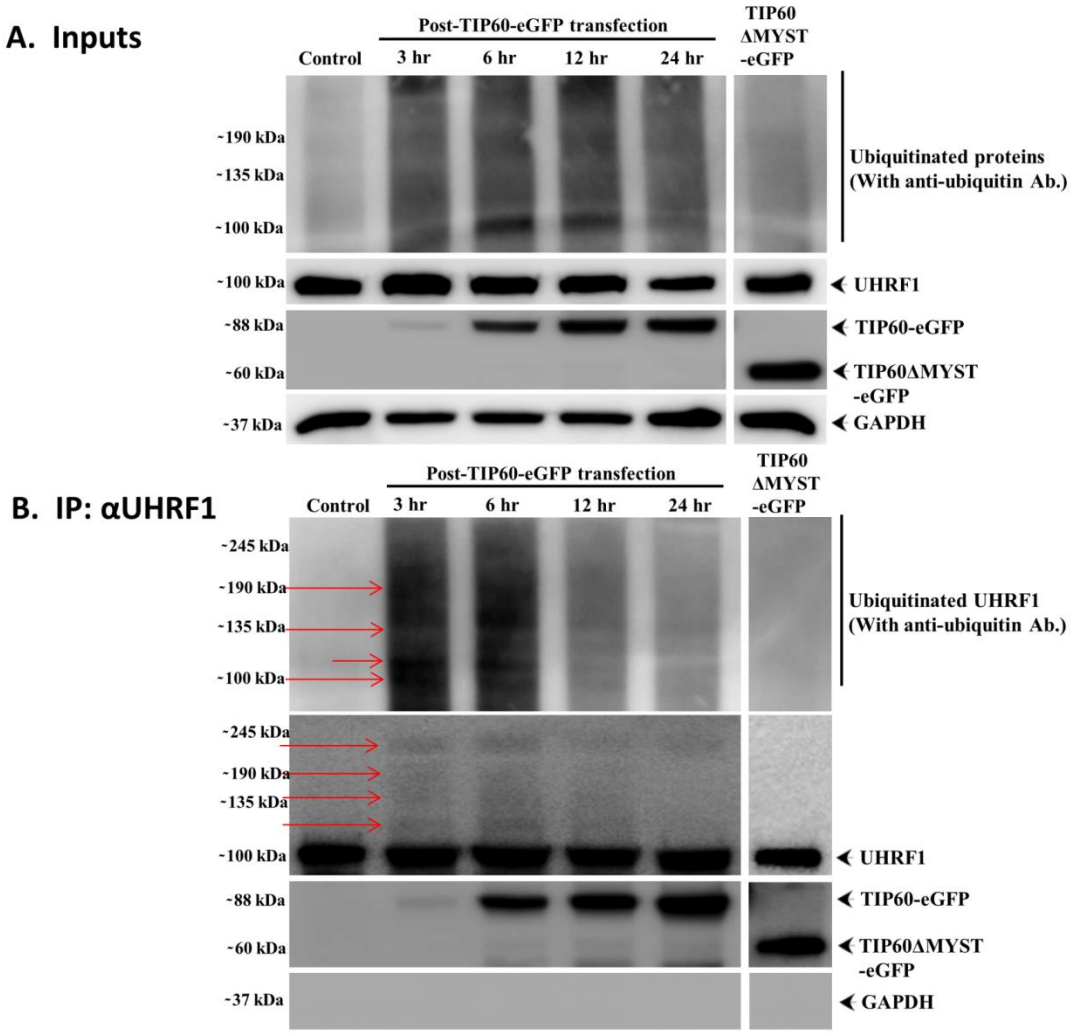

Figure 5. TIP60 induces UHRF1 ubiquitination in HeLa cells. Cells were co-transfected with either TIP60-eGFP WT or TIP60ΔMYST-eGFP mutant. All samples were treated with 10 µM of MG-132 for 8 hours before harvesting the cells. Cells were collected 3, 6, 12- and 24-hours post TIP60 transfection and 24 hours in case of TIP60ΔMYST mutant. IP was performed with anti-UHRF1 antibody. Inputs and IP samples were analyzed by SDS-PAGE and then immunoblotted with anti-UHRF1 and anti-Ubiquitin antibodies.

HeLa cells were transfected with either TIP60 WT or TIP60ΔMYST mutant. All samples were treated with MG-132. Cells were collected at different time intervals after TIP60 WT transfection. Immunoprecipitation was performed with anti-UHRF1 antibody. We observed prominent ubiquitination smear with ubiquitinated UHRF1 bands after 3 and 6 hr post TIP60 WT transfection (Figure 5B, IP lane 2 and 3). While after 12 and 24 hr post TIP60 WT transfection it was not so much prominent. In case of TIP60ΔMYST no ubiquitination of UHRF1 was observed. So collectively these results are supporting the explanation of ubiquitination-mediated degradation mechanism of UHRF1 after TIP60 overexpression.

TIP60 overexpression induced auto-ubiquitination of UHRF1

It is well known that RING domain of UHRF1 has intrinsic E3 ligase activity through which it can either ubiquitinate itself or other proteins (13,14). Therefore, we planned to investigate that down-regulation of UHRF1 levels is the consequence of UHRF1's auto-ubiquitination activity or some other E3 ligases are responsible for this. This experiment was performed using HeLa cells stably expressing either UHRF1 WT protein or UHRF1 C724A mutant protein (having impaired RING domain activity). Cells were transfected with either TIP60 WT or TIP60ΔMYST mutant and treated with MG-132. Immunoprecipitation was performed with anti-GFP antibody. We observed ubiquitination of UHRF1 WT in case of TIP60 WT overexpression as compared to either controls or ΔMYST mutant samples (Figure 6, IP lane 2). Interestingly, in case of UHRF1 C724A, no significant ubiquitination smear and bands over UHRF1 was observed (Figure 6, IP lane 4,5,6). This data indicates that after TIP60 overexpression, UHRF1 is auto-ubiquitinated due to its RING domain's intrinsic E3 ligase activity. While UHRF1 having RING domain mutation was not able to auto-ubiquitinate after TIP60 overexpression.

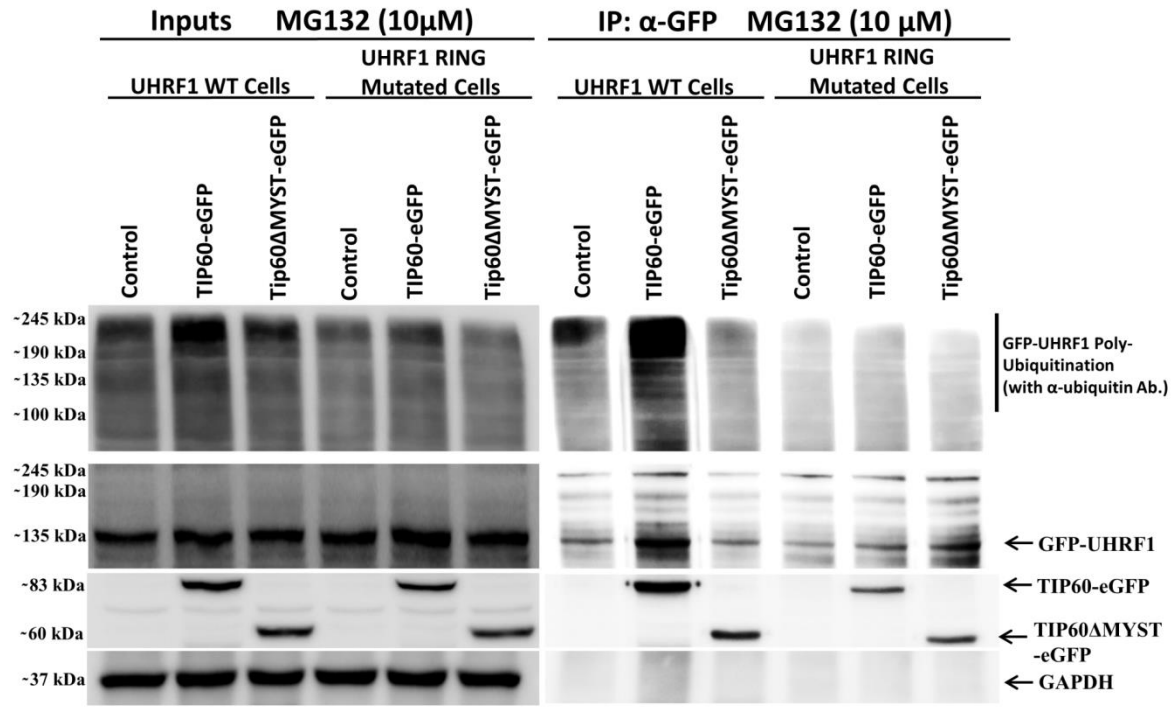

Figure 6. TIP60 induces auto-ubiquitination of UHRF1 in HeLa cells. Cells stably expressing either UHRF1 WT or UHRF1 C724A mutant proteins were transfected with either TIP60-eGFP WT or TIP60ΔMYST-eGFP mutant. All samples were treated with 10 μM of MG-132 before harvesting the cells. Whole cell lysates and immunoprecipitated samples were analyzed by SDS -PAGE and then immunoblotted with anti-GFP and anti-Ubiquitin antibodies.

UHRF1 interacts with ubiquitin

We performed FRET (Förster Resonance Energy Transfer) experiments to precisely confirm the interaction between UHRF1 and ubiquitin. FRET between GFP- and RFP- labeled proteins results only when they are less than 8nm apart, a distance relative to intermolecular protein-protein interactions (72). FRET efficiency is observed by means of decrease in fluorescence lifetime of GFP by Fluorescence Lifetime Imaging Microscopy (FLIM) (73). FLIM technique supports to derive the fluorescence lifetime (τ) through determining decrease in fluorescence. In comparison to fluorescence intensity, it does not depend on fluorophore concentration or instrumentation. τ is determined and color coded in each pixel of the image (Figure 7). HeLa cells expressing either GFP-UHRF1 WT or GFP-UHRF1 C724A mutant were used for the experiment.

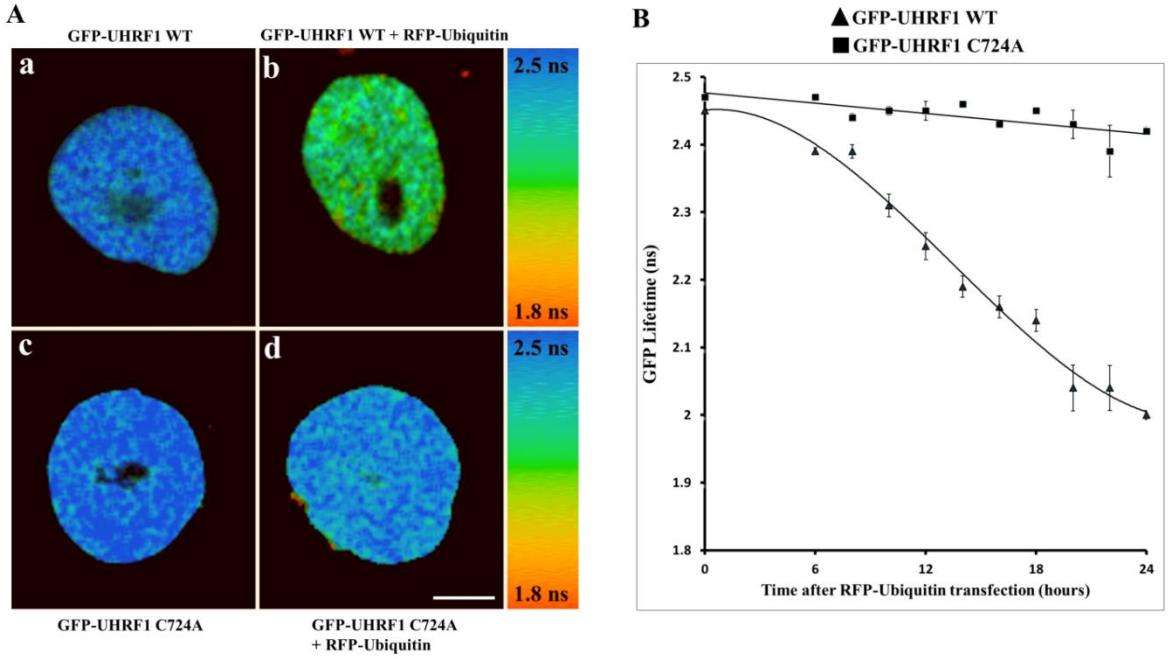

Figure 7. Interaction of UHRF1 and Ubiquitin, as determined by FRET-FLIM. **(A)** Representative 30 µm x 30 µm FLIM images of HeLa cells stably expressing GFP-UHRF1 WT (a) cells co-transfected with RFP-ubiquitin (b) HeLa cells stably expressing GFP-UHRF1 C724A (c) or cells co-transfected with RFP-ubiquitin (d). The lifetime values are shown by using a color code ranging from red (1.8 ns) to blue (2.5 ns). White bar indicates size of 10 µm. In comparison to cells expressing only GFP-UHRF1 WT (a), a strong decline in GFP lifetime and thus, a strong FRET efficiency was observed when HeLa cells were transfected with RFP-ubiquitin (b). While no significant difference in lifetime or FRET efficiency was observed in case of HeLa cells expressing only GFP-UHRF1 C724A (c) and when transfected with RFP-ubiquitin (d). FLIM data indicates that UHRF1 interacts with ubiquitin while this interaction is impaired in case of UHRF1 having RING domain mutation. **(B)** Graph representing the change in lifetime. Values are means ± S.E.M. from 2 independent experiments. (0) time interval corresponds to lifetime of either GFP-UHRF1 WT or GFP-UHRF1 C724A alone. Remaining time intervals correspond to change in lifetime of either GFP-UHRF1 WT or GFP-UHRF1 C724A post RFP-ubiquitin in a kinetic manner.

To study the interaction between UHRF1 and ubiquitin in a kinetic manner, we co-transfected the cells with RFP labeled ubiquitin and fixed the cells at different time intervals. Lifetime of GFP-UHRF1 WT used as a control was 2.45 ± 0.003 ns (n = 36 cells) (Figure 7a). This lifetime started to decline in a time dependent manner when GFP-UHRF1 WT cells were transfected with RFP-ubiquitin (Figure 7B). Significant decrease in lifetime was observed after 12 hours of RFP-ubiquitin transfection (2.25 ± 0.021 ns, n = 26 cells) and most significant decrease in lifetime was observed after 24 hours (2.0 ± 0.007 ns, 20 cells) (Figure 7b). Corresponding FRET efficiency was 8.24 ± 0.84 % and 19.40 ± 0.30 % after 12 and 24 hours of RFP-ubiquitin transfection, respectively. Data is indicating the interaction between UHRF1 and ubiquitin in the cell nucleus and this is in correlation with our IP and confocal microscopy data (Figure 3,4 and 5). Next we decided to check the interaction between RFP labeled ubiquitin and GFP labeled UHRF1 protein having RING domain mutation, in time dependent manner. Lifetime of GFP-UHRF1 C724A taken as control was 2.47 ± 0.003 ns (28 cells) (Figure 7c). Interestingly, we did not observe any significant decrease in lifetime of GFP-UHRF1 C724A after RFP-ubiquitin transfection. Post 24 hours of RFP-ubiquitin transfection, lifetime decrease was 2.42 ± 0.006 ns (18 cells) (Figure 7d) and a corresponding FRET efficiency of 2 ± 0.26 %. This low FRET value is under the commonly accepted value (5% significance limit) for protein-protein interaction (74). This data is suggesting that mutation in the RING domain of UHRF1 protein can impair its interaction with the ubiquitin. Thus, over all our FRET data suggests the interaction between UHRF1 and ubiquitin proteins inside the nuclei.

TIP60 overexpression interferes with USP7-UHRF1 association

USP7 interacts with the UHRF1 and protects the UHRF1 from ubiquitin-mediated proteasomal degradation. When this association between UHRF1 and USP7 is disrupted, then UHRF1 is degraded (65,66). We decided to check the effect of TIP60 overexpression on association between USP7 and UHRF1. This was assessed by co-immunoprecipitation experiment. HeLa cells were transfected with either TIP60-eGFP or with TIP60ΔMYST-eGFP mutant. Anti-UHRF1 antibody was used to immunoprecipitate the endogenous UHRF1 and its associated partner USP7. Association between USP7 and UHRF1 was observed in untreated sample (control) as USP7 was co-precipitated with the UHRF1 (Figure 8D). While in TIP60 overexpressed sample, there was almost negligible levels of USP7 was co-precipitated with UHRF1 (Figure 8D, lane 2). While in case of TIP60ΔMYST-eGFP mutant this association was not much affected (Figure 8D, lane 3). In a reciprocal experiment, anti-

USP7 antibody was used to immunoprecipitate the endogenous USP7 and its interacting partner protein UHRF1. After TIP60 WT overexpression, reduced levels of endogenous UHRF1 were co-precipitated as compared to control and TIP60ΔMYST-eGFP mutant sample (Figure 8E).

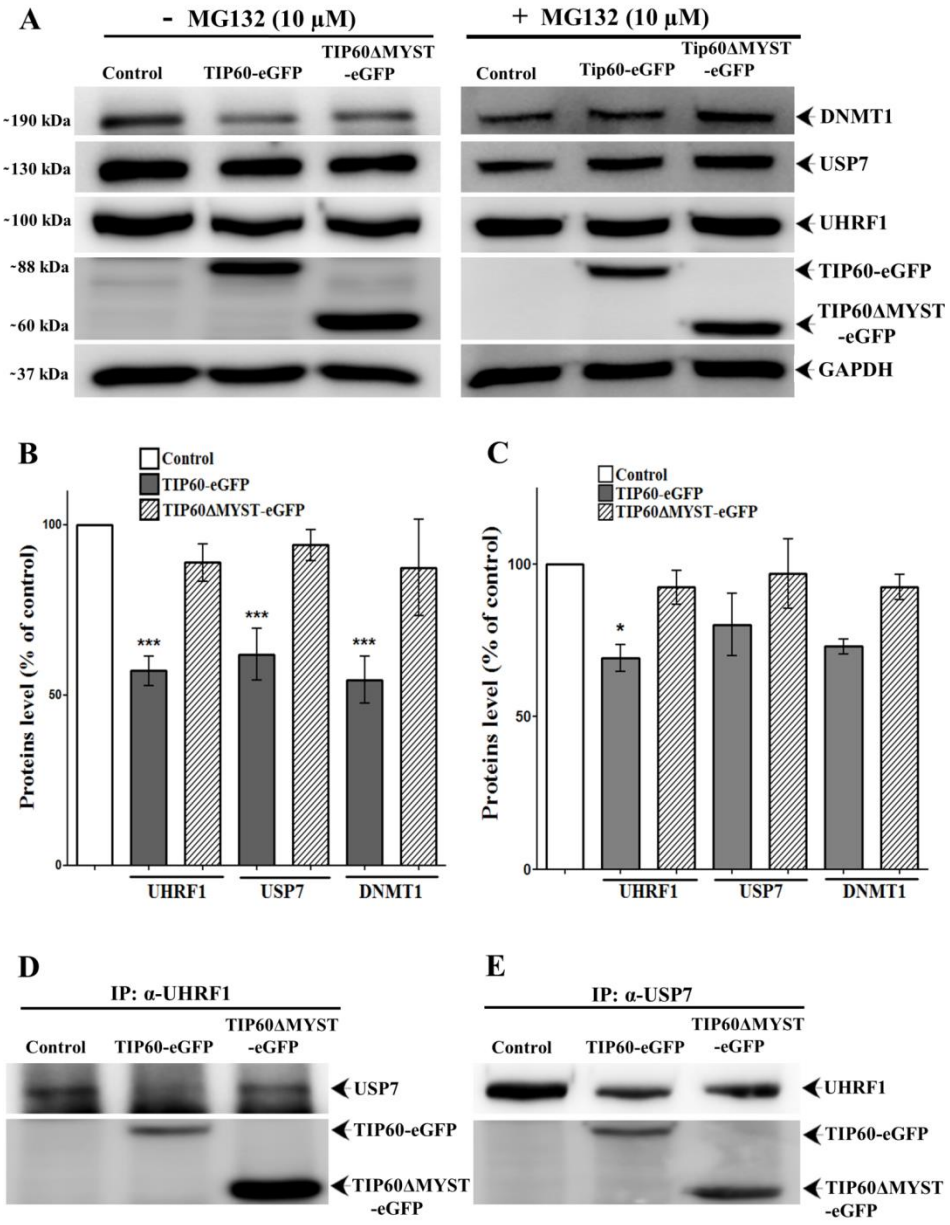

Figure 8. TIP60 interferes with UHRF1-USP7 association and their expression levels. HeLa cells were transfected with either TIP60-eGFP WT or TIP60ΔMYST-eGFP mutant. Western blot and immunoprecipitated samples were resolved by SDS-PAGE and immunoblotted with anti-UHRF1, anti-USP7 and anti-DNMT1 antibodies. **(B** and **C**) show the effect of TIP60 on UHRF1, USP7 and DNMT1 levels with or without MG-132 treatment, respectively. Results indicated are from five independent experiments which are analyzed statistically by one-way ANOVA (* $p < 0.05$; ** $p < 0.01$; *** $p < 0.001$ versus control group). **(D)** Anti-UHRF1 antibody was used to co-immunoprecipitate UHRF1 and its associating partner USP7. **(E**) In reciprocal experiment anti-USP7 antibody was used to co-immunoprecipitate USP7 and its interacting partner UHRF1.

In quantitative analysis of input fractions, we observed the significant decrease in UHRF1, USP7 and DNMT1 levels after TIP60 WT overexpression (Figure 8A, B). While MG-132 treatment fully restored USP7 and DNMT1 levels while partially restored UHRF1 levels (Figure 8A, C).

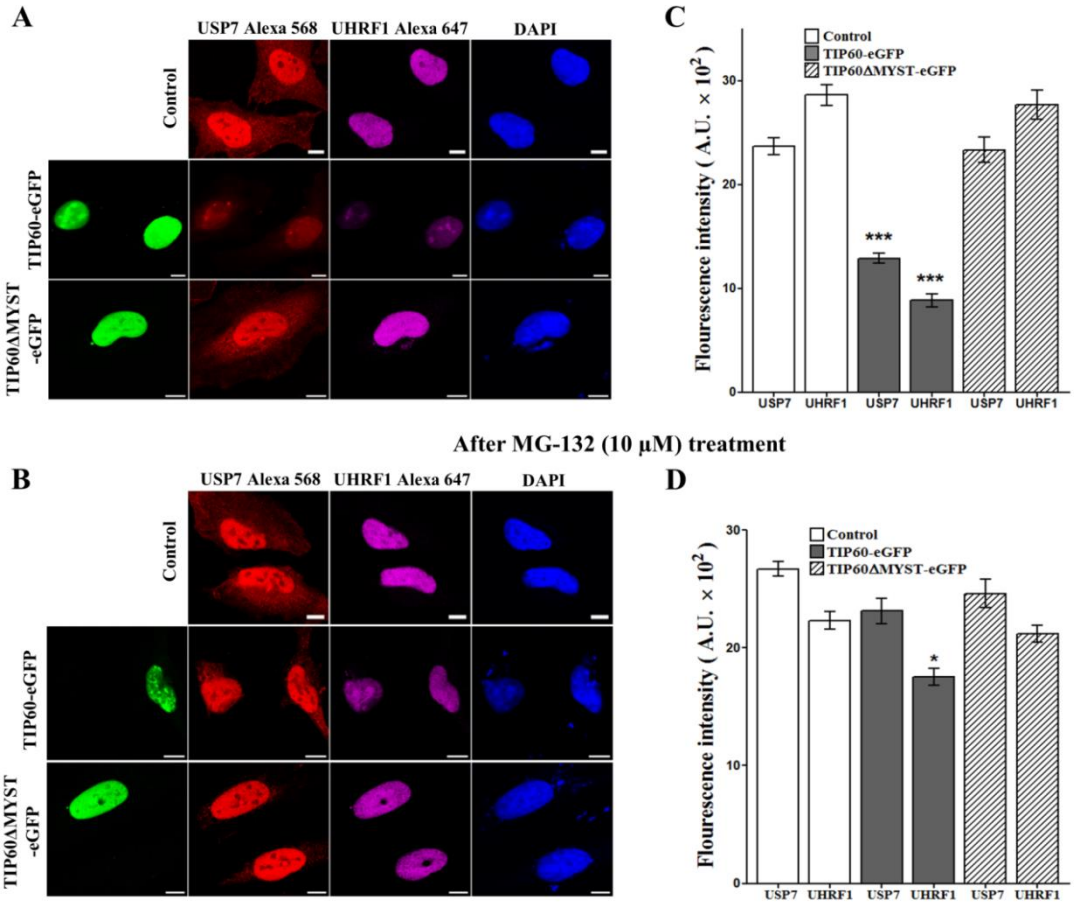

Figure 9. TIP60 down-regulates UHRF1 and USP7 levels in HeLa cells. MG-132 untreated **(A)** or treated with MG-132 10 µM for 8 hours **(B)** were immunostained with anti-USP7 or anti-UHRF1. TIP60-eGFP wild type (WT) or TIP60ΔMYST-eGFP mutant was transiently overexpressed and their effects were compared with the untransfected control cells. Cells were fixed after transfection and labeled by anti-USP7 and anti-UHRF1 antibodies. Alexa 568 and Alexa 647-labeled secondary antibodies were used as indicated in the figure to visualize corresponding proteins in confocal microscopy. White bar indicates size of 10 µm. **(C** and **D)** show mean fluorescence intensities representing the levels of USP7 and UHRF1 before and after MG-132 treatment, respectively. Values are means ± S. E. M. for three independent experiments; statistically significant: * $p < 0.05$; ** $p < 0.01$; *** $p < 0.001$ (versus control group).

Next to check the expression levels of USP7 and UHRF1 inside the cell after TIP60 overexpression, we performed the confocal microscopy experiment. The endogenous levels of UHRF1 and USP7 were checked in the same cells by labeling with respective antibodies. Based on mean fluorescence intensity of Alexa 568 and Alexa 647, USP7 and UHRF1 levels were found to decrease significantly after TIP60 overexpression (Figure 9A, C). Drop in fluorescence of USP7 (45%) and UHRF1 (60%) was comparable to that of control sample.

However, TIP60ΔMYST-eGFP mutant marginally affected the fluorescence intensity of USP7 and UHRF1 (Figure 9A, C). Thus, our data demonstrates that TIP60 overexpression can down-regulate USP7 and UHRF1 levels simultaneously. Due to its down-regulation, USP7 may be no more able to protect the UHRF1 degradation through proteasomal degradation pathway. As we observed a significant decrease in USP7 levels after TIP60 overexpression, we checked USP7 levels after treatment with MG-132. After treatment with MG-132, expression levels of USP7 were improved significantly, in TIP60 overexpressed samples (Figure 9B, D). Expression levels of UHRF1 were also improved but to a lesser extent as compared to USP7, which is giving the idea that once UHRF1 is degraded through proteasomal degradation pathway, its levels are not restored immediately (Figure 9B, D).

TIP60 overexpression induces activation of p53 and p73

p53 is an important tumor suppressor protein which maintains cellular and genomic stability by responding to a plenty of stress signals. It is activated by TIP60-mediated acetylation. While UHRF1 perturbs the interaction of TIP60 with p53 (21). As TIP60 overexpression down-regulated UHRF1 levels (3), we decided to investigate the effect of UHRF1 down-regulation on TIP60 and p53 interplay. It was observed that after TIP60 overexpression there was a significant increase in expression levels of p53 as compared to controls (Figure 10A, C). Another tumor suppressor gene p73 is also involved in the regulation of UHRF1. Higher expression levels of p73 have been reported to be involved in UHRF1 down-regulation (75). So, we also checked the effect of TIP60 on p73 levels. p73 levels were found to be upregulated after TIP60 overexpression as compared to control samples (Figure 10A, B).

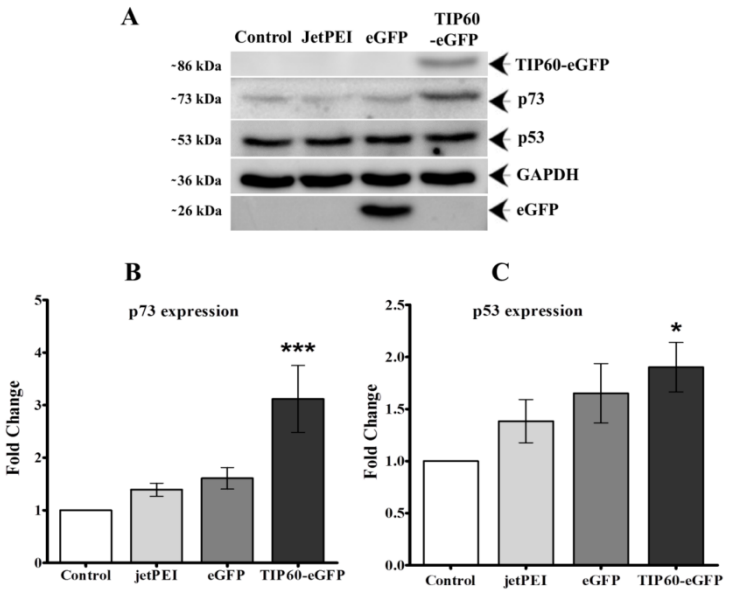

Figure 10. TIP60 activates p73, p53 proteins in HeLa cells. **(A)** Western blot showing effect of TIP60 overexpression over p73 and p53 expression in control, jetPEI treated eGFP and TIP60-eGFP transfected cells. **(B** and **C)** show analysis of TIP60 effect on p73 and p53 expression levels. Results indicated are from five independent experiments which are analyzed statistically by *Student's t-test* (* $p < 0.05$; ** $p < 0.01$; *** $p < 0.001$).

TIP60 overexpression activates p53 and p73-mediated apoptosis

Upon activation p53 and p73 can induce apoptosis in cancer cells. In order to assess the effect of TIP60 overexpression on downstream signaling pathways of p53 and p73, we performed flow cytometry experiment. TIP60-eGFP transfected cells were analyzed by FACS and compared with the cells treated with transfecting agent (jetPEI). PI and Annexin-V-iFluor^{TM} 350 staining aided us to detect late and early phases of apoptosis. A significant decrease (34 %) in cell viability was observed in TIP60 transfected cells as compared to control. Along with decrease in cell viability after TIP60 overexpression, 12 % and 16 % increase in early and late apoptotic cells was also observed, respectively (Figure 11A, B and C).

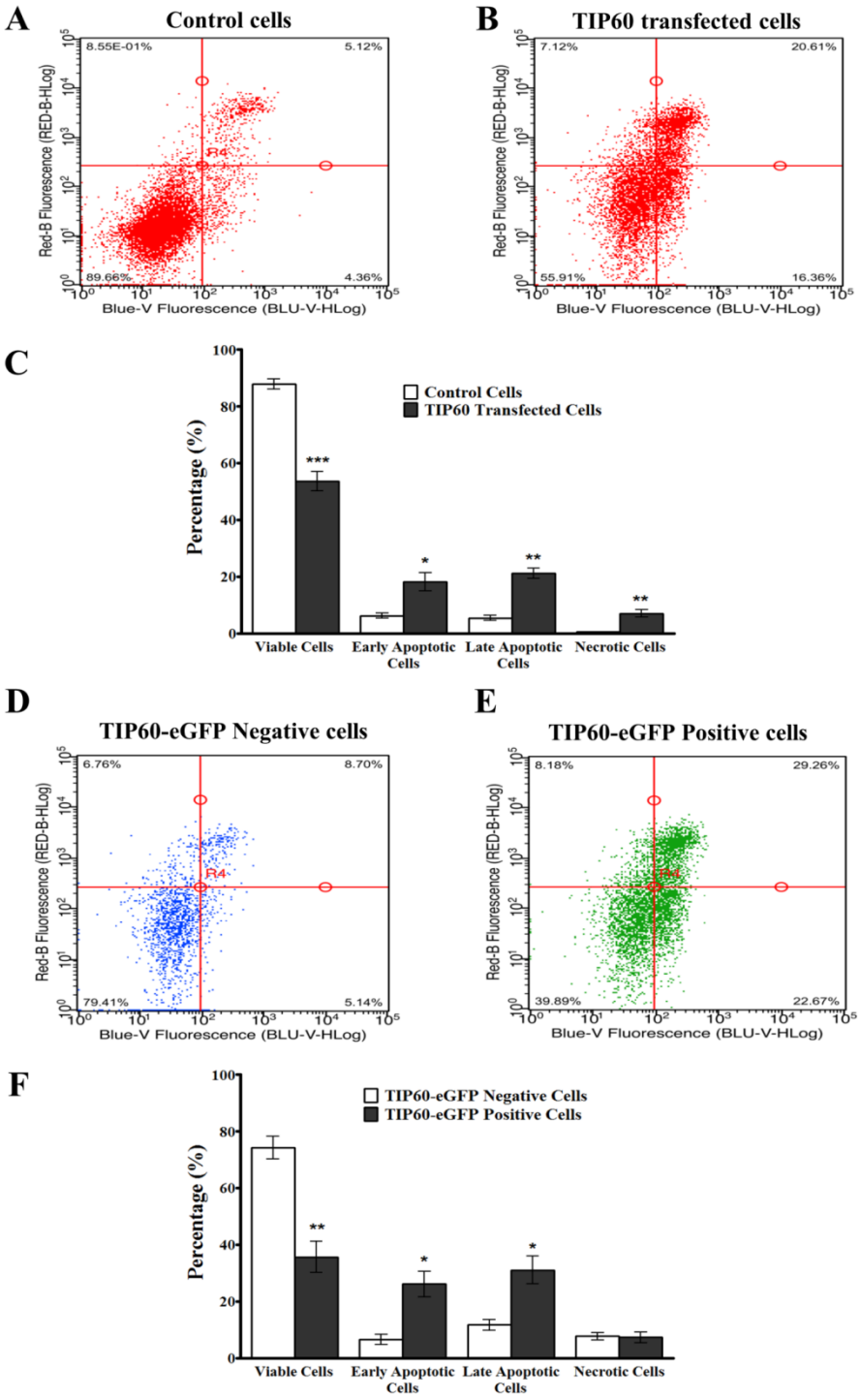

Figure 11. TIP60 overexpression induces apoptosis in cancer cells. **(A)** FACS analysis examining Annexin V-iFluor™ 350 and PI labeling in control HeLa cells (treated with jetPEI in identical manner) and **(B)** cells transfected with TIP60-eGFP for 24 hr. **(D** and **E)** FACS analysis examining Annexin V-iFluor™ 350 and PI labeling in TIP60-eGFP negative cells to TIP60-eGFP positive cells in TIP60-eGFP transfected samples. **(C** and **F)** Graph represents average values from three independent experiments which were statistically analyzed by *Student's t-test* (* $P < 0.05$; ** $P < 0.01$; *** $P < 0.001$).

To confirm the above results, we separated the total TIP60-eGFP transfected cells into TIP60-eGFP positive and TIP60-eGFP negative cells on the basis of eGFP fluorescence presence.

Analysis supported us to identify the apoptosis induction in TIP60-eGFP transfected cells as compared to cells not expressing TIP60-eGFP, in the same sample. Viability of TIP60-eGFP transfected cells was decreased by 39% as compared to cells not expressing TIP60-eGFP (Figure 11D, E). Average transfection efficiency of TIP60-eGFP was 61%. In TIP60-eGFP transfected cells, there was also an increase in early and late apoptotic cells by 20% and 19%, respectively (Figure 11E, F).

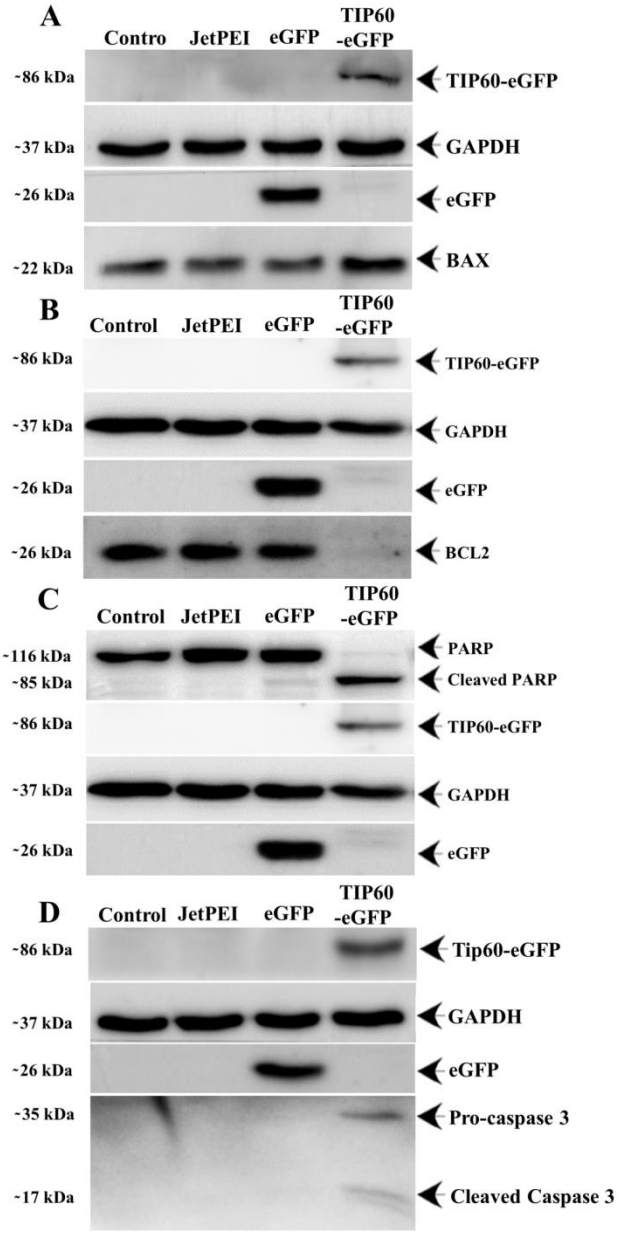

Figure 12. Effect of TIP60 overexpression on pro- and anti-apoptotic proteins. **(A)** BAX, **(B)** BCL2, **(C)** PARP and **(D)** Caspase 3 levels were analyzed by Western blot after TIP60 overexpression in HeLa cells.

Generally, p53 and p73-mediated apoptosis leads to activation of mitochondria dependent apoptotic pathway through transactivation of pro-apoptotic proteins (e.g. BAX) and down-

regulation of pro-survival proteins (e.g. BCL2). After TIP60 overexpression, the expression levels of BAX protein were increased (Figure 12A), while the expression levels of anti-apoptotic BCL2 protein were decreased (Figure 12B). To confirm the induction of apoptosis, we decided to check the expression of PARP and caspase 3. After TIP60 overexpression, caspase 3 activation from its precursor pro-caspase 3 was induced. Caspase 3 activation triggered the cleavage of PARP to induce apoptosis (Figure 12C).

Discussion

UHRF1 and TIP60 are present in the same epigenetic complex with their other interacting partners like DNMT1, USP7, HDAC1, PCNA (proliferating cell nuclear antigen) and G9a/EHMT2 (euchromatic histone-lysine N methyltransferase 2) (14,21,65,70,76). They interact with each other to maintain the epigenetic integrity. Interaction and conformation of these partners depend upon their need in genomic activity. Studies have reported higher expression levels of UHRF1 in most of cancer types (3,77) and these higher levels correspond to suppression of TSGs, tumor invasion, poor prognosis and resistance towards chemotherapy (3,24-28). In contrast to UHRF1, TIP60 expression levels are low in cancer cells. TIP60 has been believed to have a tumor suppressor role by maintaining the cellular and genomic stability (21,48,57-63). Concerning to crucial role of UHRF1 and TIP60 in cellular functions and integrity, it is of keen interest to investigate their interaction and down-stream effects of this interaction inside the cell. It is known now that UHRF1 directly interacts with TIP60 (21) and this interaction relies on MYST domain of TIP60 (3). Previously we have shown that TIP60 overexpression down-regulates UHRF1 and DNMT1 levels (3). Here we have suggested the possible mechanism involved in TIP60-mediated UHRF1 down-regulation and also proposed a model of TIP60-mediated apoptosis in cancer cells.

Western blot and confocal microscopy data had clearly shown that UHRF1 and DNMT1expression levels were decreased after TIP60 WT overexpression. Interestingly, the ΔMYST mutant (lacking acetyltransferase activity) did not show a significant effect on levels of both proteins, which is indicating that acetyltransferase activity of TIP60, is responsible for down-regulation of these proteins. Ubiquitination is a post-translational modification which adds single or multiple ubiquitin molecules to proteins marking them for proteasomal degradation, cellular trafficking, autophagy, DNA repair, receptor internalization or regulation of enzymatic activity (78,79). USP7 is a deubiquitinating enzyme which protects many proteins from ubiquitination including p53, UHRF1, PTEN, MDM2 and Myc. Its expression

levels have been reported high in many cancers. Dysregulation in ubiquitination/deubiquitination process can play a critical role in pathogenesis of several diseases including cancer (78). USP7 interacts with UHRF1 and protects it from degradation (64,66) while during M phase due to dissociation of USP7, UHRF1 is degraded (65). By performing *in vitro* acetylation assay Zhang *et al* reported that TIP60 acetylates UHRF1 at K659 and this decreases the interaction of USP7-UHRF1 (66). This convinced us to inquire the role of TIP60 overexpression in this association in HeLa cells. Our data showed that TIP60 WT overexpression has interfered with USP7 and UHRF1 association and expression levels while ΔMYST mutant failed to show any interference. Further studies are needed to understand in detail that how TIP60 acetylates UHRF1 *in vivo*.

Next we observed ubiquitination of the UHRF1 after TIP60 overexpression which is likely a consequence of TIP60-mediated interference with UHRF1-USP7 association. Due to dissociation, USP7 is no more able to protect UHRF1 from degradation through proteasomal pathway. Treatment with proteasomal inhibitor (MG-132) partially improved UHRF1 levels. Interestingly, USP7 levels were restored to normal after treatment with MG-132. This indicates that after TIP60 overexpression, once UHRF1 is degraded, its levels are not fully restored even after inhibiting proteasomal pathway. RING domain of UHRF1 has E3 ligase activity through which it can either ubiquitinate itself or other proteins (13,14). Here we show that TIP60 overexpression mediates auto-ubiquitination of UHRF1 WT while it was not observed in case of UHRF1 C724A mutant having impaired RING domain activity. FLIM-FRET analysis showed interesting aspect that interaction between UHRF1 and ubiquitin occurred in a time dependent manner. While UHRF1 protein having impaired E3 ligase activity was not able to interact with ubiquitin.

p53 is a TSG which preserves cellular and genomic integrity in response to stress conditions. TIP60 mediates p53 acetylation at K120 and this is very important for p53 induced activation of BAX and PUMA proteins and finally apoptosis (21). Another TSG p73 has been reported also to be involved in UHRF1 down-regulation and induction of apoptosis or cell cycle arrest (75). Higher UHRF1 levels directly interfere with TIP60-p53 interplay and block apoptosis.

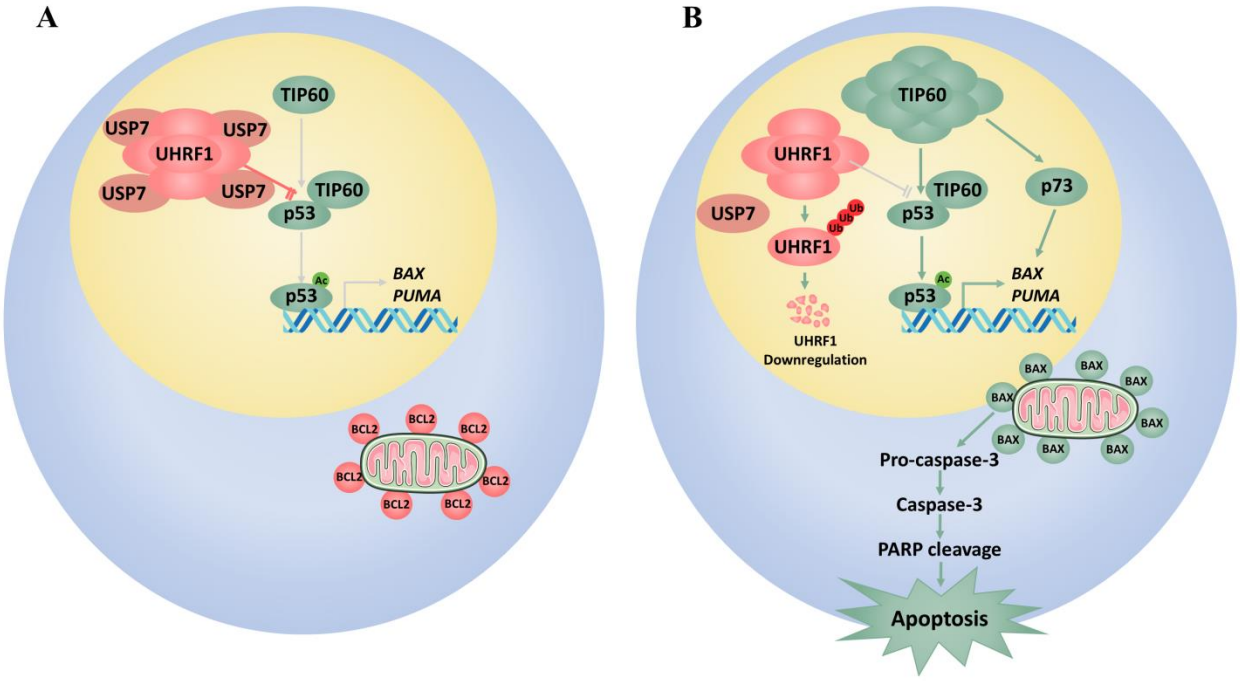

Figure 13. Schematic model of TIP60 mediated apoptosis in cancer cells. **(A)** Higher expression levels of UHRF1 in cancer inhibits TIP60-mediated p53 activation and apoptosis. **(B)** TIP60 overexpression leads to down-regulation of USP7 and UHRF1 levels. UHRF1 is degraded through proteasomal pathway. TIP60 overexpression counters inhibitory effect of UHRF1 on p53 and p73-mediated apoptosis. Gray lines indicate repressed pathway while dark lines indicate activated pathways.

UHRF1 binds with MYST domain of TIP60 and affects TIP60's ability to acetylate p53, which explains tumorogenesis role of UHRF1. Based on our observations, we have proposed a model depicting tumor suppressor role of TIP60 up-regulation in HeLa cells (Figure 13). TIP60 up-regulation induced apoptosis by activation of p53 and p73-mediated downstream signaling pathway. TIP60 overexpression led to decrease in BCL2 and increase in BAX expression which activated Caspase-3. Caspase-3 activated the cleavage of PARP and induced apoptosis.

Overall our observations suggest a tumor suppressor role of TIP60 which further can be studied in detail to therapeutically target UHRF1 which is mis-regulated in cancers. UHRF1's involvement in heterochromatin formation and transfer of DNA methylation patterns is linked with tumorogenesis (21). As UHRF1 levels are high in cancer cells while in fully differentiated cells or vital organs it is not expressed which makes it more specific and attractive target for anticancer therapy. In contrast to UHRF1, inhibitors targeting HDACs and DNMT1 have disadvantage of having less efficacy and specificity (4,26). UHRF1 also

regulates HDACs and DNMT1 proteins so targeting UHRF1 can have another benefit to control oncogenic functions of these proteins.

MATERIALS AND METHODS

Materials

MG-132 ($C_{26}H_{41}N_3O_5$) was purchased from Selleckchem.com Inhibitor Expert (S2619, USA). MG-132 was dissolved in pure DMSO (Sigma-Aldrich) and stored at -80°C. Guanidine HCl (G3272), Urea (U5378) and 2-mercaptoethanol (M6250) were purchased from Sigma-Aldrich. Propidium iodide (130-093-233) was purchased from Miltenyi Biotec while Annexin V-iFlour™ 350 conjugate (20090) was purchased from AAT Bioquest®. FxCycle™ PI/RNase staining solution (F10797) was purchased from ThermoFischer Scientific and BD Cell FIX (340181) was purchased from BD Biosciences.

Cell culture

HeLa cells (ATCC, CCL-2, Amp, Cervical Adenocarcinoma; Human) and HeLa cells stably expressing either GFP-UHRF1 WT or GFP-UHRF1 C724A protein, were grown in Dulbecco's Modified Eagle's Medium (DMEM 1X + GlutaMAX™, Pyruvate, Gibco, Lifetech, France) which was supplemented with 10% fetal bovine serum (FBS, S1810-500, Dominique Dutscher), in addition to mixture of penicillin (100 U/ml) and streptomycin (100 U/ml) (17-602E, Lonza, USA), at 37°C with 5% CO_2 in humidified environment. Plasmids were transfected with in HeLa cells with either jetPEI™ or jetPRIME (PolyPlus-transfection, France) according to the manufacturer's protocol.

Plasmid constructs

TIP60 wild type and mutants (ΔHAT, ΔMYST) were cloned into a pEGFP-N1 plasmid to express eGFP-labeled TIP60 proteins in HeLa cells. UHRF1was cloned into pCMV-mCherry vector to express UHRF1-mCherry protein. RFP-Ubiquitin was purchased from addgene (#11935).

Antibodies

Mouse monoclonal anti-UHRF1 was engineered as described previously (1). Other antibodies used include rabbit polyclonal anti-HAUSP/USP7 (Abcam, ab4080), rabbit polyclonal anti-TIP60 (Genetex, GTX 112197), mouse monoclonal anti-DNMT1 (Proteogenix, France, PTG-

MAB0079), mouse monoclonal anti-Ubiquitin (Merck, 05-944), mouse monoclonal eGFP (Proteintech, 66,002-1-Ig and Thermo Fisher Scientific A-11120), rabbit polyclonal anti-mCherry (Genetex GTX 59788), mouse monoclonal anti-GAPDH (Merck Millipore MAB374), mouse monoclonal anti-GFP (Proteintech, 66002-1-Ig), mouse monoclonal anti-p73 (BD Biosciences Pharmingen, 558785), mouse monoclonal p53 (BD Biosciences Pharmingen, 554293), rabbit polyclonal anti-Caspase 3 (Cell Signaling Technology, Danvers, MA, USA, 9661), mouse monoclonal anti-BCL2 (Merck-Millipore, 05-826), mouse monoclonal anti-PARP (BD Biosciences Pharmingen, 51-6639GR) and rabbit polyclonal anti-BAX (Merck Millipore, AB2930).

Western blotting

For Western blot, cells were collected 24 h after the transfection by trypsinization. For ubiquitination experiments, cells were treated with MG-132 (10 µM) 8 h before cells harvesting. After centrifugation, media was discarded, and cell pellet was washed with PBS. Cells were lysed with ice cold lysis buffer (10mM Tris-HCl pH 7.5, 1mM EDTA, 150 mM NaCl and 1% NP40 supplemented with protease inhibitors (11836170001, cOmplete mini EDTA-free protease inhibitor cocktail tablets, Roche Diagnostics GmbH, Germany). After denaturation for 7 min in Laemmli sample buffer (1610747, Bio-Rad Laboratories USA), 40 µg of the protein from cell lysates were loaded on 7.5% and 10% SDS-PAGE gels. Proteins were identified by anti-UHRF1, anti-Ubiquitin, anti-DNMT1, anti-USP7, anti-eGFP and anti-GAPDH antibodies, with overnight incubation at 4°C. HRP (horseradish peroxidase) conjugated secondary antibodies, anti-mouse (W402B, Promega, France) or anti-rabbit (W401B, Promega, France) were used to label primary antibodies. Signals were detected on an Image Quant LAS 4000 apparatus (GE Healthcare Life Sciences, USA) with chemiluminescent ECL system (Clarity^{TM} ECL western blotting substrate, Bio-Rad, France, 170-5060). Image Studio Lite (Li-Core Biosciences, USA) was used to analyze the images.

Immunoprecipitation (IP)

For immunoprecipitation, cells were collected and lysed by freeze shock. Mild sonication was done in ice cold PBS freshly supplemented with protease inhibitors cocktail tablet. Input controls were made by taking 40 µg of protein from each lysate. 1000 µg to 1500 µg of protein lysate were incubated with anti-UHRF1 antibody at 4°C for 3 h or with anti-USP7 antibody at 4°C for overnight. After washing and equilibration, 60 µL of Dynabeads® protein A (Thermo Fischer Scientific, Norway 1002D) were added to the lysate-antibody mixture and

incubated for 1 h at 4 °C. Later on, beads were collected and washed 3-5 times with ice cold PBS freshly supplemented with protease inhibitors tablet. Finally, beads were resuspended in Laemmli sample buffer. Proteins were denatured by heating at 95 °C for 7 min and analyzed through Western blotting.

Cell-based ubiquitination assay

Assay was performed essentially as described (21) with some modifications. HeLa cells were co-transfected with either TIP60-eGFP and His-Ubiquitin or TIP60ΔMYST-eGFP and His-Ubiquitin plasmids. All samples were treated with MG-132 (10 µM) 8 h before cell harvesting. 10% of the cells were lysed with lysis buffer and were saved as input. Remaining cell pellet was lysed with mild sonication in phosphate/guanidine buffer (10 mM Tris-HCl pH 8.0, 6 M Guanidine-HCl, 6.8 mM NaH_2PO_4, 0.1 M $Na_2HPO_4.2H_2O$, 0.2% Triton X-100 freshly supplemented with 5 mM Imidazole and 10 mM β-mercaptoethanol). To pull down His-tagged proteins, Ni-NTA beads (Qiagen 30,230) were added to sample lysates for 4h at room temperature. Phosphate/guanidine and Urea wash buffer (10 mM Tris-HCl pH 8.0, 8 M Urea, 0.1 M $Na_2HPO_4.2H_2O$, 6.8 mM NaH_2PO_4, 0.2% Triton X-100 freshly supplemented with 5 mM Imidazole and 10 mM β-mercaptoethanol) were used to wash the Ni-NTA captured fractions. Then fractions were washed thrice with Wash buffer (10 mM Tris-HCl pH 6.3, 80 mM NaH_2PO_4, 18 mM $Na_2HPO_4.2H_2O$, 0.2% Triton X-100 freshly supplemented with 5 mM Imidazole and 10 mM β-mercaptoethanol). Further, precipitates were eluted for 40 min in 60 µL of Elution buffer (0.5 M Imidazole, 0.125 M DTT). Finally, samples were analyzed by Western blotting.

UHRF1 auto-ubiquitination assay

HeLa cell lines stably expressing GFP-UHRF1 wild type and GFP-UHRF1 RING C724A mutant proteins were prepared as described elsewhere (80). HeLa cells stably expressing GFP-UHRF1 WT and GFP-UHRF1 C724A mutant proteins were transfected with either TIP60 WT or TIP60ΔMYST mutant with jetPRIME reagent. Samples were treated with 10 µM MG-132, 8h before harvesting the cells. Immunoprecipitation (as described above) was performed with anti-GFP antibody to immunoprecipitate the GFP-tagged UHRF1 protein. Samples were resolved by Western blotting.

Confocal microscopy

To study the effect of TIP60 overexpression on UHRF1 and DNMT1 levels, HeLa cells were seeded on a cover glass and transfected with eGFP or TIP60-eGFP or TIP60ΔMYST-eGFP plasmids by using jetPEI^{TM} reagent as described in manufacturer's protocol. 24 h post-transfection, cells were fixed with 4% paraformaldehyde for 10 minutes and then, permeabilized with 0.2% Triton X-100 for 20 min at room temperature. Next, blocking was done with 1% BSA for 1 hour, before incubation with a primary antibody against either UHRF1 or DNMT1 for 3 h at 4°C. After washing three times with PBS, cells were incubated with secondary antibody labeled with Alexa Fluor 568 (goat anti-mouse, A11031, Invitrogen) for 60 min at room temperature. Finally, cells were washed three times and labeled with DAPI (Hoechst stain 33258, Molecular probes). Finally, cells were imaged with a confocal Leica TCS SPE microscope equipped with a 20× air (0.7 NA) immersion lens objective. For DAPI, Alexa Flour 568 and eGFP, excitation was performed with a 405 nm laser (25 mW), 561 nm laser (10 mW) and 488 nm laser (25 mW), respectively. The detection range for the three dyes was 430-480 nm, 570-630 nm and 500-523 nm, respectively.

To check the effect of TIP60 overexpression over co-localization of UHRF1 and Ubiquitin, HeLa cells were co-transfected with either eGFP and RFP-Ubiquitin or TIP60-eGFP and RFP-Ubiquitin by using jetPEI^{TM} reagent. One group of samples was treated with MG-132 (10 μM) 8 h before cell fixation, to block the proteasomal degradation of UHRF1. Cells were labeled with anti-UHRF1 as primary antibody and Alexa Flour 647 (goat anti-mouse, A21237, Molecular probes) as secondary antibody. DAPI staining was done to stain the nucleus. All samples were imaged with a confocal Leica TCS SPE equipped with an oil immersion objective (HXC PL APO 63×/1.40 OIL CS). For DAPI, RFP, Alexa Flour 647 and eGFP, excitation was performed with a 405 nm laser (25 mW), 561 nm laser (10 mW), 635 nm laser (18 mW) and 405 nm laser (25 mW), respectively. The detection range for the four dyes was 430-480 nm, 570-630 nm, 640-702 nm and 500-523 nm, respectively.

For UHRF1-USP7 association study, HeLa cells were transfected with either TIP60-eGFP or TIP60ΔMYST-eGFP by using jetPEI^{TM} reagent. One group of samples was treated with MG-132 (10 μM) 8 h before cell fixation, to block the proteasomal degradation of UHRF1 and USP7. Cells were labeled with anti-UHRF1 (mouse) and anti-USP7 (rabbit) antibodies overnight at 4 °C. Then cells were incubated with secondary antibody labeled with Alexa Flour 568 (goat anti-rabbit, A11011, Invitrogen) for USP7 and Alexa Fluor 647 (goat anti-

mouse) for UHRF1. DAPI staining was done to stain the nucleus. All samples were imaged with a confocal Leica TCS SPE equipped with an oil immersion objective (HXC PL APO 63×/1.40 OIL CS). For DAPI, Alexa Flour 568, Alexa Flour 647 and eGFP, excitation was performed with a 405 nm laser (25 mW), 561 nm laser (10 mW), 635 nm laser (18 mW) and 405 nm laser (25 mW), respectively. The detection range for the four dyes was 430-480 nm, 570-625 nm, 644-707 nm and 500-531 nm, respectively. All the images were processed with Image J software.

Fluorescence Lifetime Imaging Microscopy (FLIM)

HeLa cells stably expressing GFP-UHRF1 were seeded (10^5 cells per dish) in a µ-dish (Ibidi) with 35 mm wells. Cells were transfected with 1 µg RFP-Ubiquitin plasmid by using jetPEI™ reagent. Cells were fixed with 4% paraformaldehyde. After fixation, cells were analyzed with a homemade two-photon excitation scanning microscope based on an Olympus IX70 inverted microscope with an 60× 1.2 NA water immersion objective operating in the descanned fluorescence collection mode as described (72,81). Two-photon excitation at 930 nm was provided by an Insight DeepSee laser (Spectra Physics). Fluorescence photons were collected using a short-pass filter with a cut-off wavelength of 680 nm (F75-680, AHF, Germany) and a band-pass filter of 520 ± 17 nm (F37-520, AHF, Germany). The fluorescence was directed to a fiber coupled APD (SPCM-AQR-14-FC, Perkin Elmer), which was connected to a time-correlated single photon counting module (SPC830, Becker & Hickl, Germany). FLIM data were analyzed using SPCImage v 7.3 (Becker & Hickel) and the Förster resonance energy transfer (FRET) efficiency was calculated according to $E=1-(\tau_{DA}/\tau_D)$, where τ_{DA} is the lifetime of the donor (GFP) in the presence of acceptor (RFP) and τ_D is the lifetime of GFP in the absence of acceptor.

Apoptosis analysis

Flow cytometry was used to analyze the TIP60 induced apoptosis. HeLa cells were seeded in six well plates. Cells were transfected with TIP60-eGFP by using jetPEI™ reagent. TIP60 transfected cells were compared to control cells or cells treated with jetPEI™ only. Cells were collected after mild trypsinization and were incubated with Propidium iodide (PI) and Annexin V-iFlour™350 conjugate. Then samples were analyzed through Guava easyCyte™ flow cytometer (Merck Millipore). InCyte Software for Guava (Merck Millipore) was used to analyze the results.

Author contributions

TA conducted biochemical and cellular experiments with the help of WA and LZ under the supervision of MM and CB. TA, CB and MM wrote most of the manuscript with guidance and help of AH and YM. All authors read and approved the final manuscript.

Conflict of interest

The authors declare that they have no conflict of interest.

FUNDING

We thank the ANR (SMFLUONA, ANR-17-CE11-0036-01) for financial support. T.A. and W.A. were supported by fellowships from HEC (Pakistan). LZ was supported by fellowships from Lebanese government.

ACKNOWLEDGEMENTS

We thank Romain Vauchelles (Plate-forme d'Imagerie Quantitative- PIQ) and Ludovic Richert for their help in Confocal and FLIM experiments.

References

1. Hopfner, R., Mousli, M., Jeltsch, J.-M., Voulgaris, A., Lutz, Y., Marin, C., Bellocq, J.-P., Oudet, P., and Bronner, C. (2000) *Cancer Research* **60**, 121-128
2. Krifa, M., Alhosin, M., Muller, C. D., Gies, J.-P., Chekir-Ghedira, L., Ghedira, K., Mély, Y., Bronner, C., and Mousli, M. (2013) *Journal of experimental & clinical cancer research : CR* **32**, 30-30
3. Ashraf, W., Ibrahim, A., Alhosin, M., Zaayter, L., Ouararhni, K., Papin, C., Ahmad, T., Hamiche, A., Mély, Y., Bronner, C., and Mousli, M. (2017) *Oncotarget* **8**, 51946-51962
4. Bronner, C., Achour, M., Arima, Y., Chataigneau, T., Saya, H., and Schini-Kerth, V. B. (2007) *Pharmacology & Therapeutics* **115**, 419-434
5. Bostick, M., Kim, J. K., Estève, P.-O., Clark, A., Pradhan, S., and Jacobsen, S. E. (2007) *Science* **317**, 1760-1764
6. Bronner, C., Alhosin, M., Hamiche, A., and Mousli, M. (2019) *Genes (Basel)* **10**, 65
7. Avvakumov, G. V., Walker, J. R., Xue, S., Li, Y., Duan, S., Bronner, C., Arrowsmith, C. H., and Dhe-Paganon, S. (2008) *Nature* **455**, 822
8. Sharif, J., Muto, M., Takebayashi, S.-i., Suetake, I., Iwamatsu, A., Endo, T. A., Shinga, J., Mizutani-Koseki, Y., Toyoda, T., Okamura, K., Tajima, S., Mitsuya, K., Okano, M., and Koseki, H. (2007) *Nature* **450**, 908
9. Arita, K., Ariyoshi, M., Tochio, H., Nakamura, Y., and Shirakawa, M. (2008) *Nature* **455**, 818
10. Nady, N., Lemak, A., Walker, J. R., Avvakumov, G. V., Kareta, M. S., Achour, M., Xue, S., Duan, S., Allali-Hassani, A., Zuo, X., Wang, Y.-X., Bronner, C., Chédin, F., Arrowsmith, C. H., and Dhe-Paganon, S. (2011) *The Journal of biological chemistry* **286**, 24300-24311

11. Rajakumara, E., Wang, Z., Ma, H., Hu, L., Chen, H., Lin, Y., Guo, R., Wu, F., Li, H., Lan, F., Shi, Y. G., Xu, Y., Patel, D. J., and Shi, Y. (2011) *Molecular Cell* **43**, 275-284
12. Hu, L., Li, Z., Wang, P., Lin, Y., and Xu, Y. (2011) *Cell research* **21**, 1374
13. Tauber, M., and Fischle, W. (2015) *Nucleus (Austin, Tex.)* **6**, 123-132
14. Du, Z., Song, J., Wang, Y., Zhao, Y., Guda, K., Yang, S., Kao, H.-Y., Xu, Y., Willis, J., Markowitz, S. D., Sedwick, D., Ewing, R. M., and Wang, Z. (2010) *Science signaling* **3**, ra80-ra80
15. Nishiyama, A., Yamaguchi, L., Sharif, J., Johmura, Y., Kawamura, T., Nakanishi, K., Shimamura, S., Arita, K., Kodama, T., Ishikawa, F., Koseki, H., and Nakanishi, M. (2013) *Nature* **502**, 249
16. Qin, W., Wolf, P., Liu, N., Link, S., Smets, M., La Mastra, F., Forné, I., Pichler, G., Hörl, D., Fellinger, K., Spada, F., Bonapace, I. M., Imhof, A., Harz, H., and Leonhardt, H. (2015) *Cell research* **25**, 911-929
17. Foster, B. M., Stolz, P., Mulholland, C. B., Montoya, A., Kramer, H., Bultmann, S., and Bartke, T. (2018) *Molecular Cell* **72**, 739-752.e739
18. Li, T., Wang, L., Du, Y., Xie, S., Yang, X., Lian, F., Zhou, Z., and Qian, C. (2018) *Nucleic acids research* **46**, 3218-3231
19. Alhosin, M., Omran, Z., Zamzami, M. A., Al-Malki, A. L., Choudhry, H., Mousli, M., and Bronner, C. (2016) *Journal of experimental & clinical cancer research : CR* **35**, 174-174
20. Alhosin, M., Sharif, T., Mousli, M., Etienne-Selloum, N., Fuhrmann, G., Schini-Kerth, V. B., and Bronner, C. (2011) *Journal of experimental & clinical cancer research : CR* **30**, 41-41
21. Dai, C., Shi, D., and Gu, W. (2013) *The Journal of biological chemistry* **288**, 19581-19592
22. Guan, D., Factor, D., Liu, Y., Wang, Z., and Kao, H. Y. (2013) *Oncogene* **32**, 3819-3828
23. Fujimori, A., Matsuda, Y., Takemoto, Y., Hashimoto, Y., Kubo, E., Araki, R., Fukumura, R., Mita, K., Tatsumi, K., and Muto, M. (1998) *Mammalian Genome* **9**, 1032-1035
24. Boukhari, A., Alhosin, M., Bronner, C., Sagini, K., Truchot, C., Sick, E., Schini-Kerth, V. B., AndrÉ, P., MÉLy, Y., Mousli, M., and Gies, J.-P. (2015) *Anticancer Research* **35**, 149-157
25. Jeanblanc, M., Mousli, M., Hopfner, R., Bathami, K., Martinet, N., Abbady, A.-Q., Siffert, J.-C., Mathieu, E., Muller, C. D., and Bronner, C. (2005) *Oncogene* **24**, 7337
26. Unoki, M., Brunet, J., and Mousli, M. (2009) *Biochemical Pharmacology* **78**, 1279-1288
27. Wang, F., Yang, Y.-Z., Shi, C.-Z., Zhang, P., Moyer, M. P., Zhang, H.-Z., Zou, Y., and Qin, H.-L. (2012) *Annals of Surgical Oncology* **19**, 2753-2762
28. Xue, B., Zhao, J., Feng, P., Xing, J., Wu, H., and Li, Y. (2019) *OncoTargets and therapy* **12**, 549-559
29. Unoki, M., Kelly, J. D., Neal, D. E., Ponder, B. A. J., Nakamura, Y., and Hamamoto, R. (2009) *British journal of cancer* **101**, 98
30. Kong, X., Chen, J., Xie, W., Brown, S. M., Cai, Y., Wu, K., Fan, D., Nie, Y., Yegnasubramanian, S., Tiedemann, R. L., Tao, Y., Chiu Yen, R.-W., Topper, M. J., Zahnow, C. A., Easwaran, H., Rothbart, S. B., Xia, L., and Baylin, S. B. *Cancer Cell*
31. Jenkins, Y., Markovtsov, V., Lang, W., Sharma, P., Pearsall, D., Warner, J., Franci, C., Huang, B., Huang, J., Yam, G. C., Vistan, J. P., Pali, E., Vialard, J., Janicot, M., Lorens, J. B., Payan, D. G., and Hitoshi, Y. (2005) *Molecular Biology of the Cell* **16**, 5621-5629
32. Tien, A. L., Senbanerjee, S., Kulkarni, A., Mudbhary, R., Goudreau, B., Ganesan, S., Sadler, K. C., and Ukomadu, C. (2011) *The Biochemical journal* **435**, 175-185
33. Mousli, M., Hopfner, R., Abbady, A. Q., Monté, D., Jeanblanc, M., Oudet, P., Louis, B., and Bronner, C. (2003) *British journal of cancer* **89**, 120-127
34. Cai, Y., Tsai, H.-C., Yen, R.-W. C., Zhang, Y. W., Kong, X., Wang, W., Xia, L., and Baylin, S. B. (2017) *Genome research* **27**, 533-544
35. Kamine, J., Elangovan, B., Subramanian, T., Coleman, D., and Chinnadurai, G. (1996) *Virology* **216**, 357-366
36. Yamamoto, T., and Horikoshi, M. (1997) *Journal of Biological Chemistry* **272**, 30595-30598
37. Hilfiker, A., Hilfiker-Kleiner, D., Pannuti, A., and Lucchesi, J. C. (1997) *The EMBO Journal* **16**, 2054-2060
38. Lee, K. K., and Workman, J. L. (2007) *Nature Reviews Molecular Cell Biology* **8**, 284

39. Doyon, Y., Selleck, W., Lane, W. S., Tan, S., and Côté, J. (2004) *Molecular and cellular biology* **24**, 1884-1896
40. Voss, A. K., and Thomas, T. (2009) *BioEssays* **31**, 1050-1061
41. Sheikh, B. N., and Akhtar, A. (2019) *Nature Reviews Genetics* **20**, 7-23
42. Kim, C.-H., Kim, J.-W., Jang, S.-M., An, J.-H., Seo, S.-B., and Choi, K.-H. (2015) *Bioscience, Biotechnology, and Biochemistry* **79**, 532-538
43. Kim, M.-Y., Ann, E.-J., Kim, J.-Y., Mo, J.-S., Park, J.-H., Kim, S.-Y., Seo, M.-S., and Park, H.-S. (2007) *Molecular and cellular biology* **27**, 6506-6519
44. Sapountzi, V., Logan, I. R., and Robson, C. N. (2006) *The International Journal of Biochemistry & Cell Biology* **38**, 1496-1509
45. Putnik, J., Zhang, C.-D., Archangelo, L. F., Tizazu, B., Bartels, S., Kickstein, M., Greif, P. A., and Bohlander, S. K. (2007) *Biochimica et Biophysica Acta (BBA) - Molecular Basis of Disease* **1772**, 1211-1224
46. Squatrito, M., Gorrini, C., and Amati, B. (2006) *Trends in Cell Biology* **16**, 433-442
47. Kimura, A., Matsubara, K., and Horikoshi, M. (2005) *The Journal of Biochemistry* **138**, 647-662
48. Ikura, T., Ogryzko, V. V., Grigoriev, M., Groisman, R., Wang, J., Horikoshi, M., Scully, R., Qin, J., and Nakatani, Y. (2000) *Cell* **102**, 463-473
49. Judes, G., Rifaï, K., Ngollo, M., Daures, M., Bignon, Y.-J., Penault-Llorca, F., and Bernard-Gallon, D. (2015) *Epigenomics* **7**, 1351-1363
50. Mouhamed, I., Khaldoun, R., Marine, D., Frédérique, P.-L., Yves-Jean, B., and Dominique, B.-G. (2018) *OMICS: A Journal of Integrative Biology* **22**, 626-628
51. Frank, S. R., Parisi, T., Taubert, S., Fernandez, P., Fuchs, M., Chan, H.-M., Livingston, D. M., and Amati, B. (2003) *EMBO reports* **4**, 575-580
52. Mo, F., Zhuang, X., Liu, X., Yao, P. Y., Qin, B., Su, Z., Zang, J., Wang, Z., Zhang, J., Dou, Z., Tian, C., Teng, M., Niu, L., Hill, D. L., Fang, G., Ding, X., Fu, C., and Yao, X. (2016) *Nature chemical biology* **12**, 226-232
53. DeRan, M., Pulvino, M., Greene, E., Su, C., and Zhao, J. (2008) *Molecular and cellular biology* **28**, 435-447
54. Niida, H., Katsuno, Y., Sengoku, M., Shimada, M., Yukawa, M., Ikura, M., Ikura, T., Kohno, K., Shima, H., Suzuki, H., Tashiro, S., and Nakanishi, M. (2010) *Genes & development* **24**, 333-338
55. Taubert, S., Gorrini, C., Frank, S. R., Parisi, T., Fuchs, M., Chan, H.-M., Livingston, D. M., and Amati, B. (2004) *Molecular and cellular biology* **24**, 4546-4556
56. Hu, Y., Fisher, J. B., Koprowski, S., McAllister, D., Kim, M.-S., and Lough, J. (2009) *Developmental dynamics : an official publication of the American Association of Anatomists* **238**, 2912-2921
57. Berns, K., Hijmans, E. M., Mullenders, J., Brummelkamp, T. R., Velds, A., Heimerikx, M., Kerkhoven, R. M., Madiredjo, M., Nijkamp, W., Weigelt, B., Agami, R., Ge, W., Cavet, G., Linsley, P. S., Beijersbergen, R. L., and Bernards, R. (2004) *Nature* **428**, 431-437
58. Sakuraba, K., Yokomizo, K., Shirahata, A., Goto, T., Saito, M., Ishibashi, K., Kigawa, G., Nemoto, H., and Hibi, K. (2011) *Anticancer Research* **31**, 77-79
59. Sakuraba, K., Yasuda, T., Sakata, M., Kitamura, Y.-H., Shirahata, A., Goto, T., Mizukami, H., Saito, M., Ishibashi, K., Kigawa, G., Nemoto, H., Sanada, Y., and Hibi, K. (2009) *Anticancer Research* **29**, 3953-3955
60. Gorrini, C., Squatrito, M., Luise, C., Syed, N., Perna, D., Wark, L., Martinato, F., Sardella, D., Verrecchia, A., Bennett, S., Confalonieri, S., Cesaroni, M., Marchesi, F., Gasco, M., Scanziani, E., Capra, M., Mai, S., Nuciforo, P., Crook, T., Lough, J., and Amati, B. (2007) *Nature* **448**, 1063
61. Kim, J. H., Kim, B., Cai, L., Choi, H. J., Ohgi, K. A., Tran, C., Chen, C., Chung, C. H., Huber, O., Rose, D. W., Sawyers, C. L., Rosenfeld, M. G., and Baek, S. H. (2005) *Nature* **434**, 921-926
62. Jha, S., Vande Pol, S., Banerjee, N. S., Dutta, A. B., Chow, L. T., and Dutta, A. (2010) *Molecular Cell* **38**, 700-711
63. Brown, J. A. L., Bourke, E., Eriksson, L. A., and Kerin, M. J. (2016) *Biochemical Society transactions* **44**, 979-986

64. Felle, M., Joppien, S., Németh, A., Diermeier, S., Thalhammer, V., Dobner, T., Kremmer, E., Kappler, R., and Längst, G. (2011) *Nucleic acids research* **39**, 8355-8365
65. Ma, H., Chen, H., Guo, X., Wang, Z., Sowa, M. E., Zheng, L., Hu, S., Zeng, P., Guo, R., Diao, J., Lan, F., Harper, J. W., Shi, Y. G., Xu, Y., and Shi, Y. (2012) *Proceedings of the National Academy of Sciences of the United States of America* **109**, 4828-4833
66. Zhang, Z.-M., Rothbart, Scott B., Allison, David F., Cai, Q., Harrison, Joseph S., Li, L., Wang, Y., Strahl, Brian D., Wang, Gang G., and Song, J. (2015) *Cell Reports* **12**, 1400-1406
67. Gelato, Kathy A., Tauber, M., Ong, Michelle S., Winter, S., Hiragami-Hamada, K., Sindlinger, J., Lemak, A., Bultsma, Y., Houliston, S., Schwarzer, D., Divecha, N., Arrowsmith, Cheryl H., and Fischle, W. (2014) *Molecular Cell* **54**, 905-919
68. Fang, J., Cheng, J., Wang, J., Zhang, Q., Liu, M., Gong, R., Wang, P., Zhang, X., Feng, Y., Lan, W., Gong, Z., Tang, C., Wong, J., Yang, H., Cao, C., and Xu, Y. (2016) *Nature Communications* **7**, 11197
69. Rothbart, S. B., Dickson, B. M., Ong, M. S., Krajewski, K., Houliston, S., Kireev, D. B., Arrowsmith, C. H., and Strahl, B. D. (2013) *Genes & development* **27**, 1288-1298
70. Achour, M., Fuhrmann, G., Alhosin, M., Rondé, P., Chataigneau, T., Mousli, M., Schini-Kerth, V. B., and Bronner, C. (2009) *Biochemical and Biophysical Research Communications* **390**, 523-528
71. Cheng, J., Yang, H., Fang, J., Ma, L., Gong, R., Wang, P., Li, Z., and Xu, Y. (2015) *Nature Communications* **6**, 7023
72. Clamme, J. P., Azoulay, J., and Mély, Y. (2003) *Biophysical journal* **84**, 1960-1968
73. Becker, W. (2015) *Advanced time-correlated single photon counting applications*, Springer
74. Voss, T. C., Demarco, I. A., and Day, R. N. (2005) *Biotechniques* **38**, 413-424
75. Alhosin, M., Abusnina, A., Achour, M., Sharif, T., Muller, C., Peluso, J., Chataigneau, T., Lugnier, C., Schini-Kerth, V. B., Bronner, C., and Fuhrmann, G. (2010) *Biochemical Pharmacology* **79**, 1251-1260
76. Kim, J. K., Estève, P.-O., Jacobsen, S. E., and Pradhan, S. (2009) *Nucleic acids research* **37**, 493-505
77. Polepalli, S., George, S. M., Valli Sri Vidya, R., Rodrigues, G. S., Ramachandra, L., Chandrashekar, R., M, D. N., Rao, P. P. N., Pestell, R. G., and Rao, M. (2019) *The International Journal of Biochemistry & Cell Biology* **114**, 105558
78. Gao, Y., Wang, Y., Zhou, C., Kong, S., Lu, J., Wang, H., and Yang, J. (2019) *Development, Growth & Differentiation* **61**, 176-185
79. Popovic, D., Vucic, D., and Dikic, I. (2014) *Nature Medicine* **20**, 1242
80. Ibrahim, A., Alhosin, M., Papin, C., Ouararhni, K., Omran, Z., Zamzami, M. A., Al-Malki, A. L., Choudhry, H., Mély, Y., Hamiche, A., Mousli, M., and Bronner, C. (2018) *Oncotarget* **9**, 28599-28611
81. El Meshri, S. E., Dujardin, D., Godet, J., Richert, L., Boudier, C., Darlix, J. L., Didier, P., Mély, Y., and de Rocquigny, H. (2015) *Journal of Molecular Biology* **427**, 1480-1494

Manuscript III: A molecular tool targeting the base-flipping activity of human UHRF1

ChemPubSoc Europe

DOI: 10.1002/chem.201902605

CHEMISTRY
A European Journal
Full Paper

DNA Binding

A Molecular Tool Targeting the Base-Flipping Activity of Human UHRF1

Liliyana Zaayter[+],[a] Mattia Mori[+],[b] Tanveer Ahmad[+],[a] Waseem Ashraf,[a] Christian Boudier,[a] Vasyl Kilin,[a] Krishna Gavvala,[a] Ludovic Richert,[a] Sylvia Eiler,[c] Marc Ruff,[c] Maurizio Botta,[b] Christian Bronner,[c] Marc Mousli,*[a] and Yves Mély*[a]

Abstract: During DNA replication, ubiquitin-like, containing PHD and RING fingers domains 1 (UHRF1) plays key roles in the inheritance of methylation patterns to daughter strands by recognizing through its SET and RING-associated domain (SRA) the methylated CpGs and recruiting DNA methyltransferase 1 (DNMT1). Herein, our goal is to identify UHRF1 inhibitors targeting the 5′-methylcytosine (5mC) binding pocket of the SRA domain to prevent the recognition and flipping of 5mC and determine the molecular and cellular consequences of this inhibition. For this, we used a multidisciplinary strategy combining virtual screening and molecular modeling with biophysical assays in solution and cells. We identified an anthraquinone compound able to bind to the 5mC binding pocket and inhibit the base-flipping process in the low micromolar range. We also showed in cells that this hit impaired the UHRF1/DNMT1 interaction and decreased the overall methylation of DNA, highlighting the critical role of base flipping for DNMT1 recruitment and providing the first proof of concept of the druggability of the 5mC binding pocket. The selected anthraquinone appears thus as a key tool to investigate the role of UHRF1 in the inheritance of methylation patterns, as well as a starting point for hit-to-lead optimizations.

Introduction

During the life of an organism, the genome undergoes a chain of epigenetic processes that shapes the function and morphology of a cell in a very diverse way. These epigenetic processes notably direct the gene expression patterns, establishing the identity of a cell that could be heritable for future generations. DNA methylation is a major epigenetic modification that controls the cell identity and fate, being responsible for many fundamental processes, such as differentiation, genome imprinting, and X-chromosome inactivation.[1] This mark is also strongly involved in cancer,[2] as it is recognized that DNA hypermethylation at specific loci is one of the hallmarks of tumorigenesis. Indeed, abnormal gain of DNA methylation in promoter regions of tumor suppressor genes plays a key role in their silencing and transcriptional repression.[3] Interestingly, the reversible nature of this epigenetic mechanism, unlike genetic ones, has earned epigenetic mediators a considerable attention as pharmaceutical targets. Different strategies can be used to target DNA methylation as numerous actors are involved in this epigenetic process, but the most effective would be to interfere with early effectors involved in the duplication of the methylation patterns. In order to achieve a faithful transmission of these patterns, the DNA methylation machinery is coordinated by a macromolecular protein complex,[4] in which UHRF1 (ubiquitin-like, containing PHD and RING fingers domains 1) is the first effector. Indeed, UHRF1 binds specifically through its SET and RING-associated domain (SRA) to CpG motifs in the hemi-methylated (HM) DNA formed by the parent and daughter strands and flips out the 5′-methylcytosine (5mC) from the DNA helix.[5] X-ray crystallography structures of SRA in complex with HM DNA helped to propose a model of DNA recognition and base flipping.[5a,6] In these structures, SRA acts as a hand grasping the DNA duplex in its palm and through its NKR finger and its thumb, it flips out the 5mC into a binding pocket located in the palm. The flipped-out 5mC is stabilized by π-stacking interactions with two aromatic residues (Y478, Y466).[6b] Besides this, UHRF1 also binds to histone H3K9me3 through its tandem Tudor and PHD domains.[7] These features promote the recruitment of DNA methyltransferase1 (DNMT1) to replication forks in the S phase of the cell cycle in order to ensure the maintenance of the methylation

[a] Dr. L. Zaayter,[+] T. Ahmad,[+] Dr. W. Ashraf, Dr. C. Boudier, Dr. V. Kilin, Dr. K. Gavvala, Dr. L. Richert, Dr. M. Mousli, Prof. Y. Mély
Laboratoire de Bioimagerie et Pathologies, UMR 7021 CNRS
Faculté de Pharmacie, Université de Strasbourg, Illkirch (France)
E-mail: marc.mousli@unistra.fr
yves.mely@unistra.fr

[b] Dr. M. Mori,[+] Dr. M. Botta
Dipartimento di Biotecnologie, Chimica e Farmacia
Dipartimento di Eccellenza 2018–2022, Università degli Studi di Siena
Via Aldo Moro 2, 53100, Siena (Italy)

[c] Dr. S. Eiler, Dr. M. Ruff, Dr. C. Bronner
Institut de Génétique et de Biologie Moléculaire et Cellulaire (IGBMC)
INSERM U964 CNRS UMR 7104, Université de Strasbourg, Illkirch (France)

[+] These authors contributed equally to this work.

Supporting information and the ORCID identification number(s) for the author(s) of this article can be found under: https://doi.org/10.1002/chem.201902605.

patterns in the newly formed DNA.[5b,7b,8] Alternatively, through the E3 ligase activity of its RING domain, UHRF1, can also mediate the ubiquitylation of H3K23 and H3K18, creating binding sites for DNMT1.[9] The presence of hemi-methylated CpG sites plays a primary role in driving UHRF1 conformational changes,[10] which consequently allow the SRA domain to flip the mC residues facilitating the recruitment of the enzyme.

Numerous emerging therapeutic strategies focus on targeting DNA methylation,[11] but to date, only demethylating agents targeting DNMTs have been disclosed. These agents include FDA-approved nucleoside analogs (azacytidine and decitabine)[12] and non-nucleoside inhibitors, such as hydralazine and procainamide[13] that majorly target DNMT1. Several limitations upon their usage, such as chemical instability, cytotoxicity, and poor selectivity[14] stimulated the search of alternative treatments with improved efficacy and fewer side effects. Due to its key role in DNA methylation and its overexpression in almost every type of tumors,[15] UHRF1 is perceived as a major target for anti-cancer therapy.[16] Several natural compounds have been reported to act on UHRF1 signaling pathways,[4b,17] but only two inhibitors have been identified to directly target the protein. One of these inhibitors is an uracil derivative that targets the SRA domain and perturbs the interaction with DNMT1,[18] whereas the second one, 4-benzylpiperidine-1-carboximidamide, targets the TTD groove and alters the binding of UHRF1 to H3K9me3.[19] Finally, mitoxantrone, a topoisomerase II inhibitor of the anthracycline family, has also been reported to alter the binding of the SRA domain to HM DNA and induce hypomethylation with subsequent re-expression of tumor suppressor genes (TSGs).[20] Very recently, a time-resolved fluorescence resonance energy transfer (TR-FRET) assay based on the binding of SRA to HM DNA was used to screen the library of pharmacologically active compounds (LOPAC).[21] This screening confirmed that mitoxantrone as well as four other topoisomerase II inhibitors of the anthracycline family can inhibit the SRA binding to HM DNA and induce dose-responsive global DNA demethylation. However, this study did not clearly identify the binding site of the anthracyclines on the protein and/or DNA.

In this context, our aim was to discover small molecules that can fit into the 5mC binding pocket of the SRA domain and characterize their molecular and cellular activity, with the goal to obtain a proof of principle that this pocket can be an appropriate target for drug development. To this aim, we established a multidisciplinary strategy that includes virtual screening and molecular modeling together with biophysical assays and cellular studies. We identified the active compound UM63 that shares some chemical features with mitoxantrone.[22] Through binding to the 5mC binding pocket, UM63 prevented base flipping with an IC_{50} value in the low micromolar range. Moreover, UM63 inhibited the DNMT1/UHRF1 interaction and decreased the DNA methylation level in HeLa cells. Therefore, UM63 emerges as a valuable tool for characterizing the role of base flipping in molecular and cellular assays and provides the first proof of concept of the druggability of the 5mC binding pocket of UHRF1.

Results

Selection of hits by virtual screening

With the aim to identify different chemotypes of UHRF1 inhibitors that target the 5mC binding pocket of the SRA domain and based on structural information available from X-ray crystallography studies,[5a,6,23] a diversity-oriented and structure-based virtual screening approach was established. The high-resolution crystallographic structure of the human SRA domain of UHRF1 bound to HM DNA[5a] was used as a rigid receptor in virtual screening. Analysis of the interactions established by the flipped 5mC in its narrow binding site within SRA revealed key pharmacophoric features, such as the aromatic ring, which is π–π stacked to the side chain of Tyr478 in a parallel displaced geometry, and several polar groups able to establish hydrogen bonds with the protein. These features were exploited to pre-screen the MolPort database of commercially available compounds and to enrich the test set with compounds endowed with a high probability to mimic the binding of 5mC within the SRA binding site. In particular, the aniline substructure was selected for filtration of the database, which was accomplished through a SMARTS-based query with the FILTER application of OMEGA from OpenEye.[24] This operation decreased the overall size of the screening library up to around 31K molecules, which were submitted to conformational analysis with OMEGA (OpenEye)[24] and were subsequently docked within the 5mC binding site by the FRED docking program from OpenEye.[25] The top-ranking 1000 compounds were further selected for visual inspection. To maximize chemical diversity in the virtual hits, these molecules were clustered based on fingerprints and a substructure search through a cheminformatics approach.[26] The combination between visual inspection and chemical diversity led to the selection of 26 small molecules for in vitro testing (Figure S1 in the Supporting Information).

Selection of hits by using an in vitro "base flipping assay"

To test the 26 compounds selected by virtual screening, we used a fluorescence-based assay highly sensitive to 5mC base flipping. This assay is based on the use of a HM DNA labeled by thienoguanosine (thG) (Figure 1 A), an isomorphic guanosine derivative that has been shown to perfectly replace the guanine residue next to the methylated cytosine in the CpG motif.[27] Addition of SRA to this labeled DNA is accompanied by a 4-fold increase in the fluorescence intensity, as a result of the SRA-induced flipping of the 5mC residue[27a] (Figures 1 B and C). Among the 26 compounds, UM63 was the most promising hit candidate, as it induced a concentration-dependent decrease in the fluorescence intensity, suggesting that it could inhibit the SRA-induced base flipping with an IC_{50} value of (4.4 ± 0.5) μM (Figure 1 B). To further evaluate the potency of UM63 to inhibit base flipping, we compared it to 5-methylcytidine, the natural ligand of the SRA binding pocket in its free form (Figure S2 in the Supporting Information). Addition of 5-methylcytidine at a concentration as high as 500 μM induced

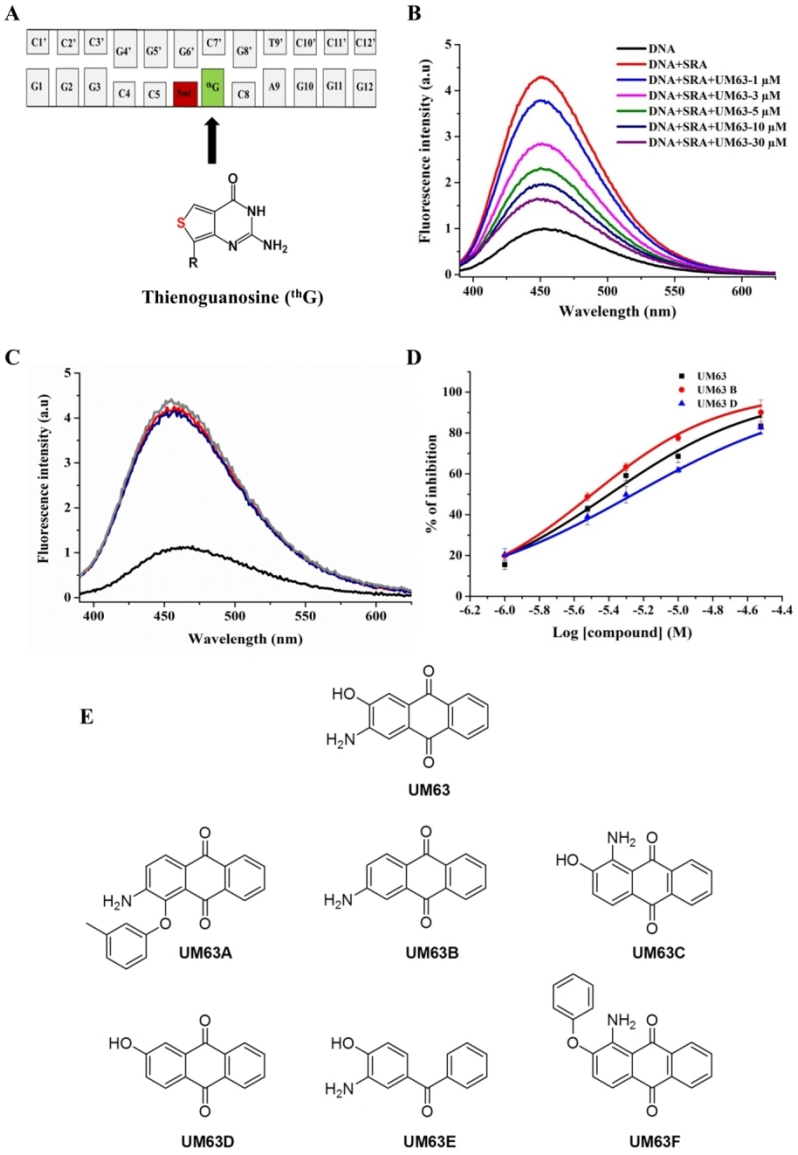

Figure 1. Effects and structures of compounds selected by virtual screening on the base-flipping assay. A) Sequence of the thG-labeled HM duplex. The guanosine at position 7 substituted by thG is highlighted in green and the methylated cytosine is in red. B) Emission spectra of thG-labeled HM DNA (1 μM) in the absence and in the presence of SRA (3 μM) before and after addition of 1, 3, 5, 10, or 30 μM of UM63. C) Emission spectra of HM thG-labeled DNA (1 μM) in the absence (black) and in the presence of SRA (3 μM) before (red) and after addition of 10 (dark blue) and 100 μM (gray) of UM63 E. D) Dose-response curve representing the inhibition of SRA base-flipping activity by the selected compounds. The solid lines correspond to the fits of the experimental points by Equation (2) in the Experimental Section. The IC_{50} values given in the text are the mean ± SEM of three independent experiments. Experiments were performed in phosphate buffer 20 mM, NaCl 50 mM, ethylenediaminetetraacetic acid (EDTA) 1 mM, tris(2-carboxyethyl)phosphine (TCEP) 2.5 mM, polyethylene glycol (PEG) 0.05 %, pH 7.5. E) Chemical structure of UM63 and six commercially available analogues of UM63 selected for in vitro tests.

only a limited inhibition of the base-flipping activity of SRA, indicating that 5-methylcytosine is far less potent than UM63. This suggests that the 5-methylcytosine base exhibits only a moderate affinity to the SRA binding pocket and that in the context of the HM, the numerous contacts with the neighbor bases of 5mC are instrumental for the base-flipping process. To further substantiate the quality of the selected scaffold, six commercially available chemical derivatives of UM63, namely UM63 A–UM63 F (Figure 1 E) were selected and tested. Whereas UM63 E was totally ineffective even at 100 μM (Figure 1 C), UM63 B and UM63 D were able to efficiently inhibit the SRA-induced base flipping, with IC_{50} values of (3.3 ± 0.3) and (6.1 ± 0.7) μM, respectively (Figures S3 A and B in the Supporting Information). Noticeably, the thG fluorescence decrease was not due to a quenching by these compounds, because none of them modified the fluorescence of the labeled duplexes in the absence of SRA (Figure S4 in the Supporting Information). The corresponding K_i values calculated from Equation (3) in the Experimental Section were, respectively, (1.45 ± 0.15), (1.05 ± 0.1), and (2.0 ± 0.2) μM for UM63, UM63 B, and UM63 D (Figure 1 D), indicating that the three compounds have similar potency in inhibiting the SRA-induced base flipping. As the three compounds have similar chemical structures, this strongly suggests that their activity is related to a specific pharmacophore.

Binding parameters of the positive hits to SRA and HM DNA

In order to determine whether the inhibitory effect of the three selected compounds on the SRA-induced base flipping is related to their binding to SRA, we determined by isothermal titration calorimetry (ITC) their thermodynamic binding parameters for SRA.

ITC titration of UM63 by SRA (Figure 2A) showed that the reaction is exothermic ($\Delta H = -18.8$ kJ mol^{-1}), with a K_d value of (0.94 ± 0.25) μM and a 1:1 stoichiometry. The reaction was also characterized by a positive entropy variation ΔS, suggesting that formation of the SRA/UM63 complex is partly driven by release of ions and water molecules. In contrast, the interaction of UM63B and UM63D with wild-type SRA was heat-silent (data not shown), preventing the determination of their K_d values. In a next step, we examined the possible interaction of UM63, UM63B, and UM63D with DNA (Figures 2C, S5A and B in the Supporting Information). The binding of the three compounds to DNA was found to be exothermic with K_d values of 0.1–0.2 μM. These strong affinities could be rationalized by the fact that anthraquinones are DNA intercalators.[28] UM63 was clearly confirmed as a DNA intercalator by its ability to displace ethidium bromide (EtBr) from DNA (Figure S6 in the Supporting Information). However, the DNA intercalating properties of these compounds appear marginal in the base-flipping inhibition (Figures 1B and S3 in the Supporting Information), because UM63E binds to DNA (Figure S5C in the Supporting Information) with an affinity comparable to the affinity of the three selected compounds but is unable to inhibit the SRA-driven base flipping of HM DNA (Figure 1C). From the clear demonstration of its binding to SRA, UM63 was selected for further studies.

UM63 binds to the SRA binding pocket and decreases the affinity of SRA to DNA

To experimentally evidence that UM63 targets the 5mC binding pocket on SRA, we replaced the wild-type SRA with a SRA-G448D mutant where the glycine 448 residue is replaced by a more bulky aspartic acid to block the binding pocket and prevent base flipping.[5a,27a] As expected, only marginal binding was observed with this mutant (Figure 2B), confirming that the 5mC binding pocket of SRA is the target of UM63, in line with molecular modeling predictions. To further explore the base-flipping inhibition by UM63, we investigated by the stopped-flow technique how UM63 alters the kinetics of the SRA-induced 5mC flipping in the thG-labeled DNA.[27a] In line with our previous study,[27a] the kinetic trace of the thG-labeled DNA in the presence of SRA showed a slow component with a rate constant of approximately 6.5 s^{-1} attributed to the 5mC base-flipping process (Figure 3, red curve). Addition of UM63 only marginally decreases the kinetic rate constant, but efficiently reduces the final fluorescence plateau in a concentration-dependent manner (Figure 3 compare blue and magenta curves with the red curve). This decrease in the plateau is consistent with the spectra in Figure 1 and the co-existence of a UM63-bound SRA population that is unable to flip the 5mC base with a population of free SRA that flips 5mC with unaltered kinetics. With increasing UM63 concentrations, the population of free active SRA decreases, explaining the decrease in the final plateau. As expected, the negative compound UM63E did not induce any change in the kinetics or the final plateau (Figure S7 in the Supporting Information). To determine whether the interaction of UM63 with the binding pocket may alter the DNA binding properties of SRA, we performed binding experiments by using the non-methylated version of the DNA duplex in Figure 1A. As no base flipping occurs with this non-methylated duplex,[27a] the effect of UM63 on the binding process can only be explored.

Accordingly, we titrated by fluorescence anisotropy the thG-labeled non-methylated DNA with increasing concentrations of SRA in the absence or in the presence of 10 μM UM63. In the absence of UM63, the equilibrium dissociation constant K_d of SRA-to-DNA was found to be (0.43 ± 0.04) μM (Figure 4A), close to the previously reported value.[27a] Addition of UM63 decreased the apparent affinity of SRA to DNA ($K_d = (1.04 \pm$

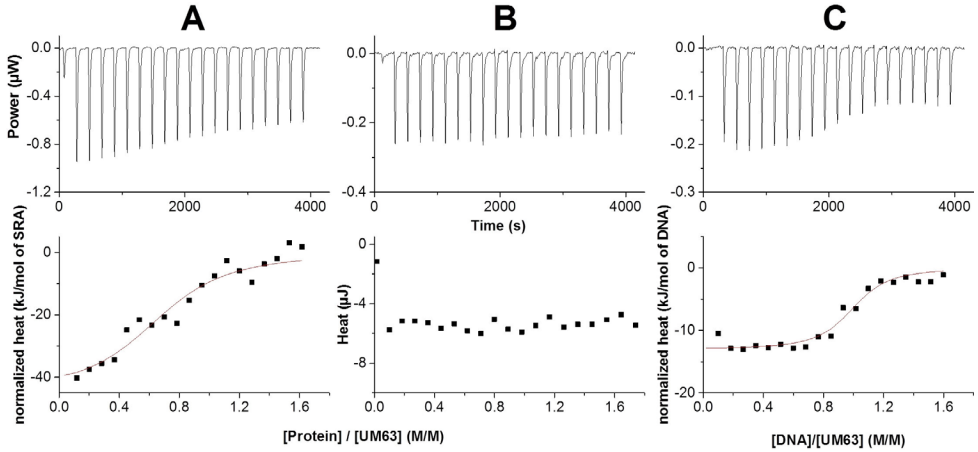

Figure 2. Binding of UM63 to A) SRA, B) SRA-G448D, and C) HM DNA, as monitored by ITC. The protein and HM DNA concentration in the syringe were 80 μM. The concentration of UM63 was 8 μM. During titration, the area of the power peaks regularly decreases, reaching a plateau value that corresponds to the dilution heats of the proteins or HM DNA into the buffer alone. The curves were fitted to the experimental normalized heat quantities by using Equation (6) in the Experimental Section. Experiments were performed at 20 °C in 20 mM phosphate buffer, NaCl 50 mM, pH 7.5.

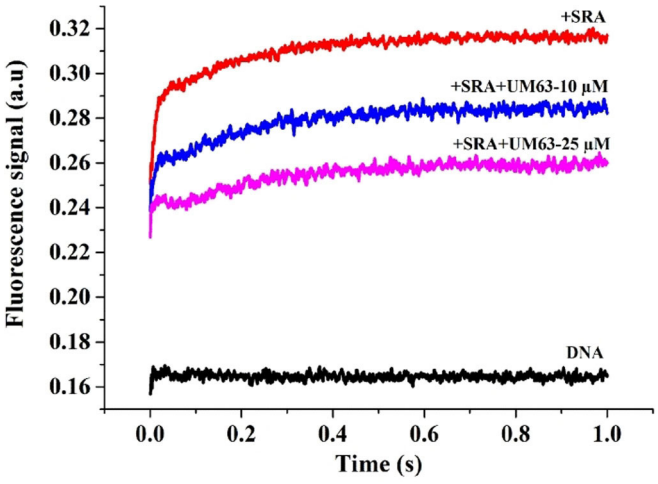

Figure 3. Stopped-flow traces showing the effect of UM63 on the base-flipping kinetics of the SRA domain. The black trace corresponds to the thG-labeled HM duplex mixed with buffer. The red trace describes the interaction of the thG-labeled HM duplex with SRA. The blue and magenta traces describe the kinetics of interaction of the thG-labeled HM duplex with SRA in the presence of 10 and 25 μM UM63. The final concentrations of the thG-labeled HM DNA and SRA were 0.2 and 1.5 μM, respectively. Experiments were performed in phosphate buffer 20 mM, NaCl 50 mM, TCEP 2.5 mM, pH 7.5.

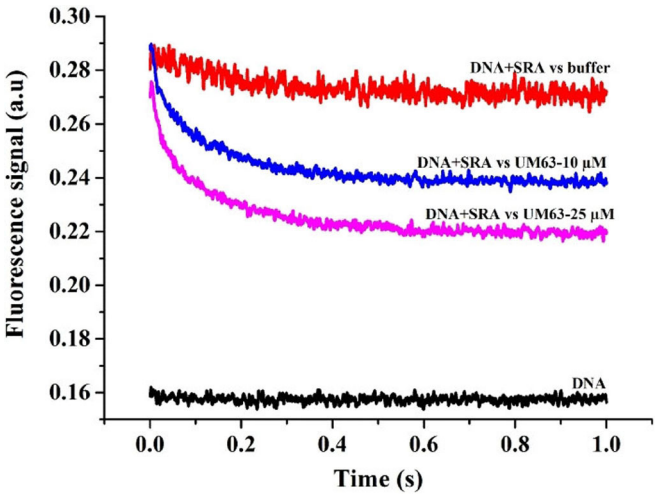

Figure 5. Stopped-flow traces for the dissociation kinetics of the DNA/SRA complex by UM63. The curves were recorded after addition of 10 and 25 μM of UM63 to a complex formed by 0.2 μM of thG-labeled HM duplex and 1.5 μM SRA. The red and black curves correspond to the DNA/SRA complex and the DNA alone mixed with buffer, respectively.

0.15) μM), indicating that UM63 alters the binding properties of SRA to DNA (Figure 4A). In contrast, no competition was observed when the thG-labeled DNA was titrated by the SRA-G448D mutant (Figure 4B), confirming that UM63 is unable to bind to this SRA mutant.

To confirm that UM63 decreases the affinity or SRA to DNA, we added 10 or 25 μM of UM63 to the pre-formed complex of SRA with the thG-labeled HM duplex and monitored the changes in the thG fluorescence with time (Figure 5).

With both concentrations, the time-dependent decrease in the thG fluorescence intensity was like that previously observed when the complex was challenged with an excess of non-labeled DNA,[27a] indicating a dissociation of the complex, when UM63 binds to the SRA binding pocket. Independently of the UM63 concentration, a dissociation rate constant of 8 s^{-1} was observed, in good agreement with the 3 s^{-1} rate constant of the flipping back of the 5mC residue, the rate-limiting step of the dissociation of the SRA/HM DNA complex.[27a] As expected, the negative compound UM63E inactive on base flipping (Figure 1C) was unable to affect the SRA/HM DNA complex, when added at a 10 μM concentration (Figure S8 in the Supporting Information).

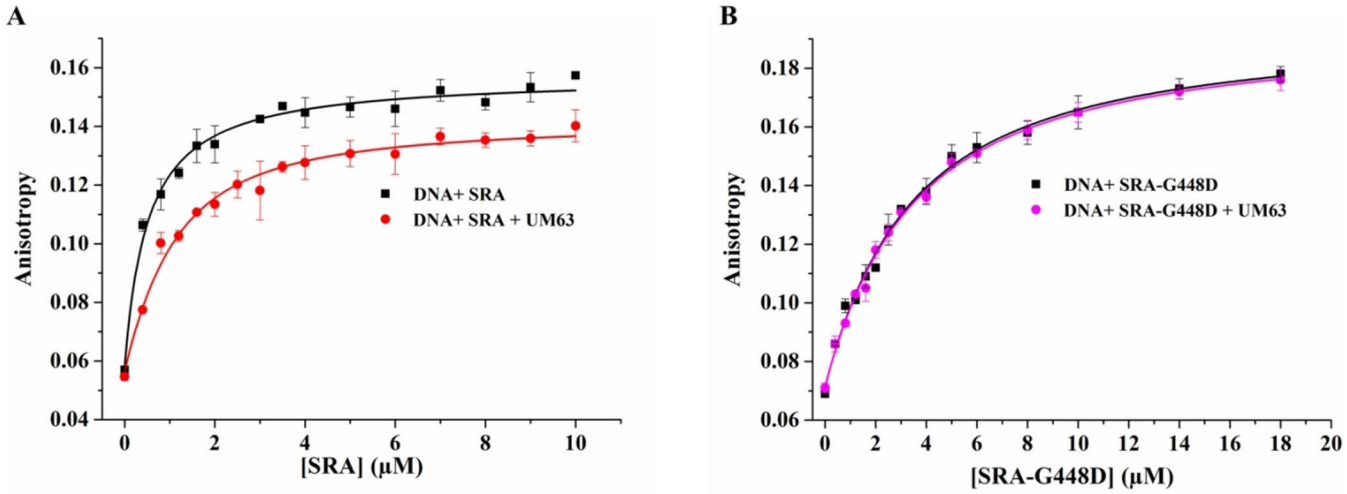

Figure 4. Effect of UM63 on the binding of SRA and SRA-G448D to non-methylated DNA, as monitored by fluorescence anisotropy. A) Titration of 1 μM DNA with SRA in the absence or in the presence of 10 μM UM63. B) Titration of 1 μM DNA with SRA-G448D in the absence or in the presence of 10 μM UM63. Experimental points are represented as means ± SEM for $n = 3$ independent experiments. The solid lines correspond to the fits of the experimental data to Equations (4) and (5) in the Experimental Section.

Binding mode of UM63 to the SRA binding pocket

The interaction of UM63 within the binding site of 5mC on SRA was further investigated by molecular modeling simulations. Compared to the virtual screening setting, a more accurate docking simulation was carried out with the FRED docking program to predict the possible binding mode of UM63. These simulations clearly show that UM63 acts as 5mC mimetic, being π–π stacked with the side chain of Tyr478 and hydrogen-bonded to key residues that are also contacted by the flipped 5mC and the backbone of HM DNA,[5a] such as Asp469, Thr479, Gly448, Gly465, and Ala463 (Figure 6). It is worth noting that the distal phenyl ring of the anthraquinone core occupies a region near the entrance of the binding site, where it sterically overlaps with the crystallographic binding of DNA phosphate backbone. The overlap is particularly important at the level of the 5mC nucleotide, which may further explain the decreased affinity of DNA to SRA in the presence of UM63 (Figure S9 in the Supporting Information).

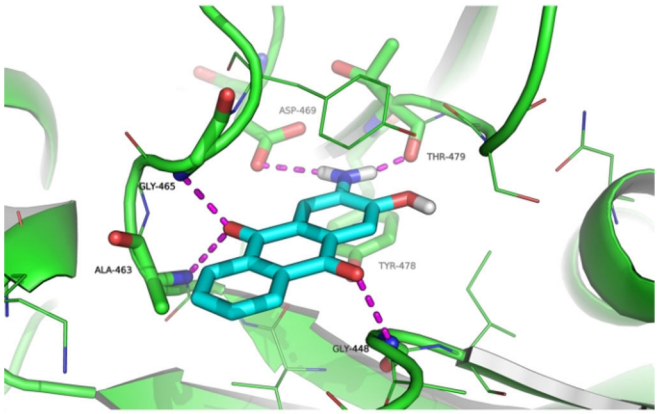

Figure 6. Docking-based binding mode of UM63 within the 5mC binding site of SRA. UM63 is shown as cyan sticks and the crystallographic structure of SRA (PDB 3CLZ) is shown as green cartoon. Residues within 5 Å from UM63 are shown as lines, whereas residues contacted by UM63 via hydrogen bonds or π–π stacking are shown as sticks and are labeled (residue numbering corresponds to the scheme adopted in the crystallographic structure). Hydrogen bonds are highlighted by magenta dashed lines.

The phenol group of UM63 does not participate in hydrogen bonding to the SRA and points towards partially accessible sub-pockets of the 5mC binding site, thus representing a possible site for hit-to-lead optimization. In contrast, the amino group and the quinone moiety are well adapted to interact with SRA residues and could less easily be modified or substituted. Overall, the binding mode of UM63 predicted by molecular docking is highly comparable to the crystallographic binding mode of 5mC. It is also consistent with the lack of detectable binding of UM63 to the G448D mutant of SRA, because the Asp488 side chain in the mutant SRA occupies the binding site and thus, prevents UM63 interaction by steric hindrance.

Inhibition of SRA activity by UM63 is associated with a drop in global DNA methylation

Considering that UM63 is a chemically stable and cell-permeable anthraquinone,[29] we decided to further investigate its effects in HeLa cells. First, we performed a trypan blue assay in HeLa cells to evaluate the cytotoxicity of UM63 and UM63 E at different concentrations. After 24 h treatment, no cytotoxicity was observed up to 10 μM of UM63 or UM63 E (Figures S10 A and B in the Supporting Information). After 48 h treatment, a significant but still moderate cytotoxicity was observed with 10 μM UM63 (Figure S10 C in the Supporting Information), but not with UM63 E, where cytotoxicity appears only at 100 μM (Figure S10 D in the Supporting Information). Based on this assay and on the nearly 1 μM affinity of UM63 for SRA, we decided to test the cellular effects of UM63 at a 10 μM concentration, as a compromise for high activity and low cytotoxicity. In a first step, we tested the effect of UM63 and UM63 E on DNA methylation. Keeping in mind that in vitro experiments and molecular modeling revealed that UM63 competed with the binding of SRA to the HM DNA and inhibited the flipping of the 5mC base, UM63 is expected to induce genomic DNA demethylation. Global DNA methylation was estimated by an immunofluorescence assay by using a specific monoclonal antibody against 5mC and Alexa488-labeled secondary antibody (Figure 7 A). Based on the mean fluorescence intensity of Alexa488, the global DNA methylation level was found to decrease after 48 h incubation with UM63 at 10 μM (Figure 7 B).

The drop in the fluorescence (43 %) was comparable to that induced by 10 μM of azacytidine (62 %), a reference DNMT1 inhibitor taken as a positive control. In contrast, there was no significant fluorescence decrease (11 %) in the sample treated with 10 μM UM63 E. Therefore, the decrease in the global genomic methylation induced by UM63 may tentatively be related to its effect on the SRA/HM DNA complexes.

UM63 prevents the interaction between UHRF1 and DNMT1 in cells

The observed inhibition of DNA methylation by UM63 could be the result of the inhibition of 5mC flipping by UHRF1, which in turn prevents the recruitment of DNMT1 that is responsible of DNA methylation. To test this hypothesis, we used first confocal microscopy to study the co-localization of eGFP-DNMT1 and UHRF1-mcherry in HeLa cells in the S phase treated with 10 μM of UM63 or UM63 E and labeled with both EdU-Alexa647 and 4′,6-Diamidine-2′-phenylindole dihydrochloride (DAPI) (Figure 8). In non-treated cells, UHRF1 and DNMT1 are well co-localized with each other, being concentrated at the replication foci evidenced by EdU-Alexa647 labeling (Figure 8, panels 1 d–g), consistent with previous observations.[5b,7b,8,30] In contrast, UM63 induces a diffuse distribution of UHRF1-mCherry in the nucleus (Figure 8, panel 2 b), with a decrease of the co-localization with EdU (Figure 8, panel 2 e), confirmed by the significant decrease of the Pearson correlation coefficient (PCC) between UHRF1 and EdU (from (0.37 ± 0.03) in non-treated cells to (0.23 ± 0.02) in UM63-treated cells, Figure S11 A in the

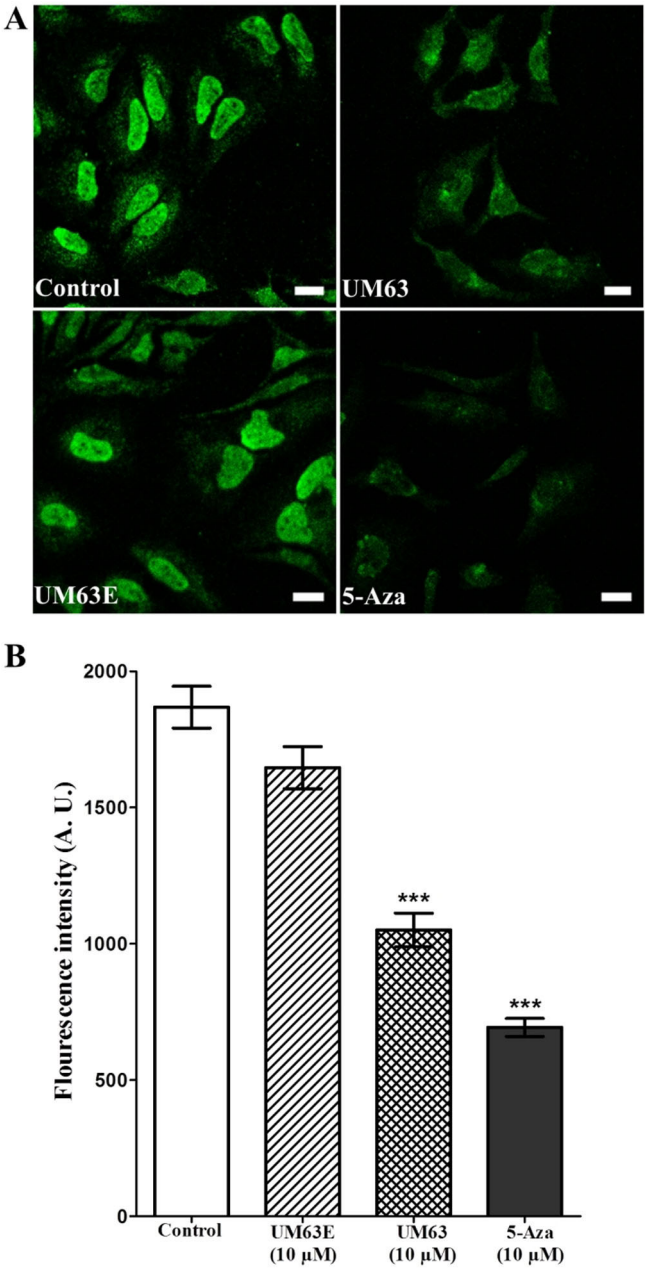

Figure 7. Effect of UM63 and UM63 E on the global DNA methylation in HeLa cells. A) Immunostaining of 5mC in HeLa cells. Non-treated HeLa cells served as negative control, whereas cells treated with 10 μM 5-azacytidine were used as a positive control and were compared to cells treated with 10 μM of UM63 and UM63 E. The cells were fixed after treatment and labeled by anti-5mC and Alexa488-labeled secondary antibodies before visualization in confocal microscopy. Scale bars = 20 μm. B) Mean fluorescence intensities representing the amount of methylated cytosine in genomic DNA. Values are mean ± SEM for three independent experiments; statistically significant: * = $p < 0.05$, ** = $p < 0.01$, *** = $p < 0.001$ (versus untreated group).

Supporting Information). A diffuse pattern (Figure 8, panel 2 a) was also observed for eGFP-DNMT1, which is concentrated in large areas, from which EdU-Alexa647 is excluded (Figure 8, panels 2 c and d). This decreased co-localization of DMNT1 and EdU was confirmed by the decrease of the PCC value from (0.57 ± 0.03) in non-treated cells to (0.45 ± 0.04) in UM63-treated cells (Figure S11 B in the Supporting Information).

Our data indicate that UM63 prevents the localization of both UHRF1 and DNMT1 at the replication foci. It should be noted that despite the redistribution of UHRF1 and DNMT1 in the nucleus, the two proteins remain well co-localized, as suggested by comparison of the PCC values (Figure S11 C in the Supporting Information). However, this co-localization cannot be interpreted in terms of direct interaction between UHRF1 and DNMT1, due to the limited resolution of confocal microscopy (300 nm). As both proteins are distributed throughout the nucleus, co-localization may simply be a consequence of the fact that all the microscopically sampled focal volumes contain both proteins, whether they interact or not. In contrast to UM63, the negative compound UM63 E showed only a limited effect on the co-localization of UHRF1 and DNMT1 at the replication foci (Figure 8, panels 3 a–g), as confirmed by the similar PCC values in the UM63 E- and non-treated cells (Figures S11 A and B in the Supporting Information). Next, the possible interaction between DNMT1 and UHRF1 was assessed in vitro by a co-immunoprecipitation assay (Figure 9). Precipitation of eGFP-DNMT1 by an anti-eGFP antibody led to the co-immunoprecipitation of UHRF1-mCherry, whereas no co-precipitation was observed when free mCherry was co-transfected with eGFP-DNMT1. This suggests a specific interaction between eGFP-DNMT1 and UHRF1-mCherry. The interaction between eGFP-DNMT1 and UHRF1-mCherry was lowered in cells treated by UM63 as a lower amount of UHRF1-mCherry was pulled down with eGFP-DNMT1, whereas treatment with UM63E only marginally impacted this interaction. To unambiguously confirm the UHRF1/DNMT1 interaction and the effect of UM63 on it, we performed Förster resonance energy transfer (FRET) experiments (Figure 10). FRET between eGFP- and mCherry-labeled proteins only occurs when they are less than 8 nm apart, a distance corresponding to intermolecular protein interactions.[31] The FRET efficiency is ideally measured through the decrease of the fluorescence lifetime of eGFP by fluorescence lifetime imaging microscopy (FLIM).[32]

By measuring the fluorescence decay at each pixel of the cell, the FLIM technique allows extracting the fluorescence lifetime (τ) that, in contrast to the fluorescence intensity, does not depend on the instrumentation or the concentration of the fluorophores. The fluorescence lifetime of eGFP was calculated and color coded in each pixel of the image (Figure 10). The lifetime of eGFP-DNMT1 used as a control was (2.55 ± 0.01) ns ($n = 21$ cells) in cells transfected with eGFP-DNMT1 alone (Figure 10 A). This lifetime was decreased to (2.10 ± 0.02) ns ($n = 32$ cells) when eGFP-DNMT1 was co-transfected with UHRF1-mCherry (Figure 10 B). This corresponds to a FRET efficiency of (18 ± 1) %, clearly confirming that UHRF1 and DNMT1 interact in the cell nucleus, in full line with our Co-IP data (Figure 9) and previous reports.[5b,8,33] When cells co-transfected with eGFP-DNMT1 and UHRF1-mCherry were treated with 10 μM UM63, the FRET strongly decreases, as the lifetime values came back to values close to those of the control (Figure 10 C).

The very low residual FRET value [(2 ± 0.3) %, $n = 31$ cells), well below the commonly accepted 5 % significance limit for protein/protein interactions,[34] clearly confirmed that UM63 impaired the interaction of UHRF1 with DNMT1. In sharp contrast,

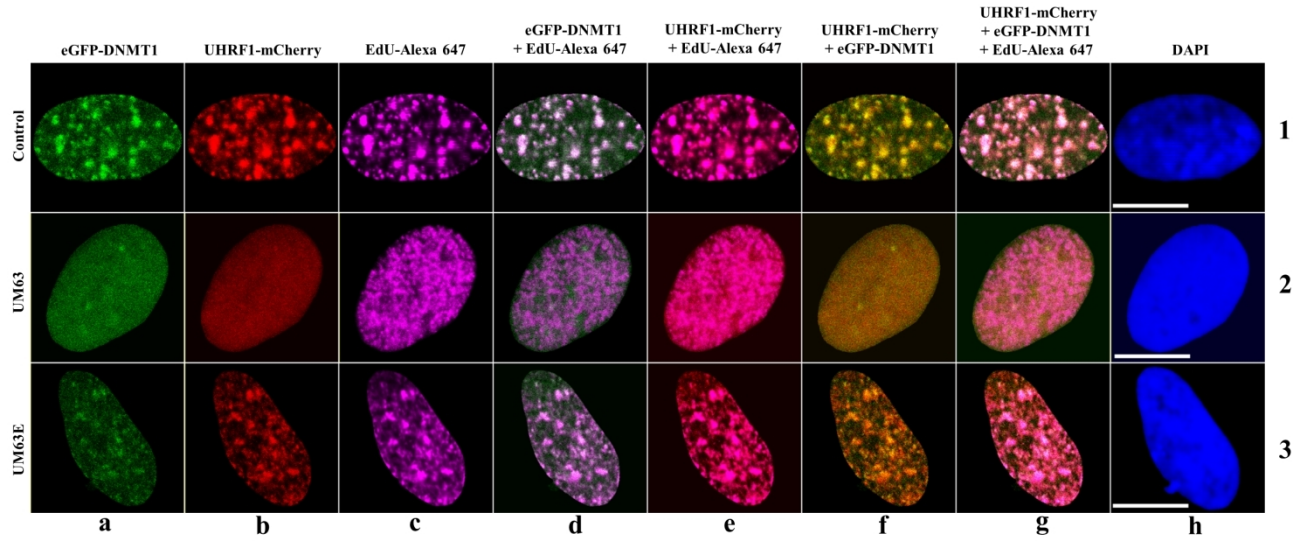

Figure 8. Effect of UM63 and UM63E on DNMT1/UHRF1 co-localization. Confocal images show the co-transfection of eGFP-DNMT1 and UHRF1-mCherry in HeLa cells labeled with EdU-Alexa 647 and DAPI. Panels 1, 2, and 3 correspond to representative control (untreated), UM63 (10 μM), and UM63E (10 μM) treated samples, respectively. Channels a), b), and c) represent eGFP-DNMT1, UHRF1-mCherry expression, and EdU-Alexa 647 (S phase) labeling, respectively. Channels d) and e) correspond to localization of eGFP-DNMT1 and UHRF1-mCherry with EdU-Alexa647, respectively. Channel f) represents co-localization of UHRF1-mCherry and eGFP-DNMT1, whereas channel g) represents co-localization of both proteins with EdU-Alexa647. Channel h) describes DAPI labeling. Scale bars = 10 μm. The number of analyzed cells was 25, 30, and 20 cells for control, UM63 treatment and UM63E treatment, respectively.

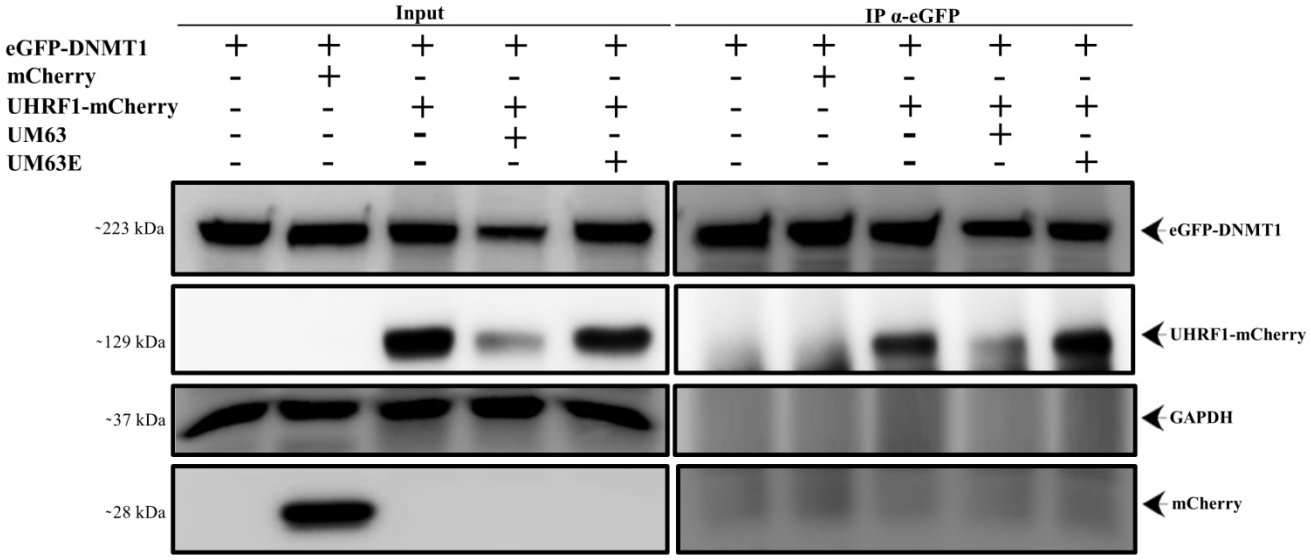

Figure 9. Effect of UM63 and UM63E on the DNMT1/UHRF1 interaction in HeLa cells, as monitored by co-immunoprecipitation. Immunoprecipitation was done with anti-eGFP antibody. Input (portion of the total cell lysate) and immunoprecipitated samples were resolved by dodecyl sulfate polyacrylamide gel electrophoresis (SDS-PAGE) and then immunoblotted with anti-eGFP and anti-mCherry antibodies to confirm the eGFP-DNMT1 and UHRF1-mCherry levels. Immunoprecipitation of eGFP-DNMT1 (223 kDa) with anti-eGFP antibody co-immunoprecipitated UHRF1-mCherry (129 kDa), which indicates an UHRF1/DNMT1 interaction. Although UM63 (10 μM) clearly decreases this interaction, UM63E (10 μM) does not show any significant effect. The co-immunoprecipitation experiments were performed two times.

addition of 10 μM UM63E did not significantly impact the FRET efficiency in cells co-transfected with eGFP-DNMT1 and UHRF1-mCherry (Figure 10D), confirming that UM63E did not impair the interaction between the two proteins, in line with the Co-IP data (Figure 9). Thus, our FRET data confirmed that UM63 but not UM63E prevented the UHRF1/DNMT1 interaction in cell nuclei.

Discussion

UHRF1 plays a key role in the inheritance of methylation marks during DNA replication by reading the DNA sequence, sensing hemi-methylated CpG motifs, and promoting the flipping of 5mC residues. Base flipping induced by the SRA domain of UHRF1 is thought to be instrumental for recruiting the DNMT1 enzyme that will methylate the opposite cytosine on the

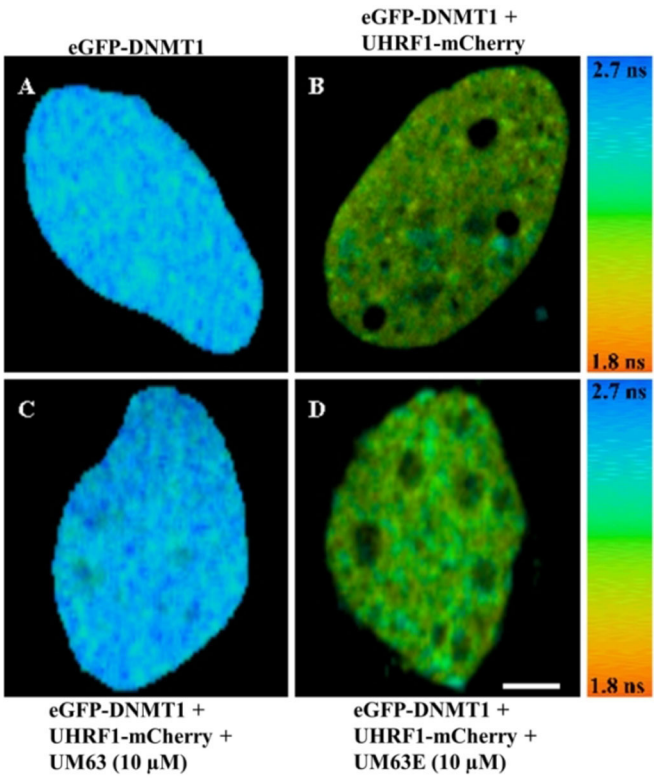

Figure 10. Effect of UM63 and UM63 E on the DNMT1/UHRF1 interaction, as assessed by FRET-FLIM. Representative FLIM images of HeLa cells transfected with A) eGFP-DNMT1 or B–D) co-transfected with UHRF1-mCherry. Cells were either untreated (A,B) or treated with 10 μM of either UM63 (C) or UM63 E (D). The lifetime values are shown by using a color code ranging from red to blue. Scale bars = 2.5 μm. In comparison to cells expressing only eGFP-DNMT1 (A), a strong decrease in the eGFP lifetime and thus, a strong FRET efficiency was observed when HeLa cells were co-transfected with eGFP-DNMT1 and UHRF1-mCherry (B). The FRET and thus, the interaction between the two labeled proteins, was preserved when cells were treated with 10 μM UM63 E (D). In contrast, treatment with 10 μM UM63 induced a strong decrease in FRET, restoring the lifetime values of free eGFP-DNMT1 (C). This indicates that UM63 prevented the interaction between the two labeled proteins.

daughter strand. In this context, the aim of the present work was to probe the druggability of the 5mC binding pocket of UHRF1 by identifying small molecules that can fit into this pocket and inhibit base flipping. To reach this aim, we combined virtual screening to select molecules able to bind to the 5mC binding pocket on the SRA domain and a fluorescence-based screening assay monitoring the SRA-induced base flipping to evaluate the molecules selected by virtual screening. Through this approach, we selected three molecules from the anthraquinone family (UM63, UM63 B, and UM63 D) that were observed to inhibit the SRA-induced based flipping with K_i values in the low μM range. The three compounds were tested by ITC for their binding to SRA and DNA. UM63 was found to be the most interesting compound, as its interaction with the wild-type SRA but not to the G448D mutant confirmed its binding to the 5mC binding pocket of SRA. This conclusion was further rationalized by molecular modeling (Figure 6), which indicated that UM63 mimics 5mC in the SRA pocket, being stabilized through a π–π stacking with the side chain of Tyr478 and several hydrogen bonds to key SRA residues also contacted by methylated DNA. Additional information on the binding of UM63 can be inferred from the ITC data. Although UM63 was found to bind exothermically to SRA (Figure 2), the binding of UM63 B and UM63 D, where, respectively, the hydroxyl and amine functions of UM63 are missing (Figure 1 E), were found to be heat-silent on binding to SRA. These data suggest that the hydrogen bonds of SRA with the amine group of UM63 strongly contribute to its exothermic binding to SRA. Moreover, although it is not directly involved in hydrogen bonding, the missing hydroxyl group in UM63 B may play a key role in the binding to SRA, by filling the pocket occupied by the methyl group in the 5mC substrate. This likely modifies the hydrogen-bond capability of the conjugated amine group, as well as the electronic properties of the aromatic system that is directly stacked to the Tyr478 residue. Moreover, UM63 can also bind to DNA with a 0.1 μM dissociation constant, likely through intercalation (Figure S6 in the Supporting Information). However, as a similar high affinity for DNA was observed with UM63 E, a compound structurally related to UM63 that has no effect on base flipping, the inhibitory effect of UM63 is thought to be mainly the consequence of its binding to SRA. The binding of UM63 to the 5mC binding pocket was further shown to decrease the affinity of SRA for DNA (Figure 4 A) and dissociate pre-formed SRA/DNA complexes (Figure 5). In addition, the inability of UM63 to perturb the binding of the G448D SRA mutant to DNA further suggests that the intercalation of UM63 into the DNA has only a marginal effect on the binding of SRA (Figure 4 B).

Interestingly, treatment of HeLa cells with UM63 was found to prevent the interaction between UHRF1 and DNMT1 (Figures 9 and 10) and their recruitment at the replication foci (Figure 8). This is likely the consequence of the binding of UM63 to the SRA domain of UHRF1, which prevents the recognition and flipping of the methylated cytosines and, the recruitment of DNMT1 through a direct interaction between SRA and the replication foci targeting sequence (RFTS) domain of DNMT1.[33c,35] In a similar manner, when an UHRF1 G448D mutant with a substitution in the SRA domain was used in HeLa cells, a loss of sensing of the hemi-methylated DNA and an important impairment of the DNA methylation maintenance were observed.[36] Prevention of mC flipping probably inhibits the transformation of UHRF1 into an active state and consequently perturbs the DNMT1 recruitment step. Indeed, the interaction of the SRA domain of UHRF1 with the CpG site is thought to trigger the conversion of the "closed form" of UHRF1 to its "open form" which can interact with DNMT1.[10] UM63 likely keeps UHRF1 in its closed form, unable to interact with DNMT1. In this context, our data clearly highlight the base flipping as a critical event for the recruitment of DNMT1 by UHRF1. As previously suggested,[27a] the base flipping is thought to allow UHRF1 to stall at the CpG sites, thus providing enough time to recruit DNMT1. In addition, it is likely that the structural changes of the SRA domain connected to the base-flipping process, such as the motion of the NKR finger, are instrumental for DNMT1 recruitment by UHRF1. By altering two crucial steps in the replication of DNA methylation pat-

terns, namely the interaction of UHRF1 with HM DNA and the recruitment of DNMT1, UM63 is thought to decrease the DNA methylation status of the cell. In line with this hypothesis, UM63 was found to decrease the global DNA methylation level by more than 40% in HeLa cells. A similar effect was observed when UHRF1 was knocked-down with shRNAs in HeLa cells,[37] or when the binding of the SRA domain to HM DNA was prevented by anthracycline derivatives,[21] highlighting the key role of UHRF1 in the maintenance of the DNA methylation level. These findings strongly suggest that UM63 can target UHRF1 in the cellular context. UM63 may thus have the same effect than interference RNAs that knockdown UHRF1.[17b,38] Similarly, natural products, such as flavonoids derived from *Limoniastrum guyonianum* and luteolin, have been shown to downregulate UHRF1 and subsequently reduce the global methylation levels in cervical cancer cells.[39]

Conclusions

Altogether, our findings suggest that UM63 acts as an UHRF1 inhibitor that binds with a nearly 1 μM affinity to the 5mC binding pocket of the SRA domain and prevents the flipping of 5mC as well as the recruitment of DNMT1 to the DNA replication foci. As a result, UM63 induces a decrease in the global methylation of DNA in cells. Therefore, UM63 can be envisioned as a key tool to investigate in molecular and cellular assays, the mechanisms in which UHRF1 is involved. UM63 will be notably very useful to carefully evaluate the effect of base flipping in reconstituted molecular complexes of UHRF1 with DNMT1 and histone partners. Moreover, UM63 can also be used as a positive control in drug screening assays targeting UHRF1. Finally, although UM63 will likely not be used as a drug due to its binding to DNA off targets and probable carcinogenicity,[40] UM63 could serve as a starting point for additional in silico screening and hit-to-lead optimizations.

Experimental Section

Materials

All compounds were dissolved in pure DMSO (Sigma–Aldrich) and kept at −20 °C. UM63 (2-amino-3-hydroxyanthra-9,10-quinone), UM63 E (3-amino-4-hydroxyphenyl)(phenyl)methanone) as well as all tested compounds were purchased from MolPort (Riga, Latvia) and Aldrich Market Select (Milwaukee, Wisconsin, USA). 5-Methylcytidine and 5-azacitidine ≥98% (HPLC) were purchased from Sigma–Aldrich. Wild-type SRA (residues 408–643 of UHRF1) and the SRA mutant (G488D) were expressed and purified in *Escherichia coli* BL21-pLysS (DE3) 3839 as previously described.[41] Their concentration was calculated by using an extinction coefficient of 43890 M^{-1} cm^{-1} at $\lambda = 280$ nm. DNA duplexes were obtained by annealing equal molar amounts of complementary oligonucleotides, heating to 90 °C for 5 min, and then cooling slowly down to room temperature. The following twelve base-pair (bp) duplex sequence was used 5′-GGGCCXGCAGGG-3′/5′-CCCTGCGGGCCC-3′ with a single CpG site that was either non-methylated (X = C) or hemi-methylated (X = 5mC). Unlabeled oligonucleotides were purchased from IBA GmbH Nucleic Acids Product Supply (Germany) in a HPLC-purified form. Labeled 5′-GGGCCXGCAGGG-3′ oligonucleotides with thG at position 7 were purchased from TriLink Biotechnologies (USA).

Absorption spectroscopy

Absorption spectra were recorded on a Cary 400 spectrophotometer (Varian). Extinction coefficients at $\lambda = 260$ nm for the non-labeled sequences 5′-GGGCCCGCAGGG-3′ and 5′-CCCTGCGGGCCC-3′ were 112500 and 97300 M^{-1} cm^{-1}, respectively. The extinction coefficient at $\lambda = 260$ nm for the single-strand DNA sequence labeled with thG at position 7 was 103000 M^{-1} cm^{-1}. Most experiments were performed at 20 °C in 20 mM phosphate buffer pH 7.5, 50 mM NaCl, 1 mM EDTA, 2.5 mM TCEP and PEG 0.05%.

Molecular modeling

The MolPort commercial library of compounds containing 6504839 entries in April 2015 (https://www.molport.com/shop/index) was downloaded in SMILES format. Filtration was performed with the FILTER application implemented in OMEGA (version 2.5.1.4) from OpenEye[24] by using the SMARTS string corresponding to the aniline substructure as query: c1ccccc1[NH2]. Filtration of the initial library led to 30947 molecules, whose protonation state was assigned by QUACPAC from OpenEye (version 1.6.3.1) (http://www.eyesopen.com). Conformational analysis was performed with OMEGA (version 2.5.1.4) keeping all default settings and allowing the storage of up to 600 conformers per molecule. The crystallographic structure of the SRA domain of UHRF1 bound to methylated DNA was retrieved from the protein data bank under the accession code 3CLZ and used as rigid receptor in molecular docking simulations. Docking-based virtual screening was performed with FRED from OpenEye (version 3.0.1) by using default settings and retaining only the best pose of each docked molecule. In-depth docking investigation of UM63 was carried out with FRED by using the highest docking resolution settings and retaining ten poses.

Steady-state fluorescence spectroscopy

Fluorescence spectra were recorded at 20 °C on a FluoroLog (Jobin Yvon) or a Fluoromax 4 spectrofluorometer equipped with a thermostated cell compartment. Excitation was set at $\lambda = 330$ nm. Spectra were corrected for buffer fluorescence, lamp fluctuations, and detector spectral sensitivity. To determine the percentage of inhibition for a given compound, the following Equation (1) was used:

$$\%\ \text{inhibition} = \frac{I_{(\text{DNA+SRA})} - I_{(\text{DNA+SRA+inhibitor})}}{I_{(\text{DNA+SRA})} - I_{(\text{DNA})}} \times 100 \quad (1)$$

where I_{DNA}, $I_{(DNA+SRA)}$, and $I_{(DNA+SRA+inhibitor)}$ correspond to the fluorescence intensity of DNA alone, the DNA/SRA complex, and the DNA/SRA complex in the presence of inhibitor, respectively. For positive hits, the percentage of inhibition was measured at several hit concentrations in order to generate a dose-response curve. This curve was then fitted by using Equation (2):

$$\%\ \text{inhibition} = A_1 + \frac{(A_2 - A_1)}{1 + 10^{((\log(IC_{50}) - C)p)}} \quad (2)$$

where A_1 and A_2 correspond to the percentage of inhibition in the absence and at the saturating concentration of the hit, respectively, C is the concentration of the hit, IC_{50} corresponds to the half maximal inhibitory concentration, and p is the Hill coefficient. From the IC_{50} value, the inhibition constant of the compound (K_i)

was then determined based on the Cheng and Prussof equation [Eq. (3)]:

$$K_i = \frac{IC_{50}}{1 + \frac{[DNA]}{K_{d(SRA/DNA)}}} \quad (3)$$

where $K_{d(SRA/DNA)}$ is the dissociation constant of SRA to the duplex and [DNA] is the DNA concentration. In order to determine the binding constant of SRA to DNA in presence of the hits, a titration was performed by monitoring the changes in the fluorescence anisotropy of a fixed amount of labeled duplex in the presence of increasing concentrations of SRA. This titration was performed in the absence and in the presence of 10 μM of the positive hit. Anisotropy values were the average of ten measurements. The excitation wavelength for thG was $\lambda = 330$ nm and emission was collected at $\lambda = 460$ nm. The affinity constants were determined by fitting the fluorescence anisotropy changes to Equation (4):

$$r = \frac{vRr_t - r_d(v-1)}{1 + Rv - v} \quad (4)$$

where r and r_d are the anisotropy values in the presence and absence of SRA, and r_t is the anisotropy at a saturating SRA concentration, R is the ratio of fluorescence intensity of the bound to the free forms and v is the fraction of bound SRA calculated given in Equation (5):

$$v = \frac{\left(K_a^{-1} + nL_t + P_t\right) - \sqrt{\left(K_a^{-1} + nL_t + P_t\right)^2 - 4nP_tL_t}}{2L_t} \quad (5)$$

where K_a is the apparent affinity constant, P_t and L_t represent the total concentrations of SRA and thG-labeled duplex, respectively, and n represents the number of DNA binding sites per SRA.[42]

Isothermal titration calorimetry

To determine the binding affinity of the hits to SRA or DNA, ITC was performed by using a Nano ITC microcalorimeter (TA instruments). Experiments were performed at 20 °C in 20 mM phosphate buffer pH 7.5, 50 mM NaCl. Solutions were prepared in a buffer containing less than 0.1% DMSO. 2.5 μL aliquots of an 80 μM SRA or HM duplex solution contained in the syringe were titrated into 8 μM of tested compound in the reaction cell. The experiment was performed under constant stirring (200 rpm) and the heat flow (μJ s^{-1}) was continuously recorded. Instrument control, data acquisition, and analysis were done with the NanoAnalyze and ITCRun software provided by the manufacturer. The molar heat of binding ΔH^0 and the equilibrium dissociation constant K_d were obtained by fitting the normalized heat accompanying each injection[43] as a function of the total protein (or DNA)/total hit molar ratio ($X_{tot}/M_{tot} = X_r$) to Equation (6):

$$\frac{dQ}{V_0\, dX_{tot}} = \Delta H^0 \left(\frac{1}{2} + \frac{1 - (1 + r)/2 - X_r/2}{(X_r^2 - 2X_r(1 - r) + (1 + r)^2)^{1/2}}\right) \quad (6)$$

V_0 is the volume of the reaction cell, Q is the released heat, and $r = K_d/nM_{tot}$ (where n is the binding stoichiometry).

Stopped flow

The kinetics of the SRA-induced base flipping in thG-labeled duplexes was monitored by using a stopped-flow apparatus (SFM-3, Bio-Logic, Claix, France). The thG excitation wavelength was set at $\lambda = 360$ nm. Fluorescence intensity was followed above 425 nm by using a long-pass filter (Kodak Wratten). The data recording frequency was 20 kHz. The dead time of the setup was 2 ms. The kinetic curves were recorded after fast mixing of 100 μL of labeled DNA solution contained in one syringe with 100 μL of SRA solution contained in the other syringe. The final concentration of labeled DNA was 0.2 μM and that of SRA was 1.5 μM. When required, 10 or 25 μM UM63 were also present. Dissociation reactions of preformed DNA/SRA complexes were triggered by the rapid addition of 10 or 25 μM UM63. Same parameters were used for both experiments. Data were recorded and processed with the Biokine software from the instrument manufacturer and the Origin software, respectively.

Cell culture

HeLa cells (ATCC, CCL-2 Amp, HeLa; Cervical Adenocarcinoma; Human) were grown in DMEM (Dulbecco's modified eagle's medium), which was supplemented with 10% FBS (fetal bovine serum), in addition to penicillin (100 U mL^{-1}) and streptomycin (100 U mL^{-1}) (Invitrogen Corporation Pontoise, France). Cells were maintained in a humid atmosphere with 5% CO_2 at 37 °C. Plasmids were transfected in HeLa cells with jetPEI™ (Life Technologies, Saint Aubin, France) according to the manufacturer's protocol.

Antibodies

Antibodies used in this study include mouse monoclonal anti-DNMT1 (Proteogenix, France, PTG-MAB0079), mouse monoclonal eGFP (Proteintech 66,002-1-Ig and Thermo Fisher Scientific A-11120), rabbit polyclonal anti-mCherry (Genetex GTX 59788), mouse monoclonal anti-GAPDH (Merck Millipore MAB374), and mouse monoclonal anti-5-methylcytocine (Active Motif 39649).

Trypan blue exclusion assay

HeLa cells (0.12×10^6 per well) were seeded in six well plates and treated with different concentrations from 0.1 to 100 μM of either UM63 or UM63E. Triton (0.1 and 1%) was used as a positive control. After 24 or 48 h of treatment, cells were collected by mild trypsinization. After centrifugation, the cell pellets were resuspended in fresh warm media. An aliquot of 50 μL of cell suspension was mixed with an equal amount of 0.4% trypan blue solution. Then, 20 μL of this mixture were loaded on a hemacytometer and examined immediately under the microscope. Living and dead (stained) cells were counted. As anthraquinones are generally referred as chemically stable compounds in physiological conditions,[29a] no further efforts were done to check the stability of UM63 and UM63E over time.

Co-immunoprecipitation (Co-IP)

For co-immunoprecipitation experiments, cells were harvested 24 h post transfection by mild trypsinization. Cells were collected and lysed by freeze shock. Sonication was done in ice-cold PBS freshly supplemented with a protease inhibitor cocktail tablet (cOmplete Mini, EDTA-free, Roche Diagnostics GmbH, Germany 11836170001). Input controls were made by taking 40 μg of protein from each lysate. For Co-IP, 900–1200 μg of protein lysate were incubated with anti-eGFP antibody at 4 °C for 4 h. After washing and equilibration, 45 μL of Dynabeads® protein A (Thermo Fischer Scientific, Norway 1002D) were added to the lysate–antibody mixture and incubated for 1 h at 4 °C. Later, beads were collected and washed five times with ice-cold PBS freshly supplemented with protease inhibitor cocktail tablet. Finally, beads were resuspended in Laemmli

sample buffer (Bio-Rad Laboratories, USA). Proteins were denatured by heating at 95 °C for 5 min and analyzed through Western blotting. Proteins were identified with anti-mCherry, anti-eGFP and anti-GAPDH antibodies with overnight incubation at 4 °C. Then, primary antibodies were labeled with secondary anti-rabbit (Promega, W401B) or anti-mouse antibodies (Promega, W402B) conjugated with horseradish peroxidase. Signals were detected with the chemiluminescent ECL system (ClarityTM ECL western blotting substrate, Biorad, 170–5060) on an Image Quant LAS 4000 apparatus.

Confocal microscopy

For methylation analysis, HeLa cells were seeded on a cover glass and then treated for 48 h with 10 μM of UM63 or UM63E or 5-azacytidine (5-Aza). Cells were fixed with 4% paraformaldehyde for 15 min. and then, permeabilized with 0.2% Triton X-100 for 15 min. Then, 2 N HCl was added for 20 min to denature DNA. The medium was then neutralized with 100 mM Tris HCl pH 8.5 for 10 min. Next, cells were blocked by using 1% BSA for one hour, before incubation with a primary antibody against 5mC (active motif) overnight at 4 °C. After washing three times with PBS, cells were incubated with secondary antibody labeled with Alexa Fluor 488 (goat anti-mouse) for 60 min. Finally, cells were washed three times and imaged with a confocal Leica TCS SPE microscope equipped with a 20× air (0.7 NA) immersion lens objective.

For localization analysis, HeLa cells co-transfected with eGFP-DNMT1 and UHRF1-mCherry were incubated for 24 h with either buffer or 10 μM of UM63 or UM63E. These cells were labeled with DAPI after fixation to stain the nucleus. Cells in the S phase were detected by labeling with the Click-iT® EdU-Alexa Fluor® 647 Imaging Kit (Thermo Fisher Scientific USA C10340) according to the manufacturer's protocol. All samples were imaged with a confocal Leica TCS SPE equipped with an oil immersion objective (HXC PL APO 63×/1.40 OIL CS). For DAPI, mCherry, and EdU-Alexa Fluor 647, the excitation was performed with a $\lambda = 405$ (25), 561 (10), and 635 nm laser (18 mW), respectively. The detection range for the three dyes was $\lambda = 430$–480, 570–625, and 644–707 nm, respectively. For eGFP and Alexa Fluor 488, excitation was performed with a $\lambda = 405$ nm laser (25 mW). The detection range was $\lambda = 500$–531 and 500–523 nm, for eGFP and Alexa Fluor 488, respectively. All the images were processed with the Image J software. Co-localization of tagged proteins was quantified by the Pearson correlation coefficient with the analysis of two colors confocal images with the "Squassh" plugin in Image J.[44] This plugin generates an R script "R_analysis.R'' used to perform one-way ANOVA for the statistical analysis of differences between datasets.

Fluorescence lifetime imaging microscopy (FLIM)

For FLIM experiments, 10^5 cells were seeded in a dish with 35 mm wells (μdish, Ibidi) and were co-transfected with 1 μg eGFP-DNMT1 and 1 μg UHRF1-mCherry plasmids by using jetPEI™ reagent. After transfection, cells were treated with 10 μM of UM63 or UM63E for 24 h. At the end of the treatment, cells were fixed with 4% paraformaldehyde. After fixation, cells were analyzed with a homemade two-photon excitation scanning microscope based on an Olympus IX70 inverted microscope with a 60× 1.2 NA water immersion objective operating in the descanned fluorescence collection mode as described.[45] Two-photon excitation at $\lambda = 930$ nm was provided by a femtosecond laser (Insight DeepSee, Spectra Physics). Fluorescence photons were collected by using a short-pass filter with a cut-off wavelength of $\lambda = 680$ nm (F75-680, AHF, Germany) and a band-pass filter of $\lambda = (520 \pm 17)$ nm (F37-520, AHF, Germany). The fluorescence was directed to a fiber-coupled APD (SPCM-AQR-14-FC, PerkinElmer), which was connected to a time-correlated single photon counting module (SPC830, Becker & Hickl, Germany). FLIM data were analyzed by using SPCImage v 7.3 (Becker & Hickl) and the Förster resonance energy transfer (FRET) efficiency was calculated according to $E = 1-(\tau_{DA}/\tau_D)$, where τ_{DA} is the lifetime of the donor (eGFP) in the presence of acceptor (mCherry) and τ_D is the lifetime of eGFP in the absence of acceptor.

Acknowledgements

We thank the ANR (SMFLUONA, ANR-17-CE11-0036-01) and Labex NIE for financial support. L.Z. and K.G. were supported by fellowships from Lebanese government and FRM, respectively. T.A. and W.A. were supported by fellowships from Higher Education Commission (HEC), Pakistan. Y.M. is grateful to the Institut Universitaire de France (IUF) for support and providing additional time to be dedicated to research. M.M. and M.B. acknowledge the partial support by MIUR Progetto Dipartimenti di Eccellenza 2018–2022. The authors thank the OpenEye Free Academic Licensing Program for providing a free academic license for molecular modeling and chemoinformatics software.

Conflict of interest

The authors declare no conflict of interest.

Keywords: base flipping inhibitors · DNA methylation · fluorescence · virtual screening

[1] a) M. Ehrlich, *J. Cell. Biochem.* **2003**, *88*, 899–910; b) I. Okamoto, A. P. Otte, C. D. Allis, D. Reinberg, E. Heard, *Science* **2004**, *303*, 644–649; c) S. K. Murphy, R. L. Jirtle, *BioEssays* **2003**, *25*, 577–588.

[2] a) A. P. Feinberg, R. Ohlsson, S. Henikoff, *Nat. Rev. Genet.* **2006**, *7*, 21–33; b) R. J. Klose, A. P. Bird, *Trends Biochem. Sci.* **2006**, *31*, 89–97.

[3] a) S. B. Baylin, P. A. Jones, *Nat. Rev. Cancer* **2011**, *11*, 726–734; b) J. Sandoval, M. Esteller, *Curr. Opin. Genet. Dev.* **2012**, *22*, 50–55.

[4] a) C. Bronner, M. Krifa, M. Mousli, *Biochem. Pharmacol.* **2013**, *86*, 1643–1649; b) M. Alhosin, T. Sharif, M. Mousli, N. Etienne-Selloum, G. Fuhrmann, V. B. Schini-Kerth, C. Bronner, *J. Exp. Clin. Cancer Res.* **2011**, *30*, 41–51.

[5] a) G. V. Avvakumov, J. R. Walker, S. Xue, Y. Li, S. Duan, C. Bronner, C. H. Arrowsmith, S. Dhe-Paganon, *Nature* **2008**, *455*, 822–825; b) J. Sharif, M. Muto, S. Takebayashi, I. Suetake, A. Iwamatsu, T. A. Endo, J. Shinga, Y. Mizutani-Koseki, T. Toyoda, K. Okamura, S. Tajima, K. Mitsuya, M. Okano, H. Koseki, *Nature* **2007**, *450*, 908–912.

[6] a) K. Arita, M. Ariyoshi, H. Tochio, Y. Nakamura, M. Shirakawa, *Nature* **2008**, *455*, 818–821; b) H. Hashimoto, J. R. Horton, X. Zhang, M. Bostick, S. E. Jacobsen, X. Cheng, *Nature* **2008**, *455*, 826–829.

[7] a) J. Cheng, Y. Yang, J. Fang, J. Xiao, T. Zhu, F. Chen, P. Wang, Z. Li, H. Yang, Y. Xu, *J. Biol. Chem.* **2013**, *288*, 1329–1339; b) X. Liu, Q. Gao, P. Li, Q. Zhao, J. Zhang, J. Li, H. Koseki, J. Wong, *Nat. Commun.* **2013**, *4*, 1563–1575; c) A. Rottach, C. Frauer, G. Pichler, I. M. Bonapace, F. Spada, H. Leonhardt, *Nucleic Acids Res.* **2010**, *38*, 1796–1804.

[8] a) M. Bostick, J. K. Kim, P. O. Esteve, A. Clark, S. Pradhan, S. E. Jacobsen, *Science* **2007**, *317*, 1760–1764; b) T. Li, L. Wang, Y. Du, S. Xie, X. Yang, F. Lian, Z. Zhou, C. Qian, *Nucleic Acids Res.* **2018**, *46*, 3218–3231.

[9] a) A. Nishiyama, L. Yamaguchi, J. Sharif, Y. Johmura, T. Kawamura, K. Nakanishi, S. Shimamura, K. Arita, T. Kodama, F. Ishikawa, H. Koseki, M. Nakanishi, *Nature* **2013**, *502*, 249–253; b) W. Qin, P. Wolf, N. Liu, S. Link, M. Smets, F. La Mastra, I. Forne, G. Pichler, D. Horl, K. Fellinger, F. Spada, I. M. Bonapace, A. Imhof, H. Harz, H. Leonhardt, *Cell Res.* **2015**, *25*, 911–929.

[10] J. Fang, J. Cheng, J. Wang, Q. Zhang, M. Liu, R. Gong, P. Wang, X. Zhang, Y. Feng, W. Lan, Z. Gong, C. Tang, J. Wong, H. Yang, C. Cao, Y. Xu, *Nat. Commun.* **2016**, *7*, 11197 – 11208.

[11] X. Yang, F. Lay, H. Han, P. A. Jones, *Trends Pharmacol. Sci.* **2010**, *31*, 536 – 546.

[12] a) J. P. Issa, H. Kantarjian, *Nat. Rev. Drug Discovery* **2005**, *4*, 275 – 276; b) H. Kantarjian, J. P. Issa, C. S. Rosenfeld, J. M. Bennett, M. Albitar, J. DiPersio, V. Klimek, J. Slack, C. de Castro, F. Ravandi, R. Helmer, L. Shen, S. D. Nimer, R. Leavitt, A. Raza, H. Saba, *Cancer* **2006**, *106*, 1794 – 1803.

[13] J. C. Chuang, C. B. Yoo, J. M. Kwan, T. W. Li, G. Liang, A. S. Yang, P. A. Jones, *Mol. Cancer Ther.* **2005**, *4*, 1515 – 1520.

[14] a) J. M. Foulks, K. M. Parnell, R. N. Nix, S. Chau, K. Swierczek, M. Saunders, K. Wright, T. F. Hendrickson, K. K. Ho, M. V. McCullar, S. B. Kanner, *J. Biomol. Screening* **2012**, *17*, 2 – 17; b) Y. Jung, J. Park, T. Y. Kim, J. H. Park, H. S. Jong, S. A. Im, K. D. Robertson, Y. J. Bang, T. Y. Kim, *J. Mol. Med.* **2007**, *85*, 1137 – 1148; c) S. S. Palii, B. O. Van Emburgh, U. T. Sankpal, K. D. Brown, K. D. Robertson, *Mol. Cell. Biol.* **2008**, *28*, 752 – 771.

[15] W. Ashraf, A. Ibrahim, M. Alhosin, L. Zaayter, K. Ouararhni, C. Papin, T. Ahmad, A. Hamiche, Y. Mely, C. Bronner, M. Mousli, *Oncotarget* **2017**, *8*, 51946 – 51962.

[16] a) C. Bronner, M. Achour, Y. Arima, T. Chataigneau, H. Saya, V. B. Schini-Kerth, *Pharmacol. Ther.* **2007**, *115*, 419 – 434; b) M. Unoki, *Recent Pat. Anti-Cancer Drug Discovery* **2011**, *6*, 116 – 130.

[17] a) M. Alhosin, A. Abusnina, M. Achour, T. Sharif, C. Muller, J. Peluso, T. Chataigneau, C. Lugnier, V. B. Schini-Kerth, C. Bronner, G. Fuhrmann, *Biochem. Pharmacol.* **2010**, *79*, 1251 – 1260; b) M. Alhosin, Z. Omran, M. A. Zamzami, A. L. Al-Malki, H. Choudhry, M. Mousli, C. Bronner, *J. Exp. Clin. Cancer Res.* **2016**, *35*, 174 – 184.

[18] V. Myrianthopoulos, P. F. Cartron, Z. Liutkeviciute, S. Klimasauskas, D. Matulis, C. Bronner, N. Martinet, E. Mikros, *Eur. J. Med. Chem.* **2016**, *114*, 390 – 396.

[19] R. S. Houliston, A. Lemak, A. Iqbal, D. Ivanochko, S. Duan, L. Kaustov, M. S. Ong, L. Fan, G. Senisterra, P. J. Brown, Y. X. Wang, C. H. Arrowsmith, *J. Biol. Chem.* **2017**, *292*, 20947 – 20959.

[20] a) B. S. Parker, S. M. Cutts, A. Nudelman, A. Rephaeli, D. R. Phillips, S. Sukumar, *Cancer Biol. Ther.* **2003**, *2*, 259 – 263; b) D. A. Walker, N. Wyhs, H. Giovinazzo, S. Yegnasubramanian, W. G. Nelson, *Cancer Res.* **2014**, *74*, 5390.

[21] H. Giovinazzo, D. Walker, N. Wyhs, J. Liu, D. M. Esopi, A. M. Vaghasia, Y. Jain, A. Bhamidipati, J. Zhou, W. G. Nelson, S. Yegnasubramanian, *Oncotarget* **2019**, *10*, 3040 – 3050.

[22] a) A. Das, S. Roy, P. Mondal, A. Datta, K. Mahali, G. Loganathan, D. Dharumadurai, P. S. Sengupta, M. A. Akbarsha, P. S. Guin, *RSC Adv.* **2016**, *6*, 28200 – 28212; b) B. J. Evison, B. E. Sleebs, K. G. Watson, D. R. Phillips, S. M. Cutts, *Med. Res. Rev.* **2016**, *36*, 248 – 299.

[23] C. Qian, S. Li, J. Jakoncic, L. Zeng, M. J. Walsh, M. M. Zhou, *J. Biol. Chem.* **2008**, *283*, 34490 – 34494.

[24] a) P. C. Hawkins, A. Nicholls, *J. Chem. Inf. Model.* **2012**, *52*, 2919 – 2936; b) OMEGA 2.5.1.4, OpenEYE Scientific Software, Santa Fe, NM, http://www.eyesopen.com.

[25] a) M. McGann, *J. Chem. Inf. Model.* **2011**, *51*, 578 – 596; b) FRED 3.0.1, OpenEYE Scientific Software, Santa Fe, NM, http://www.eyesopen.com.

[26] a) M. Stahl, H. Mauser, *J. Chem. Inf. Model.* **2005**, *45*, 542 – 548; b) M. Mori, L. Tottone, D. Quaglio, N. Zhdanovskaya, C. Ingallina, M. Fusto, F. Ghirga, G. Peruzzi, M. E. Crestoni, F. Simeoni, F. Giulimondi, C. Talora, B. Botta, I. Screpanti, R. Palermo, *Sci. Rep.* **2017**, *7*, 2213 – 2225; c) M. Mori, L. Kovalenko, S. Malancona, F. Saladini, D. De Forni, M. Pires, N. Humbert, E. Real, T. Botzanowski, S. Cianferani, A. Giannini, M. C. Dasso Lang, G. Cugia, B. Poddesu, F. Lori, M. Zazzi, S. Harper, V. Summa, Y. Mely, M. Botta, *ACS Chem. Biol.* **2018**, *13*, 253 – 266.

[27] a) V. Kilin, K. Gavvala, N. P. Barthes, B. Y. Michel, D. Shin, C. Boudier, O. Mauffret, V. Yashchuk, M. Mousli, M. Ruff, F. Granger, S. Eiler, C. Bronner, Y. Tor, A. Burger, Y. Mely, *J. Am. Chem. Soc.* **2017**, *139*, 2520 – 2528; b) D. Shin, R. W. Sinkeldam, Y. Tor, *J. Am. Chem. Soc.* **2011**, *133*, 14912 – 14915.

[28] L. W. Hsin, H. P. Wang, P. H. Kao, O. Lee, W. R. Chen, H. W. Chen, J. H. Guh, Y. L. Chan, C. P. His, M. S. Yang, T. K. Li, C. H. Lee, *Bioorg. Med. Chem.* **2008**, *16*, 1006 – 1014.

[29] a) L. L. M. Nollet, J. A. Gutiérrez-Uribe, *Phenolic Compounds in Food: Characterization and Analysis*, 1st ed., CRC, Boca Raton, **2018**, pp. 130 – 170; b) M. E. Fox, P. J. Smith, *Cancer Chemother. Pharmacol.* **1995**, *35*, 403 – 410.

[30] J. Zhang, Q. Gao, P. Li, X. Liu, Y. Jia, W. Wu, J. Li, S. Dong, H. Koseki, J. Wong, *Cell Res.* **2011**, *21*, 1723 – 1739.

[31] P. I. H. Bastiaens, A. Squire, *Trends Cell Biol.* **1999**, *9*, 48 – 52.

[32] W. Becker, *Advanced Time-Correlated Single Photon Counting Applications*, Springer, Heidelberg, **2015**.

[33] a) M. Achour, X. Jacq, P. Rondé, M. Alhosin, C. Charlot, T. Chataigneau, M. Jeanblanc, M. Macaluso, A. Giordano, A. D. Hughes, V. B. Schini-Kerth, C. Bronner, *Oncogene* **2008**, *27*, 2187 – 2197; b) B. M. Foster, P. Stolz, C. B. Mulholland, A. Montoya, H. Kramer, S. Bultmann, T. Bartke, *Mol. Cell* **2018**, *72*, 739 – 752; c) C. Bronner, M. Alhosin, A. Hamiche, M. Mousli, *Genes* **2019**, *10*, 65 – 78.

[34] T. C. Voss, I. A. Demarco, R. N. Day, *BioTechniques* **2005**, *38*, 413 – 424.

[35] P. Bashtrykov, G. Jankevicius, R. Z. Jurkowska, S. Ragozin, A. Jeltsch, *J. Biol. Chem.* **2014**, *289*, 4106 – 4115.

[36] J. S. Harrison, E. M. Cornett, D. Goldfarb, P. A. DaRosa, Z. M. Li, F. Yan, B. M. Dickson, A. H. Guo, D. V. Cantu, L. Kaustov, P. J. Brown, C. H. Arrowsmith, D. A. Erie, M. B. Major, R. E. Klevit, K. Krajewski, B. Kuhlman, B. D. Strahl, S. B. Rothbart, *eLife* **2016**, *5*, e17101.001.

[37] S. B. Rothbart, K. Krajewski, N. Nady, W. Tempel, S. Xue, A. I. Badeaux, D. Barsyte-Lovejoy, J. Y. Martinez, M. T. Bedford, S. M. Fuchs, C. H. Arrowsmith, B. D. Strahl, *Nat. Struct. Mol. Biol.* **2012**, *19*, 1155 – 1160.

[38] a) J. K. Kim, P. O. Esteve, S. E. Jacobsen, S. Pradhan, *Nucleic Acids Res.* **2009**, *37*, 493 – 505; b) W. Jin, L. Chen, Y. Chen, S. G. Xu, G. H. Di, W. J. Yin, J. Wu, Z. M. Shao, *Breast Cancer Res. Treat.* **2010**, *123*, 359 – 373; c) M. Unoki, T. Nishidate, Y. Nakamura, *Oncogene* **2004**, *23*, 7601 – 7610; d) L. Zhou, Y. Shang, Z. Jin, W. Zhang, C. Lv, X. Zhao, Y. Liu, N. Li, J. Liang, *Cancer Biol. Ther.* **2015**, *16*, 1241 – 1251.

[39] M. Krifa, A. Pizzi, M. Mousli, L. Chekir-Ghedira, L. Leloup, K. Ghedira, *Tumor Biol.* **2014**, *35*, 7877 – 7885.

[40] National Toxicology Program, *Nat. Cancer Inst. Carcinog. Tech. Rep. Ser.* **1978**, *144*, 1 – 117.

[41] a) M. Achour, G. Fuhrmann, M. Alhosin, P. Ronde, T. Chataigneau, M. Mousli, V. B. Schini-Kerth, C. Bronner, *Biochem. Biophys. Res. Commun.* **2009**, *390*, 523 – 528; b) B. Delagoutte, N. Lallous, C. Birck, P. Oudet, J. P. Samama, *Acta Crystallogr. Sect. F* **2008**, *64*, 922 – 925.

[42] N. Rochel, F. Ciesielski, J. Godet, E. Moman, M. Roessle, C. Peluso-Iltis, M. Moulin, M. Haertlein, P. Callow, Y. Mely, D. I. Svergun, D. Moras, *Nat. Struct. Mol. Biol.* **2011**, *18*, 564 – 570.

[43] T. Wiseman, S. Williston, J. F. Brandts, L. N. Lin, *Anal. Biochem.* **1989**, *179*, 131 – 137.

[44] A. Rizk, G. Paul, P. Incardona, M. Bugarski, M. Mansouri, A. Niemann, U. Ziegler, P. Berger, I. F. Sbalzarini, *Nat. Protoc.* **2014**, *9*, 586 – 596.

[45] a) S. E. El Meshri, D. Dujardin, J. Godet, L. Richert, C. Boudier, J. L. Darlix, P. Didier, Y. Mely, H. de Rocquigny, *J. Mol. Biol.* **2015**, *427*, 1480 – 1494; b) J. P. Clamme, J. Azoulay, Y. Mely, *Biophys. J.* **2003**, *84*, 1960 – 1968.

Manuscript received: June 6, 2019
Revised manuscript received: July 18, 2019
Accepted manuscript online: July 19, 2019
Version of record online: ■■ ■■, 0000

FULL PAPER

DNA Binding

L. Zaayter, M. Mori, T. Ahmad, W. Ashraf, C. Boudier, V. Kilin, K. Gavvala, L. Richert, S. Eiler, M. Ruff, M. Botta, C. Bronner, M. Mousli, Y. Mély**

■■ – ■■

A Molecular Tool Targeting the Base-Flipping Activity of Human UHRF1

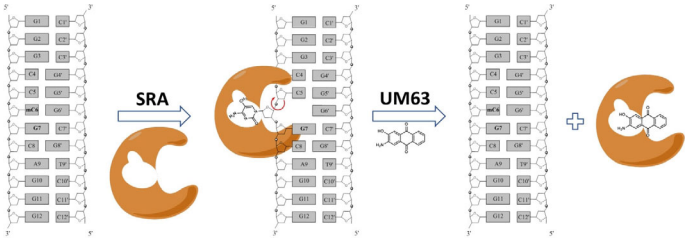

Base flipping inhibition: The anthraquinone compound UM63 binds to the 5-methylcytosine (5mC) binding pocket of the SRA domain of UHRF1 and inhibits the base-flipping process, which is crucial in the replication of DNA methylation profiles (see figure).

Supplementary Results

CHEMISTRY
A European Journal

Supporting Information

A Molecular Tool Targeting the Base-Flipping Activity of Human UHRF1

Liliyana Zaayter[+],[a] Mattia Mori[+],[b] Tanveer Ahmad[+],[a] Waseem Ashraf,[a] Christian Boudier,[a] Vasyl Kilin,[a] Krishna Gavvala,[a] Ludovic Richert,[a] Sylvia Eiler,[c] Marc Ruff,[c] Maurizio Botta,[b] Christian Bronner,[c] Marc Mousli,*[a] and Yves Mély*[a]

chem_201902605_sm_miscellaneous_information.pdf

Author Contributions

L.Z., M.M. and T.A. contributed equally. L.Z., V.K., K.G., and L.R. performed the molecular experiments. T.A., W.A., and C.Bro. performed the cellular experiments. C.Bou. supervised and analyzed the calorimetry titrations. M.Mor. and M.B. performed the virtual screening and molecular modeling. S.E. and M.R. prepared the proteins of this manuscript. M. Mou. and Y.M. supervised the project. L.Z., M.Mor., T.A., and Y.M. wrote the manuscript.

Hits selection *in silico*

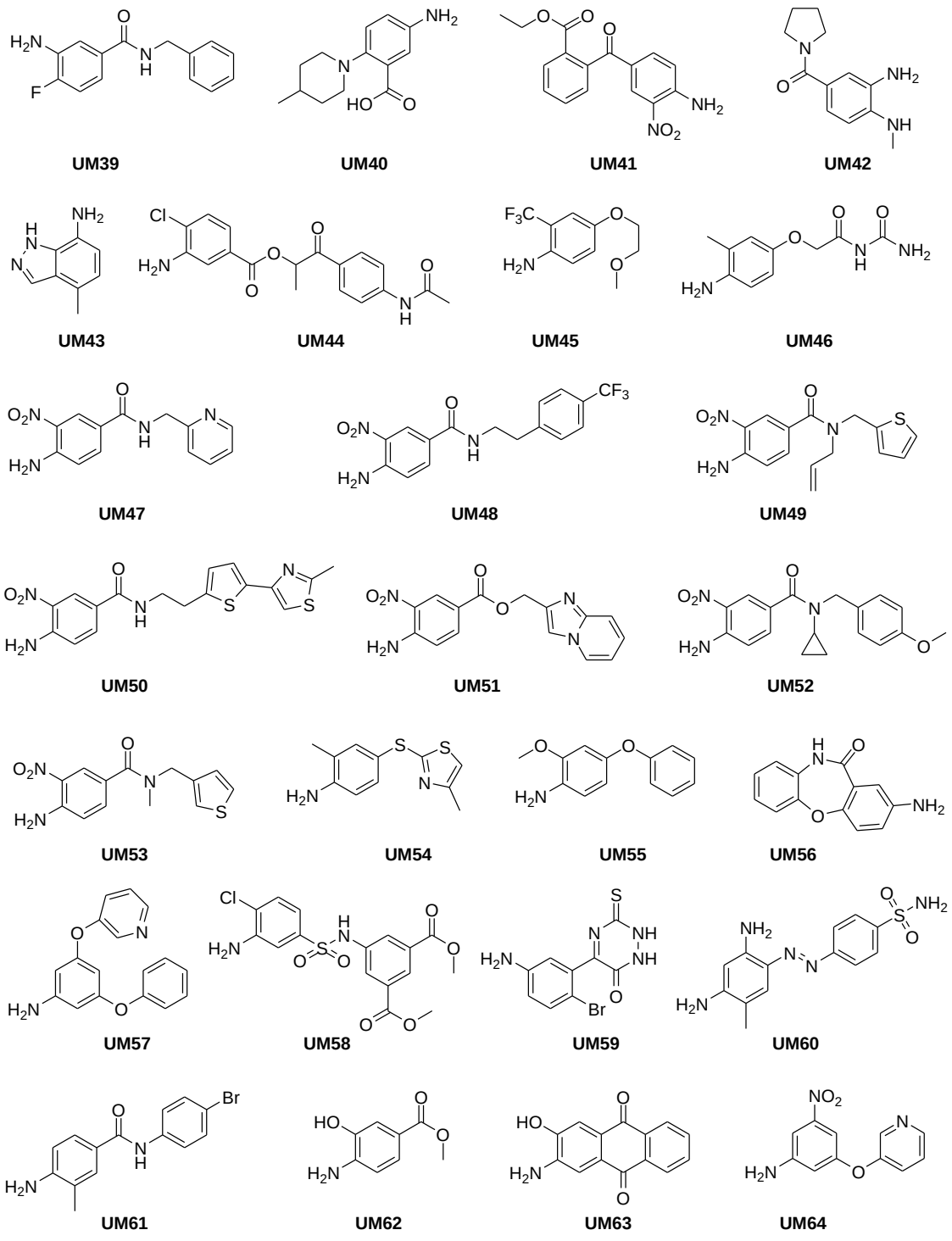

Fig. S1 Chemical structure of putative hits UM39–UM64 selected by virtual screening.

Effect of 5-methylcytidine on SRA-induced base flipping

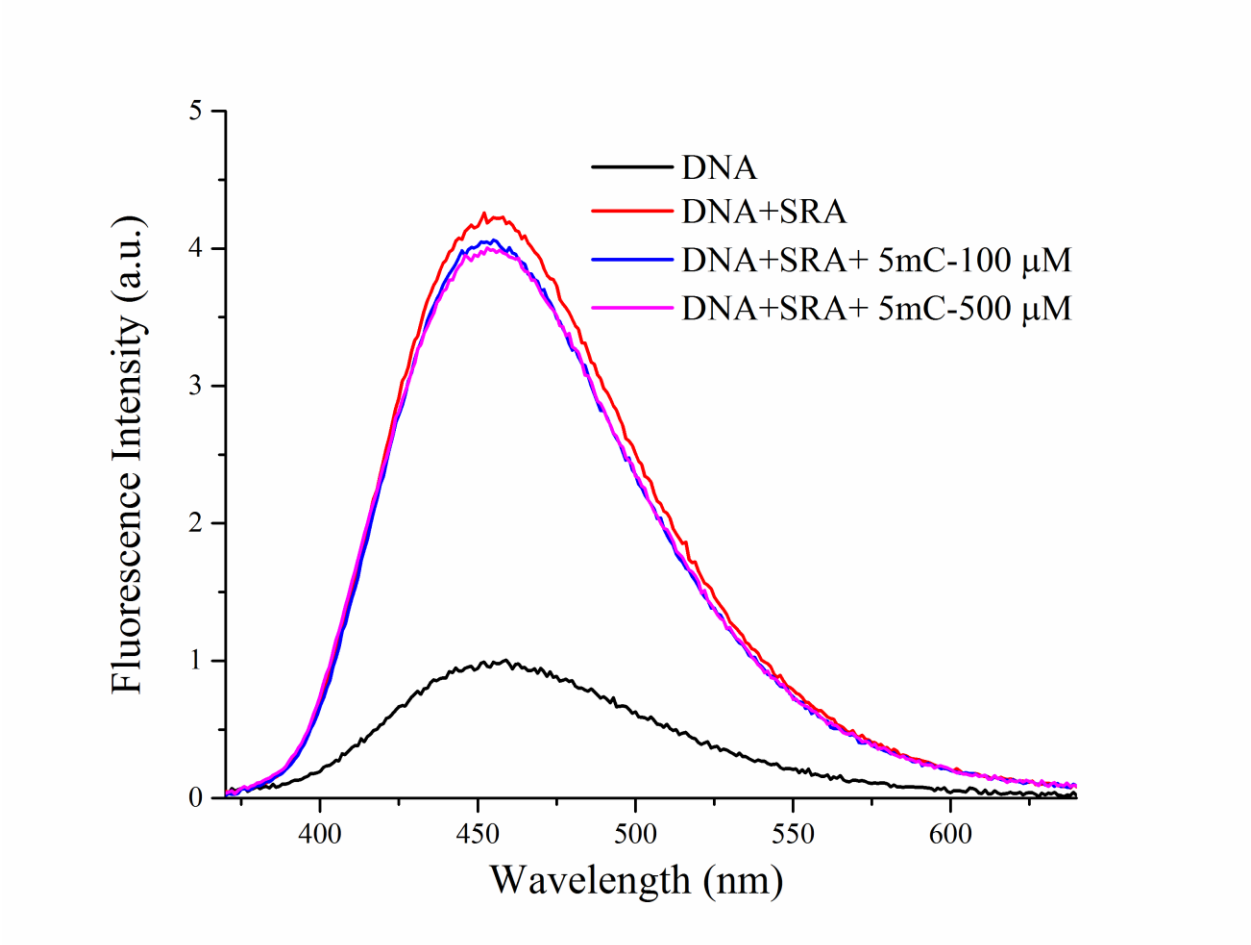

Fig. S2 Effect of 5-methylcytidine on SRA-induced base flipping. Emission spectra of thG-labeled HM DNA (1 µM) in the absence (black) and in the presence of SRA (3 µM) before (red) and after addition of 100 µM (blue) or 500 µM (magenta) of 5-methylcytidine.

Effect of UM63B and UM63D on the base flipping assay

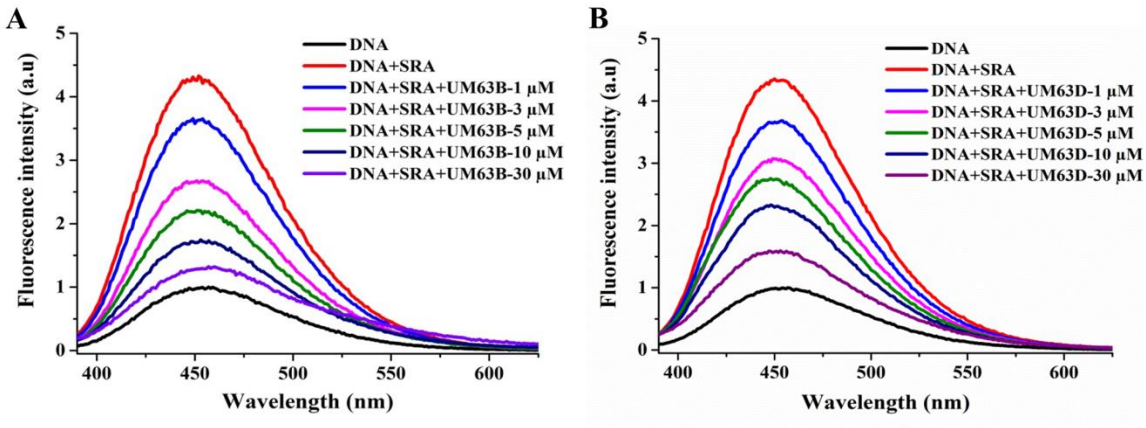

Fig. S3 Effect of UM63B and UM63D on the base flipping assay. Emission spectra of thG-labeled HM DNA (1 μM) in the absence (black) and in the presence of SRA (3 μM) before (red) and after addition of 1 μM (blue) , 3 μM (magenta) , 5 μM (green) , 10 μM (dark blue) or 30 μM (purple) of (A) UM63B and (B) UM63D.

Effect of UM63, UM63B and UM63D on the fluorescence of thG-labeled HM DNA duplexes

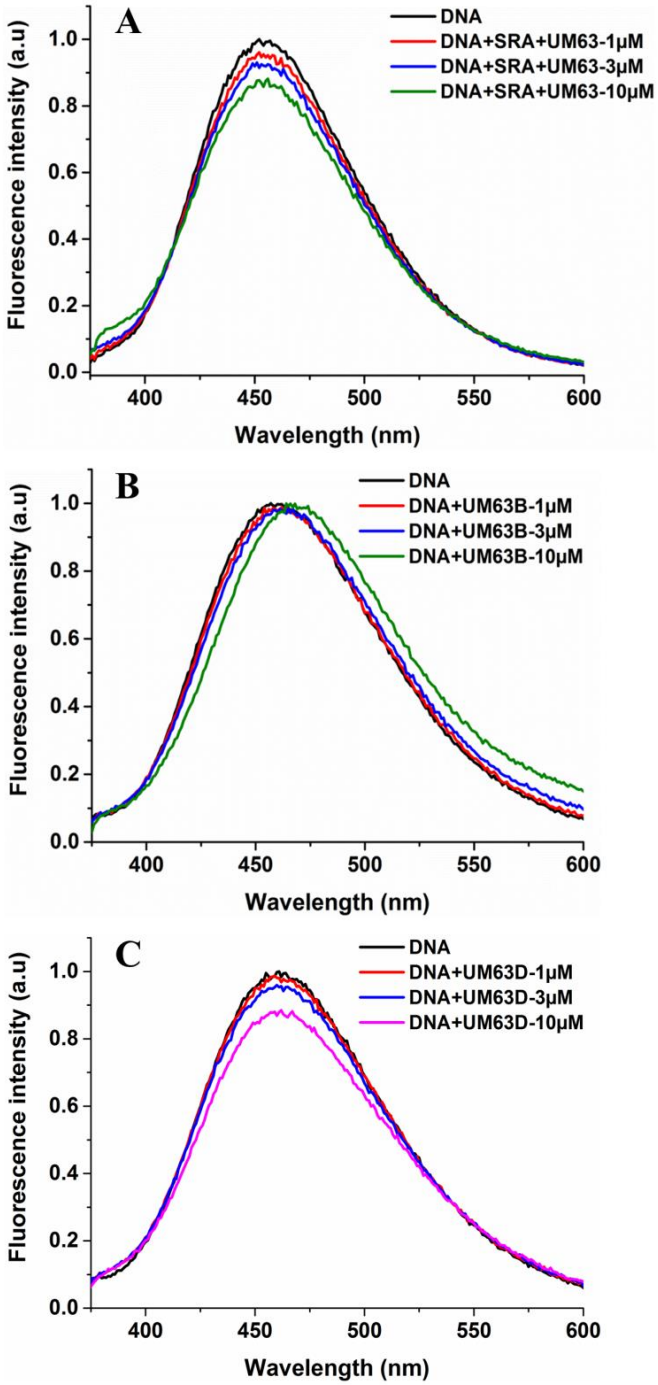

Fig. S4 Effect of UM63, UM63B and UM63D on the emission spectrum of the thG-labeled HM duplex. Emission spectra of 1 μM thG-labeled duplex in the absence (black) and in the presence of different concentrations of (A) UM63 (B) UM63B or (C) UM63D. Excitation was at 330 nm.

Binding of UM63, UM63D and UM63E to HM DNA

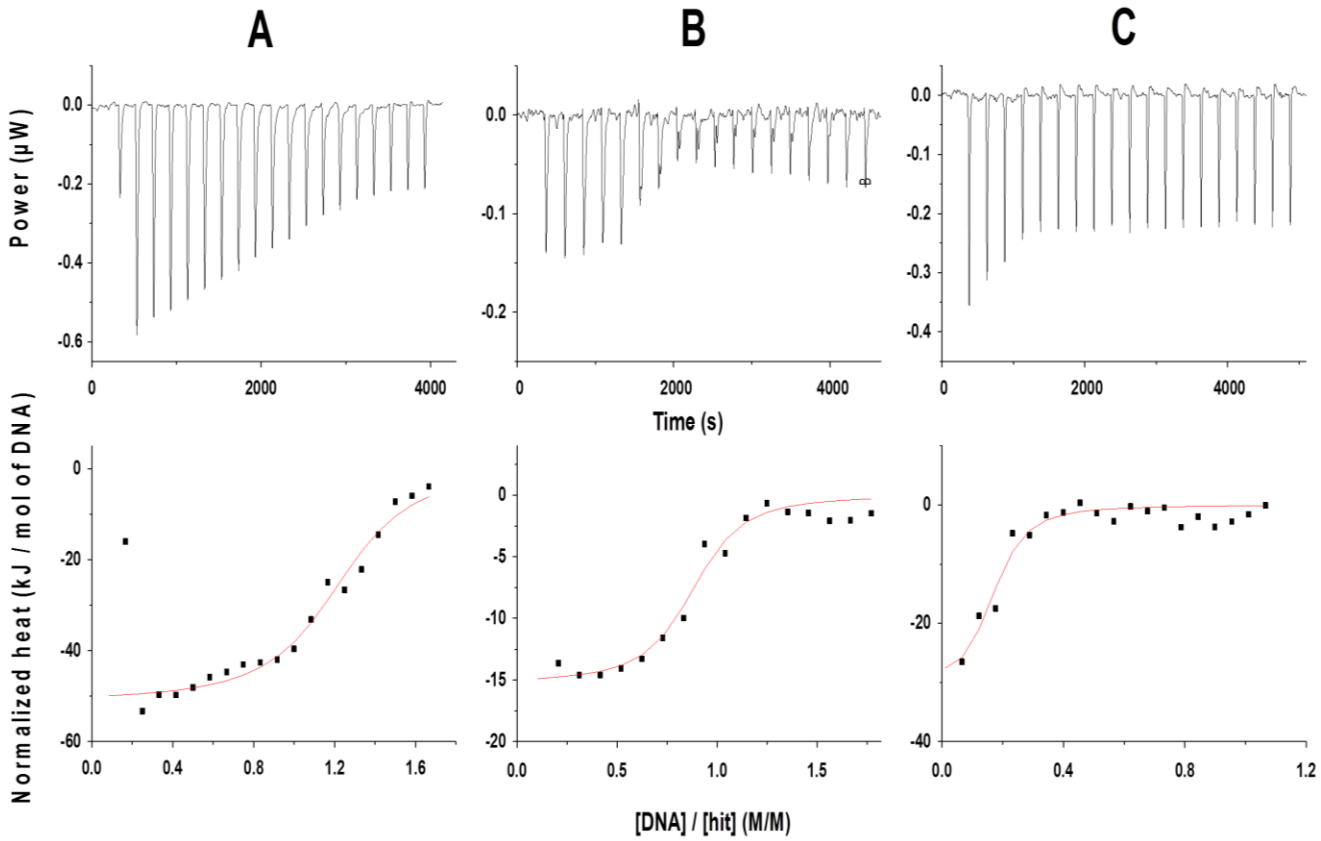

Fig. S5 Binding of UM63B (A), UM63D (B) and UM63E (C) to HM DNA as monitored by Isothermal Titration Calorimetry. In the cell, the concentration of UM63B and UM63D was 8 µM. The concentration of UM63E was 12 µM. The concentration of HM DNA in the syringe was 80 µM. The red curves were fitted to the experimental heat quantities using equation (6) giving K_d value of 0.22 µM and ΔH=-51.2 kJ/mol for UM63B, K_d = 15 µM and ΔH=15.5 kJ/mol for UM63D and K_d = 0.25 µM and ΔH=-31.5 kJ/mol for UM63E.

UM63 competes with Ethidium bromide (EtBr) to bind to DNA

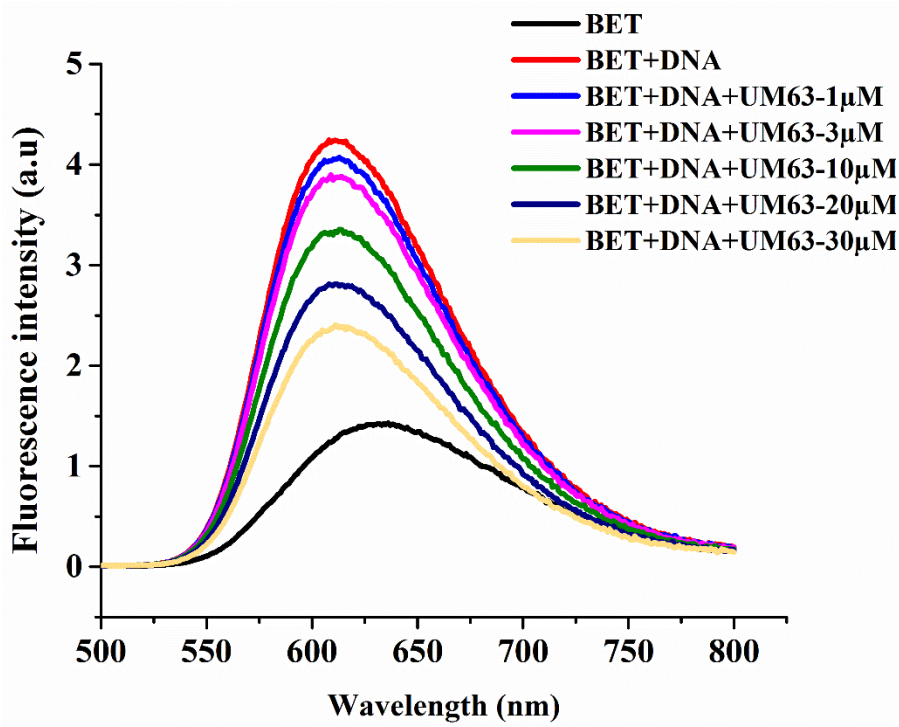

Fig. S6 UM63 competition with EtBr for DNA intercalation. Fluorescence emission spectra of 1 μM EtBr free (black line) or bound to 1 μM DNA before (red) and after addition of different concentrations of UM63.

Effect of UM63E on the base flipping kinetics of the SRA domain

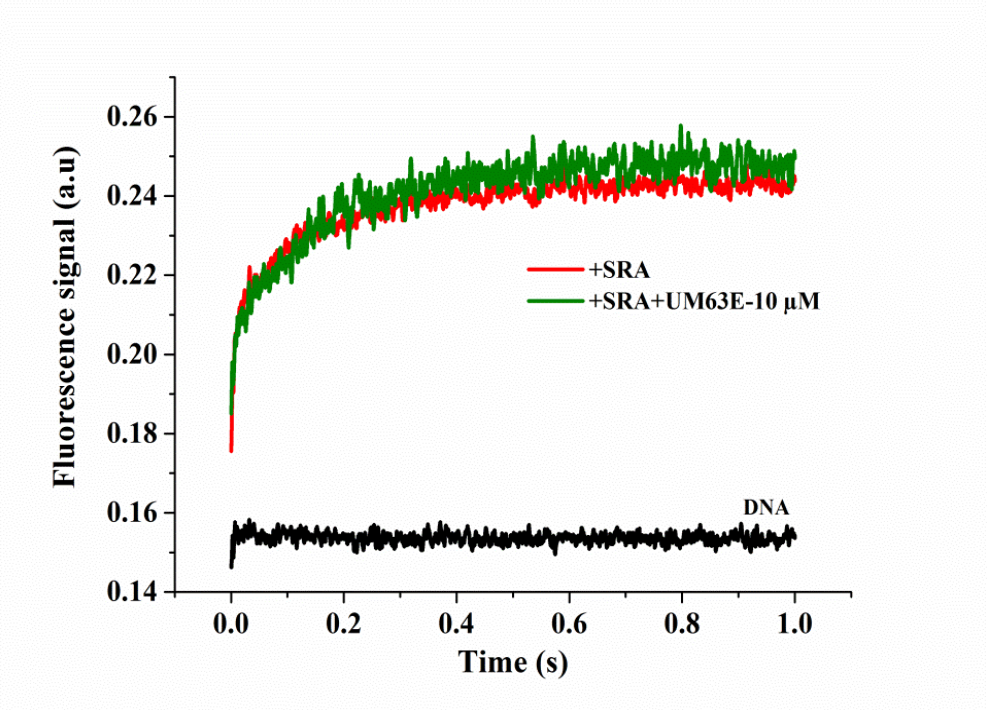

Fig. S7 Effect of UM63E on the base flipping kinetics of the SRA domain. Kinetic curves were obtained by the stopped-flow technique, monitoring the fluorescence of the thG-labeled HM duplex. The black curve corresponds to 0.2 µM HM duplex mixed with buffer. The red and green traces correspond to the mixing of 0.2 µM HM duplex with 1.5 µM SRA, respectively in the absence and the presence of 10 µM UM63E.

Effect of UM63E on the SRA/HM DNA complex

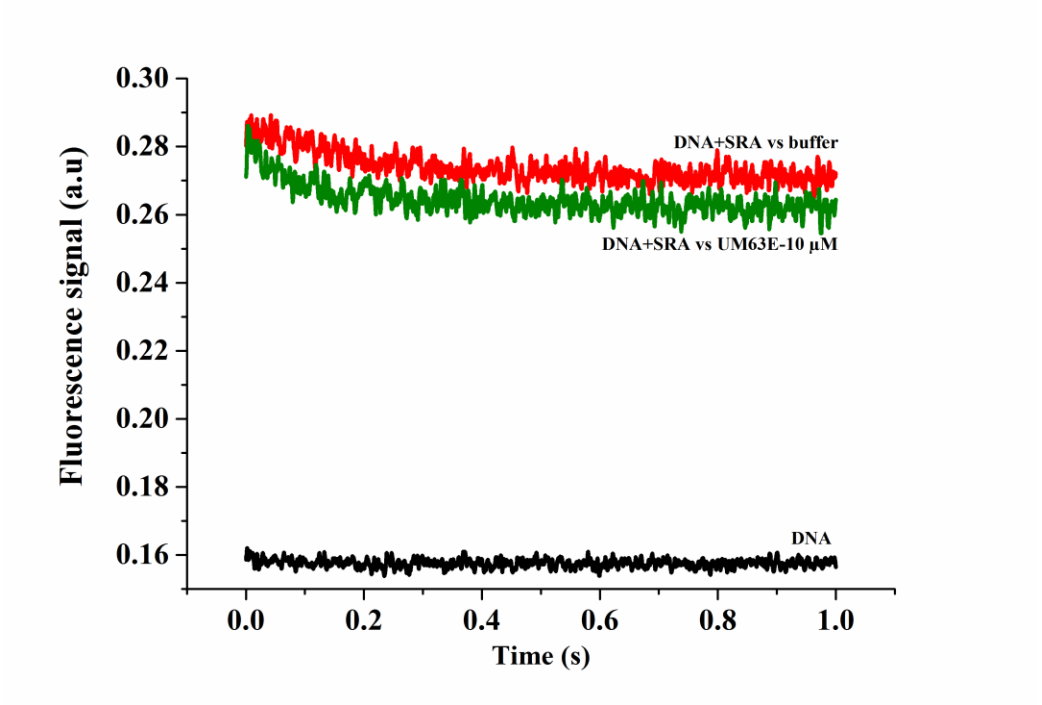

Fig. S8 Effect of UM63E on the SRA/HM DNA complex. The dissociation of the SRA/HM DNA complex was monitored by the stopped-flow technique after addition of 10 µM (green curve) of UM63E to the complex. The black curve corresponds to the DNA alone mixed with buffer. The concentrations of SRA and thG-labeled DNA were 0.2 µM and 1.5 µM, respectively.

Overlap of UM63 and HM DNA binding sites on SRA

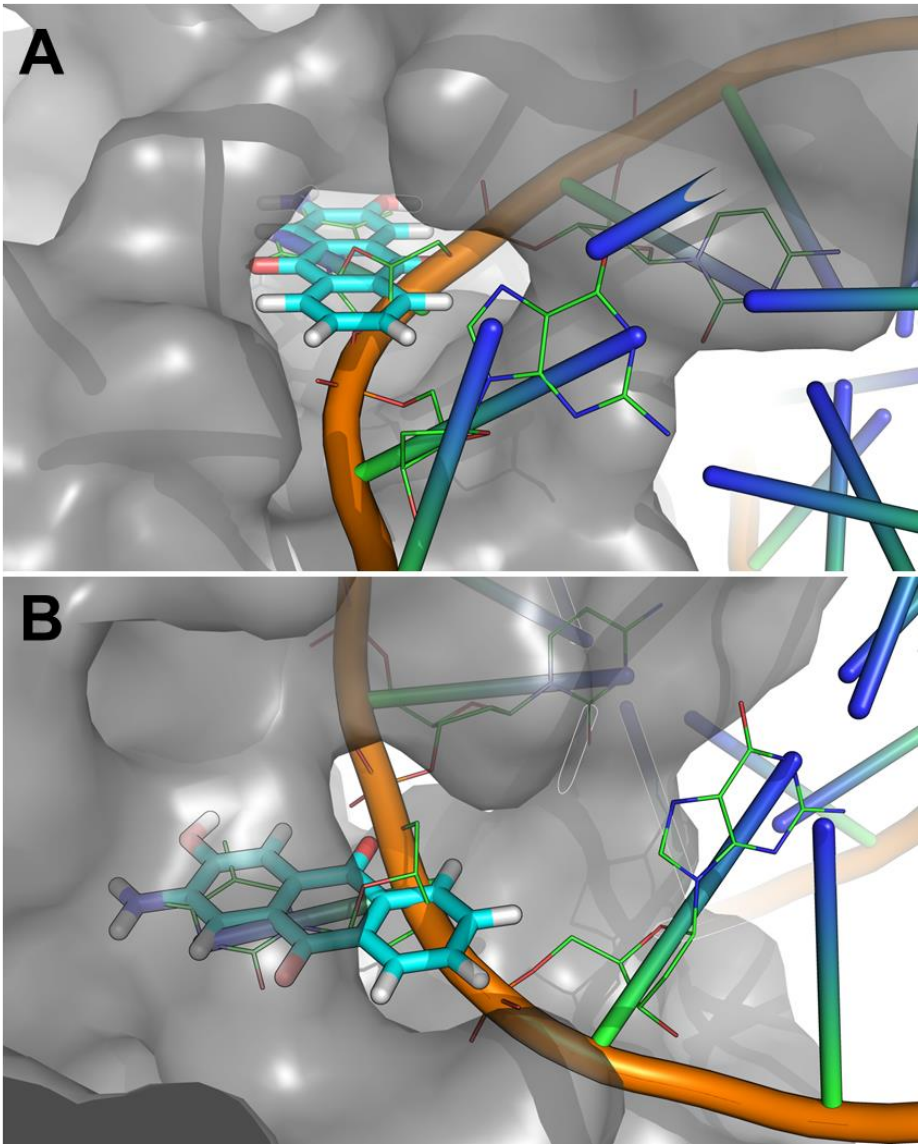

Fig. S9 UM63 and HM DNA partially overlap at the entrance of the 5mC binding site on SRA. Front (A) and side view (B) of the steric overlapping between the docking pose of UM63 and the crystallographic pose of HM DNA. UHRF1 is shown as gray surface, UM63 as cyan sticks with explicit H atoms. Crystallographic HM DNA is shown as cartoon, 5mC and the two flanking based are showed as lines.

Cytotoxic effect of UM63 and UM63E on HeLa cells

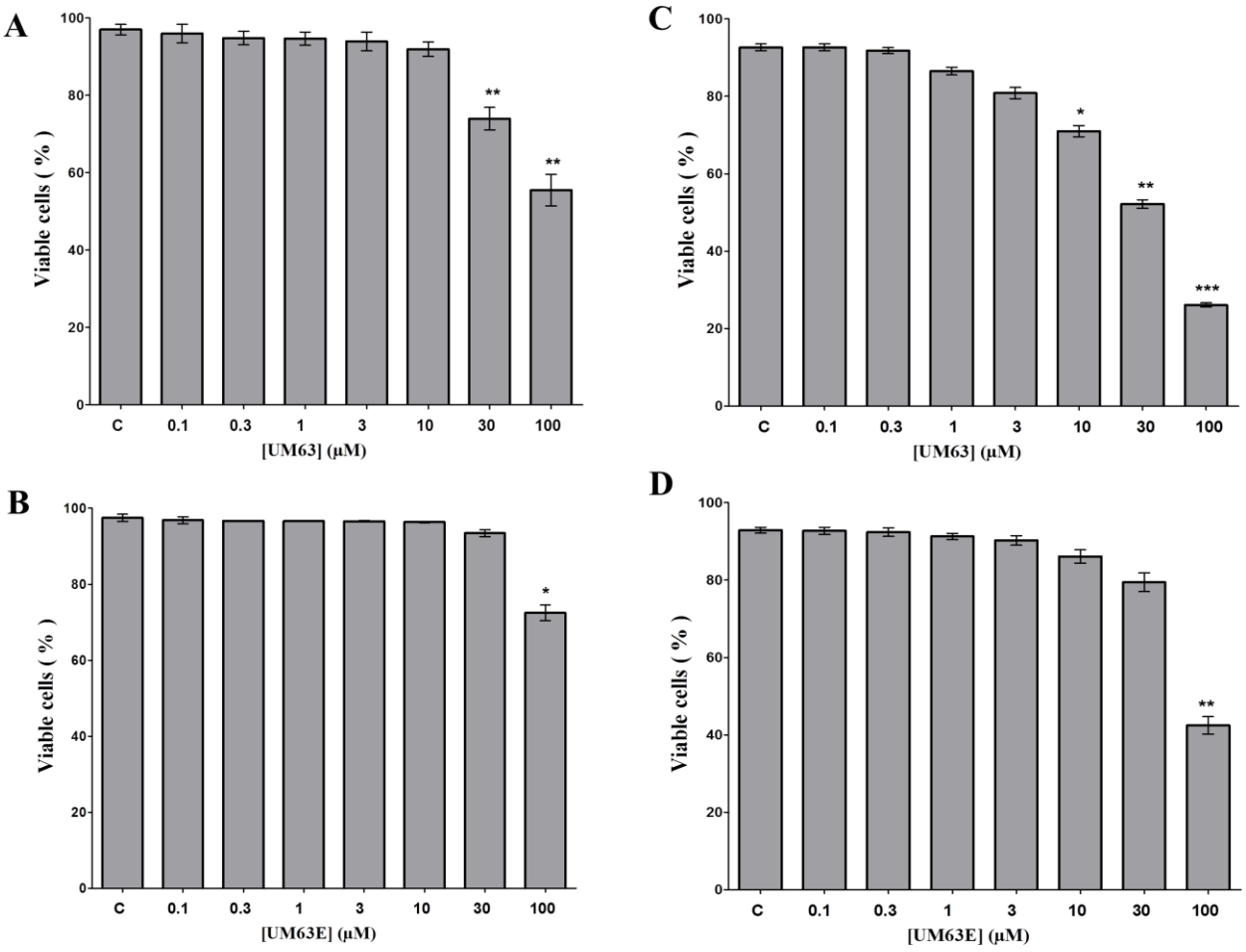

Fig. S10 Cytotoxic effect of UM63 and UM63E in HeLa cells. HeLa cells were treated with the indicated concentrations of either UM63 or UM63E, for 24 hours (A, B) and for 48 hours (C, D). Non-treated HeLa cells served as control. Trypan blue exclusion assay was performed and number of living cells was counted. Values are means ± S.E.M. for three independent experiments. Student t test was applied to analyze the data; statistically significant: * $p < 0.05$; ** $p < 0.001$; *** $p < 0.0001$ (versus untreated sample).

Co-localization analysis

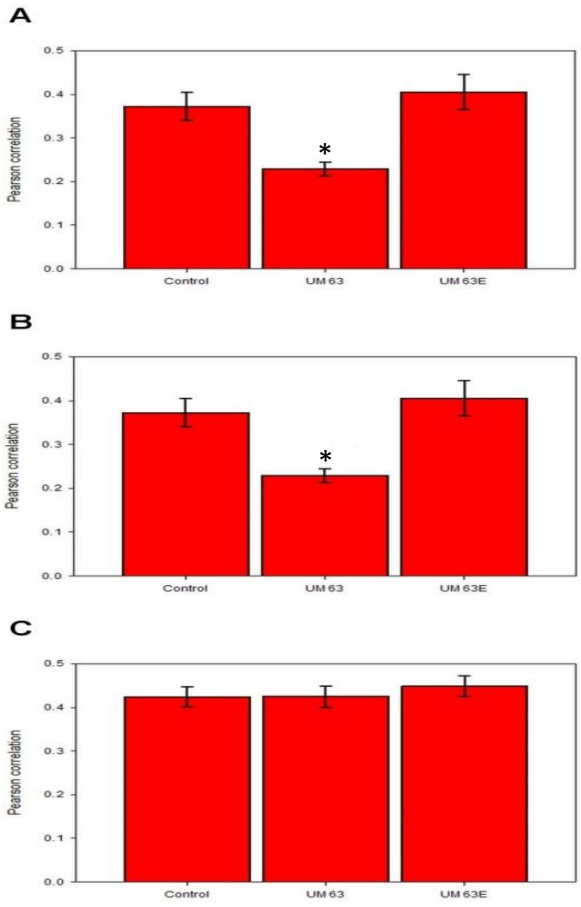

Fig. S11 Co-localization analysis on confocal images of HeLa cells co-transfected with eGFP-DNMT1 and UHRF1-mCherry and stained with EdU-Alexa 647. The data are presented in bar graphs with the mean Pearson's correlation coefficients (PCCs). Co-localization was analyzed for A) UHRF1-mCherry/ EdU-Alexa 647, B) eGFP-DNMT1 / EdU-Alexa 647 and C) eGFP-DNMT1 / UHRF1-mCherry. Non-treated cells are compared with cells treated with 10 µM UM63 or UM63E. The results show that UM63 significantly reduces the co-localization of DMNT1 and UHRF1 at the replication foci labeled with EdU-Alexa647. In contrast, UM63E does not affect the localization of both proteins at the replication foci. A Fiji/ ImageJ macro (Squassh, as described in the Methods section) was used for calculation of the mean PCCs and their standard deviation (n=12 cells). * $p<0.05$.

Manuscript IV: 2-amino-3-hydroxyanthraquinone (AHAQ) induces cell cycle arrest and apoptosis in cervical cancer cells with a re-expression of p53 and down-regulation of DNMT1/UHRF1

2-amino-3-hydroxyanthraquinone (AHAQ) induces cell cycle arrest and apoptosis in cervical cancer cells with a re-expression of p53 and down-regulation of DNMT1/UHRF1

Tanveer Ahmad[1, #], Liliyana Zaayter[1, #], Waseem Ashraf[1], Christian D. Muller[3], Christian Bronner[2], Yves Mély[1], Marc Mousli[1*]

[1]Laboratoire de Bioimagerie et Pathologies, UMR 7021 CNRS, Université de Strasbourg, Faculté de Pharmacie, 74, Route du Rhin, Illkirch-France

[2]Institut de Génétique et de Biologie Moléculaire et Cellulaire (IGBMC), INSERM U964 CNRS UMR 7104, Université de Strasbourg, Illkirch-France.

[3]Institut Pluridisciplinaire Hubert Curien, UMR 7178, Faculté de Pharmacie, CNRS-Université de Strasbourg, 74 Route du Rhin, F-67401, Illkirch Cedex, France.

# These authors contributed equally.

*Correspondence: marc.mousli@unistra.fr
Laboratory of Bioimaging and Pathologies UMR 7021 CNRS,
Faculté de Pharmacie, 74, Route du Rhin, 67401 Illkirch
Cedex, France

ABSTRACT

Anthraquinone family contains many natural and synthetic compounds that have displayed a remarkable anti-tumor profile. Yet, there is an urge to identify new derivatives in order to effectively target the cancer cells. Recently, 2-amino-3-hydroxyanthraquinone (AHAQ) has been reported as a candidate of UHRF1 inhibitor that blocks SRA domain and leads to a decrease in global methylation levels. This compound also was shown to target human breast cancer cells (MDA-MB-231) and induce death in these cells. The aim of the study is to investigate the antitumor potential of AHAQ on different types of cancer cells and to propose an underlying mechanism for these antitumor properties. In the present study, we evaluated the anti-proliferative activity of AHAQ by MTT assay on three different cancer cell lines (HeLa, A375, and Huh7) and noncancerous fibroblasts. AHAQ significantly inhibited the HeLa cell growth ($IC_{50} = 2.4 \pm 0.5$ μM) whereas other cell lines were less sensitive to AHAQ treatment. The flow cytometry cell cycle analysis shows that AHAQ induces cell cycle arrest at G0/G1 phase. Treatment with AHAQ induces apoptosis in HeLa cells which is accompanied by re-activation of caspase3, PARP, the tumor suppressor gene p53 and deactivation of Bcl2 protein. These findings were associated with a down-regulation of UHRF1 and DNMT1 which subsequently induced a global genomic demethylation. Our results suggest that AHAQ can be an interesting candidate for treatment of cervical cancer. It exerts its anti-cancer activity through induction of apoptosis and cell cycle arrest besides epigenetic modulation via UHRF1 and DNMT1. Antitumor properties of AHAQ can be further characterized for its possible application in preclinical and clinical studies.

INTRODUCTION

Anthraquinones, a family of aromatic compounds, with a planar tricyclic structure has gained considerable interest in past due to its wide anti-cancer profile (1). Doxorubicin and mitoxantrone are the two exemplified members of this family that have been widely used as chemotherapeutic agents (2). These agents are frequently recommended to treat a large variety of tumors such as multiple myeloma, breast cancers and solid tumors (2). New analogs of these anthraquinones are emerging in an attempt to improve the potency and safety of these drugs. Anthraquinones mainly exert their anti-cancer activity by interacting with DNA and interfering with the cellular machinery. In this way they target the cell proliferation by inducing apoptosis and cell cycle arrest (3). Recently, 2-amino-3-hydroxyanthraquinone (AHAQ), an anthraquinone derivative was described as an UHRF1 inhibitor that targets SRA domain and affects DNA methylation levels in cervical cancer cells. Another study of this compound has shown a possibility of AHAQ to mimic the known anthracycline drugs in terms of their anticancer effect (4). AHAQ's permeability to biological membrane is comparable to other anthracyclines and the compound exhibits antitumor effect in breast cancer cells MDAMB 231 by inhibiting cell growth and inducing of cell death (4). However, the exact mechanism of action of this anticancer effect is not well defined.

A programmed cell death is a common strategy for an anti-tumoral effect, that many anti-cancer therapies either anthraquinones-based or others proved to exert (3, 5, 6). The p53 tumor suppressor gene, a gatekeeper and caretaker of genome prevents tumorigenesis, and it is considered to be a crucial player in the cell death machinery. In response to stress, p53 controls many physiological processes through cell cycle arrest, apoptosis activation and DNA damage repair (7). An activated p53 may induce various pro-apoptotic genes that may promote intrinsic and extrinsic apoptotic pathways (8). It is noteworthy that epigenetic abnormalities are one of the recent uncovered cancer signatures that play a crucial role in developing multiple tumors (9). Besides genetic mutations, different epimutations have also been associated with almost every step of cancer progression (10). However, the epigenetic network is not so simple, and it is driven by interplay between varieties of epigenetic integrators.

Ubiquitin-like containing PHD and RING finger domains 1, (UHRF1), is a multi-domain protein recognized as one of the main epigenetic regulators. UHRF1 plays a pivotal role in faithful transmission of DNA methylation mark from the parent strand to the daughter strand

during the DNA replication by preferentially binding to hemimethylated DNA through its SRA domain and then recruiting the DNA methyltransferase (DNMT1) (11-13). In addition to this normal function, UHRF1 can play a critical role as a tumor promoter, since its levels are found to be highly expressed in majority of cancers such as hepatocellular carcinoma (14), breast cancer (15), gastric cancer (16),colorectal cancer (17), gallbladder cancer (18), and its abundance seems to correlate with tumor aggressiveness (19). The regulation of UHRF1 expression is cell cycle dependent in normal cells, but this expression remains high throughout the cell cycle in multiple tumors (20, 21). The oncogenic property of UHRF1 is also favored through regulating the function of some of tumor suppressor genes (TSGs) (22). It silences many of them including $p16^{INK4A}$ (23), HlC1 (24), RB1 (25), after DNMT1 and HDAC1 recruitment (26) leading to their promoter hypermethylation. Thus, through this repressive mechanism UHRF1 compromises the role of these genes in turmorgenesis prevention. Many studies have also underlined involvement of UHRF1 in promoting the proliferation of cancer cells by facilitating their passage through the cell cycle checkpoints (18, 27). All this highlights the putative role of UHRF1 in human malignancies (19) from where the growing interest in reconsidering UHRF1 for tumor treatments.

Accordingly, numerous investigations clearly indicate that targeting UHRF1 by siRNA, small molecules, and natural compounds in various human cancer cell lines show anti-tumor activities (28, 29). The observed consequences of UHRF1 knockdown that include upregulation of TSGs (p14, p16, and RB), inhibition of proliferation, cell cycle regulation and apoptosis initiation (22) encouraged to investigate the effect of natural compounds on UHRF1-mediated epigenetic regulation. One noted example is when a natural polyphenolic compound thymoquinone intensively down-regulated UHRF1 in Jurkat cells. Thus, leading to an arrest at G0/G1 phase of the cell cycle and induction of apoptosis through reactivation of p73 (30). However, other compounds targeting UHRF1 in human breast cancer cells, cervical cells, and leukemia cancer cells proved to inhibit cell growth through reactivation of genes such as p21, p16, p53 and consequently induce cell cycle arrest and apoptosis in these cells through their pathways (23, 31-33).

The aim of our work is to investigate whether AHAQ exerts anti-cancer effects upon UHRF1 inhibition. In our study we evaluate the anti-proliferative effect of AHAQ on different cell lines by using cervical carcinoma cells (HeLa), melanoma cells (A375) and hepatocarcinoma cells (Huh7) and we determine whether AHAQ targets UHRF1 and DNMT1 expression in

HeLa cells. We found that AHAQ induced apoptosis and cell cycle arrest in cancer cells via reactivation of tumor suppressive p53 and down-regulation of UHRF1 and DNMT1.

MATERIAL AND METHODS

1. Cell culture

HeLa (ATCC, CCL-2), A375, Huh7 and fibroblast were grown in DMEM (Dulbecco's Modified Eagle's Medium) which was supplemented with 10% FBS (fetal bovine serum), in addition to penicillin (100 U/ml) and streptomycin (100 U/ml) (penicillin/streptomycin: Invitrogen Corporation Pontoise, France). Cells were maintained in a humid atmosphere with 5% CO_2 at 37°C.

2. Antibodies

Antibodies used in this study include mouse monoclonal anti-UHRF1 which was engineered as described previously (34), mouse monoclonal anti-DNMT1 (Stressgen Canada), mouse monoclonal anti-PARP (BD Biosciences Pharmingen), mouse monoclonal anti-Bcl-2 (Merck-Millipore), rabbit polyclonal anti-caspase3 (Cell Signaling Technology, Danvers, MA, USA), mouse monoclonal anti-p53 (Delta Biolabs DB018), and mouse monoclonal anti-GAPDH (Merck Millipore MAB 374).

3. Cell proliferation by MTT assay

MTT assay was used in order to assess the proliferation state of cells after treatment with the molecules. HeLa cells were seeded in 96-well plates at a density of 5×10^3 cells/well and treated with various concentrations (0; 0.1; 0.3; 1; 3; 10; 30; 50; 100 µM) of AHAQ for 24 h. Each concentration was tested in triplicate. 100 µl of MTT reagent (5mg/10ml) dissolved in medium was added to each well and followed with incubation for 4 h at 37°C. The medium was discarded and 100µL of dimethylsulfoxide (DMSO) was added to each well. The plates were mixed gently until the dissolution of the formazan crystals. MTT reading was performed by measuring the optical density at 570 nm using Xenius plate reader. Each experiment was repeated three times and IC_{50} was calculated.

4. Cell Cycle and apoptosis analysis

Flow cytometry was used to analyze cell cycle distribution and apoptosis. HeLa cells at a density of 1.5×10^5 cells/well were seeded into a 6-well plate and treated with a concentration

of 10 µM for cell cycle and with different concentrations for apoptosis. Treated cells were compared to non-treated HeLa cells that served as control. For cell cycle, the cells were washed once with PBS, trypsinized and fixed with BD cellfix (BD Biosciences) reagent and incubated with FxCycle™ (Thermo Fisher Scientific F10797) PI/RNase staining solution for 20 min. After that DNA content was analyzed by guava easyCyte™ flow cytometer (Merck Millipore) and population percentages were determined by analyzing the results using InCyte Software for Guava® (Merck Millipore). For apoptosis, the cells were trypsinized and were incubated with PI (Miltenyi Biotec) and annexin V- FITC conjugate (Miltenyi Biotec) for 20 min. The apoptotic cells were analyzed using guava easyCyte™ flow cytometer provided with InCyte software (Merck Millipore).

5. Quantification of DNA methylation

HeLa cells were treated with 10 µM of AHAQ and 5-Azacytindine (Sigma-Aldrich), a specific demethylating agent serving as positive control. QIAamp® DNA Kit was used for DNA purification. Methylated DNA was assessed by using 200 ng of extracted DNA from non-treated cells and treated cells by using Sigma's Imprint® Methylated DNA Quantification Kit according to the manufacturer's protocol.

6. Western blot analysis

HeLa cells (1.5×10^5) were seeded into 6-well cell plates and grown for 24 h. Cells were treated with different concentrations of AHAQ for 24 h. Proteins were extracted by resuspending in ice cold lysis buffer (10 mM Tris-HCl pH 7.5, 150 mM NaCl, 1 mM EDTA and 1% NP40) containing protease inhibitors (complete mini EDTA free protease inhibitor cocktail tablets, Roche Germany). Cellular protein was quantified by Bradford method and 40 µg of proteins from cell lysate were separated on 10% SDS- polyacrylamide gel by electrophoresis after a 5 min denaturation step in Laemmli sample buffer (Bio-Rad Laboratories USA). After that, separated proteins are transferred to a (PVDF) membrane and 3% of non-fat dried milk was used to block the membrane at room temperature for 1 h. Incubation with primary antibodies a mouse monoclonal anti-UHRF1 (dilution 1:2000), anti-p53 (dilution 1:10000) , anti-DNMT1 (dilution 1:5000), anti-GAPDH (dilution 1:5000), anti-Caspase3 (dilution 1:2000), anti-BCl2 (dilution 1:2000), anti-PARP (dilution 1:10000) overnight at 4°C was followed. Primary antibodies were labeled with secondary anti-mouse (Promega, W402B) and then incubated with Horseradish Peroxidase conjugated secondary

antibody. Signals were visualized by the chemiluminescent ECL system (Clarity^{TM} ECL western blotting substrate, Biorad-USA) on Image Quant LAS 4000 apparatus. Images were analyzed and quantified by using Image Studio Lite (Li-Core Biosciences USA).

7. Statistical analysis

Data presented from at least three independent experiments and were statistically analyzed by t-Student test using GraphPadPrism (version 5.04) and Origin (version 8.6).

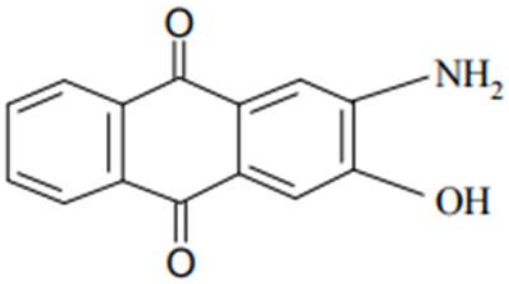

Figure 1. Chemical structure of AHAQ.

Results

1. AHAQ inhibits cell growth of cancer cells

In order to evaluate AHAQ (Fig.1) as a potential hit for anti-proliferative activity, AHAQ was assessed by MTT assay. Following a 24 h treatment with AHAQ, cell proliferation was significantly decreased in a dose-dependent manner in HeLa cancer cells (Fig. 2A). In contrast, cell proliferation was less affected in A375 cells (Fig. 2B) where the percentage of proliferation started to effectively decrease at a higher concentration than in HeLa (3 µM). In Huh7 cells (Fig. 2C), the proliferation was slightly decreased comparing to the two other cell lines, and the effect started at 10 µM of treatment. Interestingly, AHAQ exerted a less significant effect on normal (fibroblast) cells after 24 h of exposure to AHAQ (Fig. 2D). The IC_{50} values were determined graphically indicating values of 2.4±0.5 µM, 18±0.8 µM and 25±0.6 µM for HeLa, A375 and Huh7 cells respectively. These results suggest that AHAQ is controlling cell proliferation in different cancer cells. For the next experiments of our work, we chose HeLa cells as referential model.

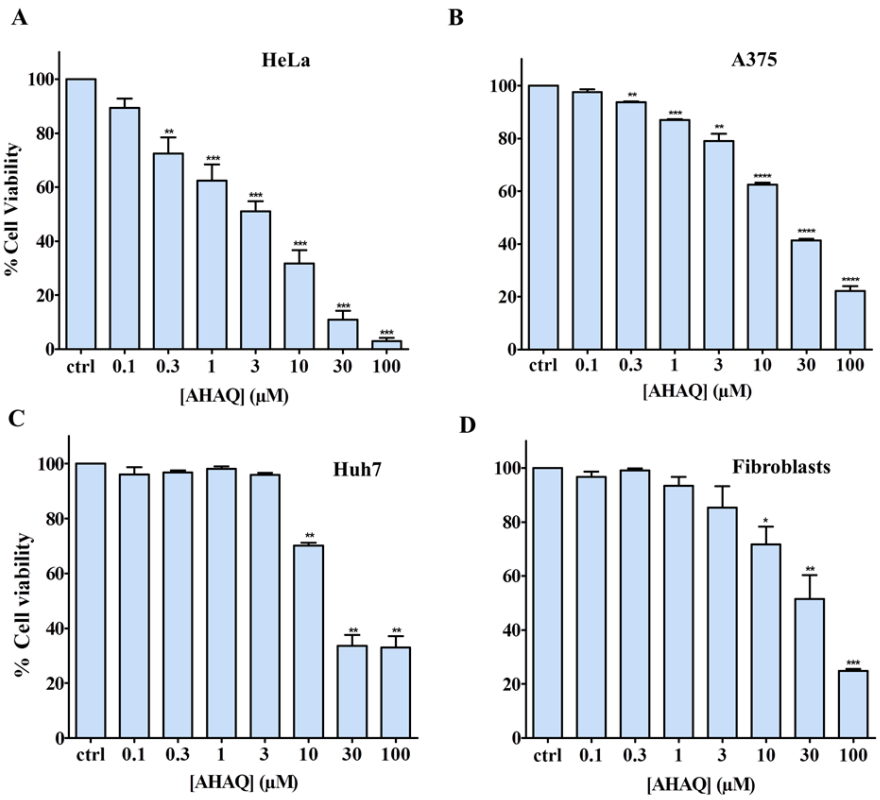

Figure 2. Concentration-dependent effect on cell viability of the AHAQ on different cancer cell lines and normal fibroblasts. (A) HeLa (B) A375 (C) Huh7 and (D) Fibroblasts cells were treated with AHAQ at the indicated concentrations for 24 h. Cell proliferation rate was assessed by colorimetry using the MTT assay. The absolute value obtained for each treated sample is expressed in a second step as percent relative to the corresponding absolute value obtained for the untreated sample and set at 100%. Values are means ±S.E.M. of three independent experiments; statistically significant * $p < 0.05$; ** $p < 0.01$; *** $p < 0.001$ (versus the corresponding untreated group).

2. AHAQ arrests HeLa cells on G0/G1 phase

Because cell proliferation is the process when cells progress through the different phases of the cell cycle, we next evaluated the effects of AHAQ on the cell cycle distribution.

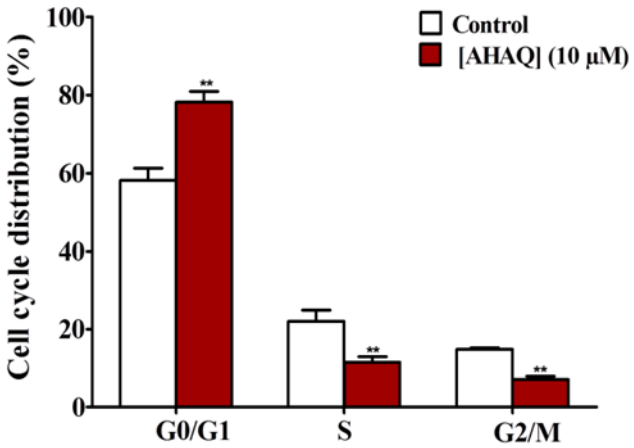

Figure 3. Effect of AHAQ on the cell cycle progression. Cells were treated with AHAQ for 24h and cell cycle distribution was assessed by a capillary cytometry detection assay. The graph shows the distribution of cells in G0/G1, S or G2/M phase; the number of cells in each phase was determined and expressed as percent relative to the total cell number. Values are means ±S.E.M. of three independent experiments; statistically significant: * $p < 0.05$; ** $p < 0.01$; *** $p < 0.001$ (versus the corresponding untreated group).

Treatment with AHAQ at 10 µM for 24 h induced an obvious cell cycle arrest at G0/G1 phase and the percentages of cells at S and G2 phase were correspondingly decreased. The percentage of G0/G1 cells increased from 58.14% to 78.23% following a decrease in G2/M population from 14.8% to 7.12% (Fig. 3). Therefore, this data suggests that AHAQ is able to inhibit the growth of HeLa cells within 24 h by promoting cell cycle arrest at the G0/G1 phase.

3. AHAQ induces apoptosis in HeLa cancer cells through caspase-3 and PARP activation and Bcl2 deactivation

Given that one of the mechanisms that lead to growth inhibition of tumor cells is by undergoing apoptosis through the reactivation of signaling pathways, we investigated whether AHAQ induces an apoptotic response in HeLa cancer cells. As shown in (Fig. 4A), AHAQ increased the number of apoptotic cells in a concentration-dependent manner. At the highest tested concentration 20 µM, AHAQ showed a significant increase in apoptosis 29%. These findings were confirmed further by western blot results that show an activation of pro-apoptotic proteins. Non treated cells show undetectable levels of cleaved caspase3; these levels start to increase after exposure to AHAQ in a dose-dependent manner (Fig. 4B). In addition, treatment with AHAQ was followed by a down-regulation of PARP with a significant increase in its cleaved form (Fig. 4D). Then, we determined the levels of the pro-survival marker Bcl2 (Fig. 4C), where the levels of the protein decreased significantly starting 2 µM. Altogether, our results suggest that the exposure of HeLa cancer cells to AHAQ induces a caspase3-dependant apoptosis.

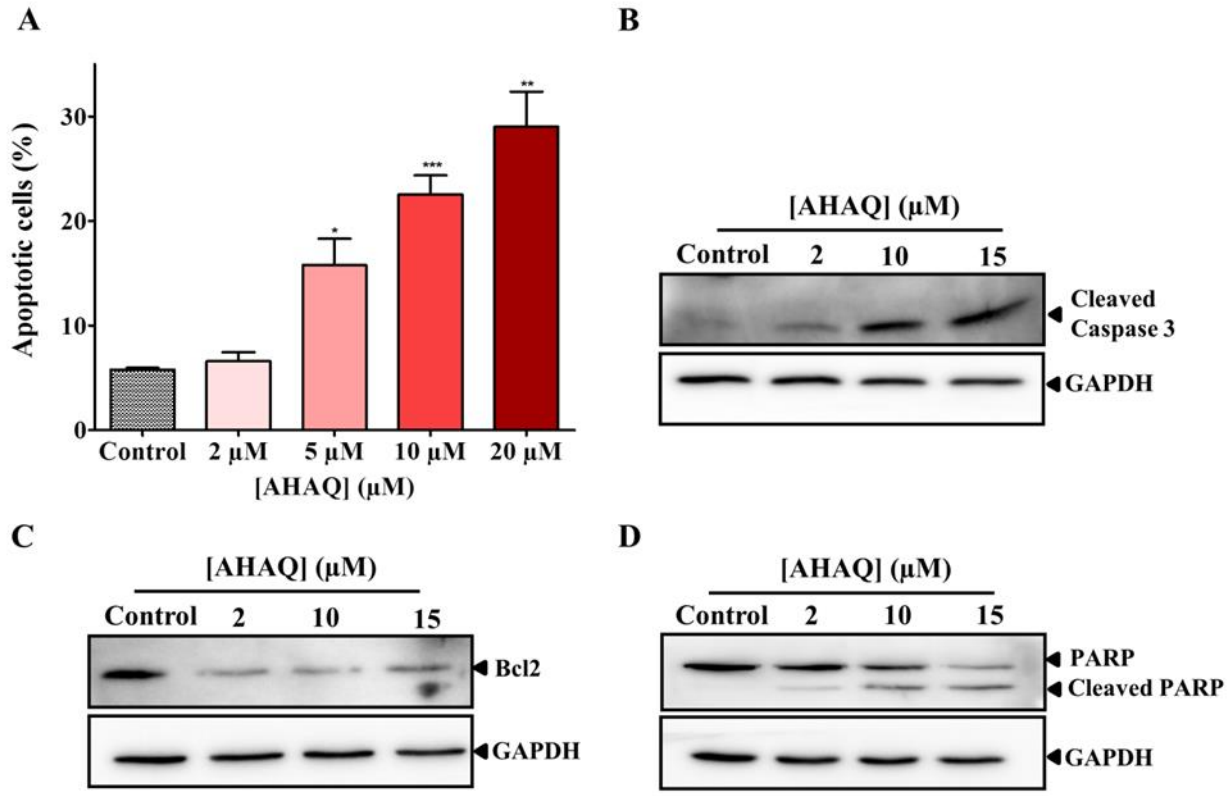

Figure 4. Effect of AHAQ on apoptosis and on expression of apoptotic protein levels in HeLa cells. Cells were treated with AHAQ at the indicated concentrations and incubated for 24 h. Cell apoptosis rate was assessed by cytometry using the Annexin V-FITC staining assay. (A) Recapitulates the number of apoptotic cells expressed as percent relative to the total cell number. Effect of AHAQ on expression levels of (B) cleaved caspase-3 (C) Bcl2 and (D) PARP. Values are means ±S.E.M. of three independent experiments; statistically significant: * $p < 0.05$; ** $p < 0.01$; *** $p < 0.001$ (versus the corresponding untreated group).

4. AHAQ induces p53 reactivation and down-regulation of UHRF1 and DNMT1 and in HeLa cells

In order to determine more precisely the molecular events activated in response to the treatment, we wanted to investigate if apoptosis is induced by activation of a tumor suppressor gene. For this we analyzed the effect of AHAQ on the expression of p53. Treatment of HeLa cells with AHAQ, reactivated p53 in an evident manner (Fig. 5) suggesting that previous results in apoptosis could be triggered through a p53-dependant pathway.

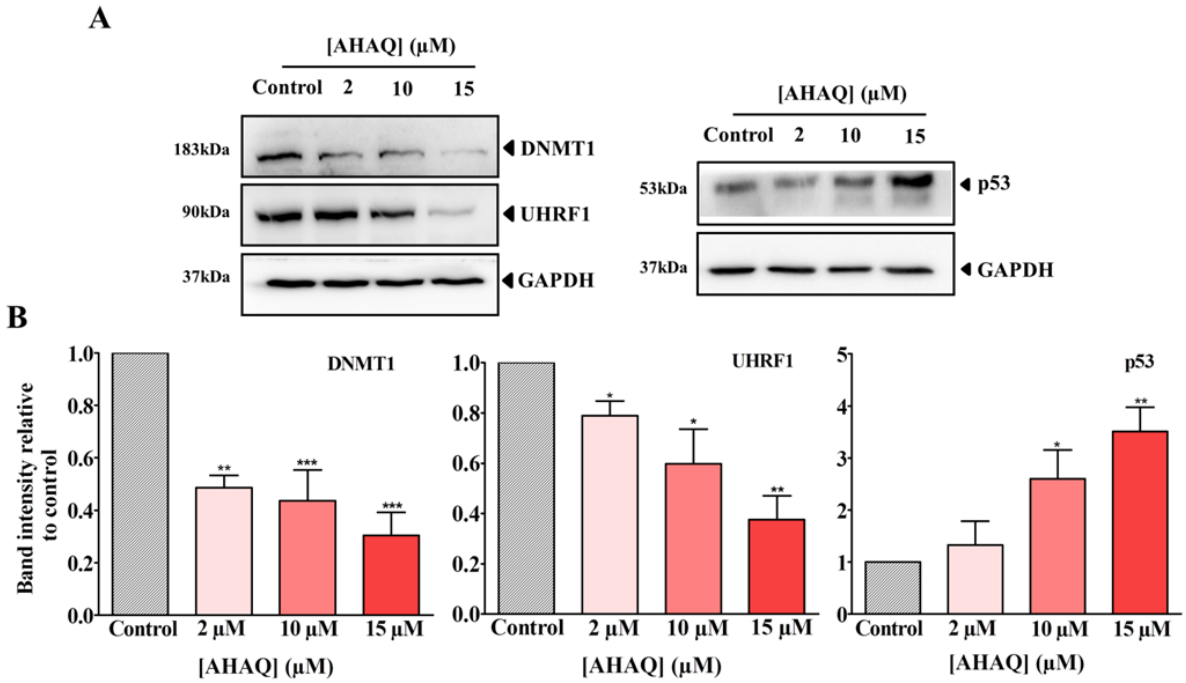

Figure 5. Concentration-dependent effects of AHAQ on the expression levels of DNMT1/ UHRF1 and on the levels of tumor suppressor p53 in HeLa cells. Cells were treated with AHAQ at the indicated concentrations and incubated for 24 h. (A) shows a representative western blot results of DNMT1/UHRF1 expression (left panel) and p53 expression (right panel). (B) shows the normalized signal for AHAQ treatment. GAPDH was used for the normalization of the expression levels of the different indicated proteins. Values are means ±S.E.M. of three independent experiments; statistically significant: * $p < 0.05$; ** $p < 0.01$; *** $p < 0.001$ (versus untreated group).

UHRF1 has been identified to be targeted by TSGs such p53 and p73, and any dysregulation of these TSGs modulates the expression of UHRF1, that can also itself control the expression of these genes by a negative feedback (22). For this, further analysis was carried out to study UHRF1 and DNMT1 proteins which are primarily involved in epigenetic modulation. HeLa cells were treated with different concentrations of AHAQ (2 µM, 10 µM, 15 µM) respectively in order to evaluate the effect on UHRF1 and DNMT1 expression in a concentration-dependent manner (Fig. 5). HeLa cells incubation with AHAQ for 24 h induced a significant reduction in DNMT1 levels. Similarly, UHRF1 expression was down-regulated gradually in the same conditions of treatment.

5. UHRF1 and DNMT1 down-regulation is associated with a decrease in global DNA methylation

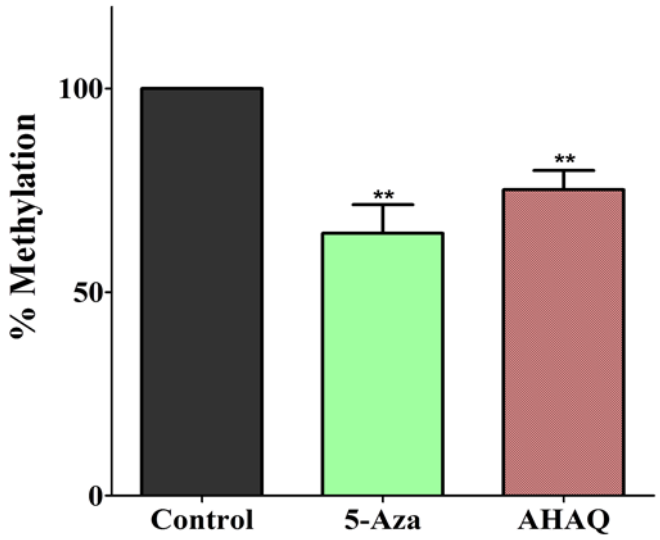

Figure 6. Effect of AHAQ on the global DNA methylation in HeLa cells. DNA was extracted from treated and non-treated cells. The graph illustrates the absorbance representing the content of methylated DNA. Values are means ±S.E.M. of three independent experiments; statistically significant: * $p < 0.05$; ** $p < 0.01$; *** $p < 0.001$ (versus untreated group).

We wanted to uncover whether the epigenetic alteration shown in our western blot result, is associated with an effect on genomic DNA methylation. For that, 5-Azacytidine, a known DNMT1 inhibitor with a demethylating effect, was used as positive control. Global DNA methylation was estimated by using Imprint Methylated DNA quantification assay after extracting the DNA from treated and untreated HeLa cells (Fig. 6). Comparing to non-treated cells, cells treated with AHAQ showed a 25.1% decrease versus a 35.7% decrease in 5-Azacytidine treated samples which is in agreement with our previously reported finding. Altogether, this data demonstrates that AHAQ leads to a reduced methylation level in the genome.

DISCUSSION

Anthraquinones have shown a great potential to be used as anti-tumor agents in different studies, however so far, their use in therapeutics is limited because of their high toxicity, poor selectivity and other side effects. Therefore, there is a need to develop new analogues which can safely and selectively target cancer cells.

Anthraquinones mostly exerts their cytotoxic effects by their ability to intercalate into the DNA bases (35), a property that has been exploited by variety of chemotherapeutic agents. A

lot of natural and synthetic anthraquinone compounds such Rhein, emodin and 1,3-dihydroxy-9,10-anthraquinone-2- carboxylic acid (DHAQC) have been reported to target various cancer cell lines (HeLa, A375, MOLT-4, MCF-7) (1, 36, 37). A recent study described that 2-amino-3-hydroxyanthraquinone AHAQ, a derivative from 9, 10 anthraquinone, impaired the cell viability of breast cancer cells (4). In this study, we also observed an evident inhibiting effect of AHAQ on proliferation of cervical cancer (HeLa), melanoma (A375) and hepatocarcinoma (Huh7). It is interesting to note that AHAQ seems not to exert evident anti-proliferative effect on non-cancer (fibroblasts) cells, which holds an opportunity for its application in chemotherapy with fewer side effects. Anyhow, further investigations should be carried out to validate this finding.

Treatment of cancer cells with AHAQ resulted in cell cycle arrest at G0/G1 phase. Anticancer drugs tend to inhibit the cell cycle progression by activation of different tumor suppressor genes and cell cycle checkpoints. For example, HeLa cells treated with aloe emodin, a natural anthraquinone, induced a G2/M arrest (38). However, the same compound arrested the hepatoma cells in G0/G1 phase after the p53 induced activation of p21 (39). Moreover, FACS analysis showed that the treatment with AHAQ also induced apoptosis in HeLa cells. Activation of apoptotic machinery is a mechanism induced in response of many anticancer drugs to kill tumors. In our study, by investigating the apoptosis related proteins, we found that the apoptotic effect is mechanistically mediated by a caspase-3 signaling pathway which is followed by a prominent PARP cleavage. In the same context, upon AHAQ exposure, Bcl2, an anti-apoptotic protein involved in mitochondrial pathway and necessary for cell survival was also found to be reduced.

p53 is an important tumor suppressor gene coordinating DNA repair, cell cycle arrest and apoptosis in cells (40). Studies have shown that in majority of the human malignancies, p53 is either mutated or suppressed to overcome its tumor preventive role in cancer (41). Upon treatment with different chemotherapeutic drugs, p53 gets activated and induces cell cycle arrest or apoptosis depending on the activating stimuli and downstream signaling initiated in response to p53 activation. Our western blot analysis demonstrated that p53 is reactivated in response to treatment with AHAQ and can be the reason for cell cycle arrest and apoptosis induction.

UHRF1, an overexpressed epigenetic regulator in cancers, plays a critical role as tumor promoter by disrupting the function of various TSGs (19, 22). Previously, it has been reported

that UHRF1 promotes oncogenesis by negatively regulating the p53 activity and suppressing p53 mediated transactivation (42). Therefore, we examined UHRF1 expression and our results showed that UHRF1 levels were down-regulated in HeLa cells after treatment with AHAQ. Accordingly, a reasonable explanation indicates the possibility of AHAQ to activate the p53 pathway by down-regulation of UHRF1. Altogether, these findings show that AHAQ probably acts by a mechanism that controls tumor suppressor genes and UHRF1.

It is important to note that DNMT1 levels were also down-regulated after treatment with AHAQ and over all global methylation reduced by 25% in these cells. DNMT1 is found upregulated in many cancers (43) and is currently being targeted by different epigenetic drugs such as azacytidine and decitabine to improve the therapeutic outcome in cancer patients. Targeting UHRF1 by siRNA, small molecules, and natural compounds have shown favorable antitumor response in various human cancer cell lines (28-30, 44, 45). Down-regulation of UHRF1 upregulates TSGs (p16, p14 and RB), inhibits the proliferation, induces cell cycle arrest and initiates apoptosis (22, 44, 46). For instance, the proliferation of MDAMB 231 cells was shown to be promoted through UHRF1 activity (47) and it is interesting to note that in a previous study treatment of AHAQ induced apoptosis of these cells (4), a finding that could be associated with UHRF1 inhibition. Similarly, in our study, targeting UHRF1 with AHAQ resulted in comparable effects by inhibiting cell growth, inducing apoptosis and cell cycle arrest. Furthermore, treatment with AHAQ down-regulated UHRF1 and DNMT1 proteins, induced global hypomethylation, thus reactivated the p53 to induce cell cycle arrest and apoptosis. However, the mechanism underlying the process of demethylation by AHAQ can be attributed to decreased levels of both proteins, additionally to the inhibition of flipping of the methylated cytosine reported previously.

In conclusion, our study clearly demonstrates that AHAQ has an anti-proliferative activity which is mediated through cell cycle arrest and apoptosis induction in HeLa cancer cells. Our findings also suggest that AHAQ is able to target the expression of epigenetic modulators UHRF1 and DNMT1 with a subsequent global DNA demethylation. Overall, these results indicate the potential of AHAQ as an UHRF1 inhibitor and as a candidate for anti-cancer research, as well as a useful reference for further investigations in order to characterize and understand the exact mechanism.

REFERENCES

1. Hussain H, Al-Harrasi A, Al-Rawahi A, et al.: A fruitful decade from 2005 to 2014 for anthraquinone patents. Expert opinion on therapeutic patents 25: 1053-1064, 2015.
2. Evison BJ, Sleebs BE, Watson KG, Phillips DR and Cutts SM: Mitoxantrone, More than Just Another Topoisomerase II Poison. Medicinal research reviews 36: 248-299, 2016.
3. Huang Q, Lu G, Shen HM, Chung MC and Ong CN: Anti-cancer properties of anthraquinones from rhubarb. Medicinal research reviews 27: 609-630, 2007.
4. Das A, Roy S, Mondal P, et al.: Studies on the interaction of 2-amino-3-hydroxy-anthraquinone with surfactant micelles reveal its nucleation in human MDA-MB-231 breast adinocarcinoma cells. RSC Advances 6: 28200-28212, 2016.
5. Koceva-Chyla A, Jedrzejczak M, Skierski J, Kania K and Jozwiak Z: Mechanisms of induction of apoptosis by anthraquinone anticancer drugs aclarubicin and mitoxantrone in comparison with doxorubicin: relation to drug cytotoxicity and caspase-3 activation. Apoptosis : an international journal on programmed cell death 10: 1497-1514, 2005.
6. Hickman JA: Apoptosis induced by anticancer drugs. Cancer metastasis reviews 11: 121-139, 1992.
7. Harris SL and Levine AJ: The p53 pathway: positive and negative feedback loops. Oncogene 24: 2899-2908, 2005.
8. el-Deiry WS: Regulation of p53 downstream genes. Seminars in cancer biology 8: 345-357, 1998.
9. Nakamura K, Nakabayashi K, Htet Aung K, et al.: DNA methyltransferase inhibitor zebularine induces human cholangiocarcinoma cell death through alteration of DNA methylation status. PloS one 10: e0120545, 2015.
10. Timp W and Feinberg AP: Cancer as a dysregulated epigenome allowing cellular growth advantage at the expense of the host. Nature reviews. Cancer 13: 497-510, 2013.
11. Arita K, Ariyoshi M, Tochio H, Nakamura Y and Shirakawa M: Recognition of hemi-methylated DNA by the SRA protein UHRF1 by a base-flipping mechanism. Nature 455: 818-821, 2008.
12. Avvakumov GV, Walker JR, Xue S, et al.: Structural basis for recognition of hemi-methylated DNA by the SRA domain of human UHRF1. Nature 455: 822-825, 2008.
13. Sharif J, Muto M, Takebayashi S, et al.: The SRA protein Np95 mediates epigenetic inheritance by recruiting Dnmt1 to methylated DNA. Nature 450: 908-912, 2007.
14. Liang D, Xue H, Yu Y, Lv F, You W and Zhang B: Elevated expression of UHRF1 predicts unfavorable prognosis for patients with hepatocellular carcinoma. International journal of clinical and experimental pathology 8: 9416-9421, 2015.
15. Geng Y, Gao Y, Ju H and Yan F: Diagnostic and prognostic value of plasma and tissue ubiquitin-like, containing PHD and RING finger domains 1 in breast cancer patients. Cancer science 104: 194-199, 2013.
16. Zhou L, Zhao X, Han Y, et al.: Regulation of UHRF1 by miR-146a/b modulates gastric cancer invasion and metastasis. FASEB journal : official publication of the Federation of American Societies for Experimental Biology 27: 4929-4939, 2013.
17. Wang F, Yang YZ, Shi CZ, et al.: UHRF1 promotes cell growth and metastasis through repression of p16(ink(4)a) in colorectal cancer. Annals of surgical oncology 19: 2753-2762, 2012.
18. Qin Y, Wang J, Gong W, et al.: UHRF1 depletion suppresses growth of gallbladder cancer cells through induction of apoptosis and cell cycle arrest. Oncology reports 31: 2635-2643, 2014.
19. Ashraf W, Ibrahim A, Alhosin M, et al.: The epigenetic integrator UHRF1: on the road to become a universal biomarker for cancer. Oncotarget, 2017.
20. Mousli M, Hopfner R, Abbady AQ, et al.: ICBP90 belongs to a new family of proteins with an expression that is deregulated in cancer cells. British journal of cancer 89: 120-127, 2003.

21. Jeanblanc M, Mousli M, Hopfner R, et al.: The retinoblastoma gene and its product are targeted by ICBP90: a key mechanism in the G1/S transition during the cell cycle. Oncogene 24: 7337-7345, 2005.
22. Alhosin M, Omran Z, Zamzami MA, et al.: Signalling pathways in UHRF1-dependent regulation of tumor suppressor genes in cancer. Journal of experimental & clinical cancer research : CR 35: 174, 2016.
23. Achour M, Mousli M, Alhosin M, et al.: Epigallocatechin-3-gallate up-regulates tumor suppressor gene expression via a reactive oxygen species-dependent down-regulation of UHRF1. Biochemical and biophysical research communications 430: 208-212, 2013.
24. Fleuriel C, Touka M, Boulay G, Guerardel C, Rood BR and Leprince D: HIC1 (Hypermethylated in Cancer 1) epigenetic silencing in tumors. The international journal of biochemistry & cell biology 41: 26-33, 2009.
25. Alhosin M, Sharif T, Mousli M, et al.: Down-regulation of UHRF1, associated with re-expression of tumor suppressor genes, is a common feature of natural compounds exhibiting anti-cancer properties. Journal of experimental & clinical cancer research : CR 30: 41, 2011.
26. Hashimoto H, Horton JR, Zhang X, Bostick M, Jacobsen SE and Cheng X: The SRA domain of UHRF1 flips 5-methylcytosine out of the DNA helix. Nature 455: 826-829, 2008.
27. Bronner C, Krifa M and Mousli M: Increasing role of UHRF1 in the reading and inheritance of the epigenetic code as well as in tumorogenesis. Biochemical pharmacology 86: 1643-1649, 2013.
28. Krifa M, Pizzi A, Mousli M, Chekir-Ghedira L, Leloup L and Ghedira K: Limoniastrum guyonianum aqueous gall extract induces apoptosis in colorectal cancer cells by inhibiting calpain activity. Tumour biology : the journal of the International Society for Oncodevelopmental Biology and Medicine 35: 7877-7885, 2014.
29. Unoki M: Current and potential anticancer drugs targeting members of the UHRF1 complex including epigenetic modifiers. Recent patents on anti-cancer drug discovery 6: 116-130, 2011.
30. Alhosin M, Abusnina A, Achour M, et al.: Induction of apoptosis by thymoquinone in lymphoblastic leukemia Jurkat cells is mediated by a p73-dependent pathway which targets the epigenetic integrator UHRF1. Biochemical pharmacology 79: 1251-1260, 2010.
31. Jang SY, Hong D, Jeong SY and Kim JH: Shikonin causes apoptosis by up-regulating p73 and down-regulating ICBP90 in human cancer cells. Biochemical and biophysical research communications 465: 71-76, 2015.
32. Kim MY, Park SJ, Shim JW, Yang K, Kang HS and Heo K: Naphthazarin enhances ionizing radiation-induced cell cycle arrest and apoptosis in human breast cancer cells. International journal of oncology 46: 1659-1666, 2015.
33. Sharif T, Auger C, Alhosin M, et al.: Red wine polyphenols cause growth inhibition and apoptosis in acute lymphoblastic leukaemia cells by inducing a redox-sensitive up-regulation of p73 and down-regulation of UHRF1. European journal of cancer 46: 983-994, 2010.
34. Hopfner R, Mousli M, Jeltsch J-M, et al.: ICBP90, a novel human CCAAT binding protein, involved in the regulation of topoisomerase IIα expression. Cancer research 60: 121-128, 2000.
35. Hsin LW, Wang HP, Kao PH, et al.: Synthesis, DNA binding, and cytotoxicity of 1,4-bis(2-amino-ethylamino)anthraquinone-amino acid conjugates. Bioorganic & medicinal chemistry 16: 1006-1014, 2008.
36. Yeap S, Akhtar MN, Lim KL, et al.: Synthesis of an anthraquinone derivative (DHAQC) and its effect on induction of G2/M arrest and apoptosis in breast cancer MCF-7 cell line. Drug design, development and therapy 9: 983-992, 2015.
37. Genov M, Kreiseder B, Nagl M, et al.: Tetrahydroanthraquinone Derivative (+/-)-4-Deoxyaustrocortilutein Induces Cell Cycle Arrest and Apoptosis in Melanoma Cells via Upregulation of p21 and p53 and Downregulation of NF-kappaB. Journal of Cancer 7: 555-568, 2016.
38. Guo JM, Xiao BX, Liu Q, Zhang S, Liu DH and Gong ZH: Anticancer effect of aloe-emodin on cervical cancer cells involves G2/M arrest and induction of differentiation. Acta pharmacologica Sinica 28: 1991-1995, 2007.

39. Kuo PL, Lin TC and Lin CC: The antiproliferative activity of aloe-emodin is through p53-dependent and p21-dependent apoptotic pathway in human hepatoma cell lines. Life sciences 71: 1879-1892, 2002.
40. Kruse JP and Gu W: Modes of p53 regulation. Cell 137: 609-622, 2009.
41. Hainaut P and Hollstein M: p53 and human cancer: the first ten thousand mutations. Advances in cancer research 77: 81-137, 2000.
42. Ma J, Peng J, Mo R, et al.: Ubiquitin E3 ligase UHRF1 regulates p53 ubiquitination and p53-dependent cell apoptosis in clear cell Renal Cell Carcinoma. Biochemical and biophysical research communications 464: 147-153, 2015.
43. Subramaniam D, Thombre R, Dhar A and Anant S: DNA methyltransferases: a novel target for prevention and therapy. Frontiers in oncology 4: 80, 2014.
44. Seo JS, Choi YH, Moon JW, Kim HS and Park SH: Hinokitiol induces DNA demethylation via DNMT1 and UHRF1 inhibition in colon cancer cells. BMC cell biology 18: 14, 2017.
45. Kofunato Y, Kumamoto K, Saitou K, et al.: UHRF1 expression is upregulated and associated with cellular proliferation in colorectal cancer. Oncology reports 28: 1997-2002, 2012.
46. Esteller M: Epigenetics in cancer. The New England journal of medicine 358: 1148-1159, 2008.
47. Li XL, Xu JH, Nie JH and Fan SJ: Exogenous expression of UHRF1 promotes proliferation and metastasis of breast cancer cells. Oncology reports 28: 375-383, 2012.

DISCUSSION AND PERSPECTIVES

V- DISCUSSION AND PERSPECTIVES

Cellular memory inheritance is characterized by faithful transmission of epigenetic marks in particular of DNA methylation patterns and histone post-translational modifications. UHRF1 is a well-recognized epigenetic integrator which is involved in governance of epigenetic modifications like DNA methylation and histone modifications. UHRF1 has preferential binding affinity towards hemi-methylated (HM) DNA. Being a "reader" UHRF1 identifies HM DNA through its SRA domain and recruits methyltransferase DNMT1 on replication strand for maintenance of DNA methylation patterns (Bostick *et al.*, 2007; Sharif *et al.*, 2007; Avvakumov *et al.*, 2008; Bronner *et al.*, 2010; Vaughan *et al.*, 2018).

TTD and PHD domains of UHRF1 also facilitate UHRF1 in methylation maintenance through reading specific modifications on H3 (Karagianni *et al.*, 2008; Hu *et al.*, 2011; Nady *et al.*, 2011; Rajakumara *et al.*, 2011; Wang *et al.*, 2011; Rothbart *et al.*, 2013; Ferry *et al.*, 2017; Jeltsch, 2019; Kori *et al.*, 2019). C-terminus RING domain of UHRF1 serves as a "writer" as it marks ubiquitination on different lysines of H3. RING-mediated H3 ubiquitination is critical for recruitment of DNMT1 on chromatin to perform methylation job (Nishiyama *et al.*, 2013; Qin *et al.*, 2015; Tauber & Fischle, 2015; Li *et al.*, 2018). UBL domain stimulates E3 ligase activity of UHRF1 and directs ubiquitin mark to H3. In combination with RING domain, it also helps in nuclear localization of DNMT1 and ultimately faithful transmission of methylation impressions (DaRosa *et al.*, 2018; Foster *et al.*, 2018; Li *et al.*, 2018). Due to its involvement in epigenetic modifications, UHRF1 takes part in a variety of functions like DNA damage, embryonic development, organogenesis and differentiation (Bronner *et al.*, 2013; Sidhu & Capalash, 2017).

UHRF1 performs these cellular functions through its interaction and coordination with other epigenetic partners such as TIP60, DNMT1, USP7, PCNA, HATs and HDAC1. All these member proteins constitute a macromolecular complex named "epigenetic code replication machinery" (ECREM) which ensures integrity of epigenome (Bronner *et al.*, 2007b; Alhosin *et al.*, 2011; Bronner *et al.*, 2013). It is well established that UHRF1 is involved in tumorogenesis and it suppresses TSGs expression (Alhosin *et al.*, 2016; Ashraf *et al.*, 2017). It promotes cellular proliferation of cancer cells and helps them to escape from apoptosis pathways. Its overexpression is also linked with poor prognosis and resistance towards chemotherapeutic drugs. Therefore, UHRF1 is an interesting therapeutic target.

An important epigenetic partner of UHRF1 is TIP60 and it was found to be present in same epigenetic complex by our team (Achour *et al.*, 2009). TIP60 is an acetyltransferase enzyme which participates in various cellular activities such as chromatin remodeling, proliferation, cell cycle, apoptosis, DNA damage response, gene expression and development (Sapountzi *et al.*, 2006; DeRan *et al.*, 2008; Sun *et al.*, 2010; Judes *et al.*, 2018). It has been believed that TIP60 has tumor suppressive activity (Avvakumov & Côté, 2007; Dai *et al.*, 2013; Wang *et al.*, 2019). Like UHRF1, TIP60 is also a multidomain protein which coordinates with various other proteins to perform its cellular responsibilities (Doyon & Côté, 2004; Sapountzi *et al.*, 2006). In this project, we have investigated interaction of UHRF1 and TIP60 as well as effects of this interaction in cancer cells. We have also screened various molecules which can inhibit base flipping activity of UHRF1.

- **UHRF1 coordinates with MYST domain of TIP60 during S phase**

Our data has revealed that UHRF1 interacts with TIP60 and this interaction is MYST domain dependent. Interaction between these epigenetic partners is developed during S phase (Ashraf *et al.*, 2017a). Co-immunoprecipitation of UHRF1 and TIP60 confirmed the presence of both proteins in same epigenetic complex. FLIM technique was used to validate this interaction inside the nucleus during S phase. *In vitro* pull-down assay shown strong interaction between UHRF1 and MYST domain of TIP60. We also observed that TIP60 overexpression in HeLa cancer cells down-regulated UHRF1 and DNMT1 expressions associated with a global hypomethylation (Ashraf *et al.*, 2017a).

MYST domain is an indispensable component of TIP60 protein. Inside the MYST domain there is a HAT domain which harbors acetyltransferase activity. MYST domain is a conserved domain which is present in some other proteins such as MOZ, MOF, HBO1 and MORF (Avvakumov & Côté, 2007; Voss & Thomas, 2009; Johnson *et al.*, 2013). Interaction of UHRF1 with MYST domain of TIP60 indicates that similar kind of UHRF1's interaction may be established with MYST domain of above four proteins. Study by Ruan has anticipated this kind of type interaction between UHRF1 and MOF. MYST domain of MOF has approximately 80% similarity with MYST domain of TIP60 (Ruan, 2015). Further studies are needed to investigate this interaction in detail. It will be interesting to check that MYST domain containing proteins are found in the complex form with UHRF1.

- **UHRF1 and its epigenetic partners TIP60 and DNMT1 are found in the same epigenetic complex**

In our study we observed that UHRF1 and its partners TIP60 and DNMT1 are present in the same macromolecular complex which is in accordance with the previous findings (Achour *et al.*, 2009; Dai *et al.*, 2013). An interesting observation was that in TIP60 transfected samples, DNMT1 expression levels were decreased but still significant amount of DNMT1 was pulled-down with UHRF1 which indicates strong association of these proteins in the complex. It is well studied that UHRF1 and DNMT1 participates in preservation of DNA methylation marks during the replication phase (S phase) of cell cycle. They are recruited to replication site through help of PCNA (Bronner *et al.*, 2013; Zhang *et al.*, 2011). With the help of FLIM technique we found that TIP60 interacts with UHRF1 during S phase of cell cycle (Ashraf *et al.*, 2017a). Thus, it gives us a clue that TIP60 can also participates in S phase activities like chromatin remodeling and conservation of epigenetic code. During chromatin replication, TIP60 provides distribution of dNTPs and histones which is very essential for DNA synthesis (DeRan *et al.*, 2008; Niida *et al.*, 2010). As discussed before, TIP60 can acetylate histones H2A, H3 and H4 at different lysine positions (Yamamoto & Horikoshi, 1997; Kimura & Horikoshi, 1998; Sapountzi *et al.*, 2006; Jacquet *et al.*, 2016) and by this way is crucial to regulate the compaction state of chromatin which impacts regulatory processes at replication fork (Ruan, 2015; Allis & Jenuwein, 2016).Overall this anticipates that these epigenetic partners interact with each other to maintain the cellular and genomic integrity.

- **TIP60 overexpression mediates down-regulation of UHRF1 and DNMT1**

We observed that TIP60 overexpression in HeLa cells down-regulated expression levels of UHRF1 and DNMT1. This down-regulation was due to the acetyltransferase activity of TIP60 as TIP60ΔMYST mutant (lacking acetyltransferase activity) was unable to affect the expression levels of these proteins. UHRF1 and TIP60 are engaged in regulation of DNMT1 and indeed these three epigenetic proteins are protected from proteasomal-mediated degradation through a deubiquitinase enzyme USP7 (Du *et al.*, 2010; Dar *et al.*, 2013; Zhang *et al.*, 2015). TIP60 interacts with and acetylates DNMT1. Acetylated DNMT1 is no more able to associate with USP7 and is degraded through E3 ligase activity of UHRF1 (Du *et al.*, 2010). In our data decrease in DNMT1 levels after TIP60 overexpression is in accordance with the above study. Similarly, decrease in UHRF1 levels may follow the same pathway as of DNMT1 degradation.

- **TIP60 overexpression interferes with association of USP7-UHRF1**

Our data showed that TIP60 overexpression can interfere with USP7-UHRF1 association. In TIP60-transfected sample, almost negligible levels of USP7 were co-immunoprecipitated with UHRF1 while TIP60 mutant lacking acetyltransferase activity did not show interference with this association. Confocal microscopy data also showed TIP60-mediated decrease in expression levels of endogenous UHRF1 and USP7. Interestingly, treatment of TIP60 transfected sample with MG-132 restored the expression levels of USP7 and partially restored UHRF1 levels. Partial restoration of UHRF1 levels may be the consequence of weak association with USP7 and once UHRF1 is dissociated, USP7 is no more available to protect it from degradation.

UHRF1 has intrinsic E3 ligase activity because of its RING domain and through this activity it can auto-ubiquitinate itself (Qin *et al.*, 2015; Tauber & Fischle, 2015). Interaction of UHRF1 with UBL 1 and UBL2 domains of USP7 can protect UHRF1 from proteasomal degradation. This interaction is established between USP7 and polybasic region (PBR) of UHRF1 located between SRA and RING domain. Inside PBR, lysine 659 is crucial for this interaction (Zhang *et al.*, 2015). This PBR localizes in the preferred sequence region of TIP60 for acetylation (Kimura & Horikoshi, 1998).

Zhang *et al* have shown that a UHRF1 polypeptide from PBR can be acetylated at K659 by TIP60. This acetylated peptide had shown weak affinity to interact with USP7 (Dai *et al.*, 2013; Zhang *et al.*, 2015). This speculates that UHRF1 may be regulated in a similar manner like DNMT1, after TIP60 overexpression. Another interesting point is that TIP60 levels are increased after accomplishment of DNA methylation (Du *et al.*, 2010). Therefore, may be TIP60's increased levels can either compete with USP7 for binding with UHRF1 or it can acetylate UHRF1, which can decrease the association of UHRF1 with USP7. Lack of this interaction may induce degradation of UHRF1.

- **TIP60 overexpression can mediate ubiquitination of UHRF1**

Like many other proteins, UHRF1 is regulated through proteasomal degradation pathway. Data from western blot, confocal microscopy and cell-based ubiquitination assay suggests that TIP60 overexpression can induce ubiquitinate of UHRF1 through its acetyltransferase activity. As in case of TIP60ΔMYST mutant-transfected sample, we did not observe ubiquitination of UHRF1. MG-132 treatment of TIP60-transfected samples also stabilized

UHRF1 levels. Overall our data suggests that, after TIP60 overexpression, UHRF1 may be acetylated and then it is down-regulated through proteasomal degradation pathway.

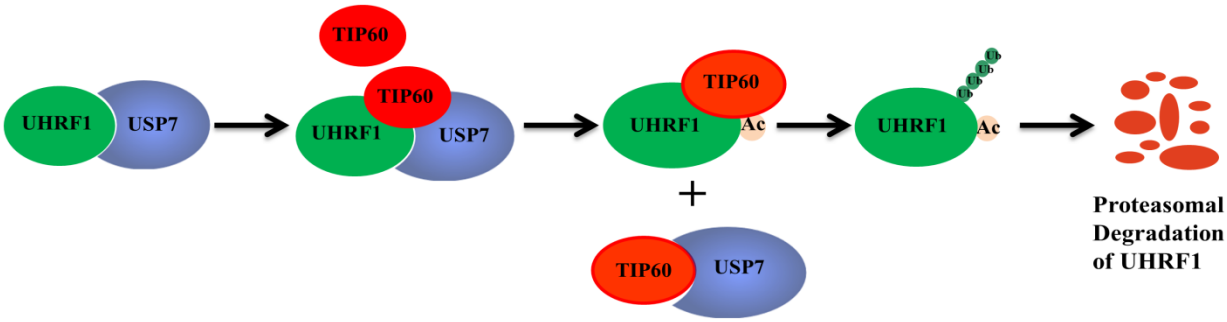

Figure 33. Projected model depicting regulation of UHRF1 inside cancer cells. When UHRF1 is associated with USP7 it is protected from ubiquitination-mediated degradation. Enhanced TIP60 levels can interfere with this association. TIP60 can compete with USP7 for binding with UHRF1 or it can make conformational change in USP7 interacting area of UHRF1 through acetylation. After dissociation from USP7, UHRF1 can be down-regulated through ubiquitination mediated by its own E3 ligase activity or any other E3 ligase present in the cells.

- **TIP60 overexpression induces p73 and p53-mediated apoptosis in cancer cells suggesting tumor suppressive potential of TIP60**

In this study, we observed an up-regulation of p73 and p53 in TIP60-transfected cancer cells. Data from flow cytometry analysis showed a significant decrease in cell viability and an increase in early and late apoptotic cells, after TIP60 overexpression. p73 and p53 induced apoptosis can lead to mitochondrial dependent apoptotic pathway through activation of BAX and down-regulation of BCL2. We observed a significant increase in expression levels of BAX protein concomitantly to a decrease in BCL2 levels after TIP60 overexpression. TIP60 also induced activation of caspase-3 from its precursor pro-caspase 3 which triggered the cleavage of PARP to induce apoptosis.

TIP60 plays an important role to maintain cellular and genomic integrity through its tumor suppressive potential. It prevents events that can lead towards malignant transformation (Sykes *et al.*, 2006; Gorrini *et al.*, 2007; Liu & Sun, 2011; Dai *et al.*, 2013). When there is a genotoxic stress event, TIP60 participates in DNA repair to conserve genomic dignity. If there is an irremediable DNA damage, TIP60 fixes this problem through activation of apoptotic pathway (Legube *et al.*, 2004; Sykes *et al.*, 2006; Tang *et al.*, 2006). In such cases TIP60 activates p53 leading to activation of cell cycle arrest or apoptotic pathway depending upon

the situation. While higher expression of UHRF1 in cancer cells interferes with TIP60-p53 interplay promoting tumorogenesis (Dai *et al.*, 2013).

p73 is also involved in regulation of UHRF1. Thymoquinone enhances p73 expression in cancer cells which subsequently induces down-regulation of UHRF1 (Alhosin *et al.*, 2010). Overall our results suggest that UHRF1 interacts with TIP60 in a MYST domain-dependent manner and undermines TIP60's ability to interact with p53 and apoptosis induction. Alternatively, TIP60 overexpression can regulate UHRF1 through activation of p53 and p73-mediated inhibition of cellular proliferation. In HeLa cells, due to presence of viral oncoproteins (HPV E6 and E7) basal expressions of TIP60 and p53 are low. With the help of EDD1 E3 ligase, HPV E6 not only favors degradation of TIP60 but also prevents p53-mediated apoptosis (Jha *et al.*, 2010; Subbaiah *et al.*, 2015). This results in down-regulation of TIP60, induction of apoptosis and immortalization of cancer cells (Rajagopalan *et al.*, 2018). A study analysis (GDS3233) submitted to GEO NCBI has revealed that TIP60 expression levels are significantly lower in cervical cancer samples as compared to normal samples (Scotto *et al*., 2008). So, overexpression of TIP60 in such cells activated p53 and p73-mediated BAX transactivation and ultimately induction of apoptosis. An interesting aspect is that through recruitment of a cellular repressor complex (Brd4), TIP60 suppresses expression of HPV E6. In response to this, virus starts degrading TIP60 to survive (Jha *et al.*, 2010). Our data indicated that overexpression of TIP60 induced p73 expression and p73 can also activate the apoptotic pathway in a similar manner (Yoon *et al.*, 2015). Our data suggested TIP60 also down-regulates expression levels of UHRF1. Previously it was reported by our group that increased p73 expression, by thymoquinone treatment, also down-regulated UHRF1 along with apoptosis (Alhosin *et al.*, 2010). Consistently with this, we have observed that TIP60 overexpression, induced apoptosis.

- **Screening of molecules inhibiting base flipping activity of UHRF1**

Domains of UHRF1 can be targeted to inhibit activity of UHRF1. It is very interesting to find small molecules that can act on these domains. And such molecules having pharmacological activities can be ideal candidates for cancer therapy. In our project we were interested to screen molecules which can act on SRA domain of UHRF1. 71 molecules were screened through biophysical and biological approaches. In first strategy, fluorescence-based tools were used to sense basic steps (recognition of hemi-methylated DNA by SRA, 5-mC flipping by SRA and recruitment of DNMT1) involved in the transmission of methylation marks (

Avvakumov *et al.*, 2008). A novel assay named "base flipping assay" assisted us to have a look on dynamics of SRA/DNA complex including base flipping in the presence of inhibitors. Three compounds (UM63, UM63B and UM63D) with an IC_{50} in a micromolar spectrum, showed inhibition of 5mC flipping. Among these three compounds only UM63 was appealing and was further characterized.

During transmission of DNA methylation impressions, flipping of 5-mC is very crucial which results due to interaction of SRA domain with hemi-methylated DNA. Our results revealed that UM63 inhibited interaction of SRA domain with DNA and flipping of methylated base (Zaayter *et al.*, 2019). Use of SRA mutant (G488D) helped us to establish the fact that UM63 binds in a specialized manner with 5-mC binding pocket inside the SRA domain. Further our data demonstrated the binding and thermodynamic mode of UM63. Displacement assay revealed that UM63 exhibits intercalating property but requires further studies.

Various anti-tumor molecules execute their effects through interference with the DNA-binding proteins. Then question arises that UM63 inhibits base flipping through blocking SRA domain or through binding with DNA? To address this question, we used an UM63's analogue UM63E which has comparable binding affinity with DNA. UM63E was not able to bind with SRA or to inhibit base flipping. Due to presence of bulky side chains, UM63E was not able to fit inside the binding pocket (Zaayter *et al.*, 2019). Therefore, our data indicates clearly that the sole binding with DNA is not enough to interfere with SRA and DNA interaction. As it is well known that UHRF1 recognizes hemi-methylated DNA through SRA domain and then it helps to recruit DNMT1 through interacting with RFTS domain of DNMT1. UM63 not only blocked SRA but also interfered with UHRF1/DNMT1 interaction as demonstrated by immunoprecipitation, confocal microscopy and FLIM data (Zaayter *et al.*, 2019). This suggests that the base flipping is required for optimal interaction of UHRF1 with DNMT1. Next we decided to check the effect of this interference on global DNA methylation levels. We observed that UM63 significantly decreased the methylation levels in HeLa cells while UM63E did not impacted methylation. Decrease in global methylation may be correlated with UM63-induced interference with SRA and DNA complex (Zaayter *et al.*, 2019).

During cell viability assay only UM12, UM48 and UM63 were able to inhibit cell proliferation. UM48 was excluded as it did not show any effect on UHRF1/DNMT1 levels and methylation status. UM12 showed a demethylating effect but without having any effect

over UHRF1/DNMT1 proteins. UM63 with an IC_{50} in micromolar range showed anti-proliferative activity in HeLa, A375 and Huh7 cell lines. This activity varied according to the cell line. Use of different cell lines can help to investigate membrane permeability, selectivity and non-specific protein binding of UM63. Time dependent studies can reveal a more detailed insight about effects of UM63 at the cellular level. As a perspective, it will be very interesting to study the mechanism of UM63-induced down-regulation of UHRF1 and DNMT1 proteins. As UHRF1 exhibits intrinsic E3 ligase activity so it can be investigated whether UHRF1, after UM63 treatment, is going to be down-regulated in a ubiquitination-dependent manner or not. And if it undergoes ubiquitination pathway, then further it can be explored that it is either auto-ubiquitination or any other E3 ligase is involved.

As described earlier, targeting UHRF1 expression through natural compounds can result in reactivation of TSGs, cell cycle arrest and induction of apoptosis(Gali-Muhtasib *et al*., 2006; Alhosin *et al*., 2010; Achour *et al*., 2013; Krifa *et al*., 2013 ; Krifa *et al*., 2014 ; Alhosin *et al*., 2015; Ibrahim *et al*., 2018). Our results showed that UM63 treatment in HeLa cells led to reactivation of p53 with a cell cycle arrest in G_0/G_1 phase and induced apoptosis in caspase-3 dependent manner. As a future perspective it will be interesting to study that p53 reactivation is due to demethylation of its promoter region? Along with p53, it will be also appealing to investigate the effect of UM63 on other TSGs which can be reactivated through down-regulation of UHRF1. In conclusion, our results suggest that UM63 can act as UHRF1 inhibitor which can bind with 5mC binding pocket with an affinity in micromolar range. It blocks base flipping and DNMT1 recruitment and induces a decrease in global genomic methylation. UM63 can be used to investigate effect of base flipping on UHRF1/DNMT1/histones. Finally, UM63 can be considered as a tool to screen new molecules targeting UHRF1 and hit-to-lead optimizations.

VI-References

Abbady, AQ., Bronner, C., Bathami, K., Muller, C.D., Jeanblanc, M., Mathieu, E., Klein, J. P., Candolfi, E., & Mousli, M., 2005. TCR pathway involves ICBP90 gene down-regulation via E2F binding sites. *Biochem Pharmacol,* 70(4), 570-579.

Abusnina, A., Alhosin, M., Keravis, T., Muller, C.D., Fuhrmann, G., Bronner, C., & Lugnier, C., 2011. Down-regulation of cyclic nucleotide phosphodiesterase PDE1A is the key event of p73 and UHRF1 deregulation in thymoquinone-induced acute lymphoblastic leukemia cell apoptosis. *Cell Signal,* 23(1), 152-160.

Abusnina, A., Keravis, T., Yougbaré, I., Bronner, C., & Lugnier, C. 2011. Anti-proliferative effect of curcumin on melanoma cells is mediated by PDE1A inhibition that regulates the epigenetic integrator UHRF1. *Mol Nutr Food Res,* 55(11), 1677-1689.

Acharya, D., Nera, B., Milstone, Z.J., Bourke, L., Yoon, Y., Rivera-Pérez, J.A., Trivedi, CM., & Fazzio, T.G., 2018. TIP55, a splice isoform of the KAT5 acetyltransferase, is essential for developmental gene regulation and organogenesis. *Sci Rep,* 8(1), 14908.

Achour, M., Fuhrmann, G., Alhosin, M., Rondé, P., Chataigneau, T., Mousli, M., Schini-Kerth, V. B., & Bronner, C., 2009. UHRF1 recruits the histone acetyltransferase Tip60 and controls its expression and activity. *Biochem Biophys Res Commun,* 390(3), 523-528.

Achour, M., Mousli, M., Alhosin, M., Ibrahim, A., Peluso, J., Muller, C. D., Schini-Kerth, V. B., Hamiche, A., Dhe-Paganon, S., & Bronner, C., 2013. Epigallocatechin-3-gallate up-regulates tumor suppressor gene expression via a reactive oxygen species-dependent down-regulation of UHRF1. *Biochem Biophys Res Commun,* 430(1), 208-212.

Akhtar, A., Zink, D., & Becker, P. B., 2000. Chromodomains are protein–RNA interaction modules. *Nature,* 407(6802), 405-409.

Alhosin, M., Abusnina, A., Achour, M., Sharif, T., Muller, C., Peluso, J., Chataigneau, T., Lugnier, C., Schini-Kerth, V. B., Bronner, C., & Fuhrmann, G., 2010. Induction of apoptosis by thymoquinone in lymphoblastic leukemia Jurkat cells is mediated by a p73-dependent pathway which targets the epigenetic integrator UHRF1. *Biochem Pharmacol,* 79(9), 1251-1260.

Alhosin, M., León-González, A. J., Dandache, I., Lelay, A., Rashid, S. K., Kevers, C., Pincemail, J., Fornecker, L.M., Mauvieux, L., Herbrecht, R., & Schini-Kerth, V. B., 2015. Bilberry extract (Antho 50) selectively induces redox-sensitive caspase 3-related apoptosis in chronic lymphocytic leukemia cells by targeting the Bcl-2/Bad pathway. *Sci Rep,* 5, 8996.

Alhosin, M., Omran, Z., Zamzami, M. A., Al-Malki, A. L., Choudhry, H., Mousli, M., & Bronner, C., 2016. Signalling pathways in UHRF1-dependent regulation of tumor suppressor genes in cancer. *J Exp Clin Cancer Res,* 35(1), 174-184.

Alhosin, M., Sharif, T., Mousli, M., Etienne-Selloum, N., Fuhrmann, G., Schini-Kerth, V. B., & Bronner, C., 2011. Down-regulation of UHRF1, associated with re-expression of tumor suppressor genes, is a common feature of natural compounds exhibiting anti-cancer properties. *J Exp Clin Cancer Res,* 30(1), 41-41.

Allis, C. D., & Jenuwein, T., 2016. The molecular hallmarks of epigenetic control. *Nat Rev Genet,* 17, 487-500.

Arima, Y., Hirota, T., Bronner, C., Mousli, M., Fujiwara, T., Niwa, S.-i., Ishikawa, H., & Saya, H., 2004. Down-regulation of nuclear protein ICBP90 by p53/p21Cip1/WAF1-dependent DNA-damage checkpoint signals contributes to cell cycle arrest at G1/S transition. *Genes Cells,* 9(2), 131-142.

Arita, K., Ariyoshi, M., Tochio, H., Nakamura, Y., & Shirakawa, M., 2008. Recognition of hemi-methylated DNA by the SRA protein UHRF1 by a base-flipping mechanism. *Nature,* 455, 818-821.

Arita, K., Isogai, S., Oda, T., Unoki, M., Sugita, K., Sekiyama, N., Kuwata, K., Hamamoto, R., Tochio, H., Sato, M., Ariyoshi, M., & Shirakawa, M., 2012. Recognition of modification

status on a histone H3 tail by linked histone reader modules of the epigenetic regulator UHRF1. *Proc Natl Acad Sci U S A,* 109(32), 12950-12955.

Ashraf, W., Bronner, C., Zaayter, L., Ahmad, T., Richert, L., Alhosin, M., Ibrahim, A., Hamiche, A., Mely, Y., & Mousli, M., 2017a. Interaction of the epigenetic integrator UHRF1 with the MYST domain of TIP60 inside the cell. *J Exp Clin Cancer Res,* 36(1), 188-201.

Ashraf, W., Ibrahim, A., Alhosin, M., Zaayter, L., Ouararhni, K., Papin, C., Ahmad, T., Hamiche, A., Mély, Y., Bronner, C., & Mousli, M., 2017b. The epigenetic integrator UHRF1: on the road to become a universal biomarker for cancer. *Oncotarget,* 8(31), 51946-51962.

Audia, J. E., & Campbell, R. M., 2016. Histone Modifications and Cancer. *Cold Spring Harb Perspect Biol,* 8(4), 019521-019521.

Avvakumov, G. V., Walker, J. R., Xue, S., Li, Y., Duan, S., Bronner, C., Arrowsmith, C. H., & Dhe-Paganon, S., 2008. Structural basis for recognition of hemi-methylated DNA by the SRA domain of human UHRF1. *Nature,* 455, 822-825.

Avvakumov, N., & Côté, J., 2007. The MYST family of histone acetyltransferases and their intimate links to cancer. *Oncogene,* 26, 5395-5407.

Babbio, F., Pistore, C., Curti, L., Castiglioni, I., Kunderfranco, P., Brino, L., Oudet, P., Seiler, R., Thalman, G. N., Roggero, E., Sarti, M., Pinton, S., Mello-Grand, M., Chiorino, G., Catapano, C. V., Carbone, G. M., & Bonapace, I. M., 2012. The SRA protein UHRF1 promotes epigenetic crosstalks and is involved in prostate cancer progression. *Oncogene,* 31(46), 4878-4887.

Bagacean, C., Tempescul, A., Le Dantec, C., Bordron, A., Mohr, A., Saad, H., Olivier, V., Zdrenghea, M., Cristea, V., Cartron, P.-F., Douet-Guilbert, N., Berthou, C., & Renaudineau, Y., 2017. Alterations in DNA methylation/demethylation intermediates predict clinical outcome in chronic lymphocytic leukemia. *Oncotarget,* 8(39), 65699-65716.

Barthes, N. P., Michel, B. Y., Shaya, J., Martinet, N., & Burger, A., 2016. Génétique et épigénétique. *l'actualité chimique,*412, 20.

Bashtrykov, P., Jankevicius, G., Jurkowska, R. Z., Ragozin, S., & Jeltsch, A., 2014. The UHRF1 protein stimulates the activity and specificity of the maintenance DNA methyltransferase DNMT1 by an allosteric mechanism. *J Biol Chem,* 289(7), 4106-4115.

Bashtrykov, P., Jankevicius, G., Smarandache, A., Jurkowska, Renata Z., Ragozin, S., & Jeltsch, A., 2012. Specificity of Dnmt1 for methylation of hemimethylated CpG sites resides in its catalytic domain. *Chem Biol,* 19(5), 572-578.

Bassi, C., Li, Y. T., Khu, K., Mateo, F., Baniasadi, P. S., Elia, A., Mason, J., Stambolic, V., Pujana, M. A., Mak, T. W., & Gorrini, C., 2016. The acetyltransferase Tip60 contributes to mammary tumorigenesis by modulating DNA repair. *Cell Death Differ,* 23(7), 1198-1208.

Bennett, R. L., & Licht, J. D., 2018. Targeting Epigenetics in Cancer. *Annu Rev of Pharmacol Toxicol,* 58(1), 187-207.

Berkyurek, A. C., Suetake, I., Arita, K., Takeshita, K., Nakagawa, A., Shirakawa, M., & Tajima, S., 2014. The DNA methyltransferase Dnmt1 directly interacts with the SET and RING finger-associated (SRA) domain of the multifunctional protein Uhrf1 to facilitate accession of the catalytic center to hemi-methylated DNA. *J Biol Chem,* 289(1), 379-386.

Berndsen, C. E., Albaugh, B. N., Tan, S., & Denu, J. M., 2007. Catalytic mechanism of a MYST family histone acetyltransferase. *Biochemistry,* 46(3), 623-629.

Berns, K., Hijmans, E. M., Mullenders, J., Brummelkamp, T. R., Velds, A., Heimerikx, M., Kerkhoven, R. M., Madiredjo, M., Nijkamp, W., Weigelt, B., Agami, R., Ge, W., Cavet, G., Linsley, P. S., Beijersbergen, R. L., & Bernards, R., 2004. A large-scale RNAi screen in human cells identifies new components of the p53 pathway. *Nature,* 428(6981), 431-437.

Bhoumik, A., Singha, N., O'Connell, M. J., & Ronai, Z. e. A., 2008. Regulation of TIP60 by ATF2 modulates ATM activation. *J Biol Chem,* 283(25), 17605-17614.

Bigey, P., Ramchandani, S., Theberge, J., Araujo, F. D., & Szyf, M., 2000. Transcriptional regulation of the human DNA Methyltransferase (dnmt1) gene. *Gene,* 242(1), 407-418.

Bird, A. (2002). DNA methylation patterns and epigenetic memory. *Genes Dev,* 16(1), 6-21.

Bird, A. (2007). Perceptions of epigenetics. *Nature,* 447, 396-398.

Biswas, S., & Rao, C. M., 2017. Epigenetics in cancer: Fundamentals and Beyond. *Pharmacol Ther,* 173, 118-134.

Bochtler, M., Kolano, A., & Xu, G.L., 2017. DNA demethylation pathways: Additional players and regulators. *BioEssays,* 39(1),1600178.

Bogdanović, O., & Lister, R., 2017. DNA methylation and the preservation of cell identity. *Curr Opin Genet Deve,* 46, 9-14.

Bostick, M., Kim, J. K., Estève, P.O., Clark, A., Pradhan, S., & Jacobsen, S. E., 2007. UHRF1 Plays a role in maintaining DNA methylation in mammalian cells. *Science,* 317(5845), 1760-1764.

Botezatu, A., Iancu, I. V., Plesa, A., Manda, D., Popa, O., Bostan, M., Mihaila, M., Albulescu, A., Fudulu, A., & Vladoiu, S. V., 2019. Methylation of tumour suppressor genes associated with thyroid cancer. *Cancer Biomark,* 25 (1), 53-65.

Brady, M. E., Ozanne, D. M., Gaughan, L., Waite, I., Cook, S., Neal, D. E., & Robson, C. N., 1999. Tip60 is a nuclear hormone receptor coactivator. *J Biol Chem,* 274(25), 17599-17604.

Brauns-Schubert, P., Schubert, F., Wissler, M., Weiss, M., Schlicher, L., Bessler, S., Safavi, M., Miething, C., Borner, C., Brummer, T., & Maurer, U., 2018. CDK9-mediated phosphorylation controls the interaction of TIP60 with the transcriptional machinery. *EMBO Rep,* 19(2), 244-256.

Brenner, C., Luciani, J., Bizet, M., Ndlovu, M., Josseaux, E., Dedeurwaerder, S., Calonne, E., Putmans, P., Cartron, P.-F., Defrance, M., Fuks, F., & Deplus, R., 2016. The interplay between the lysine demethylase KDM1A and DNA methyltransferases in cancer cells is cell cycle dependent. *Oncotarget,* 7(37), 58939-58952.

Bronner, C., Achour, M., Arima, Y., Chataigneau, T., Saya, H., & Schini-Kerth, V. B., 2007a. The UHRF family: Oncogenes that are drugable targets for cancer therapy in the near future? *Pharmacol Ther,* 115(3), 419-434.

Bronner, C., Alhosin, M., Hamiche, A., & Mousli, M., 2019. Coordinated dialogue between UHRF1 and DNMT1 to ensure faithful inheritance of methylated DNA patterns. *Genes,* 10(1), 65-78.

Bronner, C., Chataigneau, T., Schini-Kerth, V.B., Landry, L., 2007b. The "Epigenetic Code Replication Machinery", ECREM: a promising drugable target of the epigenetic cell memory. *Curr Med Chem,* 14(25), 2629-2641.

Bronner, C., Fuhrmann, G., Chédin, F. L., Macaluso, M., & Dhe-Paganon, S., 2010. UHRF1 links the histone code and DNA methylation to ensure faithful epigenetic memory inheritance. *Genet Epigenet,* 2009(2), 29-36.

Bronner, C., Krifa, M., & Mousli, M., 2013. Increasing role of UHRF1 in the reading and inheritance of the epigenetic code as well as in tumorogenesis. *Biochem Pharmacol,* 86(12), 1643-1649.

Bronner, C., Trotzier, M.-A., Filhol, O., Cochet, C., Rochette-Egly, C., SchÖLler-Guinard, M., Klein, J.-P., & Mousli, M., 2004. The antiapoptotic protein ICBP90 is a target for protein kinase 2. *Ann N Y Acad Sci,* 1030(1), 355-360.

Butler, J. S., Lee, J.-H., & Skalnik, D. G., 2008. CFP1 interacts with DNMT1 independently of association with the Setd1 Histone H3K4 methyltransferase complexes. *DNA Cell Biol,* 27(10), 533-543.

Cartron, P.-F., Nadaradjane, A., Lepape, F., Lalier, L., Gardie, B., & Vallette, F. M., 2013. Identification of TET1 partners that control its DNA-demethylating function. *Genes Cancer,* 4(5-6), 235-241.

Charvet, C., Wissler, M., Brauns-Schubert, P., Wang, S.-J., Tang, Y., Sigloch, F. C., Mellert, H., Brandenburg, M., Lindner, S. E., Breit, B., Green, D. R., McMahon, S. B., Borner, C., Gu, W., & Maurer, U., 2011. Phosphorylation of Tip60 by GSK-3 determines the induction of PUMA and apoptosis by p53. *Mol Cell,* 42(5), 584-596.

Chen, G., Cheng, Y., Tang, Y., Martinka, M., & Li, G., 2012. Role of Tip60 in human melanoma cell migration, metastasis, and patient survival. *J Investig Dermatol,* 132(11), 2632-2641.

Chen, H., Ma, H., Inuzuka, H., Diao, J., Lan, F., Shi, Y. G., Wei, W., & Shi, Y., 2013. DNA damage regulates UHRF1 stability via the SCF(β-TrCP) E3 ligase. *Mol Cell Biol,* 33(6), 1139-1148.

Cheng, Z., Ke, Y., Ding, X., Wang, F., Wang, H., Ahmed, K., Liu, Z., Xu, Y., Aikhionbare, F., Yan, H., Liu, J., Xue, Y., Powell, M., Liang, S., Reddy, S. E., Hu, R., Huang, H., Jin, C., & Yao, X., 2007. Functional characterization of TIP60 sumoylation in UV-irradiated DNA damage response. *Oncogene,* 27, 931-941.

Cheray, M., Nadaradjane, A., Bonnet, P., Routier, S., Vallette, F. M., & Cartron, P.-F., 2014. Specific inhibition of DNMT1/CFP1 reduces cancer phenotypes and enhances chemotherapy effectiveness. *Epigenomics*, 6(3), 267-275.

Cheray, M., Pacaud, R., Nadaradjane, A., Vallette, F. M., & Cartron, P.-F., 2013. Specific inhibition of one DNMT1-including complex influences tumor initiation and progression. *Clin Epigenet*, 5(1), 9.

Chin, H. G., Ponnaluri, V. K. C., Zhang, G., Estève, P.-O., Schaus, S. E., Hansen, U., & Pradhan, S., 2016. Transcription factor LSF-DNMT1 complex dissociation by FQI1 leads to aberrant DNA methylation and gene expression. *Oncotarget*, 7(50), 83627-83640.

Choudhry, H., Zamzami, M. A., Omran, Z., Wu, W., Mousli, M., Bronner, C., & Alhosin, M., 2018. Targeting microRNA/UHRF1 pathways as a novel strategy for cancer therapy. *Oncol Lett*, 15(1), 3-10.

Chu, J., Loughlin, E. A., Gaur, N. A., SenBanerjee, S., Jacob, V., Monson, C., Kent, B., Oranu, A., Ding, Y., Ukomadu, C., & Sadler, K. C., 2012. UHRF1 phosphorylation by cyclin A2/cyclin-dependent kinase 2 is required for zebrafish embryogenesis. *Mol Biol Cell*, 23(1), 59-70.

Clamme, J. P., Azoulay, J., & Mély, Y., 2003. Monitoring of the formation and dissociation of polyethylenimine/DNA complexes by two photon fluorescence correlation spectroscopy. *Biophys J*, 84(3), 1960-1968.

Col, E., Caron, C., Chable-Bessia, C., Legube, G., Gazzeri, S., Komatsu, Y., Yoshida, M., Benkirane, M., Trouche, D., & Khochbin, S., 2005. HIV-1 Tat targets Tip60 to impair the apoptotic cell response to genotoxic stresses. *EMBO J*, 24(14), 2634-2645.

Cole, H. A., Cui, F., Ocampo, J., Burke, T. L., Nikitina, T., Nagarajavel, V., Kotomura, N., Zhurkin, V. B., & Clark, D. J., 2016. Novel nucleosomal particles containing core histones and linker DNA but no histone H1. *Nucleic Acids Res*, 44(2), 573-581.

Creaven, M., Hans, F., Mutskov, V., Col, E., Caron, C., Dimitrov, S., & Khochbin, S., 1999. Control of the histone-acetyltransferase activity of Tip60 by the HIV-1 transactivator protein, Tat. *Biochemistry*, 38(27), 8826-8830.

Cui, H., Guo, M., Xu, D., Ding, Z.-C., Zhou, G., Ding, H.-F., Zhang, J., Tang, Y., & Yan, C., 2015. The stress-responsive gene ATF3 regulates the histone acetyltransferase Tip60. *Nature Commun*, 6, 6752.

Cui, H., Li, X., Han, C., Wang, Q.-E., Wang, H., Ding, H.-F., Zhang, J., & Yan, C., 2016. The stress-responsive gene ATF3 mediates dichotomous UV responses by regulating the Tip60 and p53 proteins. *J Biol Chem*, 291(20), 10847-10857.

Dai, C., Shi, D., & Gu, W., 2013. Negative regulation of the acetyltransferase TIP60-p53 interplay by UHRF1 (ubiquitin-like with PHD and RING finger domains 1). *J Biol Chem*, 288(27), 19581-19592.

Dar, A., Shibata, E., & Dutta, A., 2013. Deubiquitination of Tip60 by USP7 determines the activity of the p53-dependent apoptotic pathway. *Mol Cellular Biol*, 33(16), 3309-3320.

Darakhshan, S., Bidmeshki Pour, A., Hosseinzadeh Colagar, A., & Sisakhtnezhad, S., 2015. Thymoquinone and its therapeutic potentials. *Pharmacol Res*, 95-96, 138-158.

DaRosa, P. A., Harrison, J. S., Zelter, A., Davis, T. N., Brzovic, P., Kuhlman, B., & Klevit, R. E., 2018. A Bifunctional role for the UHRF1 UBL domain in the control of hemi-methylated DNA-dependent histone ubiquitylation. *Mol Cell*, 72(4), 753-765.

Daskalos, A., Oleksiewicz, U., Filia, A., Nikolaidis, G., Xinarianos, G., Gosney, J. R., Malliri, A., Field, J. K., & Liloglou, T., 2011. UHRF1-mediated tumor suppressor gene inactivation in nonsmall cell lung cancer. *Cancer*, 117(5), 1027-1037.

Dawson, Mark A., & Kouzarides, T., 2012. Cancer epigenetics: from mechanism to therapy. *Cell*, 150(1), 12-27.

Deissler, H., Kafka, A., Schuster, E., Sauer, G., Kreienberg, R., & Zeillinger, R., 2004. Spectrum of p53 mutations in biopsies from breast cancer patients selected for preoperative chemotherapy analysed by the functional yeast assay to predict therapeutic response. *Oncol Rep*, 11(6), 1281-1286.

DeRan, M., Pulvino, M., Greene, E., Su, C., & Zhao, J., 2008. Transcriptional activation of histone genes requires NPAT-dependent recruitment of TRRAP-Tip60 complex to histone promoters during the G1/S phase transition. *Mol Cell Biol*, 28(1), 435-447.

De Vos, M., El Ramy, R., Quénet, D., Wolf, P., Spada, F., Magroun, N., Babbio, F., Schreiber, V., Leonhardt, H., Bonapace, I. M., & Dantzer, F., 2014. Poly(ADP-ribose) polymerase 1 (PARP1) associates with E3 ubiquitin-protein ligase UHRF1 and modulates UHRF1 biological functions. *J Biol Chem,* 289(23), 16223-16238.

Ding, G., Chen, P., Zhang, H., Huang, X., Zang, Y., Li, J., Li, J., & Wong, J., 2016. Regulation of ubiquitin-like with plant homeodomain and RING finger domain 1 (UHRF1) protein stability by heat shock protein 90 chaperone machinery. *J Biol Chem,* 291(38), 20125-20135.

Doyon, Y., & Côté, J., 2004. The highly conserved and multifunctional NuA4 HAT complex. *Curr Opin Genet Deve,* 14(2), 147-154.

Du, S., Xu, G., Zou, W., Xiang, T., & Luo, Z., 2017. Effect of dihydroartemisinin on UHRF1 gene expression in human prostate cancer PC-3 cells. *Anti-cancer drugs,* 28(4), 384-391.

Du, Z., Song, J., Wang, Y., Zhao, Y., Guda, K., Yang, S., Kao, H.-Y., Xu, Y., Willis, J., Markowitz, S. D., Sedwick, D., Ewing, R. M., & Wang, Z., 2010. DNMT1 stability is regulated by proteins coordinating deubiquitination and acetylation-driven ubiquitination. *Sci Signal,* 3(146), 1-21.

Dubrez, L., 2017. Regulation of E2F1 Transcription Factor by Ubiquitin Conjugation. *Intl J Mol Sci*, 18(10), 2188-2196.

Dubrez, L., Causse, S., Borges Bonan, N., Dumétier, B., & Garrido, C., 2019. Heat-shock proteins: chaperoning DNA repair. *Oncogene*. doi: 10.1038/s41388-019-1016-y.

Edmond, V., Moysan, E., Khochbin, S., Matthias, P., Brambilla, C., Brambilla, E., Gazzeri, S., & Eymin, B., 2011. Acetylation and phosphorylation of SRSF2 control cell fate decision in response to cisplatin. *EMBO J,* 30(3), 510-523.

Edwards, J. R., Yarychkivska, O., Boulard, M., & Bestor, T. H., 2017. DNA methylation and DNA methyltransferases. *Epigenet Chromatin,* 10, 23.

Ehrlich, M., 2009. DNA hypomethylation in cancer cells. *Epigenomics,* 1(2), 239-259.

Ehrlich, M., 2019. DNA hypermethylation in disease: mechanisms and clinical relevance. *Epigenetics*, 1-23.

El Meshri, S. E., Dujardin, D., Godet, J., Richert, L., Boudier, C., Darlix, J. L., Didier, P., Mély, Y., & de Rocquigny, H., 2015. Role of the nucleocapsid domain in HIV-1 Gag oligomerization and trafficking to the plasma membrane: a Fluorescence Lifetime Imaging Microscopy investigation. *J Mol Biol,* 427(6), 1480-1494.

Esteller, M., 2008. Epigenetics in cancer. *N Engl J Med,* 358(11), 1148-1159.

Eymin, B., Claverie, P., Salon, C., Leduc, C., Col, E., Brambilla, E., Khochbin, S., & Gazzeri, S., 2006. p14ARF activates a Tip60-dependent and p53-independent ATM/ATR/CHK pathway in response to genotoxic stress. *Mol Cell Biol,* 26(11), 4339-4350.

Fang, J., Cheng, J., Wang, J., Zhang, Q., Liu, M., Gong, R., Wang, P., Zhang, X., Feng, Y., Lan, W., Gong, Z., Tang, C., Wong, J., Yang, H., Cao, C., & Xu, Y., (2016). Hemi-methylated DNA opens a closed conformation of UHRF1 to facilitate its histone recognition. *Nature Commun,* 7, 11197-11197.

Fang, X., Lu, G., Ha, K., Lin, H., Du, Y., Zuo, Q., Fu, Y., Zou, C., & Zhang, P., 2018. Acetylation of TIP60 at K104 is essential for metabolic stress-induced apoptosis in cells of hepatocellular cancer. *Exp Cell Res,* 362(2), 279-286.

Fang, Z., Xing, F., Bronner, C., Teng, Z., & Guo, Z., 2009. ICBP90 mediates the ERK1/2 signaling to regulate the proliferation of Jurkat T cells. *Cell Immunol,* 257(1), 80-87.

Fatemi, M., Hermann, A., Pradhan, S., & Jeltsch, A., 2001. The activity of the murine DNA methyltransferase Dnmt1 is controlled by interaction of the catalytic domain with the N-terminal part of the enzyme leading to an allosteric activation of the enzyme after binding to methylated DNA. *J Mol Biol,* 309(5), 1189-1199.

Felle, M., Joppien, S., Németh, A., Diermeier, S., Thalhammer, V., Dobner, T., Kremmer, E., Kappler, R., & Längst, G., 2011. The USP7/Dnmt1 complex stimulates the DNA methylation activity of Dnmt1 and regulates the stability of UHRF1. *Nucleic Acids Res,* 39(19), 8355-8365.

Ferry, L., Fournier, A., Tsusaka, T., Adelmant, G., Shimazu, T., Matano, S., Kirsh, O., Amouroux, R., Dohmae, N., Suzuki, T., Filion, G. J., Deng, W., de Dieuleveult, M., Fritsch, L., Kudithipudi, S., Jeltsch, A., Leonhardt, H., Hajkova, P., Marto, J. A., Arita, K., Shinkai, Y., & Defossez,

P.-A., 2017. Methylation of DNA ligase 1 by G9a/GLP recruits UHRF1 to replicating DNA and regulates DNA methylation. *Mol Cell*, 67(4), 550-565.

Foster, B. M., Stolz, P., Mulholland, C. B., Montoya, A., Kramer, H., Bultmann, S., & Bartke, T., 2018. Critical role of the UBL domain in stimulating the E3 ubiquitin ligase activity of UHRF1 toward chromatin. *Mol Cell*, 72(4), 739-752.

Frank, S. R., Parisi, T., Taubert, S., Fernandez, P., Fuchs, M., Chan, H.-M., Livingston, D. M., & Amati, B., 2003. MYC recruits the TIP60 histone acetyltransferase complex to chromatin. *EMBO Rep*, 4(6), 575-580.

Gali-Muhtasib, H., Roessner, A., & Schneider-Stock, R., 2006. Thymoquinone: A promising anti-cancer drug from natural sources. *Int J Biochem Cell Biol*, 38(8), 1249-1253.

Gali-Muhtasib, H. U., Kheir, W. G. A., Kheir, L. A., Darwiche, N., & Crooks, P. A., 2004. Molecular pathway for thymoquinone-induced cell-cycle arrest and apoptosis in neoplastic keratinocytes. *Anti-cancer drugs*, 15(4), 389-399.

Gao, L., Tan, X.-F., Zhang, S., Wu, T., Zhang, Z.-M., Ai, H.-W., & Song, J., 2018. An intramolecular interaction of UHRF1 reveals dual control for Its histone association. *Structure*, 26(2), 304-311.

Gao, Y., Koppen, A., Rakhshandehroo, M., Tasdelen, I., van de Graaf, S. F., van Loosdregt, J., van Beekum, O., Hamers, N., van Leenen, D., Berkers, C. R., Berger, R., Holstege, F. C. P., Coffer, P. J., Brenkman, A. B., Ovaa, H., & Kalkhoven, E., 2013. Early adipogenesis is regulated through USP7-mediated deubiquitination of the histone acetyltransferase TIP60. *Nature Commun*, 4, 2656.

García-Martínez, A., Sottile, J., Sánchez-Tejada, L., Fajardo, C., Cámara, R., Lamas, C., Barberá, V. M., & Picó, A., 2018. DNA methylation of tumor suppressor genes in pituitary neuroendocrine tumors. *J Clin Endocrinol Metab*, 104(4), 1272-1282.

Gaughan, L., Brady, M. E., Cook, S., Neal, D. E., & Robson, C. N., 2001. Tip60 is a co-activator specific for class I nuclear hormone receptors. *J Biol Chem*, 276(50), 46841-46848.

Gaughan, L., Logan, I. R., Cook, S., Neal, D. E., & Robson, C. N. 2002. Tip60 and histone deacetylase 1 regulate androgen receptor activity through changes to the acetylation status of the receptor. *J Biol Chem*, 277(29), 25904-25913.

Gelato, Kathy A., Tauber, M., Ong, Michelle S., Winter, S., Hiragami-Hamada, K., Sindlinger, J., Lemak, A., Bultsma, Y., Houliston, S., Schwarzer, D., Divecha, N., Arrowsmith, Cheryl H., & Fischle, W., 2014. Accessibility of different histone H3-binding domains of UHRF1 is allosterically regulated by phosphatidylinositol 5-phosphate. *Mol Cell*, 54(6), 905-919.

Gévry, N., Chan, H. M., Laflamme, L., Livingston, D. M., & Gaudreau, L., 2007. p21 transcription is regulated by differential localization of histone H2A.Z. *Genes Deve*, 21(15), 1869-1881.

Giovinazzo, H., Walker, D., Wyhs, N., Liu, J., Esopi, D. M., Vaghasia, A. M., Jain, Y., Bhamidipati, A., Zhou, J., Nelson, W. G., & Yegnasubramanian, S., 2019. A high-throughput screen of pharmacologically active compounds for inhibitors of UHRF1 reveals epigenetic activity of anthracycline derivative chemotherapeutic drugs. *Oncotarget*, 10(32), 3040-3050.

Goldstein, G., Scheid, M., Hammerling, U., Schlesinger, D. H., Niall, H. D., & Boyse, E. A., 1975. Isolation of a polypeptide that has lymphocyte-differentiating properties and is probably represented universally in living cells. *Proc Nat Acad Sci U S A*, 72(1), 11-15.

Goll, M. G., Kirpekar, F., Maggert, K. A., Yoder, J. A., Hsieh, C.-L., Zhang, X., Golic, K. G., Jacobsen, S. E., & Bestor, T. H., 2006. Methylation of tRNAAsp by the DNA methyltransferase homolog Dnmt2. *Science*, 311(5759), 395-408.

Gorrini, C., Squatrito, M., Luise, C., Syed, N., Perna, D., Wark, L., Martinato, F., Sardella, D., Verrecchia, A., Bennett, S., Confalonieri, S., Cesaroni, M., Marchesi, F., Gasco, M., Scanziani, E., Capra, M., Mai, S., Nuciforo, P., Crook, T., Lough, J., & Amati, B., 2007. Tip60 is a haplo-insufficient tumour suppressor required for an oncogene-induced DNA damage response. *Nature*, 448, 1063-1070.

Grant, T. J., Bishop, J. A., Christadore, L. M., Barot, G., Chin, H. G., Woodson, S., Kavouris, J., Siddiq, A., Gredler, R., Shen, X.-N., Sherman, J., Meehan, T., Fitzgerald, K., Pradhan, S., Briggs, L. A., Andrews, W. H., Sarkar, D., Schaus, S. E., & Hansen, U., 2012. Antiproliferative small-molecule inhibitors of transcription factor LSF reveal oncogene addiction to LSF in hepatocellular carcinoma. *Proc Nat Acad Sci U S A*, 109(12), 4503-4508.

Greiner, V. J., Kovalenko, L., Humbert, N., Richert, L., Birck, C., Ruff, M., Zaporozhets, O. A., Dhe-Paganon, S., Bronner, C., & Mély, Y., 2015. Site-Selective monitoring of the interaction of the SRA domain of UHRF1 with target DNA sequences labeled with 2-Aminopurine. *Biochemistry,* 54(39), 6012-6020.

Guan, D., Factor, D., Liu, Y., Wang, Z., & Kao, H. Y., 2013. The epigenetic regulator UHRF1 promotes ubiquitination-mediated degradation of the tumor-suppressor protein promyelocytic leukemia protein. *Oncogene,* 32(33), 3819-3828.

Hashimoto, H., Horton, J. R., Zhang, X., Bostick, M., Jacobsen, S. E., & Cheng, X., 2008. The SRA domain of UHRF1 flips 5-methylcytosine out of the DNA helix. *Nature*, 455(7214), 826-829.

Hermann, A., Goyal, R., & Jeltsch, A., 2004. The Dnmt1 DNA-(cytosine-C5)-methyltransferase methylates DNA processively with high preference for hemimethylated target sites. *Journal of Biological Chemistry, 279*(46), 48350-48359.

Hermann, A., Schmitt, S., & Jeltsch, A. (2003). The human Dnmt2 has residual DNA-(cytosine-C5) methyltransferase activity. *J Biol Chem,* 278(34), 31717-31721.

Hervouet, E., Cheray, M., Vallette, F. M., & Cartron, P.-F., 2013. DNA methylation and apoptosis resistance in cancer cells. *Cells,* 2(3), 545-573.

Hervouet, E., Lalier, L., Debien, E., Cheray, M., Geairon, A., Rogniaux, H., Loussouarn, D., Martin, S. A., Vallette, F. M., & Cartron, P.-F., 2010. Disruption of Dnmt1/PCNA/UHRF1 interactions promotes tumorigenesis from human and mice glial cells. *PloS one,* 5(6), e11333-e11333.

Hervouet, E., Peixoto, P., Delage-Mourroux, R., Boyer-Guittaut, M., & Cartron, P.-F., 2018. Specific or not specific recruitment of DNMTs for DNA methylation, an epigenetic dilemma. *Clin Epigenet,* 10, 17-17.

Hervouet, E., Vallette, F. M., & Cartron, P.-F., 2009. Dnmt3/transcription factor interactions as crucial players in targeted DNA methylation. *Epigenetics,* 4(7), 487-499.

Hopfner, R., Mousli, M., Garnier, J.-M., Redon, R., du Manoir, S., Chatton, B., Ghyselinck, N., Oudet, P., & Bronner, C., 2001. Genomic structure and chromosomal mapping of the gene coding for ICBP90, a protein involved in the regulation of the topoisomerase IIα gene expression. *Gene,* 266(1), 15-23.

Hopfner, R., Mousli, M., Jeltsch, J.-M., Voulgaris, A., Lutz, Y., Marin, C., Bellocq, J.-P., Oudet, P., & Bronner, C., 2000. ICBP90, a novel human CCAAT binding protein, involved in the regulation of Topoisomerase IIα expression. *Cancer Res,* 60(1), 121-128.

Houliston, R. S., Lemak, A., Iqbal, A., Ivanochko, D., Duan, S., Kaustov, L., Ong, M. S., Fan, L., Senisterra, G., Brown, P. J., Wang, Y.-X., & Arrowsmith, C. H., 2017. Conformational dynamics of the TTD-PHD histone reader module of the UHRF1 epigenetic regulator reveals multiple histone-binding states, allosteric regulation, and druggability. *J Biol Chem,* 292(51), 20947-20959.

Hu, L., Li, Z., Wang, P., Lin, Y., & Xu, Y., 2011. Crystal structure of PHD domain of UHRF1 and insights into recognition of unmodified histone H3 arginine residue 2. *Cell Res,* 21, 1374-1380.

Ibrahim, A., Alhosin, M., Papin, C., Ouararhni, K., Omran, Z., Zamzami, M. A., Al-Malki, A. L., Choudhry, H., Mély, Y., Hamiche, A., Mousli, M., & Bronner, C., 2018. Thymoquinone challenges UHRF1 to commit auto-ubiquitination: a key event for apoptosis induction in cancer cells. *Oncotarget,* 9(47), 28599-28611.

Idrissou, M., Rifaï, K., Daures, M., Penault-Llorca, F., Bignon, Y.-J., & Bernard-Gallon, D., 2018. Exciting history of Tip60 and its companions in carcinogenesis across the heterochromatin landscapes. *J Integ Biol,* 22(9), 626-628.

Ikura, T., Ogryzko, V. V., Grigoriev, M., Groisman, R., Wang, J., Horikoshi, M., Scully, R., Qin, J., & Nakatani, Y., 2000. Involvement of the TIP60 histone acetylase complex in DNA repair and apoptosis. *Cell*, 102(4), 463-473.

Inbar-Feigenberg, M., Choufani, S., Butcher, D. T., Roifman, M., & Weksberg, R., 2013. Basic concepts of epigenetics. *Fertil Steril,* 99(3), 607-615.

Jacquet, K., Fradet-Turcotte, A., Avvakumov, N., Lambert, J.-P., Roques, C., Pandita, R. K., Paquet, E., Herst, P., Gingras, A.-C., Pandita, T. K., Legube, G., Doyon, Y., Durocher, D., & Côté, J.,

2016. The TIP60 complex regulates bivalent chromatin recognition by 53BP1 through direct H4K20me binding and H2AK15 acetylation. *Mol Cell*, 62(3), 409-421.
Jaiswal, B., & Gupta, A., 2018. Modulation of nuclear receptor function by chromatin modifying factor TIP60. *Endocrinology*, 159(5), 2199-2215.
Jakovcevski, M., & Akbarian, S., 2012. Epigenetic mechanisms in neurological disease. *Nat Med*, 18(8), 1194-1204.
Jang, S. Y., Hong, D., Jeong, S. Y., & Kim, J.-H., 2015. Shikonin causes apoptosis by up-regulating p73 and down-regulating ICBP90 in human cancer cells. *Biochem Biophys Res Commun*, 465(1), 71-76.
Jeltsch, A., 2002. Beyond Watson and Crick: DNA methylation and molecular enzymology of DNA methyltransferases. *Chembiochem*, 3(4), 274-293.
Jeltsch, A., 2006. On the enzymatic properties of Dnmt1: specificity, processivity, mechanism of linear diffusion and allosteric regulation of the enzyme. *Epigenetics*, 1(2), 63-66.
Jeltsch, A., 2019. Novel insights into peptide binding and conformational dynamics of UHRF1. *Structure*, 27(3), 408-410.
Jeltsch, A., & Jurkowska, R. Z., 2014. New concepts in DNA methylation. *Trends Biochem Sci*, 39(7), 310-318.
Jeltsch, A., & Jurkowska, R. Z., 2016. Allosteric control of mammalian DNA methyltransferases – a new regulatory paradigm. *Nucleic Acids Res*, 44(18), 8556-8575.
Jenkins, Y., Markovtsov, V., Lang, W., Sharma, P., Pearsall, D., Warner, J., Franci, C., Huang, B., Huang, J., Yam, G. C., Vistan, J. P., Pali, E., Vialard, J., Janicot, M., Lorens, J. B., Payan, D. G., & Hitoshi, Y., 2005. Critical role of the ubiquitin ligase activity of UHRF1, a nuclear RING finger protein, in tumor cell growth. *Mol Biol Cell*, 16(12), 5621-5629.
Jeong, K. W., Kim, K., Situ, A. J., Ulmer, T. S., An, W., & Stallcup, M. R., 2011. Recognition of enhancer element–specific histone methylation by TIP60 in transcriptional activation. *Nat Struct Mol Biol*, 18, 1358-1365.
Jha, S., Vande Pol, S., Banerjee, N. S., Dutta, A. B., Chow, L. T., & Dutta, A., 2010. Destabilization of TIP60 by human papillomavirus E6 results in attenuation of TIP60-dependent transcriptional regulation and apoptotic pathway. *Mol Cell*, 38(5), 700-711.
Jiang, X., Sun, Y., Chen, S., Roy, K., & Price, B. D., 2006. The FATC domains of PIKK proteins are functionally equivalent and participate in the Tip60-dependent activation of DNA-PKcs and ATM. *J Biol Chem*, 281(23), 15741-15746.
Jimenji, T., Matsumura, R., Kori, S., & Arita, K. (2019). Structure of PCNA in complex with DNMT1 PIP box reveals the basis for the molecular mechanism of the interaction. *Biochem Biophys Res Commun*, 516(2), 578-583.
Jin, B., & Robertson, K. D., 2013. DNA methyltransferases, DNA damage repair, and cancer. *Adv Exp Med Biol*, 754, 3-29.
Johnson, A. A., Sarthi, J., Pirooznia, S. K., Reube, W., & Elefant, F., 2013. Increasing Tip60 HAT levels rescues axonal transport defects and associated behavioral phenotypes in a Drosophila Alzheimer's disease model. *J Neurosci*, 33(17), 7535-7547.
Johnstone, R. W., 2002. Histone-deacetylase inhibitors: novel drugs for the treatment of cancer. *Nat Rev Drug Discov*, 1, 287-299.
Jones, P. A., & Liang, G., 2009. Rethinking how DNA methylation patterns are maintained. *Nature Rev. Genet*, 10(11), 805-811.
Judes, G., Dubois, L., Rifaï, K., Idrissou, M., Mishellany, F., Pajon, A., Besse, S., Daures, M., Degoul, F., Bignon, Y.-J., Penault-Llorca, F., & Bernard-Gallon, D., 2018. TIP60: an actor in acetylation of H3K4 and tumor development in breast cancer. *Epigenomics*, 10(11), 1415-1430.
Jung, J. K., Arora, P., Pagano, J. S., & Jang, K. L., 2007. Expression of DNA methyltransferase 1 is activated by hepatitis B virus X protein via a regulatory circuit involving the p16INK4a-Cyclin D1-CDK 4/6-pRb-E2F1 Pathway. *Cancer Res*, 67(12), 5771.
Jurkowska, R. Z., & Jeltsch, A. (2016). Enzymology of Mammalian DNA Methyltransferases. In A. Jeltsch & R. Z. Jurkowska (Eds.), *DNA Methyltransferases - Role and Function* (pp. 87-122). Cham: Springer International Publishing.

Jurkowska, R. Z., Jurkowski, T. P., & Jeltsch, A., 2011. Structure and function of mammalian DNA methyltransferases. *Chembiochem*, 12(2), 206-222.

Kaidi, A., & Jackson, S. P., 2013. KAT5 tyrosine phosphorylation couples chromatin sensing to ATM signalling. *Nature*, 498(7452), 70-74.

Kamine, J., Elangovan, B., Subramanian, T., Coleman, D., & Chinnadurai, G., 1996. Identification of a cellular protein that specifically interacts with the essential cysteine region of the HIV-1 Tat transactivator. *Virology*, 216(2), 357-366.

Karagianni, P., Amazit, L., Qin, J., & Wong, J., 2008. ICBP90, a novel methyl K9 H3 binding protein linking protein ubiquitination with heterochromatin formation. *Mol Cell Biol*, 28(2), 705-717.

Kilin, V., Gavvala, K., Barthes, N. P. F., Michel, B. Y., Shin, D., Boudier, C., Mauffret, O., Yashchuk, V., Mousli, M., Ruff, M., Granger, F., Eiler, S., Bronner, C., Tor, Y., Burger, A., & Mély, Y., 2017. Dynamics of methylated cytosine flipping by UHRF1. *J Amer Chem Soc*, 139(6), 2520-2528.

Kim, C.-H., Kim, J.-W., Jang, S.-M., An, J.-H., Seo, S.-B., & Choi, K.-H., 2015. The chromodomain-containing histone acetyltransferase TIP60 acts as a code reader, recognizing the epigenetic codes for initiating transcription. *Biosci, Biotechnol, Biochem*, 79(4), 532-538.

Kim, G.-D., Ni, J., Kelesoglu, N., Roberts, R. J., & Pradhan, S., 2002. Co-operation and communication between the human maintenance and de novo DNA (cytosine-5) methyltransferases. *EMBO J*, 21(15), 4183-4195.

Kim, J.-W., Jang, S.-M., Kim, C.-H., An, J.-H., Kang, E.-J., & Choi, K.-H., 2012. New molecular bridge between RelA/p65 and NF-κB target genes via histone acetyltransferase TIP60 cofactor. *J Biol Chem*, 287(10), 7780-7791.

Kim, J. H., Kim, B., Cai, L., Choi, H. J., Ohgi, K. A., Tran, C., Chen, C., Chung, C. H., Huber, O., Rose, D. W., Sawyers, C. L., Rosenfeld, M. G., & Baek, S. H., 2005. Transcriptional regulation of a metastasis suppressor gene by Tip60 and β-catenin complexes. *Nature*, 434(7035), 921-926.

Kim, J. K., Estève, P.-O., Jacobsen, S. E., & Pradhan, S., 2009. UHRF1 binds G9a and participates in p21 transcriptional regulation in mammalian cells. *Nucleic Acids Res*, 37(2), 493-505.

Kim, K.-B., Son, H.-J., Choi, S., Hahm, J. Y., Jung, H., Baek, H. J., Kook, H., Hahn, Y., Kook, H., & Seo, S.-B., 2015. H3K9 methyltransferase G9a negatively regulates UHRF1 transcription during leukemia cell differentiation. *Nucleic Acids Res*, 43(7), 3509-3523.

Kim, M. Y., Park, S.-J., Shim, J. W., Yang, K., Kang, H. S., & Heo, K., 2015. Naphthazarin enhances ionizing radiation-induced cell cycle arrest and apoptosis in human breast cancer cells. *Int J Oncol*, 46(4), 1659-1666.

Kim, Y.-C., Gerlitz, G., Furusawa, T., Catez, F., Nussenzweig, A., Oh, K.-S., Kraemer, K. H., Shiloh, Y., & Bustin, M., 2009. Activation of ATM depends on chromatin interactions occurring before induction of DNA damage. *Nat Cell Biol*, 11(1), 92-96.

Kimura, A., & Horikoshi, M., 1998. Tip60 acetylates six lysines of a specific class in core histones in vitro. *Genes Cells*, 3(12), 789-800.

Kimura, Y., & Tanaka, K., 2010. Regulatory mechanisms involved in the control of ubiquitin homeostasis. *J Biochem*, 147(6), 793-798.

Kirkin, V., & Dikic, I., 2011. Ubiquitin networks in cancer. *Curr Opin Genet Deve*, 21(1), 21-28.

Klein Hesselink, E. N., Zafon, C., Villalmanzo, N., Iglesias, C., van Hemel, B. M., Klein Hesselink, M. S., Montero-Conde, C., Buj, R., Mauricio, D., Peinado, M. A., Puig-Domingo, M., Riesco-Eizaguirre, G., Reverter, J. L., Robledo, M., Links, T. P., & Jordà, M., 2017. Increased global DNA hypomethylation in distant metastatic and dedifferentiated thyroid cancer. *J Clin Endocrinol Metab*, 103(2), 397-406.

Kohli, R. M., & Zhang, Y., 2013. TET enzymes, TDG and the dynamics of DNA demethylation. *Nature*, 502(7472), 472-479.

Kori, S., Ferry, L., Matano, S., Jimenji, T., Kodera, N., Tsusaka, T., Matsumura, R., Oda, T., Sato, M., Dohmae, N., Ando, T., Shinkai, Y., Defossez, P.-A., & Arita, K., 2019. Structure of the UHRF1 tandem Tudor domain bound to a methylated non-histone protein, LIG1, reveals rules for binding and regulation. *Structure*, 27(3), 485-496.

Krifa, M., Alhosin, M., Muller, C. D., Gies, J.-P., Chekir-Ghedira, L., Ghedira, K., Mély, Y., Bronner, C., & Mousli, M., 2013. *Limoniastrum guyonianum* aqueous gall extract induces apoptosis in human cervical cancer cells involving p16 INK4A re-expression related to UHRF1 and DNMT1 down-regulation. *J Exp Clin Cancer Res*, 32(1), 30-30.

Krifa, M., Leloup, L., Ghedira, K., Mousli, M., & Chekir-Ghedira, L., 2014. Luteolin induces apoptosis in BE colorectal cancer cells by downregulating calpain, UHRF1, and DNMT1 expressions. *Nutr Cancer*, 66(7), 1220-1227.

Lallous, N., Legrand, P., McEwen, A. G., Ramón-Maiques, S., Samama, J.-P., & Birck, C., 2011. The PHD finger of human UHRF1 reveals a new subgroup of unmethylated histone H3 tail readers. *PloS one*, 6(11), e27599.

Langenstroth-Röwer, D., Gromoll, J., Wistuba, J., Tröndle, I., Laurentino, S., Schlatt, S., & Neuhaus, N., 2017. De novo methylation in male germ cells of the common marmoset monkey occurs during postnatal development and is maintained in vitro. *Epigenetics*, 12(7), 527-539.

Leduc, C., Claverie, P., Eymin, B., Col, E., Khochbin, S., Brambilla, E., & Gazzeri, S., 2005. Le gène suppresseur de tumeur p14ARF induit l'accumulation de la protéine RB en inhibant son acétylation médiée par Tip60. *Rev Mal Respir*, 22(5), 868.

Lee, J.-S., Smith, E., & Shilatifard, A., 2010. The language of histone crosstalk. *Cell*, 142(5), 682-685.

Lee, M. S., Seo, J., Choi, D. Y., Lee, E. W., Ko, A., Ha, N. C., Bok Yoon, J., Lee, H. W., Pyo Kim, K., & Song, J., 2012. Stabilization of p21 (Cip1/WAF1) following Tip60-dependent acetylation is required for p21-mediated DNA damage response. *Cell Death Differ*, 20 (4), 620-629.

Legube, G., Linares, L. K., Lemercier, C., Scheffner, M., Khochbin, S., & Trouche, D., 2002. Tip60 is targeted to proteasome-mediated degradation by Mdm2 and accumulates after UV irradiation. *EMBO J*, 21(7), 1704-1712.

Legube, G., Linares, L. K., Tyteca, S., Caron, C., Scheffner, M., Chevillard-Briet, M., & Trouche, D., 2004. Role of the histone acetyl transferase Tip60 in the p53 pathway. *J Biol Chem*, 279(43), 44825-44833.

Legube, G., & Trouche, D., 2003. Identification of a larger form of the histone acetyl transferase Tip60. *Gene*, 310, 161-168.

Leitao, M. M., Soslow, R. A., Baergen, R. N., Olvera, N., Arroyo, C., & Boyd, J., 2004. Mutation and expression of the TP53 gene in early stage epithelial ovarian carcinoma. *Gynecol Oncol*, 93(2), 301-306.

Lemercier, C., Legube, G., Caron, C., Louwagie, M., Garin, J., Trouche, D., & Khochbin, S., 2003. Tip60 acetyltransferase activity is controlled by phosphorylation. *J Biol Chem*, 278(7), 4713-4718.

Leonhardt, H., Page, A. W., Weier, H.-U., & Bestor, T. H., 1992. A targeting sequence directs DNA methyltransferase to sites of DNA replication in mammalian nuclei. *Cell*, 71(5), 865-873.

Lewinska, A., Adamczyk-Grochala, J., Kwasniewicz, E., Deregowska, A., Semik, E., Zabek, T., & Wnuk, M., 2018. Reduced levels of methyltransferase DNMT2 sensitize human fibroblasts to oxidative stress and DNA damage that is accompanied by changes in proliferation-related miRNA expression. *Redox Biol*, 14, 20-34.

Li, C., Fan, Y., Li, G., Xu, X., Duan, J., Li, R., Kang, X., Ma, X., Chen, X., Ke, Y., Yan, J., Lian, Y., Liu, P., Zhao, Y., Zhao, H., Chen, Y., Yu, Y., & Liu, J., 2018. DNA methylation reprogramming of functional elements during mammalian embryonic development. *Cell Discov*, 4(1), 41.

Li, H., Cuenin, C., Murr, R., Wang, Z.-Q., & Herceg, Z., 2004. HAT cofactor Trrap regulates the mitotic checkpoint by modulation of Mad1 and Mad2 expression. *EMBO J*, 23(24), 4824-4834.

Li, J., Huang, Q., Zeng, F., Li, W., He, Z., Chen, W., Zhu, W., & Zhang, B., 2014. The prognostic value of global DNA hypomethylation in cancer: a meta-analysis. *PloSone*, 9(9), e106290.

Li, M. L., Jiang, Q., Bhanu, N. V., Wu, J., Li, W., Garcia, B. A., & Greenberg, R. A., 2018. Phosphorylation of TIP60 suppresses 53BP1 localization at DNA damage sites. *Mol Cell Biol*, 39(1), 209-218.

Li, T., Wang, L., Du, Y., Xie, S., Yang, X., Lian, F., Zhou, Z., & Qian, C., 2018. Structural and mechanistic insights into UHRF1-mediated DNMT1 activation in the maintenance DNA methylation. *Nucleic Acids Res*, 46(6), 3218-3231.

Li, Y., Mori, T., Hata, H., Homma, Y., & Kochi, H., 2004. NIRF induces G1 arrest and associates with Cdk2. *Biochem Biophys Res Commun*, 319(2), 464-468.

Li, Y., Sun, W., Sun, D., & Yin, D., 2019. Ras–ERK1/2 signaling promotes the development of uveal melanoma by downregulating H3K14ac. *J Cell Physiol*, 234(9), 16011-16020.

Liang, Z., Yu, Q., Ji, H., & Tian, D., 2019. Tip60-siRNA regulates ABCE1 acetylation to suppress lung cancer growth via activation of the apoptotic signaling pathway. *Exp Ther Med*, 17(4), 3195-3202.

Liao, J., Karnik, R., Gu, H., Ziller, M. J., Clement, K., Tsankov, A. M., Akopian, V., Gifford, C. A., Donaghey, J., Galonska, C., Pop, R., Reyon, D., Tsai, S. Q., Mallard, W., Joung, J. K., Rinn, J. L., Gnirke, A., & Meissner, A., 2015. Targeted disruption of DNMT1, DNMT3A and DNMT3B in human embryonic stem cells. *Nat Genet*, 47(5), 469-478.

Lin, S.-Y., Li, T. Y., Liu, Q., Zhang, C., Li, X., Chen, Y., Zhang, S.-M., Lian, G., Liu, Q., Ruan, K., Wang, Z., Zhang, C.-S., Chien, K.-Y., Wu, J., Li, Q., Han, J., & Lin, S.-C., 2012. GSK3-TIP60-ULK1 signaling pathway links growth factor deprivation to autophagy. *Science*, 336(6080), 477-481.

Lin, Y., Chen, W., Wang, Z., & Cai, P., 2017. Emodin promotes the arrest of human lymphoma Raji cell proliferation through the UHRF1‑DNMT3A‑ΔNp73 pathways. *Mol Med Rep*, 16(5), 6544-6551.

Liu, N., Wang, J., Wang, J., Wang, R., Liu, Z., Yu, Y., & Lu, H., 2013. ING5 is a Tip60 cofactor that acetylates p53 in response to DNA damage. *Cancer Res*, 73(12), 3749-3760.

Liu, Z., & Sun, Y., 2011. Role of Tip60 tumor suppressor in DNA repair pathway. *Chinese Sci Bull*, 56(12), 1212-1215.

Liyanage, C., Wathupola, A., Muraleetharan, S., Perera, K., Punyadeera, C., & Udagama, P., 2019. Promoter hypermethylation of tumor suppressor genes p16(INK4a), RASSF1A, TIMP3, and PCQAP/MED15 in salivary DNA as a quadruple biomarker panel for early detection of oral and oropharyngeal cancers. *Biomolecules*, 9(4), 148.

LLeonart, M., Vidal, F., Gallardo, D., Diaz-Fuertes, M., Rojo, F., Cuatrecasas, M., Lopez-Vicente, L., Kondoh, H., Blanco, C., & Carnero, A., 2006. New p53 related genes in human tumors: significant downregulation in colon and lung carcinomas. *Oncol Rep*, 16(3), 603-608.

Lu, R., & Wang, G. G., 2013. Tudor: a versatile family of histone methylation 'readers'. *Trends Biochem Sci*, 38(11), 546-555.

Luger, K., Mäder, A. W., Richmond, R. K., Sargent, D. F., & Richmond, T. J., 1997. Crystal structure of the nucleosome core particle at 2.8 Å resolution. *Nature*, 389(6648), 251-260.

Lund, A. H., & van Lohuizen, M., 2004. Epigenetics and cancer. *Genes Dev*, 18(19), 2315-2335.

Lyko, F., Foret, S., Kucharski, R., Wolf, S., Falckenhayn, C., & Maleszka, R., 2010. The honey bee epigenomes: differential methylation of brain DNA in queens and workers. *PLOS Biol*, 8(11), e1000506.

Ma, H.-S., Wang, E. L., Xu, W.-F., Yamada, S., Yoshimoto, K., Qian, Z. R., Shi, L., Liu, L.-L., & Li, X.-H., 2018. Overexpression of DNA (cytosine-5)-methyltransferase 1 (DNMT1) and DNA (cytosine-5)-methyltransferase 3A (DNMT3A) is associated with aggressive behavior and hypermethylation of tumor suppressor genes in human pituitary adenomas. *Med Sci Monit*, 24, 4841-4850.

Ma, H., Chen, H., Guo, X., Wang, Z., Sowa, M. E., Zheng, L., Hu, S., Zeng, P., Guo, R., Diao, J., Lan, F., Harper, J. W., Shi, Y. G., Xu, Y., & Shi, Y., 2012. M phase phosphorylation of the epigenetic regulator UHRF1 regulates its physical association with the deubiquitylase USP7 and stability. *Proc Nat Acad Sci U S A*, 109(13), 4828-4833.

Mattera, L., Escaffit, F., Pillaire, M. J., Selves, J., Tyteca, S., Hoffmann, J. S., Gourraud, P. A., Chevillard-Briet, M., Cazaux, C., & Trouche, D., 2009. The p400/Tip60 ratio is critical for colorectal cancer cell proliferation through DNA damage response pathways. *Oncogene*, 28, 1506-1517.

Mauray, A., Milenkovic, D., Besson, C., Caccia, N., Morand, C., Michel, F., Mazur, A., Scalbert, A., & Felgines, C., 2009. Atheroprotective effects of Bilberry extracts in Apo E-deficient mice. *J Agri Food Chem*, 57(23), 11106-11111.

Meilinger, D., Fellinger, K., Bultmann, S., Rothbauer, U., Bonapace, I. M., Klinkert, W. E. F., Spada, F., & Leonhardt, H., 2009. Np95 interacts with de novo DNA methyltransferases, Dnmt3a and Dnmt3b, and mediates epigenetic silencing of the viral CMV promoter in embryonic stem cells. *EMBO Rep*, 10(11), 1259-1264.

Meng, H., Harrison, D. J., & Meehan, R. R. (2015). MBD4 interacts with and recruits USP7 to heterochromatic foci. *J Cell Biochem*, 116(3), 476-485.

Merlo, A., Herman, J. G., Mao, L., Lee, D. J., Gabrielson, E., Burger, P. C., Baylin, S. B., & Sidransky, D., 1995. 5′ CpG island methylation is associated with transcriptional silencing of the tumour suppressor p16/CDKN2/MTS1 in human cancers. *Nat Med*, 1(7), 686-692.

Meyers, F. J., Chi, S.-G., Fishman, J. R., White, R. W. d., & Gumerlock, P. H., 1993. p53 mutations in benign prostatic hyperplasia. *J Natl Cancer Inst*, 85(22), 1856-1858.

Michalak, E. M., Burr, M. L., Bannister, A. J., & Dawson, M. A., 2019. The roles of DNA, RNA and histone methylation in ageing and cancer. *Nat Rev Mol Cell Bio*. 10.1038/s41580-019-0143-1.

Miyamoto, N., Izumi, H., Noguchi, T., Nakajima, Y., Ohmiya, Y., Shiota, M., Kidani, A., Tawara, A., & Kohno, K., 2008. Tip60 is regulated by circadian transcription factor clock and is involved in cisplatin resistance. *J Biol Chem*, 283(26), 18218-18226.

Mo, F., Zhuang, X., Liu, X., Yao, P. Y., Qin, B., Su, Z., Zang, J., Wang, Z., Zhang, J., Dou, Z., Tian, C., Teng, M., Niu, L., Hill, D. L., Fang, G., Ding, X., Fu, C., & Yao, X., 2016. Acetylation of Aurora B by TIP60 ensures accurate chromosomal segregation. *Nat Chem Biol*, 12(4), 226-232.

Mori, T., Ikeda, D. D., Fukushima, T., Takenoshita, S., & Kochi, H., 2011. NIRF constitutes a nodal point in the cell cycle network and is a candidate tumor suppressor. *Cell Cycle*, 10(19), 3284-3299.

Mori, T., Ikeda, D. D., Yamaguchi, Y., & Unoki, M., 2012. NIRF/UHRF2 occupies a central position in the cell cycle network and allows coupling with the epigenetic landscape. *FEBS Lett*, 586(11), 1570-1583.

Mori, T., Li, Y., Hata, H., Ono, K., & Kochi, H., 2002. NIRF, a novel RING finger protein, is involved in cell-cycle regulation. *Biochem Biophys Res Commun*, 296(3), 530-536.

Morrissey, C., Gallis, B., Solazzi, J. W., Kim, B. J., Gulati, R., Vakar-Lopez, F., Goodlett, D. R., Vessella, R. L., & Sasaki, T., 2010. Effect of artemisinin derivatives on apoptosis and cell cycle in prostate cancer cells. *Anticancer Drugs*, 21(4), 423-432.

Mousli, M., Hopfner, R., Abbady, A. Q., Monté, D., Jeanblanc, M., Oudet, P., Louis, B., & Bronner, C., 2003. ICBP90 belongs to a new family of proteins with an expression that is deregulated in cancer cells. *Br J Cancer*, 89(1), 120-127.

Myrianthopoulos, V., Cartron, P. F., Liutkevičiūtė, Z., Klimašauskas, S., Matulis, D., Bronner, C., Martinet, N., & Mikros, E., 2016. Tandem virtual screening targeting the SRA domain of UHRF1 identifies a novel chemical tool modulating DNA methylation. *Eur J Med Chem*, 114, 390-396.

Nady, N., Lemak, A., Walker, J. R., Avvakumov, G. V., Kareta, M. S., Achour, M., Xue, S., Duan, S., Allali-Hassani, A., Zuo, X., Wang, Y.-X., Bronner, C., Chédin, F., Arrowsmith, C. H., & Dhe-Paganon, S., 2011. Recognition of multivalent histone states associated with heterochromatin by UHRF1 protein. *J Biol Chem*, 286(27), 24300-24311.

Nagashima, M., Shiseki, M., Pedeux, R. M., Okamura, S., Kitahama-Shiseki, M., Miura, K., Yokota, J., & Harris, C. C., 2003. A novel PHD-finger motif protein, p47ING3, modulates p53-mediated transcription, cell cycle control, and apoptosis. *Oncogene*, 22(3), 343-350.

Naidu, S. R., Lakhter, A. J., & Androphy, E. J. (2012). PIASy-mediated Tip60 sumoylation regulates p53-induced autophagy. *Cell Cycle*, 11(14), 2717-2728.

Nielsen, P. R., Nietlispach, D., Mott, H. R., Callaghan, J., Bannister, A., Kouzarides, T., Murzin, A. G., Murzina, N. V., & Laue, E. D., 2002. Structure of the HP1 chromodomain bound to histone H3 methylated at lysine 9. *Nature*, 416(6876), 103-107.

Niida, H., Katsuno, Y., Sengoku, M., Shimada, M., Yukawa, M., Ikura, M., Ikura, T., Kohno, K., Shima, H., Suzuki, H., Tashiro, S., & Nakanishi, M., 2010. Essential role of Tip60-dependent

recruitment of ribonucleotide reductase at DNA damage sites in DNA repair during G1 phase. *Genes Dev*, 24(4), 333-338.

Nishiyama, A., Yamaguchi, L., Sharif, J., Johmura, Y., Kawamura, T., Nakanishi, K., Shimamura, S., Arita, K., Kodama, T., Ishikawa, F., Koseki, H., & Nakanishi, M., 2013. Uhrf1-dependent H3K23 ubiquitylation couples maintenance DNA methylation and replication. *Nature*, 502(7470), 249-253.

Pacaud, R., Brocard, E., Lalier, L., Hervouet, E., Vallette, F. M., & Cartron, P.-F., 2014. The DNMT1/PCNA/UHRF1 disruption induces tumorigenesis characterized by similar genetic and epigenetic signatures. *Sci Rep*, 4, 4230-4230.

Pacaud, R., Sery, Q., Oliver, L., Vallette, F. M., Tost, J., & Cartron, P.-F., 2014. DNMT3L interacts with transcription factors to target DNMT3L/DNMT3B to specific DNA sequences: Role of the DNMT3L/DNMT3B/p65-NFκB complex in the (de-)methylation of TRAF1. *Biochimie*, 104, 36-49.

Pandey, A. K., Zhang, Y., Zhang, S., Li, Y., Tucker-Kellogg, G., Yang, H., & Jha, S., 2015. TIP60-miR-22 axis as a prognostic marker of breast cancer progression. *Oncotarget*, 6(38), 41290-41306.

Papait, R., Pistore, C., Negri, D., Pecoraro, D., Cantarini, L., & Bonapace, I. M., 2007. Np95 is implicated in pericentromeric heterochromatin replication and in major satellite silencing. *Mol Biol Cell*, 18(3), 1098-1106.

Parashar, G., & Capalash, N., 2016. Promoter methylation-independent reactivation of PAX1 by curcumin and resveratrol is mediated by UHRF1. *Clin Exp Med*, 16(3), 471-478.

Park, J. H., Sun, X.-J., & Roeder, R. G., 2010. The SANT domain of p400 ATPase represses acetyltransferase activity and coactivator function of TIP60 in basal p21 gene expression. *Mol Cell Biol*, 30(11), 2750-2761.

Parker, B. S., Cutts, S. M., Nudelman, A., Rephaeli, A., Phillips, D. R., & Sukumar, S., 2003. Mitoxantrone mediates demethylation and re-expression of Cyclin D2, estrogen receptor 14.3.3 sigma in breast cancer cells. *Cancer Biol Ther*, 2(3), 259-263.

Patel, J. H., Du, Y., Ard, P. G., Phillips, C., Carella, B., Chen, C.-J., Rakowski, C., Chatterjee, C., Lieberman, P. M., Lane, W. S., Blobel, G. A., & McMahon, S. B., 2004. The c-MYC oncoprotein is a substrate of the acetyltransferases hGCN5/PCAF and TIP60. *Mol Cell Biol*, 24(24), 10826-10834.

Patnaik, D., Estève, P.-O., & Pradhan, S., 2018. Targeting the SET and RING-associated (SRA) domain of ubiquitin-like, PHD and ring finger-containing 1 (UHRF1) for anti-cancer drug development. *Oncotarget*, 9(40), 26243-26258.

Pei, J.-H., Luo, S.-Q., Zhong, Y., Chen, J.-H., Xiao, H.-W., & Hu, W.-X., 2011. The association between non-Hodgkin lymphoma and methylation of p73. *Tumor Biol*, 32(6), 1133-1138.

Pérez, R. F., Tejedor, J. R., Bayón, G. F., Fernández, A. F., & Fraga, M. F., 2018. Distinct chromatin signatures of DNA hypomethylation in aging and cancer. *Aging Cell*, 17(3), e12744.

Periasamy, A., Mazumder, N., Sun, Y., Christopher, K. G., & Day, R. N., 2015. FRET Microscopy: basics, issues and advantages of FLIM-FRET Imaging. *Advanced Time-Correlated Single Photon Counting Applications*. *Springer Intl Pub*. 249-276.

Pichler, G., Wolf, P., Schmidt, C. S., Meilinger, D., Schneider, K., Frauer, C., Fellinger, K., Rottach, A., & Leonhardt, H., 2011. Cooperative DNA and histone binding by Uhrf2 links the two major repressive epigenetic pathways. *J Cell Biochem*, 112(9), 2585-2593.

Polepalli, S., George, S. M., Valli Sri Vidya, R., Rodrigues, G. S., Ramachandra, L., Chandrashekar, R., M, D. N., Rao, P. P. N., Pestell, R. G., & Rao, M., 2019. Role of UHRF1 in malignancy and its function as a therapeutic target for molecular docking towards the SRA domain. *Intl J Biochem Cell Biol*, 114, 105558.

Popovic, D., Vucic, D., & Dikic, I., 2014. Ubiquitination in disease pathogenesis and treatment. *Nat Med*, 20, 1242-1253.

Portela, A., & Esteller, M., 2010. Epigenetic modifications and human disease. *Nat Biotechnol*, 28, 1057-1068.

Qadi, S. A., Hassan, M. A., Sheikh, R. A., Baothman, O. A., Zamzami, M. A., Choudhry, H., Al-Malki, A. L., Albukhari, A., & Alhosin, M., 2019. Thymoquinone-induced reactivation of

tumor suppressor genes in cancer cells involves epigenetic mechanisms. *Epigenet Insights*, 12, 1-9.

Qin, J., Wen, B., Liang, Y., Yu, W., & Li, H., 2019. Histone Modifications and their role in colorectal cancer. *Pathol Oncol Res*. 1-11. 10.1007/s12253-019-00663-8.

Qin, W., Leonhardt, H., & Pichler, G., 2011. Regulation of DNA methyltransferase 1 by interactions and modifications. *Nucleus*, 2(5), 392-402.

Qin, W., Wolf, P., Liu, N., Link, S., Smets, M., La Mastra, F., Forné, I., Pichler, G., Hörl, D., Fellinger, K., Spada, F., Bonapace, I. M., Imhof, A., Harz, H., & Leonhardt, H., 2015. DNA methylation requires a DNMT1 ubiquitin interacting motif (UIM) and histone ubiquitination. *Cell Res*, 25(8), 911-929.

Rajagopalan, D., Pandey, A. K., Xiuzhen, M. C., Lee, K. K., Hora, S., Zhang, Y., Chua, B. H., Kwok, H. S., Bhatia, S. S., Deng, L. W., Tenen, D. G., Kappei, D., & Jha, S., 2017. TIP60 represses telomerase expression by inhibiting Sp1 binding to the TERT promoter. *PLoS Pathog*, 13(10), e1006681.

Rajagopalan, D., Tirado-Magallanes, R., Bhatia, S. S., Teo, W. S., Sian, S., Hora, S., Lee, K. K., Zhang, Y., Jadhav, S. P., Wu, Y., Gan, Y.-H., Karnani, N., Benoukraf, T., & Jha, S., 2018. TIP60 represses activation of endogenous retroviral elements. *Nucleic Acids Res*, 46(18), 9456-9470.

Rajakumara, E., Wang, Z., Ma, H., Hu, L., Chen, H., Lin, Y., Guo, R., Wu, F., Li, H., Lan, F., Shi, Y. G., Xu, Y., Patel, D. J., & Shi, Y., 2011. PHD finger recognition of unmodified histone H3R2 links UHRF1 to regulation of euchromatic gene expression. *Mol Cell*, 43(2), 275-284.

Ran, Q., & Pereira-Smith, O. M., 2000. Identification of an alternatively spliced form of the Tat Interactive Protein (Tip60), Tip60(β). *Gene*, 258(1), 141-146.

Ravichandran, P., & Ginsburg, D., 2015. Tip60 overexpression exacerbates chemotherapeutic drug treatment in breast, pancreatic, and lung cancer cell lines. *FASEB J*, 29(1), 725.721.

Ren, W., Gao, L., & Song, J., 2018. Structural basis of DNMT1 and DNMT3A-mediated DNA methylation. *Genes*, 9(12), 620-639.

Robertson, K. D., 2005. DNA methylation and human disease. *Nat Rev Genet*, 6(8), 597-610.

Robertson, K. D., Uzvolgyi, E., Liang, G., Talmadge, C., Sumegi, J., Gonzales, F. A., & Jones, P. A., 1999. The human DNA methyltransferases (DNMTs) 1, 3a and 3b: coordinate mRNA expression in normal tissues and overexpression in tumors. *Nucleic Acids Research*, 27(11), 2291-2298.

Rothbart, S. B., Krajewski, K., Nady, N., Tempel, W., Xue, S., Badeaux, A. I., Barsyte-Lovejoy, D., Martinez, J. Y., Bedford, M. T., Fuchs, S. M., Arrowsmith, C. H., & Strahl, B. D., 2012. Association of UHRF1 with methylated H3K9 directs the maintenance of DNA methylation. *Nat Struct Mol Biol*, *19*, 1155-1160.

Rottach, A., Frauer, C., Pichler, G., Bonapace, I. M., Spada, F., & Leonhardt, H., 2010. The multi-domain protein Np95 connects DNA methylation and histone modification. *Nucleic Acids Research*, 38(6), 1796-1804.

Ruan, Y., 2015. Investigating the regulation of UHRF1 in cell cycle. The University of Hong Kong (Pokfulam, Hong Kong).

Russo, V., Martienssen, R., & Riggs, A., 1996. Epigenetic mechanisms of gene regulation. *Cold Spring Harbor Laboratory Press NY*.

Sakuraba, K., Yasuda, T., Sakata, M., Kitamura, Y.-H., Shirahata, A., Goto, T., Mizukami, H., Saito, M., Ishibashi, K., Kigawa, G., Nemoto, H., Sanada, Y., & Hibi, K., 2009. Down-regulation of Tip60 gene as a potential marker for the malignancy of colorectal cancer. *Anticancer Res*, 29(10), 3953-3955.

Sakuraba, K., Yokomizo, K., Shirahata, A., Goto, T., Saito, M., Ishibashi, K., Kigawa, G., Nemoto, H., & Hibi, K., 2011. TIP60 as a potential marker for the malignancy of gastric cancer. *Anticancer Res*, 31(1), 77-79.

Santhekadur, P. K., Rajasekaran, D., Siddiq, A., Gredler, R., Chen, D., Schaus, S. E., Hansen, U., Fisher, P. B., & Sarkar, D., 2012. The transcription factor LSF: a novel oncogene for hepatocellular carcinoma. *Amer J Cancer Res*, 2(3), 269-285.

Santoro, R., & Grummt, I., 2001. Molecular mechanisms mediating methylation-dependent silencing of ribosomal gene transcription. *Mol Cell*, 8(3), 719-725.

Sapountzi, V., Logan, I. R., & Robson, C. N., 2006. Cellular functions of TIP60. *Intl J Biochem Cell Biol*, 38(9), 1496-1509.

Schlechte, H., Lenk, S. V., Löning, T., Schnorr, D., Rudolph, B. D., Ditscherlein, G., & Loening, S. A., 1998. p53 tumour suppressor gene mutations in benign prostatic hyperplasia and prostate cancer. *Eur Urol*, 34(5), 433-440.

Schuermann, D., Weber, A. R., & Schär, P., 2016. Active DNA demethylation by DNA repair: facts and uncertainties. *DNA Repair*, 44, 92-102.

Scotto, L., Narayan, G., Nandula, S. V., Arias-Pulido, H., Subramaniyam, S., Schneider, A., Kaufmann, A. M., Wright, J. D., Pothuri, B., Mansukhani, M., & Murty, V. V., 2008. Identification of copy number gain and overexpressed genes on chromosome arm 20q by an integrative genomic approach in cervical cancer: Potential role in progression. *Genes Chromosomes Cancer*, 47(9), 755-765.

Senisterra, G., Zhu, H. Y., Luo, X., Zhang, H., Xun, G., Lu, C., Xiao, W., Hajian, T., Loppnau, P., Chau, I., Li, F., Allali-Hassani, A., Atadja, P., Oyang, C., Li, E., Brown, P. J., Arrowsmith, C. H., Zhao, K., Yu, Z., & Vedadi, M., 2018. Discovery of small-molecule antagonists of the H3K9me3 binding to UHRF1 tandem Tudor domain. *SLAS Discov*, 23(9), 930-940.

Seo, J. S., Choi, Y. H., Moon, J. W., Kim, H. S., & Park, S.-H., 2017. Hinokitiol induces DNA demethylation via DNMT1 and UHRF1 inhibition in colon cancer cells. *BMC Cell Biol*, 18(1), 14-25.

Sharif, J., Muto, M., Takebayashi, S.-i., Suetake, I., Iwamatsu, A., Endo, T. A., Shinga, J., Mizutani-Koseki, Y., Toyoda, T., Okamura, K., Tajima, S., Mitsuya, K., Okano, M., & Koseki, H., 2007. The SRA protein Np95 mediates epigenetic inheritance by recruiting Dnmt1 to methylated DNA. *Nature*, 450, 908-912.

Sharif, T., Alhosin, M., Auger, C., Minker, C., Kim, J.-H., Etienne-Selloum, N., Bories, P., Gronemeyer, H., Lobstein, A., Bronner, C., Fuhrmann, G., & Schini-Kerth, V. B., 2012. Aronia melanocarpa juice induces a redox-sensitive p73-related caspase 3-dependent apoptosis in human leukemia cells. *PloS One*, 7(3), e32526.

Sharif, T., Auger, C., Alhosin, M., Ebel, C., Achour, M., Étienne-Selloum, N., Fuhrmann, G., Bronner, C., & Schini-Kerth, V. B., 2010. Red wine polyphenols cause growth inhibition and apoptosis in acute lymphoblastic leukaemia cells by inducing a redox-sensitive up-regulation of p73 and down-regulation of UHRF1. *Eur J Cancer*, 46(5), 983-994.

Sharma, S., Kelly, T. K., & Jones, P. A., 2010. Epigenetics in cancer. *Carcinogenesis*, 31(1), 27-36.

Sheng, Y., Wang, H., Liu, D., Zhang, C., Deng, Y., Yang, F., Zhang, T., & Zhang, C. (2016). Methylation of tumor suppressor gene CDH13 and SHP1 promoters and their epigenetic regulation by the UHRF1/PRMT5 complex in endometrial carcinoma. *Gynecol Oncol*, 140(1), 145-151.

Sheridan, A. M., Force, T., Yoon, H. J., O'Leary, E., Choukroun, G., Taheri, M. R., & Bonventre, J. V., 2001. PLIP, a novel splice variant of Tip60, interacts with group IV cytosolic phospholipase A(2), induces apoptosis, and potentiates prostaglandin production. *Mol Cell Biol*, 21(14), 4470-4481.

Shin, S. H., & Kang, S. S., 2013. Phosphorylation of Tip60 tyrosine 327 by Abl kinase inhibits HAT activity through association with FE65. *Biochem J*, 7, 66-72.

Shiota, M., Yokomizo, A., Masubuchi, D., Tada, Y., Inokuchi, J., Eto, M., Uchiumi, T., Fujimoto, N., & Naito, S., 2010. Tip60 promotes prostate cancer cell proliferation by translocation of androgen receptor into the nucleus. *Prostate*, 70(5), 540-554.

Shoieb, A. M., Elgayyar, M., Dudrick, P. S., Bell, J. L., & Tithof, P. K., 2003. In vitro inhibition of growth and induction of apoptosis in cancer cell lines by thymoquinone. *Intl J Oncol*, 22(1), 107-113.

Sidhu, H., & Capalash, N., 2017. UHRF1: The key regulator of epigenetics and molecular target for cancer therapeutics. *Tumor Biol*, 39(2), 1-11.

Singer, B. D., 2019. A practical guide to the measurement and analysis of DNA methylation. *Amer J Respir Cell Mol Biol*. 10.1165/rcmb.2019-0150TR.

Slaby, O., Laga, R., & Sedlacek, O., 2017. Therapeutic targeting of non-coding RNAs in cancer. *Biochem J*, 474(24), 4219-4251.

Smets, M., Link, S., Wolf, P., Schneider, K., Solis, V., Ryan, J., Meilinger, D., Qin, W., & Leonhardt, H., 2017. DNMT1 mutations found in HSANIE patients affect interaction with UHRF1 and neuronal differentiation. *Hum Mol Genet,* 26(8), 1522-1534.

Song, J., Rechkoblit, O., Bestor, T. H., & Patel, D. J., 2011. Structure of DNMT1-DNA complex reveals a role for autoinhibition in maintenance DNA methylation. *Science (New York, N.Y.), 331*(6020), 1036-1040. doi: 10.1126/science.1195380

Song, J., Teplova, M., Ishibe-Murakami, S., & Patel, D. J. (2012). Structure-based mechanistic insights into DNMT1-mediated maintenance DNA methylation. *Science*, 335(6069), 709-712.

Stefansson, O. A., Hermanowicz, S., van der Horst, J., Hilmarsdottir, H., Staszczak, Z., Jonasson, J. G., Tryggvadottir, L., Gudjonsson, T., & Sigurdsson, S., 2017. CpG promoter methylation of the ALKBH3 alkylation repair gene in breast cancer. *BMC Cancer,* 17(1), 469-469.

Stefansson, O. A., Jonasson, J. G., Olafsdottir, K., Hilmarsdottir, H., Olafsdottir, G., Esteller, M., Johannsson, O. T., & Eyfjord, J. E., 2011. CpG island hypermethylation of BRCA1 and loss of pRb as co-occurring events in basal/triple-negative breast cancer. *Epigenetics,* 6(5), 638-649.

Subbaiah, V. K., Zhang, Y., Rajagopalan, D., Abdullah, L. N., Yeo-Teh, N. S. L., Tomaić, V., Banks, L., Myers, M. P., Chow, E. K., & Jha, S., 2015. E3 ligase EDD1/UBR5 is utilized by the HPV E6 oncogene to destabilize tumor suppressor TIP60. *Oncogene,* 35, 2062-2074.

Sun, Y., Jiang, X., Chen, S., Fernandes, N., & Price, B. D., 2005. A role for the Tip60 histone acetyltransferase in the acetylation and activation of ATM. *Proc Natl Acad Sci U S A,* 102(37), 13182-13187.

Sun, Y., Jiang, X., & Price, B. D., 2010. Tip60: connecting chromatin to DNA damage signaling. *Cell Cycle,* 9(5), 930-936.

Sun, Y., Xu, Y., Roy, K., & Price, B. D., 2007. DNA damage-induced acetylation of lysine 3016 of ATM activates ATM kinase activity. *Mol Cell Biol,* 27(24), 8502-8509.

Sykes, M., Szot, G., Swenson, K., Pearson, D., & Wekerle, T., 1998. Separate regulation of peripheral hematopoietic and thymic engraftment. *Exper Hematol,* 26(6), 457-465.

Sykes, S. M., Mellert, H. S., Holbert, M. A., Li, K., Marmorstein, R., Lane, W. S., & McMahon, S. B., 2006. Acetylation of the p53 DNA-binding domain regulates apoptosis induction. *Mol Cell,* 24(6), 841-851.

Szyf, M., Bozovic, V., & Tanigawa, G., 1991. Growth regulation of mouse DNA methyltransferase gene expression. *J Biolog Chem,* 266(16), 10027-10030.

Takebayashi, S.-i., Tamura, T., Matsuoka, C., & Okano, M., 2007. Major and essential role for the DNA methylation mark in mouse embryogenesis and stable association of DNMT1 with newly replicated regions. *Mol Cell Biol,* 27(23), 8243-8258.

Takeshita, K., Suetake, I., Yamashita, E., Suga, M., Narita, H., Nakagawa, A., & Tajima, S., 2011. Structural insight into maintenance methylation by mouse DNA methyltransferase 1 (Dnmt1). *Proc Natl Acad Sci U S A,* 108(22), 9055-9059.

Takino, T., Nakada, M., Li, Z., Yoshimoto, T., Domoto, T., & Sato, H., 2016. Tip60 regulates MT1-MMP transcription and invasion of glioblastoma cells through NF-κB pathway. *Clin Exp Metast,* 33(1), 45-52.

Tam, L. M., Jiang, J., Wang, P., Li, L., Miao, W., Dong, X., & Wang, Y., 2017. Arsenite binds to the zinc finger motif of TIP60 histone acetyltransferase and induces its degradation via the 26S proteasome. *Chem Res Toxicol,* 30(9), 1685-1693.

Tang, Y., Luo, J., Zhang, W., & Gu, W., 2006. Tip60-dependent acetylation of p53 modulates the decision between cell-cycle arrest and apoptosis. *Molecular Cell,* 24(6), 827-839.

Taniue, K., Kurimoto, A., Sugimasa, H., Nasu, E., Takeda, Y., Iwasaki, K., Nagashima, T., Okada-Hatakeyama, M., Oyama, M., Kozuka-Hata, H., Hiyoshi, M., Kitayama, J., Negishi, L., Kawasaki, Y., & Akiyama, T., 2016. Long noncoding RNA UPAT promotes colon tumorigenesis by inhibiting degradation of UHRF1. *Proc Natl Acad Sci U S A,* 113(5), 1273-1278.

Tauber, M., & Fischle, W., 2015. Conserved linker regions and their regulation determine multiple chromatin-binding modes of UHRF1. *Nucleus,* 6(2), 123-132.

Taubert, S., Gorrini, C., Frank, S. R., Parisi, T., Fuchs, M., Chan, H.-M., Livingston, D. M., & Amati, B., 2004. E2F-dependent histone acetylation and recruitment of the Tip60 acetyltransferase complex to chromatin in late G1. *Mol Cell Biol*, 24(10), 4546-4556.

Trotzier, M.-A., Bronner, C., Bathami, K., Mathieu, E., Abbady, A.-Q., Jeanblanc, M., Muller, C. D., Rochette-Egly, C., & Mousli, M., 2004. Phosphorylation of ICBP90 by protein kinase A enhances topoisomerase IIα expression. *Biochem Biophys Res Commun*, 319(2), 590-595.

Unoki, M., 2019. Recent Insights into the Mechanisms of De Novo and Maintenance of DNA Methylation in Mammals DNA Methylation Mechanism: *IntechOpen.*

Unoki, M., Brunet, J., & Mousli, M., 2009. Drug discovery targeting epigenetic codes: The great potential of UHRF1, which links DNA methylation and histone modifications, as a drug target in cancers and toxoplasmosis. *Biochem Pharmacol*, 78(10), 1279-1288.

Unoki, M., Kelly, J. D., Neal, D. E., Ponder, B. A. J., Nakamura, Y., & Hamamoto, R., 2009. UHRF1 is a novel molecular marker for diagnosis and the prognosis of bladder cancer. *Br J Cancer*, 101, 98-105.

Unoki, M., Nishidate, T., & Nakamura, Y., 2004. ICBP90, an E2F-1 target, recruits HDAC1 and binds to methyl-CpG through its SRA domain. *Oncogene*, 23(46), 7601-7610.

Van Den Broeck, A., Eymin, B., Khochbin, S., Brambilla, E., & Gazzeri, S., 2008. L'Histone Acétyltransférase Tip60 régule l'activité biologique du facteur de transcription E2F1. *Rev Mal Respir*, 25(9), 1165.

Van Den Broeck, A., Nissou, D., Brambilla, E., Eymin, B., & Gazzeri, S., 2011. Activation of a Tip60/E2F1/ERCC1 network in human lung adenocarcinoma cells exposed to cisplatin. *Carcinogenesis*, 33(2), 320-325.

Van Den Broeck, A., Ozenne, P., Eymin, B., & Gazzeri, S., 2010. Lung cancer: a modified epigenome. *Cell Adh Mig*, 4(1), 107-113.

Vaughan, R. M., Dickson, B. M., Whelihan, M. F., Johnstone, A. L., Cornett, E. M., Cheek, M. A., Ausherman, C. A., Cowles, M. W., Sun, Z.-W., & Rothbart, S. B., 2018. Chromatin structure and its chemical modifications regulate the ubiquitin ligase substrate selectivity of UHRF1. *Proc Natl Acad Sci U S A*, 115(35), 8775-8780.

Vaughan, R. M., Rothbart, S. B., & Dickson, B. M., 2019. The finger loop of the SRA domain in the E3 ligase UHRF1 is a regulator of ubiquitin targeting and is required for maintaining DNA methylation. *J Biol Chem*, 1-16. 10.1074/jbc.RA119.010160.

Veland, N., Hardikar, S., Zhong, Y., Gayatri, S., Dan, J., Strahl, B. D., Rothbart, S. B., Bedford, M. T., & Chen, T., 2017. The arginine methyltransferase PRMT6 regulates DNA methylation and contributes to global DNA hypomethylation in cancer. *Cell Rep*, 21(12), 3390-3397.

von Meyenn, F., Iurlaro, M., Habibi, E., Liu, N. Q., Salehzadeh-Yazdi, A., Santos, F., Petrini, E., Milagre, I., Yu, M., Xie, Z., Kroeze, L. I., Nesterova, T. B., Jansen, J. H., Xie, H., He, C., Reik, W., & Stunnenberg, H. G., 2016. Impairment of DNA methylation maintenance is the main cause of global demethylation in naive embryonic stem cells. *Mol Cell*, 62(6), 848-861.

Wade, P. A., 2001. Methyl CpG-binding proteins and transcriptional repression. *BioEssays*, 23(12), 1131-1137.

Walter, A., Etienne-Selloum, N., Brasse, D., Khallouf, H., Bronner, C., Rio, M.-C., Beretz, A., & Schini-Kerth, V. B., 2010. Intake of grape-derived polyphenols reduces C26 tumor growth by inhibiting angiogenesis and inducing apoptosis. *FASEB J*, 24(9), 3360-3369.

Wang, C., Shen, J., Yang, Z., Chen, P., Zhao, B., Hu, W., Lan, W., Tong, X., Wu, H., Li, G., & Cao, C., 2011. Structural basis for site-specific reading of unmodified R2 of histone H3 tail by UHRF1 PHD finger. *Cell Res*, 21(9), 1379-1382.

Wang, C., Wang, X., Su, Z., Fei, H., Liu, X., & Pan, Q., 2015. The novel mTOR inhibitor Torin-2 induces autophagy and downregulates the expression of UHRF1 to suppress hepatocarcinoma cell growth. *Oncol Rep*, 34(4), 1708-1716.

Wang, J., & Chen, J., 2010. SIRT1 regulates autoacetylation and histone acetyltransferase activity of TIP60. *J Biol Chem*, 285(15), 11458-11464.

Wang, P., Bao, H., Zhang, X. P., Liu, F., & Wang, W., 2019. Regulation of Tip60-dependent p53 acetylation in cell fate decision. *FEBS Lett*, 593(1), 13-22.

Wang, Z., 2018. Diverse roles of regulatory non-coding RNAs. *J Mol Cell Biol*, 10(2), 91-92.
Wapenaar, H., & Dekker, F. J., 2016. Histone acetyltransferases: challenges in targeting bi-substrate enzymes. *Clin Epigenet*, 8, 59-59.
Watt, F., & Molloy, P. L., 1988. Cytosine methylation prevents binding to DNA of a HeLa cell transcription factor required for optimal expression of the adenovirus major late promoter. *Genes Dev*, 2(9), 1136-1143.
Wilkinson, K. A., & Henley, J. M., 2010. Mechanisms, regulation and consequences of protein SUMOylation. *Biochem J*, 428(2), 133-145.
Wilson, V. G., 2017. Introduction to Sumoylation. *SUMO Regulation of Cellular Processes*, Springer Intl Pub, 1-12.
Xiao, H., Chung, J., Kao, H.-Y., & Yang, Y.-C., 2003. Tip60 is a co-repressor for STAT3. *J Biol Chem*, 278(13), 11197-11204.
Xu, C.-C., Deng, T., Fan, M.-L., Lv, W.-B., Liu, J.-H., & Yu, B.-Y., 2016. Synthesis and in vitro antitumor evaluation of dihydroartemisinin-cinnamic acid ester derivatives. *Eur J Med Chem*, 107, 192-203.
Xu, F., Mao, C., Ding, Y., Rui, C., Wu, L., Shi, A., Zhang, H., Zhang, L., & Xu, Z., 2010. Molecular and enzymatic profiles of mammalian DNA methyltransferases: structures and targets for drugs. *Curr Med Chem*, 17(33), 4052-4071.
Xu, L., Chen, Y., Song, Q., Xu, D., Wang, Y., & Ma, D., 2009. PDCD5 interacts with Tip60 and functions as a cooperator in acetyltransferase activity and DNA damage-induced apoptosis. *Neoplasia*, 11(4), 345-354.
Xu, Y., Liao, R., Li, N., Xiang, R., & Sun, P., 2014. Phosphorylation of Tip60 by p38α regulates p53-mediated PUMA induction and apoptosis in response to DNA damage. *Oncotarget*, 5(24), 12555-12572.
Xu, Y., Zhang, S., Lin, S., Guo, Y., Deng, W., Zhang, Y., & Xue, Y., 2017. WERAM: a database of writers, erasers and readers of histone acetylation and methylation in eukaryotes. *Nucleic Acids Res*, 45(1), 264-270.
Xue, B., Zhao, J., Feng, P., Xing, J., Wu, H., & Li, Y., 2019. Epigenetic mechanism and target therapy of UHRF1 protein complex in malignancies. *Onco Targets Ther*, 12, 549-559.
Yamada, H. Y., 2012. Human Tip60 (NuA4) complex and cancer. *Colorectal Cancer Biology-From Genes to Tumor*. 10.5772/28295.
Yamamoto, T., & Horikoshi, M., 1997. Novel substrate specificity of the histone acetyltransferase activity of HIV-1-Tat interactive protein Tip60. *J Biol Chem*, 272(49), 30595-30598.
Yan, Y., Barlev, N. A., Haley, R. H., Berger, S. L., & Marmorstein, R., 2000. Crystal structure of yeast Esa1 suggests a unified mechanism for catalysis and substrate binding by histone acetyltransferases. *Mol Cell*, 6(5), 1195-1205.
Yan, Y., Harper, S., Speicher, D. W., & Marmorstein, R., 2002. The catalytic mechanism of the ESA1 histone acetyltransferase involves a self-acetylated intermediate. *Nat Struct Biol*, 9(11), 862-869.
Yang, C., Wu, J., & Zheng, Y. G., 2012. Function of the active site lysine autoacetylation in Tip60 catalysis. *PloS One*, 7(3), e32886.
Yang, J., Liu, K., Yang, J., Jin, B., Chen, H., Zhan, X., Li, Z., Wang, L., Shen, X., Li, M., Yu, W., & Mao, Z., 2017. PIM1 induces cellular senescence through phosphorylation of UHRF1 at Ser311. *Oncogene*, 36(34), 4828-4842.
Yang, Y., Sun, J., Chen, T., Tao, Z., Zhang, X., Tian, F., Zhou, X., & Lu, D., 2017. Tat-interactive protein-60KDA (TIP60) regulates the tumorigenesis of lung cancer in vitro. *J Cancer*, 8(12), 2277-2281.
Yi, J., Huang, X., Yang, Y., Zhu, W.-G., Gu, W., & Luo, J., 2014. Regulation of histone acetyltransferase TIP60 function by histone deacetylase 3. *J Biol Chem*, 289(49), 33878-33886.
Yoon, M.-K., Ha, J.-H., Lee, M.-S., & Chi, S.-W., 2015. Structure and apoptotic function of p73. *BMB Rep*, 48(2), 81-90.
Yu, C., Xing, F., Tang, Z., Bronner, C., Lu, X., Di, J., Zeng, S., & Liu, J., 2013. Anisomycin suppresses Jurkat T cell growth by the cell cycle-regulating proteins. *Pharmacol Rep*, 65(2), 435-444.

Zaayter, L., Mori, M., Ahmad, T., Ashraf, W., Boudier, C., Kilin, V., Gavvala, K., Richert, L., Eiler, S., Ruff, M., Botta, M., Bronner, C., Mousli, M., & Mely, Y., 2019. A molecular tool targeting the base flipping activity of human UHRF1. *Chem Eur J*, 10.1002/chem.201902605.

Zhang, J., Gao, Q., Li, P., Liu, X., Jia, Y., Wu, W., Li, J., Dong, S., Koseki, H., & Wong, J., 2011. S phase-dependent interaction with DNMT1 dictates the role of UHRF1 but not UHRF2 in DNA methylation maintenance. *Cell Res*, 21(12), 1723-1739.

Zhang, H., Gao, Q., Tan, S., You, J., Lyu, C., Zhang, Y., Han, M., Chen, Z., Li, J., Wang, H., Liao, L., Qin, J., Li, J., & Wong, J., 2019. SET8 prevents excessive DNA methylation by methylation-mediated degradation of UHRF1 and DNMT1. *Nucleic Acids Res*. doi: 10.1093/nar/gkz626.

Zhang, H., Liu, H., Chen, Y., Yang, X., Wang, P., Liu, T., Deng, M., Qin, B., Correia, C., Lee, S., Kim, J., Sparks, M., Nair, A. A., Evans, D. L., Kalari, K. R., Zhang, P., Wang, L., You, Z., Kaufmann, S. H., Lou, Z., & Pei, H., 2016. A cell cycle-dependent BRCA1–UHRF1 cascade regulates DNA double-strand break repair pathway choice. *Nat Commun*, 7, 1-14.

Zhang, Y., Ji, G., Han, S., Shao, Z., Lu, Z., Huo, L., Zhang, J., Yang, R., Feng, Q., Shen, H., Wang, H., & Li, X., 2018. Tip60 suppresses cholangiocarcinoma proliferation and metastasis via PI3k-AKT. *Cell Physiol Biochem*, 50(2), 612-628.

Zhang, Y., Lei, M., Yang, X., Feng, Y., Yang, Y., Loppnau, P., Li, Y., Yang, Y., Min, J., & Liu, Y., 2018. Structural and histone binding studies of the chromo barrel domain of TIP60. *FEBS Lett*, 592(7), 1221-1232.

Zhang, Z.-M., Rothbart, Scott B., Allison, David F., Cai, Q., Harrison, Joseph S., Li, L., Wang, Y., Strahl, Brian D., Wang, Gang G., & Song, J., 2015. An allosteric interaction links USP7 to deubiquitination and chromatin targeting of UHRF1. *Cell Rep*, 12(9), 1400-1406.

Zhao, H., Jin, S., & Gewirtz, A. M., 2012. The histone acetyltransferase TIP60 interacts with c-Myb and inactivates its transcriptional activity in human leukemia. *J Biol Chem*, 287(2), 925-934.

Zheng, H., Seit-Nebi, A., Han, X., Aslanian, A., Tat, J., Liao, R., Yates, J. R., 3rd, & Sun, P., 2013. A posttranslational modification cascade involving p38, Tip60, and PRAK mediates oncogene-induced senescence. *Mol Cell*, 50(5), 699-710.

Zhou, T., Xiong, J., Wang, M., Yang, N., Wong, J., Zhu, B., & Xu, R.-M., 2014. Structural basis for hydroxymethylcytosine recognition by the SRA domain of UHRF2. *Mol Cell*, 54(5), 879-886.

ANNEXURE

VII-ANNEXURE

VII.A. UHRF1 as a diagnostic tool for cancer

UHRF1 expression levels are high in proliferative cells while its levels are almost undetectable in differentiated tissues and in vital organs (Hopfner *et al.*, 2000). It is believed to have an oncogenic potential. Many studies have reported high expression levels of UHRF1 in breast, bladder, colorectal, ESSC, gastric, gynecological, liver, prostate, renal cancers and osteosarcomas, lymphoblastic leukemia and melanomas (Ashraf *et al.*, 2017b; Polepalli *et al.*, 2019; Xue *et al.*, 2019). Higher UHRF1 levels are linked with cancer cell proliferation, suppression of TSGs, tumor invasion, DNA methylation anomalies, poor prognosis and resistance towards chemotherapeutic agents (Bronner *et al.*, 2007; Alhosin *et al.*, 2016).

Early detection in cancer can help to cure tumor in a better way. Various epigenetic marks and biomolecules are in process of exploration to use them as a biomarker in cancer. Ideally a biomarker should be able to differentiate between pathological and normal state. It should have the capacity to detect the malignancy and prognosis with accuracy. As UHRF1 levels are high in proliferative cells as compared to normal cells so it has the potential to be used as a biomarker for cancer diagnosis and prognosis (Unoki *et al.*, 2009; Ashraf *et al.*, 2017b). In our review, we compared UHRF1 expression levels in different cancerous tissues versus levels in normal tissues. We propose UHRF1 as a diagnostic and prognostic cancer biomarker which can detect malignancy, tumor risk assessment as well as indicate about intervention at different stages of cancer (Ashraf *et al.*, 2017b).

Review Article: The epigenetic integrator UHRF1: on the road to become a universal biomarker for cancer

www.impactjournals.com/oncotarget/ Oncotarget, 2017, Vol. 8, (No. 31), pp: 51946-51962

Review

The epigenetic integrator UHRF1: on the road to become a universal biomarker for cancer

Waseem Ashraf[1], Abdulkhaleg Ibrahim[2], Mahmoud Alhosin[3,4,5], Liliyana Zaayter[1], Khalid Ouararhni[2], Christophe Papin[2], Tanveer Ahmad[1], Ali Hamiche[2], Yves Mély[1], Christian Bronner[2,*] and Marc Mousli[1,*]

[1] Laboratory of Biophotonics and Pharmacology, Faculty of Pharmacy, University of Strasbourg, Illkirch, France

[2] Institute of Genetics and Molecular and Cellular Biology, University of Strasbourg, Illkirch-Graffenstaden, France

[3] Department of Biochemistry, Faculty of Sciences, King Abdulaziz University, Jeddah, Saudi Arabia

[4] Cancer Metabolism and Epigenetic Unit, King Abdulaziz University, Jeddah, Saudi Arabia

[5] Cancer and Mutagenesis Unit, King Fahd Centre for Medical Research, King Abdulaziz University, Jeddah, Saudi Arabia

[*] These authors are co-last authors

***Correspondence to**: Marc Mousli, **email**: marc.mousli@unistra.fr*

Keywords: cancer, biomarkers, epigenetics, UHRF1, DNA methylation

***Received**: February 03, 2017* ***Accepted**: April 02, 2017* ***Published**: April 24, 2017*

ABSTRACT

Cancer is one of the deadliest diseases in the world causing record number of mortalities in both developed and undeveloped countries. Despite a lot of advances and breakthroughs in the field of oncology still, it is very hard to diagnose and treat the cancers at early stages. Here in this review we analyze the potential of Ubiquitin-like containing PHD and Ring Finger domain 1 (UHRF1) as a universal biomarker for cancers. UHRF1 is an important epigenetic regulator maintaining DNA methylation and histone code in the cell. It is highly expressed in a variety of cancers and is a well-known oncogene that can disrupt the epigenetic code and override the senescence machinery. Many studies have validated UHRF1 as a powerful diagnostic and prognostic tool to differentially diagnose cancer, predict the therapeutic response and assess the risk of tumor progression and recurrence. Highly sensitive, non-invasive and cost effective approaches are therefore needed to assess the level of UHRF1 in patients, which can be deployed in diagnostic laboratories to detect cancer and monitor disease progression.

INTRODUCTION

In cancer, the prognosis of the disease is highly dependent on the type and location of the cancer along with the stage at which it is diagnosed. The survival rate and the treatment response is better if the cancer is diagnosed early when the tumor is localized and small. Nowadays many biomolecules and epigenetic patterns are being explored as "biomarkers" to help in early diagnosis of cancers along with currently employed techniques of imaging and cytology [1]. An ideal biomarker for cancer detection must be able to differentiate between normal and tumoral cells and it should be able to predict the malignant potential and prognosis of the disease.

All cells of a multicellular mammalian organism, except germinal cells, contain the same DNA in terms of nucleotide sequence. Considering the fact that DNA is the layer of heredity and cell identity, how can cell diversity and differentiation arise from the same DNA sequence is an important question challenging the scientific community. Epigenetics is the research field that tries to answer this question by deciphering a tremendous number of cellular mechanisms of gene regulation embedded in the chromatin but not related to changes in DNA sequences. In other words, it refers to external modifications of DNA that turn *genes* "on" or "off. At the molecular level, "off" means that the genes are silenced, by means of DNA methylation and histone methylation, *e.g.,* di- and tri-methylation of lysines 9 & 27 of histone H3 (H3K9me2, H3K9me3, H3K27me2, H3K27me3) as well as chromatin structure, micro RNA and histone variants [2-5]. However, gene expression does not function as a simple "on-off" dichotomy but rather through a complex language dictated by the degree of DNA methylation and a set of epigenetic

marks appearing on the N-terminal tails of histones present in the nucleosome [3]. This complex language allows the cell to express genes as a function of precise needs during cell cycle or during lifespan and no more or less than it is required for the cell to work adequately. This complex language is profoundly modified in various diseases, including cancer [3-5].

Indeed, cancer cells exhibit profound changes in epigenetic profiles, as much on the DNA methylation side as on histone code side [6]. Cancer cells undergo global DNA hypomethylation, whereas some regions, on the contrary, undergo hypermethylation, *e.g.* promoters of tumor suppressor genes [7, 8]. On the histone code versant, several modifications have been reported in various types of cancer [9].

There are increased evidences that DNA methylation appears as an ideal biomarker for various types of cancers [10-13]. DNA methylation in mammals preferentially occurs in a CpG context, meaning that both DNA strands are methylated in an asymmetrical manner, which represents one of the layers of epigenetic information. Methylation of cytosine is slightly mutagenic, explaining the loss of CpG sites in mammalian genomes during evolution. As a consequence, CpG sites in human genome are globally found 3–4 times less often than statistically expected, except in CpG islands, which are often located in gene promoters [2, 14].

The mechanism of inheritance of the methylation patterns is relatively well documented regarding DNA but is still elusive concerning histones, although several models are under investigation for definitive validation [15]. Duplication of DNA methylation patterns in a CpG context, is subjected to prior DNA replication generating hemi-methylated DNA, *i.e.,* only one DNA strand is methylated, a state that is specifically recognized by Ubiquitin-like containing PHD and Ring Finger domain protein 1 (UHRF1) [16-20]. The sensing of hemi-methylated DNA by UHRF1, induces the recruitment of DNA methyltransferase 1 (DNMT1) which methylates the opposite unmethylated DNA strand, and consequently CpG dinucleotides are methylated on both strands. Through these properties, the tandem UHRF1/DNMT1 plays a role during cell proliferation and therefore in development and cancer [21].

THE EPIGENETIC INTEGRATOR UHRF1

Structure of UHRF1

Among the different epigenetic modulators, UHRF1, which is also known as Inverted CCAAT box Binding Protein of 90 kDa (ICBP90) or nuclear protein of 95kDa (Np95) [22-24] has gained a considerable attention during the past few years because of its high expression in most of the cancers and its ability to link important epigenetic processes such as DNA methylation and histone modifications [25].

Initially, UHRF1 was identified as a transcription factor regulating the expression of topoisomerase IIα by binding to an inverted CCAAT box located in its promoter [22]. UHRF1 was further shown to critically participate in various epigenetic processes by its different structural domains (Figure 1). Indeed, UHRF1 is composed of an N-terminal ubiquitin-like domain that is coming before the tandem tudor domain (TTD) and plant homeodomain (PHD). These domains are followed by the unique set and ring associated (SRA) domain and the really interesting new gene (RING) finger domain at the C-terminus [25]. Except for the RING domain exhibiting an E3 ligase activity towards histone H3 on lysine 23 or on lysine 18, no further enzymatic activity has been so far identified for any of the other domains. Instead, interesting binding activities were identified for each domain conferring unique capacities of readout [26-28]. One key property of UHRF1 is its ability to sense the presence of hemi-methylated DNA at the replication fork, thanks to the SRA domain [19, 20]. Concomitantly, it can also sense the di- and tri- methylated lysine 9 of histone H3 (H3K9me2/H3K9me3) in the chromatin by help of its tandem tudor domain [29-31]. Association of UHRF1 with methylated H3K9 through TTD facilitates the maintenance of DNA methylation but primarily it is the SRA domain that recruits UHRF1 to hemi-methylated DNA [32]. Indeed, we have shown that the binding of SRA domain does not induce distortion of the DNA, which is in favor of a sliding behavior along the DNA seeking for hemi-methylated CpG sites and subsequent flipping of the methylated cytosine, thus facilitating the recruitment of DNMT1 [33, 34]. It has also been shown that UHRF1, through its SRA domain, is capable of recognizing hydroxymethylcytosine [35]. The relevance of this latter remains elusive but it might bring new insights in DNA methylation maintenance, once resolved.

Beside this role, UHRF1 is considered to play a pivotal role in the epigenetic inheritance as it coordinates the action of different chromatin modifying proteins [36]. It interacts, among many others, with DNA methyltransferases (DNMTs), proliferating cell nuclear antigen (PCNA), histone deacetylase 1 (HDAC1), ubiquitin specific protease 7 (USP7), euchromatic histone-lysine N methyltransferase 2 (G9a/EHMT2) and Tat Interacting Protein 60 (Tip60) to maintain DNA methylation patterns and histone epigenetic marks in various physiological and pathological conditions [18, 19, 37-42]. Together with its partners, UHRF1 ensures the regulation, through "silencing" of a high number of tumor suppressor genes and long non-coding RNAs, including *RB1* [43], *p16* (*CDKN2A)* [44-48], *CDH13* and *SHP1* [49], *SOCS3* and *3OST2* [50], *BRCA1* [51], *CDX2, RUNX3, FOXO4, PPARG* and *PML* [52, 53], *MEG3* [54]

and *14-3-3σ* [55]. Moreover, *KISS1*, functioning as a metastasis suppressor in various cancers, also looks to be under the control of UHRF1 [56]. Altogether, these studies highlight UHRF1 as a conductor of tumor suppressor gene silencing in cancers through a DNA methylation-dependent mechanism.

UHRF1 as a tumor promoter

UHRF1 is mostly expressed in proliferating cells, while it is not found in fully differentiated tissues [22]. Levels of UHRF1 expression positively co-relate with the proliferative potential of cells. In cancer cells, UHRF1 is overexpressed and promotes the proliferation and dedifferentiation of cells [22]. In non-cancerous proliferating cells, UHRF1 expression is cell cycle regulated and peaks in late G1 and G2/M phase, while in cancerous cells, UHRF1 is continuously expressed at all stages of cell cycle [57]. UHRF1 is considered to be essential for G1/S phase transition as its depletion or down-regulation by activation of p53/p21$^{Cip1/WAF1}$ dependent DNA damage response leads to cell cycle arrest at the G1/S phase transition [58, 59]. Similarly, in another study it has been reported that depletion of UHRF1 in HCT116 cells leads to the activation of DNA damage response with subsequent cell cycle arrest at G2/M phase and induction of caspase 8-dependent apoptosis [60]. Conversely, overexpression of UHRF1 in human fibroblasts or its orthologue Np95 in terminally differentiated mouse myotubes facilitates the entry of these cells in S-phase and induces cell proliferation [43, 58].The possibility that UHRF1 behaves as an oncogene has been questioned for a while [61]. However, it is now clearly demonstrated through a recent series of studies that UHRF1 is a tumor promoter. Indeed, it was shown that overexpressed UHRF1 causes DNA hypomethylation, a hallmark of cancer cells; instead of normal maintenance of DNA methylation. Overexpressed UHRF1, through its E3 ligase activity, ubiquitinylates DNMT1 and DNMT3. Thus, by destabilizing and delocalizing them, UHRF1 induces global DNA hypomethylation [62, 63].

Several studies have also revealed that disruption of UHRF1 function results in hypersensitivity to DNA damage [64-69] supporting the idea that UHRF1 plays a critical role in the maintenance of genome stability. This is not surprising, considering that a native protein has first a physiological role before a deleterious role. The deleterious role is coming from an abnormal level of UHRF1 rather than from its function itself.

The abnormally high level of UHRF1 may result from the aberrant activity of various transcription factors regulating the expression of UHRF1 in cancers (Figure 2). E2F transcription factor 1 (E2F1) and E2F transcription factor 8 (E2F8) are upregulated in many cancers and stimulate *UHRF1* expression by directly binding to different sites in its promoter region [37, 57, 70]. Specificity protein 1 (SP1) and Forkhead Box M1 (FOXM1) also potentiate UHRF1 expression in different cancers [71, 72]. Repression of SP1 activity by T3 receptor pathway activation downregulates UHRF1, relieves p21 from UHRF1-mediated silencing and induces cell cycle arrest at G0/G1 phase in liver cancer cells [71]. Similarly, our recent study suggests that activation of highly expressed membrane integrin CD47 in astrocytoma activates NFκB-mediated signaling and UHRF1 expression, which in turn represses p16, thereby strengthening the tumor promoter role of UHRF1 [48]. High UHRF1 levels are also attributed to downregulation of its epigenetic regulator H3K9 methyltransferase (G9a) in various cancers which works along with Yin Yang transcription factor 1 (YY1) as negative upstream regulator of UHRF1 [73].

Besides increased expression of *UHRF1*, increased stability of *UHRF1 mRNA* through down-regulation of regulatory micro RNAs and increased stability of UHRF1 protein also contribute to abnormal high levels of UHRF1 in different cancers (Figure 2) [8, 74-79]. UHRF1 protein levels are controlled in normal cells by coordination of ubiquitinylating and deubiquitinylating enzymes which

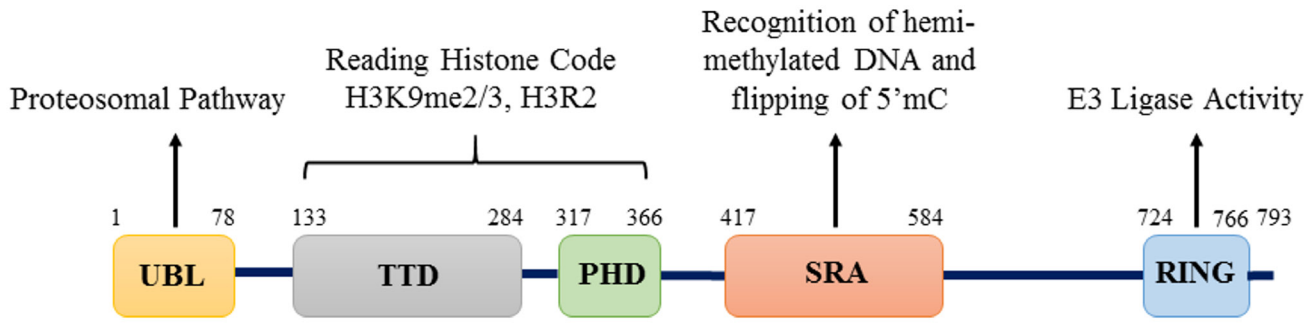

Figure 1: Structure of UHRF1 protein. Structure of UHRF1 protein showing the different domains and their functions. The protein contains 793 amino acids and five major domains: UBL (ubiquitin-like) domain, TTD (Tandem Tudor Domain), PHD (Plant Homeodomain), SRA (Set and Ring Associated) domain and RING (Really Interesting New Gene) domain.

regulate its proteosomal degradation (Figure 2). $SCF^{\beta\text{-}TrCP}$ E3 ligase or intrinsic activity of UHRF1 RING domain can induce degradation of UHRF1 by ubiquitinylation [26, 65]. Phosphorylation of serine residue at 108 by casein kinase 1δ helps $SCF^{\beta\text{-}TrCP}$ E3 ligase to recognize and ubiquitinate UHRF1 for degradation [65]. On the other hand, UHRF1 is stabilized and recruited to chromatin by its association with deubiquitinating enzyme USP7. M phase specific kinase CDK1-cyclin B which phosphorylates UHRF1 at serine 652 in the interacting region of USP7 can disrupt this association and lead to degradation of UHRF1 [40, 80]. Considering that USP7 is upregulated in many cancers, this might be one of the possible reason for high levels of UHRF1 in cancer cells [81-83]. UHRF1 is also stabilized by its interaction with long noncoding RNA UPAT (UHRF1 Protein Associated Transcript), which promotes colon tumorigenesis through inhibition of UHRF1 degradation [84]. Pharmacological inhibition of heat shock protein (HSP90) also destabilizes UHRF1 and suppress cancer cell proliferation predicting a role of HSP90 in UHRF1 turnover [85]. Altogether these events result in abnormal high level of UHRF1 in cancers which appears now to be exploitable as a biomarker.

We will now review the potential of UHRF1 to fulfil the features of a biomarker in various types of cancer.

UHRF1 EXPRESSION IN DIFFERENT CANCERS

UHRF1 in lung cancer

Lung cancer is the most common and fatal among different types of cancers with an average 5-year survival rate of around 15% [86]. According to latest data, over 1.8 million new cases of lung cancer were reported worldwide in 2012, while in the same year the death toll of lung cancer was around 1.59 million [86]. High smoking incidences and late diagnosis of cancer are major factors contributing to its high mortality rate. Various novel proteins are now being investigated, in search of a superior biomarker and

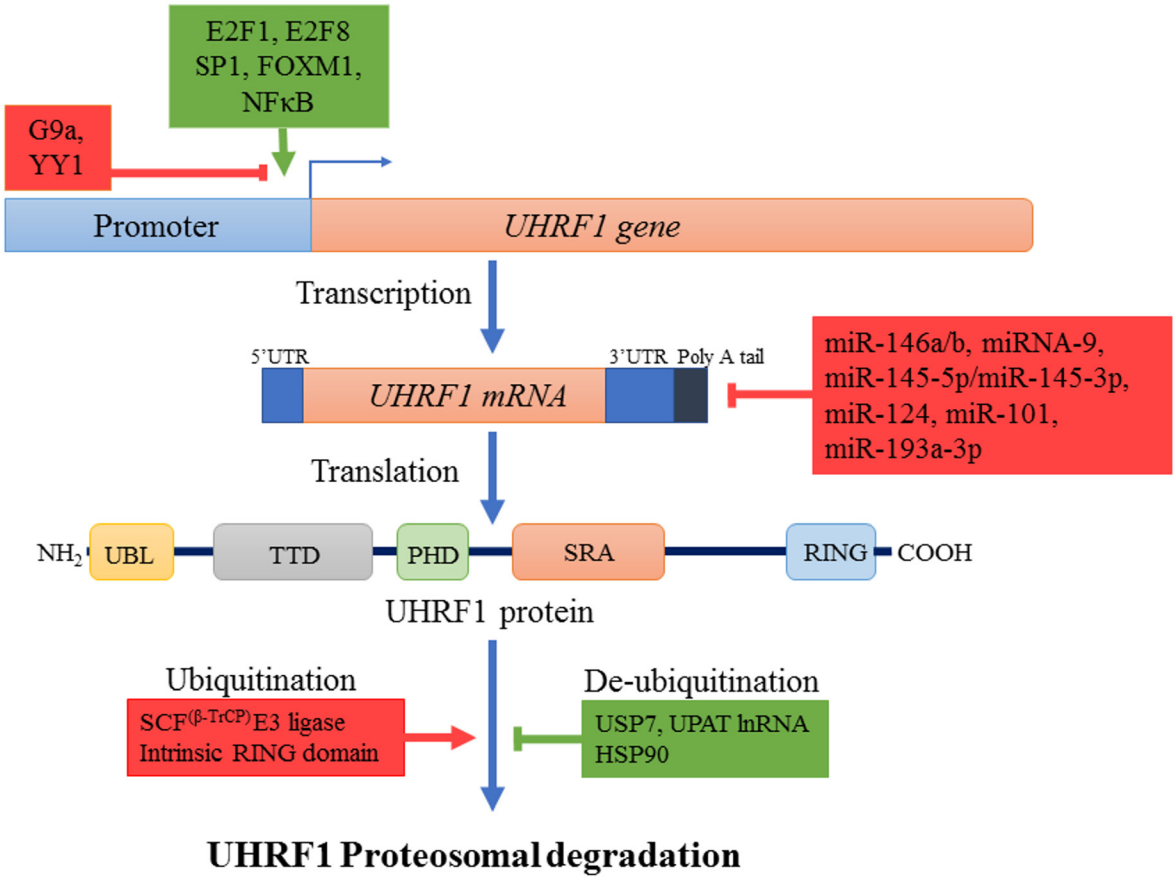

Figure 2: Regulation mechanisms of UHRF1. Different transcription factors like E2F1, E2F8, Sp1, FOXM1, NFκB (indicated in green) enhance while others such as YY1 along with lysine methyl transferase G9a (indicated in red) repress the expression of *UHRF1* at transcription level. Many small non-coding microRNAs also decrease *UHRF1* expression by destabilizing *UHRF1 mRNA* through binding to 3'UTR region. UHRF1 protein is degraded by proteosomal pathway after autoubiquitinylation or ubiquitinylation by $SCF^{\beta\text{-}TrCP}$ E3 ligase. Ubiquitinylated UHRF1 is stabilized in cells by USP7, HSP90 or UPAT lnRNA. Increased transcription factor expression, downregulation of miRNAs and increased levels of stabilizing factors (all indicated in green) result in overexpression of UHRF1.

among them UHRF1 has shown encouraging results. Immunohistochemistry (IHC) analysis of 322 lung cancer tissues from Japan and 56 samples from US, revealed an overexpression of UHRF1 in all histological types of non-small cell lung cancer (NSCLC) especially in non-adenocarcinomas [87]. Transcript analysis of samples also showed marked increase of UHRF1 mRNA in 70% of lung cancer cases. As enhanced expression significantly correlated with the advanced stages and malignancy of the cancer, authors proposed UHRF1 as a prognostic biomarker for lung cancer [87]. Similarly, a recent study in Taiwan has predicted a six-gene signature including *ABCC4*, *ADRBK2*, *KLHL23*, *PDS5A*, *UHRF1* and *ZNF551* as better prognostic marker in NSCLC for overall survival time and treatment outcome [88].

UHRF1 overexpression was also confirmed in another study including 105 NSCLC tissues (55 adenocarcinomas and 50 squamous cell carcinomas) along with DNMT1, DNMT3A and DNMT3B [89]. This overexpression resulted in silencing of tumor suppressor genes such as *RASSF1* and *p16*, via promoter hypermethylation in 32.4% and 26% of cases, respectively. Accordingly, in a cell model of lung cancer, knockdown of UHRF1 in A549 cells prevented the tumor suppressor genes *RASSF1*, *CYGB*, and *CDH13* promoters from hypermethylation [89].

UHRF1 in liver cancer

Hepatocellular carcinoma (HCC) is one of the most prevalent cancers with multiple etiological factors and is the second leading cause of cancer related deaths worldwide [86]. So far, many studies have been carried out to understand the complex nature and poor prognosis of this disease but it is still elusive. A recent study reported overexpression of UHRF1 in HCC of various etiologies and described UHRF1 as an oncogene, that drives global DNA hypomethylation by delocalizing DNMT1 [62]. In this study, expression of UHRF1 was assessed in 109 human HCC cases by qPCR and results revealed abnormally high expression of UHRF1 (averagely 2-fold higher than normal) in 95.41% (104/109) of the cases [62]. UHRF1 protein levels in samples were also in accordance with mRNA levels and were found significantly higher in 73% of tumors but were barely detectable in normal tissue

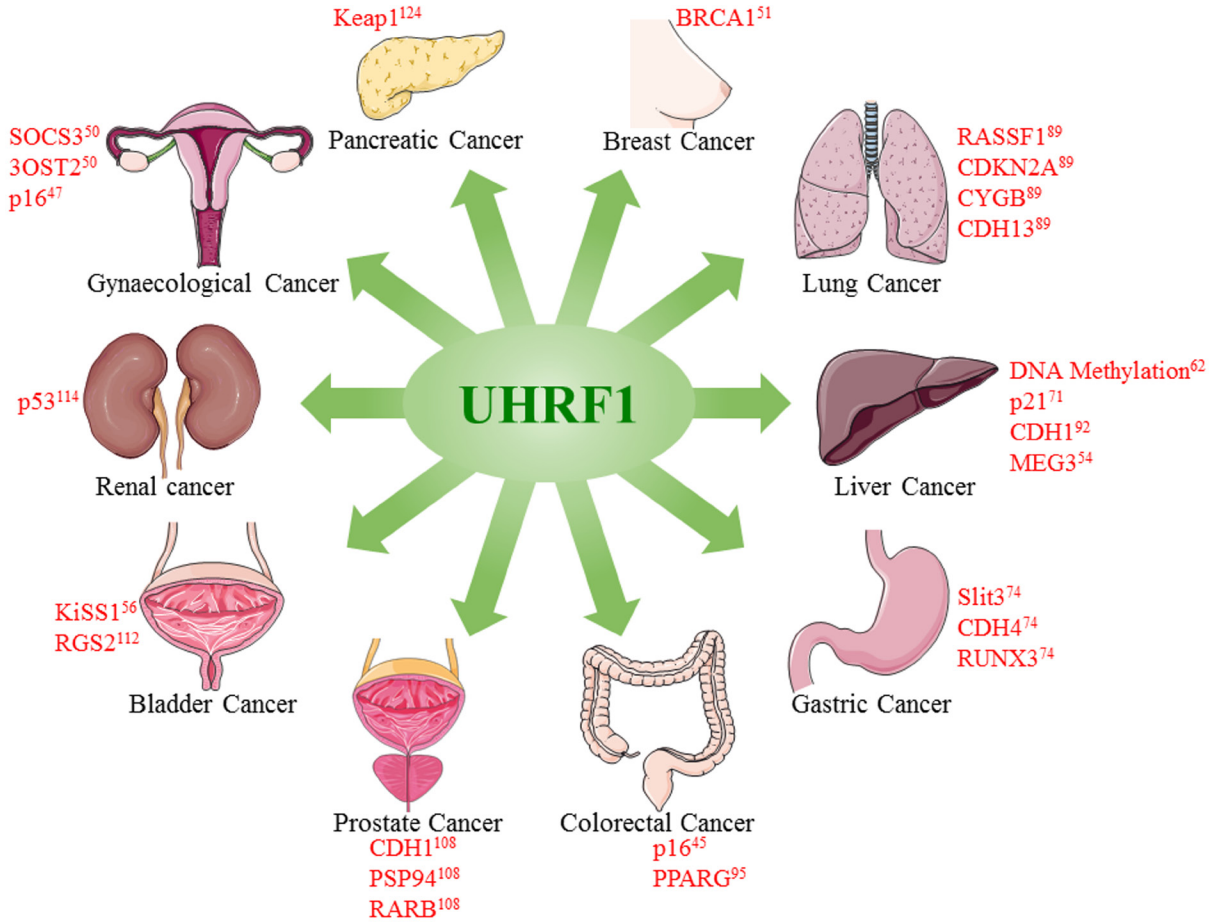

Figure 3: Overexpression of UHRF1 promotes tumorigenesis in different cancers. UHRF1 overexpression leads to epigenetic abnormalities including DNA methylation and downregulation of tumor suppressor genes or lnRNAs. Figure is made using images taken with permission from Servier Medical Arts http://servier.com/Powerpoint-image-bank.

samples [62]. Tumors with higher expression of UHRF1 also had poor prognosis with higher recurrence rate, alpha fetoprotein, microvascular invasion and lower survival rate emphasizing the diagnostic and prognostic potential of UHRF1 in HCC [62]. Similarly, high levels of UHRF1 mRNA were reported in 160 HCC patients notably during later stages II & III of cancer [71]. UHRF1 protein level were also significantly upregulated in 75.7% (52 of 70) of samples when analyzed by western blot [71]. Results were further confirmed by immunohistochemistry analysis of 136 HCC tissue samples which showed high expression of UHRF1 in tumor samples, positively correlating with tumor size, fetoprotein levels and HBV infection [71]. The diagnostic and prognostic capacities of UHRF1, as a novel biomarker in HCC, were also highlighted by a study on Chinese population including 68 HCC specimens [90]. In this study, significantly higher levels of UHRF1 were found in HCC samples by HPLC compared with the adjacent non-cancerous tissues. Of note, the levels of UHRF1 correlated with distant metastasis, tumor area and HBV [90]. Furthermore, elevated levels of UHRF1 also predicted poor prognosis as after 5 years of follow up, the survival rate in high UHRF1 expression group was 29.8% as compared with 81% in low UHRF1 expression group [90]. Another group also reported similar findings where UHRF1 mRNA expression was found significantly increased in 67% (54/80, $P < 0.05$) of HCC specimens [91]. Immunohistochemical staining of 102 pairs of HCC samples included in study also revealed significantly higher staining of UHRF1 protein in cancerous tissues (57.8% vs 32.7%) when compared to non-cancerous tissue. Like previous studies, overexpression of UHRF1 positively correlated with tumor size, staging and poor survival rate of patients [92].

On a cellular aspect, knockdown of UHRF1 inhibited the tumor growth *in vivo* and *in vitro* and induced cell cycle arrest at G2/M phase confirming the oncogenic potential of UHRF1. Targeting of UHRF1 also decreased the migration and invasion of cancer cells by hampering endothelial to mesenchymal transition (EMT) as evidenced by up regulation of (EMT opposing) E-cadherin and down regulation of (EMT favoring) β-catenin, vimentin, N-cadherin and snail in UHRF1 knockdown cells [92]. Overexpression of UHRF1 in hepatocellular carcinoma also negatively regulated the levels of tumor suppressive long non-coding RNA maternally expressed gene 3 (MEG3) via promoter hypermethylation which exerts its tumor suppressive role by induction of p53 [54, 93].

UHRF1 in gastric cancer

Gastric cancer is one of the most fatal cancers among all malignant diseases, and is accounted for approximately 723,000 world-wide deaths each year. Eastern Asian countries like China, Japan, Taiwan and Philippines have higher incidences of gastric cancer as compared with western countries [86]. In 2013, a study reported high levels of UHRF1 in gastric cancers and explored miR-146a/b mediated regulation of UHRF1 as a novel therapeutic approach in preventing metastasis and treating such cancers [74]. Immunohistochemistry staining of 106 gastric tumors revealed higher expression of UHRF1 in cancer tissues compared with adjacent normal tissues, which correlated with poor differentiation, cancer staging, increased lymph node and tissue metastasis [74]. Kaplan-Meier analysis showed that patients with higher expression of UHRF1 had poor prognosis and shorter overall survival time as compared with patients having relatively lower expression of UHRF1, suggesting abnormal high levels of UHRF1 as independent diagnostic and prognostic marker for gastric cancer [74].

At the cellular level, overexpression of UHRF1 was observed in aggressive gastric cancer cell lines (GC9811-P and MKN28M), which has been suggested to enhance the proliferating capacity of these cells [74]. Reduced levels of UHRF1, induced by miR-146a/b, reactivated tumor suppressor genes like *SLIT3*, *CDH4*, and *RUNX3* via promoter hypomethylation [74]. Consistently, with this notion, same authors further explored the prognostic value of UHRF1 expression in a study including 238 gastric cancer patients [52]. Immunohistochemistry labelling for UHRF1 was found positive in 82% of samples and significantly correlated with poor differentiation and metastasis. Indeed, patients with higher expression of UHRF1 had a very low 5-year survival rate of 19% as compared to patients with negative (38%) or low expression of UHRF1 (30%) suggesting UHRF1 as a significant predictor of gastric cancer prognosis [52].

UHRF1 in colorectal cancer

Epigenetic silencing of tumor suppressor genes via promoter hypermethylation is commonly reported besides the genetic aberrations in colorectal carcinogenesis and many mechanisms have been proposed for this deregulation. UHRF1 overexpression in colorectal cancer has been observed in several studies and is considered to be involved in promoter hypermethylation mediated repression of TSGs [7, 8, 94]. Wang *et al* first reported the overexpression of UHRF1 in colorectal cancer and suggested its use as a biomarker and a possible therapeutic target for diagnosis and treatment of colorectal cancer [45]. The authors observed a significantly increased UHRF1 expression at both transcriptomic and proteomic levels in colon cancer tissues and found positive association of this overexpression with metastasis, poor clinical staging and *p16* silencing [45]. Overexpression of UHRF1 was also observed in LoVo, DLD1, SW480 and SW620 colon cancer cell lines. Inhibition of UHRF1 in these cells led to upregulation of *p16*, decreased proliferation and migration capacity, as well as cell cycle arrest at G0/G1 and apoptosis [45]. Similarly, in colorectal cells,

overexpressed UHRF1 negatively regulated peroxisome proliferator-activated receptor gamma *(PPARG),* through epigenetic-dependent mechanisms [95]. The consequences were increased endothelial to mesenchymal transition (EMT), growth and cell viability. Furthermore, prognostic values were more significant when both UHRF1 overexpression and PPARG down-regulation were taken into account [95]. Another study in which 231 colorectal cancer tissues and 40 adenoma specimens were analyzed for UHRF1 levels reported similar results [96]. Indeed, immunohistochemistry showed high expression of UHRF1 in the nucleus of 65.8% (152/231) colorectal cancer tissues and of 87.5% (35/40) adenoma samples while little or no expression was found in normal colonic mucosa [96]. Expression of UHRF1 positively correlated with the depth of invasion and E2F-1 levels [96]. So far it is not yet clear why UHRF1 is up-regulated in cancer but some interesting leads are emerging. For instance, an inverse relationship between the levels of UHRF1 and the regulatory miRNA-9 has been reported in colorectal cells, for which high levels of UHRF1 are associated with poor survival rate of patients [75].

UHRF1 in breast cancer

Like for other cancers, many studies have reported the association of UHRF1 with breast cancer which is one of the leading causes of cancer related deaths in women world-wide, killing around 0.5 million women each year [86]. In 2003, we first reported increased expression of UHRF1 in breast cancer tissues and found a relationship between its expression and pathological grade of cancer [57]. Later UHRF1 overexpression in breast cancer patients was reported by cDNA microarray and qRT-PCR [37]. Overexpressed UHRF1 was further confirmed by the immunohistochemical staining and correlated with poor differentiation of tumors [37]. Recently, a study has investigated UHRF1 as a diagnostic and prognostic marker for breast cancer [97]. In this study, 62 tissue samples were analyzed and compared with 24 adjacent non-cancerous tissues. Higher expression of UHRF1 was observed at both mRNA and protein level in cancerous tissues which significantly correlated with stage of disease and c-erb2 status but was independent of age, menopause, estrogen and progesterone receptor levels [97].

The origin of the enhanced UHRF1 expression in breast cancer remains elusive in contrast to the down-stream events. Notably, increased expression of UHRF1 in breast cancers is believed to aggravate the pathogenesis by silencing *BRCA1* and modulating the estrogen receptor-α expression [51, 98]. UHRF1 overexpression also increased the proliferation and migration potential of breast cancer cells as exogenous expression of UHRF1 in MDA-MB-231 breast cancer cells facilitated their passage through the cell cycle by induction of cyclin D1 and prevention of apoptosis [99]. UHRF1 also confers radioresistance to breast cancer cells by promoting the expression of DNA damage repair proteins Lupus Ku autoantigen protein p70 (Ku-70) and Lupus Ku autoantigen protein p80 (Ku-80) repairing the chromosomal aberrations and also by down-regulating the expression of BAX and other pro-apoptotic proteins [100]. Similarly, it has been observed that specific inhibition of UHRF1, by mRNA targeting, decreased the oncogenic capacity in breast cancer cells and increased their sensitivity to chemotherapy [101, 102].

UHRF1 in gynecological tumors

UHRF1 expression in cervical cancer is also a good indicator for cellular proliferation and malignancy. Notably, an analysis of 99 cervical biopsies showed UHRF1 as a useful biomarker to discriminate low grade intraepithelial lesions from normal tissues with a sensitivity of 71.4% and to discriminate low grade intraepithelial lesions from high grade intraepithelial lesions with a sensitivity of 97.6% [103]. Another study on cervical squamous cell carcinoma (CSCC) also reported high expression of UHRF1 at both mRNA and protein level in 47 samples and found that silencing of UHRF1 in cervical cancer cells inhibited cell proliferation and induced apoptosis [104]. The reasons why UHRF1 is overexpressed in cervical cancer, is still not yet elucidated and again it is rather the downstream events that have been deciphered in cellular models. Indeed, polyphenolic extracts from plant sources were found to downregulate UHRF1 in the cervical cancer HeLa cell line [47]. This in turn upregulated the tumor suppressor gene *p16* and ultimately halted the progression of the cell cycle and induced apoptosis [47]. Moreover, UHRF1 overexpression in HeLa cells was shown to decrease their radio-sensitivity to γ-radiation by increasing the expression of the DNA repair proteins XRCC4, thus, enhancing the capability of these cells to repair the DNA damaged by radiation [105]. It is remarkable to notice that a paradigm is emerging concerning the decreased sensitivity of cancer cells to chemotherapy through control of the DNA repair machinery by UHRF1.

Besides cervical cancer, the diagnostic and prognostic capabilities of UHRF1 as biomarker have also been evaluated in ovarian cancer, which is the major worldwide contributor in gynecological tumors posing serious threat to the life of women. In a study including 80 samples from ovarian cancer tissues, significantly higher expression of UHRF1 was found at both transcriptomic and protein levels in tumors as compared with adjacent normal tissues. Knockdown of UHRF1 in ovarian cancer cells inhibited their proliferation and induced apoptosis, suggesting UHRF1 as a general indicator of malignancy and an attractive therapeutic target for ovarian cancers [106].

UHRF1 in prostate cancer

Prostate cancer undergoes profound epigenetic modifications via aberrant DNA methylation and histone post-translational modifications resulting in silencing of tumor suppressor genes [107]. Expression analysis by immunohistochemistry in tissue microarrays of 226 prostate tumor samples revealed significant overexpression of UHRF1 in almost half of tissue samples [108]. This overexpression correlated with poor clinical prognosis as patients with high expression of UHRF1 had reduced median survival rates (10.4 years) as compared to patients with low expression of UHRF1 (12.4 years) [108]. Recently Wan *et al* reported similar results after analyzing expression of UHRF1 in 225 prostate cancer specimens [109]. UHRF1 staining was found in 47.1% of specimens which positively correlated with the Gleason score and the pathological stage of the disease [109]. Patients with higher levels of UHRF1 were found to be at higher risk for biochemical recurrence after radical prostatectomy. Mean biochemical recurrence (BCR) free time in UHRF1-positive patients was around 23.0 months versus 38.9 months in UHRF1-negative patients while 5-year BCR-free survival rate was 12.4% in UHRF1-positive patients as compared with 51.8% in UHRF1-negative patients. These results support UHRF1 as a valuable independent prognostic factor to predict prostate cancer outcome after radical prostatectomy [109].

At the cellular level, overexpression of UHRF1 has also been reported in aggressively proliferating, androgen-independent cell lines of prostate cancer (DU145 and PC3), while low expression of UHRF1 was found in immortalized normal prostate epithelial cells (LHS) or androgen-dependent prostate adenocarcinoma cells with low metastatic potential (LNCaP and 22Rv1 cells) [108, 109]. Overexpression of UHRF1 accompanied with downregulation of tumor suppressor genes and increased expression of EZH2 (H3K27 methyltransferase) in prostate cancer cells contributed to the poor clinical prognosis and lethal progression disease. UHRF1 also recruited SUV39H1 (H3K9 methyltransferase) and DNMTs to the promoter region of many tumor suppressor genes *(CDH1, PSP94, RARB)* resulting in increased methylation of histones and DNA with subsequent silencing of TSGs [108]. Altogether these results suggest that UHRF1 may serve as a useful biomarker and therapeutic target for prostate cancer as it plays an important role in epigenetic silencing of TSGs via histone and DNA modifications

UHRF1 in bladder cancer

UHRF1 has also been described as a 'novel' diagnostic and prognostic marker for the bladder cancer, which is the second most common cancer of the urinary system [110]. Expression of UHRF1 was found significantly increased in the cancer cells and was positively correlated with histological and pathological grade, as higher expression was observed in later stages of cancer. Increased expression of UHRF1 was also associated with poor prognosis of disease as patients having higher levels of UHRF1 had poor survival rate and higher recurrence [110]. UHRF1 levels evaluated by qRT-PCR or immunohistochemistry based detection methods in surgical sections showed UHRF1 as a specific and sensitive biomarker for bladder cancer. Significantly higher levels of UHRF1 were detectable in specimens with non-invasive or superficially invasive cancers at very early stages compared to normal cells [110]. Similarly, in non-muscle-invasive bladder cancer (NMIBC) increased expression of UHRF1 was found in cancer cells, which was directly related with tumor malignancy [111]. Indeed, patients with UHRF1 overexpression had shorter survival duration (mean survival time 42.59 months) and higher incidences of recurrence (41 out of 70 cases) as compared with patients with relatively lower expression of UHRF1, who had greater survival time (mean survival time 71.36 months) and lower chances of recurrence (29 out of 70 cases) [111]. This suggests UHRF1 as an independent prognostic marker for the bladder cancers.

Other studies reported similar overexpression of UHRF1 in bladder cancers and in invasive cell lines, such as 253J, T24, KU7, along with silencing of tumor suppressor genes *e.g., KISS1* and *RGS2* [56, 112, 113]. Altogether, these studies emphasize UHRF1 as an attractive biomarker and therapeutic target for bladder cancers.

UHRF1 in renal cancer

Each year 338,000 new cases of kidney cancers, with a majority of renal cell carcinomas (RCC) are reported worldwide with a high prevalence in developed countries [86]. First evidence of UHRF1 overexpression in kidney tumors has been reported by Unoki *et al* [110]. By investigating mRNA levels, UHRF1 overexpression was found to be associated with several characteristics of kidney tumor patients, including 5-year survival rates, pathological staging and histological grade [110]. Later Ma *et al* found elevated levels of UHRF1 mRNA in 70% of RCC cases [114]. Overexpression was further confirmed by staining of UHRF1 in histological samples, which showed 74.2 % positive staining in RCC carcinoma tissues [114]. Similarly, UHRF1 overexpression, in metastatic renal cancer tissues as compared with non-metastatic tissues, correlated with downregulation of non-coding miR-146a-5p, which targets UHRF1 transcription [115]. However, another miRNA might also be involved in UHRF1 overexpression in RCC. Indeed, miRNA-101 has also been shown to regulate UHRF1 expression since its downregulation leads to UHRF1 upregulation [78]. Interestingly, in this study UHRF1 overexpression

was confirmed in sunitinib-treated RCC tissues and was associated with shorter overall survival after surgery for RCC [78].

UHRF1 in other cancers

Few studies have also predicted UHRF1 as a diagnostic and prognostic marker for various other types of cancers. Representational difference analysis (RDA) of different pathological grades of astrocytoma revealed *UHRF1* and four other genes to be differentially expressed in astrocytoma cancer tissues [116]. Results were confirmed by qPCR analysis in which 7 normal brain tissues, 9 grade I (pilocytic astrocytoma), 9 grade II (low grade astrocytoma), 11 grade III (anaplastic astrocytoma), and 22 grade IV (glioblastoma multiforme) samples were analyzed. Significant overexpression of UHRF1 was observed in cancerous tissues as compared with normal cells showing the possibility to use this differential expression of UHRF1 as a diagnostic marker for astrocytoma [116].

The diagnostic and prognostic value of UHRF1 has also been evaluated in medulloblastoma, a common malignant brain tumor. Out of 168 formalin-fixed, paraffin-embedded medulloblastoma, high levels of UHRF1 were found in 108 cases while lower expression of UHRF1 was observed in the remaining 60 samples, whilst normal cerebellum tissue samples lacked UHRF1 staining [117]. Kaplan–Meier survival analysis showed that patients with high levels of UHRF1 had poor overall survival and progression free survival rate illustrating UHRF1 as a potential independent prognostic marker for medulloblastoma [117].

UHRF1 has also been proposed as a biomarker and potential therapeutic target for gallbladder cancer, which is well known for its poor prognosis and high mortality rate [118]. Immunohistochemical results showed UHRF1-positive staining in 63.2% of cancerous tissue samples [118]. UHRF1 was overexpressed in cancerous tissues and correlated with the advanced stage and lymph node metastasis. Enhanced expression of UHRF1 was also observed at both mRNA and protein level in GBC-SD and NOZ cell lines and depletion of UHRF1 by siRNA or shRNA markedly reduced their migration potential *in vitro* and tumor forming capabilities [118]. Interestingly, knockdown of UHRF1 promoted the expression of *promyelocytic leukemia protein* (PML) and *p21* (*CDKN1A)* tumor suppressor genes, resulting in cell cycle arrest at G1 [118]. UHRF1 depletion also induced apoptosis in these cells by activating both intrinsic and extrinsic pathways for apoptosis, in accordance with previous studies suggesting that UHRF1 exhibits anti-apoptotic properties [119]. All this information suggests an oncogenic role of UHRF1 in gallbladder cancer and increased expression of UHRF1 as an independent biomarker for diagnosis and a therapeutic target of gallbladder cancers.

Correlation of UHRF1 expression with tumorigenesis has also been demonstrated in laryngeal squamous cell carcinomas (LSCC), through analysis of 60 LSCC samples [120]. UHRF1 overexpression was found in 78.3% (47/60) of cancer tissue samples, whereas remaining 13 samples had relatively lower expression of UHRF1 and in normal tissues, UHRF1 expression was barely detectable [120]. UHRF1 overexpression also correlated with the histological and pathological stages of cancer and was found in undifferentiated cells in advanced stages of cancer [120].

Similar findings were reported in esophageal squamous cell carcinoma (ESCC) where increased expression of UHRF1 was observed in 67% of human ESCC samples and overexpression positively correlated with advanced pathological and histological stages of the cancer, poor differentiation and lymph node metastasis [121]. Accordingly, overexpressed UHRF1 was also related to the radiotherapy resistance in patients with ESCC. Furthermore, results were validated by lentivirus mediated targeting of UHRF1 by shRNA in a TE-1 cell line inducing radio-sensitivity and apoptosis in ESCC derived cell line [121]. Another cohort study of 160 ESCC patients demonstrated that UHRF1 is as an attractive prognostic marker and potential target for cancer therapy as high levels of UHRF1 corresponded to poor survival rate [122].

High levels of UHRF1 have also been reported in several studies on pancreatic cancer, supporting the use of UHRF1 as a diagnostic marker for pancreatic cancer. For instance, power blot assay identified UHRF1 among differentially expressed proteins in pancreatic adenocarcinoma, which is extremely aggressive and difficult to diagnose with survival rate of less than 5% in five years [123]. Moreover, UHRF1 was selectively overexpressed in pancreatic adenocarcinoma tissues while it was not detectable in normal pancreatic tissue or chronic pancreatitis specimens [123]. UHRF1 overexpression was found at both proteomic and transcriptomic level in 80% of pancreatic ductal adenosarcoma cases and high UHRF1 levels correlated with neoplastic grade and lesion [123]. Similarly, UHRF1 overexpression was observed in 86% (114 of 132) of malignant pancreatic tumors samples [124] and 158 pancreatic cancer samples [125]. Furthermore, high UHRF1 levels positively correlated with short survival time of patients [124, 125]. All these results suggest UHRF1 as a valuable independent diagnostic marker for pancreatic cancer in clinical settings.

Similar findings were reported in thyroid cancers cells as microarray analysis showed significant upregulation of UHRF1 to identify gene expression profile that favors the progression of well differentiated tumors to aggressive, poorly differentiated or undifferentiated cancer cells [126]. UHRF1 levels were significantly higher in both differentiated and poorly differentiated cancer cells as compared with normal cells, suggesting a good

Table 1: Summary of studies describing diagnostic and prognostic potential of UHRF1 in various cancers

Cancer	Methods	Potential of UHRF1	Downregulated TSGs	Reference
Lung Cancer	qRT-PCR, IHC	UHRF1 overexpression relates to tumor stages, metastasis and poor prognosis.	*RASSF1, p16, CYGB CDH13*	[87-89]
Liver Cancer	qRT-PCR, IHC, Immunoblot assay, HPLC	UHRF1 overexpression relates to tumor size, metastasis, α-fetoprotein, relapse and short survival time.	*p21, CDH1, MEG3*	[54, 62, 71, 90-92]
Gastric Cancer	qRT-PCR, IHC	UHRF1 overexpression relates to poor differentiation, tumor stages, metastasis and low survival rate.	*SLIT3, CDH4, RUNX3, p16, FOXO4, PPARG, BRCA1, PML*	[52, 74]
Colorectal Cancer	qRT-PCR, IHC	UHRF1 overexpression relates to metastasis, tumor stage, E2F1 levels and poor survival rate.	*p16, PPARG*	[45, 75, 95, 96]
Breast Cancer	qPCR, Western Blot, IHC	UHRF1 overexpression relates to tumor stages, low survival rate and resistance to radiotherapy.	*BRCA1*	[37, 51, 97, 100]
Cervical Cancer	qRT-PCR, Western Blot, IHC	UHRF1 overexpression relates to tumor stages, poor prognosis and resistance to radiotherapy.	*p16*	[47, 103-105]
Ovarian Cancer	qRT-PCR, Western Blot	UHRF1 overexpression relates to progression of cancer.		[106]
Prostate Cancer	qRT-PCR IHC	UHRF1 overexpression relates to high Gleason score, tumor stages, recurrence and low survival rate.	*CDH1, PSP94, RARB*	[107-109]
Bladder Cancer	qRT-PCR, IHC	UHRF1 overexpression relates to tumor stages, risk of recurrence and low survival rate.	*KISS1, RGS2*	[56, 76, 77, 110-113]
Renal Cell Carcinoma	qRT-PCR, Western Blot, IHC	UHRF1 overexpression relates to tumor stages of cancer, drug (sunitinib) resistance and low survival rate	*p53*	[78, 114, 115]
Astrocytoma	RDA, qRT-PCR	UHRF1 overexpression relates to stages of cancer.		[116]
Medulloblastoma	IHC	UHRF1 overexpression relates to shorter survival and progression free time.		[117]
Gall Bladder Carcinoma	qRT-PCR, Western Blot, IHC	UHRF1 overexpression relates to tumor stages and lymph node metastasis.	*PML, p21*	[118]
Laryngeal Squamous Cell Carcinoma	qRT-PCR, IHC	UHRF1 overexpression relates to tumor stages, metastasis and low survival rate.		[120]
Esophageal Squamous Cell Carcinoma	qRT-PCR, IHC	UHRF1 overexpression relates to poor differentiation, pathological stage, low survival rate and resistance to radiotherapy.		[121, 122]
Pancreatic Carcinoma	qRT-PCR, IHC	UHRF1 overexpression relates to tumor size, metastasis, stages of cancer and low survival rate.	*RASSF1, p16, KEAP1*	[123-125]
Thyroid Cancer	qRT-PCR, IHC	UHRF1 overexpression relates to tumor stage.		[126, 127]

Abbreviations: qRT-PCR: quantitative reverse-transcriptase polymerase chain reaction; IHC: immunohistochemistry; RDA: representational difference analysis

diagnostic value for UHRF1 in thyroid cancers [126]. These results were in agreement with another study in a Chinese population showing high expression of UHRF1 in poorly differentiated anaplastic thyroid cancer cells versus papillary thyroid cancer and normal cells [127]. Targeting UHRF1 in these cells resulted in suppression of dedifferentiation and stem cell marker expression such as CD97, SOX2, OCT4 and NANOG, highlighting UHRF1 as an attractive target for thyroid cancer therapy [127].

CONCLUSIONANDFUTUREDIRECTIONS

UHRF1 overexpression is found in majority, if not all, of cancers, thus predicting UHRF1 as an independent universal diagnostic and prognostic biomarker for cancer detection, disease progression and therapeutic response monitoring (Table 1). High UHRF1 mRNA and protein levels are detected in early stages of many tumors suggesting UHRF1 as a valuable diagnostic marker for the timely detection of cancers. It is also employed to predict the prognosis of cancer as high level of UHRF1 is generally correlated to poor survival rate, resistance to therapy and recurrence of malignancy.

UHRF1 levels have been well correlated with Ki67 and PCNA which are widely used proliferation markers in cancers [52, 95, 104]. However, UHRF1 overexpression is a better diagnosis and prognostic biomarker in cancers as compared with Ki67 and PCNA since it fulfills the requirement of an independent factor. However, so far no universal biomarker is available for cancer early-onset diagnostic. Ratio of Ki67-staining vs UHRF1-staining might differentiate well between normal proliferating cells and cancer cells. Indeed, overexpression of UHRF1 is maintained throughout the cell cycle in cancer cells but not in normal cells [57]. Thus, one might expect that UHRF1-staining should be lower than Ki67 in normal tissues and as much as Ki67 or above in cancer cells. This interesting direction requires further investigations but may represent the basis for the development of a diagnostic kit.

UHRF1 overexpression has also proven to be a barrier to cure cancer because of its ability to silence tumor suppressor genes depending on the cancer type (Figure 3) or to counteract pro-apoptotic genes and to induce therapy resistance. It is therefore essential to target UHRF1 overexpression to achieve therapeutic goals in cancer patients. Many strategies can be designed to target UHRF1, including use of small molecules [128]. Therefore, following UHRF1 levels in fluids or tissues during cancer treatment could be of help in a theranostic context.

Abbreviations

UHRF1: ubiquitin-like containing PHD and Ring Finger domain protein 1; DNMT1: DNA methyltransferase 1; qRT-PCR: quantitative reverse-transcriptase polymerase chain reaction; IHC: immunohistochemistry; RDA: representational difference analysis; NSCLC: non-small cell lung cancer; HCC: hepatocellular carcinoma, NMIBC: non-muscle-invasive bladder cancer; RCC: renal cell carcinoma; ESCC: esophageal squamous cell carcinoma; LSCC: laryngeal squamous cell carcinomas.

ACKNOWLEDGMENTS

Our work on UHRF1 was supported by the Agence National de la Recherche (ANR Fluometadn), the Fondation pour la Recherche Médicale (FRM DCM20111223038), Ligue contre le Cancer and by the grant ANR-10-LABX-0030-INRT, a French State fund managed by the Agence Nationale de la Recherche under the frame program Investissements d'Avenir ANR-10-IDEX-0002-02.

CONFLICTS OF INTEREST

All authors report no conflicts of interest.

REFERENCES

1. Sandoval J, Peiro-Chova L, Pallardo FV, Garcia-Gimenez JL. Epigenetic biomarkers in laboratory diagnostics: emerging approaches and opportunities. Expert Rev Mol Diagn. 2013; 13: 457-71. doi: 10.1586/erm.13.37.
2. Jeltsch A, Jurkowska RZ. New concepts in DNA methylation. Trends Biochem Sci. 2014; 39: 310-8. doi: 10.1016/j.tibs.2014.05.002.
3. Zane L, Sharma V, Misteli T. Common features of chromatin in aging and cancer: cause or coincidence? Trends Cell Biol. 2014; 24: 686-94. doi: 10.1016/j.tcb.2014.07.001.
4. Lawrence M, Daujat S, Schneider R. Lateral thinking: how histone modifications regulate gene expression. Trends Genet. 2016; 32: 42-56. doi: 10.1016/j.tig.2015.10.007.
5. Zink LM, Hake SB. Histone variants: nuclear function and disease. Curr Opin Genet Dev. 2016; 37: 82-9. doi: 10.1016/j.gde.2015.12.002.
6. Dawson MA, Kouzarides T. Cancer epigenetics: from mechanism to therapy. Cell. 2012; 150: 12-27. doi: 10.1016/j.cell.2012.06.013.
7. Alhosin M, Sharif T, Mousli M, Etienne-Selloum N, Fuhrmann G, Schini-Kerth VB, Bronner C. Down-regulation of UHRF1, associated with re-expression of tumor suppressor genes, is a common feature of natural compounds exhibiting anti-cancer properties. J Exp Clin Cancer Res. 2011; 30: 41. doi: 10.1186/1756-9966-30-41.
8. Alhosin M, Omran Z, Zamzami MA, Al-Malki AL, Choudhry H, Mousli M, Bronner C. Signalling pathways in UHRF1-dependent regulation of tumor suppressor genes in cancer. J Exp Clin Cancer Res. 2016; 35: 174. doi: 10.1186/s13046-016-0453-5.
9. Chervona Y, Costa M. Histone modifications and cancer: biomarkers of prognosis? Am J Cancer Res. 2012; 2: 589-97.
10. Amacher DE. A 2015 survey of established or potential epigenetic biomarkers for the accurate detection of human cancers. Biomarkers. 2016; 21: 387-403. doi:

10.3109/1354750X.2016.1153724.

11. Angulo JC, Lopez JI, Ropero S. DNA Methylation and urological cancer, a step towards personalized medicine: current and future prospects. Mol Diagn Ther. 2016; 20: 531-49. doi: 10.1007/s40291-016-0231-2.
12. Lam K, Pan K, Linnekamp JF, Medema JP, Kandimalla R. DNA methylation based biomarkers in colorectal cancer: a systematic review. Biochim Biophys Acta. 2016; 1866: 106-20. doi: 10.1016/j.bbcan.2016.07.001.
13. Wu P, Cao Z, Wu S. New progress of epigenetic biomarkers in urological cancer. Dis Markers. 2016; 2016: 9864047. doi: 10.1155/2016/9864047.
14. Willbanks A, Leary M, Greenshields M, Tyminski C, Heerboth S, Lapinska K, Haskins K, Sarkar S. The evolution of epigenetics: from prokaryotes to humans and its biological consequences. Genet Epigenet. 2016; 8: 25-36. doi: 10.4137/GEG.S31863.
15. Probst AV, Dunleavy E, Almouzni G. Epigenetic inheritance during the cell cycle. Nat Rev Mol Cell Biol. 2009; 10: 192-206. doi: 10.1038/nrm2640.
16. Bostick M, Kim JK, Esteve PO, Clark A, Pradhan S, Jacobsen SE. UHRF1 plays a role in maintaining DNA methylation in mammalian cells. Science. 2007; 317: 1760-4. doi: 10.1126/science.1147939.
17. Sharif J, Muto M, Takebayashi S, Suetake I, Iwamatsu A, Endo TA, Shinga J, Mizutani-Koseki Y, Toyoda T, Okamura K, Tajima S, Mitsuya K, Okano M, Koseki H. The SRA protein Np95 mediates epigenetic inheritance by recruiting Dnmt1 to methylated DNA. Nature. 2007; 450: 908-12. doi: 10.1038/nature06397.
18. Arita K, Ariyoshi M, Tochio H, Nakamura Y, Shirakawa M. Recognition of hemi-methylated DNA by the SRA protein UHRF1 by a base-flipping mechanism. Nature. 2008; 455: 818-21. doi: 10.1038/nature07249.
19. Avvakumov GV, Walker JR, Xue S, Li Y, Duan S, Bronner C, Arrowsmith CH, Dhe-Paganon S. Structural basis for recognition of hemi-methylated DNA by the SRA domain of human UHRF1. Nature. 2008; 455: 822-5. doi: 10.1038/nature07273.
20. Hashimoto H, Horton JR, Zhang X, Bostick M, Jacobsen SE, Cheng X. The SRA domain of UHRF1 flips 5-methylcytosine out of the DNA helix. Nature. 2008; 455: 826-9. doi: 10.1038/nature07280.
21. Kent B, Magnani E, Walsh MJ, Sadler KC. UHRF1 regulation of Dnmt1 is required for pre-gastrula zebrafish development. Dev Biol. 2016; 412: 99-113. doi: 10.1016/j.ydbio.2016.01.036.
22. Hopfner R, Mousli M, Jeltsch JM, Voulgaris A, Lutz Y, Marin C, Bellocq JP, Oudet P, Bronner C. ICBP90, a novel human CCAAT binding protein, involved in the regulation of topoisomerase IIalpha expression. Cancer Res. 2000; 60: 121-8.
23. Hopfner R, Mousli M, Garnier JM, Redon R, du Manoir S, Chatton B, Ghyselinck N, Oudet P, Bronner C. Genomic structure and chromosomal mapping of the gene coding for ICBP90, a protein involved in the regulation of the topoisomerase IIalpha gene expression. Gene. 2001; 266: 15-23.
24. Hopfner R, Mousli M, Oudet P, Bronner C. Overexpression of ICBP90, a novel CCAAT-binding protein, overcomes cell contact inhibition by forcing topoisomerase II alpha expression. Anticancer Res. 2002; 22: 3165-70.
25. Bronner C, Krifa M, Mousli M. Increasing role of UHRF1 in the reading and inheritance of the epigenetic code as well as in tumorogenesis. Biochem Pharmacol. 2013; 86: 1643-9. doi: 10.1016/j.bcp.2013.10.002.
26. Jenkins Y, Markovtsov V, Lang W, Sharma P, Pearsall D, Warner J, Franci C, Huang B, Huang J, Yam GC, Vistan JP, Pali E, Vialard J, et al. Critical role of the ubiquitin ligase activity of UHRF1, a nuclear RING finger protein, in tumor cell growth. Mol Biol Cell. 2005; 16: 5621-9. doi: 10.1091/mbc.E05-03-0194.
27. Nishiyama A, Yamaguchi L, Sharif J, Johmura Y, Kawamura T, Nakanishi K, Shimamura S, Arita K, Kodama T, Ishikawa F, Koseki H, Nakanishi M. Uhrf1-dependent H3K23 ubiquitylation couples maintenance DNA methylation and replication. Nature. 2013; 502: 249-53. doi: 10.1038/nature12488.
28. Qin W, Wolf P, Liu N, Link S, Smets M, La Mastra F, Forne I, Pichler G, Horl D, Fellinger K, Spada F, Bonapace IM, Imhof A, et al. DNA methylation requires a DNMT1 ubiquitin interacting motif (UIM) and histone ubiquitination. Cell Res. 2015; 25: 911-29. doi: 10.1038/cr.2015.72.
29. Hashimoto H, Horton JR, Zhang X, Cheng X. UHRF1, a modular multi-domain protein, regulates replication-coupled crosstalk between DNA methylation and histone modifications. Epigenetics. 2009; 4: 8-14.
30. Nady N, Lemak A, Walker JR, Avvakumov GV, Kareta MS, Achour M, Xue S, Duan S, Allali-Hassani A, Zuo X, Wang YX, Bronner C, Chedin F, et al. Recognition of multivalent histone states associated with heterochromatin by UHRF1 protein. J Biol Chem. 2011; 286: 24300-11. doi: 10.1074/jbc.M111.234104.
31. Karagianni P, Amazit L, Qin J, Wong J. ICBP90, a novel methyl K9 H3 binding protein linking protein ubiquitination with heterochromatin formation. Mol Cell Biol. 2008; 28: 705-17. doi: 10.1128/MCB.01598-07.
32. Zhao Q, Zhang J, Chen R, Wang L, Li B, Cheng H, Duan X, Zhu H, Wei W, Li J, Wu Q, Han JD, Yu W, et al. Dissecting the precise role of H3K9 methylation in crosstalk with DNA maintenance methylation in mammals. Nat Commun. 2016; 7: 12464. doi: 10.1038/ncomms12464.
33. Greiner VJ, Kovalenko L, Humbert N, Richert L, Birck C, Ruff M, Zaporozhets OA, Dhe-Paganon S, Bronner C, Mely Y. Site-selective monitoring of the interaction of the SRA domain of UHRF1 with target DNA sequences labeled with 2-aminopurine. Biochemistry. 2015; 54: 6012-20. doi: 10.1021/acs.biochem.5b00419.

34. Kilin V, Gavvala K, Barthes NP, Michel BY, Shin D, Boudier C, Mauffret O, Yashchuk V, Mousli M, Ruff M, Granger F, Eiler S, Bronner C, et al. Dynamics of methylated cytosine flipping by UHRF1. J Am Chem Soc. 2017; 139: 2520-8. doi: 10.1021/jacs.7b00154.

35. Frauer C, Hoffmann T, Bultmann S, Casa V, Cardoso MC, Antes I, Leonhardt H. Recognition of 5-hydroxymethylcytosine by the Uhrf1 SRA domain. PLoS One. 2011; 6: e21306. doi: 10.1371/journal.pone.0021306.

36. Unoki M, Brunet J, Mousli M. Drug discovery targeting epigenetic codes: the great potential of UHRF1, which links DNA methylation and histone modifications, as a drug target in cancers and toxoplasmosis. Biochem Pharmacol. 2009; 78: 1279-88. doi: 10.1016/j.bcp.2009.05.035.

37. Unoki M, Nishidate T, Nakamura Y. ICBP90, an E2F-1 target, recruits HDAC1 and binds to methyl-CpG through its SRA domain. Oncogene. 2004; 23: 7601-10. doi: 10.1038/sj.onc.1208053.

38. Achour M, Fuhrmann G, Alhosin M, Ronde P, Chataigneau T, Mousli M, Schini-Kerth VB, Bronner C. UHRF1 recruits the histone acetyltransferase Tip60 and controls its expression and activity. Biochem Biophys Res Commun. 2009; 390: 523-8. doi: 10.1016/j.bbrc.2009.09.131.

39. Kim JK, Esteve PO, Jacobsen SE, Pradhan S. UHRF1 binds G9a and participates in p21 transcriptional regulation in mammalian cells. Nucleic Acids Res. 2009; 37: 493-505. doi: 10.1093/nar/gkn961.

40. Ma H, Chen H, Guo X, Wang Z, Sowa ME, Zheng L, Hu S, Zeng P, Guo R, Diao J, Lan F, Harper JW, Shi YG, et al. M phase phosphorylation of the epigenetic regulator UHRF1 regulates its physical association with the deubiquitylase USP7 and stability. Proc Natl Acad Sci U S A. 2012; 109: 4828-33. doi: 10.1073/pnas.1116349109.

41. Dai C, Shi D, Gu W. Negative regulation of the acetyltransferase TIP60-p53 interplay by UHRF1 (ubiquitin-like with PHD and RING finger domains 1). J Biol Chem. 2013; 288: 19581-92. doi: 10.1074/jbc.M113.476606.

42. Pacaud R, Brocard E, Lalier L, Hervouet E, Vallette FM, Cartron PF. The DNMT1/PCNA/UHRF1 disruption induces tumorigenesis characterized by similar genetic and epigenetic signatures. Sci Rep. 2014; 4: 4230. doi: 10.1038/srep04230.

43. Jeanblanc M, Mousli M, Hopfner R, Bathami K, Martinet N, Abbady AQ, Siffert JC, Mathieu E, Muller CD, Bronner C. The retinoblastoma gene and its product are targeted by ICBP90: a key mechanism in the G1/S transition during the cell cycle. Oncogene. 2005; 24: 7337-45. doi: 10.1038/sj.onc.1208878.

44. Achour M, Jacq X, Ronde P, Alhosin M, Charlot C, Chataigneau T, Jeanblanc M, Macaluso M, Giordano A, Hughes AD, Schini-Kerth VB, Bronner C. The interaction of the SRA domain of ICBP90 with a novel domain of DNMT1 is involved in the regulation of VEGF gene expression. Oncogene. 2008; 27: 2187-97. doi: 10.1038/sj.onc.1210855.

45. Wang F, Yang YZ, Shi CZ, Zhang P, Moyer MP, Zhang HZ, Zou Y, Qin HL. UHRF1 promotes cell growth and metastasis through repression of p16(ink(4)a) in colorectal cancer. Ann Surg Oncol. 2012; 19: 2753-62. doi: 10.1245/s10434-011-2194-1.

46. Achour M, Mousli M, Alhosin M, Ibrahim A, Peluso J, Muller CD, Schini-Kerth VB, Hamiche A, Dhe-Paganon S, Bronner C. Epigallocatechin-3-gallate up-regulates tumor suppressor gene expression via a reactive oxygen species-dependent down-regulation of UHRF1. Biochem Biophys Res Commun. 2013; 430: 208-12. doi: 10.1016/j.bbrc.2012.11.087.

47. Krifa M, Alhosin M, Muller CD, Gies JP, Chekir-Ghedira L, Ghedira K, Mely Y, Bronner C, Mousli M. Limoniastrum guyonianum aqueous gall extract induces apoptosis in human cervical cancer cells involving p16 INK4A re-expression related to UHRF1 and DNMT1 down-regulation. J Exp Clin Cancer Res. 2013; 32: 30. doi: 10.1186/1756-9966-32-30.

48. Boukhari A, Alhosin M, Bronner C, Sagini K, Truchot C, Sick E, Schini-Kerth VB, Andre P, Mely Y, Mousli M, Gies JP. CD47 activation-induced UHRF1 over-expression is associated with silencing of tumor suppressor gene p16INK4A in glioblastoma cells. Anticancer Res. 2015; 35: 149-57.

49. Sheng Y, Wang H, Liu D, Zhang C, Deng Y, Yang F, Zhang T, Zhang C. Methylation of tumor suppressor gene CDH13 and SHP1 promoters and their epigenetic regulation by the UHRF1/PRMT5 complex in endometrial carcinoma. Gynecol Oncol. 2016; 140: 145-51. doi: 10.1016/j.ygyno.2015.11.017.

50. Chen H, Zhang C, Sheng Y, Yao S, Liu Z, Zhang C, Zhang T. Frequent SOCS3 and 3OST2 promoter methylation and their epigenetic regulation in endometrial carcinoma. Am J Cancer Res. 2015; 5: 180-90.

51. Jin W, Chen L, Chen Y, Xu SG, Di GH, Yin WJ, Wu J, Shao ZM. UHRF1 is associated with epigenetic silencing of BRCA1 in sporadic breast cancer. Breast Cancer Res Treat. 2010; 123: 359-73. doi: 10.1007/s10549-009-0652-2.

52. Zhou L, Shang Y, Jin Z, Zhang W, Lv C, Zhao X, Liu Y, Li N, Liang J. UHRF1 promotes proliferation of gastric cancer via mediating tumor suppressor gene hypermethylation. Cancer Biol Ther. 2015; 16: 1241-51. doi: 10.1080/15384047.2015.1056411.

53. Guan D, Factor D, Liu Y, Wang Z, Kao HY. The epigenetic regulator UHRF1 promotes ubiquitination-mediated degradation of the tumor-suppressor protein promyelocytic leukemia protein. Oncogene. 2013; 32: 3819-28. doi: 10.1038/onc.2012.406.

54. Zhuo H, Tang J, Lin Z, Jiang R, Zhang X, Ji J, Wang P, Sun B. The aberrant expression of MEG3 regulated by UHRF1 predicts the prognosis of hepatocellular carcinoma. Mol Carcinog. 2016; 55: 209-19. doi: 10.1002/mc.22270.

55. Qin L, Dong Z, Zhang JT. Reversible epigenetic regulation of 14-3-3sigma expression in acquired gemcitabine resistance by uhrf1 and DNA methyltransferase 1. Mol Pharmacol. 2014; 86: 561-9. doi: 10.1124/mol.114.092544.

56. Zhang Y, Huang Z, Zhu Z, Zheng X, Liu J, Han Z, Ma X, Zhang Y. Upregulated UHRF1 promotes bladder cancer cell invasion by epigenetic silencing of KiSS1. PLoS One. 2014; 9: e104252. doi: 10.1371/journal.pone.0104252.

57. Mousli M, Hopfner R, Abbady AQ, Monte D, Jeanblanc M, Oudet P, Louis B, Bronner C. ICBP90 belongs to a new family of proteins with an expression that is deregulated in cancer cells. Br J Cancer. 2003; 89: 120-7. doi: 10.1038/sj.bjc.6601068.

58. Bonapace IM, Latella L, Papait R, Nicassio F, Sacco A, Muto M, Crescenzi M, Di Fiore PP. Np95 is regulated by E1A during mitotic reactivation of terminally differentiated cells and is essential for S phase entry. J Cell Biol. 2002; 157: 909-14. doi: 10.1083/jcb.200201025.

59. Arima Y, Hirota T, Bronner C, Mousli M, Fujiwara T, Niwa S, Ishikawa H, Saya H. Down-regulation of nuclear protein ICBP90 by p53/p21Cip1/WAF1-dependent DNA-damage checkpoint signals contributes to cell cycle arrest at G1/S transition. Genes Cells. 2004; 9: 131-42.

60. Tien AL, Senbanerjee S, Kulkarni A, Mudbhary R, Goudreau B, Ganesan S, Sadler KC, Ukomadu C. UHRF1 depletion causes a G2/M arrest, activation of DNA damage response and apoptosis. Biochem J. 2011; 435: 175-85. doi: 10.1042/BJ20100840.

61. Bronner C, Achour M, Arima Y, Chataigneau T, Saya H, Schini-Kerth VB. The UHRF family: oncogenes that are drugable targets for cancer therapy in the near future? Pharmacol Ther. 2007; 115: 419-34. doi: 10.1016/j.pharmthera.2007.06.003.

62. Mudbhary R, Hoshida Y, Chernyavskaya Y, Jacob V, Villanueva A, Fiel MI, Chen X, Kojima K, Thung S, Bronson RT, Lachenmayer A, Revill K, Alsinet C, et al. UHRF1 overexpression drives DNA hypomethylation and hepatocellular carcinoma. Cancer Cell. 2014; 25: 196-209. doi: 10.1016/j.ccr.2014.01.003.

63. Jia Y, Li P, Fang L, Zhu H, Xu L, Cheng H, Zhang J, Li F, Feng Y, Li Y, Li J, Wang R, Du JX, et al. Negative regulation of DNMT3A de novo DNA methylation by frequently overexpressed UHRF family proteins as a mechanism for widespread DNA hypomethylation in cancer. Cell Discov. 2016; 2: 16007. doi: 10.1038/celldisc.2016.7.

64. Muto M, Fujimori A, Nenoi M, Daino K, Matsuda Y, Kuroiwa A, Kubo E, Kanari Y, Utsuno M, Tsuji H, Ukai H, Mita K, Takahagi M, et al. Isolation and characterization of a novel human radiosusceptibility gene, NP95. Radiat Res. 2006; 166: 723-33. doi: 10.1667/RR0459.1.

65. Chen H, Ma H, Inuzuka H, Diao J, Lan F, Shi YG, Wei W, Shi Y. DNA damage regulates UHRF1 stability via the SCF(beta-TrCP) E3 ligase. Mol Cell Biol. 2013; 33: 1139-48. doi: 10.1128/MCB.01191-12.

66. Tian Y, Paramasivam M, Ghosal G, Chen D, Shen X, Huang Y, Akhter S, Legerski R, Chen J, Seidman MM, Qin J, Li L. UHRF1 contributes to DNA damage repair as a lesion recognition factor and nuclease scaffold. Cell Rep. 2015; 10: 1957-66. doi: 10.1016/j.celrep.2015.03.038.

67. Zhang H, Liu H, Chen Y, Yang X, Wang P, Liu T, Deng M, Qin B, Correia C, Lee S, Kim J, Sparks M, Nair AA, et al. A cell cycle-dependent BRCA1-UHRF1 cascade regulates DNA double-strand break repair pathway choice. Nat Commun. 2016; 7: 10201. doi: 10.1038/ncomms10201.

68. Liang CC, Zhan B, Yoshikawa Y, Haas W, Gygi SP, Cohn MA. UHRF1 is a sensor for DNA interstrand crosslinks and recruits FANCD2 to initiate the Fanconi anemia pathway. Cell Rep. 2015; 10: 1947-56. doi: 10.1016/j.celrep.2015.02.053.

69. Wang KY, Chen CC, Tsai SF, Shen CJ. Epigenetic enhancement of the post-replicative DNA mismatch repair of mammalian genomes by a hemi-mCpG-Np95-Dnmt1 axis. Sci Rep. 2016; 6: 37490. doi: 10.1038/srep37490.

70. Park SA, Platt J, Lee JW, Lopez-Giraldez F, Herbst RS, Koo JS. E2F8 as a novel therapeutic target for lung cancer. J Natl Cancer Inst. 2015; 107: djv151. doi: 10.1093/jnci/djv151.

71. Wu SM, Cheng WL, Liao CJ, Chi HC, Lin YH, Tseng YH, Tsai CY, Chen CY, Lin SL, Chen WJ, Yeh YH, Huang CY, Chen MH, et al. Negative modulation of the epigenetic regulator, UHRF1, by thyroid hormone receptors suppresses liver cancer cell growth. Int J Cancer. 2015; 137: 37-49. doi: 10.1002/ijc.29368.

72. Sanders DA, Gormally MV, Marsico G, Beraldi D, Tannahill D, Balasubramanian S. FOXM1 binds directly to non-consensus sequences in the human genome. Genome Biol. 2015; 16: 130. doi: 10.1186/s13059-015-0696-z.

73. Kim KB, Son HJ, Choi S, Hahm JY, Jung H, Baek HJ, Kook H, Hahn Y, Kook H, Seo SB. H3K9 methyltransferase G9a negatively regulates UHRF1 transcription during leukemia cell differentiation. Nucleic Acids Res. 2015; 43: 3509-23. doi: 10.1093/nar/gkv183.

74. Zhou L, Zhao X, Han Y, Lu Y, Shang Y, Liu C, Li T, Jin Z, Fan D, Wu K. Regulation of UHRF1 by miR-146a/b modulates gastric cancer invasion and metastasis. FASEB J. 2013; 27: 4929-39. doi: 10.1096/fj.13-233387.

75. Zhu M, Xu Y, Ge M, Gui Z, Yan F. Regulation of UHRF1 by microRNA-9 modulates colorectal cancer cell proliferation and apoptosis. Cancer Sci. 2015; 106: 833-9. doi: 10.1111/cas.12689.

76. Matsushita R, Yoshino H, Enokida H, Goto Y, Miyamoto K, Yonemori M, Inoguchi S, Nakagawa M, Seki N. Regulation of UHRF1 by dual-strand tumor-suppressor microRNA-145 (miR-145-5p and miR-145-3p): Inhibition of bladder cancer cell aggressiveness. Oncotarget. 2016; 7: 28460-87. doi: 10.18632/oncotarget.8668.

77. Wang X, Wu Q, Xu B, Wang P, Fan W, Cai Y, Gu X, Meng F. MiR-124 exerts tumor suppressive functions on the cell

proliferation, motility and angiogenesis of bladder cancer by fine-tuning UHRF1. FEBS J. 2015; 282: 4376-88. doi: 10.1111/febs.13502.

78. Goto Y, Kurozumi A, Nohata N, Kojima S, Matsushita R, Yoshino H, Yamazaki K, Ishida Y, Ichikawa T, Naya Y, Seki N. The microRNA signature of patients with sunitinib failure: regulation of UHRF1 pathways by microRNA-101 in renal cell carcinoma. Oncotarget. 2016; 7: 59070-86. doi: 10.18632/oncotarget.10887.
79. Deng W, Yan M, Yu T, Ge H, Lin H, Li J, Liu Y, Geng Q, Zhu M, Liu L, He X, Yao M. Quantitative proteomic analysis of the metastasis-inhibitory mechanism of miR-193a-3p in non-small cell lung cancer. Cell Physiol Biochem. 2015; 35: 1677-88. doi: 10.1159/000373981.
80. Zhang ZM, Rothbart SB, Allison DF, Cai Q, Harrison JS, Li L, Wang Y, Strahl BD, Wang GG, Song J. An allosteric interaction links USP7 to deubiquitination and chromatin targeting of UHRF1. Cell Rep. 2015; 12: 1400-6. doi: 10.1016/j.celrep.2015.07.046.
81. Zhao GY, Lin ZW, Lu CL, Gu J, Yuan YF, Xu FK, Liu RH, Ge D, Ding JY. USP7 overexpression predicts a poor prognosis in lung squamous cell carcinoma and large cell carcinoma. Tumour Biol. 2015; 36: 1721-9. doi: 10.1007/s13277-014-2773-4.
82. Song MS, Salmena L, Carracedo A, Egia A, Lo-Coco F, Teruya-Feldstein J, Pandolfi PP. The deubiquitinylation and localization of PTEN are regulated by a HAUSP-PML network. Nature. 2008; 455: 813-7. doi: 10.1038/nature07290.
83. Nicholson B, Suresh Kumar KG. The multifaceted roles of USP7: new therapeutic opportunities. Cell Biochem Biophys. 2011; 60: 61-8. doi: 10.1007/s12013-011-9185-5.
84. Taniue K, Kurimoto A, Sugimasa H, Nasu E, Takeda Y, Iwasaki K, Nagashima T, Okada-Hatakeyama M, Oyama M, Kozuka-Hata H, Hiyoshi M, Kitayama J, Negishi L, et al. Long noncoding RNA UPAT promotes colon tumorigenesis by inhibiting degradation of UHRF1. Proc Natl Acad Sci U S A. 2016; 113: 1273-8. doi: 10.1073/pnas.1500992113.
85. Ding G, Chen P, Zhang H, Huang X, Zang Y, Li J, Li J, Wong J. Regulation of Ubiquitin-like with plant homeodomain and RING finger domain 1 (UHRF1) protein stability by heat shock protein 90 chaperone machinery. J Biol Chem. 2016; 291: 20125-35. doi: 10.1074/jbc.M116.727214.
86. Ferlay J, Soerjomataram I, Dikshit R, Eser S, Mathers C, Rebelo M, Parkin DM, Forman D, Bray F. Cancer incidence and mortality worldwide: sources, methods and major patterns in GLOBOCAN 2012. Int J Cancer. 2015; 136: E359-86. doi: 10.1002/ijc.29210.
87. Unoki M, Daigo Y, Koinuma J, Tsuchiya E, Hamamoto R, Nakamura Y. UHRF1 is a novel diagnostic marker of lung cancer. Br J Cancer. 2010; 103: 217-22. doi: 10.1038/sj.bjc.6605717.
88. Huang P, Cheng CL, Chang YH, Liu CH, Hsu YC, Chen JS, Chang GC, Ho BC, Su KY, Chen HY, Yu SL. Molecular gene signature and prognosis of non-small cell lung cancer. Oncotarget. 2016; 7: 51898-907. doi: 10.18632/oncotarget.10622.
89. Daskalos A, Oleksiewicz U, Filia A, Nikolaidis G, Xinarianos G, Gosney JR, Malliri A, Field JK, Liloglou T. UHRF1-mediated tumor suppressor gene inactivation in nonsmall cell lung cancer. Cancer. 2011; 117: 1027-37. doi: 10.1002/cncr.25531.
90. Liang D, Xue H, Yu Y, Lv F, You W, Zhang B. Elevated expression of UHRF1 predicts unfavorable prognosis for patients with hepatocellular carcinoma. Int J Clin Exp Pathol. 2015; 8: 9416-21.
91. Chen X, Cheung ST, So S, Fan ST, Barry C, Higgins J, Lai KM, Ji J, Dudoit S, Ng IO, Van De Rijn M, Botstein D, Brown PO. Gene expression patterns in human liver cancers. Mol Biol Cell. 2002; 13: 1929-39. doi: 10.1091/mbc.02-02-0023.
92. Liu X, Ou H, Xiang L, Li X, Huang Y, Yang D. Elevated UHRF1 expression contributes to poor prognosis by promoting cell proliferation and metastasis in hepatocellular carcinoma. Oncotarget. 2017; 8: 10510-22. doi: 10.18632/oncotarget.14446.
93. Chang L, Wang G, Jia T, Zhang L, Li Y, Han Y, Zhang K, Lin G, Zhang R, Li J, Wang L. Armored long non-coding RNA MEG3 targeting EGFR based on recombinant MS2 bacteriophage virus-like particles against hepatocellular carcinoma. Oncotarget. 2016; 7: 23988-4004. doi: 10.18632/oncotarget.8115.
94. Shen L, Toyota M, Kondo Y, Lin E, Zhang L, Guo Y, Hernandez NS, Chen X, Ahmed S, Konishi K, Hamilton SR, Issa JP. Integrated genetic and epigenetic analysis identifies three different subclasses of colon cancer. Proc Natl Acad Sci U S A. 2007; 104: 18654-9. doi: 10.1073/pnas.0704652104.
95. Sabatino L, Fucci A, Pancione M, Carafa V, Nebbioso A, Pistore C, Babbio F, Votino C, Laudanna C, Ceccarelli M, Altucci L, Bonapace IM, Colantuoni V. UHRF1 coordinates peroxisome proliferator activated receptor gamma (PPARG) epigenetic silencing and mediates colorectal cancer progression. Oncogene. 2012; 31: 5061-72. doi: 10.1038/onc.2012.3.
96. Kofunato Y, Kumamoto K, Saitou K, Hayase S, Okayama H, Miyamoto K, Sato Y, Katakura K, Nakamura I, Ohki S, Koyama Y, Unoki M, Takenoshita S. UHRF1 expression is upregulated and associated with cellular proliferation in colorectal cancer. Oncol Rep. 2012; 28: 1997-2002. doi: 10.3892/or.2012.2064.
97. Geng Y, Gao Y, Ju H, Yan F. Diagnostic and prognostic value of plasma and tissue ubiquitin-like, containing PHD and RING finger domains 1 in breast cancer patients. Cancer Sci. 2013; 104: 194-9. doi: 10.1111/cas.12052.
98. Macaluso M, Montanari M, Noto PB, Gregorio V, Bronner C, Giordano A. Epigenetic modulation of estrogen receptor-

alpha by pRb family proteins: a novel mechanism in breast cancer. Cancer Res. 2007; 67: 7731-7. doi: 10.1158/0008-5472.CAN-07-1476.

99. Li XL, Xu JH, Nie JH, Fan SJ. Exogenous expression of UHRF1 promotes proliferation and metastasis of breast cancer cells. Oncol Rep. 2012; 28: 375-83. doi: 10.3892/or.2012.1792.

100. Li X, Meng Q, Rosen EM, Fan S. UHRF1 confers radioresistance to human breast cancer cells. Int J Radiat Biol. 2011; 87: 263-73. doi: 10.3109/09553002.2011.530335.

101. Yan F, Tan XY, Geng Y, Ju HX, Gao YF, Zhu MC. Inhibition effect of siRNA-downregulated UHRF1 on breast cancer growth. Cancer Biother Radiopharm. 2011; 26: 183-9. doi: 10.1089/cbr.2010.0886.

102. Fang L, Shanqu L, Ping G, Ting H, Xi W, Ke D, Min L, Junxia W, Huizhong Z. Gene therapy with RNAi targeting UHRF1 driven by tumor-specific promoter inhibits tumor growth and enhances the sensitivity of chemotherapeutic drug in breast cancer in vitro and in vivo. Cancer Chemother Pharmacol. 2012; 69: 1079-87. doi: 10.1007/s00280-011-1801-y.

103. Lorenzato M, Caudroy S, Bronner C, Evrard G, Simon M, Durlach A, Birembaut P, Clavel C. Cell cycle and/or proliferation markers: what is the best method to discriminate cervical high-grade lesions? Hum Pathol. 2005; 36: 1101-7. doi: 10.1016/j.humpath.2005.07.016.

104. Ge TT, Yang M, Chen Z, Lou G, Gu T. UHRF1 gene silencing inhibits cell proliferation and promotes cell apoptosis in human cervical squamous cell carcinoma CaSki cells. J Ovarian Res. 2016; 9: 42. doi: 10.1186/s13048-016-0253-8.

105. Li XL, Meng QH, Fan SJ. Adenovirus-mediated expression of UHRF1 reduces the radiosensitivity of cervical cancer HeLa cells to gamma-irradiation. Acta Pharmacol Sin. 2009; 30: 458-66. doi: 10.1038/aps.2009.18.

106. Yan F, Wang X, Shao L, Ge M, Hu X. Analysis of UHRF1 expression in human ovarian cancer tissues and its regulation in cancer cell growth. Tumour Biol. 2015; 36: 8887-93. doi: 10.1007/s13277-015-3638-1.

107. Adjakly M, Ngollo M, Dagdemir A, Judes G, Pajon A, Karsli-Ceppioglu S, Penault-Llorca F, Boiteux JP, Bignon YJ, Guy L, Bernard-Gallon D. Prostate cancer: the main risk and protective factors-Epigenetic modifications. Ann Endocrinol (Paris). 2015; 76: 25-41. doi: 10.1016/j.ando.2014.09.001.

108. Babbio F, Pistore C, Curti L, Castiglioni I, Kunderfranco P, Brino L, Oudet P, Seiler R, Thalman GN, Roggero E, Sarti M, Pinton S, Mello-Grand M, et al. The SRA protein UHRF1 promotes epigenetic crosstalks and is involved in prostate cancer progression. Oncogene. 2012; 31: 4878-87. doi: 10.1038/onc.2011.641.

109. Wan X, Yang S, Huang W, Wu D, Chen H, Wu M, Li J, Li T, Li Y. UHRF1 overexpression is involved in cell proliferation and biochemical recurrence in prostate cancer after radical prostatectomy. J Exp Clin Cancer Res. 2016; 35: 34. doi: 10.1186/s13046-016-0308-0.

110. Unoki M, Kelly JD, Neal DE, Ponder BA, Nakamura Y, Hamamoto R. UHRF1 is a novel molecular marker for diagnosis and the prognosis of bladder cancer. Br J Cancer. 2009; 101: 98-105. doi: 10.1038/sj.bjc.6605123.

111. Yang GL, Zhang LH, Bo JJ, Chen HG, Cao M, Liu DM, Huang YR. UHRF1 is associated with tumor recurrence in non-muscle-invasive bladder cancer. Med Oncol. 2012; 29: 842-7. doi: 10.1007/s12032-011-9983-z.

112. Ying L, Lin J, Qiu F, Cao M, Chen H, Liu Z, Huang Y. Epigenetic repression of regulator of G-protein signaling 2 by ubiquitin-like with PHD and ring-finger domain 1 promotes bladder cancer progression. FEBS J. 2015; 282: 174-82. doi: 10.1111/febs.13116.

113. Saidi S, Popov Z, Janevska V, Panov S. Overexpression of UHRF1 gene correlates with the major clinicopathological parameters in urinary bladder cancer. Int Braz J Urol. 2017; 43: 224-9. doi: 10.1590/S1677-5538.IBJU.2016.0126.

114. Ma J, Peng J, Mo R, Ma S, Wang J, Zang L, Li W, Fan J. Ubiquitin E3 ligase UHRF1 regulates p53 ubiquitination and p53-dependent cell apoptosis in clear cell Renal Cell Carcinoma. Biochem Biophys Res Commun. 2015; 464: 147-53. doi: 10.1016/j.bbrc.2015.06.104.

115. Wotschofsky Z, Gummlich L, Liep J, Stephan C, Kilic E, Jung K, Billaud JN, Meyer HA. Integrated microRNA and mRNA signature associated with the transition from the locally confined to the metastasized clear cell renal cell carcinoma exemplified by miR-146-5p. PLoS One. 2016; 11: e0148746. doi: 10.1371/journal.pone.0148746.

116. Oba-Shinjo SM, Bengtson MH, Winnischofer SM, Colin C, Vedoy CG, de Mendonca Z, Marie SK, Sogayar MC. Identification of novel differentially expressed genes in human astrocytomas by cDNA representational difference analysis. Brain Res Mol Brain Res. 2005; 140: 25-33. doi: 10.1016/j.molbrainres.2005.06.015.

117. Zhang ZY, Cai JJ, Hong J, Li KK, Ping Z, Wang Y, Ng HK, Yao Y, Mao Y. Clinicopathological analysis of UHRF1 expression in medulloblastoma tissues and its regulation on tumor cell proliferation. Med Oncol. 2016; 33: 99. doi: 10.1007/s12032-016-0799-8.

118. Qin Y, Wang J, Gong W, Zhang M, Tang Z, Zhang J, Quan Z. UHRF1 depletion suppresses growth of gallbladder cancer cells through induction of apoptosis and cell cycle arrest. Oncol Rep. 2014; 31: 2635-43. doi: 10.3892/or.2014.3145.

119. Abbady AQ, Bronner C, Trotzier MA, Hopfner R, Bathami K, Muller CD, Jeanblanc M, Mousli M. ICBP90 expression is downregulated in apoptosis-induced Jurkat cells. Ann N Y Acad Sci. 2003; 1010: 300-3.

120. Pi JT, Lin Y, Quan Q, Chen LL, Jiang LZ, Chi W, Chen HY. Overexpression of UHRF1 is significantly associated with poor prognosis in laryngeal squamous cell carcinoma.

Med Oncol. 2013; 30: 613. doi: 10.1007/s12032-013-0613-9.

121. Yang C, Wang Y, Zhang F, Sun G, Li C, Jing S, Liu Q, Cheng Y. Inhibiting UHRF1 expression enhances radiosensitivity in human esophageal squamous cell carcinoma. Mol Biol Rep. 2013; 40: 5225-35. doi: 10.1007/s11033-013-2559-6.

122. Nakamura K, Baba Y, Kosumi K, Harada K, Shigaki H, Miyake K, Kiyozumi Y, Ohuchi M, Kurashige J, Ishimoto T, Iwatsuki M, Sakamoto Y, Yoshida N, et al. UHRF1 regulates global DNA hypomethylation and is associated with poor prognosis in esophageal squamous cell carcinoma. Oncotarget. 2016; 7: 57821-31. doi: 10.18632/oncotarget.11067.

123. Crnogorac-Jurcevic T, Gangeswaran R, Bhakta V, Capurso G, Lattimore S, Akada M, Sunamura M, Prime W, Campbell F, Brentnall TA, Costello E, Neoptolemos J, Lemoine NR. Proteomic analysis of chronic pancreatitis and pancreatic adenocarcinoma. Gastroenterology. 2005; 129: 1454-63. doi: 10.1053/j.gastro.2005.08.012.

124. Abu-Alainin W, Gana T, Liloglou T, Olayanju A, Barrera LN, Ferguson R, Campbell F, Andrews T, Goldring C, Kitteringham N, Park BK, Nedjadi T, Schmid MC, et al. UHRF1 regulation of the Keap1-Nrf2 pathway in pancreatic cancer contributes to oncogenesis. J Pathol. 2016; 238: 423-33. doi: 10.1002/path.4665.

125. Cui L, Chen J, Zhang Q, Wang X, Qu J, Zhang J, Dang S. Up-regulation of UHRF1 by oncogenic Ras promoted the growth, migration, and metastasis of pancreatic cancer cells. Mol Cell Biochem. 2015; 400: 223-32. doi: 10.1007/s11010-014-2279-9.

126. Pita JM, Banito A, Cavaco BM, Leite V. Gene expression profiling associated with the progression to poorly differentiated thyroid carcinomas. Br J Cancer. 2009; 101: 1782-91. doi: 10.1038/sj.bjc.6605340.

127. Wang BC, Lin GH, Wang B, Yan M, He B, Zhang W, Yang AK, Long ZJ, Liu Q. UHRF1 suppression promotes cell differentiation and reduces inflammatory reaction in anaplastic thyroid cancer. Oncotarget. 2016 Jul 18. doi: 10.18632/oncotarget.10674. [Epub ahead of print].

128. Myrianthopoulos V, Cartron PF, Liutkeviciute Z, Klimasauskas S, Matulis D, Bronner C, Martinet N, Mikros E. Tandem virtual screening targeting the SRA domain of UHRF1 identifies a novel chemical tool modulating DNA methylation. Eur J Med Chem. 2016; 114: 390-6. doi: 10.1016/j.ejmech.2016.02.043.

Manuscript V: Maritime pine tannin extract from bark exhibits anticancer properties by inducing expression of p73 and targeting UHRF1 and DNMT1 of epigenetic machinery in cancer cells.

Maritime pine tannin extract from bark exhibits anticancer properties by inducing expression of p73 and targeting UHRF1 and DNMT1 of epigenetic machinery in cancer cells.

Waseem Ashraf [1], Mounira Krifa [1,2], Tanveer Ahmad [1], Liliyana Zaayter [1], Antonio Pizzi [3,] Christian D. Muller [4], Yves Mély [1], Christian Bronner [5], Marc Mousli [1*]

[1]Laboratory of Bioimaging and Pathologies, UMR 7021 CNRS, Université de Strasbourg, Faculté de Pharmacie, Illkirch France

[2]Division of Pharmacognosy and Molecular Biology, Faculty of Pharmacy at Monastir, Monastir, Tunisia

[3]ENSTIB/LERMAB, Epinal, France

[4] Institut Pluridisciplinaire Hubert Curien, UMR 7178 CNRS Université de Strasbourg, Illkirch, France

[5]Institut de Génétique et de Biologie Moléculaire et Cellulaire (IGBMC), INSERM U964 CNRS UMR 7104, Université de Strasbourg, Illkirch-France

*Correspondence: marc.mousli@unistra.fr
Laboratory of Bioimaging and Pathologies UMR 7021 CNRS,
Faculté de Pharmacie, 74, Route du Rhin, 67401 Illkirch
Cedex, France

ABSTRACT

Maritime pine bark is a rich source of polyphenolic compounds and it is commonly employed as herbal supplement worldwide. This study was designed to check the potential of maritime pine tannin extract (MPTE) for anticancer therapy and to determine the underlying mechanism of action. Our results demonstrated an inhibitory effect of MPTE on the proliferation of cancer cells as its treatment induced cell cycle arrest in G2/M phase. Treatment with MPTE also induced apoptosis in a concentration-dependent manner in cancer human cell lines as evident by an enhanced activation of caspase 3 and cleavage of PARP along with down-regulation of antiapoptotic protein BCL2. MPTE showed a pro-oxidant role in cancer cells and promoted the expression of p73 tumor suppressor gene in p53-deficient cells. It also down-regulated the proto-oncogenic UHRF1 and DNMT1, mediators of DNA methylation machinery and reduced global methylation levels in HeLa cells. Altogether, our results show that maritime pine tannin extract can play a favorable role in cancer treatment to be further explored by pharmaceutical industry for anticancer therapy.

INTRODUCTION

Cancer related diseases are among the major causes of death around the world. Though modern therapies have improved the patient care and therapeutic outcomes, still the majority of tumors are untreatable (Ferlay *et al.*, 2015, Gali-Muhtasib *et al.*, 2015). Continuous efforts are being made to find effective and safer therapies for cancer related disease. Naturally occurring compounds from plants are being thoroughly explored for this purpose and many drugs of natural origin have entered the clinical use (Wang *et al.*, 2012). Indeed, some of the effective anticancer drugs such as vincristine, vinblastine, docetaxel, paclitaxel are derivatives of plant kingdom and are in clinical use today for diverse types of cancers (Greenwell and Rahman, 2015). Treatment with these anticancer drugs inhibit the proliferation of tumors by halting the cell cycle and inducing the apoptosis (Moudi *et al.*, 2013, Iqbal *et al.*, 2017, Xie and Zhou, 2017).

Pinus *pinaster* tree (synonym Pinus *maritimus,* maritime pine) is well-known in traditional herbal medicine for multiple biological activities. Maritime pine trees are commonly found in Mediterranean countries such as France, Italy, Spain and Portugal, and in some northern African countries including Tunisia, Algeria and Morocco (Chupin *et al.*, 2013). Its bark is rich in polyphenolic compounds and is believed to possess anti-inflammatory, antioxidant, antidiabetic, anticancer and antiallergic properties (Packer *et al.*, 1999). The dry extract from bark is available commercially by the name of Pycnogenol® and is commonly indicated for multiple disease including asthma, allergies, skin disease, diabetes, osteoarthritis, erectile dysfunction and venous disease (Rohdewald, 2015). Polyphenolic constituents of this extract are divided into monomer or condensed (procyanidin) flavonoids. Monomers are generally catechin, epicatechin, epigallocatechin and epicatechin gallate along with small proportions of fisetinidin and taxifolin while the procyanidin are polymer of flavan-3-ol units of (+)-catechin or epicatechin of various lengths (Navarrete *et al.*, 2010, Chupin *et al.*, 2013, de la Luz Cadiz-Gurrea *et al.*, 2014).

Anticancer activities of French maritime pine bark have been predicted in few studies due to its polyphenolic content. It induced apoptosis in breast cancer cells, leukemic and fibrosarcoma cells and also prevented the oncogenic transformation of ovarian cells on exposure to carcinogenic talc (Huynh and Teel, 2000, Huang *et al.*, 2005, Buz'Zard and Lau, 2007, Harati *et al.*, 2015). Treatment with bark extract also lowered the incidence of side effects related to anticancer therapy (Belcaro *et al.*, 2008). Despite a beneficial role of

maritime pine bark in cancer suggested by these studies, a detailed study on anticancer properties of this bark content is lacking.

Cancer cells are well known for their tendency to evade the normal growth regulatory mechanisms to proliferate indefinitely by escaping the immune system and simultaneously invading the surrounding tissues. Besides different genetic alterations, various epigenetic perturbations in response to endogenous or exogenous stress signals also predispose the normal cells to acquire these oncogenic properties (Dawson and Kouzarides, 2012). Unlike the genetic abnormalities, epigenetic alterations can be reversed and led to the foundation of new class of compounds that can target these epigenetic alterations to treat cancer. Aberrant hypermethylation of the promoters of tumor suppressor genes is one of the hallmarks of cancer as it represses the function of these genes and leads to unopposed proliferation of cancer tissues (Sharma *et al.*, 2010, Sandoval and Esteller, 2012). DNMT1 and UHRF1 are the integral part of the DNA methylation machinery. UHRF1 identifies the hemi-methylated cytosine on the parent DNA strand and recruits the DNMT1 to the non-methylated cytosine at the daughter strand for the transfer of methylation pattern to newly form strand during the DNA replication (Bronner *et al.*, 2013). UHRF1 and DNMT1 levels are also upregulated in cancers which make them attractive target for anticancer therapy (Unoki, 2011, Ashraf *et al.*, 2017). Currently, 5-azacytidine and 5-aza-2'-deoxycytidine (Decitabine) two DNMTs inhibitor are already in market for the treatment of cancers by targeting this DNA methylation machinery (Pechalrieu *et al.*, 2017). Among many compounds of plant origin, few polyphenolic compounds such as epigallocatechin-3-gallate (EGCG) and luteolin have been reported for their ability to target this UHRF1/DNMT1 tandem to correct the faulty methylation pattern in cells and induce anti-proliferative response in cancer cells (Fang *et al.*, 2003, Achour *et al.*, 2013, Krifa *et al.*, 2013).

Here, we analyze the anticancer activity of maritime pine tannin extract. Polyphenolic compounds present in this bark inhibit the proliferation of cancer cells by inducing arrest in G2/M phase of cell cycle. MPTE treatment also induces activation of p73 tumor suppressor genes and activates the apoptotic pathway in HeLa cells. This extract also down-regulates the levels of epigenetic proteins, like UHRF1 and DNMT1 involved in maintenance of DNA methylation, ultimately leading to a global hypomethylation of the treated cells.

MATERIAL AND METHODS

1. Maritime Pine Tannin extract preparation

Maritime pine (Pinus maritimus) bark was obtained from “Les Landes”, a region situated in the southwest region of France. It was dried initially and crushed mildly to form coarse chips of bark which were later completely dried till a constant weight was obtained. Tannins were extracted from dried ground bark by completely immersing it in 2% sodium bisulphite and 0.5% sodium bicarbonate water solution with continuous stirring in an industrial reactor (Biolandes, France). Final solution was spray-dried to obtain the tannins in the form of dark reddish-brown powder which was later used for studies.

2. Cell culture and MPTE treatment

HeLa cells (ATCC, CCL-2), U2OS and fibroblast were cultured in DMEM (Dulbecco’s Modified Eagle’s Medium), supplemented with 10% FBS (fetal bovine serum), in addition to penicillin (100 U/ml) and streptomycin (100 U/ml) (Invitrogen). Cells were maintained at 37°C in a humid atmosphere with a continuous supply of CO_2 maintained at 5%.

MPTE solutions were always freshly prepared for the treatment of cells. 10 mg of extract powder was first mixed with 50 µL of DMSO by sonication and later this solution was then diluted in 10 mL of preheated DMEM by brief vortex to obtain a concentration of 1 mg/mL. Extract solution was then sterilized by passing through Millex-GP, 0.22 µm syringe filters (Merck-Millipore) and diluted to required concentrations with additional DMEM media. Prepared solutions of desired concentration were then added to seeded cells while the control samples were replaced with fresh media, without the addition of extract.

3. Antibodies:

Different antibodies used in this study include mouse monoclonal anti-PARP (BD Biosciences Pharmingen), rabbit polyclonal anti-caspase3 (Cell Signaling), mouse monoclonal anti-UHRF1 engineered as described previously (Hopfner *et al.*, 2000), mouse monoclonal anti-DNMT1 (Proteogenix France), mouse monoclonal anti-BCL-2 (Merck-Millipore), mouse monoclonal anti-GAPDH (Merck Millipore), polyclonal anti-mouse (Promega) and polyclonal anti-rabbit (promega) antibodies.

4. Cellular proliferation test

Effect of MPTE treatment on cellular proliferation was assayed by help of colorimetric MTT assay. In this assay, viable cells are identified by their ability to reduce the tetrazolium dye MTT 3-(4,5-dimethylthiazol-2-yl)-2,5-diphenyltetrazolium bromide to insoluble purple color formazan crystals. These crystals are later dissolved in DMSO and quantified by measuring absorption at 570 nm. Cell were seeded in 96 well plate at a density of $5x10^3$ cells per well and incubated with different concentrations (12.5, 25, 50, 75, 100, 150, 300, 400 and 500 µg/mL) of MPTE extract. Negative control wells were also replaced with fresh media without addition of extract. After 24 hr of treatment, old media was replaced by 100 µL of MTT (5mg/10mL) containing media in each well and incubated for further 4 hr. Formazan crystals formed after incubation with MTT were later dissolved in 100 µL of DMSO and the absorption at 570 nm was determined by Xenius plate reader. Each experiment was repeated three times and percentage viability in the treated samples was calculated with reference to untreated samples. The cytotoxicity was expressed as IC_{50}, which is the concentration required to reduce the absorbance of treated cells by 50% with reference to the control (untreated cells). Average IC_{50} values were then statistically determined from the dose response curves obtained in Origin software (version 8.6).

5. Cell cycle and apoptosis analysis

For cell cycle analysis, HeLa cells were seeded in 6-well plate at a density of 10^5 cells per well and were treated with 75, 150 and 300 µg/mL of MPTE along with control samples. At the end of 24 hr of treatment, cells were washed with PBS and mildly trypsinized to collect the cells which were then fixed in BD cellfix (BD Biosciences) reagent. Fixed cells were then incubated with FxCycle™ PI/RNase staining solution (Thermo Fisher Scientific) for 20 mins before analysis on Guava 12HT capillary cytometer with the EasyCyte™ software (Merck-Millipore). Fractions of cells in different phase of cell cycle were quantified by using InCyte Software for Guava® (Merck Millipore).

For apoptosis analysis, cells were seeded and treated as mentioned above. Cells from the plate and culture media were collected and incubated with PI and annexin V-FITC™ (Miltenyi Biotec) for 20 mins to label cells undergoing apoptosis which were then analyzed on Guava capillary cytometer and computed with the easyCyte™ software (Merck Millipore) to determine percentage of cells in different phase of apoptosis.

6. Analysis of reactive oxygen species (ROS) production

HeLa cells were seeded and treated in 6-well plate as described in pervious section. ROS production was determined by dihydroethidium (DHE) staining through flow cytometry. Cells were incubated with 10 µM concentration of DHE for 30 mins at 37°C before collection and analysis on Guava 12HT cytometer (Merck Millipore).

7. Western blot

HeLa cells were seeded in a 6-well plate and treated with 75, 150 and 300 µg/mL of MPTE for 24 hr as described earlier. After treatment, cells were collected by trypsinization and incubated with lysis buffer 10 mM Tris-HCl pH 7.5, 150 mM NaCl, 1 mM EDTA and 1% NP40 supplemented with protease inhibitors (complete mini EDTA free protease inhibitor cocktail tablets, Roche Germany) for 30 min on ice to harvest the proteins. After quantifying the isolated proteins by help of standard BSA curve, 40 µg of total protein lysate from each sample was resolved on 10% SDS-PAGE and transferred onto PVDF membranes. Membranes were blocked for 1 hr with 3% blotting-grade blocker (Bio-Rad) in TBST buffer before incubating them overnight with the primary antibodies at 4°C. Membranes were then washed with TBST for three times and incubated with respective secondary antibodies for 1 hr at room temperature. After washing the membranes with TBST, membranes were imaged with the help of chemiluminescent ECL system (Clarity^{TM} ECL western blotting substrate, Biorad, 170-5060) on ImageQuant™ LAS 4000 system (GE Healthcare). Images were quantified using the Image Studio Lite (LiCore Biosciences, USA).

8. Global Methylation Assay:

For global methylation assay HeLa cells were seeded in six well plate and treated as described earlier. DNA was extracted from the treated and non-treated samples by using QIAamp® DNA Kit (Qiagen). 200 µg of the purified DNA from each sample was then analyzed for global methylation levels by using Sigma's Imprint® methylated DNA quantification kit (Sigma-Aldrich) according to manufacturer's protocol.

9. Statistical Analysis:

All experiments were repeated three times and results between groups were statistically compared by one-way ANOVA with post-hoc Tukey test using GraphPad-Prism (version 5.04) and Origin (version 8.6) software.

RESULTS

1. Effect of Maritime Pine tannin extract (MPTE) on cell proliferation

Firstly, the effect of maritime pine tannin extract on cellular proliferation was determined by MTT assay on different cell lines including cervical cancer cell line HeLa, osteosarcoma U2OS cells, and normal fibroblasts cells. Cells were treated with 12.5, 25, 50, 75, 100, 150, 300, 400 and 500 µg/mL of extract for 24 hr and the inhibitory effect was determined by comparing the cell viability with the untreated cells. Results of MTT assay showed that MPTE inhibited the proliferation of these cells in a dose dependent manner (Fig. 1). IC_{50} values were graphically determined for each cell line and it was observed that MPTE significantly reduced the proliferation of HeLa and U2OS cells at relatively low concentration (Fig. 1A-B) as compared to normal fibroblast cells (Fig. 1C). The mean IC_{50} values for HeLa and U2OS cells were 153 ± 16 µg/mL and 218 ± 5 µg/mL respectively as compared to normal fibroblast cells in which the IC_{50} value was 490 ± 26 µg/mL. This shows a selective response of MPTE towards the rapidly dividing cancer cells and prompted us to evaluate its antitumor potential in HeLa cells.

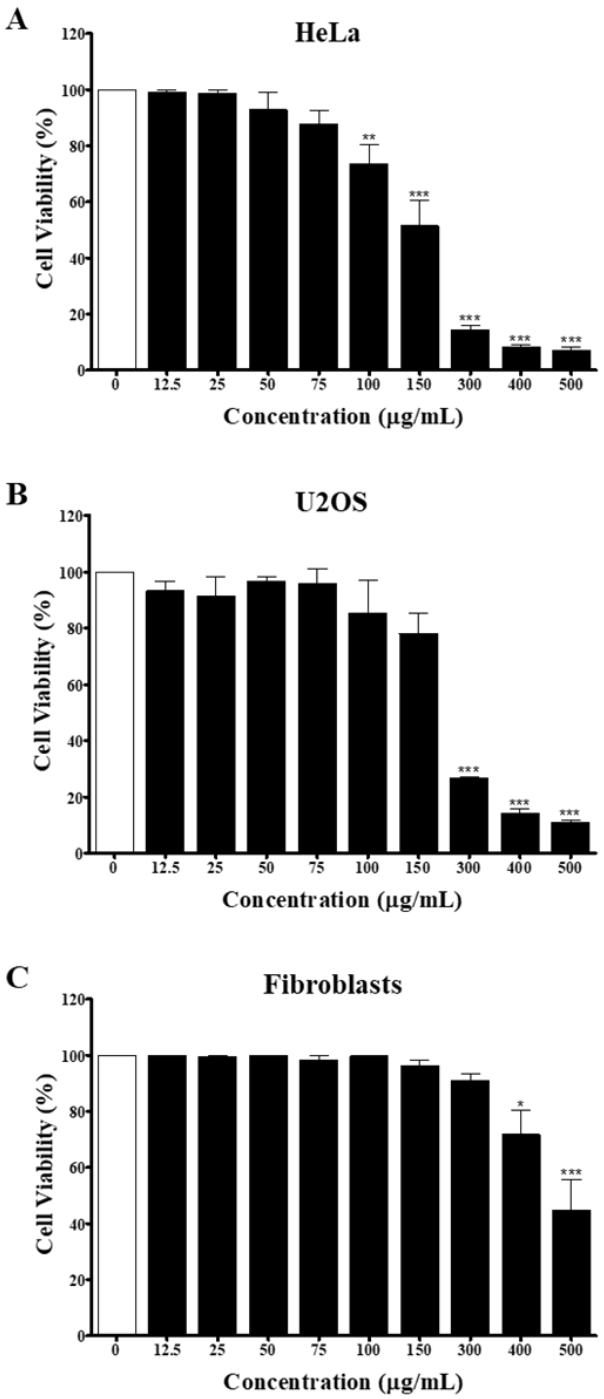

Figure 1. MPTE inhibits the proliferation of cancer cells. HeLa (A), U2OS (B) and fibroblasts cells (C) were treated with MPTE for 24 hr. and the inhibition of proliferation was determined by colorimetric MTT assay. Values are represented in terms of percentage with reference to untreated samples serving as control. Values shown are mean ± SEM of three independent experiments. Statistical significance is represented as * $P < 0.05$, ** $P < 0.01$, *** $P < 0.001$ versus the corresponding control group.

2. MPTE induces cell cycle arrest in G2/M phase

In order to further explore the inhibitory effect of MPTE on cellular proliferation we analyzed the distribution of cells in different phases of cell cycle treated or not with 75, 150 and 300 µg/mL of MPTE. Cytometric analysis revealed that treatment of MPTE for 24 hr. reduced the cellular population in G0/G1 phase while the population in G2/M phase was increased in a dose dependent manner (Fig. 2). Indeed, cellular fraction in G0/G1 phase was significantly reduced from 57% in control cells to 30% and 27% in cells treated with 150 and 300 µg/mL of MPTE respectively. While the cellular population in G2/M phase significantly increased from 18% in control cells to 38% and 34% in HeLa cells treated with 150 and 300 µg/mL of MPTE respectively. This suggests that treatment of MPTE inhibits proliferation of cells by inducing cell cycle arrest at G2/M phase.

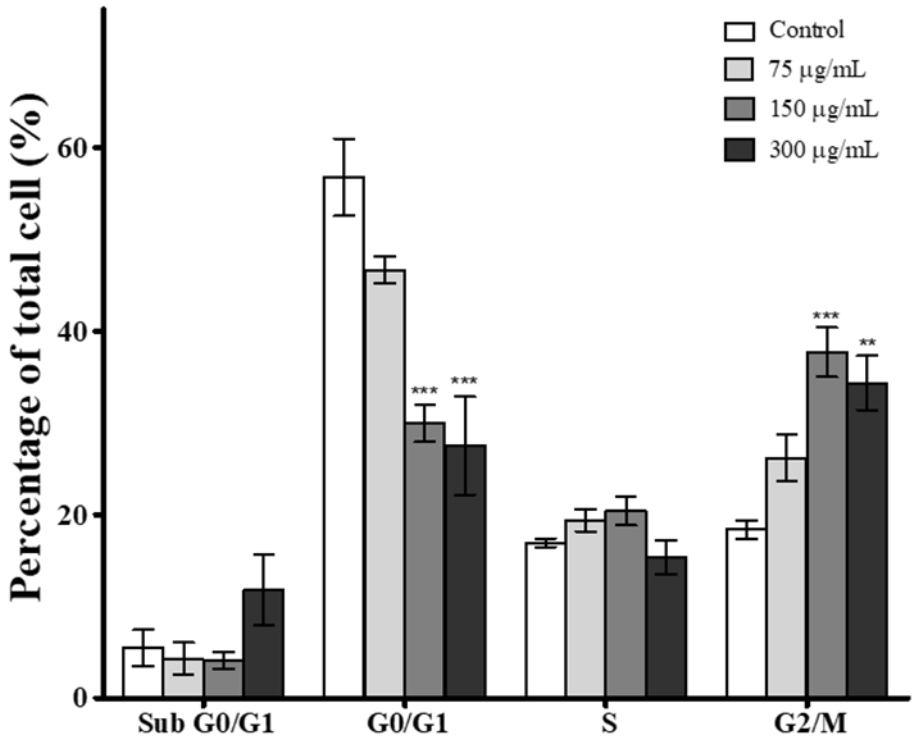

Figure 2. MPTE treatment induced cell cycle arrest. HeLa cells were treated with indicated concentrations of MPTE for 24 hr. Distribution of cells in different phases of cell cycle was determined by cytometric analysis. Cellular distribution in each phase was represented in terms of percentage relative to the total number of cells. Values are expressed as mean ± SEM of three independent experiments. Statistical significance is represented as * $P < 0.05$, ** $P < 0.01$, *** $P < 0.001$ versus the corresponding control group.

3. MPTE treatment induced apoptosis in cells

The potential cytotoxic effect of MPTE treatment was also determined by cytometry through labelling of annexin-FITC and propidium iodide. Treatment with MPTE decreased the viability of cells and induced apoptosis in HeLa cells in a concentration dependent manner (Fig. 3A). Viable cells were significantly reduced from 92% in control cells to 76%, 48% and 27% in cells treated with 75, 150 and 300 µg/mL of MPTE respectively. Accordingly, the early apoptotic cells were also increased from 1.8% in control to 8%, 8.7% and 5.2% in cells treated with 75, 150 and 300 µg/mL of MPTE respectively (Fig. 3A). The percentage of late apoptotic cells and necrotic cells also increased significantly by 24 hr. treatment with 150 and 300 µg/mL of MPTE showing the ability of this extract to induce death in proliferating cells (Fig. 3A).

We also confirmed the induction of apoptosis by analyzing the activation of caspase 3, cleavage of PARP and levels of antiapoptotic protein like BCL2 in the proteins isolated from control and MPTE treated cells (Fig. 3B). Western blot analysis revealed evident activation of caspase 3 from its precursor protein after treating the cells with 150 µg/mL or higher concentration of MPTE. PARP cleavage also became visible in response to MPTE treatment and became more prominent with increasing concentration of MPTE. Indeed, BCL2 levels were also found evidently reduced with treatment of MPTE. These results confirmed the induction of apoptosis in response to MPTE treatment.

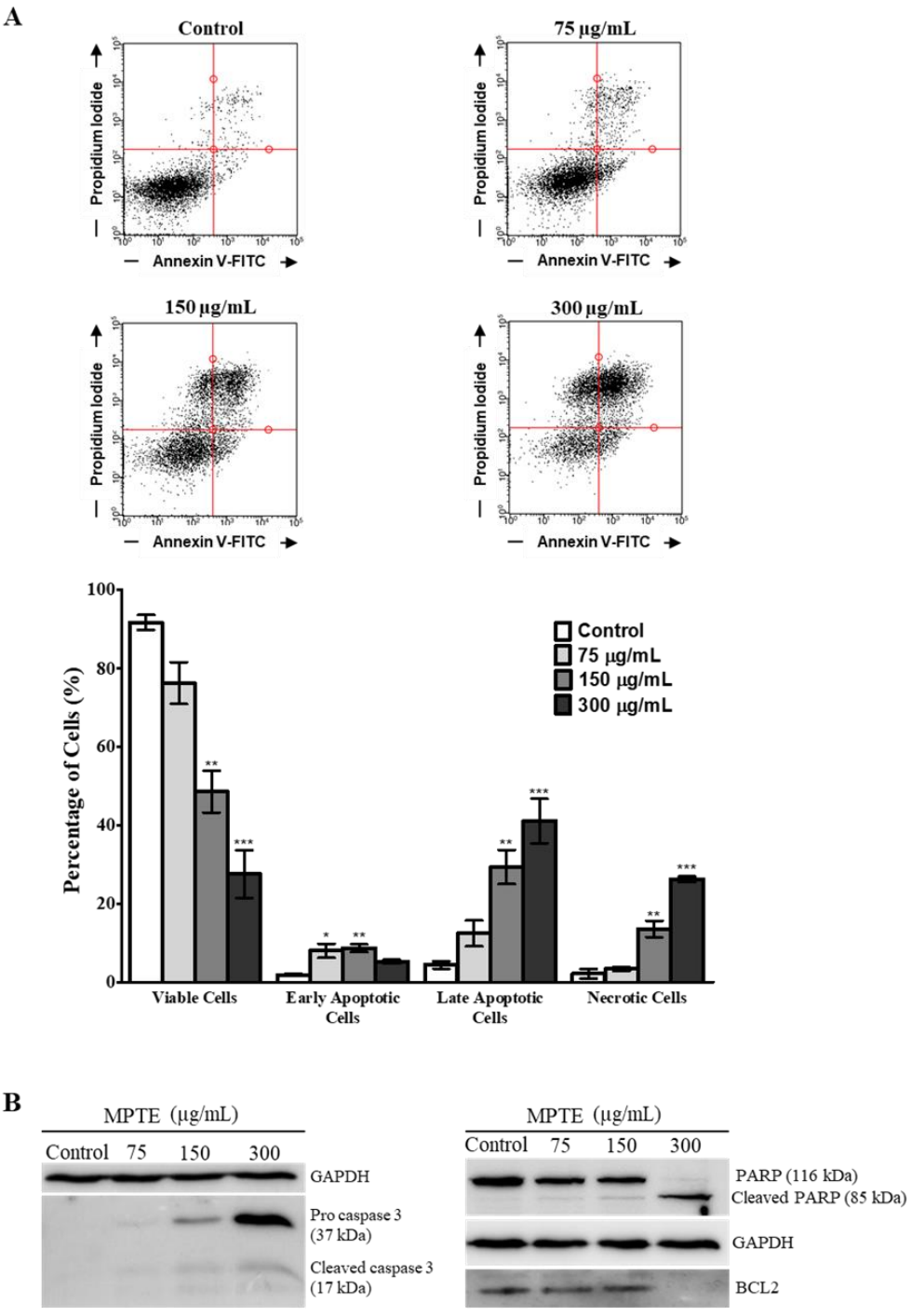

Figure 3. MPTE treatment induced apoptosis in HeLa cells. A, HeLa cells were incubated with indicated concentrations of MPTE for 24 hr. and viable cells along with fraction of cells undergoing apoptosis were determined by annexin V-FITC and PI labeling through cytometry. Values are expressed as mean ± SEM of three independent experiments. Statistical significance is represented as * $P < 0.05$, ** $P < 0.01$, *** $P < 0.001$ versus the corresponding control group. B, Western blots showing cleavage of procaspase 3 and PARP along with down-regulation of BCL2 protein with treatment MPTE in HeLa cells.

4. MPTE treatment induced ROS generation

In order to further determine the mechanism of apoptosis, we checked by cytometric analysis the levels of reactive oxygen species (ROS) generation in cells treated with MPTE by using dihydroethidium (DHE) staining. DHE gets oxidized inside the cells on exposure to ROS and changes to 2-hydroxyethidium or ethidium which gets incorporated into the DNA and fluorescently labels the cells. Cytometric analysis of HeLa cells treated with MPTE revealed significant production of ROS when incubated with higher concentrations of MPTE for 24 hr (Fig. 4A-B). Indeed, the ROS levels increased by 1.5 and 2 folds with the 24 hr treatment of 150 and 300 µg/mL of MPTE respectively as compared to controls (Fig. 4B). The granularity of the cells is usually increased with ROS generation and is often considered as indicator of senescence or apoptosis (Gosselin *et al.*, 2009). Side scatter plot revealed that granularity of cells increased after 24 hr with the treatment of 150 and 300 µg/mL of MPTE in a pattern similar to increase in ROS levels indicating that high ROS levels by MPTE treatment induced apoptosis in these cells (Fig. 4C-D).

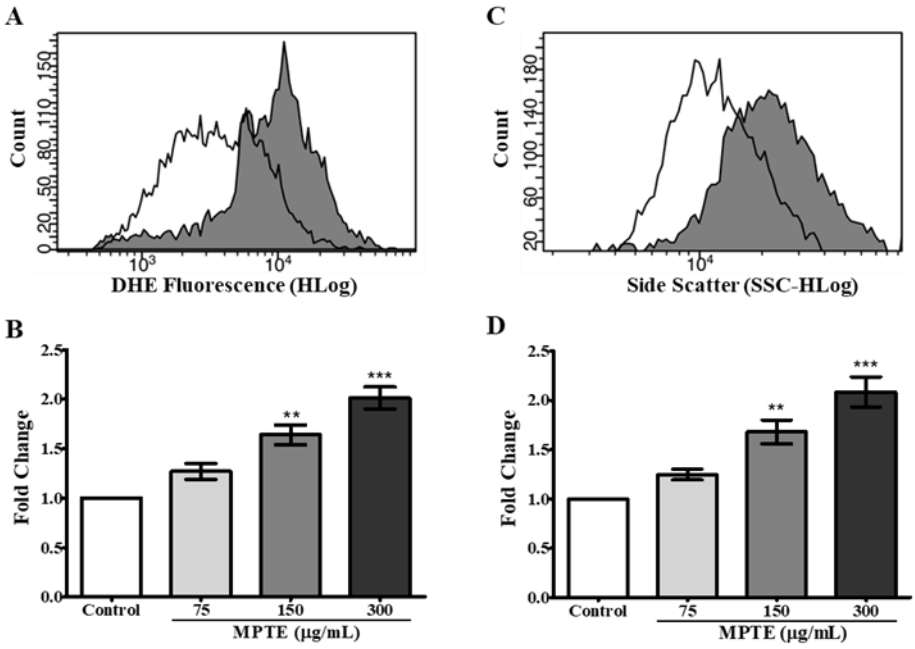

Figure 4. MPTE treatment increased ROS levels and granularity in treated cells. A, Cytogram showing DHE labeling in control (represented by white area under graph) and MPTE treated cells (300 µg/mL, represented by gray area under graph). B, Bar graph showing fold change in DHE labeling by treatment of MPTE at different concentration with respect to control. C, Cytogram showing side scatter in control (represented by white area under graph) and MPTE treated cells (300 µg/mL, represented by gray area under graph). D, Bar graph showing fold change in side scatter by treatment of MPTE at different concentration with respect to control. Values indicated are from three independent experiments and were analyzed by one-way ANOVA with post-hoc Tukey test. (* $P < 0.05$, ** $P < 0.01$, *** $P < 0.001$).

5. MPTE treatment upregulated p73 and down-regulated UHRF1 and DNMT1 in HeLa cells

Previously, it has been reported that naturally occurring polyphenolic compounds inhibit the proliferation and activate apoptosis in p53 deficient cancer cells by inducing the expression of its analogue p73 (Alhosin *et al.*, 2010, Achour *et al.*, 2013). So, to check this effect as possible mechanism for induction of cell cycle arrest and apoptosis we evaluated the effect of MPTE treatment on expression of p73 in these cells. Cells were treated with 75, 150 and 300 µg/mL of MPTE for 24 hr and western blot results of the proteins isolated from these cells revealed that treatment of MPTE induced upregulation of p73 in HeLa cells (Fig. 5A-B). Increase in p73 expression was found most significant with treatment of 300 µg/mL of MPTE which upregulated p73 levels by five folds as compared to controls (Fig. 5B).

In our previous studies, we have observed that polyphenolic compounds can also target the UHRF1/DNMT1 tandem responsible for the maintenance of DNA methylation patterns in cells through tumor suppressor genes such as p53 and p73 (Alhosin *et al.*, 2010, Achour *et al.*, 2013). So, we also analyzed the levels of these epigenetic proteins after MPTE exposure to cells and observed significant down-regulation of UHRF1 and DNMT1 in a dose dependent manner (Fig. 5A, C-D). Treatment with 75 µg/mL of MPTE induced significant decrease in UHRF1 and DNMT1 levels as compared to controls which became more prominent with higher concentration of extract (Fig. 5C-D).

Since, UHRF1 and DNMT1 are primarily involved in the maintenance of DNA methylation pattern during the replication; we also checked the effect of UHRF1 and DNMT1 down-regulation on global DNA methylation level in cells by using Imprint® Methylated DNA Quantification assay. After treatment with different concentration of extract for 24 hr, our results indicated a decrease in the global methylation levels (Fig. 5E). The effect was more prominent at concentration of 150 µg/mL, as the global methylation levels were averagely 25% less than the levels in control samples. Treatment with 300 µg/mL of MPTE for 24 hr further reduced the global methylation levels by 33% when compared with control samples.

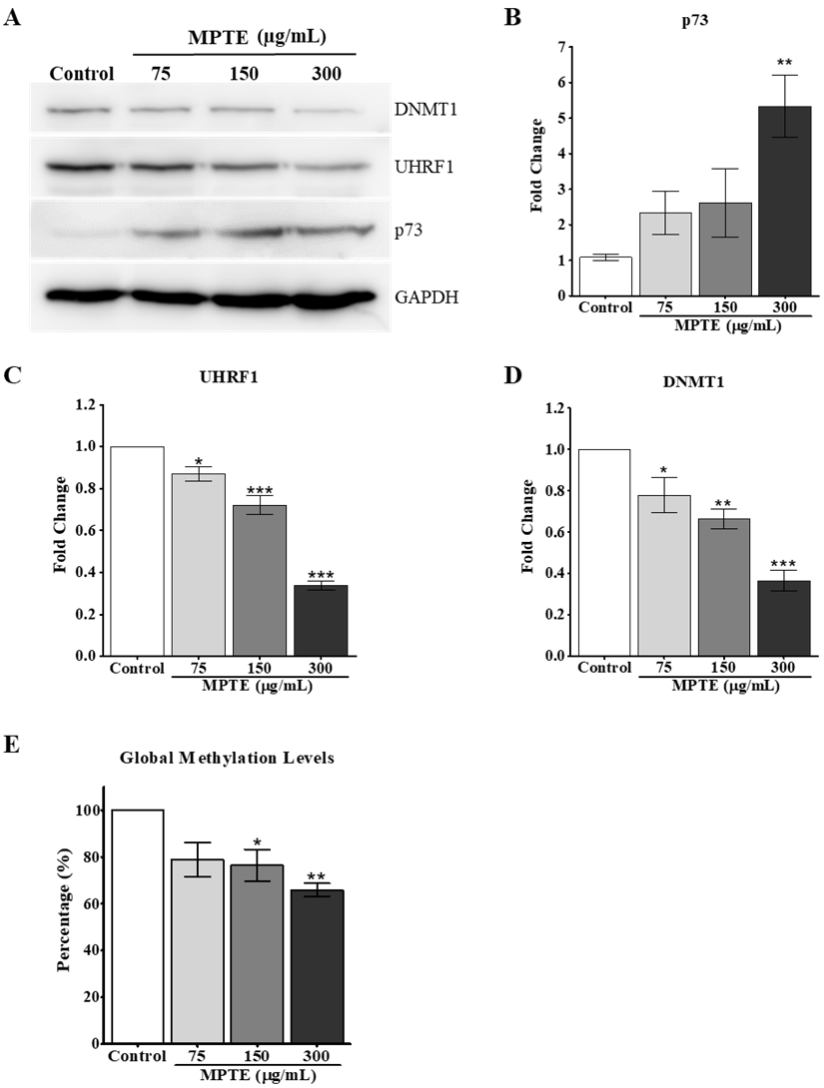

Figure 5. MPTE upregulated p73 along with down-regulation of UHRF1 and DNMT1 in cancer cells. A, Western blot analysis of proteins isolated from HeLa cells were treated with 75, 150 and 300 µg/mL of MPTE for 24 hr. along with untreated cells. B, Effect of MPTE treatment on p73 levels with respect to controls. C, Effect of MPTE treatment on UHRF1 levels with respect to controls. D, Effect of MPTE treatment on DNMT1 levels with respect to controls. E, Effect of MPTE treatment on global methylation levels. Values indicated are from three independent experiments and were analyzed by one-way ANOVA with post-hoc Tukey test. (* $P < 0.05$, ** $P < 0.01$, *** $P < 0.001$).

DISCUSSION

Many studies have shown a beneficial role of polyphenolic plant products in prevention and cure of cancers. Such products are now being thoroughly explored for their possible application in treatment of tumors by identifying their active ingredients and their possible mechanism of action (Asensi *et al.*, 2011, Zhou *et al.*, 2016). Maritime pine bark has been previously reported to induce differentiation and apoptosis in cancer cells (Huynh and Teel,

2000, Huang *et al.*, 2005, Buz'Zard and Lau, 2007, Harati *et al.*, 2015). The aim of this study was to check the potential of tannin extract from its bark for the anticancer therapy. MPTE has been well characterized chemically, MALDI-TOF and 13C NMR analysis of this extract revealed that it contains mixture of condensed tannins (procyanidins) made up of varying subunits of catechin, epicatechin, epigallocatechin, epicatechin gallate and fisetinidin monomers (Fig. 6) (Navarrete *et al.*, 2010).

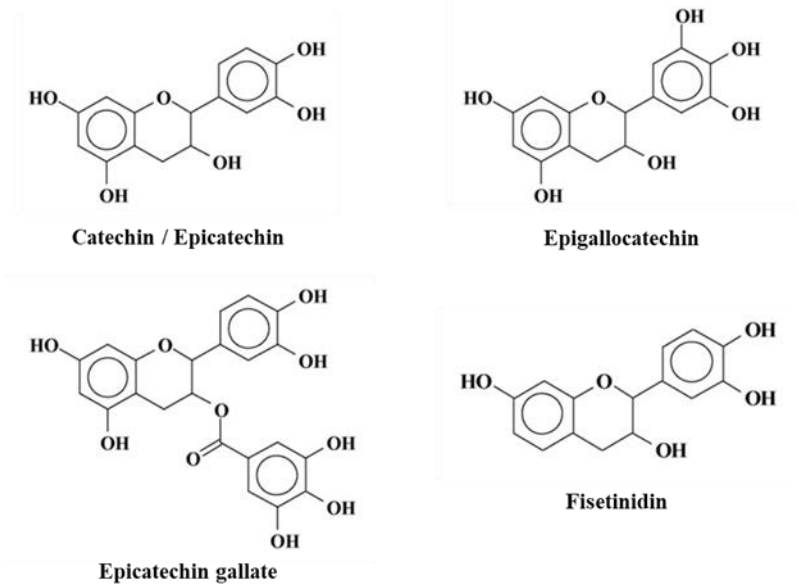

Figure 6. Major catechol monomers forming the procyanidins oligomers in maritime pine tannin extract.

Different physiological properties of maritime pine bark extract such as antioxidant, anti-inflammatory, antidiabetic and cardioprotective effects have been attributed to the presence of these polyphenolic compounds (Packer *et al.*, 1999, Rohdewald, 2015). These compounds are also present in naturally different combinations in leaves of green tea where they have shown their anticancer properties in different studies (Achour *et al.*, 2013, Yang and Wang, 2016). It is also observed that these compounds work better in the form of natural combination in plant product rather than tested individually, as in combination they are effective at lower dose and cause less toxicity (Bode and Dong, 2009).

In our results we observed that treatment with MPTE inhibited the proliferation of cervical cancer HeLa and osteosarcoma U2OS cell lines at low concentration as compared to the primary fibroblasts showing a specific response towards the rapidly proliferating cancer cells. Inhibition of proliferation on treatment with MPTE also resulted in accumulation of the cells in G2/M phase which is commonly observed by the treatment of anticancer compounds

(Senese *et al.*, 2014). Catechins and other polyphenolic compounds and from different plant sources have also been reported to induce arrest in G2/M phase of cell cycle in similar studies (Shan *et al.*, 2015, Takanashi *et al.*, 2017). Along with it, MPTE also induced apoptosis in HeLa cells as indicated by increased labeling of annexin V and PI in flow cytometry analysis. Western blot results further confirmed the induction of apoptosis as it revealed the activation of caspase 3 and cleavage of PARP in a dose dependent manner in MPTE treated cells. Levels of pro-survival protein BCL2 were also decreased on MPTE treatment which is necessary for the maintenance of mitochondrial membrane integrity. Loss of BCL2 results in release of cytochrome c and thus leads to apoptosis. In a similar manner, many polyphenolic compounds e.g. (-) epigallocatechin gallate, butein and curcumin have been shown to induce apoptosis in variety of cancer cells by activating caspase 3 and PARP cleavage along with down-regulation of BCL-2 protein (Halder *et al.*, 2008, Chen *et al.*, 2012, Wang *et al.*, 2015, Zhu *et al.*, 2015, Wang *et al.*, 2018).

Contrary to previously reported antioxidant activity of maritime pine bark extract, we observed a pro-oxidant role of MPTE in cancer cells which was evident by dose dependent increase in ROS staining with treatment of MPTE (Packer *et al.*, 1999). Polyphenols rich extracts from tea leaves, grapes, fruits and berries have already been reported to induce ROS production and induce apoptosis in cancer cells besides having predominantly antioxidant effect in normal cells (Leon-Gonzalez *et al.*, 2015). Polyphenols can act as both antioxidant and pro-oxidant depending upon the nature of cells. In normal cells, polyphenolic compounds prevent the cellular material from oxidative stress because of its anti-oxidant activity while in cancer cells they may behave as pro-oxidant compound and can kill the tumor cells because of high pH and increased level of redox active transient metals (Leon-Gonzalez *et al.*, 2015, Eghbaliferiz and Iranshahi, 2016). This specific targeting of cancer cells makes the polyphenolic compounds an interesting candidate for anticancer therapy. Increased ROS is also associated with increase granularity in the cells indicating the early sign of apoptosis as previously it has been reported that increase in ROS generation leads to senescence by increased granulation of cells (Gosselin *et al.*, 2009, Raghuram *et al.*, 2010).

It is also interesting to note that treatment of MPTE induced the expression of p73, tumor suppressor genes in p53 deficient HeLa cells. Previously, it has been shown that increase ROS production can activate the p73 expression in HeLa cells and induce apoptosis through mitochondrial pathway by activation of caspase 9 and 3 (Singh *et al.*, 2007). Activation of p73 has also been observed with different plant products including thymoquinone,

epigallocatechin-3-gallate and polyphenolic extracts from grapes and berries in p53 deficient cancer cells where it induced apoptosis by p73 dependent mechanism (Alhosin *et al.*, 2010, Sharif *et al.*, 2012, Achour *et al.*, 2013, Leon-Gonzalez *et al.*, 2017).

Earlier, we have observed in different studies that p53 and p73 also negatively regulates the epigenetic mediator UHRF1 in cancer cells (Alhosin *et al.*, 2010, Achour *et al.*, 2013). In this study, we also observed down-regulation of UHRF1 upon MPTE treatment in HeLa cells along with upregulation of p73, correlating with the previous data. UHRF1 is mostly found upregulated in cancers and promotes oncogenesis of cells by facilitating their passage through cell cycle (Ashraf *et al.*, 2017). High levels of UHRF1 directly interfere in function of tumor suppressor genes (TSGs) or induce down-regulation of variety of TSGs through their promoter hypermethylation. UHRF1 upregulation in cancer cells also makes the cells resistive to anticancer therapy by facilitating the DNA damage repair, highlighting its potential as a target for anticancer therapy (Bronner *et al.*, 2013, Ashraf *et al.*, 2017). Therefore, knockdown of UHRF1 by siRNA or other plant products such as ECGC, thymoquinone or polyphenolic extracts induced the apoptosis in cancer cells and improved the response of resistive tumor cells to anticancer therapy (Alhosin *et al.*, 2010, Achour *et al.*, 2013, Bronner *et al.*, 2013). In our current study, we observed a down-regulation of UHRF1 with chatechin and epicatechin associated monomers and polymers enriched in MPTE and we observed blockade of cells in G2/M phase which is in agreement with a previous finding where depletion of UHRF1 resulted in cell cycle arrest in G2/M phase of cell cycle (Tien *et al.*, 2011). MPTE also down-regulated the expression of DNMT1, important epigenetic partner of UHRF1. It is through the mutual coordination with DNMT1 that UHRF1 silences different TSGs through promoter hypermethylation (Unoki, 2011, Bronner *et al.*, 2013). We have also observed that down-regulation of UHRF1 and DNMT1 was followed by global hypomethylation on treatment with MPTE. Catechol containing dietary polyphenols has been well described previously to interfere in the DNA methylation process (Stefanska *et al.*, 2012). Catechol groups can be methylated by catechol-O-methyltransferase (COMT) to methylated catechols. This process depletes the S-adenosyl-L-methionine (SAM), the methyl group donor in the body for DNA methylation and converts it into S-adenosyl-L-homocysteine (SAH) which is a potent inhibitor of DNA methylation by feedback mechanism (Lee and Zhu, 2006). Additionally, gallic acid moiety containing catechol analogues such as (-)-epigallocatechin-3-O-gallate can also directly inhibit DNMT1 by tethering into the hydrophilic binding pocket of DNMT1 through Mg^{+2} stabilized interaction (Lee *et al.*, 2005,

Fang *et al.*, 2007). MPTE is rich in this catechol containing compounds and by affecting the important actors of DNA methylation machinery including UHRF1 and DNMT1; it can interfere in the global methylation patterns of the cells.

In conclusion, we demonstrate here anticancer properties of maritime pine tannin extract and establish, in HeLa cells, that MPTE specifically inhibits the proliferation of cancer cells by inducing cell cycle arrest in G2/M phase along with ROS mediated activation of mitochondrial apoptotic pathway. MPTE increases the expression of p73 tumor suppressor gene while it down-regulates oncogenic UHRF1 and DNMT1 in cancer cells and reduces the global DNA methylation levels. Maritime pine bark extract has been used in traditional herbal medicine for a long time. Easy availability in nature along with unique capability to inhibit cancer cells and regulate the DNA methylation patterns make MPTE an interesting candidate for pharmaceutical research to explore it for anticancer therapy.

REFERENCES

Achour, M., Mousli, M., Alhosin, M., Ibrahim, A., Peluso, J., Muller, C.D., Schini-Kerth, V.B., Hamiche, A., Dhe-Paganon, S. & Bronner, C., 2013. Epigallocatechin-3-gallate up-regulates tumor suppressor gene expression via a reactive oxygen species-dependent down-regulation of UHRF1. *Biochem Biophys Res Commun,* 430**,** 208-12.

Alhosin, M., Abusnina, A., Achour, M., Sharif, T., Muller, C., Peluso, J., Chataigneau, T., Lugnier, C., Schini-Kerth, V.B., Bronner, C. & Fuhrmann, G., 2010. Induction of apoptosis by thymoquinone in lymphoblastic leukemia Jurkat cells is mediated by a p73-dependent pathway which targets the epigenetic integrator UHRF1. *Biochem Pharmacol,* 79**,** 1251-60.

Asensi, M., Ortega, A., Mena, S., Feddi, F. & Estrela, J.M., 2011. Natural polyphenols in cancer therapy. *Crit Rev Clin Lab Sci,* 48**,** 197-216.

Ashraf, W., Ibrahim, A., Alhosin, M., Zaayter, L., Ouararhni, K., Papin, C., Ahmad, T., Hamiche, A., Mely, Y., Bronner, C. & Mousli, M., 2017. The epigenetic integrator UHRF1: on the road to become a universal biomarker for cancer. *Oncotarget,* 8**,** 51946-51962.

Belcaro, G., Cesarone, M.R., Genovesi, D., Ledda, A., Vinciguerra, G., Ricci, A., Pellegrini, L., Gizzi, G., Ippolito, E., Dugall, M., Cacchio, M., Di Renzo, A. & Stuard, S., 2008. Pycnogenol may alleviate adverse effects in oncologic treatment. *Panminerva Med,* 50**,** 227-34.

Bode, A.M. & Dong, Z., 2009. Epigallocatechin 3-gallate and green tea catechins: United they work, divided they fail. *Cancer Prev Res (Phila),* 2**,** 514-7.

Bronner, C., Krifa, M. & Mousli, M., 2013. Increasing role of UHRF1 in the reading and inheritance of the epigenetic code as well as in tumorogenesis. *Biochem Pharmacol,* 86**,** 1643-9.

Buz'zard, A.R. & Lau, B.H., 2007. Pycnogenol reduces talc-induced neoplastic transformation in human ovarian cell cultures. *Phytother Res,* 21**,** 579-86.

Chen, Y.H., Yeh, C.W., Lo, H.C., Su, S.L., Hseu, Y.C. & Hsu, L.S., 2012. Generation of reactive oxygen species mediates butein-induced apoptosis in neuroblastoma cells. *Oncol Rep,* 27**,** 1233-7.

Chupin, L., Motillon, C., Charrier-El Bouhtoury, F., Pizzi, A. & Charrier, B., 2013. Characterisation of maritime pine (Pinus pinaster) bark tannins extracted under different conditions by spectroscopic methods, FTIR and HPLC. *Industrial Crops and Products,* 49**,** 897-903.

Dawson, M.A. & Kouzarides, T., 2012. Cancer epigenetics: from mechanism to therapy. *Cell,* 150**,** 12-27.

De La Luz Cadiz-Gurrea, M., Fernandez-Arroyo, S. & Segura-Carretero, A., 2014. Pine bark and green tea concentrated extracts: antioxidant activity and comprehensive characterization of bioactive compounds by HPLC-ESI-QTOF-MS. *Int J Mol Sci,* 15**,** 20382-402.

Eghbaliferiz, S. & Iranshahi, M., 2016. Prooxidant Activity of Polyphenols, Flavonoids, Anthocyanins and Carotenoids: Updated Review of Mechanisms and Catalyzing Metals. *Phytother Res,* 30**,** 1379-91.

Fang, M., Chen, D. & Yang, C.S., 2007. Dietary polyphenols may affect DNA methylation. *J Nutr,* 137**,** 223S-228S.

Fang, M.Z., Wang, Y., Ai, N., Hou, Z., Sun, Y., Lu, H., Welsh, W. & Yang, C.S., 2003. Tea polyphenol (-)-epigallocatechin-3-gallate inhibits DNA methyltransferase and reactivates methylation-silenced genes in cancer cell lines. *Cancer Res,* 63**,** 7563-70.

Ferlay, J., Soerjomataram, I., Dikshit, R., Eser, S., Mathers, C., Rebelo, M., Parkin, D.M., Forman, D. & Bray, F., 2015. Cancer incidence and mortality worldwide: sources, methods and major patterns in GLOBOCAN 2012. *Int J Cancer,* 136**,** E359-86.

Gali-Muhtasib, H., Hmadi, R., Kareh, M., Tohme, R. & Darwiche, N., 2015. Cell death mechanisms of plant-derived anticancer drugs: beyond apoptosis. *Apoptosis,* 20**,** 1531-62.

Gosselin, K., Deruy, E., Martien, S., Vercamer, C., Bouali, F., Dujardin, T., Slomianny, C., Houel-Renault, L., Chelli, F., De Launoit, Y. & Abbadie, C., 2009. Senescent keratinocytes die by autophagic programmed cell death. *Am J Pathol,* 174**,** 423-35.

Greenwell, M. & Rahman, P.K., 2015. Medicinal Plants: Their Use in Anticancer Treatment. *Int J Pharm Sci Res,* 6**,** 4103-4112.

Halder, B., Bhattacharya, U., Mukhopadhyay, S. & Giri, A.K., 2008. Molecular mechanism of black tea polyphenols induced apoptosis in human skin cancer cells: involvement of Bax translocation and mitochondria mediated death cascade. *Carcinogenesis,* 29**,** 129-38.

Harati, K., Slodnik, P., Chromik, A.M., Behr, B., Goertz, O., Hirsch, T., Kapalschinski, N., Klein-Hitpass, L., Kolbenschlag, J., Uhl, W., Lehnhardt, M. & Daigeler, A., 2015. Proapoptotic effects of pycnogenol on HT1080 human fibrosarcoma cells. *Int J Oncol,* 46**,** 1629-36.

Hopfner, R., Mousli, M., Jeltsch, J.M., Voulgaris, A., Lutz, Y., Marin, C., Bellocq, J.P., Oudet, P. & Bronner, C., 2000. ICBP90, a novel human CCAAT binding protein, involved in the regulation of topoisomerase IIalpha expression. *Cancer Res,* 60**,** 121-8.

Huang, W.W., Yang, J.S., Lin, C.F., Ho, W.J. & Lee, M.R., 2005. Pycnogenol induces differentiation and apoptosis in human promyeloid leukemia HL-60 cells. *Leuk Res,* 29**,** 685-92.

Huynh, H.T. & Teel, R.W., 2000. Selective induction of apoptosis in human mammary cancer cells (MCF-7) by pycnogenol. *Anticancer Res,* 20**,** 2417-20.

Iqbal, J., Abbasi, B.A., Mahmood, T., Kanwal, S., Ali, B., Shah, S.A. & Khalil, A.T., 2017. Plant-derived anticancer agents: A green anticancer approach. *Asian Pacific Journal of Tropical Biomedicine,* 7**,** 1129-1150.

Krifa, M., Alhosin, M., Muller, C.D., Gies, J.P., Chekir-Ghedira, L., Ghedira, K., Mely, Y., Bronner, C. & Mousli, M., 2013. Limoniastrum guyonianum aqueous gall extract induces apoptosis in human cervical cancer cells involving p16 INK4A re-expression related to UHRF1 and DNMT1 down-regulation. *J Exp Clin Cancer Res,* 32**,** 30.

Lee, W.J., Shim, J.Y. & Zhu, B.T., 2005. Mechanisms for the inhibition of DNA methyltransferases by tea catechins and bioflavonoids. *Mol Pharmacol,* 68**,** 1018-30.

Lee, W.J. & Zhu, B.T., 2006. Inhibition of DNA methylation by caffeic acid and chlorogenic acid, two common catechol-containing coffee polyphenols. *Carcinogenesis,* 27**,** 269-77.

Leon-Gonzalez, A.J., Auger, C. & Schini-Kerth, V.B., 2015. Pro-oxidant activity of polyphenols and its implication on cancer chemoprevention and chemotherapy. *Biochem Pharmacol,* 98**,** 371-80.

Leon-Gonzalez, A.J., Jara-Palacios, M.J., Abbas, M., Heredia, F.J. & Schini-Kerth, V.B., 2017. Role of epigenetic regulation on the induction of apoptosis in Jurkat leukemia cells by white grape pomace rich in phenolic compounds. *Food Funct,* 8**,** 4062-4069.

Moudi, M., Go, R., Yien, C.Y. & Nazre, M., 2013. Vinca alkaloids. *Int J Prev Med,* 4**,** 1231-5.

Navarrete, P., Pizzi, A., Pasch, H., Rode, K. & Delmotte, L., 2010. MALDI-TOF and 13C NMR characterization of maritime pine industrial tannin extract. *Industrial Crops and Products,* 32**,** 105-110.

Packer, L., Rimbach, G. & Virgili, F., 1999. Antioxidant activity and biologic properties of a procyanidin-rich extract from pine (Pinus maritima) bark, pycnogenol. *Free Radic Biol Med,* 27**,** 704-24.

Pechalrieu, D., Etievant, C. & Arimondo, P.B., 2017. DNA methyltransferase inhibitors in cancer: From pharmacology to translational studies. *Biochem Pharmacol,* 129**,** 1-13.

Raghuram, G.V., Pathak, N., Jain, D., Panwar, H., Pandey, H., Jain, S.K. & Mishra, P.K., 2010. Molecular mechanisms of isocyanate induced oncogenic transformation in ovarian epithelial cells. *Reprod Toxicol,* 30**,** 377-86.

Rohdewald, P.J., 2015. Update on the clinical pharmacology of Pycnogenol(R). *Medical Research Archives*.

Sandoval, J. & Esteller, M., 2012. Cancer epigenomics: beyond genomics. *Curr Opin Genet Dev,* 22**,** 50-5.

Senese, S., Lo, Y.C., Huang, D., Zangle, T.A., Gholkar, A.A., Robert, L., Homet, B., Ribas, A., Summers, M.K., Teitell, M.A., Damoiseaux, R. & Torres, J.Z., 2014. Chemical dissection of the cell cycle: probes for cell biology and anti-cancer drug development. *Cell Death Dis,* 5**,** e1462.

Shan, H.M., Shi, Y. & Quan, J., 2015. Identification of green tea catechins as potent inhibitors of the polo-box domain of polo-like kinase 1. *ChemMedChem,* 10**,** 158-63.

Sharif, T., Alhosin, M., Auger, C., Minker, C., Kim, J.H., Etienne-Selloum, N., Bories, P., Gronemeyer, H., Lobstein, A., Bronner, C., Fuhrmann, G. & Schini-Kerth, V.B., 2012. Aronia melanocarpa juice induces a redox-sensitive p73-related caspase 3-dependent apoptosis in human leukemia cells. *PLoS One,* 7**,** e32526.

Sharma, S., Kelly, T.K. & Jones, P.A., 2010. Epigenetics in cancer. *Carcinogenesis,* 31**,** 27-36.

Singh, M., Sharma, H. & Singh, N., 2007. Hydrogen peroxide induces apoptosis in HeLa cells through mitochondrial pathway. *Mitochondrion,* 7**,** 367-73.

Stefanska, B., Karlic, H., Varga, F., Fabianowska-Majewska, K. & Haslberger, A., 2012. Epigenetic mechanisms in anti-cancer actions of bioactive food components--the implications in cancer prevention. *Br J Pharmacol,* 167**,** 279-97.

Takanashi, K., Suda, M., Matsumoto, K., Ishihara, C., Toda, K., Kawaguchi, K., Senga, S., Kobayashi, N., Ichikawa, M., Katoh, M., Hattori, Y., Kawahara, S.I., Umezawa, K., Fujii, H. & Makabe, H., 2017. Epicatechin oligomers longer than trimers have anti-cancer activities, but not the catechin counterparts. *Sci Rep,* 7**,** 7791.

Tien, A.L., Senbanerjee, S., Kulkarni, A., Mudbhary, R., Goudreau, B., Ganesan, S., Sadler, K.C. & Ukomadu, C., 2011. UHRF1 depletion causes a G2/M arrest, activation of DNA damage response and apoptosis. *Biochem J,* 435**,** 175-85.

Unoki, M., 2011. Current and potential anticancer drugs targeting members of the UHRF1 complex including epigenetic modifiers. *Recent Pat Anticancer Drug Discov,* 6**,** 116-30.

Wang, H., Khor, T.O., Shu, L., Su, Z.Y., Fuentes, F., Lee, J.H. & Kong, A.N., 2012. Plants vs. cancer: a review on natural phytochemicals in preventing and treating cancers and their druggability. *Anticancer Agents Med Chem,* 12**,** 1281-305.

Wang, J., Pan, Y., Hu, J., Ma, Q., Xu, Y., Zhang, Y., Zhang, F. & Liu, Y., 2018. Tea polyphenols induce S phase arrest and apoptosis in gallbladder cancer cells. *Braz J Med Biol Res,* 51**,** e6891.

Wang, J., Xie, Y., Feng, Y., Zhang, L., Huang, X., Shen, X. & Luo, X., 2015. (-)-Epigallocatechingallate induces apoptosis in B lymphoma cells via caspase-dependent pathway and Bcl-2 family protein modulation. *Int J Oncol,* 46**,** 1507-15.

Xie, S. & Zhou, J., 2017. Harnessing Plant Biodiversity for the Discovery of Novel Anticancer Drugs Targeting Microtubules. *Front Plant Sci,* 8**,** 720.

Yang, C.S. & Wang, H., 2016. Cancer Preventive Activities of Tea Catechins. *Molecules,* 21.

Zhou, Y., Zheng, J., Li, Y., Xu, D.P., Li, S., Chen, Y.M. & Li, H.B., 2016. Natural Polyphenols for Prevention and Treatment of Cancer. *Nutrients,* 8.

Zhu, L., Han, M.B., Gao, Y., Wang, H., Dai, L., Wen, Y. & Na, L.X., 2015. Curcumin triggers apoptosis via upregulation of Bax/Bcl-2 ratio and caspase activation in SW872 human adipocytes. *Mol Med Rep,* 12**,** 1151-6.

RESUME DE THESE

VIII-RÉSUMÉ DE THÈSE

VIII.A. Introduction

L'épigénétique est définie comme une modification héréditaire de la fonction des gènes qui n'impliquent pas une altération de la séquence de l'ADN. Les modifications épigénétiques comme la méthylation de l'ADN, les modifications des histones et l'expression non codante de l'ARN peuvent modifier la structure de la chromatine et l'expression des génes. Les aberrations dans le méthylome peuvent favoriser la transformation oncogènique des cellules de l'organisme en inhibant les gènes suppresseurs de tumeurs (TGSs) ou en induisant l'expression des oncogènes. L'inversion de ces aberrations épigénétiques peut constituer un objectif thérapeutique prometteur de la thérapie anticancéreuse.

L'intégrateur nucléaire épigénétique UHRF1 (Ubiquitin-like, containing PHD and RING Finger domains 1) joue un rôle important dans la maintenance de la méthylation de l'ADN, les modifications des histones, le cycle cellulaire et la réparation aux dommages de l'ADN. La protéine UHRF1 (Figure 1) est considérée comme ayant un potentiel oncogènique car ses niveaux d'expression sont élevés dans de nombreux cancers et elle favorise la prolifération cellulaire. Elle inhibe les gènes suppresseurs de tumeurs (TSGs) comme la p73, RB1, $p16^{INK4A}$ et $p14^{ARF}$ par hypermethylation de leurs régions promotrices. UHRF1 se lie spécifiquement par l'intermédiaire de son domaine SET and RING Associated (SRA) aux sites CpGs de l'ADN hémi-méthylé (HM) et fait basculer la 5'-méthylcytosine (5mC) dans le grand sillon de l'hélice d'ADN. UHRF1 se lie également à l'histone H3K9me3 par l'intermédiaire de son domaine Tandem Tudor. UHRF1 est stabilisé par l'enzyme désubiquitinase connue sous le nom d'USP7 (Ubiquitin-specific peptidase 7) qui protège UHRF1 de la dégradation protéasomique. Avec ses autres partenaires, UHRF1, avec TIP60, DNMT1, PCNA, USP7 et HDAC1, forment un complexe macromoléculaire et jouent un rôle important dans la stabilité et la régulation de la DNMT1.

La protéine TIP60 (Tat-interacting protein of 60 kDa) (Figure 1) appartient à la famille MYST (MOZ, YBF2, SAS2 et TIP60) ayant une activité acétyltransférase. Au départ, elle a été identifiée comme un partenaire de la protéine Tat du VIH-1. En raison de son activité acétyltransférase, TIP60 joue un rôle clé dans de nombreuses fonctions cellulaires telles que la transmission de signaux cellulaires, le cycle cellulaire, la réparation des dommages à l'ADN et l'apoptose. Dans les cellules cancéreuses, les niveaux d'expression de TIP60 sont bas.

TIP60 est une protéine multi-domaine, ayant un domaine CRD (chromodomaine) sur sa partie N-terminale, et un domaine MYST. A l'intérieur du domaine MYST, on trouve un domaine en doigt de zinc et un domaine catalytique connu sous le nom de domaine HAT (histone acétyltransférase). TIP60 peut acétyler de nombreuses protéines, y compris des histones (H2AK5, H3K14 et H4K) et d'autres protéines non-histones comme DNMT1, p53, ATM, c-Myc et AR. TIP60 acétyle la p53 en position K120 conduisant à l'activation de la voie p21 (arrêt de croissance) ou à l'activation de la voie PUMA (apoptose). Ainsi, TIP60 maintient la stabilité génomique et inhibe la tumorigenèse.

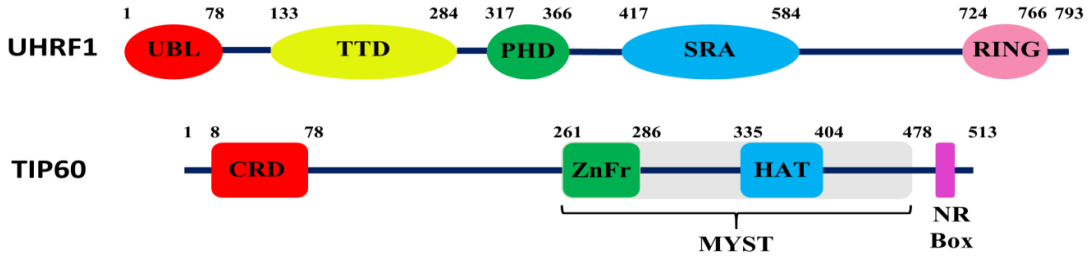

Figure 1. Schéma des structures protéiques d'UHRF1 et de TIP60.

VIII.B. Objectifs

Les principaux objectifs de ce projet étaient les suivants:

1. Etude de l'interaction d'UHRF1 et TIP60 dans les cellules par FLIM (Fluorescent lifetime imaging microscopie). Les deux protéines avec DNMT1 existent dans le même complexe épigénétique et sont associées à la réplication du code épigénétique pendant la phase S.
2. Identification du domaine de TIP60 interagissant avec UHRF1.
3. Etude de l'effet de la surexpression de TIP60 dans les cellules cancéreuses. La TIP60 présente un potentiel prometteur de suppresseur des tumeurs grâce à l'inhibition des TSG et à la prolifération des cellules tumorales. L'expression de TIP60 est faible dans la plupart des cancers ; par conséquent, la surexpression de TIP60 dans les cellules cancéreuses pourrait modifier le fonctionnement normal des TSG et contrôler la prolifération.
4. Etude de l'effet de la surexpression de TIP60 sur les taux d'UHRF1 et identification d'un autre mécanisme possible impliqués dans la régulation de l'UHRF1 par le TIP60.
5. Identification de petites molécules inhibitrices à l'aide d'un outil fluorescent précis, le "test de base-flipping assay". Cet outil permet d'étudier la dynamique d'interaction du

domaine SRA avec l'ADN. Les résultats positifs seront étudiés à l'aide de techniques biophysiques (calorimétrie isotherme, spectroscopie de fluorescence en régime permanent, anisotropie et FLIM-FRET).

6. Évaluation du potentiel anticancéreux des molécules positives sur les lignées cellulaires cancéreuses. Évaluation de l'effet de la molécule cible sur la prolifération cellulaire, l'apoptose, le cycle cellulaire et l'expression d'UHRF1 et DNMT1. Effet du candidat sur l'interaction UHRF1-DNMT1 et son impact sur le maintien de la méthylation de l'ADN.

VIII.C. Méthodologie et Résultats

i) Interaction d'UHRF1 avec son partenaire épigénétique TIP60

La technique de FLIM-FRET (Fluorescence Life time Imaging Microscopie- Fluorescence Resonance Energy Transfer) a été utilisée pour mettre en évidence l'interaction de TIP60 avec UHRF1, *in vivo* dans les cellules HeLa. TIP60-eGFP était le donneur et UHRF1-mCherry était le fluorophore accepteur. Selon le principe de FLIM-FRET, la durée de vie du fluorophore donneur est significativement réduite si le fluorophore accepteur est très proche (<8 nm) du donneur. L'expérience a montré qu'en présence d'UHRF1-mCherry, la durée de vie de TIP60-eGFP a été significativement réduite, confirmant l'interaction entre les deux protéines pendant la phase S (Figure 2).

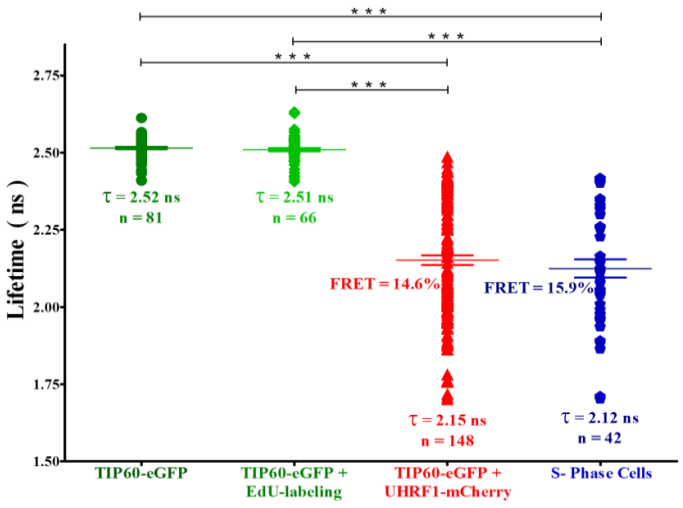

Figure 2. L'interaction entre TIP60-eGFP et UHRF1-mCherry dans la phase S du cycle cellulaire des cellules HeLa. Distribution du temps de vie de fluorescence de TIP60-eGFP (●), des cellules TIP60-eGFP marquées par EdU (♦), des cellules co-transfectées par TIP60-eGFP + UHRF1-mCherry (▲) et des cellules co-transfectées

dans la phase S du cycle cellulaire (⬣).Les valeurs sont les moyennes ± SEM de cinq expériences indépendantes. Pour l'analyse statistique, un test *t Student* a été réalisé (*** P< 0.001)

Des expériences biochimiques de co-immunoprécipitation (Co-IP) ont également été réalisées pour vérifier l'interaction entre les deux protéines exprimées de façon exogène. Les protéines UHRF1 endogène et exogène (UHRF1-mCherry) ont été co-immunoprécipitées par l'anti-TIP60-eGFP. Des expériences, *in vivo* par FLIM-FRET et *in vitro*, par Co-IP avec la protéine TIP60WT et ses mutants ont montré que l'interaction de TIP60 avec UHRF1 dépend fortement de son doigt de zinc et du domaine MYST (Figure 3).

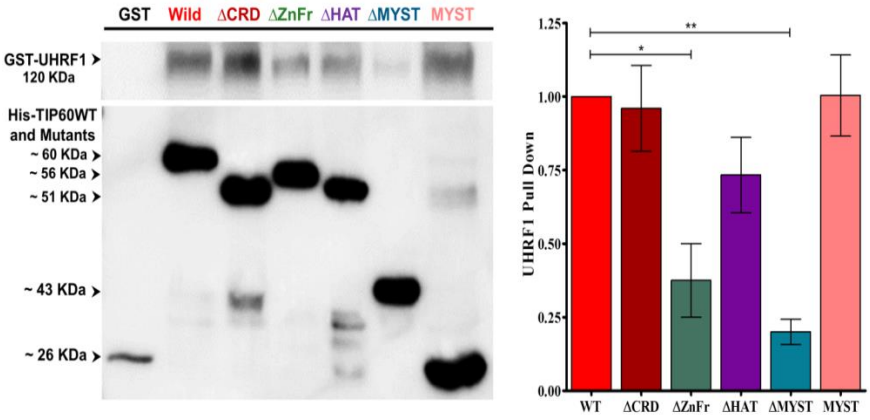

Figure 3. Analyse *in vitro* de l'interaction entre His-TIP60WT/mutants et la GST-UHRF1.

Nos résultats du Western-blot ont également montré que l'augmentation des niveaux de TIP60 dans les cellules cancéreuses entraîne une régulation à la baisse des niveaux d'UHRF1 et de DNMT1. De plus, nos données d'expériences confocales ont confirmé de même que les niveaux d'UHRF1 et de DNMT1 étaient en baisse par rapport au contrôle, lorsque TIP60-eGFP était sur-exprimée dans les cellules HeLa (Figure 4). Bien qu'il n'y ait eu aucun effet sur les taux des deux protéines lorsque le mutant TIP60ΔMYST-eGFP était surexprimé (ΔMYST mutant n'ayant aucune activité acétyltransférase).

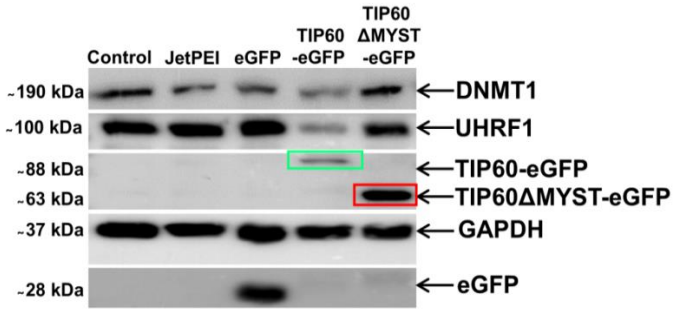

Figure 4. La surexpression de TIP60 inhibe l'expression de ses partenaires épigénétiques UHRF1 et DNMT1.

Ensuite, nous avons réalisé des expériences d'immunoprécipitation pour observer l'association d'USP7 et UHRF1 en présence de TIP60. Tout d'abord, nous avons utilisé un anticorps anti-UHRF1 pour immuno-précipiter UHRF1 et ses partenaires. Des taux réduits d'USP7 ont été observés dans l'échantillon de TIP60 par rapport au témoin et à ΔMYST mutant. Ensuite, la même expérience a été réalisée en utilisant l'anticorps anti-USP7 pour immuno-précipiter USP7 et sa protéine d'interaction UHRF1. Nous avons observé des taux plus faibles d'UHRF1 dans l'échantillon surexprimant TIP60 WT que dans l'échantillon témoin et mutant (Figure 5). Ces résultats montrent que la surexpression du TIP60 WT interfère avec l'association USP7-UHRF1.

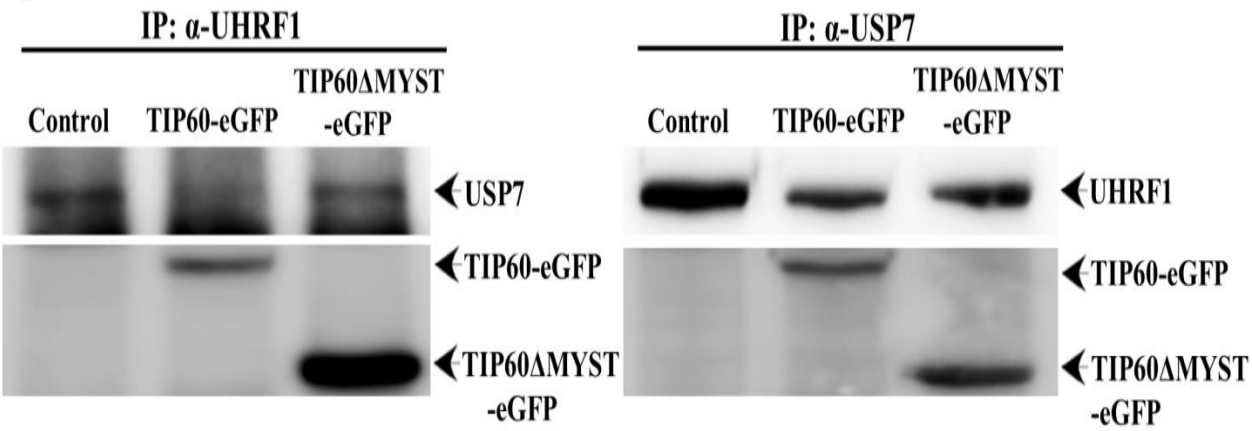

Figure 5. TIP60 interfère avec l'association UHRF1-USP7 et leurs niveaux d'expression.

Comme pour la plupart des protéines nucléaires, UHRF1 est également régulée par la voie de dégradation protéasomique. Comme nous avons montré que la surexpression TIP60 conduit à la baisse les taux d'UHRF1 dans les cellules cancéreuses, nous avons donc décidé d'évaluer en détail le mécanisme possible impliquant une inhibition d'UHRF1 par ubiquitination. Le traitement au MG-132 (inhibiteur de la dégradation protéasomique) nous montre que l'ubiquitination d'UHRF1 dépend de TIP60 ce qui a été confirmé par la suite par un test d'ubiquitination spécifique (Figure 6).

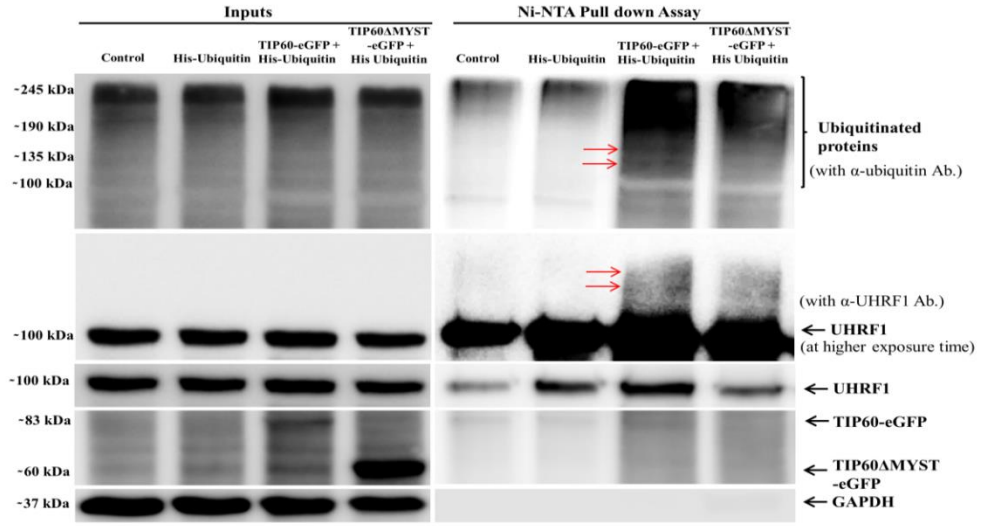

Figure 6. TIP60 induit l'ubiquitination d'UHRF1 dans les cellules HeLa. Les cellules ont été co-transfectées avec le mutant TIP60-eGFP WT ou TIP60ΔMYST-eGFP en combinaison avec His-Ubiquitin. Tous les échantillons ont été traités avec 10 µM de MG-132 pendant 8 heures avant le prélèvement des cellules. Des extraits de cellules entières et des fractions purifiées par affinité Ni-NTA ont été analysés par SDS-PAGE, puis immunoblottés avec des anticorps anti-UHRF1 et anti-ubiquitine.

L'ubiquitination est un événement rapide et dynamique, nous avons donc décidé de vérifier l'effet de la surexpression de TIP60 sur l'ubiquitination d'UHRF1 en fonction du temps. Nous avons observé des bandes UHRF1 ubiquitinées après 3 et 6 heures après la transfection TIP60 WT (Figure 7, voies 2 et 3). Dans le cas de TIP60ΔMYST, aucune ubiquitination d'UHRF1 n'a été observée. Ensemble, ces résultats soutiennent le mécanisme de dégradation de l'UHRF1 par l'ubiquitination après surexpression de TIP60.

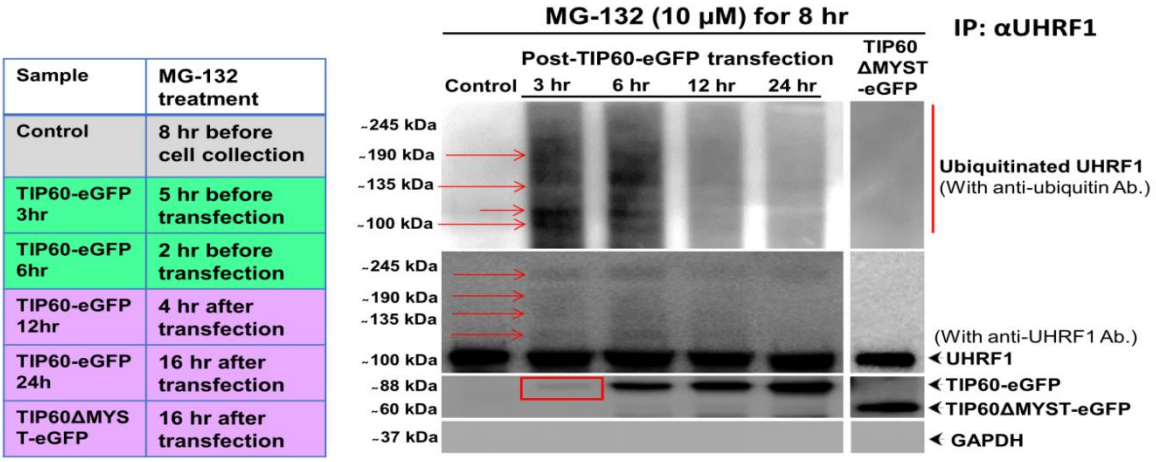

Figure 7. TIP60 induit l'ubiquitination de l'UHRF1 dans les cellules HeLa. Les cellules ont été co-transfectées avec le mutant TIP60-eGFP WT ou TIP60ΔMYST-eGFP. Tous les échantillons ont été traités avec 10 µM de MG-132 pendant 8 heures avant le prélèvement des cellules. Les cellules ont été prélevées 3, 6, 12 et 24 heures après la transfection TIP60 et 24 heures dans le cas de TIP60ΔMYST mutant. L'immuno-précipitation a été réalisée avec un anticorps anti-UHRF1.

Il est bien connu que le domaine RING d'UHRF1 possède une activité ligase E3 intrinsèque par laquelle la protéine peut s'ubiquitiner elle-même ou ubiquitiner d'autres protéines. Nous avions envisagé de vérifier qu'après la surexpression de TIP60, UHRF1 soit auto-ubiquitinée ou bien il existerait une autre ligase E3 capable d'ubiquitiner UHRF1. Des lignées cellulaires HeLa exprimant de façon stable la mutation C724A, H741A de GFP-UHRF1 ou GFP-UHRF1 (sans activité ligase E3) ont été créées. L'expérience d'immunoprécipitation a permis d'observer qu'après surexpression de TIP60 WT, UHRF1 était auto-ubiquitinée (Figure 8).

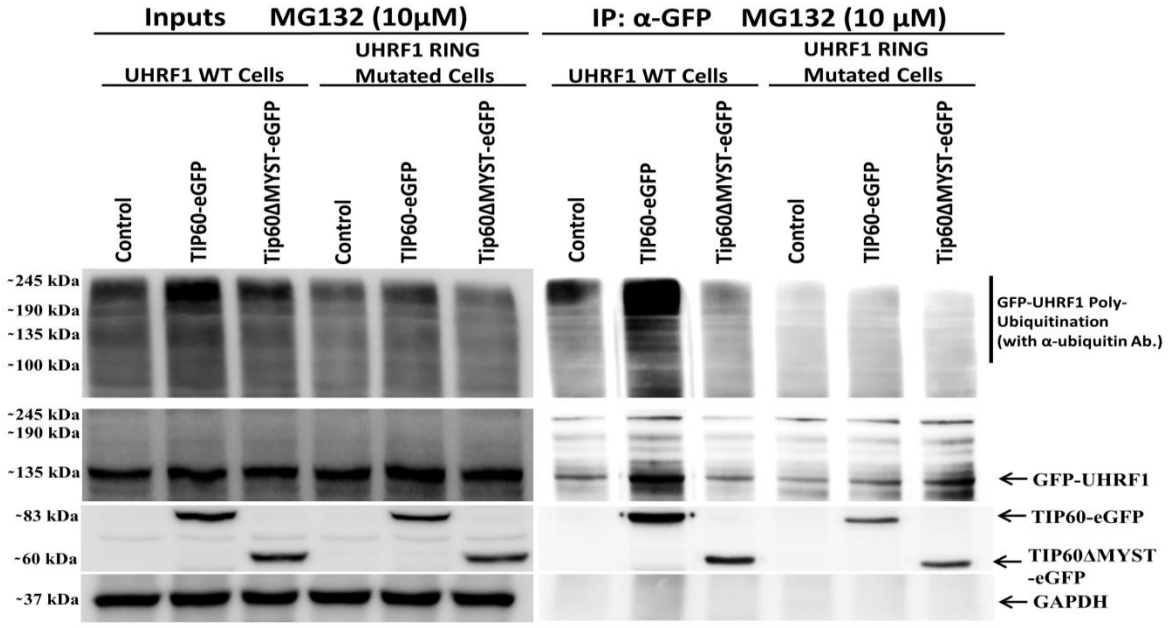

Figure 8. TIP60 induit l'auto-ubiquitination d'UHRF1 dans les cellules HeLa. Des cellules exprimant de façon stable les protéines mutantes UHRF1 WT ou UHRF1 C724A, H741A et H741A ont été transfectées avec un mutant TIP60-eGFP WT ou TIP60ΔMYST-eGFP. Tous les échantillons ont été traités avec 10 μM de MG-132 avant le prélèvement des cellules. Les lysats de cellules entières et les échantillons immunoprécipités ont été analysés par SDS -PAGE, puis immunoblotés avec des anticorps anti-GFP et anti-Ubiquitine.

La surexpression d'UHRF1 dans les cancers inhibe l'expression de nombreux gènes suppresseurs de tumeurs. Comme la surexpression de TIP60 réduisait les niveaux d'UHRF1, nous avons donc décidé d'étudier l'effet de TIP60 sur l'activation des TSG *p53* et *p73*. La surexpression de TIP60 augmente les niveaux d'expression de p53 et p73. Lors de l'activation, p53 et p73 peuvent induire l'apoptose dans les cellules cancéreuses. Nous avons donc étudié l'effet de la surexpression de TIP60 sur l'apoptose par cytométrie de flux. La viabilité des cellules transfectées par TIP60 a diminué de 39 %. Dans les cellules transfectées par TIP60, on a également observé une augmentation des cellules apoptotiques précoces et tardives. La surexpression de TIP60 augmente le niveau de p53 et induit l'apoptose via la p73 dans les cellules cancéreuses. En général, l'apoptose dépend de *p53* et *p73* entraîne l'activation

de la voie apoptotique dépendante des mitochondries par la transactivation de la protéine pro-apoptotique (BAX) et la régulation négative de la protéine anti-apoptotique (BCL2). Après surexpression de TIP60, les niveaux d'expression de la protéine BAX ont augmenté tandis que les niveaux d'expression de BCL2 ont diminué. Pour confirmer l'induction de l'apoptose, nous avons décidé de vérifier l'expression du PARP et de la caspase 3. Après surexpression de TIP60, l'activation de caspase 3 à partir de son précurseur pro-caspase 3 a été induite. L'activation de caspase 3 a déclenché le clivage de PARP pour induire l'apoptose.

Nos résultats nous permettent de proposer un modèle décrivant le rôle suppresseur de tumeur induit par la surexpression de TIP60 dans les cellules HeLa (Figure 9). La surexpression de TIP60 entraîne la dissociation d'UHRF1 de USP7 et après cela UHRF1 est dégradée par auto-ubiquitination. TIP60 induit l'apoptose par l'activation des voies de signalisation p53 et p73 en aval.

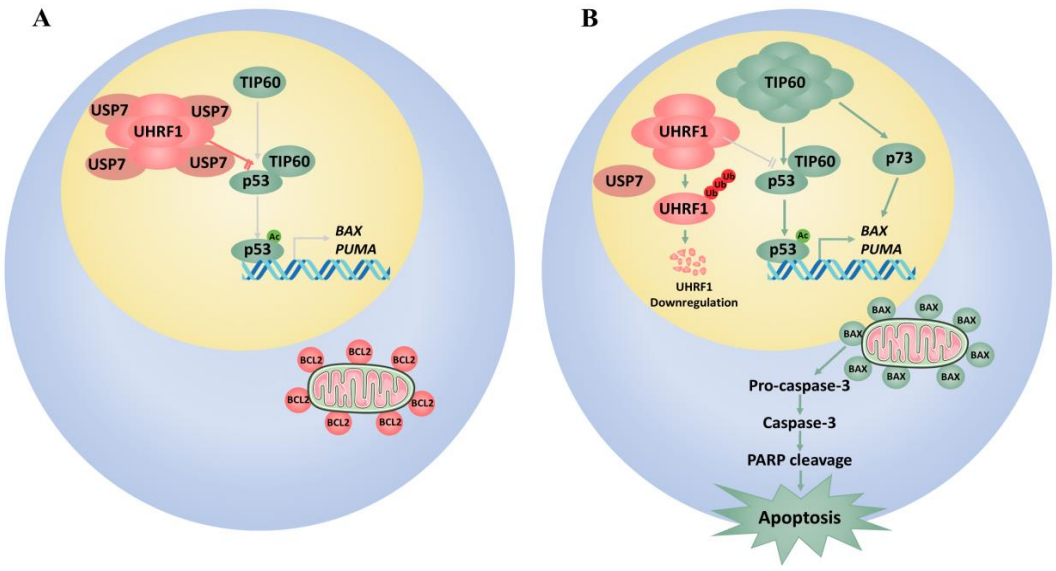

Figure 9. Modèle schématique de l'apoptose par TIP60 dans les cellules cancéreuses. **(A)** Des niveaux d'expression plus élevés de UHRF1 dans le cancer inhibent l'activation et l'apoptose par TIP60. **(B)** La surexpression TIP60 conduit à une baisse des niveaux USP7 et UHRF1. La protéine UHRF1 est dégradée par voie protéasomique. La surexpression TIP60 neutralise l'effet inhibiteur d'UHRF1 sur l'apoptose via *p53* et *p73*. Les lignes grises indiquent une voie d'inhibition tandis que les lignes foncées indiquent une voie activée.

ii) Cibler l'activité d'UHRF1 par les épi-drogues

Le but de cette étude était d'identifier et de tester de nouvelles molécules inhibitrices de l'activité du domaine SRA de la protéine UHRF1 afin de prévenir une méthylation anormale

de l'ADN. Nous avons criblé 71 molécules à l'aide d'un test spécifique « base flipping ». Parmi ces molécules, l'UM63 était le candidat le plus prometteur. Son dérivé UM63E étant inefficace, il a servi de contrôle négatif. Comme l'UM63 inhibe le base flipping, cela empêche à son tour le recrutement de la DNMT1 qui est responsable de la méthylation du brin d'ADN néo-synthétisé par duplication de ce dernier. Pour étudier cela, nous avons réalisé une expérience de microscopie confocale pour vérifier la co-localisation d'UHRF1 et DNMT1 aux fourches de réplication. Les cellules HeLa ont été co-transfectées avec eGFP-DNMT1 et UHRF1-mCherry. Dans les cellules non traitées, UHRF1 et DNMT1 sont bien co-localisées entre elles au niveau des foyers de réplication. Le traitement avec l'UM63 induit une distribution diffuse d'UHRF1 et de DNMT1 et empêche leur co-localisation au niveau des fourches de réplication. Le traitement par l'UM63E exerce un effet faible sur la co-localisation des deux protéines (Figure 10).

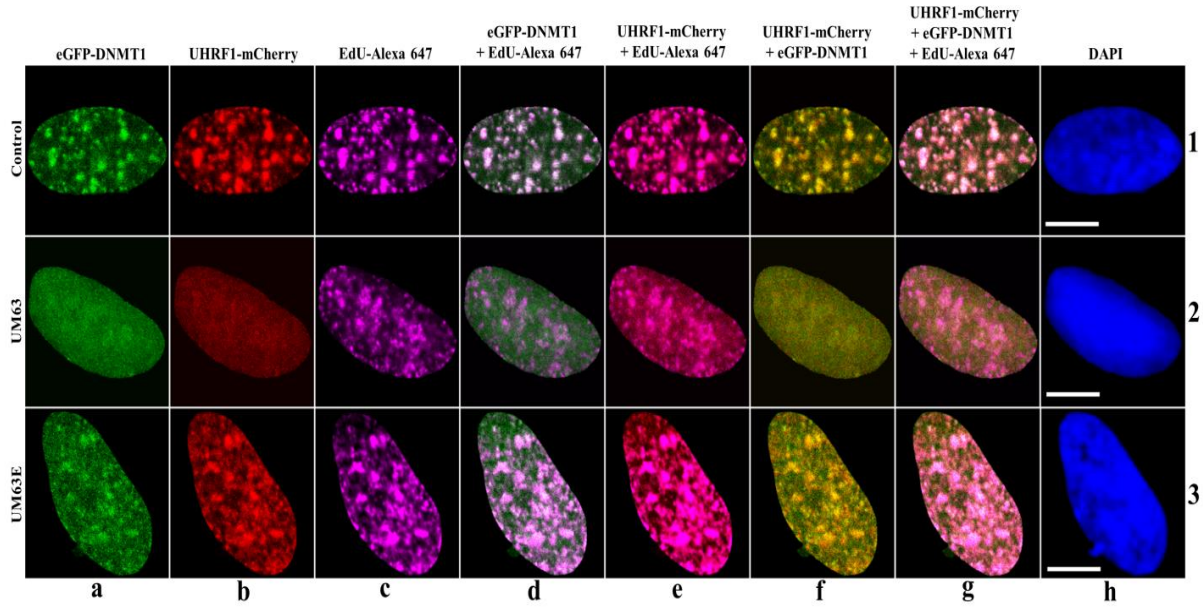

Figure 10. Effet des UM63 et UM63E sur la co-localisation de DNMT1/UHRF1. Les images confocales montrent la co-transfection d'eGFP-DNMT1 et UHRF1-mCherry dans des cellules HeLa marquées avec EdU-Alexa 647 et DAPI. Les panneaux 1, 2 et 3 correspondent aux échantillons témoins (non traités), UM63 (10 µM) et UM63E (10 µM) traités. Les canaux (a), (b) et (c) représentent respectivement eGFP-DNMT1, UHRF1-mCherry expression et EdU-Alexa 647 (phase S) marquage. Les canaux (d) et (e) correspondent respectivement à la localisation d'eGFP-DNMT1 et UHRF1-mCherry avec EdU-Alexa 647. Le canal (f) représente la co-localisation d'UHRF1-mCherry et eGFP-DNMT1, tandis que le canal (g) représente la co-localisation des deux protéines avec EdU-Alexa 647. Le canal (h) décrit l'étiquetage DAPI. La barre blanche indique une taille de 10 µm.

Ensuite, l'interaction possible entre UHRF1 et DNMT1 a été évaluée par co-immunoprécipitation. Les cellules HeLa ont été co-transfectées avec eGFP-DNMT1 et

UHRF1-mCherry avec et sans traitement UM63. La précipitation d'eGFP-DNMT1 par un anticorps anti-eGFP a entraîné la co-immunoprécipitation d'UHRF1-mCherry par rapport aux témoins. Cela suggère une interaction spécifique entre UHRF1 et DNMT1. Cette interaction a été réduite dans les cellules traitées avec UM63 alors qu'UM63E a eu un impact marginal sur cette interaction (Figure 11).

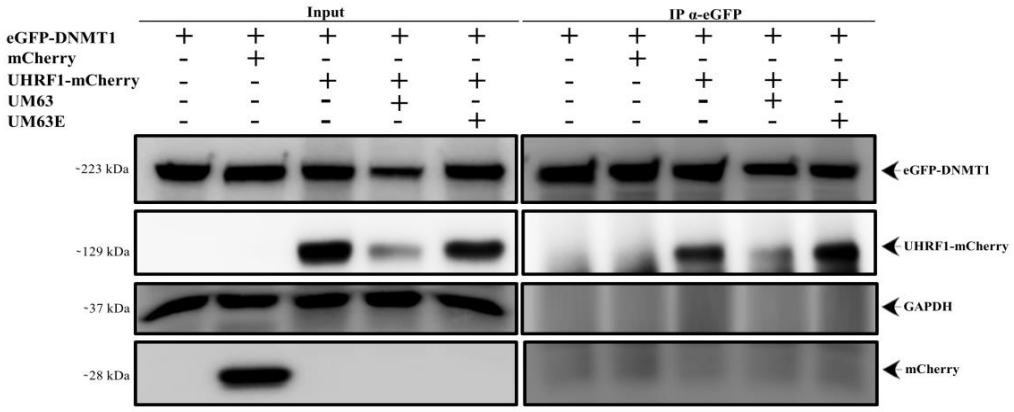

Figure 11. Effet de l'UM63 et de l'UM63E sur l'interaction DNMT1/UHRF1 dans les cellules HeLa, suivi par co-immunoprécipitation.

Pour confirmer l'interaction des deux protéines, nous avons réalisé l'expérience de FRET-FLIM. eGFP-DNMT1 a servi de donneur et UHRF1-mCherry d'accepteur.

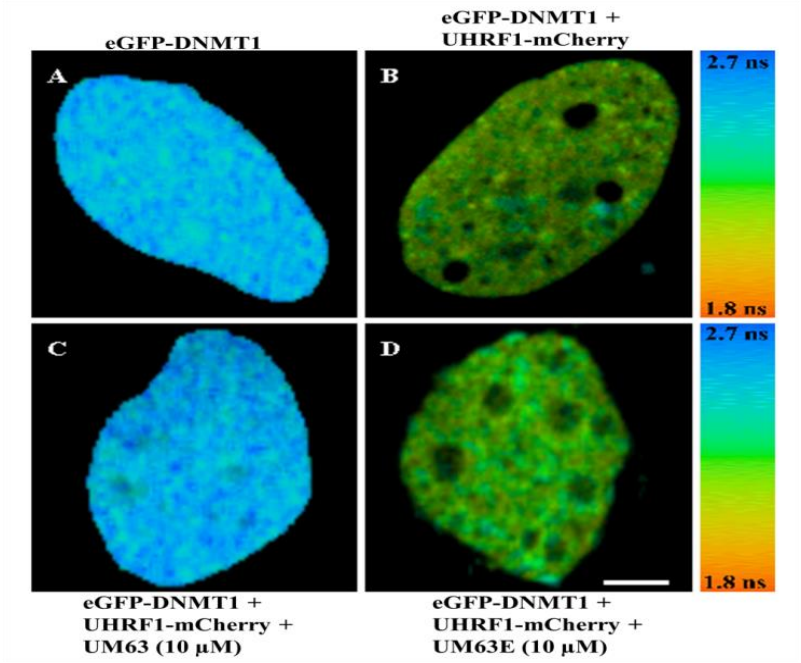

Figure 12. Effet de l' UM63 et de l'UM63E sur l'interaction DNMT1/UHRF1 analysée par FRET-FLIM.

La durée de vie d'eGFP-DNMT1 utilisé comme témoin était de 2,54 ns. Cette durée de vie a été réduite à 2,2 ns lorsqu'eGFP-DNMT1 a été co-transfectées avec UHRF1-mCherry, ce qui confirme clairement l'interaction entre les deux protéines *in vivo* dans la cellule. Le traitement UM63 dans des cellules co-transfectées eGFP-DNMT1 et UHRF1-mCherry a inhibé cette interaction car le temps de vie de la GFP est revenue à une valeur plus proche de la valeur témoin. Le traitement par UM63E n'a pas eu d'impact sur cette interaction (Figure 12).

Comme l'UM63 inhibait l'interaction UHRF1/DNMT1, une diminution globale de la méthylation de l'ADN était attendue. Pour étudier l'effet de l'UM63 sur la méthylation de l'ADN, un test d'immunofluorescence a été réalisé en utilisant un anticorps monoclonal spécifique contre 5-mC. Après le traitement par UM63, on a observé une diminution de 43 % de la méthylation globale de l'ADN, ce qui est comparable à une diminution de 60 % obtenue avec la 5-azacytidine témoin positive. UM63E n'a pas montré de diminution significative des niveaux de méthylation (Figure 13).

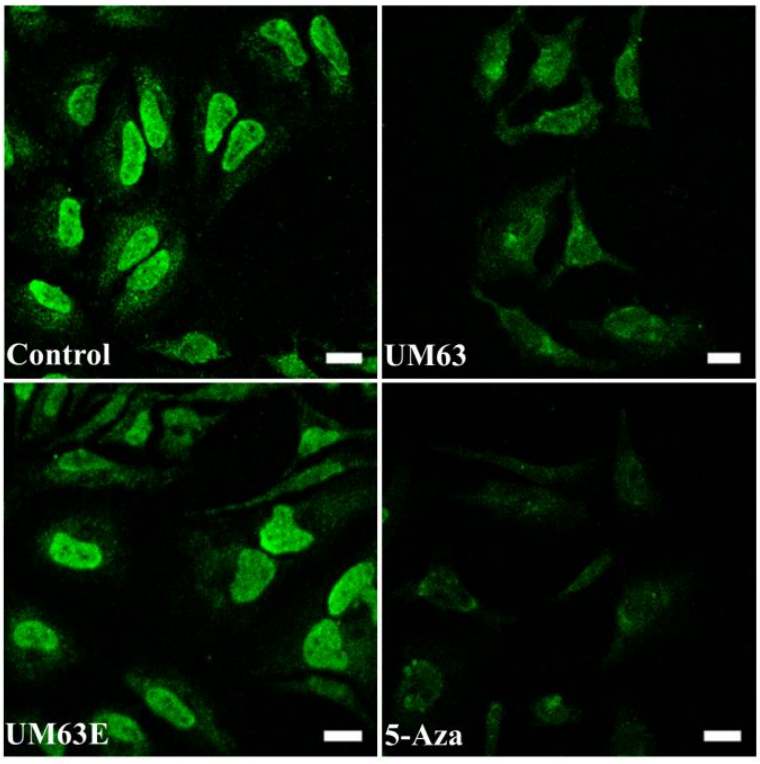

Figure 13. Effet de l''UM63 et de l'UM63E sur la méthylation globale de l'ADN dans les cellules HeLa. Immunoccytochimie de 5 mC dans les cellules HeLa. Les cellules HeLa non traitées ont servi de témoin négatif, tandis que les cellules traitées avec 10 µM de 5-Azacytidine ont été utilisées comme témoin positif et comparées aux cellules traitées avec 10 µM d'UM63 et UM63E.

VIII.D. Conclusion et Perspectives

Nos résultats suggèrent qu'UHRF1 et TIP60 avec DNMT1 sont présents dans le même complexe épigénétique (Figure 14). TIP60 est un véritable partenaire d'interaction de l'UHRF1 qui interagit avec l'UHRF1 à travers son domaine MYST. La surexpression de TIP60 interfère avec l'association USP7-UHRF1. TIP60 régule à la baisse les taux d'UHRF1 (grâce à l'auto-ubiquitination de l'UHRF1) et induit l'apoptose, ce qui pourrait contrer le potentiel oncogène de l'UHRF1 dans le cancer.

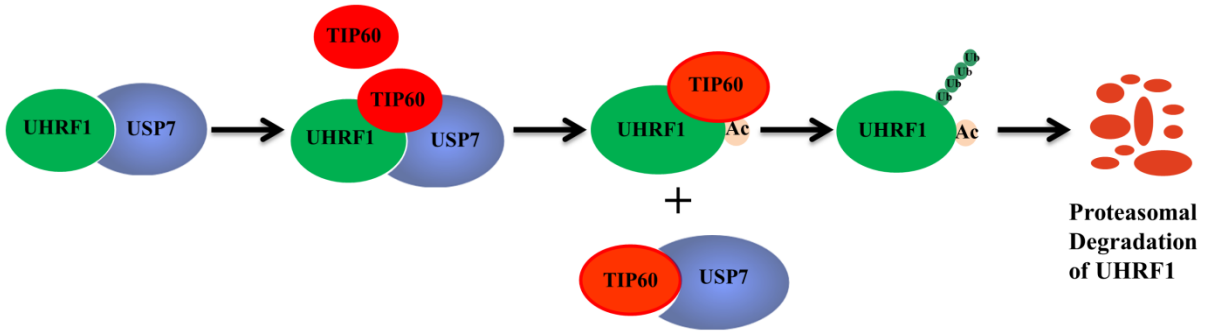

Figure 14. Modèle illustrant la régulation d'UHRF1 dans les cellules cancéreuses. Lorsqu'UHRF1 est associée à USP7, UHRF1 est protégée contre la dégradation due à l'ubiquitination. Les niveaux augmentés de TIP60 peuvent interférer avec cette association. TIP60 peut rivaliser avec USP7 pour la liaison avec UHRF1 ou il peut faire un changement conformationnel dans la zone d'interaction USP7 de UHRF1 par acétylation. Après dissociation d'USP7, UHRF1 peut être régulée à la baisse par ubiquitination médiée par sa propre activité E3 ligase ou par toute autre ligase E3 présente dans les cellules.

UM63 peut agir comme un inhibiteur de UHRF1 en se localisant dans la poche de liaison de 5mC avec une affinité de l'ordre du micromolaire. Il bloque ainsi le basculement de 5 mC et le recrutement subséquent de la DNMT1. UM63 interfère avec l'interaction UHRF1/DNMT1 et induit une diminution de la méthylation génomique globale.

Dans la perspective de ce projet, il serait intéressant d'étudier l'effet de l'inhibition de l'activité de TIP60 (en utilisant un inhibiteur spécifique de TIP60) sur UHRF1 et sur l'interaction avec l'ubiquitine par FRET-FLIM. Le mécanisme de régulation de l'UHRF1 peut être élucidé dans des lignées de cellules cancéreuses « knockdown » pour TIP60. Il sera intéressant également d'étudier *in vivo* l'acétylation de UHRF1 médiée par TIP60. De plus, le recrutement d'UHRF1 et de TIP60 pourra être étudié dans la réponse aux dommages de l'ADN et d'autres activités cellulaires importantes. UM63 peut être utilisé pour étudier l'effet du basculement de la base sur UHRF1/DNMT1/histones. Enfin, UM63 peut être considéré comme un outil de criblage de nouvelles molécules ciblant l'UHRF1 et sur fond d'optimisations « hit-to-lead ».

Tanveer AHMAD

Inhibition de la protéine UHRF1 par les partenaires épigénétiques et les épi-drogues

Résumé

UHRF1 est protéine nucléaire sur-exprimée dans les cellules cancereuses. Elle joue un rôle essentiel dans la méthylation de l'ADN, favorise la prolifération cellulaire et inhibe l'expression des gènes suppresseurs de tumeurs. TIP60 est un partenaire important d'UHRF1 qui participe au remodelage de la chromatine, à la régulation transcriptionnelle des gènes et à d'autres activités cellulaires grâce à son activité acétyltransférase. Les deux protéines sont impliquées dans la régulation de l'activité et la stabilité d'importantes protéines telles que la DNMT1 et la p53. Le but de cette thèse était d'étudier le mécanisme d'interaction de TIP60 avec UHRF1 et d'explorer l'effet de la surexpression de TIP60 dans la régulation d'UHRF1. Un autre objectif était de dépister et de développer des inhibiteurs de l'UHRF1 qui puisse cibler son activité. Pour atteindre ces objectifs, nous avons utilisé diverses approches, y compris des techniques biologiques et biophysiques. Les résultats ont révélé qu'UHRF1 interagit avec le domaine MYST de TIP60 durant la phase S du cycle cellulaire. La surexpression de TIP60 régule la dégradation d'UHRF1 (un oncogène) de manière dépendent d'une ubiquitination, expliquant ainsi son rôle suppresseur de tumeur. De plus, un inhibiteur d'UHRF1 appartenant à la famille des anthraquinones a été identifié. Cette molécule inhibe l'activité de basculement de la cytosine méthylée réalisée par le domaine SRA d'UHRF1. Elle a également altéré l'interaction UHRF1/DNMT1 et réduit les niveaux de méthylation globaux.

Résumé en anglais

UHRF1 is a nuclear protein that is in cancer cells. It plays an essential role in DNA methylation, promotes cell proliferation and inhibits the expression of tumor suppressor genes. TIP60 is an important partner of UHRF1 which participates in chromatin remodeling, transcriptional gene regulation and other cellular activities through its acetyltransferase activity. Both proteins are involved in regulating the activity and stability of important proteins such as DNMT1 and p53. The purpose of this thesis was to study the interaction mechanism of TIP60 with UHRF1 and to explore the effect of overexpression of TIP60 in the regulation of UHRF1 expression. Another objective was to identify and develop UHRF1 inhibitors that could target its activity. To achieve these objectives, we used different approaches, including biological and biophysical techniques. The results revealed that UHRF1 interacts with the MYST domain of TIP60 during the S phase of the cell cycle. The overexpression of TIP60 induces the degradation of UHRF1 (an oncogene), in a poly-ubiquitination dependent way, explaining in parts its tumor suppressing role. In addition, an anthraquinone UHRF1 inhibitor was found. This molecule inhibits the flipping activity of methylated cytosine produced by SRA domain of UHRF1. It also altered the UHRF1/DNMT1 interaction and reduced global methylation levels.

Keywords: UHRF1, TIP60, DNMT1, Protein-Protein interaction, Ubiquitination, DNA methylation, Histone acetyltransferase (HAT), FLIM, FRET